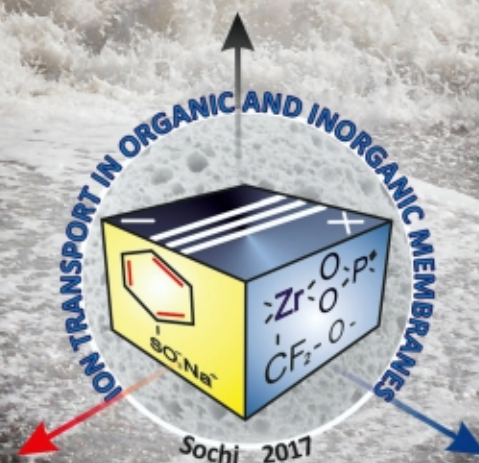


ISBN 978-5-9906777-6-0

ION TRANSPORT IN ORGANIC AND INORGANIC MEMBRANES

CONFERENCE PROCEEDING



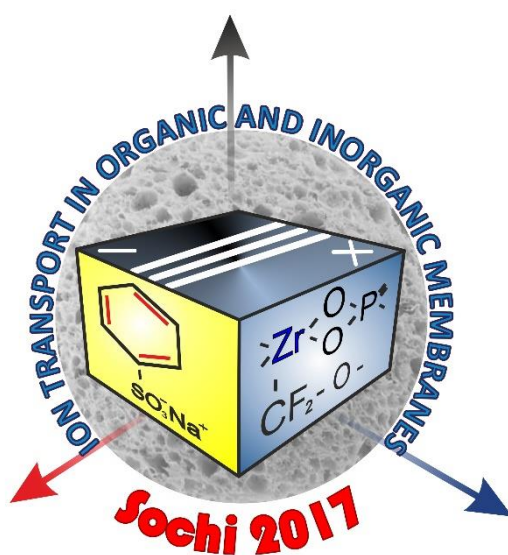
RUSSIAN ACADEMY OF SCIENCES
SECTION "MEMBRANES AND MEMBRANE TECHNOLOGIES" OF D.I.
MENDELEEV RUSSIAN CHEMICAL SOCIETY
RUSSIAN FOUNDATION FOR BASIC RESEARCH
FEDERAL AGENCY FOR SCIENTIFIC ORGANIZATIONS
RAS SCIENTIFIC COUNCIL ON PHYSICAL CHEMISTRY
RUSSIAN MEMBRANE NETWORK
KUBAN STATE UNIVERSITY
KURNAKOV INSTITUTE OF GENERAL AND INORGANIC CHEMISTRY RAS
«MEMBRANE TECHNOLOGY» INNOVATION ENTERPRISE

INTERNATIONAL CONFERENCE

Ion transport in organic and inorganic membranes

Conference Proceedings

23 - 27 May 2017



Krasnodar 2017

SCIENTIFIC/ORGANIZING COMMITTEE

Chairman YAROSLAVTSEV A.B. (*Russia*)
Co-chairman ZABOLOTSKY V.I. (*Russia*)

POURCELLY G. (*France*)

NIKONENKO V.V. (*Russia*)

Scientific secretary KONONENKO N.A. (*Russia*)

AGEEV E.P. (*Russia*)

OZERIN A.N. (*Russia*)

BILDYUKEVICH A.V. (*Belarus*)

PISMENSKAYA N.D. (*Russia*)

BOBRESHOVA O.V. (*Russia*)

ROLDUGHIN V.I. (*Russia*)

CRETIN M. (*France*)

RUBINSTEIN I. (*Israel*)

DAMMAK L. (*France*)

SHAPOSHNIK V.A. (*Russia*)

FILIPPOV A.N. (*Russia*)

SHELDESHOV N.V. (*Russia*)

GRAFOV B.M. (*Russia*)

STAROV V.M. (*UK*)

GRANDE D. (*France*)

TSKHAY A.A. (*Kazakhstan*)

KHOHLOV A.R. (*Russia*)

VOLFKOVICH Yu.M. (*Russia*)

NOVAK L. (*Czech Republic*)

VOLKOV V.V. (*Russia*)

Local organizing committee (*Krasnodar, Russia*)

ACHOH A.R.

LOZA N.V.

BELASHOVA E.D.

LOZA S.A.

DOLGOPOLOV S.V.

MAREEV S.A.

ETEREVSKOVA S.I.

MELNIKOV S.S.

FALINA I.V.

NEBAVSKAYA K.A.

KOZMAI A.E.

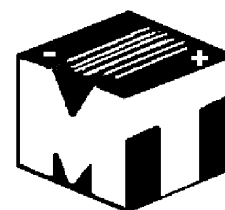
SHKIRSKAYA S.A.

Sponsors:

RUSSIAN FOUNDATION
FOR BASIC RESEARCH

FEDERAL AGENCY FOR
SCIENTIFIC ORGANIZATIONS

«MEMBRANE TECHNOLOGY»
INNOVATION ENTERPRISE



Мероприятие проводится при финансовой поддержке Российского фонда
фундаментальных исследований, Проект № 17-08-20100

Preface



May 8, 2017 is the 70th anniversary of Victor Ivanovich Zabolotsky, the permanent chairman of our conference for almost 30 last years. Over these years, the conference survived the difficult times of the 90s, it has become international and is now again on the rise. The membership of the conference is constantly expanding, and it is becoming more attractive not only for the Russian academic and technological world, but also for colleagues from the near and far abroad. This development is largely due to the well-balanced harmonious approach to the selection of the conference scope, the possibility of discussions and to a broader representation of young scientists. Great merit in the success of the conference belongs to Victor Ivanovich, his large scientific vision and erudition. In 1970, V.I. Zabolotsky graduated from the

Chemical Faculty at the Far Eastern State University (Vladivostok) with a degree in Chemistry. After the graduate school and defense of its PhD thesis at the Leningrad Institute of Technology in 1973, he has been working for 44 years at the Kuban State University. Victor Ivanovich began his scientific work at KubSU as a young research fellow under the direction of the father of membrane electrochemistry, Nikolai Petrovich Gnusin. In 1987, Victor Ivanovich became a doctor of science, and starting from 1988, he is the head of the Department of Physical Chemistry at KubSU. Since 1986, for 13 years, he worked as the vice-rector for science at this university. At present, he is the director of the Membrane Research Institute at KubSU, a full member of the International Academy of Sciences of the Higher School, a member of the European Membrane Society, Membrane Club of France. Victor Ivanovich is the Honored Worker of Science of the Russian Federation, Honored Worker of the Higher School of Russia, Honored Inventor of the Russian Federation, Honored Worker of Science of the Kuban. He is a member of the editorial board of the "Membranes and Membrane Technologies" journal, chairman of the Dissertation Council D212.101.10 on the defense of doctoral and candidate dissertations on two specialties, Electrochemistry and Inorganic Chemistry. Victor Ivanovich is the author of more than 300 articles in peer-reviewed Russian and international journals, 62 patents and copyright certificates for inventions and 2 monographs. Under his leadership, 3 doctoral and more than 20 candidate dissertations were defended. The undoubted merit of Victor Ivanovich is the fact that the department headed by him occupies the 3rd place in the world on the publication activity in the field of electro dialysis and ion-exchange membranes (Scopus).

V.I. Zabolotsky made a significant contribution to the development of membrane electrochemistry. He developed, together with N.P. Gnusin, the concept of generalized conductivity for describing the transport processes in real microheterogeneous membranes, a theory of water splitting at the interphase boundaries of bipolar and monopolar membranes. As a result of comprehensive studies of coupled phenomena of concentration polarization in the overlimiting state of electromembrane systems, new non-hydrodynamic methods of increasing mass transfer in dilute solutions were discovered and implemented into the practice of electro dialysis, which made it possible to significantly expand the scope of electro dialysis. Under the direction of V.I. Zabolotsky, a reagent-free electromembrane technology for the deionized and ultrapure water production directly from tap water was developed for the first time in the world practice. Installations of various capacities have been introduced at the enterprises of the chemical industry, heat power engineering, electronic industry, in hemodialysis departments of regional hospitals, in the production of heavy-duty polyaramid fibers, high-quality alcohol and alcohol-free drinks, in obtaining drinking water of the highest quality category.

The organizing committee of the international conference "Ion transport in organic and inorganic membranes" heartily congratulates Victor Ivanovich on this remarkable anniversary and wishes him good health and new creative successes in the development of membrane science and technology.



Contents

1.	Dmitriy Abonosimov, Sergey Lazarev, Irina Khorokhorina Study for the hydrodynamic structure of the flow in the membrane element of tubular type (<i>Tambov, Russia</i>)	16
2.	Oleg Abonosimov, Sergey Lazarev, Sergey Kotenev Investigation of kinetic characteristics the reverse osmosis desalination-concentration of solutions chemical water treatment (<i>Tambov, Russia</i>)	19
3.	Aslan Achoh, Victor Zabolotsky, Stanislav Melnikov, Konstantin Lebedev Verification of phenomenological model of competitivetransport of ions in sulfate-nitrate solutions of electrolytes (<i>Krasnodar, Russia</i>)	22
4.	Evgeny Ageev, Nadezhda Strusovskaya, Natalia Matushkina Visualization and removal of hydrophilic admixtures from hydrophobic isotactic polypropylene films (<i>Moscow, Russia</i>)	25
5.	Denis Ainetdinov, Marina Kardash, Tatyana Yakunina, Artem Morozov, Roman Polnyi Influence of modifying additives on structure and properties of multifunctional nanocomposites "Polikon K" (<i>Saratov, Russia</i>)	27
6.	Elmara Akberova, Elena Goleva, Vladimir Kolganov, Dmitrii Korotkov Spectral properties of concentration field fluctuations in stratified electromembrane systems with strongly basic anion-exchange membranes after temperature treatment (<i>Voronezh, Russia</i>)	29
7.	Elmara Akberova, Elena Goleva, Vera Vasil'eva Diffusion boundary layers in the solution on the interphase with sulfocation exchange membranes after temperature modification (<i>Voronezh, Russia</i>)	31
8.	Elmara Akberova, Vera Vasil'eva, Mikhail Malykhin Effect of the changes in chemical nature of the ionogenic groups for anion-exchange membranes after temperature treatment on the size of the electroconvective instability region in high-current modes (<i>Voronezh, Russia</i>)	34
9.	Anastasia Alekseenko, Vladimir Guterman, Vadim Volochaev, Angelina Pavlets, Kirill Paperj Optimization of composition and microstructure with the aim of increasing the specific electrochemical characteristics of catalysts with a low content of platinum (<i>Rostov-on-Don, Russia</i>)	37
10.	Diana Aleshkina, Veronika Sarapulova, Natalia Pismenskaya Effect of anthocyanins on the morphology and chemical composition of AMX-Sb membrane surface (<i>Krasnodar, Russia</i>)	40
11.	Marina Andreeva, Lasaad Dammak, Christian Larchet, Natalia Kononenko Impact of pulsed electric field modes on scaling formation during electro dialysis (<i>Krasnodar, Russia; Thiais, France</i>)	43
12.	Natalia Anisimova, Anna Korovkina, Stanislav Rybtsev, Tolera Badessa, Vladimir Shaposhnik Electrical resistivity of multilayer monopolar ion-exchange membranes (<i>Voronezh, Russia; Arba Minch, Ethiopia</i>)	46
13.	Tatiana Anokhina, Tatiana Pleshivtseva, Alexey Yushkin, Viktoria Ignatenko, Sergey Antonov, Alexey Volkov Study of dissolution of cellulose in ionic liquid/DMSO system and preparation of dense membranes (<i>Moscow, Russia</i>)	48
14.	Anatoly Antipov, Mikhail Vorotyntsev Bromate anion electroreduction on rotation disc electrode: Asymptotic behavior for very high currents (<i>Moscow, Chernogolovka, Russia; Dijon, France</i>)	51
15.	Anatoly Antipov, Mikhail Vorotyntsev Bromate electroreduction via catalytic redox-mediator (EC') mechanism (<i>Moscow, Chernogolovka, Russia; Dijon, France</i>)	54
16.	Anatoly Antipov, Mikhail Vorotyntsev Theory of steady-state convective-diffusion transport for bromate electroreduction at rotating disc electrode. Equal	56

- diffusion coefficients approximation (*Moscow, Chernogolovka, Russia; Dijon, France*)
17. **Irina Antropova, Olga Koshkina, Eldar Magomedbekov, Tatiyana Dmitrieva, Yurii Birukov, Sergey Lakeev, Aleksei Shepelev, Vyacheslav Minashkin, Aleksandr Smolyanskii** Comparative research of regularities of passing of hydrosols nano-/microparticles of silver through nuclear and aerosol filters (*Moscow, Russia*) 59
 18. **Pavel Apel, Irina Blonskaya, Nikolay Lizunov, Oleg Orelovich, Christina Trautmann** The role of osmotic effects in asymmetric track etching (*Dubna, Russia; Darmstadt, Germany*) 61
 19. **Artem Atlaskin, Maxim Trubyanov, Pavel Drozdov, Ilya Vorotyntsev, Vladimir Vorotyntsev** Membrane cascade type of "continuous membrane column" (*Nizhny Novgorod, Russia*) 64
 20. **Stepan Bazhenov, Danila Bakhtin, Alexey Volkov** Ionic liquids as CO₂ solvents for high pressure gas-liquid pvtms-membrane contactors (*Moscow, Russia*) 67
 21. **Myriam Bdiri, Lasâad Dammak, Christian Larchet, Lobna Chaabane, Fayçal Hellal** Characterization of ion-exchange membranes used in food industry and contribution to the cleaning membranes using chemical solutions (*Thiais, France; Tunisie*) 70
 22. **Ekaterina Belashova, Sergey Mikhaylin, Victor Nikonenko, Natalia Pismenskaya, Laurent Bazinet** Impact of membrane scaling nature on the water splitting and electroconvection development at the surface of the cation exchange membrane (*Krasnodar, Russia; Quebec, Canada*) 72
 23. **Mikhail Berekchiian, Dmitrii Petukhov, Andrei Eliseev** Study of ion diffusion through anodic alumina membranes (*Moscow, Russia*) 75
 24. **Sergey Bessarabov, Vita Borisova, Valeriya Plotnikova** Justification of the nano-filtration membranes application at small recreational facilities under conditions of the Krasnodar territory climate (*Novocherkassk, Russia*) 76
 25. **Anastasia Bocharova, Irina Falina, Olga Demina** Conductive properties of MK-40 heterogeneous membrane in different ionic forms (*Krasnodar, Russia*) 78
 26. **Yuliya Bogdanova, Valentina Dolzhikova** The relationship of energy characteristics of surfaces of continuous polymer membranes and their transport properties (*Moscow, Russia*) 80
 27. **Daniil Bograchev, Yurii Volfkovich, Alexey Rychagov, Alexey Mikhailin, Valentin Sosenkin** Development of mathematical model of water capacitive deionization (*Moscow, Russia*) 83
 28. **Denis Bondarev, Victor Zabolotsky, Alexander Bepalov, Anastasia But** Optimal conditions adjustment for synthesis of polymeric modifiers for anion-exchangemembranes (*Krasnodar, Russia*) 86
 29. **Ilya Borisov, Evgenia Grushevenko, Georgy Golubev, Danila Bakhtin, Vladimir Volkov** Thermopervaporation membranes based on syndiotactic polybutadiene and polymethylsiloxane for removal of chlororganic from water (*Moscow, Russia*) 88
 30. **Ilya Borisov, Anna Ovcharova, Stepan Bazhenov, Rustem Ibragimov, Galina Bondarenko, Alexandr Bildyukevich, Vladimir Volkov** Highly efficient composite ptmsp membranes on polysulfone supports for gas-liquid membrane contactors (*Moscow, Kazan, Russia; Minsk, Belarus*) 91
 31. **Ilya Borisov, Nikolai Ushakov, Evgenia Grushevenko, Vladimir Volkov, Eugene Finkelshtein** Polydimethylsilalkylene-dimethylsiloxanes - new membrane materials for separation butanol from water via thermopervaporation (*Moscow, Russia*) 94

32. **Denis Bouyer** Polymeric membrane formation - interplay between process conditions and final morphology. A coupling between experimental and modeling approaches (*Montpellier, France*) 97
33. **Anastasya Boyarishcheva, Nikita Kovalev, Nikolay Sheldeshov, Victor Zabolotsky** Water splitting in MB-2 bipolar membrane, modified by chromium(III) hydroxide (*Krasnodar, Russia*) 100
34. **Dmitrii Butylskii, Semyon Mareev, Christian Larchet, Lasaad Dammak, Natalia Pismenskaya, Victor Nikonenko** Experimental and theoretical investigation of surface geometrical heterogeneity of homogeneous ion-exchange membranes using scanning electrochemical microscopy method (*Krasnodar, Russia; Thiais, France*) 103
35. **Marc Cretin** Nanomaterials for electrochemical applications in energy conversion and waste water treatment (*Montpellier, France*) 105
36. **Lasaad Dammak, Mona Chérif, Anton Kozmai, Lobna Chaabane, Christian Larchet, Victor Nikonenko** The neutralization dialysis process: State of the art and perspectives (*Thiais, France; Krasnodar, Russia*) 107
37. **Ekaterina Dankovtseva, Svetlana Shkirskaya** Investigation of selectivity of perfluorinated membranes modified by polyaniline (*Krasnodar, Russia*) 110
38. **Umit Demirci** Boron hydrides for energy: Focus on membranes, an underinvestigated field (*Montpellier, France*) 112
39. **Tatyana Denisova, Ekaterina Safronova, Anna Parshina, Olga Bobreshova** The influence of proton-acceptor properties and concentration of dopants introduced into MF-4SC membranes on the cross sensitivity of DP-sensors to ions in alkaline solutions of glutamic and aspartic acids (*Voronezh, Moscow, Russia*) 113
40. **Maria Dmitrieva, Ekaterina Zolotukhina, Ekaterina Gerasimova, Aleksey Terentyev, Yuriy Dobrovolsky** Electrocatalytic properties of extracts obtained from *E.Coli* BB culture at mediated glucose oxidation (*Chernogolovka, Russia*) 114
41. **Nikita Faddeev, Alexandra Kuriganova, Nina Smirnova** Electrochemical oxidation of alcohols on Pd/C catalysts synthesized by pulse alternating current technique (*Novocherkassk, Russia*) 116
42. **Irina Falina, Olga Demina, Victor Zabolotsky** Verification of capillary model of free solvent electroosmotic transfer in ion-exchange membranes (*Krasnodar, Russia*) 118
43. **Irina Fedorova, Lyubov Safonova** Study of the proton transfer processes in non-aqueous solutions of Brønsted acid (*Ivanovo, Russia*) 120
44. **Patrick Fievet, Anthony Szymczyk, Sébastien Déon** Theoretical and experimental tools for investigating transport properties through nanofiltration membranes (*Besançon, Rennes, France*) 123
45. **Anatoly Filippov** Synthesis and prediction of transport properties of hybrid bilayer ion-exchange membranes on the base of MF-4SC, halloysite and platinum (*Moscow, Russia*) 125
46. **Anatoly Filippov, Tamara Philippova** Cell method to calculation of electric conductivity of ion-exchange membranes (*Moscow, Russia*) 129
47. **Elizaveta Frants, Georgy Ganchenko, Vladimir Shelistov, Evgeny Demekhin** Asymptotic and numerical investigation of electrophoresis in a weak electric field (*Krasnodar, Moscow, Russia*) 132
48. **Anna Gaidamaka, Irina Bagryantseva, Valentina Ponomareva** Phase composition, thermal and transport properties of rubidium mono and dihydrogen phosphates system (*Novosibirsk, Russia*) 134
49. **Igor Galushka, Denis Terin, Marina Kardash, Larisa Karpenko-Jereb, Denis Ambarnov, Artem Morozov, Sergey Tsyplyaev** Evaluation of 135

- modification of materials "Polykon A" by porous silicon nanoparticles (*Saratov, Russia; Graz, Austria*)
50. **Georgy Ganchenko, Ekaterina Gorbacheva, Evgeny Demekhin** Two-layer flow of the electrolyte-dielectice system under ac electric field (*Krasnodar, Russia*) 138
 51. **Nataly Ganchenko, Georgy Ganchenko, Evgeny Demekhin** Investigation of electrolyte near nonideal ionselective surfaces (*Krasnodar, Russia*) 139
 52. **Violetta Gil, Victor Nikonenko, Natalia Pismenskaya** The influence of the current density on the diffusion boundary layer structure in sodium, calcium and magnesium chloride solutions (*Krasnodar, Russia*) 140
 53. **Elena Goleva, Vera Vasil'eva** Transport of sodium chloride and phenylalanine through ion-exchange membranes in neutralization dialysis (*Voronezh, Russia*) 143
 54. **Daniel Golubenko, Andrey Yaroslavtsev** Polymethylpentene: the optimum material for ion exchange membranes fabrication by UV post-grafting (*Moscow, Russia*) 146
 55. **Georgy Golubev, Ilya Borisov, Vladimir Vasilevsky, Vladimir Volkov** Thermopervaporation process with semi-automatic adsorption method for bio-butanol recovery from fermentation broth (*Moscow, Russia*) 149
 56. **Andrey Gorobchenko, Semyon Mareev, Andrey Kononov** Simulation of liquid flow in the channel of a laboratory electrodyalysis cell (*Krasnodar, Russia*) 152
 57. **Evgenia Grushevenko, Ilya Borisov, Danila Bahtin, George Shandryuk, Galina Bondarenko, Alexey Volkov** Silicone rubbers with alkyl and silicon-containing side chains substituents for hydrocarbons separation (*Moscow, Russia*) 154
 58. **Farhad Heidary** Synthesis of Fe₃O₄ nanostructures by sono-chemical method and its application in cellulose acetate polymeric nanocomposite membrane (*Arak, Iran*) 157
 59. **Farhad Heidary, Behrouz Heidari, Siavash Heidary, Elahe Naseri, Maryam Ansari** Preparation of nanocomposite membrane containing magnetite nanoparticles for removal of metal ions (*Arak, Iran*) 159
 60. **Olga Istakova, Dmitry Konev, Mikhail Vorotyntsev** Preparation of cobalt (II) polyporphine films by electrochemical method and their catalytic properties (*Chernogolovka, Moscow, Russia*) 161
 61. **Larisa Karpenko-Jereb** Effect of polymer and counter-ion nature on the structural features of the polymer electrolyte membranes (*Graz, Austria*) 164
 62. **Larisa Karpenko-Jereb, Eduard Schatt, Clemens Fink, Peter Urthaler, Alexander Bergmann, Reinhard Tatschl** Impact of ionomer in catalyst layer on performance of a polymer electrolyte fuel cell (*Graz, Austria*) 167
 63. **Olesya Kharchenko, Ekaterina Belashova, Natalia Pismenskaya** Mass transfer characteristics of anion exchange membranes in NaCl and NaH₂PO₄ solutions (*Krasnodar, Russia*) 168
 64. **Serezha Kirakosyan, Sergey Belenov, Vladimir Guterman** Synthesis and investigation of the catalytic properties of novel Pt-Co nanoparticles with gradient structure (*Rostov-on-Don, Russia*) 171
 65. **Anastasia Klevtsova, Veronika Sarapulova, Natalia Pismenskaya** Investigation of the interactions of anthocyanins with some ion-exchange materials using color indication technique (*Krasnodar, Russia*) 173
 66. **Denis Kolot, Stanislav Melnikov, Elena Nosova** Changes in transport-structural characteristics of heterogeneous ion-exchange membranes after contact with solutions containing anions of carboxylic acids (*Krasnodar, Russia*) 176
 67. **Natalia Kononenko, Olga Demina, Irina Falina, Svetlana Shkirskaya, Anatoly Filippov** Experimental and theoretical investigations of diffusion and electroosmotic permeability of ion-exchange membranes (*Krasnodar, Russia*) 179

68. **Natalia Kononenko, Daniel Grande, Victor Nikonenko** Investigation of correlation between structural and electrotransport properties of modified ion-exchange membranes (*Krasnodar, Russia; Thiais, France*) 181
69. **Andrey Kononov, Semyon Mareev, Andrey Gorobchenko, Victor Nikonenko** 1D galvanostatic model of ion transport in membrane system at overlimiting current modes (*Krasnodar, Russia*) 183
70. **Olga Koshkina, Irina Antropova, Dariya Nebaikina, Phyo Myint O, Eldar Magomedbekov, Aleksandr Smolyanskii** Transport through nuclear filters of the nanoparticles of silver synthesized in water-alcoholic solutions *murraya paniculata* (*Moscow, Russia*) 184
71. **Margarita Kostyanaya, Inna Petrova, Vladimir Volkov, Andrey Yaroslavtsev** Preparation of the bimetallic catalysts on polymeric support for the process of nitrate removal from water (*Moscow, Russia*) 186
72. **Anna Kovalenko, Makhmet Urtenov, Alexander Pismenskiy** Evaluation of the possibility of the emergence of gravitational convection due to the recombination of hydrogen ions and hydroxyl (*Krasnodar, Russia*) 189
73. **Anna Kovalenko, Makhmet Urtenov, Natalia Seidova, Alexander Pismenskiy** Influence of dissociation / recombination of water molecules on the transport of binary salt ions in membrane systems (*Krasnodar, Russia*) 191
74. **Nikita Kovalev, Anna Akimova, Nuriyet Hapacheva, Anton Serdiuk, Nikolay Sheldeshov, Victor Zabolotsky** Dissociation of alcohols and water in organic solutions (*Krasnodar, Russia*) 193
75. **Alina Kozlova, Maxim Shalygin, Vladimir Teplaykov** The study of water and ethanol vapors diffusion in polymeric membranes (*Moscow, Russia*) 196
76. **Anton Kozmai, Mona Chérif, Lasaad Dammak, Myriam Bdiri, Victor Nikonenko, Christian Larchet, Ulia Aniskina** Stationary and non-stationary models of ion transfer in neutralization dialysis (*Krasnodar, Russia*) 198
77. **Tamara Kravchenko** Catalytical, chemical and electrochemical activity of metal (Ag, Cu) nanoparticles in ion-exchange matrixes (*Voronezh, Russia*) 201
78. **Olga Kristavchuk, Ilya Nikiforov, Vladimir Kukushkin, Alexander Nechaev, Pavel Apel** Composite track-etched membranes with silver nanoparticles (*Dubna, Chernogolovka, Russia*) 204
79. **Dina Kritskaya, Emil Abdrashitov, Veslav Bokun, Ardalion Ponomarev, Eugeny Sanginov, Yury Dobrovolsky** Water and water saturated vapor transfer rate through proton exchange polymer membranes (*Chernogolovka, Russia*) 207
80. **Larissa Kushakova, Anna Reznichenko, Natalia Sizikova, Olesya Brailko** Application of sorption and extraction processes in the flowsheets of hydrometallurgical processing of ores of deposits of Kazakhstan (*Ust-Kamenogorsk, Kazakhstan*) 209
81. **Sergey Lazarev, Urii Golovin, Olga Kovaleva, Valerii Polikarpov, Irina Khorokhorina** Evaluation of structural changes for nanofiltration membranes by the diffractometry method (*Tambov, Russia*) 210
82. **Sergey Lazarev, Olga Kovaleva, Roman Popov, Sergey Kovalev** Investigation of the process of ultrafiltration separation of technological solutions in the production of alcohol from molasses (*Tambov, Russia*) 212
83. **Denis Lebedev, Alexey Shiverskiy, Mikhail Simunin, Victoria Bykanova, Vera Solodovnichenko, Ilya Ryzhkov** Ion-selective and electrochemical properties of carbon coated alumina nanofiber membranes (*Krasnoyarsk, Russia*) 215
84. **Konstantin Lebedev, Victor Zabolotsky, Nikolay Sheldeshov, Vera Vasil'eva, Michail Kasparov** Mathematical model of ion transport through the interface: the ion exchange membrane / strong electrolyte (*Krasnodar, Voronezh, Russia*) 217

85. **Natalia Loza, Nazar Romanyuk, Sergey Loza** Competitive electromass transfer of cations of hydrogen and phenylammonium through the perfluorated membrane MF-4SK (*Krasnodar, Russia*) 220
86. **Sergey Loza, Kristina Dmitrieva, Alexander Korzhov, Natalia Loza, Victor Zabolotsky** Energy generation by reverse electro dialysis (*Krasnodar, Russia*) 223
87. **Aleksandra Lytkina, Natalia Orekhova, Margarita Ermilova, Ilya Petriev, Mikhail Baryshev, Andrey Yaroslavtsev** Hydrogen production via metanol steam reforming with the use of membrane catalysis (*Moscow, Krasnodar, Russia*) 225
88. **Sofia Makulova, Yulia Karavanova, Andrey Yaroslavtsev, Igor Ponomarev** Ionic conductivity of polynaphthaleneimid membranes modified with silica (*Moscow, Russia*) 228
89. **Alexander Malakhov, Stepan Bazhenov, Alexey Volkov** CO₂ stripping from the ionic liquid using a dense membrane contactor (*Moscow, Russia*) 230
90. **Semyon Mareev, Anton Kozmai, Vladlen Nichka, Victor Nikonenko** Three-dimensional model of impedance of the ion exchange membrane with electrically inhomogeneous surface (*Krasnodar, Russia*) 233
91. **Svetlana Markova, Alexander Kharitonov, Vladimir Teplyakov** Selective gas permeability of poly(4-methyl-1-pentene) modified by gas phase fluorination (*Moscow, Chernogolovka, Russia*) 234
92. **Vladislav Menshchikov, Sergey Belenov, Anastasia Alekseenko, Vadim Volochaev** Bimetallic Pt-based catalysts: structure, activity in the oxygen reduction reaction and methanol electrooxydation (*Rostov-on-Don, Russia*) 236
93. **Olga Mikhaleva, Svetlana Shkirskaya, Stanislav Melnikov, Sergey Dolgopopov** Diffusion permeability of Ralex anion exchange membranes, modified by MF-4SC and polyaniline (*Krasnodar, Russia*) 238
94. **Tatyana Mochalova, Alexander Bespalov, Nikolay Sheldeshov, Victor Zabolotsky** Influence of the modification of the anion-exchange layer of the bipolar membrane on the dissociation rate of water molecules in the bipolar region (*Krasnodar, Russia*) 241
95. **Mariya Moshareva, Svetlana Novikova, Andrey Yaroslavtsev** Ionic transport in solid electrolytes Li_{1+x}Al_xGe_{2-x}(PO₄)₃ with nasicon structure (*Moscow, Russia*) 244
96. **Ekaterina Nazyrova, Svetlana Shkirskaya, Viktoria Soloshko** Influence of modifiers in ion-exchange membranes on structure of hydrate complex fixed ion – counter ion (*Krasnodar, Russia*) 246
97. **Ksenia Nebavskaya, Natalia Pismenskaya, Konstantin Sabbatovskiy, Vladimir Sobolev, Victor Nikonenko** Accounting for membrane conductivity in determination of surface charge via streaming potential measurements (*Krasnodar, Moscow, Russia*) 248
98. **Andrey Nebavskiy, Semyon Mareev, Vladlen Nichka, Ksenia Nebavskaya** Comparison of chronopotentiometric curves of heterogeneous ion-exchange membranes with hydrophobic or hydrophilic non-conductive surface areas. 2D simulation (*Krasnodar, Russia*) 251
99. **Vladlen Nichka, Semyon Mareev, Andrey Nebavskiy, Dmitrii Butylskii, Natalia Pismenskaya, Victor Nikonenko** The phenomenon of two transition times in chronopotentiometry of systems with electrically inhomogeneous ion exchange membranes. Experiment and model (*Krasnodar, Russia*) 254
100. **Sabukhi Niftaliev, Olga Kozaderova, Kseniya Kim** The study of ion transport in the system "heterogeneous ion-exchange membrane - ammonium nitrate solution" (*Voronezh, Russia*) 256
101. **Victor Nikonenko, Aminat Uzdenova, Ksenia Nebavskaya, Marina Andreeva, Lasaad Dammak** Impact of current density, solution concentration and surface

- charge density on the mechanism of electroconvection in membrane systems. Perspectives in fighting scaling (*Krasnodar, Russia; Thiais, France*)
102. **Eduard Novitsky, Ilya Borisov, Georgy Golubev, Dmitry Matveev, Alexey Volkov** Concentration of mineral salts in a membrane distiller with the porous condenser (*Moscow, Russia*) 261
103. **Ivan Novomlinskiy, Irina Gerasimova, Vladimir Guterman** Composite SnO₂/C carrier, obtained by electrochemical method, and supported platinum catalysts (*Rostov-on-Don, Russia*) 263
104. **Kseniia Otvagina, Alla Mochalova, Tatyana Sazanova, Artem Atlaskin, Ilya Vorotyntsev** Transport properties of asymmetry and composite membranes based on chitosan copolymers with vinyl monomers (*Nizhny Novgorod, Russia*) 265
105. **Anna Ovcharova, Ilya Borisov, Stepan Bazhenov, Rustem Ibragimov, Vladimir Vasilevsky, Alexandr Bildyukevich, Vladimir Volkov** Hydrophobization of porous polysulfone hollow fiber membranes: Low temperature plasma treatment (*Moscow, Kazan, Russia; Minsk, Belarus*) 268
106. **Anna Ovcharova, Vladimir Vasilevsky, Ilya Borisov, Stepan Bazhenov, Alexey Volkov, Alexandr Bildyukevich, Vladimir Volkov** Polysulfone porous hollow fiber membranes for ethylene-ethane separation in a gas-liquid membrane contactor (*Moscow, Russia; Minsk, Belarus*) 271
107. **Anna Parshina, Ekaterina Safronova, Olga Bobreshova** The influence of moisture content and transport properties of perfluorated membranes on the DP-sensors characteristics depending on the analites nature and solution pH (*Voronezh, Moscow, Russia*) 274
108. **Natalia Pismenskaya, Ekaterina Belashova, Olesya Kharchenko, Victor Nikonenko** Anomalous current-voltage and chronopotentiometric curves of homogeneous anion-exchange membrane in monosodium phosphate solution (*Krasnodar, Russia*) 275
109. **Alexander Pismenskiy, Mahamet Urtenov, Anna Kovalenko, Ekaterina Belashova** Modeling of mass transfer processes in electro dialysis of ampholites with the account of nonisothermal deprotoning-protoning reactions (*Krasnodar, Russia*) 278
110. **Roman Pichugov, Mikhail Petrov, Dmitry Konev, Anatoly Antipov, Mikhail Vorotyntsev** Effect of acidity on the regeneration process in bromate fuel cells (*Moscow, Chernogolovka, Russia; Dijon, France*) 281
111. **Roman Pichugov, Mikhail Petrov, Dmitry Konev, Anatoly Antipov, Mikhail Vorotyntsev** Spectrophotometric analysis of bromine species in concentrated aqueous solutions at different pH (*Moscow, Chernogolovka, Russia; Dijon, France*) 282
112. **Tatiana Plisko, Alexandr Bildyukevich, Svetlana Aponovich, Stepan Bazhenov** Modification of ultrafiltration membranes by addition of polyelectrolytes to the coagulation bath (*Minsk, Belarus; Moscow, Russia*) 283
113. **Tatiana Plisko, Alexandr Bildyukevich, Yana Isaichykava, Anna Ovcharova** Preparation of high flux polyphenylsulfone membranes using upper and lower critical solution temperature systems: effect of coagulation bath temperature (*Minsk, Belarus; Moscow, Russia*) 286
114. **Kristina Pogosyan, Natalia Kononenko, Vera Vasil'eva** Influence of heat treatment on structural characteristics of ion-exchange membranes (*Krasnodar, Voronezh, Russia*) 289
115. **Valentina Ponomareva, Galina Lavrova, Elena Shutova** The functional properties of new proton electrolytes based on cesium dihydrogen phosphate and high water retention matrix (*Novosibirsk, Russia*) 291

116. **Valentina Ponomareva, Irina Bagryantseva, Elena Shutova** Phase composition, transport and thermal properties of barium doped cesium dihydrogen phosphate system (*Novosibirsk, Russia*) 292
117. **Valentina Ponomareva, Galina Lavrova, Boris Zakharov, Irina Bagryantseva** New proton conducting electrolytes in cesium mono and dihydrogen phosphates system (*Novosibirsk, Russia*) 294
118. **Ludmila Ponomarova, Yuliya Dzyazko, Yurii Volfkovich, Valentin Sosenkin** Organic-inorganic ion-exchanger based on weakly and strongly acidic resins (*Sumy, Kyiv, Ukraine; Moscow, Russia*) 295
119. **Darya Popova, Irina Falina, Natalia Loza, Marya Salashenko** Investigation of anisotropic perfluorinated membranes modified by polyaniline by spectral methods (*Krasnodar, Russia*) 298
120. **Mikhail Porozhnyy, Stefano Deabate, Patrice Huguet, Victor Nikonenko** Concentration dependence of conductivity and diffusion permeability of ion exchange membranes embedded with mineral or organic nanoparticles. Modelling and experiment (*Krasnodar, Russia; Montpellier, France*) 300
121. **Gérald Pourcelly, Victor Nikonenko** Membrane-based processes for desalination & water treatment and sustainable power generation (*Montpellier, France; Krasnodar, Russia*) 303
122. **Ivan Prikhno, Ekaterina Safronova, Andrey Yaroslavtsev** Hybrid membranes based on Nafion powder and different dopants obtained by hot pressing (*Moscow, Russia*) 305
123. **Vjacheslav Roldughin, Larisa Karpenko-Jereb, Tat'yana Kharitonova** On the Schroeder paradox for ion-exchange and nonionic polymers (*Moscow, Russia; Graz, Austria*) 307
124. **Vjacheslav Roldughin, Vladimir Zhdanov, Andrey Shabatin** Generalized dusty-gas model for gas mixture flow through nanoporous bodies (*Moscow, Russia*) 310
125. **Vjacheslav Roldughin, Vladimir Zhdanov, Andrey Shabatin** Non-equilibrium thermodynamics of heat and mass transfer through the membrane surface for two-component mixture (*Moscow, Russia*) 313
126. **Valeriia Rostovtseva, Alexandra Pulyalina, Ludmila Vinogradova, Galina Polotskaya** Influence of hybrid fullerene-containing modifiers on physico-chemical and transport properties of polyphenylene oxide membranes (*Saint Petersburg, Russia*) 316
127. **Ilya Ryzhkov, Denis Lebedev, Victoria Bykanova, Vera Solodovnichenko, Alexey Shiverskiy, Mikhail Simunin** Ion transport in carbon coated alumina nanofiber membranes: mathematical modelling and experiment (*Krasnoyarsk, Moscow, Russia*) 319
128. **Konstantin Sabbatovskiy, Polina Epifanova, Nadezhda Golovaneva, Vladimir Sobolev, Elena Farnosova, Georgy Kagramanov** The effect of the concentration of nickel chloride on the surface charge and the selectivity of the nanofiltration membrane (*Moscow, Russia*) 322
129. **Artemiy Samarov, Maria Sokolova, Michael Smirnov, Oleg Medvedev, Alexander Toikka** Choline chloride based deep eutectic solvents and their influence on the transport properties of chitosan membranes (*St. Petersburg, Russia*) 324
130. **Veronika Sarapulova, Mariya Fomenko, Liudmila Arzaniaeva, Natalia Pismenskaya** Effect of ampholyte nature on transport characteristics of anion-exchange membranes (*Krasnodar, Russia*) 326
131. **Veronika Sarapulova, Ekaterina Nevakshenova, Natalia Pismenskaya, Anton Kozmai, Philippe Sizat** Use of impedance spectroscopy for studying the 329

- electrochemical behavior of ion-exchange membranes after their contact with wine
(*Krasnodar, Russia; Montpellier, France*)
132. **Tatyana Sazanova, Alsu Akhmetshina, Artem Atlaskin, Ksenia Otvagina, Ilya Vorotyntsev** The correlation of gas separation properties of nonporous polymeric membranes with its topography (*Nizhny Novgorod, Russia*) 332
133. **Valentin Sedelkin, Dmitry Cherkasov, Olga Lebedeva** Investigation of ion biocidal activity of chitosan membranes (*Engels, Russia*) 335
134. **Valentin Sedelkin, Olga Lebedeva, Dmitry Cherkasov** Amorphous-crystalline structure of the filtration membrane made of a chitosan in salt and the basic form (*Engels, Russia*) 338
135. **Olga Sereda, Natalia Sherstneva, Dmitry Konev, Anatoly Antipov, Mikhail Vorotyntsev** Stability of bromate anion in strongly acidic solutions (*Moscow, Chernogolovka, Russia; Dijon, France*) 340
136. **Vladimir Shaposhnik** Supramolecular chemistry of ion exchange membranes (*Voronezh, Russia*) 343
137. **Nikolay Sheldeshov, Konstantin Lebedev, Victor Zabolotsky** Ions' transport through ion exchange membranes in the systems used to obtaining organic acids and bases by bipolar electro dialysis (*Krasnodar, Russia*) 345
138. **Vladimir Sobolev, Inessa Sergeeva** The effect of surface charge on the cationic polyelectrolyte adsorption (*Moscow, Russia*) 347
139. **Vera Solodovnichenko, Denis Lebedev, Victoria Bykanova, Alexey Shiverskiy, Ilya Ryzhkov, Tatiana Azarova, Sergei Azarov, Vladimir Prozorovich, Elena Krivoshapkina, Andrei Ivanets** Synthesis and characterization of composite alumina–mullite and alumina–cordierite membranes (*Krasnoyarsk, Syktyvkar, Russia; Belarus*) 349
140. **Vera Solodovnichenko, Alexey Shiverskiy, Mikhail Simunin, Denis Lebedev, Victoria Bykanova, Ilya Ryzhkov** Synthesis of ion–selective ceramic membranes based on alumina nanofibers (*Krasnoyarsk, Moscow, Russia*) 351
141. **Natalia Talagaeva, Ekaterina Zolotukhina, Mikhail Vorotyntsev** Electrochemical properties of prussian blue–polypyrrole composite (*Chernogolovka, Moscow, Russia*) 353
142. **Denis Terin, Sergey Korchagin** Synergetic approach in analysis of composite materials fractal morphology (*Saratov, Russia*) 356
143. **Sergej Timofeev, Gennadiy Belyakov, Vladimir Gursky** Experience of solid-polymer water electrolyzers using with MF-4SK membranes (*St. Petersburg, Moscow, Sosnovyi Bor, Russia*) 358
144. **Ekaterina Titskaya, Irina Falina, Anatoly Phillipov** Transport properties of perfluorinated membranes modified by halloysite nanotubes (*Krasnodar, Moscow, Russia*) 359
145. **Yuriy Tolmachev, Oleg Tripachev, Olga Istakova, Dmitry Konev, Anatoly Antipov, Mikhail Vorotyntsev** Flow battery of a novel type prospective for stationary energy storage, fully electric vehicles and direct solar-to-chemical energy conversion (*Moscow, Chernogolovka, Russia; Dijon, France*) 361
146. **Sergey Tsyplyaev, Marina Kardash, Ilya Strilets** Design and fabrication of multifunctional nanocomposite materials «Polikon A» (*Saratov, Russia*) 362
147. **Anna Ulyankina, Nina Smirnova** Electrochemical synthesis of copper oxides and their electrocatalytic properties in direct alcohol fuel cells (*Novocherkassk, Russia*) 363
148. **Makhamet Urtenov, Anna Kovalenko, Alexander Pismenskiy** 2D modelling of the main coupled effects of concentration polarization in electromembrane systems and their impact on ion transport in binary electrolytes (*Krasnodar, Russia*) 365
149. **Stanislav Utin, Sergey Loza, Victor Zabolotsky, Alexander Bepalov, Victor Dotsenko** Influence of the degree of functionalization of carboxylated

- hyperbrached polymers on electrochemical characteristics of asymmetrical bipolar membranes (*Krasnodar, Russia*)
150. **Aminat Uzdenova, Makhamet Urtenov, Anna Kovalenko, Victor Nikonenko** 370
Two-dimensional mathematical model of overlimiting transfer in membrane systems taking into account electroconvection and forced flow for the galvanostatic mode (*Karachaevsk, Krasnodar, Russia*)
151. **Dmitrii Vakhnin, Valeriya Pridorogina, Lev Polyanskii, Tamara Kravchenko** 371
New redox-sorption model as water deoxygenation description method (*Voronezh, Russia*)
152. **Vladimir Vasilevsky, Eduard Novitsky, Evgeniy Trofimenko, Evgenia Grushevenko, Kirill Kutuzov, Alexey Volkov** 374
The configuration of the laboratory unit for reverse electro dialysis process (*Moscow, Russia*)
153. **Vera Vasil'eva, Elmara Akberova, Evgeniya Kozhuhova, Lubos Novak, Victor Zabolotsky, Konstantin Lebedev** 376
The surface analysis of the cm pes ion exchange membranes with the different degree of ion exchanger dispersion by SEM and AFM methods (*Voronezh, Krasnodar, Russia; Strazh pod Ralskem, Czech Republic*)
154. **Alexander Vilensky** 379
The study of radiolysis products in the tracks of polyethylene terephthalate and polycarbonate as the distance from the ion trajectory (*Moscow, Russia*)
155. **Yurii Volfkovich, Alexey Rychagov, Alexey Mikhailin, Marina Kardash, Natalia Kononenko, Denis Ainetdinov, Svetlana Shkirkaya, Valentin Sosenkin** 382
Capacitive deionization of water using membrane of mosaic structure (*Moscow, Engels, Krasnodar, Russia*)
156. **Mikhail Vorotyntsev, Yuriy Tolmachev, Dmitry Konev, Anatoly Antipov** 385
Bromate anion reduction via autocatalytic cycle and its implications for electrical energy sources (*Moscow, Chernogolovka, Russia; Dijon, France*)
157. **Alexander Vvedenskii, Anastasiya Fedoseeva, Natalya Morozova, Elvira Leschenko, Alexey Dontsov** 388
Influence of the phase composition on the parameters of hydrogen permeability of Pd53Cu film electrodes (*Voronezh, Russia*)
158. **Andrey Yaroslavtsev, Daniil Golubenko, Andrey Ilyin, Irina Stenina, Vladimir Tverskoy** 391
The relationship between protoncontaining groups structure, mobility and transport properties of ion-exchange membranes (*Moscow, Russia*)
159. **Ala Yaskevich, Victor Kasperchik, Aleksandr Bilydukevich** 394
Variation of the ultrafiltration polyacrylonitrile membranes properties by the diamine modification (*Minsk, Belarus*)
160. **Ivan Yasnev, Vladimir Gursky** 396
Deoxygenation of high-purity water using membrane electrode units (*Sosnovyi Bor, Russia*)
161. **Andrey Yatsev, Vera Vasil'eva, Elmara Akberova** 398
The changes in surface and transport properties of ion-exchange membranes used at electro dialysis treatment of natural waters (*Voronezh, Russia*)
162. **Polina Yurova, Yulia Karavanova, Andrey Yaroslavtsev** 400
Synthesis and diffusion properties of cation-exchange membranes modified with protonactert and protondonor dopants (*Moscow, Russia*)
163. **Alexey Yushkin, Danila Bakhtin, Mikhail Efimov, Lev Zemtsov, Alexey Volkov** 402
Influence of IR radiation on membranes based on polyacrylonitrile (*Moscow, Russia*)
164. **Victor Zabolotsky, Anastasia But, Lubos Novak, Vera Vasil'eva** 405
Electroconvection in systems with heterogeneous and homogenous ion-exchange membranes (*Krasnodar, Voronezh, Russia; Strazh pod Ralskem, Czech Republic*)
165. **Victor Zabolotsky, Stanislav Melnikov, Stanislav Utin** 408
Influence of nature of cation exchange layer on electrochemical characteristics of asymmetric bipolar membranes (*Krasnodar, Russia*)

166. **Victor Zabolotsky, Oleg Mugtamov, Stanislav Melnikov** Stabilization of copper nanoparticles in ion exchange membrane matrix to create composite materials with dual function - ion transport and electrocatalysis of nitrate ion reduction reaction (*Krasnodar, Russia*) 411
167. **Victor Zabolotsky, Nikolay Sheldeshov, Stanislav Melnikov, Stanislav Utin** Reagent-free electro-membrane technology of pH-correction of water and water-organic solutions (*Krasnodar, Russia*) 414
168. **Victor Zabolotsky, Polina Vasilenko, Stanislav Utin, Konstantin Lebedev** Theoretical and experimental investigation of the pH correction process of softened water in long electro-dialysis channels with bipolar membranes (*Krasnodar, Russia*) 417
169. **Dmitri Zagorskiy, Sergey Bedin, Sergey Kruglikov, Ilya Doludenko** Galvanic deposition of multicomponent alloys into the nano-sized pores of track membranes (*Moscow, Russia*) 419
170. **Evgenia Zhelonkina, Svetlana Shishkina** Effect of the type of functional groups on scaling during electro-dialysis (*Kirov, Russia*) 421
171. **Natalia Zhilyaeva, Elena Mironova, Margarita Ermilova, Natalia Orekhova, Nina Shevlyakova, Margarita Dyakova, Vladimir Tverskoy, Andrey Yaroslavtsev** Influence of humidity and pressure on separation of ethylene/ ethane mixtures with sulfocationite membranes (*Moscow, Russia*) 423
172. **Ekaterina Zolotukhina, Konstantin Gor'kov, Ekaterina Sakardina, Sofia Kleinikova** Functional matrix activity of nanocomposites silver-ion exchanger in low-temperature formaldehyde oxidation (*Chernogolovka, Moscow, Russia*) 426
173. **Svetlana Zyryanova, Dmitriy Butylskii, Victor Nikonenko, Natalia Pismenskaya** Experimental study of the effect of pulsed electric field on chronoamperograms of Nafion 438 (*Krasnodar, Russia*) 428
174. **Danila Bakhtin, Alexey Volkov, Vladimir Volkov, Valeriy Khotimskiy, Leonid Kulikov, Anton Maksimov, Eduard Karakhanov** Thin film composite ptmsp/paf membranes: study of physical aging (*Moscow, Russia*) 431

STUDY FOR THE HYDRODYNAMIC STRUCTURE OF THE FLOW IN THE MEMBRANE ELEMENT OF TUBULAR TYPE

Dmitriy Abonosimov, Sergey Lazarev, Irina Khorokhorina

Tambov state technical university, Tambov, Russia, E-mail: geometry@mail.nnn.tstu.ru

Introduction

The hydrodynamics structure of the flow for a tubular-type reverse-osmosis apparatus based on OPMN-P membranes at operating pressures of process from 1 MPa to 4 MPa is investigated. Experimental data are obtained for the response curves and the longitudinal mixing coefficient depending on the flow speed of solution and the pressure in the separation module. These data allowed to obtain a criterial equation for the longitudinal mixing coefficient calculating.

Experiments

In the experimental studies of the longitudinal mixing coefficient, the pulse tracer method (20% NaCl aqueous solution) was used, followed by the registration of the response curve at the outlet from the membrane module.

The scheme of the original tubular-type experimental module for determining the longitudinal mixing coefficient is shown on Fig. 1 and consists from a dosing cylinder (1), an inlet valve (2), membrane tubular elements (3), a body of the apparatus (4) and a measuring cells (5).

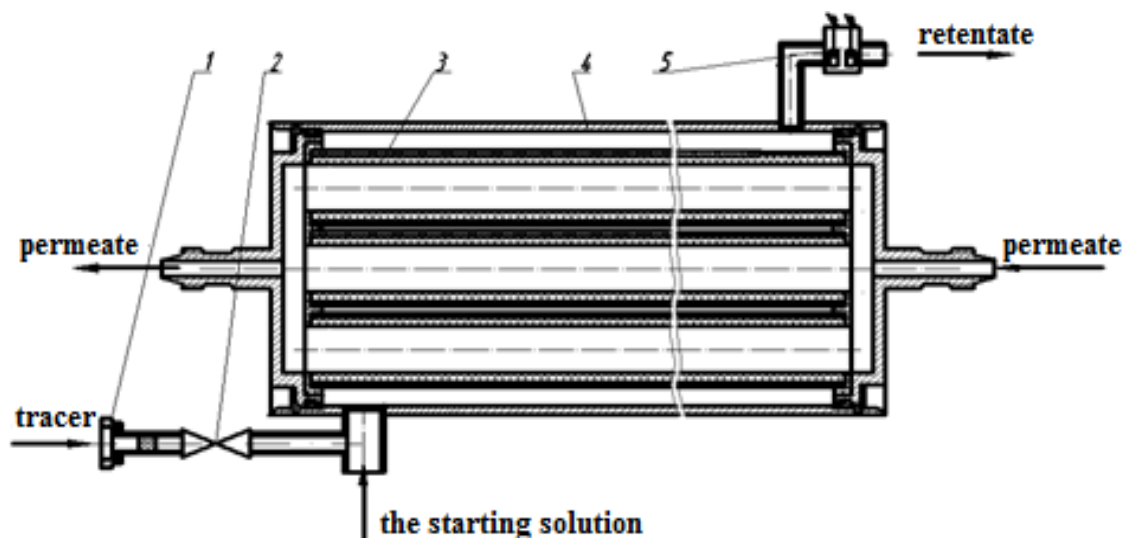


Figure. 1 - Design of a tubular type module

Results and Discussion

An important characteristic for the hydrodynamic structure of the flow for a solution in reverse osmosis modules is the longitudinal mixing coefficient. It can be calculated through the statistical parameters of the differential distribution function of the residence time of the substance in the apparatus, obtained experimentally with the aid of the pulsed method [1-2].

As a result of the experimental studies, the response curves were obtained, depending on the flow rate of the solution in the intermembrane channel and the pressure of the solution for two types of membrane modules at different pressures. The results of experimental studies are presented in Figs. 2 and 3 for tubular elements based on the OPMN-P membrane for pressures of 1, 2, 3, 4 MPa.

The value of the longitudinal mixing coefficient was calculated using the dependence:

$$D_{\Pi} = \frac{LU}{Pe}, \quad (1)$$

where L – the length of the module, m; U – the speed of the solution in the module channel, m/s.

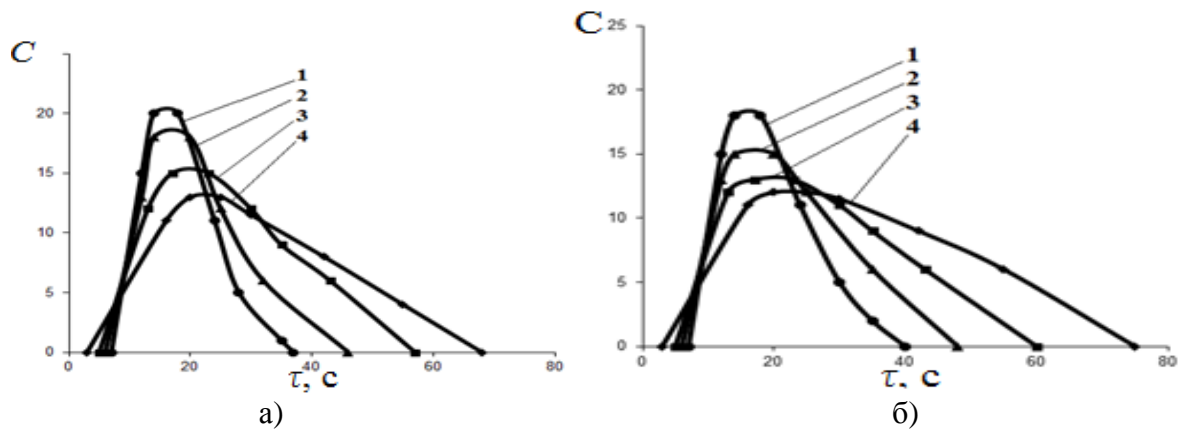


Figure. 2 - Response curves for a tubular membrane element at a solution speed, m / s : 1 - 0.08; 2 - 0.12; 3 - 0.18; 4 - 0.28; a) $P = 1 \text{ MPa}$; б) $P = 2 \text{ MPa}$

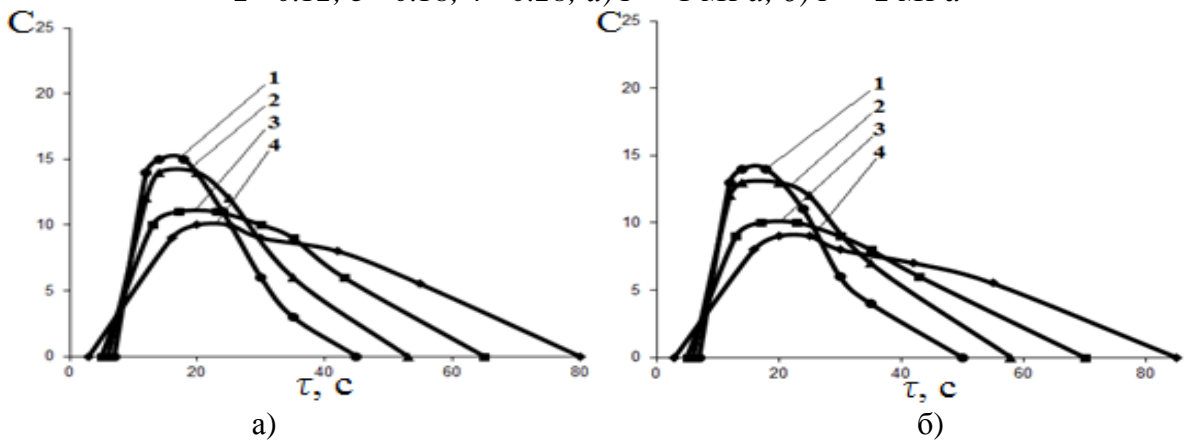


Figure. 3 - Response curves for a tubular membrane element at a solution speed, m / s : 1 - 0.08; 2 - 0.12; 3 - 0.18; 4 - 0.28; a) $P = 3 \text{ MPa}$; б) $P = 4 \text{ MPa}$

The results of experimental studies to determine the dependence of the longitudinal mixing coefficient from the speed and pressure of the solution in the module are shown graphically in Fig. 4. As can be seen in the graphs, the longitudinal mixing coefficient increases significantly with increasing fluid flow speed in the module. This can be explained by the fact that as the fluid speed increases, turbulent mixing in the intermembrane channels of the tubular elements increases also.

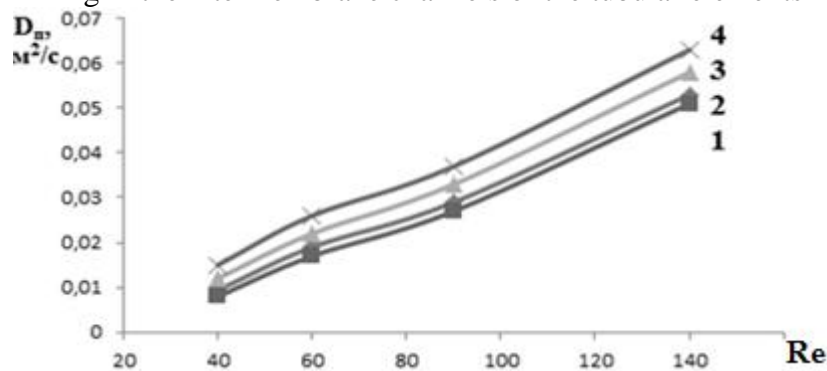


Figure. 4 - Dependence of the longitudinal mixing coefficient on the speed of solution and pressure: 1 - 1 MPa; 2 - 2 MPa; 3 - 3 MPa; 4 - 4 MPa

When considering the dependences of the longitudinal mixing coefficient for different pressures in the module, the coefficient values increase with increasing pressure. When creating pressure in the module, an additional factor appears that affects the coefficient of longitudinal mixing. With increasing pressure in the module, there is a flow of permeate, gradually depleting the main flow along the length of the module. The permeate flow is directed from the core of the flow in the intermembrane channel through the membrane, that is perpendicular to the main stream. Therefore, due to the permeate flow, further mixing of the liquid flow takes place in the membrane

module. At a higher pressure, the permeate flow increases, which leads to an increase for the longitudinal mixing coefficient [3].

According to the experimental data, the dependence of the longitudinal mixing coefficient on the pressure and speed of the solution was obtained, for a tube-type baromembrane module:

$$D_n = b \cdot \text{Re}^n \cdot \left(\frac{P}{P_0} \right)^m, \quad (2)$$

where b , n – the empirical coefficients of the Reynolds criterion, m – the empirical coefficient of hydrostatic pressure, P_0 – the working pressure and pressure, assumed to be 0,1 MPa, respectively.

References

1. Application of membrane technologies in waste water treatment of galvanic production / S.I. Lazarev, D.O. Abonosimov // Vestnik TSTU - 2014, T.20, №2-P.306-311.
2. Lazarev K.S. Investigation of the kinetic coefficients of reverse osmosis separation of solutions on membranes MGA-95, MGA-100 and OPM-K / K.S. Lazarev, S.V. Kovalev, A.A. Arzamestsev // Vestnik TSTU, Tambov: 2011.P.1-2
3. Abonosimov O.A. Problems of hydrodynamics of solution flow in baromembrane apparatus of a roll type / O.A. Abonosimov, S.I. Lazarev, D.O. Abonosimov // Ivanovo: Chemistry and Chemical Technology, T.53, no. 7, 2010.- P. 76-79

INVESTIGATION OF KINETIC CHARACTERISTICS THE REVERSE OSMOSIS DESALINATION-CONCENTRATION OF SOLUTIONS CHEMICAL WATER TREATMENT

Oleg Abonosimov, Sergey Lazarev, Sergey Kotenev

Tambov state technical university, Tambov, Russia, E-mail: abontam@inbox.ru

Introduction

Modern membrane plants for industrial sewage treatment of chemical industries, especially reverse osmosis plants, are increasingly attracting the attention of specialists due to their versatility, as well as the possibility of creating a circulating water supply system at enterprises [1].

With engineering methods for calculating the process of reverse osmosis separation, it is necessary to have experimental data on the kinetic parameters of mass transfer. One of the components of mass transfer in the reverse osmosis separation is the specific membrane productivity and the retention factor [1-3].

Experiments

In order to study the main kinetic characteristics of the reverse osmosis separation, an experiment on desalination-concentration of wastewater from the chemical water treatment plant "VNIPIsera" in Lviv, containing chlorides and sodium sulfates, was carried out. For the study, a laboratory reverse osmosis roll type installation was used, the scheme of which is shown in Fig. 1.

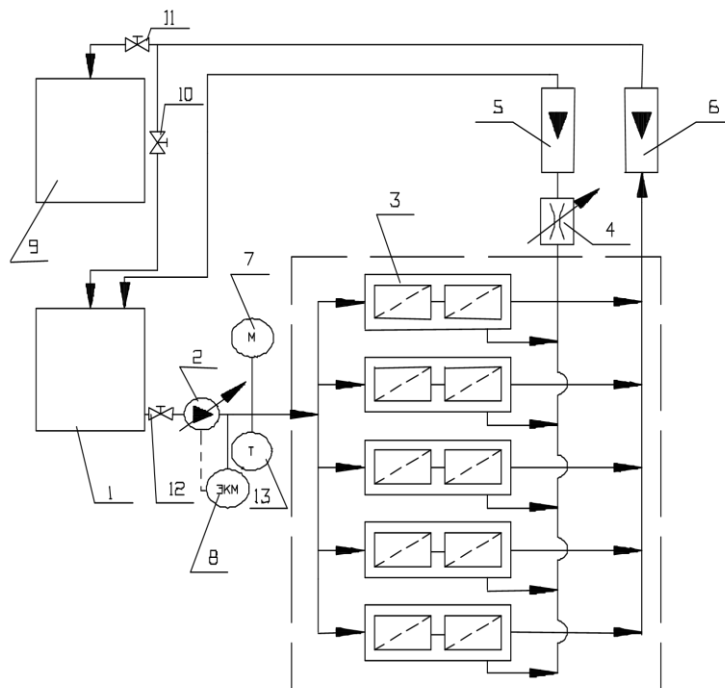


Figure 1. Scheme of laboratory reverse osmosis installation of roll type:

1 - capacity of the initial solution; 2 - high-pressure pump; 3 - separating module; 4 - throttle; 5,6 - rotameter; 7,8-sample and electrocontact manometer; 9 - capacity of permeate collection; 10,11,12 - the valve; 13 - thermometer

The main separating element of the installation is the reverse osmosis module 3, in which two reverse osmosis rolls of the type ERO-E-6,5 / 900A with membranes MGA-95 were installed. From the tank 1, the stock solution was pumped into the reverse osmosis module 3 by a plunger pump type 2, ND-2.5, which provided a solution in the range from 0 to 2.5 m³/h and created a pressure of up to 6 MPa. With the help of the throttle 4 in the reverse osmosis module, the required working pressure of the solution was set, which was controlled by an electrocontacte manometer 8. The flow rate of the solution was monitored by a rotameter 5 and the temperature was measured by a thermometer 13. The permeate flow after the modules was monitored by a rotameter 6 and

collected in a container 9. Experimental studies were carried out with varying concentrations And the speed of the solution. To determine the mean values, a series of three experiments was carried out.

The value of specific membrane productivity G was calculated from the dependence [1, 3]:

$$G = \frac{V}{F_m \cdot \tau}, \quad (1)$$

where G - the specific productivity of the membrane, $\text{m}^3 / \text{m}^2\text{s}$; V - volume of collected permeate, m^3 ; F_m - the area of the membrane, m^2 ; τ - the time of the experiment, s.

The retention factor was determined by the formula:

$$k = 1 - \frac{C_{per}}{C_{in}}, \quad (2)$$

where k - the retention factor, S_{per} - the concentration of the dissolved substance in the permeate, kg / m^3 , S_{in} - the concentration of the dissolved substance in the initial solution, kg / m^3 .

Results and Discussion

In Fig. 2, 3 shows the dependences of the specific productivity and the retention coefficient of the MGA-95 membrane on the concentration at different solution rates over the membrane.

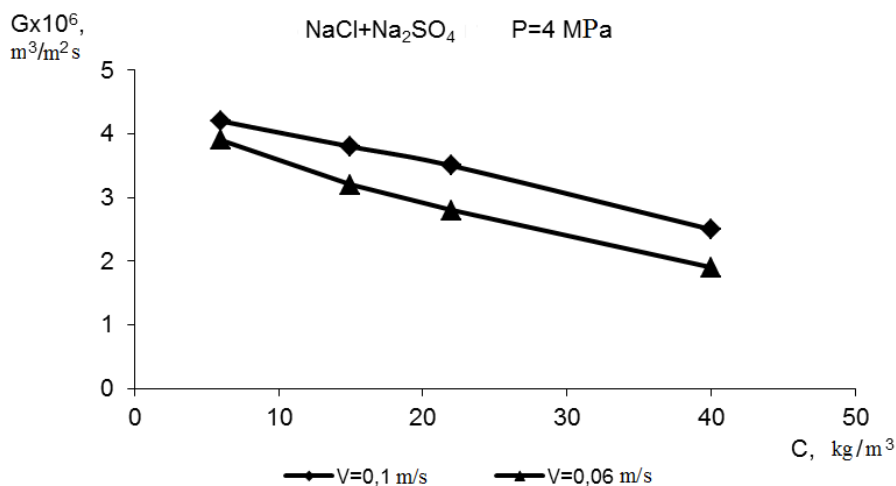


Figure 2. Dependence of specific productivity of membrane MGA-95 on concentration

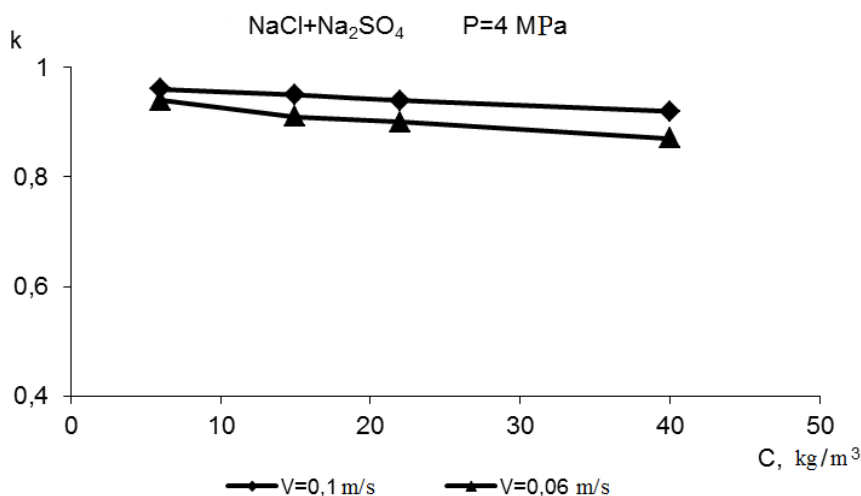


Figure 3. Dependence of the coefficient of retention of the membrane MGA-95 on concentration.

According to the presented dependences, it is evident that with increasing concentration of solution, the specific productivity falls significantly and, to a lesser extent, the retention factor.

The decrease in specific productivity and the retention factor is explained by the fact that when the concentration is increased within the prescribed limits, the increase in the osmotic pressure of the solution, and, consequently, the decrease in the driving force of the separation process, has a significant effect [4, 5]. In addition, the viscosity of the solution increases, the effect of concentration polarization increases, which can cause precipitation on the surface of the membrane of dissolved salts. At higher solution velocities above the membrane, as can be seen from the given dependences, the effect of concentration polarization and the specific yield and retention factor is somewhat higher than at a lower rate.

In conclusion of the article it should be noted that, based on the results of the research, a 5-step desalination-concentration scheme for wastewater from the chemical water purification plant "VNIPIsera" in Lviv was designed, which meets the requirements for the volume of effluent and total salt content in the permeate.

References

1. *Dytner'skii Yu. I.* Membrane processes of separation of liquid mixtures. M.: Chemistry, 1975. 252 p.
2. *Hvang S.-T., Kammermeier K.* Membrane separation processes. / Trans. From the English / Ed. Yu.I. Dytner'skii. M.: Chemistry, 1981. 464 p.
3. *Mulder M.* Introduction to Membrane Technology (translated from English by Leont'ev A.Yu., Yampolskaya G.P., edited by Yampolsky Yu.P., Dubyagi V.P.) 2001. 350 p.
4. *Abonosimov D.O., Lazarev S.I.* Application of membrane technologies in the purification of waste water galvanoproizvodstv // Bulletin of TSTU. Tambov. 2014. T.20. №2. P.306-313.
5. *Kovalev S.V., Lazarev S.I., Lazarev K.S., Popov R.V.* Specific flux and retention factor of the membrane MGA-95 in the electrobaromembrane separation of an aqueous solution of zinc sulphate // Bulletin of TSTU. 2015. Vol. 21. No. 1. P. 112-120.

VERIFICATION OF PHENOMENOLOGICAL MODEL OF COMPETITIVE TRANSPORT OF IONS IN SULFATE-NITRATE SOLUTIONS OF ELECTROLYTES

Aslan Achoh, Victor Zabolotsky, Stanislav Melnikov, Konstantin Lebedev
Kuban State University, Krasnodar, Russia

Introduction

Ion-exchange membranes with a modified surface are promising materials for the development of new generation electromembrane processes, such as "selectodialysis" [1]. The effectiveness of this process is determined by the selectivity of the transfer of one of the components of the mixture through the ion-exchange membrane. Membranes used in such a process must have high selectivity to ions with a charge greater than one.

Recent work [1-3] show that the selective and transport properties of ion-exchange membranes are mostly determined by the thin (up to several nanometers) surface layer. Therefore, the most promising direction concerning changing the properties of the membrane and giving it selective properties is its surface modification.

The purpose of this paper is to verify the theoretical model of competing ion transport through anion-exchange membranes obtained by depositing a thin (4, 15 and 40 μm thick) cation exchange layer on the surface of an anion-exchange membrane in sulfate-nitrate solutions of electrolytes.

Theory

Mathematical modeling is carried out within the framework of the Nernst-Planck system of equations with the condition of preservation of electroneutrality for two counter ions $j = 1, 2$ and cation $j = C$. The model is described in detail in [4]. Here we note that the equations of ion transfer are recorded for a membrane and two diffusion layers surrounding the membrane. In each layer, the electroneutrality condition is assumed, the electric current flow equation operates. The influence of the modified layer is characterized by the phenomenological coefficient of conductivity L'_j . The equation for the transfer of ions of type j through the modifying layer has the

following form in the model $j_j = L'_j \frac{\Delta\mu'_j}{d'}$ where the quantities (electrochemical potential jumps, thickness) with a stroke refer to the modifying layer. Writing this formula for ions 1 and 2 and excluding the electric potential from the obtained system, we obtain an analog of Nikol'skii's equation.

$$\frac{(C_{SO_4}^n)^{1/z_{SO_4}}}{(C_{NO_3}^n)^{1/z_{NO_3}}} = K_{12} \exp[-(R_1 T_1 - R_2 T_2) I] \frac{(C'_{SO_4})^{1/z_{SO_4}}}{(C'_{NO_3})^{1/z_{NO_3}}}$$

where $R_j = \frac{d' i_{np}^0}{z_j^2 F R T L'_j}$ – the dimensionless resistance of the layer with respect to the ions of type j . I

is the dimensionless current density normalized to the limiting current density in an ideal system impermeable to ions. At zero current ($i = 0$), the exponential factor in is equal to a unit and the modified layer does not affect the ionic equilibrium. If the current flows through the membrane and $R_1 > R_2$, the modified layer weakly retards singly charged ions. But when the current flows through the membrane, the shape of the concentration profiles begins to depend on the electrodiffusion resistance and the current density (Figure 1). Diffusion through the modified sulfate ion layer decreases, and the diffusion of the singly charged nitrate ion increases.

Figure 2 shows the dependence of the selectivity coefficients of doubly charged sulfate ions on the dimensionless current density for different values of R_1 ($R_1 \gg R_2$). It is seen that with increasing R_1 the coefficient of selectivity for doubly charged ions with a fixed current i decreases. But at a current close to the current limit, the selective properties of the system are determined by the properties of the solution and do not depend on the separation properties of the membrane, regardless of the presence of the modifying layer.

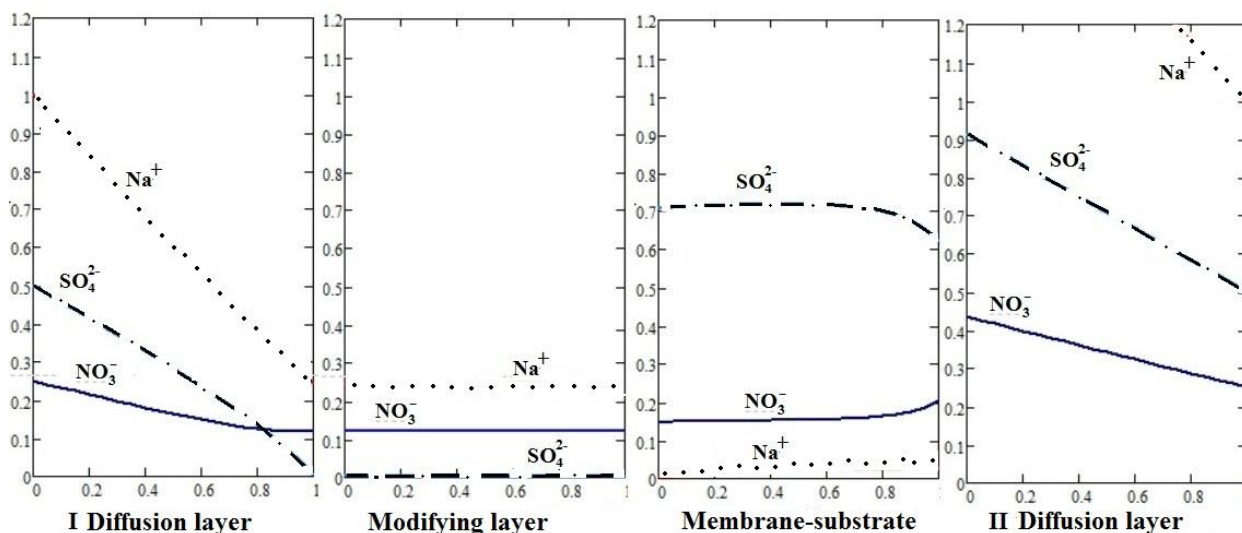


Figure 1. Distribution of concentrations of competing counterions SO_4^{2-} and NO_3^- , and of the co- Na^+ in a membrane system with a modified layer of $15 \mu m$. Concentrations of the modifying layer do not change.

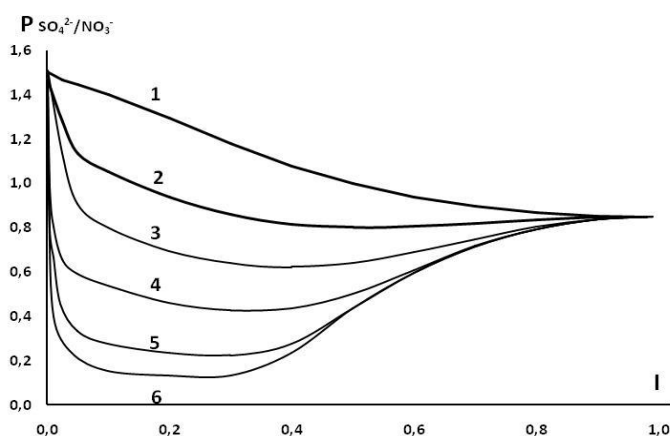


Figure 2. Dependence of the selectivity coefficient for sulphate ions on the dimensionless current density at different values R_1 : $R_1=1$; $R_1=5$; $R_1=10$; $R_1=20$; $R_1=50$; $R_1=100$. $R_2=0$.

Results and discussion

The studies were carried out using the rotating membrane disk method, which allows to maintain a constant thickness of the diffusion layer, and also allows continuous determination of the composition of the chambers (anodic and cathodic) and determine the Hittorf's transfer numbers for each ion. The ion concentrations were determined by liquid chromatography. Concentrations of substances in solution are given by constant and known $NaNO_3 - 0.01M$, $Na_2SO_4 - 0.005M$. The thicknesses of all layers are also known. The thickness of both diffusion layers is $\delta=0,053$ cm, the thickness of the modifying layer was set differently, depending on the experiment, the membrane thickness $d = 0.45$ cm.

Diffusion coefficients in solution and diffusion layers (cm^2/s): $D_{NO_3} = 1.902 \cdot 10^{-5}$, $D_{SO_4} = 1.065 \cdot 10^{-5}$, $D_{Na} = 1.334 \cdot 10^{-5}$. In the modifying layer $D_{Na^+} = 1.102 \cdot 10^{-6}$ and the substrate membrane $D_{SO_4} = 3.43 \cdot 10^{-6}$, $D_{NO_3} = 3.63 \cdot 10^{-6}$.

Numerical experiments show that the selective properties of a membrane with a modifying film are influenced by factors such as thickness and charge (concentration of fixed groups) of the film. The dependence of the selectivity coefficient on the dimensionless current density does not linearly

depend on the thickness of the modifying film, which is also confirmed by the experimental data (Fig. 3).

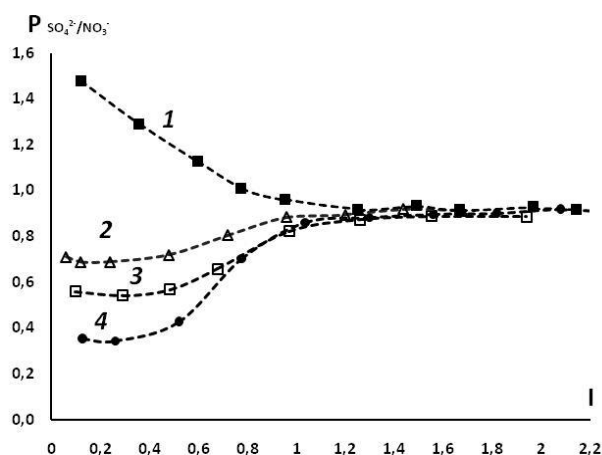


Figure 3. Dependence of the selectivity coefficient for sulfate ions on the dimensionless current density for the MA-41 membrane with different thicknesses of the cation-exchange film: 1- initial membrane MA-41; 2- film thickness 4 μm ; 3- thickness of the film 15 microns; 4 film thickness 40 μm).

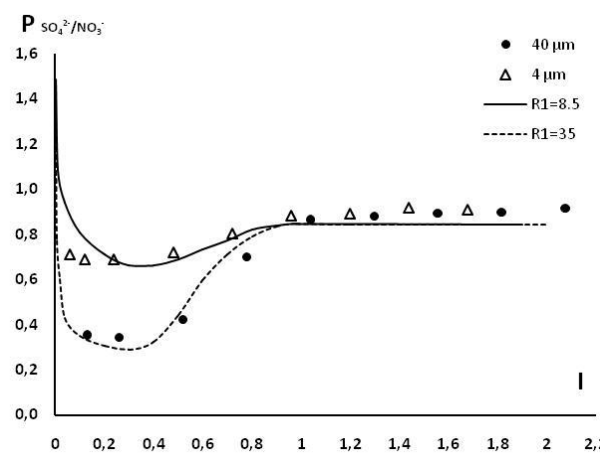


Figure 4. Dependence of the selectivity coefficient for sulfate ions on the dimensionless current density for the MA-41 membrane with different thicknesses of the cation-exchange film: the points are experimental data; Curves - calculated by model.

Comparison of numerical calculations on the model with experimental data, shown in Fig. 4, shows that the electrodiffusion transfer of singly charged co-ions through the modifying layer and, as a consequence, the bilayer membrane as a whole, increases with allowance for the thickness of the modifying layer both on the experimental data and on the experimental data calculated by theory. These data support the above-described model.

Acknowledgements

The present work is supported by the State Task of the Ministry of Education and Science of the Russian Federation, project No. 10.3091.2017 / PP.

References

1. Zhang Y., Paepen S., Pinoy L., Meesschaert B., Van Der Bruggen B. // Sep. Purif. Technol., 2012, V. 88, P. 191.
2. Mulyati, S., Takagi R., Fujii A., Ohmukai Y., Matsuyama H. // J. Membr. Sci. 2013. V. 431, P. 113.
3. Mizutani, Y. // J. Membr. Sci. 1990. V. 54, P. 233.
4. Nikonenko V.V., Zabolotsky V.I., Lebedev K.A., // Elektrokhimiya. 1996. V. 32, №2, P. 258.

VISUALIZATION AND REMOVAL OF HYDROPHILIC ADMIXTURES FROM HYDROPHOBIC ISOTACTIC POLYPROPYLENE FILMS

Evgeny Ageev, Nadezhda Strusovskaya, Natalia Matushkina

M. V. Lomonosov Moscow State University, Chemistry Department, Moscow, Russia

E-mail: ageev@phys.chem.msu.ru

Subject of the investigation – industrial large-scale product – films from stereoregular isotactic polypropylene (PP) grade 01030.

Method of the investigation – the sequence of routes of molecules-probes providing a possibility to interpret the experimental results.

Instrument of the investigation – analytical balance.

Goal of the investigation – to substantiate the mechanism of the discovered new effect – decrease of the mass of the sorbent that sorbs a sorbate! To utilize this effect to remove admixtures from isotactic PP films. To visualize the presence of hydrophilic admixtures in hydrophobic polymer.

Results of investigation

The discovered effect is due to the presence of impregnated particles-sorbents in the polymer. The following sequence of processes takes place: transfer of a substance-probe from the solution into the polymer, formation of a localized sorption complex sorbate – impregnated particle-sorbent, disruption of the attraction forces of the sorption complex and the polymer, delocalization of the complex sorbate-particle, its return into the solution. In the flux from the solution into the polymer only one sorbate is present, and in the reverse flux from the polymer into the solution appears the sorbate with the admixture. As opposed to desorption, the reverse flow is called reverse sorption. In the proposed mechanism for the first time used delocalized (moving!) particles-sorbents, and the inversion of the gradient of chemical potential upon formation of delocalized particles determines the direction of the reverse mass transfer.

The presented kinetic curves of swelling refer to the same sorbate – to water in figure 1 and to acetone in figure 2 – but to different unknown sorbents included into impregnated admixtures of the polymer. They were formed from the rest of Ziegler–Natta catalyst and other substances, which were present in the process of production of the end product. These substances pass into the category of useless admixtures because later on they are not needed.

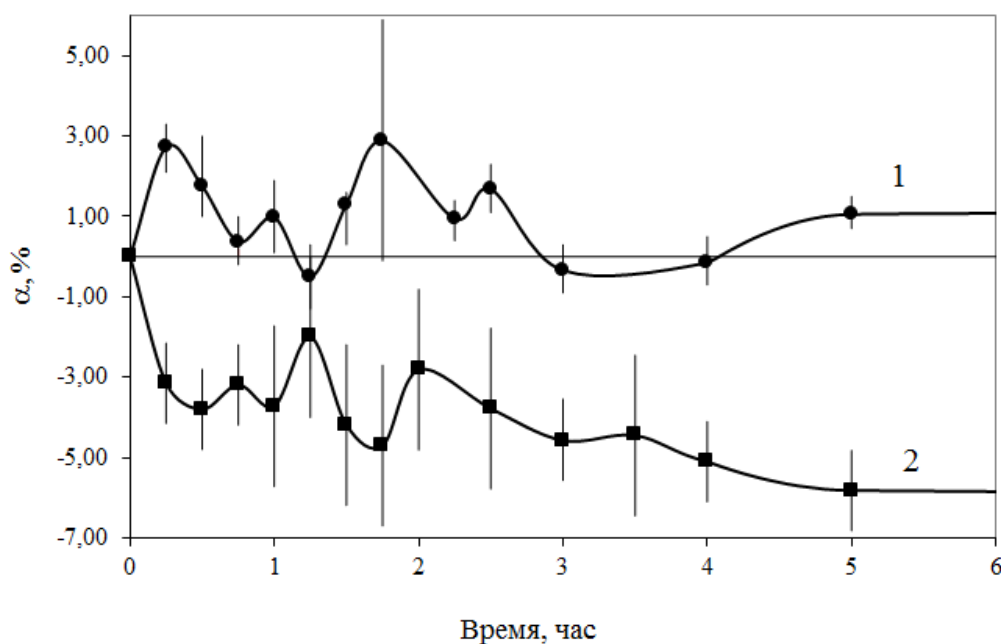


Fig. 1. Kinetics of swelling of water by hydrophilic admixtures in PP films: 1 – localized sorption; 2 – reverse sorption of delocalized admixtures.

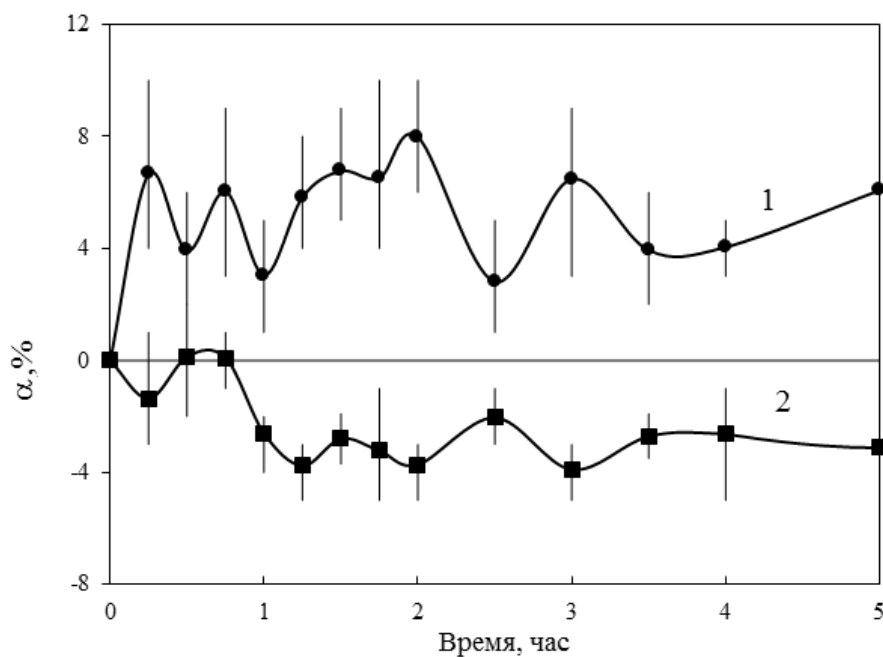


Fig. 2. Kinetics of swelling of acetone by PP films: 1 – localized sorption with participation of polymer and its hydrophobic and hydrophilic admixtures; 2 – reverse sorption with participation of hydrophilic groups of PP.

The points corresponding to the positive degree of swelling α refer to localized sorption (curves 1 of figures 1 and 2), and the corresponding negative values of α – to delocalized reverse sorption (curves 2 of figures 1 and 2).

The specificity of the data for acetone consists in the fact that acetone is diphilic sorbate, i. e. it has a hydrophilic carbonyl group and two hydrophobic methyl groups. This leads to the fact that the experimental data for curve 1 are shifted to the region of localized sorption.

INFLUENCE OF MODIFYING ADDITIVES ON STRUCTURE AND PROPERTIES OF MULTIFUNCTIONAL NANOCOMPOSITES "POLIKON K"

Denis Ainetdinov, Marina Kardash, Tatyana Yakunina, Artem Morozov, Roman Polnyi
Engels Tehnological Institute of Yuri Gagarin State Technical University of Saratov, Russia
E-mail: denis-ajjnetdinov@rambler.ru; E-mail:m_kardash@mail.ru

Introduction

Recently the demand for polymeric ion exchange materials is increasing. They have an important place in modern water treatment and water purification technologies. Regardless of the fact that there exists a manifold of such materials, they do not always satisfy the increasing requirements of consumers. Today obtaining of polymeric composite materials with a unique set of properties is actual and scientific and technical task. Therefore, in recent years, intensive studies on the synthesis of new polymeric membranes on the base hybrid materials that include nanodispersed inorganic additives [1].

Experiments

For improvement of the spatial structure of "Polikon K» the material and increase the electrical conductivity of nanodispersive proposed implementation of a number of additives (Ni and Fe), and carry out the process in the volume phenol-formaldehyde novolac fibers. Nanoparticulate additive synthesis step have implemented.

Results and Discussion

The influence the nanoparticles on the kinetics and the thermodynamics of the synthesis processes and curing by differential scanning calorimetry was investigated. According to the nature heat total thermal peak is divided into 3 sections, each characterized by its speed of the reaction. Nickel ultradispersed particles catalyze the synthesis process while iron supplements accelerate the curing process, as compared to the unmodified fibers. This is because the implementation nano-sized particles cause significant changes in polymer structure due to the formation of additional crosslinks epicenters during the formation the polymer matrix. The investigations showed that ultra-additive effect on synthesis processes and the formation of cationite matrix which occur at a higher rate than unmodified fiber (Figure 1).

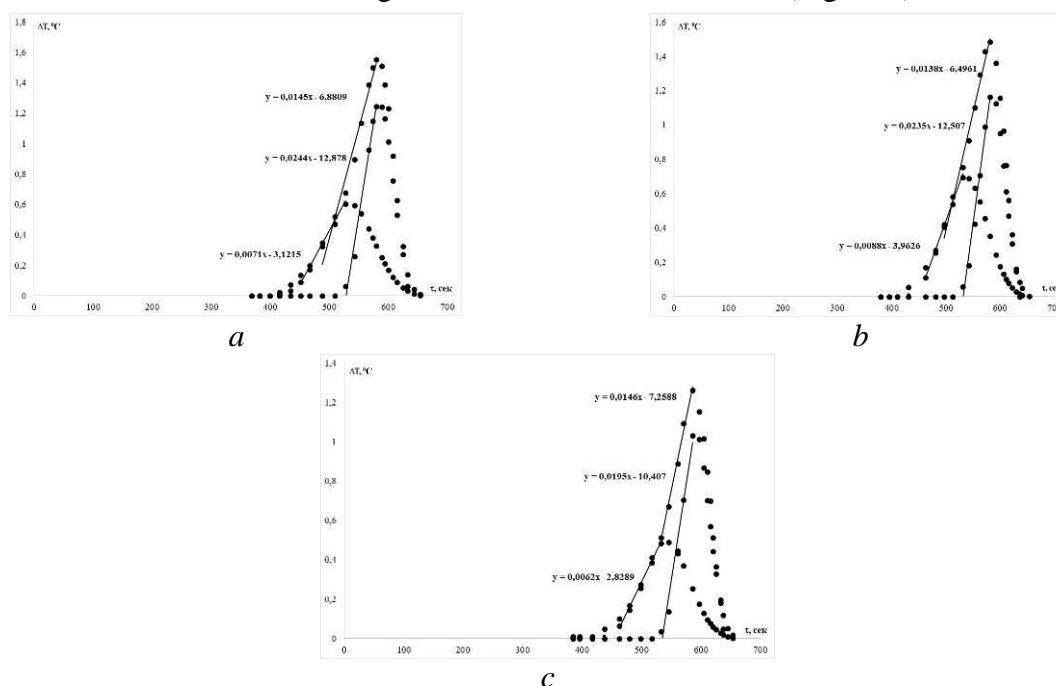


Figure 1. Approximation of Gaussian peaks of the experimental data obtained by differential scanning calorimetry materials "Polikon K" with ultrafine additives:
a - 0% ultrafine additives; b - 1,5% Ni; c - 1,5% Fe

The diffusion process of the monomers in the structure of the fiber reinforcing fabric scanning electron microscopy was found. It is shown that a branched structure formed during polycondensation process with the introduction of additives ultrafine. Branched structure consisting of fibers and ion exchange binder with nanoparticles. Nanoparticles are additional epicenters crosslinking. Occurs a significant strengthening the polymer backbone of the nanocomposite (Figure 2).

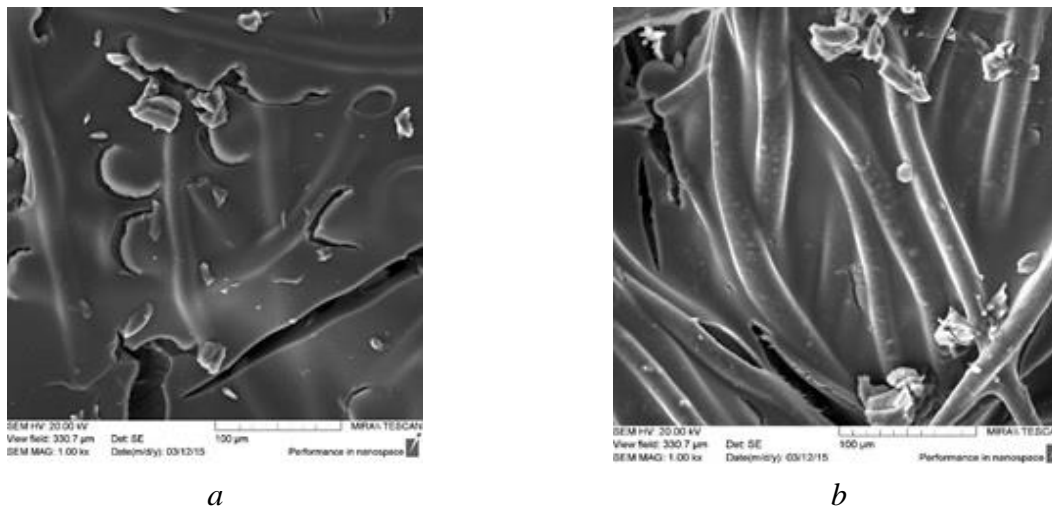


Figure 2. SEM images: a - "Polikon K" on the NFF fiber; b - "Polikon K" + Fe (1,5%)

For ion-exchange materials of one of the indicators of their performance is the exchange capacity. Analysis of the results indicates (Fig. 3) that the material "Polikon K" ultrafine particles when implementing Ni and Fe, have higher sorption characteristics (14% and 16% respectively).

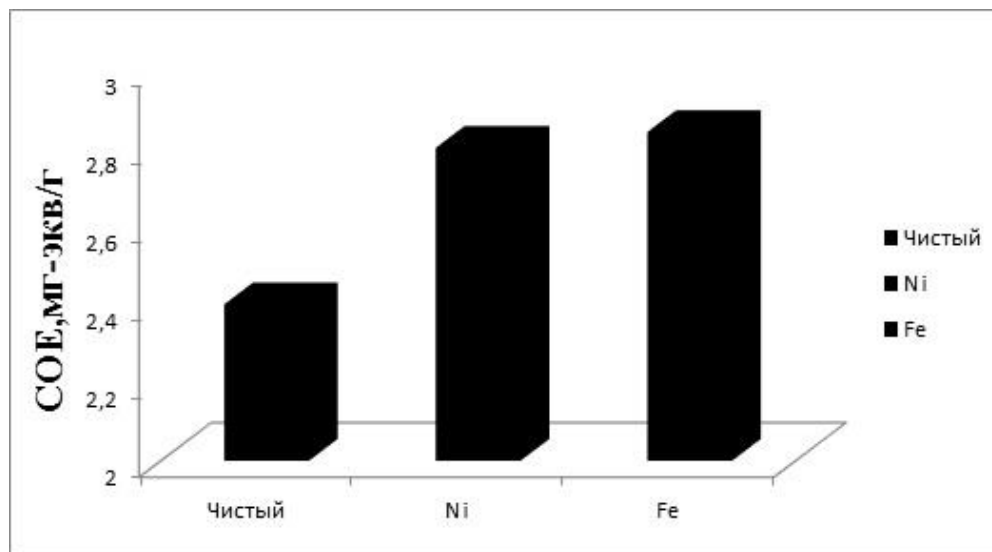


Figure 3. Static exchange capacity

References

1. Kardash M.M., Ambarnov D.V., Ainetdinov D.V. Structural and Absorption Features of Policon K Nanocomposites // Fibre Chemistry. -2016. –Vol. 47, № 6. –P.486-488

SPECTRAL PROPERTIES OF CONCENTRATION FIELD FLUCTUATIONS IN STRATIFIED ELECTROMEMBRANE SYSTEMS WITH STRONGLY BASIC ANION-EXCHANGE MEMBRANES AFTER TEMPERATURE TREATMENT

Elmara Akberova, Elena Goleva, Vladimir Kolganov, Dmitrii Korotkov

Voronezh State University, Voronezh, Russia, E-mail: elmara_09@inbox.ru

The purpose of this study was to investigate the influence of changes of surface properties and chemical composition for heterogeneous strongly basic anion-exchange membranes after temperature effect on the spectral composition of concentration field fluctuations using Fourier analysis. The objects of the study were samples of anion-exchange membranes containing quaternary ammonium groups: MA-41 (produced by ShchekinoAzot, Russia), experimental samples of MA-41P and chemically and thermally stable surface modified membrane MA-41M. Samples of membranes were thermostatically controlled at 100 °C in distilled water for 50 h.

Experiments were carried out in a horizontally oriented electro dialysis cell at a concentration-temperature stable stratification. Visualization of a hydrodynamic picture of interphase boundaries was carried out by using of Mach – Zender type interferometric set up. The results of measurements of the interference fringes fluctuations (optical noise) were recorded in the form of time series. To study optical noise there was applied Fourier analysis, which led us to the conclusion about the frequency composition of the noise, averaged over the entire recording time of oscillatory process.

For strongly basic anion-exchange membranes subjected to heat treatment, differences in the formation of the concentration field were revealed in comparison with the initial conditioned samples. It has been established that for the membranes after temperature effect, the amplitude and average frequency of the oscillations of the interference fringe decreased in practically the entire range of currents (Fig. 1).

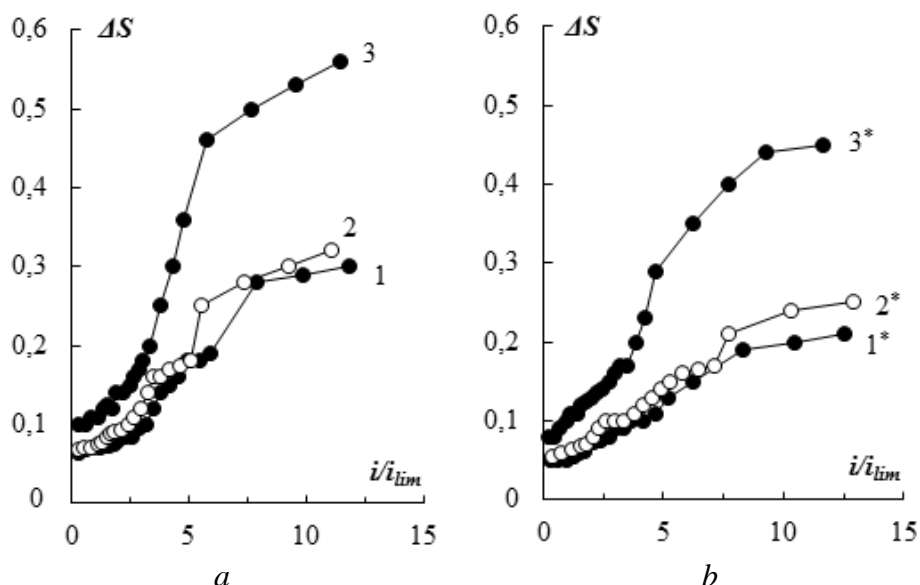


Figure 1. The amplitude of oscillations of the interference fringe in the solution at the interface with the anion-exchange membranes at stable stratification of the system in the gravitational field: $C_0(\text{NaCl})=2.0 \cdot 10^{-2} \text{M}$, $V=1.3 \cdot 10^{-3} \text{m/s}$, $h=2 \cdot 10^{-3} \text{m}$. MA-41 (1, 1*), MA-41M (2, 2*), MA-41P (3, 3*) membrane samples: after conditioning (a), thermal treatment in water at 100°C during 50 h (b)

The maximum values of the amplitude and the average frequency of the oscillations of the interference fringe before and after the temperature treatment were observed in the solution at the interface with the MA-41P membrane, the minimum values at the interface with MA-41. For the MA-41P membrane at current densities in the range of $3.0 < i/i_{lim} < 12.0$ amplitude of oscillations was less by 1.5 ± 0.2 times in comparison with the conditioned sample. For the MA-41 membrane amplitude of oscillations decreased by 1.2 ± 0.1 times at current densities in the range of $1.0 <$

$i/i_{lim} < 13.0$ The average frequency of interference fringe oscillations at these currents changed by 1.14 ± 0.05 times in comparison with the conditioned sample.

According to the methodology of flicker noise spectroscopy [1] parameter n , characterizing the transition from laminar fluid motion to extremely turbulent, defined as the slope of the high-frequency portion of the spectrum. The value $n = 3$ describes a chaotic bulk turbulent mixing of the solution. An analysis of the spectral composition of the fluctuations of the concentration field revealed an increase in the characteristic slope of the spectral region and an increase in the exponent n with an increase in the multiplicity of the excess of the limiting diffusion current density. The minimum degree of turbulent character of the solution was detected at the surface of the membrane after thermal treatment (Fig. 2b).

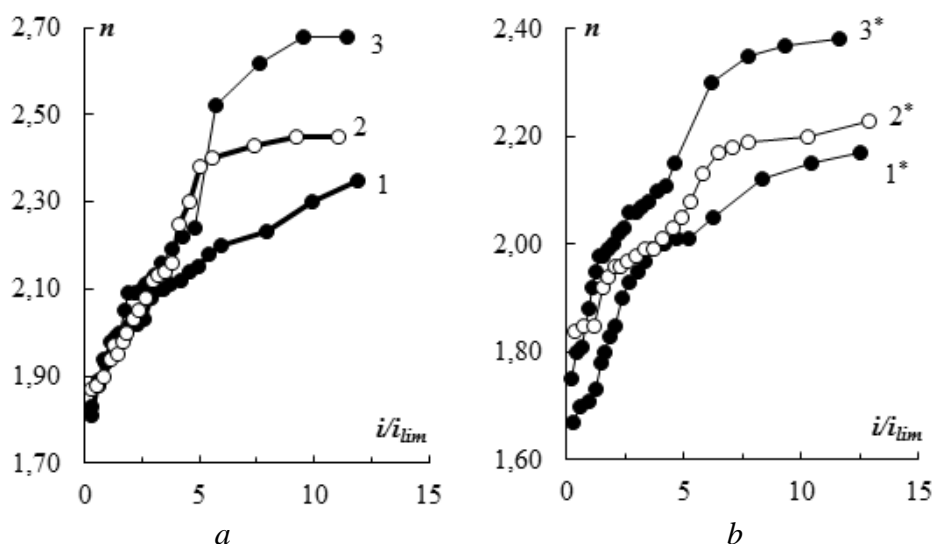


Figure 2. Comparison of the parameter n of interference fringes fluctuation at the surface of the strongly basic membranes at $C_0(\text{NaCl}) = 2.0 \cdot 10^{-2} \text{ M}$, $V = 1.3 \cdot 10^{-3} \text{ m/s}$, $h = 2.0 \cdot 10^{-3} \text{ m}$. MA-41 (1, 1*), MA-41M (2, 2*), MA-41P (3, 3*) membrane samples: after conditioning (a), thermal treatment in water at 100°C during 50 h (b)

For strongly basic anion-exchange membranes after the temperature treatment an increase in the fraction of conducting surface area by 8 and 26% for MA-41P and MA-41 membranes, respectively, and an increase of the geometric surface inhomogeneity by more than two times were established. But during the heat treatment of these membranes, quaternary amino groups are converted to catalytically active tertiary amino groups [2, 3]. It leads to an increase in the generation of H^+ and OH^- ions during the reaction of heterolytic dissociation of water and, as a consequence, to a decrease in the intensity of the electroconvective instability in the solution at the interface with the investigated strongly basic membranes.

Acknowledgements

The present work is supported by the RFBR (project No 16-38-00572 mol_a).

References

1. Timashev S.F., Grigoriev V.V., Prudnikov E.Y. Flicker noise spectroscopy in the analysis of fluctuation dynamics of the electric potential in electromembrane system under "overlimiting" current density // Russ. J. Phys. Chem. 2002. Vol. 76. №3. P. 554-561. [in Russian]
2. Vasil'eva V.I., Pismenskaya N.D., Akberova E.M., Nebavskaya K.A. Effect of thermochemical treatment on the surface morphology and hydrophobicity of heterogeneous ion-exchange membranes // Russ. J. Phys. Chem. A. 2014. Vol. 88. No 8. P. 1293-1299.
3. Vasil'eva V.I., Akberova E.M., Zabolotskii V.I. Electroconvection in systems with heterogeneous ion-exchange membranes after thermal modification // Russ. J. Electrochem. 2017. Vol. 53. No. 4. P. 398-410.

DIFFUSION BOUNDARY LAYERS IN THE SOLUTION ON THE INTERPHASE WITH SULFOCATION EXCHANGE MEMBRANES AFTER TEMPERATURE MODIFICATION

Elmara Akberova, Elena Goleva, Vera Vasil'eva

Voronezh State University, Voronezh, Russia, E-mail: elmara_09@inbox.ru

Introduction

Occurrence of convective instability in electromembrane systems has been visualized in researches by means of optical methods of the analysis [1, 2]. Application of laser interferometry allowed visualization the process of formation and development of the diffusion layers in a solution near the surface of an ion-exchange membrane in a wide range of current densities [3]. One of the main factors determining behavior of the ion-exchange membranes at the overlimiting current density are the properties of their surfaces. In particular, the electrical heterogeneity of the membrane surface intensifies the development of electroconvective vortexes near its surface [4]. Changes of microstructure of membranes can be reached by temperature modifying [5]. The aim of the present work is an investigation of dynamics of a development of the convective instability region and measurement thickness of the diffusion boundary layer at high-intensity regimes of an electro dialysis by the method of laser interferometry.

Experiments

The objects of the study were samples of heterogeneous ion-exchange MK-40 membrane with low catalytic activity in the water dissociation reaction sufficiently thermostable fixed sulfur groups. The used membranes were chemically conditioned by sequential treatment with solutions of acids and alkalis. Then the samples of membranes were thermostated at 100 °C in distilled water for 50 hours.

Visualization of a hydrodynamic picture of interphase boundaries was carried out by using of Mach – Zender type interferometric set up, that allowed defining the characteristic size of the convective instability region arising at high-intensity regimes of an electro dialysis. The size of convective instability region d is defined as distance from a membrane surface on which a concentration profile has unstable, oscillatory character. It is possible to find the Nernst δ_N and the total δ thicknesses of diffusion boundary layer. Nernst thickness δ_N is obtained as the intersection of a tangent to the concentration profile drawn from interphase surface to the straight line corresponding to the initial concentration, δ is defined as the distance from the surface to the point in solution where $c=0.99c_0$. At overlimiting current regimes the dimensions of the total diffusion layers δ and linear Nernst approximations δ_N obtained as the intersection of a tangent to the concentration profile drawn from interphase convective instability zone and stable diffusion layer to the straight line corresponding to the initial concentration [6, 7]. Experiments were carried out in a horizontally oriented electro dialysis cell at a concentration-temperature stable stratification.

Results and Discussion

The study of development of convective vortices in the membrane channel consisting from the MK-40 cation-exchange membrane before and after temperature modifying and the MA-41 anion-exchange membrane, has detected their dependence on effect of membrane surface properties after temperature treatment.

Figure 1 presents experimentally obtained dependence of the total (δ), effective (δ_N) thickness of the diffusion boundary layer and the size of convective instability zone (d) on the non-dimensional current density under stable stratification of electromembrane systems. At the current densities lower than the limiting current density i_{lim} the value of the total diffusion layer δ increases significantly with i , while that of δ_N increases more slightly. At $i > i_{lim}$ the increase of the convection instability region of the solution in the vicinity of the membrane surface and the decrease of thicknesses of the diffusion layer with the uprising of the current density in an overlimiting region has been revealed experimentally. When the dimensions of the convective instability region

correspond to the thickness of the boundary layer, the concept of the diffusion layer thickness loses its meaning and its complete destruction occurs. After the temperature treatment, the thickness drop and then the destruction of the diffusion layer are fixed at a degree of membrane polarization one and a half times smaller than for the conditioned membrane.

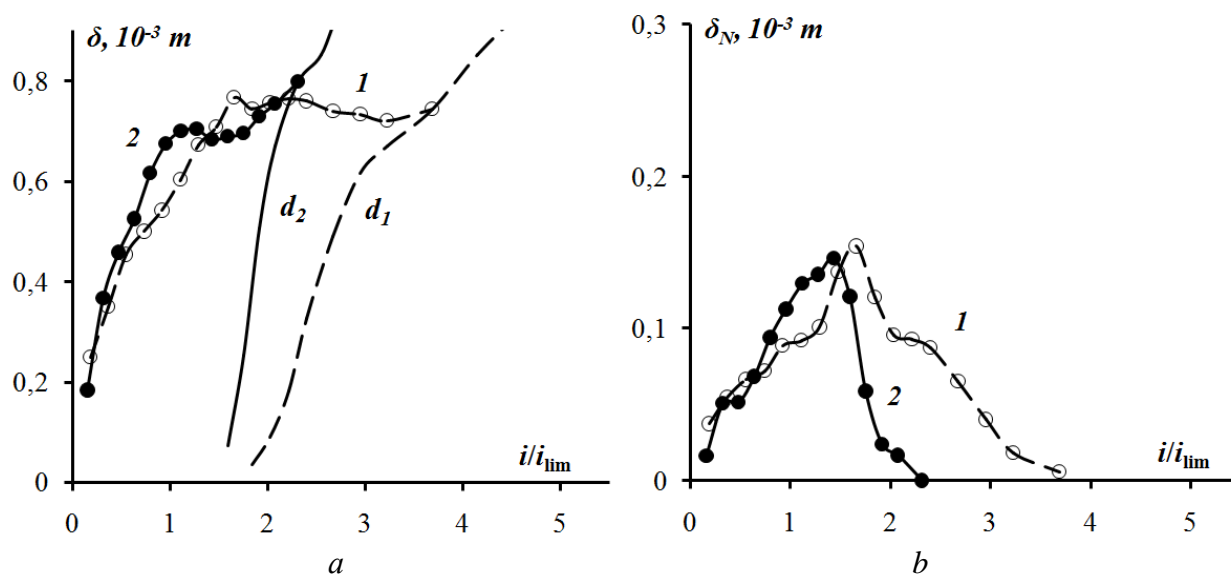


Figure 1. Total (a) and the Nernst (b) thickness of the diffusion layer and the size of convective instability zone (d) near the MK-40 cation-exchange membranes after conditioning (1) and temperature treatment in water at 100 °C (2): $C_0(\text{NaCl})=0.02\text{M}$, $V=0.13\text{ cm/s}$, $h=0.2\text{ cm}$

Significant changes in the structure of diffusion layers of MK-40 membrane with sufficiently thermostable fixed sulfur groups were caused by changes in the surface morphology and microrelief of membrane after temperature effect (Table 1). It was found that action of elevated temperature leads to an increase in the porosity by 3 times, while the conductive surface proportion S_c (ion exchange material plus spacing between the ion-exchanger and inert binding agent) is increased by 40%. Amplitude and the average oscillation frequency of the interference fringe in a wide range of currents for membranes MK-40 exceeded the corresponding values for the initial sample.

Table 1: Microstructure of the swollen membranes surface after temperature treatment at 100 °C (50 h)

Samples	S, %	P, %	S_c , %	\bar{R} , μm	\bar{r} , μm	R_a , nm	R_y , nm
Before treatment	13.2±0.9	1.9±0.2	14.8±0.9	3.3±0.3	1.8±0.2	54	813
After treatment	15.5±0.9	6.5±0.3	20.8±0.9	4.0±0.2	2.4±0.1	182	2028

where S and S_c are the proportion of the ion exchanger and conductive phase, respectively, P is the porosity; \bar{R} and \bar{r} are the radii of the ion exchangers and pores, respectively; R_a is the maximum height, R_y is the arithmetic mean roughness.

Thus, under intensive current regimes, the parameters of diffusion layers depend on the properties of the membrane surface that determine the intensity of electroconvection, such as electrical and geometric inhomogeneity.

Acknowledgements

The present work is financially supported by the RFBR (project No 15-08-05031 and 16-38-00572 mol_a).

Microphotographs of the membranes surface were obtained at the CCUSE of VSU.

References

1. *Pevnitskaya M.V.* Intensification mass transfer at an electrodialysis of the diluted solutions // *Electrokhimiya*. 1992. Vol.28. №1. P. 1708-1715. (in Russian)
2. *Rubinstein S.M., Manukyan G., Staicu A., Rubinstein I., Zaltzman B., Lammertink R.G.H., Mugele F., Wessling M.* Direct Observation of a Nonequilibrium Electro-Osmotic Instability // *Physical Review Letters*. 2008. Vol. 101. P. 236101.
3. *Vasil'eva V.I., Shaposhnik V.A., Grigorchuk O.V., Petrunya I.P.* The membrane-solution interface under high-performance current regimes of electrodialysis by means of laser interferometry // *Desalination*. 2006. Vol. 192. № 1-3. P. 408-414.
4. *Rubinstein I., Zaltsman B.* Electro-osmotically induced convection at a permselective membrane // *Phys. Rev. E*. 2000. Part A, Vol. 62, No 2. P. 2238-2251.
5. *Vasil'eva V. I., Akberova E. M., Zabolotskii V. I.* Electroconvection in systems with heterogeneous ion-exchange membranes after thermal modification // *Russ. J. Electrochem.* 2017. Vol. 53. No. 4. P. 398-410.
6. *Nikonenko V.V., Vasil'eva V.I., Akberova E.M., Uzdenova A.M., Urtenov M.K., Kovalenko A.V., Pismenskaya N.P., Mareev S.A., Pourcelly G.* Competition between diffusion and electroconvection at an ion-selective surface in intensive current regimes // *Advances in Colloid and Interface Science*. 2016. Vol. 235. P. 233-246.
7. *Vasil'eva V., Zhiltsova A., Shaposhnik V., Zabolotsky V., Lebedev K., Malykhin M.* Direct observation of convective instability in electromembrane systems by laser interferometry // *Ion Transport in Organic and Inorganic Membranes: Intern. Conf. : Conf. Proc., 28 May-2 June 2012. Krasnodar, 2012. P. 233-235.*

EFFECT OF THE CHANGES IN CHEMICAL NATURE OF THE IONOGENIC GROUPS FOR ANION-EXCHANGE MEMBRANES AFTER TEMPERATURE TREATMENT ON THE SIZE OF THE ELECTROCONVECTIVE INSTABILITY REGION IN HIGH-CURRENT MODES

Elmara Akberova, Vera Vasil'eva, Mikhail Malykhin

Voronezh State University, Voronezh, Russia, E-mail: *viv155@mail.ru*

Introduction

According to modern views, the intensity of electroconvection decreases because of water dissociation at the membrane–solution interface. The main factors determining the rate of the heterolytic water dissociation are the nature of the ionogenic groups of membranes and the current density [1-4]. The aim of this study was to investigate the influence of the changes in nature of the ionogenic groups of membranes with different catalytic activities in heterolytic water dissociation due to temperature treatment on the dynamics of the development of electroconvective instability and the size of its region in high-current modes by laser interferometry.

Experiments

Anion-exchange membranes containing quaternary ammonium groups were selected as the objects of investigation: MA-41 (produced by ShchekinoAzot, Russia), experimental samples of MA-41P and chemically and thermally stable surface modified membrane MA-41M. Samples of membranes were thermostatically controlled at 100 °C in distilled water for 50 h.

The study of concentration field in a solution at the boundary with the membrane was performed by laser interferometry with the use of interferometric set up of Mach-Zender type. The obtained interferograms were presented as separate subject videos. Interference band represented the profile of the refractive index and concentration, respectively. Thickness of convective instability region at the interphase boundary membrane-solution d was determined as the distance from membrane surface where the interference band and concentration profile, respectively, are of unstable, oscillation character.

Experiments were made in electro-dialyzer divided into seven compartments with alternating cation-exchange and anion-exchange membranes. The investigated central compartment consisted of one-type membranes and it was located horizontally under the stable concentration-temperature stratification. The height of membrane channel L was of $4,1 \cdot 10^{-2}$ m, width was of $2,4 \cdot 10^{-2}$ m, intermembrane distance was $h = 2,0 \cdot 10^{-3}$ m. Sodium chloride solutions with the initial concentration of $2,0 \cdot 10^{-2}$ M were supplied with the rate of $1,3 \cdot 10^{-3}$ m/s, that corresponds to laminar flow ($Re=3$). Electrodialysis was performed in galvanostatic mode.

The experimental studies of surface morphology of hydrated membranes were conducted using the method of scanning electron microscopy at JSM-6380 LV microscope (Japan) equipped with regulated pressure. Fraction of conducting surface was estimated by means of an original software system. The membrane surface was also investigated via AFM using a Solver P47 Pro microscope (Zelenograd, Russia) on dry samples in the semicontact mode.

Results and Discussion

A comparative analysis of current-voltage curves and dimensions of the region of electroconvective instability in the solution at the boundary with the conditioned samples of strongly basic anion exchange membranes shows that the limiting-current plateau length, the resistance in the regions of current-voltage curves, and the intensity of electroconvection are determined predominantly by the catalytic activity of fixed membrane groups in the heterolytic reaction of water dissociation (Fig. 1). The substitution of quaternary amines, which are bidentately bound to the membrane matrix, for unstable quaternary ammonium bases in the surface layer of MA-41 membrane provides a low rate of heterolytic reaction of water dissociation and the generation of convective stirring at the interface with MA-41M membrane at a lower polarization of electromembrane system. Therefore, the modified MA-41M membrane with a weak catalytic effect in the heterolytic reaction of water dissociation is characterized by the smallest plateau

length and the lowest electric resistance R_2 corresponding to the plateau. The experimental data on the thickness of convective instability region support the fact of more intense electroconvective stirring of solution at the boundary with the modified anion exchange membrane (Fig. 1b).

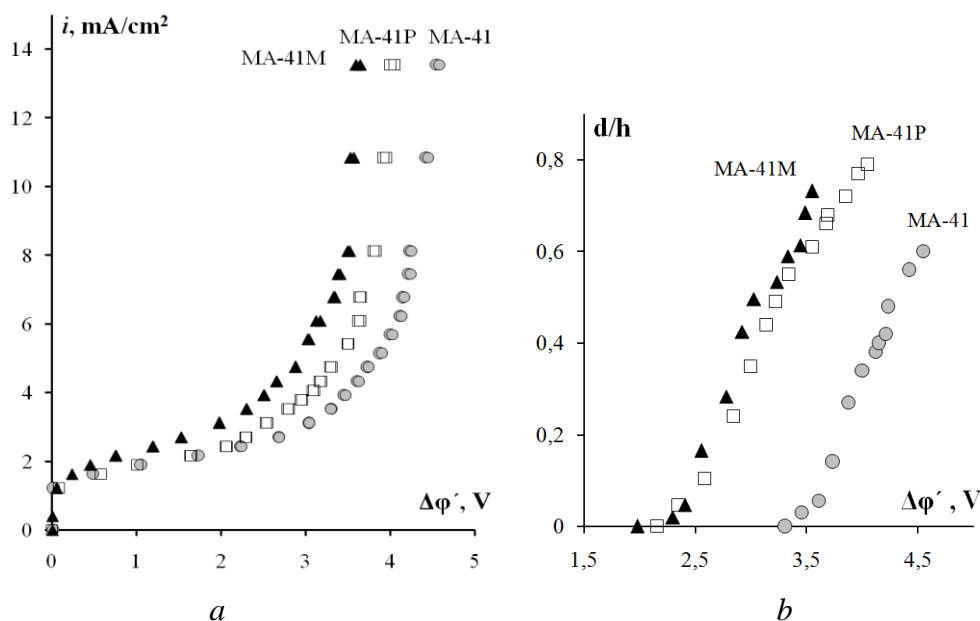


Figure 1. Current-voltage curves (a) and thickness of the convective instability region normalized to the intermembrane distance h (b) in solution at the boundary with conditioned strongly basic anion-exchange membranes

The original samples of MA-41 and MA-41P heterogeneous membranes differ in the content of a fraction of weakly basic groups α and in the parameters of electrical and geometrical surface inhomogeneity due to different degrees of cross-linking of AV-17 anion-exchanger, which is contained in the membranes. For the conditioned specimen of MA-41 membrane based on a stronger cross-linked anion exchanger, a fraction of secondary and ternary amino groups is 0.17, which is by 40% larger than for a weaker cross-linked MA-41P membrane. The data on the difference in the solution pH value between the inlet and outlet of the concentrating section adjacent to the section under investigation (Fig. 2) are the evidence for weaker generation of H^+ and OH^- ions at the boundary of MA-41P membrane due to a lower content of secondary and ternary amines. A fraction of conducting surface area of strongly basic MA-41P membrane based on the weakly cross-linked ion-exchanger is by 1.6 times larger than that of the specimen of MA-41 membrane based on the strongly cross-linked ion-exchanger; the peak-to-peak height on the MA-41P membrane surface is by 1.5 times larger. These factors provide more intense development of electroconvection in the solution at the boundary with the MA-41P membrane. This is manifested by a decrease in the length and an increase in the slope of the plateau in the current-voltage curve and a larger dimension of the region of electroconvective solution stirring as compared with the MA-41 membrane (Fig. 1).

For strongly basic anion-exchange membranes due to the thermal destruction of their fixed groups after the temperature treatment, in spite of an increase in the fraction of conducting surface area by 8 and 26% for MA-41P and MA-41 membranes, respectively, and an increase of the geometric surface inhomogeneity by more than two times, the dimensions of electroconvective instability region decrease for both membranes.

In accordance with the series [2] of catalytic activity of ionogenic groups in the heterolytic reaction of water molecule dissociation the conversion of benzene trimethyl ammonium into weakly basic amino groups by the degradation reaction during the thermal treatment of strongly basic membranes leads to more intense generation of H^+ and OH^- ions in the solution near the membrane surface that hampers the development of electroconvection. An increase in the concentration of the products of water molecule dissociation near the surface of strongly basic

membranes after their thermal treatment is supported by the measured pH values of solution in the adjacent concentrating section (Fig. 2).

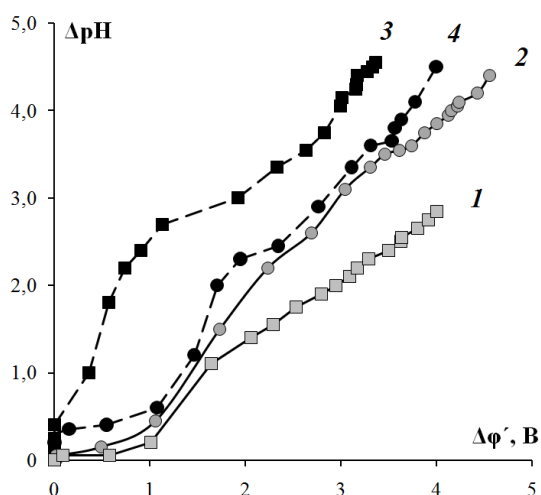


Figure 2. Difference between the pH values of solution at the outlet and inlet of concentrating section adjacent to the membrane under investigation. The membrane samples: conditioned MA-41P (1) and MA-41(2); after thermal treatment MA-41P (3) and MA-41(4).

A linear correlation is found between the thickness of electroconvective instability region and a fraction of fixed weakly basic functional amino groups in the strongly basic anion-exchange membranes. The dimensions of electroconvective instability region decrease with the formation of fixed weakly basic amino groups, which are catalytically active in the reaction of water dissociation, as a result of thermal destruction of strongly basic anion-exchange membranes.

It is found that the thickness of electroconvective instability region decreases and the currents/potentials of its initiation increase with increasing contribution of degradation to the thermal destruction of fixed groups of strongly basic membranes. Thus, the variation of the surface chemical composition in the course of thermal treatment of heterogeneous strongly basic membranes is the main factor that determines the conditions for generation and the intensity of development of electroconvection under the overlimiting current modes.

Acknowledgements

The present work is financially supported by the RFBR (project No 15-08-05031 and 16-38-00572 mol_a).

References

1. Simons R. Electric field effects on proton transfer between ionizable groups and water in ion exchange membranes // *Electrochim. Acta*. 1984. Vol. 29. P. 151-158. [in Russian]
2. Zabolotskii V.I., Shel'deshov N.V., Gnusin N.P. Dissociation of water molecules in systems with ion-exchange membranes // *Uspekhi Khimii*. 1988. Vol. 57. P. 1403-1414. [in Russian]
3. Zabolotskii V.I., Bugakov V.V., Sharafan M.V., Chermit R.Kh. Transfer of electrolyte ions and water dissociation in anion-exchange membranes under intense current conditions // *Russ. J. Electrochem.* 2012. Vol. 48. P. 650-659.
4. Vasil'eva V. I., Zhil'tsova A. V., Malykhin M. D., Zabolotskii V. I., Lebedev K. A., Chermit R. Kh., Sharafan M. V. Effect of the chemical nature of the ionogenic groups of ion-exchange membranes on the size of the electroconvective instability region in high-current modes // *Russ. J. Electrochem.* 2014. Vol. 50. P. 120-128.

OPTIMIZATION OF COMPOSITION AND MICROSTRUCTURE WITH THE AIM OF INCREASING THE SPECIFIC ELECTROCHEMICAL CHARACTERISTICS OF CATALYSTS WITH A LOW CONTENT OF PLATINUM

Anastasia Alekseenko, Vladimir Guterman, Vadim Volochaev, Angelina Pavlets, Kirill Paperj

Southern Federal University, Rostov-on-Don, Zorge st.,7, Russia

E-mail: an-an-alekseenko@yandex.ru

Introduction

In recent years an actual problem of modern electrochemical power engineering is a preparation of electrocatalysts for low temperature fuel cells, which have desired characteristics for modern technologies [1, 2]. A development of new and optimization of well-known synthesis methods are the most promising directions in the field of preparation and study of these materials [2]. Pt-based alloy catalysts has attracted the most attention in the research of material with low content noble metal. The composition, size, shape and fine structure (architecture) of Pt and Pt-alloys nanoparticles (NPs) are the most important parameters, which affect the basic characteristics of catalysts [1, 3]. Preparation of Pt-based electrocatalysts, containing bimetallic NPs with special structure (core-shell, alloy, hollow NPs and other) is primarily seen as a good possibility to reduce the loading of expensive platinum in the final material. At the same time this is opportunity to increase the electrochemical characteristics due to structural and electronic effects [1, 4].

Experimental section

A number of Pt(Cu)/C materials with an assumed gradient distribution of components in nanoparticles were obtained during the study. Both final materials and intermediate products were examined. Carbon black (Vulcan XC-72) was used as a support for nanoparticles. Ethylene glycol was used as a solvent for the preparation of these suspensions. Synthesis was carried out in 4 stages with successive addition of metal precursors. It is supposed that the gradient particles would consist of a massive copper core, then two Cu + Pt layers with different ratios of the components, and the last layer - pure Pt. At each stage, metal precursors reduction was carried out with an excess of NaBH₄ (reducing agent) in organic-aqueous medium at room temperature.

It was supposed that such materials would be characterized by a gradual increase in the concentration of platinum from the center of the nanoparticle to the surface. The architecture and composition of obtained materials are shown in Fig. 1. For comparison, sample A5 of similar composition was prepared by simultaneous reduction of copper and platinum (alloy structure).

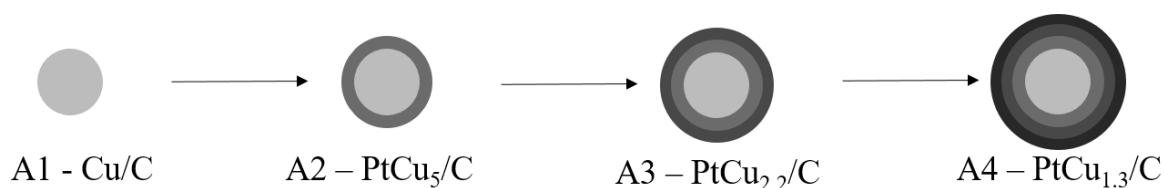


Figure 1. Schematic representation of obtaining a gradient nanoparticle.

Further, the structural and electrochemical characteristics of the obtained Pt(Cu)/C materials were studied.

Results and Discussion

Prepared Pt(Cu)/C materials contained from 10 to 29 wt. of metals (4.6 – 21 % wt. Pt). An average crystallites size calculated by XRD data was from 1.8 to 3 nm (Tab. 1).

We measured the electrochemically active surface area of the Pt(Cu)/C catalysts and studied characteristics of their electrochemical behavior. An electroactive surface area (ECSA) of Pt determined by the amount of electricity expended in electrochemical adsorption and desorption of adsorbed atomic hydrogen was measured by hydrogen electrodesorption method in the process of

registering of the 2nd cyclic voltammograms at a scan rate 20 mV/s. The values of ECSA were from 71 to 196 m²g⁻¹(Pt) (Fig.2a). The abnormally high value of the active surface area of sample A3 is due to very low content of platinum.

It is known that dissolution of copper from the non-protected by platinum surface of cores occurs during the electrochemical measurement. To detect this fact, the composition of materials after electrochemical measurements was measured.

Table 1: Some characteristics of Pt(Cu)/C catalysts

Sample	Material composition	Metal's loading in the catalyst, % wt	Pt loading in the catalyst, % wt	Average size of crystallites, nm	ECSA, m ² g ⁻¹ (Pt)	ECSA ₅₀₀₀ /ECSA _{max} , %
A1	Cu	10.0	-	-	-	-
A2	PtCu ₅	12.2	4.6	1.8	-	-
A3	PtCu _{2.2}	15.3	8.9	2.2	196	-
A4	PtCu _{1.3}	28.8	20.2	2.3	96	82
A5	PtCu _{0.98}	27.7	21.0	3.1	71	64
E-TEK (commercial sample)	Pt	-	20	2.8	87	74

It turned out that the sample containing nanoparticles with a gradient structure demonstrated an increased content of copper after electrochemical measurements in comparison with the catalyst with alloy structure. This is because the copper is more effectively protected by a platinum-shell which prevents its dissolution.

A comparative study of the durability for the synthesized Pt(Cu)/C materials in the process of long-term (more than 5000 cycles) voltammetric cycling were performed (Tab. 1). Sample A4 is characterized by increased stability during the stress test in comparison with “alloy” A5 and E-TEK materials.

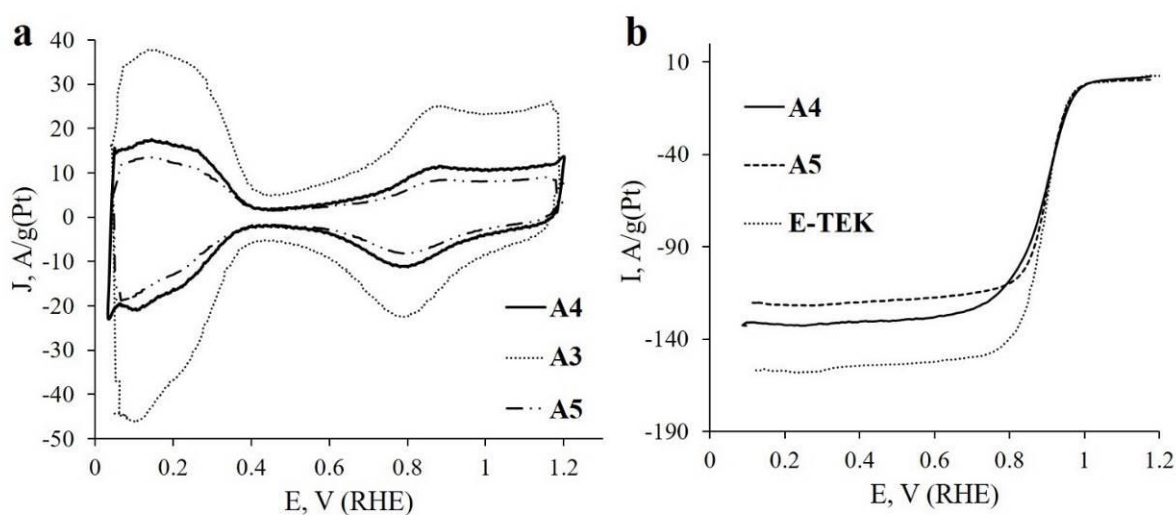


Figure 2. Cyclic voltammograms of Pt(Cu)/C electrocatalysts in Ar-saturated 0.1 M HClO₄, 20mV/s (a). LSV of Pt-Cu/C samples and commercial Pt/C electrocatalysts. 1600 rpm, 20 mV/s, O₂-saturated 0.1 M HClO₄ (b).

The catalytic activity of the Pt(Cu)/C electrocatalysts in ORR was evaluated by linear sweep voltammetric measurements at 20 mV/s in O₂-saturated 0.1 M HClO₄ electrolyte at 1600 rpm (rotating disk electrode (RDE)). The data are compared with the same for commercial Pt/C (E-TEK) in Figure 2b.

In according with results of our study, materials with gradient architecture of two-component nanoparticles can be a promising direction in electrocatalysis. Such materials can exhibit high

specific characteristics, while being characterized by a reduced content of platinum and a low percentage of d-metal dissolution.

The work was carried out within the framework of the Ministry of Education and Science of the Russian Federation (assignment No. 13.2005.2017/PCh).

References

1. Junga N., Chung D.Y., Ryua J., Yoo S.J., Sung Y. Pt-based nanoarchitecture and catalyst design for fuel cell applications // *Nano Today*. 2014. V. 9. P. 433–56.
2. Yaroslavtsev A.B., Dobrovolsky Y.A., Shaglaeva N.S., Frolova L.A., Gerasimova E.V., Sanginov E.A. Nanostructured materials for low-temperature fuel cells // *Russian Chemical Reviews*. 2012. V. 81. P. 191–220.
3. Guterman V.E., Lastovina T.A., Belenov S.V., Tabachkova N.Yu., Vlasenko V.G., Khodos I.I., Balakshina E.N. PtM/C (M = Ni, Cu, or Ag) Electrocatalysts: Effects of Alloying Components on Morphology and Electrochemically Active Surface Areas // *J. of Solid State Electrochemistry*. 2014. V. 18. P. 1307–1317.
4. Guterman V.E., Belenov S.V., Pakharev A.Yu., Min M., Tabachkova N.Yu., et al. Pt-M/C (M = Cu, Ag) electrocatalysts with an inhomogeneous distribution of metals in the nanoparticles // *Int. J. of Hydrogen Energy*. 2016. V. 41. P. 1609–26.

EFFECT OF ANTHOCYANINS ON THE MORPHOLOGY AND CHEMICAL COMPOSITION OF AMX-Sb MEMBRANE SURFACE

Diana Aleshkina, Veronika Sarapulova, Natalia Pismenskaya

Institute of Membranes, Kuban State University, Krasnodar, Russia, E-mail: lerd2@yandex.ru

Introduction

Anion-exchange membranes are increasingly used in the processes of purification, stabilization and conditioning concentrating liquid media in the food industry. As a rule, a fouling of membranes accompanies these processes. We assume that the contact of membranes with the components of the wine, in particular anthocyanins, should lead to a change in the morphology and chemical composition of its surface. The aim of this paper is to test this hypothesis.

Experiments

The object of the study was homogeneous anion exchange membrane AMX-Sb AEM (Astom, Tokuyama Corp., Japan). We used 10% solutions of anthocyanins with pH 3; 6; 9. It was obtained by extraction of anthocyanins from marc of black grape. The pH of the initial solution was adjusted by solutions of acid (HCl) or alkali (NaOH). The sample of the membrane under study was equilibrated with each of these solutions. The initial solutions of anthocyanins and samples of equilibrated membranes were dried at a temperature of 40 degrees. FT-IR Spectroscopy Attenuated Total Reflectance (ATR) of solutions and membranes were obtained using the spectrometer Vertex-70 (Bruker Optics, Germany) with ATR diamond crystal. The determination was made in the range 4500-350 cm^{-1} . The spectra obtained were normalized to the baseline using the OPUS™ software. AFM JEOL 5400 was used to estimate morphology of pristine and fouled membranes. We have obtained at least three images of each surface of the sample, which area was $5 \times 5 \mu\text{m}^2$. Then we made five sections on them and determined the parameters of the surface roughness using software. The data obtained were processed using statistical analysis.

Results and Discussion

It is known that the structure and color of anthocyanins can depend on the medium. Figure 1 shows the proposed structure and the color scale of the investigated anthocyanins as a function of pH (Fig 1).

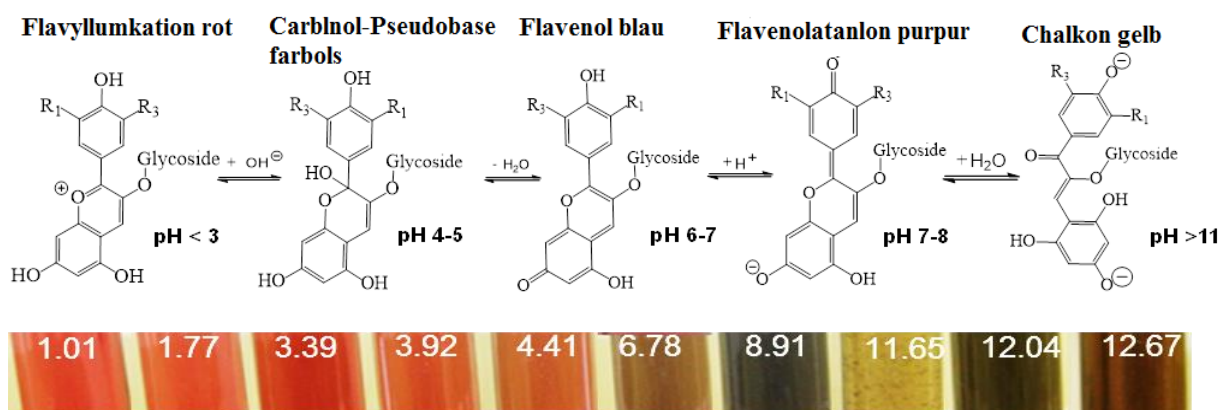


Figure 1. Different states of anthocyanin molecule and the color of aqueous solution of anthocyanins depending on pH

Our studies have shown that the structure of anthocyanins really depends strongly on the medium pH (Fig 2).

The spectrum of AMX-Sb membrane before and after contact with antocianyns have different shape (Fig. 3) due to the interaction of the components of AEM with anthocyanins. Methyl and methylene groups of the membrane absorb near $1450-1420\text{cm}^{-1}$ and 1380cm^{-1} . On the spectrum of fouled membrane, the intensity of the absorption band increases near 1600cm^{-1} , and also $1225-950\text{cm}^{-1}$, which corresponds to stretching vibrations of the C-C bond of the benzene ring. The

appearance of an intense peak at 1039 cm^{-1} corresponds to stretching vibrations of the C-O group ($1230\text{-}1000\text{ cm}^{-1}$), which is also intense in the anthocyanin spectrum.

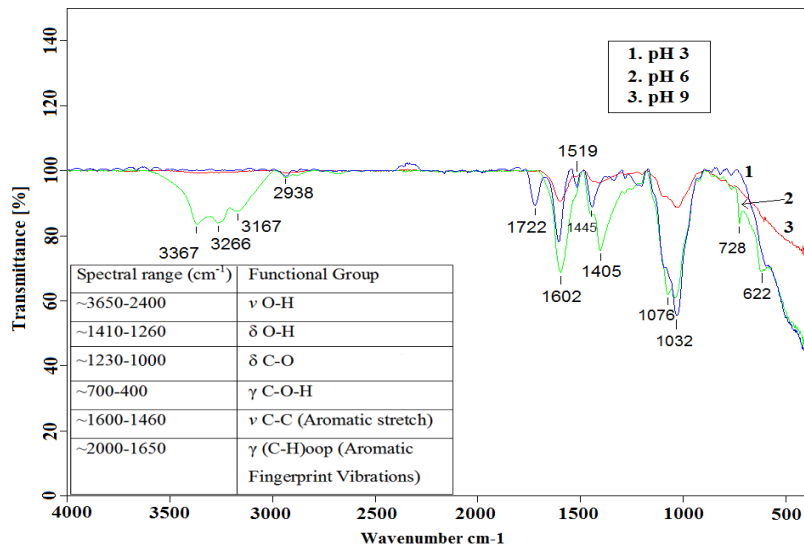


Figure 2. Effect pH on the shape of the FT-IR ATR spectra of anthocyanins

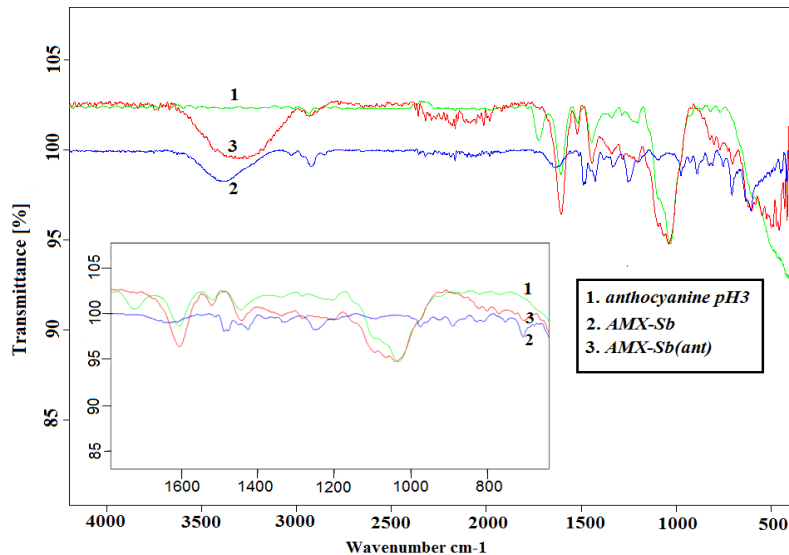


Figure 3. FT-IR ATR spectra of anthocyanine (pH= 3), pristine (AMX-Sb) and equilibrated with this anthocyanine (AMX-Sb ant) membrane in air-dry state .

Images of the surfaces of the initial and anthocyanin-contacted membranes are shown in Fig. 4. Surface roughness parameters of pristine and anthocyanin-contacted membranes data are summarized in the table 1. From the data obtained, it follows that the morphology of the surface changes markedly after the membrane is contacted with anthocyanins.

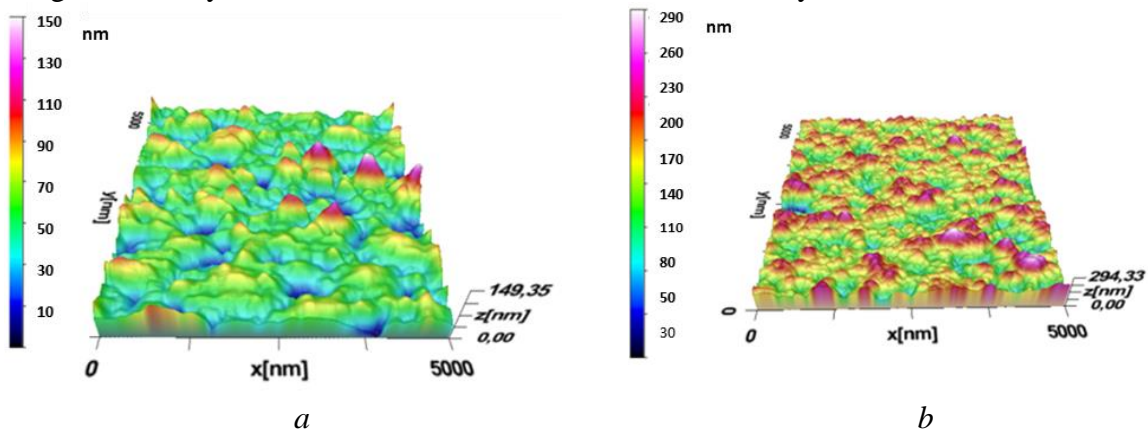


Figure 4. Images of the surfaces of the pristine (a) and anthocyanin-contacted (b) membranes

Table 1. Surface roughness parameters of pristine and anthocyanin-contacted membranes

membrane parameter	AMX-Sb	AMX-Sb(ant)
R_a , nm	14,5±3,9	25,02±3,5
R_z , nm	88,9±23,3	148,13±22,6
S_{ratio}	1,03±0,01	1,1±0,01
R_q	18,5±4,9	31,35±4,3
$R_{z_{ij}}$	55,2±12,1	91,79±13,63

R_a – arithmetical mean roughness value;
 R_z – mean roughness depth;
 S_{ratio} – factor of the roughness;
 R_q – root mean square roughness;
 $R_{z_{ij}}$ – 10-point height of irregularities.

Thus, the contact of membranes with anthocyanins does indeed lead to a noticeable change in the chemical composition and parameters of the roughness of their surface.

Acknowledgements

The study was realized within French-Russian laboratory “Ion-exchange membranes and related processes”. We are grateful to CNRS, France, and to RFBR (grant № 15-58-16019_NCNIL) for financial support.

We thank the employees of the Center for Collective Use "Diagnostics of the Structure and Properties of Nanomaterials" (Kuban State University) for the equipment and useful discussions.

IMPACT OF PULSED ELECTRIC FIELD MODES ON SCALING FORMATION DURING ELECTRODIALYSIS

^{1,2}Marina Andreeva, ²Lasaad Dammak, ²Christian Larchet, ¹Natalia Kononenko

¹Institute of Membranes, Kuban State University, Krasnodar, Russia

E-mail: andreeva_marina_90@bk.ru

²Institute de Chimie et des Matériaux de Paris Est, UMR 7182 CNRS-Université Paris-Est, Thiais, France

Introduction

Recent studies have shown that electrodialysis (ED) is one of the effective approaches to treating reverse osmosis brines and reaching near zero liquid discharge [1]. Nevertheless, precipitation of scaling compounds on ion exchange membrane surface (or in its bulk) is a major block in ED performance. Pulsed electric field (PEF) modes can be applied for increasing mass transfer rate and reducing fouling/scaling in ED [2]. In addition, Lee et al. [3] reported the humate fouling mitigation on anion exchange membrane when applying PEF mode in ED treatment. The purpose of this work is to study the effect of pulsed currents on the concentration polarization phenomena and, as consequence, deposit formation on the cation exchange membrane surface in desalination ED compartment.

Experiments

A four-compartment electrodialysis cell [4] was used in this study. It comprises two MK-40 cation exchange heterogeneous membranes (Shchekinoazot, Russia) and a MA-41 anion exchange heterogeneous membrane (Shchekinoazot, Russia). Membrane positions in the cell are described in Fig. 1.

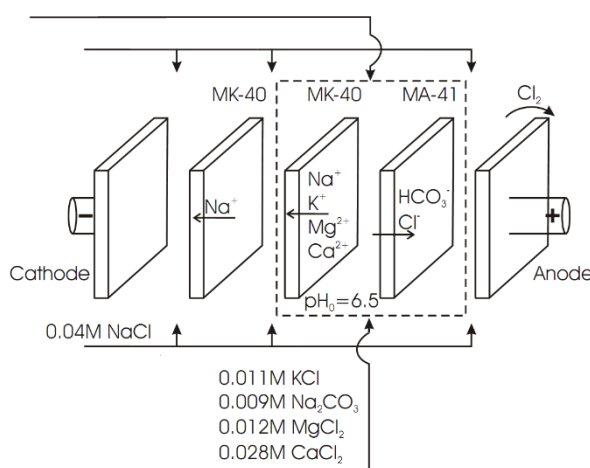


Figure 1. Electrodialysis cell configuration

This arrangement involves two closed loops containing the model mixed salt solution (desalinating stream) and 0.04 M NaCl solution (concentrating stream and electrode rinse stream). The model mixed salt solution was composed of 0.011 M KCl, 0.009 M Na₂CO₃, 0.028 M CaCl₂ and 0.012 M MgCl₂ ($pH_0=6.5$). The intermembrane distance in the desalination channel was 6.5 mm. The flow velocity of the solution was 30 mL·min⁻¹. The desalination length was 2.0 cm. The pH of the solution in the intermediate tank was registered as a function of time using a pHM210 MeterLab pH-meter. The limiting current density (i_{lim}^{Lev}) was calculated by the Lévêque equation. The potential drop (PD), $\Delta\phi$, was measured between the tips of two Luggin's capillaries installed from both sides of the membrane under study.

Results and Discussion

The chronopotentiometric responses of MK-40 membrane are obtained in the range from 0.25 to 2.5 i_{lim}^{Lev} . If the current density $i < 1.4 i_{lim}^{Lev}$ and $i > 2.1 i_{lim}^{Lev}$, the shape of the curves is typical one as shown in Fig. 2a. In the interval from 1.4 to 2.1 i_{lim}^{Lev} , the reduced PD ($\Delta\phi' = \Delta\phi - \Delta\phi_{Ohm}$) does not reach its steady-state value, but slowly increases during one experimental run (900

seconds). In this interval of currents, the pH of the desalinating solution has approximately constant value; if $i > 2.1 i_{lim}^{Lev}$, the pH decreases with time (Fig. 2b).

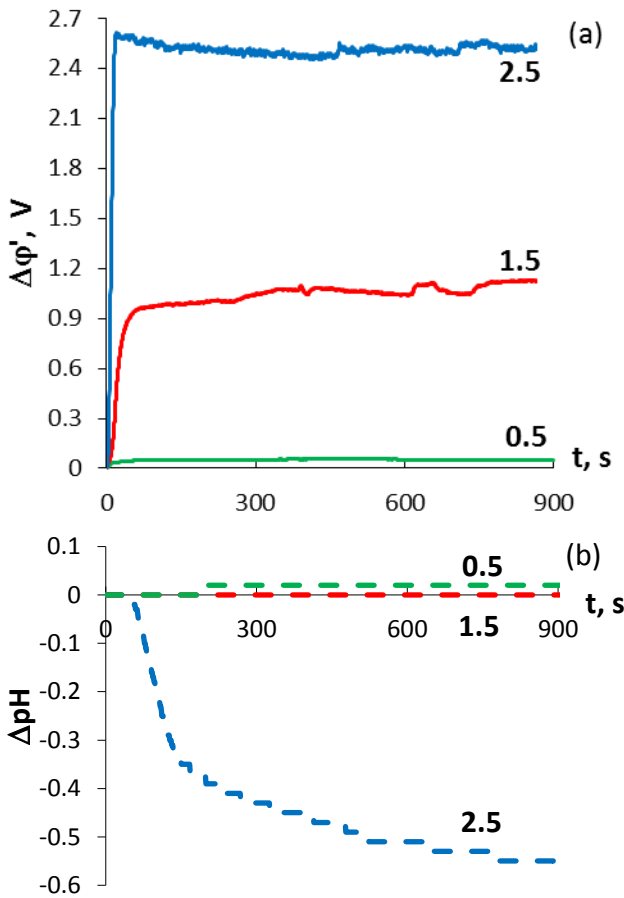


Figure 2. The chronopotentiograms of MK-40 (a) and ΔpH variation with time for the desalination channel (b). The numbers on the curves denote the values of i/i_{lim}^{Lev} .

The slow increase in PD for $1.4 < i < 2.1 i_{lim}^{Lev}$ is probably related to the formation of precipitate at the MK-40 membrane surface. Visualization of the membrane surface by scanning electron microscope after a 5-hour experiment run at $i = 1.5 i_{lim}^{Lev}$ has shown the presence of scaling compounds on the MK-40 membrane surface facing desalinating solution (Fig. 3a). A precipitate was also detected on the MA-41 membrane surface facing the same solution (Fig. 3b).

Figure 4 presents the changes of the $\Delta\phi'$ and the ΔpH of desalination channel with time in steady state mode (Fig. 4a) and in PEF mode when using four pulse/pause conditions: 15 min / 15 min (Fig. 4b), 15 min / 7.5 min (Fig. 4b), 5 min / 5min (Fig. 4c), 1 min / 1 min (Fig. 4c) at $i = 1.5 i_{lim}^{Lev}$.

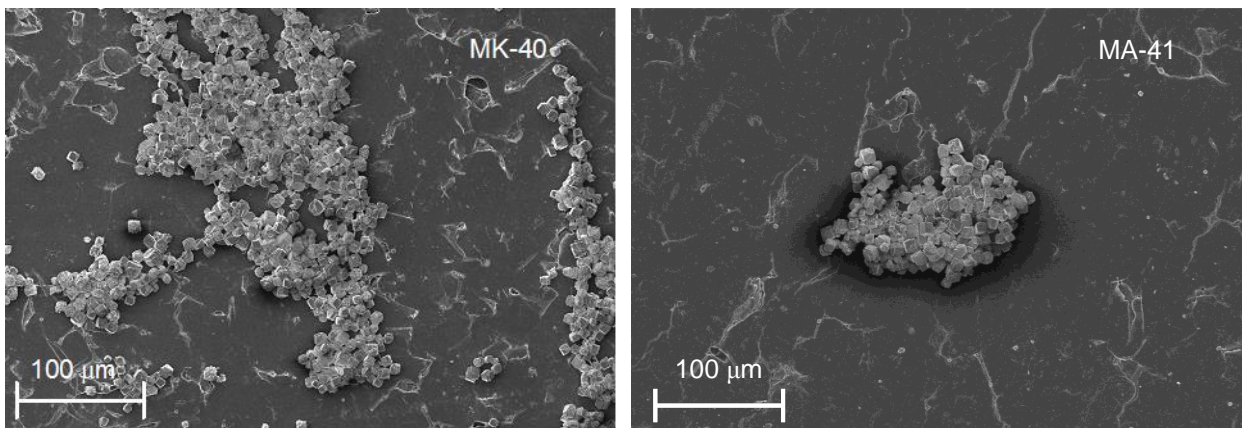


Figure 3. SEM images of scaled MK-40 and MA-41 membranes after experiment at $i = 1.5 i_{lim}^{Lev}$

As the result of precipitation formation, the $\Delta\phi'$ slowly increases in the steady state mode. The scale blocks the ion pathways on the membrane surface. The precipitation on the membrane surface directly enhances water splitting. There are two causes for this effect: 1) the local current density strongly increases in the presence of scale; 2) it is possible that the scale contains compounds, which catalyzes water splitting process. On the contrary, there is no global variation of $\Delta\phi'$ in PEF mode.

Figs. 4a, b and c show that the time-averaged value of PD in the case of PEF mode is lower than that in the case of steady-state mode, under condition that the current density is the same. The use of pulsation and an extended relaxation time allow membrane scaling mitigation. The least averaged PD was found for the minimum period studied (2 min) in the 1 min / 1 min condition. In this condition, there is no variation of the pH of desalinating solution (Fig. 4c), which means that the water splitting rate at the MK-40 membrane depleted surface is lower than in the case of steady-state mode.

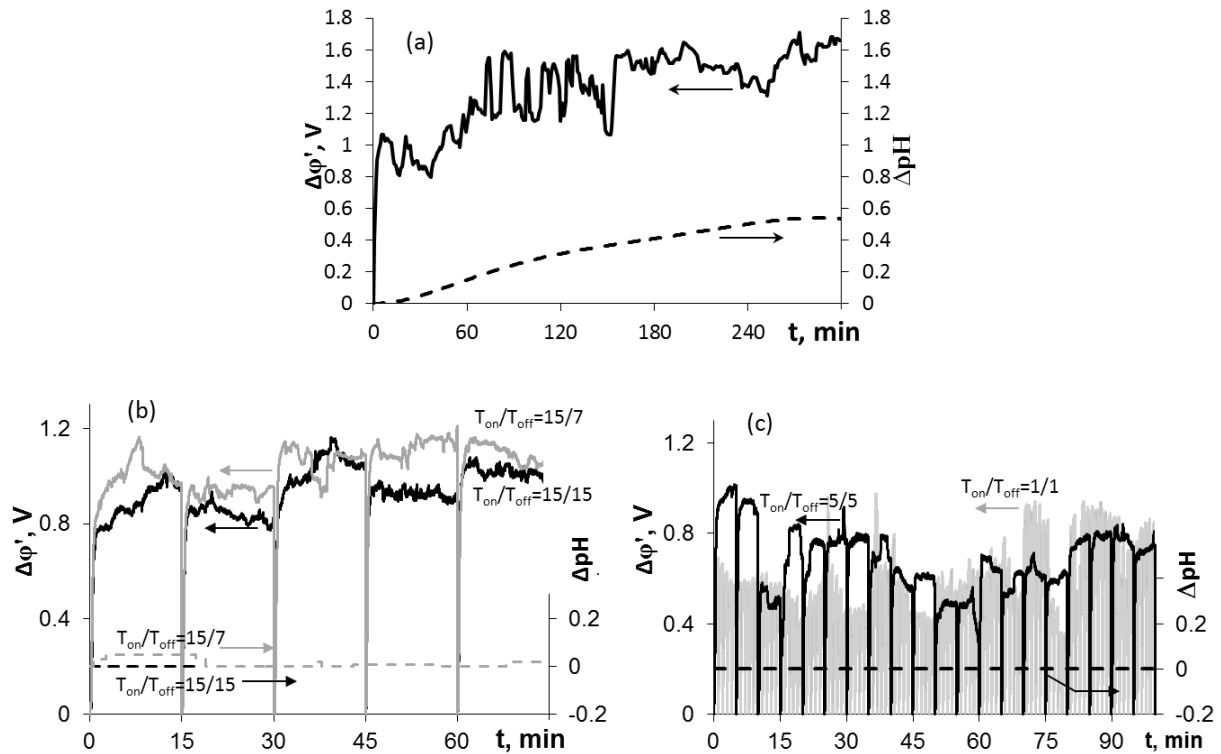


Figure 4. The chronopotentiograms (solid curve) of MK-40 and ΔpH (dashed curve) for the desalination channel at $i = 1.5 i_{lim}^{Lev}$ in steady state mode (a), and in pulsed current modes: 15 min / 15 min (b), 15 min / 7.5 min (b), 5 min / 5 min (c), 1 min / 1 min (c)

Acknowledgments

This investigation was realized within French-Russian International Associated Laboratory "Ion-exchange membranes and related processes". The authors are grateful to CNRS, France, and to RFBR, Russia (grant № 17-08-01442_a).

References

1. Oren Y., Korngold E., Daltrophe N., Messalem R., Volkman Y., Aronov L., et al. Pilot studies on high recovery BWRO-EDR for near zero liquid discharge approach // *Desalination*. 2010. V. 261. P. 321-330.
2. Mikhaylin S., Nikonenko V., Pourcelly G., Bazinet L. Intensification of demineralization process and decrease in scaling by application of pulsed electric field with short pulse/pause conditions // *J. Membr. Sci.* 2014. V. 468. P. 389-399.
3. Lee H.J., Moon S.H., Tsai S.P. Effects of pulsed electric fields on membrane fouling in electrodialysis of NaCl solution containing humate // *Sep. Pur. Technol.* 2002. V. 27. P.89-95.
4. Gil V. V., Andreeva M. A., Pismenskaya N. D., Nikonenko V. V., Larchet C., Dammak L. Effect of counterion hydration number on the development of electroconvection near the surface of heterogeneous cation-exchange membrane modified by a MF-4SK film // *Membranes and membrane technology*. 2016. V. 6. №2. P.181-192.

ELECTRICAL RESISTIVITY OF MULTILAYER MONOPOLAR ION-EXCHANGE MEMBRANES

¹Natalia Anisimova, ¹Anna Korovkina, ¹Stanislav Rybtsev, ²Tolera Badessa, ¹Vladimir Shaposhnik

¹Voronezh State University, Russia, E-mail: v.a.shaposhnik@gmail.com

²Arba Minch University, Ethiopia

Contact, difference [1] and contact-difference methods [2] are known methods for measuring the electrical resistance of membranes. The disadvantage of difference method is the occurrence of large errors in measuring the electrical resistances of ion-exchange membranes in equilibrium with infinite dilution. The necessity of measuring electrical resistivity of membrane in pure water is the rejection of Donnan sorbed electrolyte that makes the membrane complex system comprising both counter ions and non-exchangeable sorbed electrolytes that causes the membrane to have high electrical conductivity. When measuring the electrical conductivity of membrane using a contact method there is a systematic error that can be the main problem due to the presence of resistance of the solution film between the metal electrode and the membrane. The contact-difference method is free from these problems. Measuring the electrical conductivity of membrane using contact-difference method involves the measurement of electrical resistivity of two and one membranes, and then their difference gives the actual electrical resistance of ion-exchange membrane [2, 3]. According to the authors of the monograph [1], the disadvantage of contact-difference method is that the possible errors that are related to the existence of additional electrical resistivity found at the inter-membrane boundaries. Therefore, this work is focusing on the investigation of the electrical resistivity at the inter-membrane boundaries.

The measurements were carried out in the measuring cell described in [2, 3]. The membranes were placed between platinum electrodes of the cell filled with equilibrated solution or pure water that is connected to thermostatically controlling thermostat. Then the measurements of electrical resistances were made using TESLA 509 impedance meter. Finally from the obtained measurements of two and one membranes, the Nyquist coordinates at a frequency of 1 KHz found the active component of the impedance by vector subtraction [3]. The constant value of the electrical resistivity was reached at a pressure of 350 kPa on the membrane, which corresponded to the load of 350 g platform.

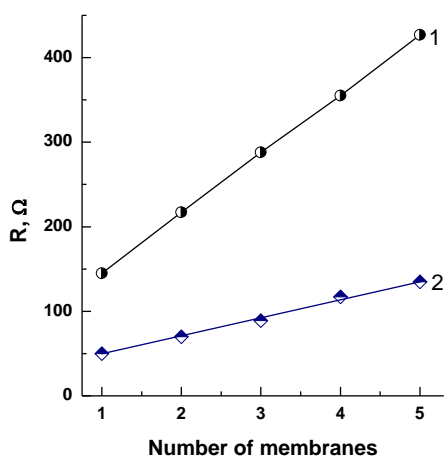


Figure 1. Dependence of electrical resistance of cation-exchange membrane MK-40 in the form of sodium ions on their numbers in the pure water (1) and 0.001 M NaCl

For the measurements, a series of cation-exchange membranes of MK-40 brand made from the composites of strongly acidic cation exchanger KU-2 (2/3) and polyethylene were taken. The membrane samples were prepared following the standard procedures [4], and then the measurements were conducted in the form of sodium ions. Fig. 1 shows the dependence of the electrical resistance of MK-40 membranes in pure water (1) and equilibrated with 0.001 mol /L

sodium chloride solution (2) that is washed with clean water on their number. The linear dependence of electrical resistances indicates that the contact-difference is good method to measure the actual electrical resistance of the membrane by neglecting the additional electrical resistances raise from inter-membrane boundaries.

References

1. *V.I. Zabolotsky, V.V. Nikonenko*. Transport of ions in membranes. Moscow, Nauka, 1996
2. *V.A. Shaposhnik, D.E. Emel'anov, I.V. Drobysheva*. Contact-difference method of measuring the electrical conductivity of membranes // *Rus. Colloid J.* 1984. V. 46. P. 820.- 822.
3. *Badessa T.S., Shaposhnik V.A.* Electrical conductance studies on ion exchange membrane using contact-difference method // *Electrochimica Acta.* 2017. V.211. P. 453-459.
4. *N.A.Kononenko, O.A. Demina, N.V. Loza, I.V. Falina, S.A. Shkirskeya*. Membrane Electrochemistry, Krasnodar, 2015.

STUDY OF DISSOLUTION OF CELLULOSE IN IONIC LIQUID/DMSO SYSTEM AND PREPARATION OF DENSE MEMBRANES

Tatiana Anokhina, Tatiana Pleshivtseva, Alexey Yushkin, Viktoria Ignatenko, Sergey Antonov, Alexey Volkov

A.V.Topchiev Institute of Petrochemical Synthesis RAS, Moscow, Russia

E-mail: tsanokhina@ips.ac.ru

Introduction

Cellulose (Fig. 1) is a polysaccharide obtained from plant feedstock. Cellulose macromolecules are long, having no branched chains [1]. This polymer is one of the most abundant, renewable, inexpensive and biodegradable organic materials and considered as an almost inexhaustible source of raw material for the increasing demand for environmentally friendly and biocompatible products. A distinctive property of cellulose is its chemical resistance to a wide range of solvents [1]. This property represents a great interest in such membrane process as organic solvent nanofiltration (non-aqueous) (OSN).

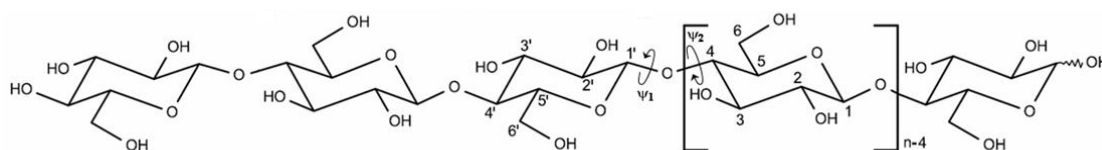


Figure 1. The structural formula of cellulose

However, the unique chemical resistance of this material significantly complicates its recycling and molding of membranes based on it. Unfortunately, there are only limited number of solvent systems capable of dissolving cellulose: DMAA/LiCl [3], DMSO/paraformaldehyde [4], H₃PO₄ [5], and N-methylmorpholine-N-oxide (MMO) [6]. Most of these systems are characterized by high cost, toxicity, and difficulty of solvent recovery. Therefore, in recent years, more and more attention has been attracted to the method of dissolving cellulose with ionic liquids (ILs), which is also considered more environmentally friendly. The most common ILs used for this purpose are 1-n-butyl-3-methylimidazolium chloride [Bmim]Cl, 1-n-allyl-3-methylimidazolium chloride [Amim]Cl, 1-n-ethyl-3-methylimidazolium chloride [Emim]Cl, 1-ethyl-3-methylimidazolium acetate [Emim]OAc. When these ILs are used, the dissolution process is carried out at elevated temperatures from 60 to 150 °C. In addition, to reduce the cost of the dissolution process and the viscosity of the molding solution, a cosolvent is often added to the IL. Therefore, the aim of this study was to investigate the process of dissolving cellulose in ILs mixtures with co-solvents and creation of cellulosic nanofiltration membranes obtained molding solutions

Experiments

In this paper, for the preparation of solutions two ionic liquids 1-Butyl-3-methylimidazolium acetate [Bmim]OAc and 1-Ethyl-3-methylimidazolium chloride [Emim]Cl were used (Fig.2). Dimethylsulfoxide (DMSO) was added as cosolvents to IL. Cosolvent concentration, C_{cos}, wt%, was calculated as follows:

$$C_{\text{cos}} = \frac{m_{\text{cos}}}{m_{\text{cos}} + m_{\text{IL}}} \cdot 100\% \quad (1)$$

where m_i is the weight of the component. Polymer concentration was calculated as following:

$$C_{\text{Cell}} = \frac{m_{\text{Cell}}}{m_{\text{Cell}} + m_{\text{cos}} + m_{\text{IL}}} \cdot 100\% \quad (2)$$

Cosolvent content in the mixture was varied from 0 to 90%. The solutions were prepared at a temperature of 80 - 100°C. To create a membrane solution applied via a squeegee blade onto the hot glass. The coagulating bath was water. Obtained membrane was washed in water and dried.



Figure 2. The structural formula of ILs

The filtration experiments were carried out in the set-up with dead-end filtration cells described elsewhere [7]. Helium was used to pressurize the liquid above the membrane due to insignificant difference in solubility of the gas in ethanol. The chamber above the membrane was filled with liquid (solvent or its dye solution). The permeate collector was arranged so as to minimize solvent evaporation; the volume of each collected liquid sample was 2.5 ± 0.5 ml. Figure 3 shows the solvents using which the permeability of cellulosic membranes have been studied.

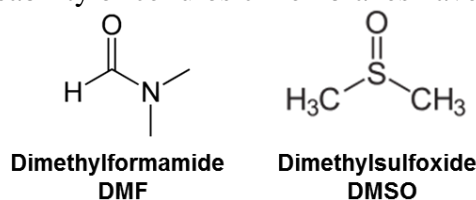


Figure 3. The solvents used in the work

For retention experiments, dye with a concentration in solvents of 10 mg/l was used –Orange II (MW 350, anionic). The dye concentration in the feed and permeate was determined using UV–VIS spectroscopy at the λ_{\max} experimentally obtained for each dye. To estimate actual feed concentration for each single experiment, changes of dye content in the feed during filtration were calculated based on mass balance. The dye retention values were calculated using the following equation:

$$R(\%) = \left(1 - \frac{C_p}{C_f} \right) \cdot 100\%$$

where C_p and C_f are the dye concentration in the permeate and the feed, respectively. All filtration tests with a selected dye were repeated for each membrane sample until steady-state data were reached – deviation in retention less than 2%. All reported results are steady-state data, and an average obtained using at least two different membrane samples.

Results and Discussion

At the first stage of the work, dissolution of 8% by weight of cellulose in pure [Bmim] OAc and in a mixture of this IL with DMSO at a concentration of 50% at a temperature of 80 ° C was investigated. This concentration of the polymer and co-solvent was selected based on literature data as one of the most optimal for the preparation of membrane materials from a mixture with an ionic liquid. Table 1 shows that when 50% DMSO is added, the dissolution time is reduced by almost 4 times. It should be noted that no complete dissolution was achieved in pure DMSO.

The results for the dissolution of cellulose can be interpreted in terms of the interaction of an aprotic solvent with the ionic liquid. The formation of hydrogen bonds is more preferably between the acetate anion and the hydroxyl group of the cellulose. At the same time, the main role of the aprotic solvent DMSO is to facilitate the dissociation of the ionic liquid and the subsequent solvation of the ions. Thus, it can be concluded that the addition of DMSO to the [Bmim] OAc increases the degree of dissociation of the ionic liquid, and thus, its solvent power, which reduces the time for dissolving cellulose.

Table 1: Dependence of the dissolution time of cellulose on the DMSO content in a mixture with [Bmim]OAc

Concentration [Bmim]OAc, %	Concentration DMSO, %	Dissolution time, h
100	0	92
50	50	25

When replacing [Bmim] OAc with a solid IL [Emim]Cl with the addition of 50% DMSO, cellulose was not dissolved at 80 °C. To completely dissolve the cellulose, the temperature was increased to 100 °C and the preparation time of the 8% cellulose solution was about 100 hours. Thus, it can be assumed that anion chloride is less effective in dissolving cellulose than an acetate anion.

After preparation of molding solutions with different cellulose contents, membranes were created and characterized from the viewpoint of the DMF permeability and the retention of the anionic dye of Orange II. It was shown that as the concentration of cellulose in the molding solution increases, the permeability of DMF decreases and the retention rate increases.

This work was supported by the Russian Foundation for Basic Research, project no. 17-08-00499 A.

References

1. Klemm, D. *Comprehensive Cellulose Chemistry: 2 vols. Vol. 1-2* / D. Klemm, B. Philipp, T. Heinze, U. Heinze, W. Wagenknecht. – Weinheim: Wiley-VCH, 1998.
2. A. Pinkert, K.N. Marsh, S. Pang, M.P. Staiger // *Chem. Rev.* 2009. V. 109. P. 6712.
3. T. Nishino, I. Matsuda, K. Hirao // *Macromolecules.* 2004. V. 37. P. 7683.
4. J.F. Masson, R.S. John Manley // *Macromolecules.* 1991. V. 24. P. 5914.
5. Vinogradov V.V., Akaev O.P., Mizerovskii L.N. // *Fibre Chemistry.* 2002. V. 34. № 3. P. 167.
6. Lewandowski Z. // *J Appl Polym Sci.* 2002. V. 83. P. 2762.
7. Volkov A. Application of negative retention in organic solvent nanofiltration for solutes fractionation. // *Sep. Purif. Tech.* 2014. V. 124. P. 43

BROMATE ANION ELECTROREDUCTION ON ROTATION DISC ELECTRODE: ASYMPTOTIC BEHAVIOR FOR VERY HIGH CURRENTS

^{1,2,*}Anatoly Antipov, ^{1-4,**}Mikhail Vorotyntsev

¹D. I. Mendeleev University of Chemical Technology of Russia, Moscow, Russia

²M. V. Lomonosov Moscow State University, Moscow, Russia

³Institute of Problems of Chemical Physics, Russian Academy of Sciences, Chernogolovka, Russia

⁴ICMUB, UMR 6302 CNRS-Université de Bourgogne, Dijon, France

*E-mail: 89636941963antipov@gmail.com, ** E-mail: mivo2010@yandex.com

Theoretical analysis [1] has been developed for the bromate anion electroreduction process on RDE under steady-state conditions owing to catalytic cycle, which consists of a reversible redox bromine / bromide reaction:



and irreversible comproportionation reaction



It has been shown [1] that under certain hydrodynamical conditions, i.e. for a fixed value of the RDE revolution frequency, f , the steady-state current density of this process, j , increases monotonously as a function of the electrode potential, E , its shape corresponding to a typical cathodic voltammetric wave, in particular the current density, j , tends to a “maximal” (potential-independent) value, j^{\max} , for sufficiently high cathodic overpotentials (see Fig. 1a).

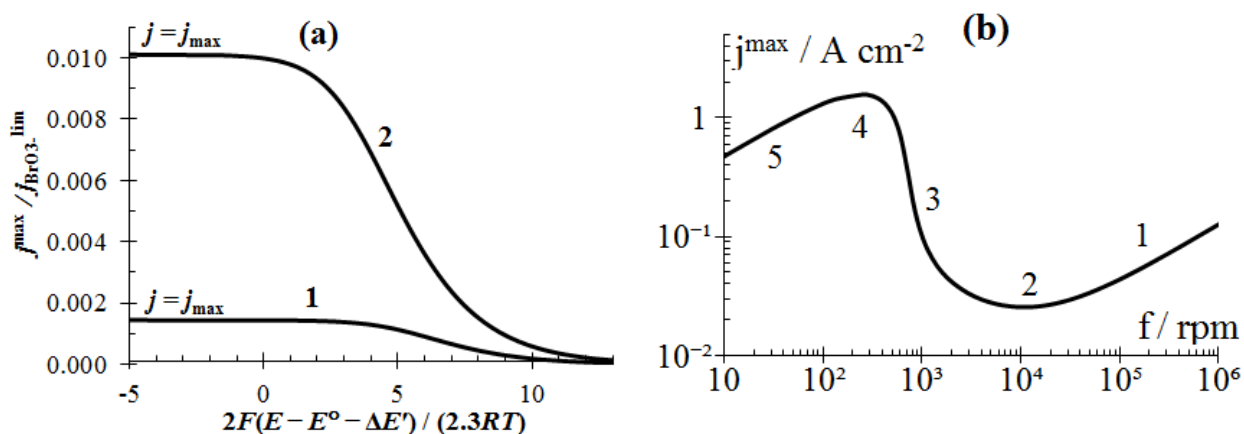


Figure 1. (a) Polarization curves for different values of the diffusion layer and kinetic layer thicknesses ratio x_{dk} equal to 1 (line 1), 4 (line 2). (b) Relation between the maximal current, j^{\max} , and the RDE frequency, f , for the proton excess case and 2M BrO_3^- bulk concentration.

At the same time, the dependence of this maximal current density, j^{\max} , on the rotation frequency, f , has revealed astonishing features which are in disparity with the conventional results where a weaker agitation of the solution, i.e. diminution of f , leads always to a smaller current density, or at least to a practical constancy of j^{\max} within an interval of f values (for the catalytic EC' mechanism).

On the contrary, our theory for the bromate electroreduction has predicted a complicated shape for the $j^{\max}(f)$ dependence (see Fig. 1b). While the conventional Levich-type behavior, $j^{\max} \sim f^{1/2}$, are observed for the interval of sufficiently large (line 1 in Fig. 1b corresponds to the diffusion limited current $j_{\text{Br}_2}^{\text{lim}}$ of bromine) and sufficiently small (line 5 in Fig. 1b corresponds the diffusion limited current $j_{\text{BrO}_3^-}^{\text{lim}}$ of bromate) f values, for the intermediate frequency range the $j^{\max}(f)$ plot passes through a **minimum** (point 2 in Fig. 1b) and a **maximum** (point 4 in Fig. 1b), which are separated by an **anomalous** branch where j^{\max} **increases** by several orders of magnitude for **decrease** of the frequency, f (line 3 in Fig. 1b).

These surprising results originate from the **autocatalytic** nature of the cycle [1], i.e. due to transformation of the principal reactant, BrO_3^- , via reaction (2) into a component of the mediator redox couple, Br_2 . As a result, even for a tracer amount of bromine in the bulk solution the passing

current can reach *enormous* values for high BrO_3^- concentrations, restricted by the diffusion limited current $j_{\text{BrO}_3^-}^{\text{lim}}$ of bromate across the diffusion layer.

One should keep in mind that these results have been obtained on the basis of an *approximate analytical theory* [1]. Its analysis shows that they are justified within certain ranges of parameters, in particular for any possible current density, j , if the diffusion layer thickness, z_d , is smaller than, or comparable with the kinetic layer one, z_k . At the same time for very large diffusion layer thicknesses, $z_d \gg z_k$, the previously derived results [1] can only be used if the current density, j , is smaller than the bromate diffusion limited one, $j_{\text{BrO}_3^-}^{\text{lim}}$.

Therefore, this theory [1] left without description an important situation where $z_d \gg z_k$ and $j > j_{\text{BrO}_3^-}^{\text{lim}}$, in particular for the maximal current density, j^{max} . We have compared predictions of the analytical theory with results of numerical calculations [2,3]. As it has been expected, the analytical analysis is reliably confirmed for small and intermediate ratios of the diffusion and kinetic layer thicknesses, x_{dk} , as well as for the weak currents regime. On the contrary, for sufficiently high x_{dk} and very high currents numerical results demonstrate *essentially new* behavior for the profiles of concentrations (See Fig.2a). (see Fig.2a). The bromate concentration almost vanishes within the kinetic layer while the bromide concentration is very small outside this spatial area. As a consequence, the comproportionation reaction is localized within a narrow spatial zone located at the boundary of these two ranges (see Fig. 2b).

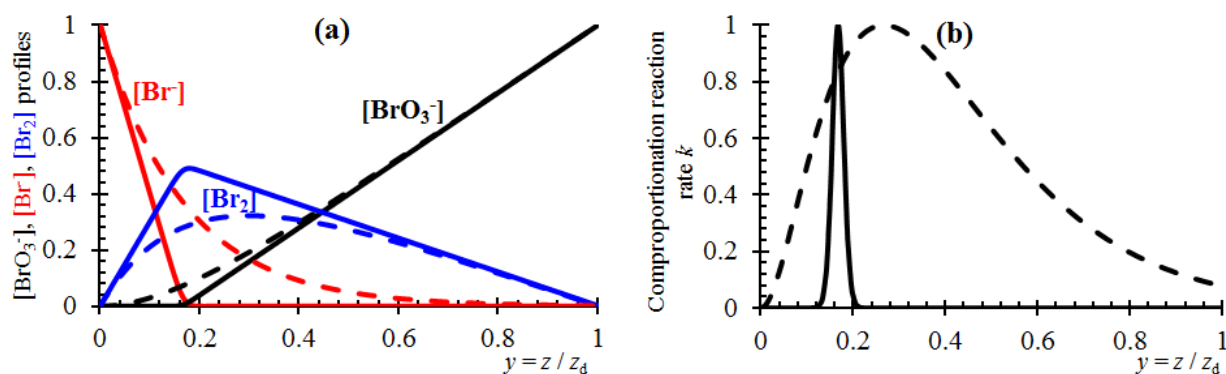


Figure 2. Dimensionless concentration profiles (a) and spatial variation of the normalized comproportionation rate (b), calculated analytically for thin kinetic layer approximation [1] (dashed lines) and numerically (solid lines) for $j = j^{\text{max}}$ and very large $x_{\text{dk}} = 1000$.

To obtain the numerical solution of the set of nonlinear equations with boundary conditions for the concentrations of the components we used the COMSOL Multiphysics software package [2]. It allows one to find a galvanostatic mode solution (at a given current density). In particular one can get an expression for the dependence, $j^{\text{max}}(f)$, for each set of values for the parameters.

Therefore, in this study [2], the goal was to find out to which numerical value the ratio $j^{\text{max}}/j_{\text{BrO}_3^-}^{\text{lim}}$ tends for large values of the parameter $x_{\text{dk}} = z_d/z_k$ (see Fig. 3). We note that this range of values of x_{dk} corresponds to both the extremely thick diffusion layer thickness z_d (for a fixed thickness z_k) and the extremely large values of the reaction rate k constant (for a fixed layer thickness z_d).

As a result, the ratio of the maximum current density to the density of the diffusion limited current for the electroreduction of the bromate anion to bromine was found and, firstly not only it exceeds intuitively expected value of 1, but the "critical" value of 1.2, which formally corresponds to the diffusion limited current for the electroreduction of it to the bromide anion (although the actual final product of the process is bromine) and, secondly, it depends not only on the bulk bromate concentration, but also on the bulk bromine concentration.

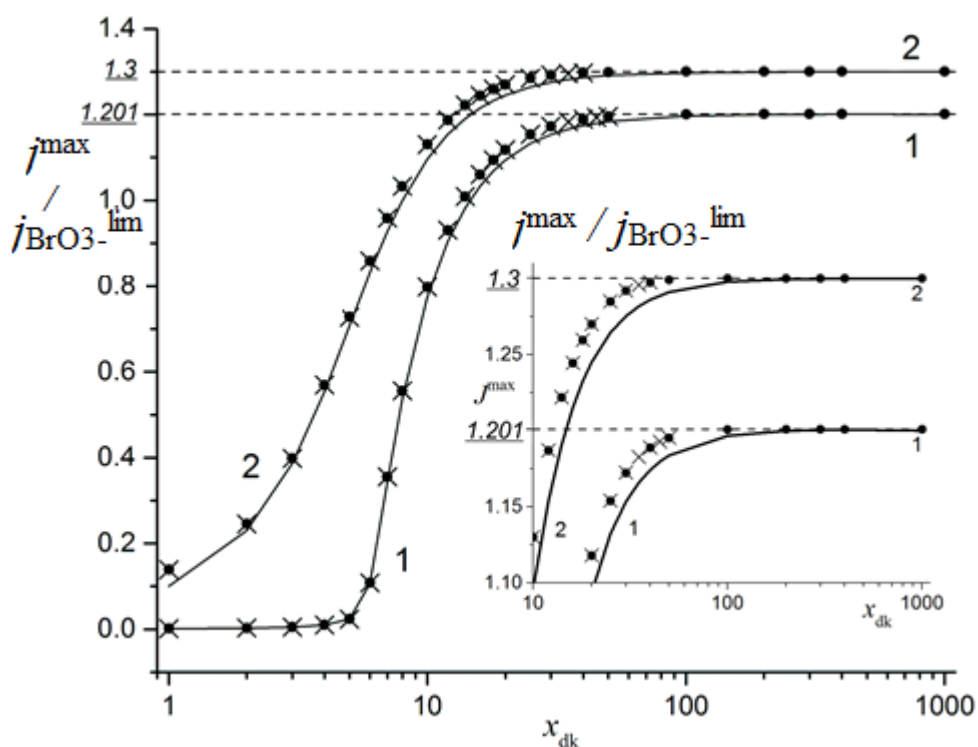


Figure 3. Dependence of the maximum cathode current density $j^{\max} / j_{\text{BrO}_3^-}^{\text{lim}}$ as a function of parameter $x_{\text{dk}} = z_{\text{d}} / z_{\text{k}}$. Solid lines correspond to analytical predictions (see (17f -dim) in [1]) for $j_{\text{Br}_2}^{\text{lim}} / j_{\text{BrO}_3^-}^{\text{lim}} = 10^{-3}$ (line 1) and 10^{-1} (line 2), symbols correspond to numerical results, obtained with COMSOL package [2] (dots) and previously proposed Fortran algorithm [3] (crosses), for corresponding $j_{\text{Br}_2}^{\text{lim}} / j_{\text{BrO}_3^-}^{\text{lim}}$. The main figure shows the general view of the dependences, the inset corresponds to the limit of very high x_{dk} , where horizontal dashed lines correspond to the predicted limiting values of j^{\max} .

Acknowledgements

The study was financially supported by the RF president council grant № 14.W01.16.6741-MK.

References.

1. Vorotyntsev M. A., Konev D. V., Tolmachev Y. V. // *Electrochim. Acta*. 2015. Vol. 173. P. 779–795.
2. Antipov A. E., Vorotyntsev M. A. // *Russ. J. Electrochem.* 2017, in press.
3. Antipov A. E., Vorotyntsev M. A. // *Russ. J. Electrochem.*, 52 (2016), 925–932.

BROMATE ELECTROREDUCTION VIA CATALYTIC REDOX-MEDIATOR (EC') MECHANISM

^{1,2,*}Anatoly Antipov, ^{1-4,**} Mikhail Vorotyntsev

¹D. I. Mendeleev University of Chemical Technology of Russia, Moscow, Russia

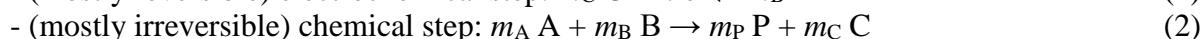
²M. V. Lomonosov Moscow State University, Moscow, Russia

³Institute of Problems of Chemical Physics, Russian Academy of Sciences, Chernogolovka, Russia

⁴ICMUB, UMR 6302 CNRS-Université de Bourgogne, Dijon, France

*E-mail: 89636941963antipov@gmail.com, ** E-mail: mivo2010@yandex.com

Recent theoretical studies of the bromate electroreduction from strongly acidic solution have been overviewed in view of very high redox-charge and energy densities of this process making it attractive for electric energy sources [1]. All these attractive features of the bromate anion as oxidant for cathode are counterbalanced by the lack of its electroactivity within the potential range positive with respect to the hydrogen electrode, for all tested electrode materials including noble metals. The conventional solution to overcome this problem of non-electroactivity of the principal reactant (denoted as A) is to apply the EC' mechanism of electrochemical reactions which is based on addition of a reversible redox couple, C and B, into solution which triggers a combination of electrochemical and chemical steps. In the most general case the reaction scheme may be written down in the form:



This mechanism has been extensively studied for various regimes of the process, mostly assuming that all stoichiometric coefficients, m_i , are assumed to be equal to 1 while the general qualitative features of the mechanism are remaining the same for other values of the coefficients, in particular for the non-equal values of m_C and m_B , too. On the other hand, it is crucially important that the ratio of the coefficients in front of C and B, m_C / m_B , is *the same* in Eqs (1) and (2). Then, the passage of the cycle composed of reactions (1) and (2) does *not change* the total amount of the components of the redox couple, $m_C C + m_B B$, so that this couple plays the role of a *redox-mediator catalyst*.

For such systems the bulk solution contains (for the reduction process) both the electrochemically inactive oxidant, A, of a high concentration, A° , and the oxidized component of the reversible redox couple, C, the latter concentration, C° , being much lower than that of the former one, A° .

In the frame of the present analytical study for illustration of predictions of such systems the EC' process was considered taking place at a rotating disk electrode (RDE) under steady-state conditions. To simplify the analysis the convective effects are simulated within the framework of the "stagnant Nernst layer model" where the concentrations of all species are assumed to be constant outside the (Nernst) diffusion layer (for $z > z_d$) while the convective terms are disregarded inside the layer (for $z < z_d$).

Firstly we have got analytic expressions for all concentration distributions for the components for weak current regime, when passing current is so weak that the consumption of species A near the electrode surface does not lead to a significant gradient of its concentration so that the overall drop of its concentration across the diffusion layer is small compared to its bulk concentration ($A^\circ - A(0) \ll A^\circ$), which imposes a limitation to the current density to be small compared to the diffusion-limited one for species A, j_A^{lim} .

Secondly, the concentration profiles were also derived in the thin kinetic layer regime approximation (for both weak and strong currents), when kinetic layer thickness z_k is much thinner than the diffusion one z_d , which implies the condition: $x_{dk} = z_d / z_k \gg 1$.

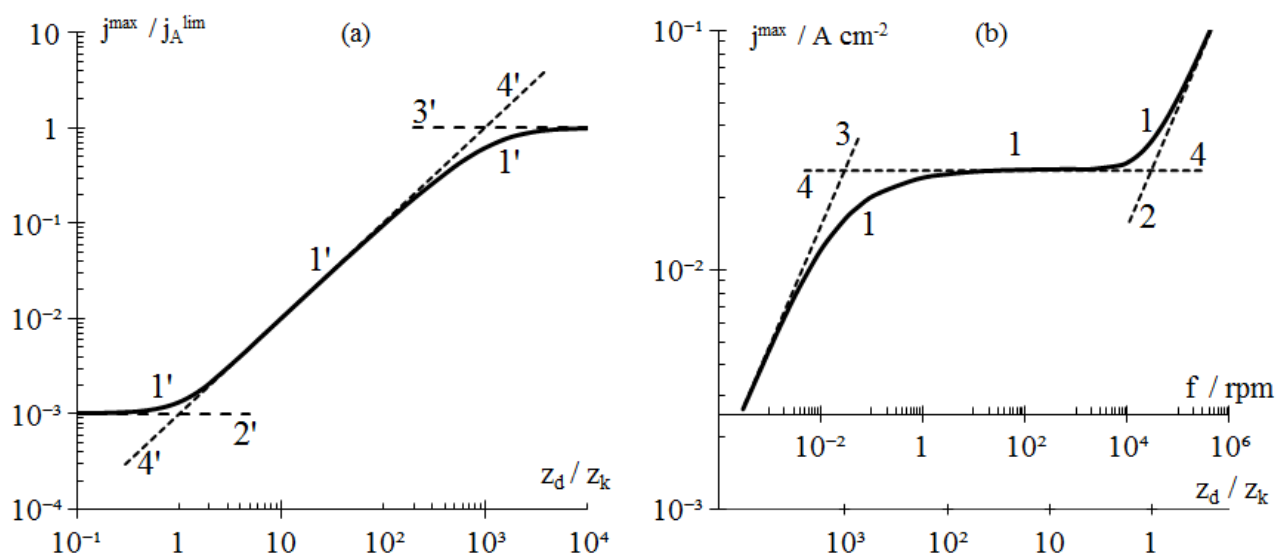


Figure 1. Plots for the maximal current density, j^{\max} , in bilogarithmic coordinates: (a) dimensionless value, $j^{\max} / j_A^{\text{lim}}$, as a function of $x_{\text{dk}} = z_d / z_k$ (line 1'); (b) j^{\max} vs. RDE frequency, f (line 1). Dashed straight lines: asymptotic behavior of plots 1' and 1 in various ranges: $j^{\max} = j_C^{\text{lim}}$ (lines 2' and 2), $j^{\max} = j_A^{\text{lim}} + j_C^{\text{lim}}$ (lines 3' and 3), $j^{\max} = j^{\text{cat}}$ (lines 4' and 4), where j_A^{lim} is diffusion-limited current for bromate anion species, j_C^{lim} and j^{cat} are the diffusion-limited current for bromine species across the diffusion and kinetic layer (correspondingly).

It was shown that for each value of the principal parameter, $x_{\text{dk}} = z_d / z_k$, the interval of possible values of the current density, j , is limited from above by the value which is called "the maximal current density", j^{\max} . This dependence in the form of $j^{\max} / j_A^{\text{lim}}$ vs. x_{dk} , is shown as line 1' in Fig. 1a. In view of relation between the RDE revolution rate, f , and the diffusion layer thickness, z_d , (according to the Levich formula [2]) the above results for the concentration profiles and for the maximal current allows one to predict their dependence on f . In particular, line 1 in Fig. 1b represents a plot for j^{\max} vs. the RDE revolution rate, f . This figure also shows the relationship between j^{\max} and x_{dk} .

As a whole, the plots for the maximal current density (lines 1' and 1 in Figs. 1a,b) demonstrate the existence of **three** characteristic ranges separated by two transition zones where $x_{\text{dk}} \sim 1$ and $x_{\text{dk}} \sim j_A^{\text{lim}} / j_C^{\text{lim}}$. The latter value which is proportional to the ratio of the bulk concentrations of species A and C, A^0 / C^0 , is usually very large, i.e. $J_{\text{CA}} = j_C^{\text{lim}} / j_A^{\text{lim}} \ll 1$, to minimize the amount of the added redox couple. Then, the medium interval of frequencies, f , or x_{dk} where the maximal current is independent of the diffusion layer thickness and it is close to the "catalytic one", $j^{\max} \cong j^{\text{cat}}$, is very extended: the ratio of their values for transitions (line 2 to line 4 and line 4 to line 3) is J_{CA}^{-1} (i.e. 1000 in Fig. 1a) for the x_{dk} axis and J_{CA}^{-2} (i.e. 10^6 in Fig. 1b).

Acknowledgements

The study was financially supported by the RFBR (project 16-33-00975).

References

1. Vorotyntsev M. A., Konev D. V., Tolmachev Y. V. // *Electrochim. Acta*. 2015. Vol. 173. P. 779–795.
2. Levich V.G. *Physicochemical hydrodynamics*, New York: Prentice-Hall, 1962.

THEORY OF STEADY-STATE CONVECTIVE-DIFFUSION TRANSPORT FOR BROMATE ELECTROREDUCTION AT ROTATING DISC ELECTRODE. EQUAL DIFFUSION COEFFICIENTS APPROXIMATION

^{1,2,*}Anatoly Antipov, ^{1-4,**}Mikhail Vorotyntsev

¹D. I. Mendeleev University of Chemical Technology of Russia, Moscow, Russia

²M. V. Lomonosov Moscow State University, Moscow, Russia

³Institute of Problems of Chemical Physics, Russian Academy of Sciences, Chernogolovka, Russia

⁴ICMUB, UMR 6302 CNRS-Université de Bourgogne, Dijon, France

*e-mail: 89636941963antipov@gmail.com, **e-mail: mivo2010@yandex.com

The process of the steady-state electroreduction of bromate-anion at rotating disk electrode (RDE) has been described for the first time on the basis of *convective diffusion transport equations* for solute components, bromate (A species) and bromide (B species) ions as well as bromine (C species) in the frames of the *same diffusion coefficients for all species approximation* [1]. Bulk solution contains high concentrations of bromate anion (A°) and a strong acid (which are non-electroactive at the electrode) as well as a trace amount of bromine ($C^{\circ} \ll A^{\circ}$). The current passes owing to bromine which is reduced to bromide ion that participates further in the comproportionation reaction with bromate anion, with regeneration of bromine.

Approximate analytical solutions for all concentration distributions have been derived in the approximation of the same diffusion coefficients for all species. It has been demonstrated that the passage of the bromate process depends *crucially* on the values of the ratios of two characteristic lengths: diffusion-layer thickness, z_d , determined by *an interplay of the diffusion and convection* mechanisms, and kinetic layer thickness, z_k , where the comproportionation reaction takes place.

We define a diffusion layer thickness z_d via Levich formula [2], where D is corresponding diffusion coefficient. Then, one can introduce the dimensionless parameter equal to the ratio of the diffusion and kinetic layer thicknesses for each component: $x_{dk} = z_d / z_k$.

The exact relations between concentration profiles of the species A, B and C are obtained for the equal diffusion coefficients assumption for all of the components, that allows one to reduce the problem to the solution of the nonlinear second-order equation for the bromide (B) concentration with boundary conditions on the surface of the electrode and in the bulk solution.

Obtained concentration profiles (see Fig.1) for all of the components for the set of current densities are used to calculate stationary polarization curves (see Fig.2) and the maximal current dependence on the rotation frequency of RDE. As a result of the analysis *the effect of convection* on the concentration profiles of components is clearly seen *at a distance* from the electrode surface comparable to the thickness of the diffusion layer, whereas when approaching the surface of the electrode the effect becomes *negligibly small* compared to the stagnant Nernst layer model [3,4]. The unexpected predictions made earlier by the analytical theory of achieving enormous cathode current densities j in the system due to the autocatalytic effects many orders of magnitude higher than diffusion limited current for bromine, $j_{Br_2}^{lim}$, and up to the values of *“formally” defined* diffusion limited current for bromate anion $j_{BrO_3^-}^{lim}$, [3], *remain valid* also with *consecutive consideration of convective transport* of substances in the system for the relatively large diffusion layer and kinetic layer thicknesses ratios (x_{dk}).

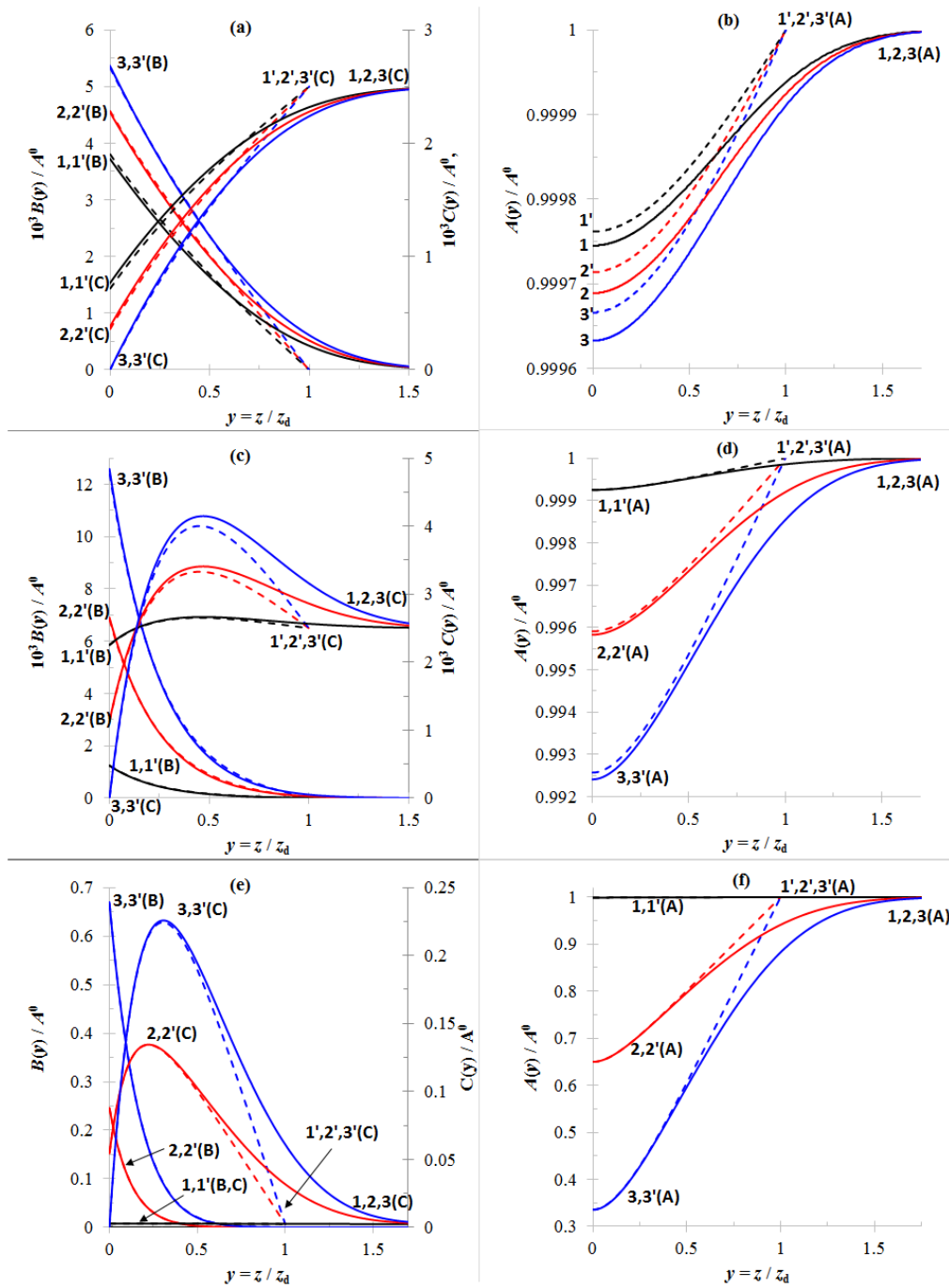


Figure 1. Concentration profiles dependences from spatial coordinate $y = z / z_d$ of bromate anion A species (Figs. (b),(d),(f)), bromide anion B species and bromine C species (Figs (a),(c),(e)), normalized to bromate bulk concentration A^0 . Solid lines 1-3 represent the convective-diffusion set of transport equations solution, dashed lines 1'-3' correspond to the stagnant Nernst layer model [3]. Symbols A, B or C after the line number determine the component, to which corresponds the particular concentration profile. The bromate bulk excess case is under study, while the bulk concentration of bromine is insignificant. Parameter x_{dk} equals 1 (Figs. a, b), 4 (Figs. c,d) or 10 (Figs. e, f), that corresponds to maximal current density $j^{\max} / j_{\text{BrO}_3}^{\text{lim}}$ equal to, $1.4 \cdot 10^{-3}$, $1.0 \cdot 10^{-2}$ or 0.8, correspondingly. The current density j is equal to $j_{\text{Br}_2}^{\text{lim}}$ (lines 1, 1'), $0.5 (j^{\max} - j_{\text{Br}_2}^{\text{lim}})$ (lines 2, 2') or j^{\max} (lines 3, 3').

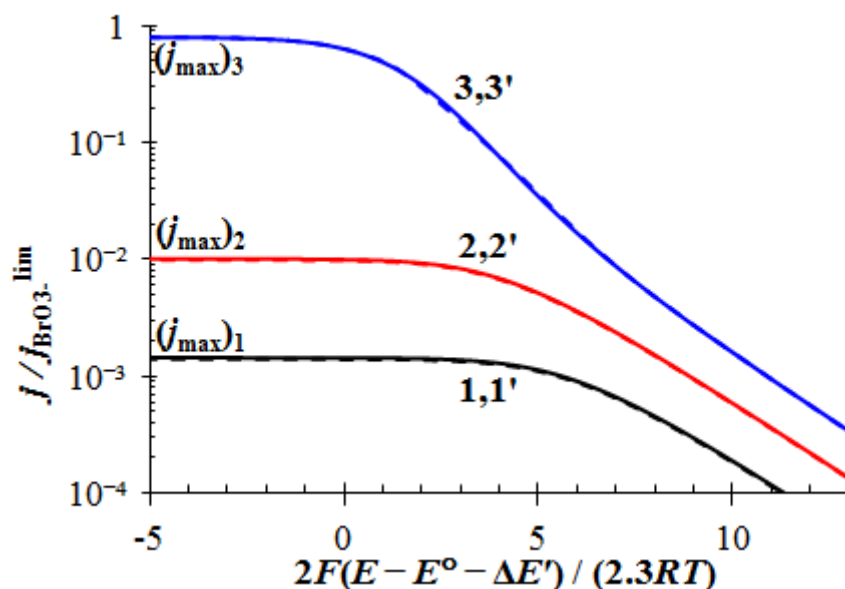


Figure 2. Polarization curves for different values of the diffusion layer and kinetic layer thicknesses ratio x_{dk} equal to 1 (lines 1, 1'), 4 (lines 2, 2') or 10 (lines 3, 3'). Solid lines 1, 2 and 3 are calculated via solution of convective diffusion set of equations, dashed lines are calculated for the stagnant Nernst layer model [3].

Acknowledgements

The study was financially supported by the RF president council grant № 14.W01.16.6741-MK.

References

1. Antipov A. E., Vorotyntsev M. A. // Russ. J. Electrochem. 2017, in press.
2. V.G. Levich Physicochemical hydrodynamics, , New York: Prentice-Hall, 1962.
3. Vorotyntsev M. A., Konev D. V., Tolmachev Y. V. // Electrochim. Acta. 2015. Vol. 173. P. 779–795.
4. Antipov A. E., Vorotyntsev M. A. // Russ. J. Electrochem., 52 (2016), 925–932.

COMPARATIVE RESEARCH OF REGULARITIES OF PASSING OF HYDROSOLS NANO-/MICROPARTICLES OF SILVER THROUGH NUCLEAR AND AEROSOL FILTERS

¹Irina Antropova, ¹Olga Koshkina, ¹Eldar Magomedbekov, ²Tatiana Dmitrieva, ³Yurii Birukov, ³Sergey Lakeev, ⁴Aleksei Shepelev, ³Vyacheslav Minashkin, ^{1,3}Aleksandr Smolyanskii

¹D.Mendeleev University of Chemical Technology of Russia, Moscow, E-mail: antropovai@inbox.ru

²PLC "Systems for microscopy and analysis", Moscow, Russia

³Branch of JSC "Karpov Institute of Physical Chemistry", Moscow, 105064, Russia, E-mail: fizhimiya-2010@mail.ru

⁴NRC "Kurchatov Institute", Moscow, Russia.

Introduction

The aim of this work was to study the transport patterns of the hydrosols of nano-modified particles of silver (Ag-NMP) through the micropores of nuclear filters (NF), the surface-modified layer of nano-microfibers fluoroplastic.

Experiments

In experiments using samples NF by irradiation stream of accelerated ions of xenon polyethylene terephthalate film brand "Hostaphan" with a thickness of 12 μm , Dubna. The average size of the micropores NF was 0.22 μm , surface density $\sim 4,6 \cdot 10^7 \text{ cm}^{-2}$.

Surface modification of samples NF in the form of discs $\varnothing 25 \text{ mm}$ was performed by the method of electrotorture. Through the application of the microfibers based on PTFE F-42V, after manufacture, on a substrate of NF. As a result, the surface of the NF was formed a layer of PTFE microfibers. Before the experiment, the samples of initial and surface-modified NP were placed in the filter holder.

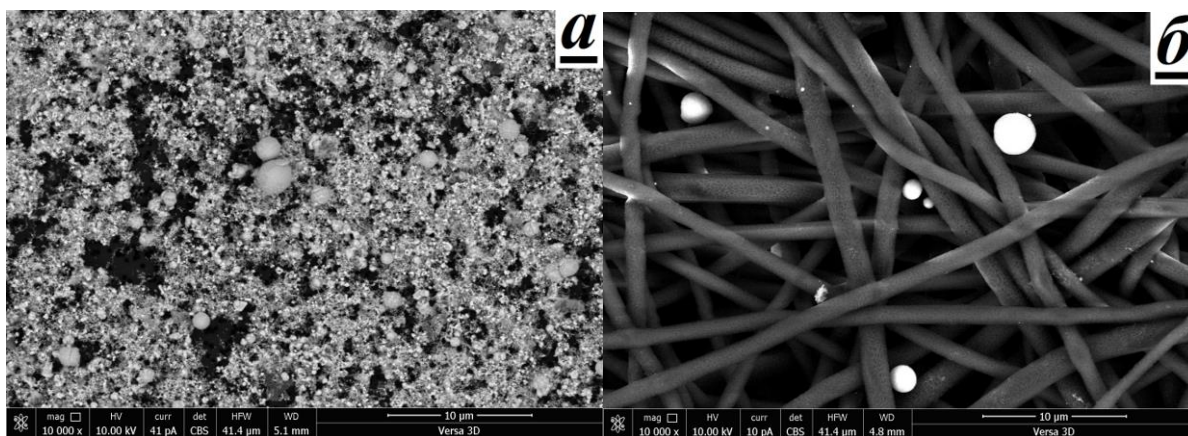


Figure 1. Images of the surface initial (a) and surface-modified microfibers of the PTFE (b) NP samples after passing the sample of Hydrosol silver. Photos obtained by scanning electron microscopy. The conditions of the measurements are shown in the images

Hydrosols Ag-HMP received by passing the aerosol of silver synthesized using a spark aerosol generator in air, at room temperature, through a Tishchenko flask to which was added 100 ml of distilled water. The composition of aerosols was monitored using a diffusion spectrometer of aerosols DAS 2720. The obtained colloidal solutions Ag-HMP kept in the dark for three months in air at room temperature. Immediately before the filtration of colloidal solutions of Ag-HMP was treated in ULTRASONIC bath for 10 minutes.

The composition of the samples of the initial colloid solution and the filtrate of the Ag-HMP was examined using the analyzer of the shape and size of the particles Eyetechnology production company Ambivalu (Netherlands) in laser and visible range (from 0.1 to 300 μm). Before analysis the samples were treated in ULTRASONIC bath.

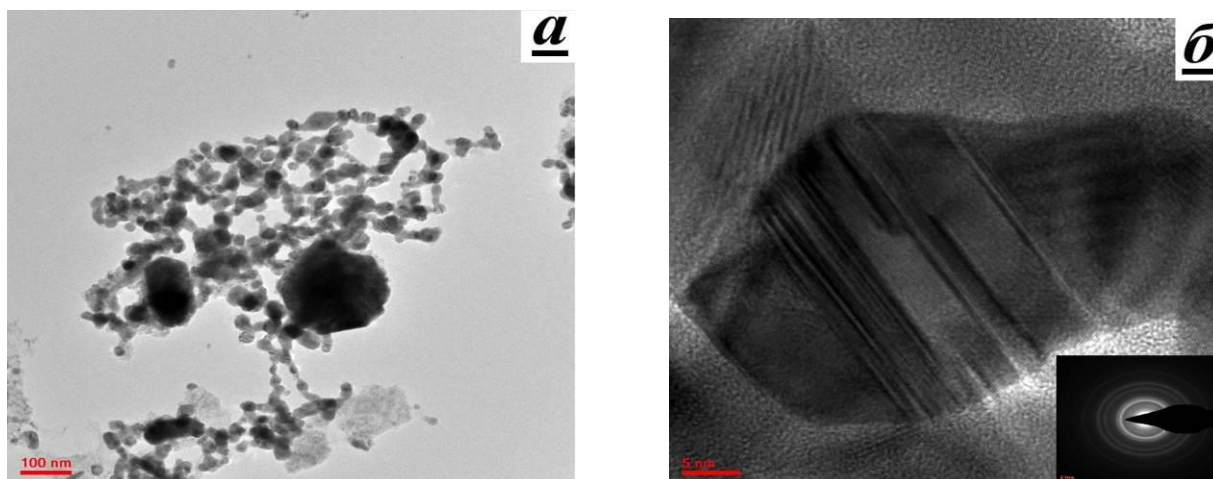


Figure 2. Nanostructures (fractal aggregates) of nanoparticles of silver formed in silver hydrosols (a). Image of silver nanoparticles in the growth process. The inset shows the electronic diffraction pattern of the surface of the particles (b)

Results and discussions

As follows from the results of the study NF the scanning electron microscopy, transmission of the silver Hydrosol through the original NF leads to the formation on the surface of the layer of Ag-HMP (Fig. 1, a), with surface-modified NF Ag-HMP are localized in cavities between the microfibers (Fig. 1, b), also Ag-HMP deposited on the surface of microfibers. The spherical shape Ag-HMP due to the method of producing aerosol in the spark discharge. Analysis of the elemental composition of the surface of the initial X-ray fluorescence method according to the technology EDAX confirms the presence of silver.

The method of translucent electronic microscopy discovered that Ag-HMP form in both the original and the filtered Hydrosol of silver fractal aggregates as a result of processes of coagulation Ag-HMP in clusters and the subsequent interaction of clusters with each other (Fig. 2, a). Fractal dimension amounted to 1,807, which is evidence in favor of the proposed method of formation of the fractal aggregates in the framework of the "cluster – cluster" Association of particles performing Brownian motion in three-dimensional space.

It is possible to detect Ag-HMP irregular shape, which may be associated with the growth processes of the particles (Fig. 2, b). By electron diffraction it was shown that the growth process of the particles is accompanied by the formation of crystals of silver (Fig. 2, b, inset). While on the surface of the particles observed horizontal degree, the nature of which may be associated with the growing faces of the crystals of silver.

It is the processes of formation and growth of fractal aggregates occurring during the storage of the original and the filtered Hydrosol Ag-HMP, lead to the unexpected sight of functions of distribution of particles in size, which was determined using the analyzer of the shape and size of the particles Eyeteck. In favor of this assumption is evidenced by the shift of the peak of functions of distribution of particles filtrate from 2 to ~4.5 μm compared to of functions of distribution of particles source of Hydrosol Ag-HMP, in the case of using NF source Application for purification of Hydrosol Ag-HMP sample NF, surface-modified microfibers of PTFE significantly reduces the intensity of the processes of formation and concentration of fractal aggregates in the filtrate.

We can conclude that the surface modification of the NP microfibers fluoroplastic synthesized by electrospinning, is an effective means of improving the quality of cleaning of Hydrosol Ag-HMP, reducing the likelihood of undesirable side processes and reactions in the filtrate.

The present study was supported by the Russian Foundation for basic research (project No. 17-07-00524).

THE ROLE OF OSMOTIC EFFECTS IN ASYMMETRIC TRACK ETCHING

^{1,2}Pavel Apel, ¹Irina Blonskaya, ¹Nikolay Lizunov, ¹Oleg Orelovich, ³Christina Trautmann

¹Flerov Laboratory of Nuclear Reactions, JINR, Dubna, Russia; *E-mail: apel@jinr.ru*

²Dubna State University, Dubna, Russia

³GSI Helmholtzzentrum für Schwerionenforschung GmbH, Darmstadt, Germany

Introduction

The ion track technology provides unique opportunities for developing engineered micro- and nanoporous membranes the transport properties of which can be finely tuned. In recent years, special interest was paid to the so-called conical pores. Their fabrication includes the irradiation of a polymer foil with accelerated ions followed by one-sided chemical etching. When etching, the ion-irradiated foil separates the two compartments of a conductometric cell where one side contains the alkaline etchant and the other side a stopping solution [1]. When the etchant breaks through to the foil, the newborn nanopore is detected as an ionic current of 0.1-1 nA between the electrodes. Thus obtained approximately conical channels have a large opening of the order of hundreds of nanometers and a small opening (i.e. the tip) of several nanometers in diameter. The pores possess ionic selectivity and exhibit ionic current rectification effects in electrolyte solutions, which is regarded as the basis of many potential applications [2]. The process of pore formation remains a subject of further studies. Very recently it was found that under the asymmetric etching conditions an intense osmotic flux develops and has a strong effect on the nanopore geometry [3]. The observed phenomenon is an example of osmotic flow through leaky channels, i.e. the process that - in contrast to the well-known osmosis through semipermeable membranes - has been little studied so far. In this paper we report on experiments aimed at better understanding the role of osmotic phenomena in asymmetric track-etched nanopores.

Experiments

Polyethylene terephthalate (PET) biaxially oriented films (12- μ m-thick Hostaphan RNK, Mitsubishi Polyester Films) were irradiated with 11 MeV/u Au ions at the UNILAC accelerator of GSI (Darmstadt) and 1.2 MeV/u Xe and Kr ions at the IC-100 cyclotron of FLNR JINR (Dubna). Chemical etching of ion-irradiated samples was performed in an electrolytic cells at room temperature. Before etching, all samples were exposed to soft ultraviolet radiation to stabilize the track-to-bulk etch rate ratio. One compartment of the cell was filled with 9 M NaOH and the other compartment contained a stopping solution. Either neutral (1M KCl) or acidic (2 M KCl + 2 M HCOOH (50:50, v/v)) stopping solutions were used. The cell was equipped with a capillary, with a 2 mm inner diameter, inserted into the compartment with the alkaline etchant. The working area of foil samples was 1 cm².

Geometry of the obtained asymmetric pores was investigated using field emission electron microscopy (FESEM). An FESEM instrument (Hitachi SU8020, Japan) equipped with an energy dispersive X-rays microanalysis system was employed.

Table 1: Parameters of ions used to produce tracks in PET foil

Ion	Specific energy, MeV/u	Energy loss, keV/nm
¹⁹⁷ Au	5-11.4	15-17
¹³² Xe	1.2	8-11
⁸⁴ Kr	1.2	6-7

Results and Discussion

Because the electrolyte concentrations on the two sides of the asymmetrically etched foil are significantly different, a gradient of the chemical potential of water across the foil exists and the osmotic pressures of the etching and stopping solutions are important parameters which should be considered. According to the van't Hoff equation the osmotic pressure difference $\Delta\Pi$ is

$$\Delta\Pi = \Delta c R T \quad (1)$$

where Δc is the difference in solute concentrations, R is the universal gas constant, T is the temperature. The difference in solute concentrations between the two halves of the cell is so large that the differential osmotic pressure could reach tens of bars.

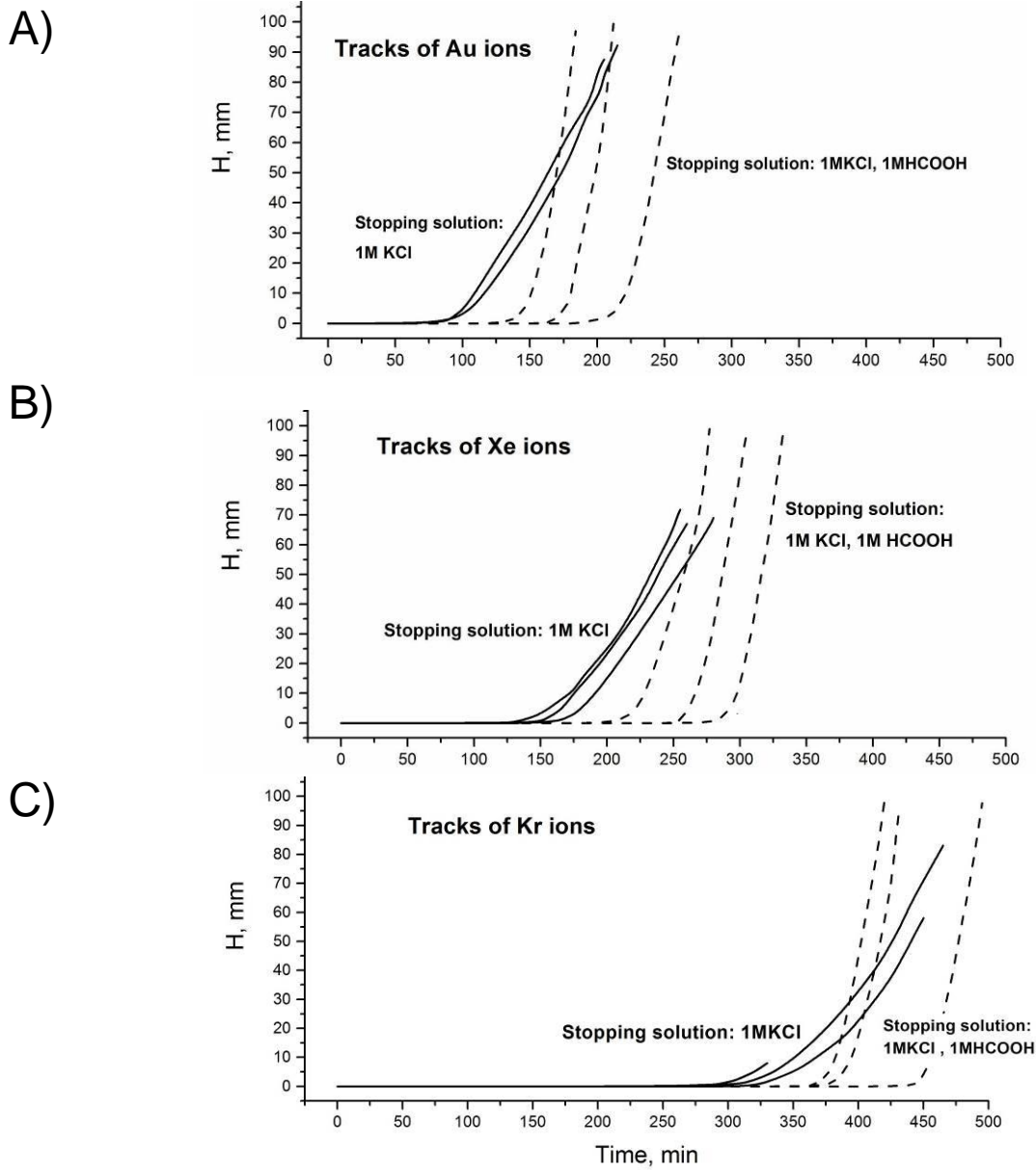


Figure 1. The build-up of solution level H in the alkaline compartment of the cell as a function of time of asymmetric etching. Etchant: 9M NaOH. Stopping solution: 1M KCl (solid lines), 1M KCl/1M HCOOH (dashed lines). PET foil with $\sim 10^8$ tracks of Au (A), Xe (B) and Kr (C) ions. Results of several parallel experiments for each set of parameters (ion and stopping solution) are shown.

Fig. 1 shows the solution build-up in the capillary as a function of the etching time. The array of 10^8 Au ion tracks shows a well-pronounced osmotic flow that started at 90-100 and 140-200 min for neutral and acidic stopping solutions, respectively. Tracks of lighter ions (Xe and Kr, that possess lower energy losses in polymer) are etched through slower, however the resulting pores show a similar osmotic flow. Remarkable is that the effect of acidic stopping solution on the breakthrough time decreases with decreasing energy loss of the ion that produced the track.

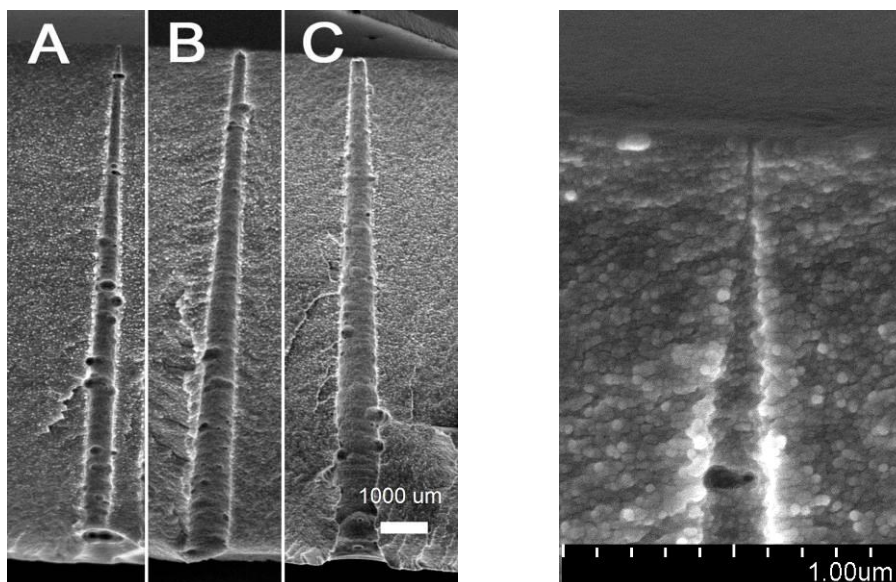


Figure 2. FESEM images of pores produced by asymmetric etching. Left: Full pore profiles. Time of etching after osmotic flow started: 20 min (A), 60 min (B), and 100 min (C). Etchant: 9M NaOH. Stopping solution: 1M KCl/1M HCOOH. Right: pore tip at a higher magnification. Time of etching after osmotic flow started: ~ 20 min.

A number of important conclusions can be drawn from these experiments:

1. Asymmetric etching conditions provide a considerable gradient of water chemical potential across the foil with ion tracks, which generates osmotic flow after through pores are formed.
2. Continuation of asymmetric etching after breakthrough results in a rapid transformation of the pore tip shape, while the wide part of the pore remains conical.
3. Due to osmotically driven flow of water into the pore, the alkali concentration gradient in the pore is essentially non-linear, namely the concentration is almost constant along the wide part of the pore and dramatically decreases in the pore tip region.
4. Osmotic flux of $(1-7) \cdot 10^{-12} \text{ cm}^3 \cdot \text{s}^{-1}$ per single pore is observed, which corresponds to a linear flow velocity of the order of 1 cm/s in the pore lumen.
5. The osmotic flow plays a decisive role in the conservation of the tip radius at a level of several nanometers after the etching and stopping solutions meet each other.
6. Low pH of stopping solution slows down the etching rate along the track, which indicates that soaking the latent track with acid significantly alters its permeability to alkaline electrolyte. This effect is especially pronounced for heavier ions that produce heavier damage and generate a larger free volume in tracks.
7. To our knowledge, clear osmotic effects caused by inorganic salts in track-etched membranes have not been observed before.

References

1. *Apel P.Yu., Korchev Yu.E., Siwy Z., Spohr R., Yoshida M.* // Nucl. Instrum. Meth. Phys. Res. 2001. V. B184. P. 337-341
2. *Choi Y., Baker L.A., Hillebrenner H., Martin C.R.* // Phys. Chem. Chem. Phys. 2006. V. 8. P. 4976-88.
3. *Apel P.Yu., Bashevoy V.V., Blonskaya I.V., Lizunov N.E., Orelovitch O.L., Trautmann C.* // Phys. Chem. Chem. Phys. 2016. V. 18. P. 25421-33.

MEMBRANE CASCADE TYPE OF "CONTINUOUS MEMBRANE COLUMN"

Artem Atlaskin, Maxim Trubyanov, Pavel Drozdov, Ilya Vorotyntsev, Vladimir Vorotyntsev

Nizhny Novgorod State Technical University n.a. R.E. Alekseev, Nizhny Novgorod, Russia
E-mail: atlaskin@gmail.com

Introduction

Strengthening of environmental regulations, improvement of product specification level, and the need to reduce production costs in the current economic situation set the task for chemical engineers to intensify the implementation of energy-efficient separation methods and search for novel ways of optimizing the existing technological solutions. Membrane gas separation has recently drawn a great attention in the field of high-purity gases production in conjunction with developing continuous non-waste technologies capable to provide small-scale point-of-use supply of high-purity gases. It has been shown that new single-stage schemes, such as unsteady-state membrane gas separation[1] and absorbing pervaporation[2] have a great potential in gas separation applications, but the separation efficiency of the single stage membrane processes is limited by the selectivity of the membrane at a given pressure ratio, hence the high purity product can be obtained only by multi-stage systems. However, this leads to a material-intensive configurations and high capital costs, which makes the membrane process noncompetitive. Another approach to increase the separation efficiency is the use of a continuous membrane column[3,4] which has similar configuration to a distillation column. The purpose of the current work is to present novel concepts for realization of purification process by gas separation in multi-stage membrane cascades which are promising and competitive prototypes of countercurrent distillation columns.

Experiments

Gases high purification experiments were carried out using the set-up presented at Fig. 1. The gas flow direction is indicated by arrows. This membrane cascade consists of three membrane elements: single module for extraction section and two elements in enrichment section.

Gas mixture composition determination was carried out by gas chromatography, using helium carrier gas, a thermal conductivity detector and a Porapak Q packed column.

In the experiments an argon-propane model mixture was used with concentration 0.02 – 1% of propane.

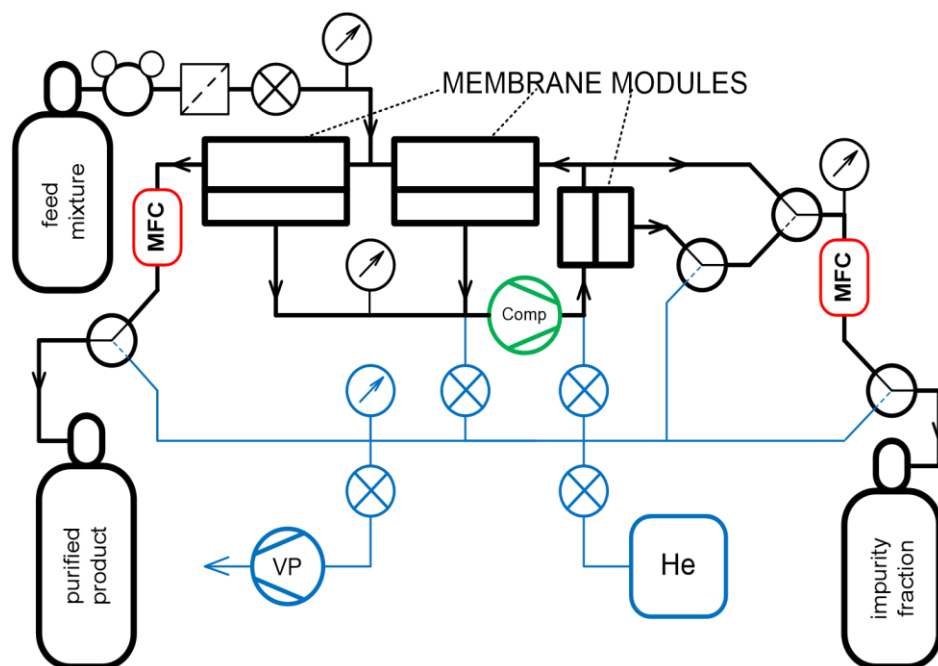


Figure 1. Principal scheme of membrane cascade type of «continuous membrane column»

Results and Discussion

A cascade of the membrane column (MC) type is shown in Fig. 2a, and a cascade of the three-module membrane column (TMC) type is shown in Fig. 2b. Fig. 2c presents the scheme of a two-membrane column (TwMC) in which the membranes in the elements in both section have opposite properties, in contrast to the preceding cascades: the contaminant passes through the membrane better than the basic component in the extraction section and worse in the enrichment section.

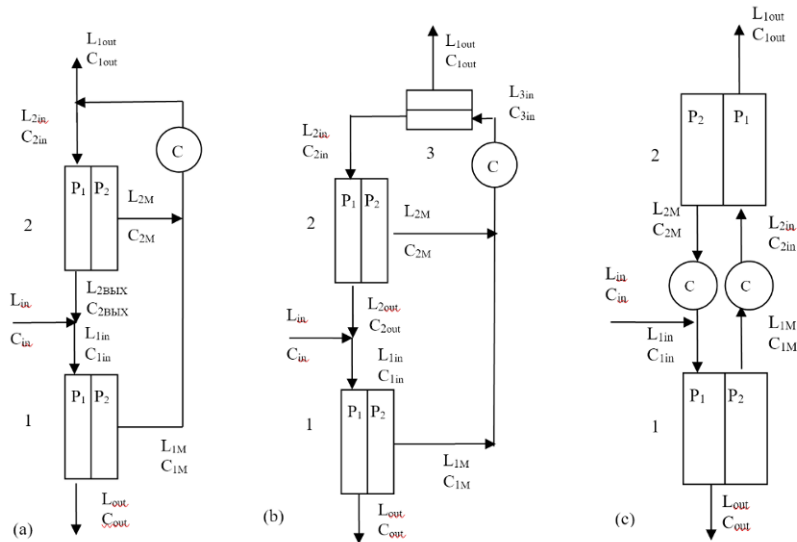


Figure 2. Diagram of MC (a), TMC (b), and TwMC (c) cascades. *K*, compressor; *P1*, HPC; *P2*, LPC.

The cascade separation efficiency as a function of stage-cut (θ) is presented in Fig. 3, where F_1 is extraction section separation factor, F_2 enrichment section separation factor and F is the set-up separation factor. Separation factor of extraction and enrichment sections is determined by the inlet and outlet gas mixture concentration ratio. Cascade separation factor is the ratio of impurity concentration in impurity fraction and product fraction.

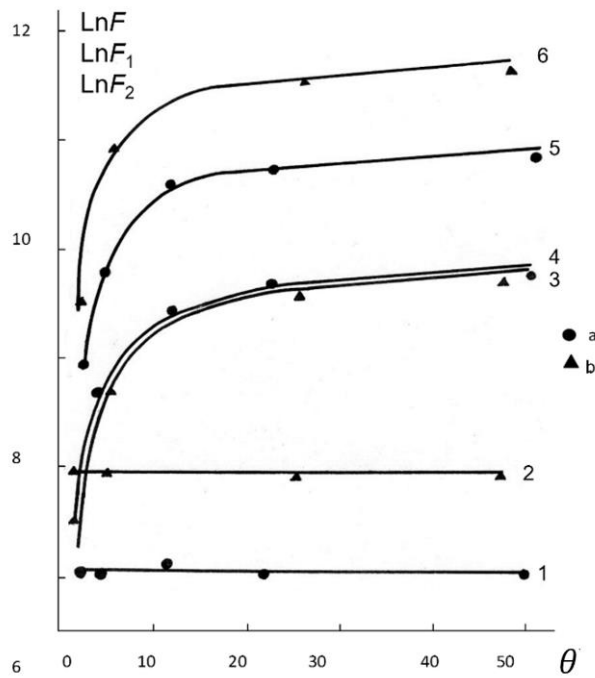


Figure 3. The dependence of the separation factor of the extraction section (F_1), enrichment section (F_2), and the setup as a whole (F) on the parameter $\theta = l/l_0$: (a) experimental data for the MC mode; (b) TMC mode: (1, 2) F_2 ; (3, 4) F_1 ; (5, 6) F .

It is shown that with an increase of stage-cut value (or with a decrease in the rate of product and concentrate withdrawal), the separation efficiency of the extraction section increases, and its value for the enrichment section varies insignificantly. The separation factor of the set-up is also increasing. The degree of separation of the enrichment section of the TMC-type cascade is higher than that of the MC-type cascade. The degree of separation of the extraction section of the cascades of both types is practically the same. A small difference is explained by a decrease in the withdrawal degree of the concentrate and, correspondingly, an increase in the withdrawal rate of the purified product in a cascade of the TMC type in comparison with MC for the same stage-cut value parameter.

The experimental results are in good agreement with the calculated data. The maximum separation factor is $1.8 \cdot 10^4$ in the MC cascade and $8.5 \cdot 10^4$ in the TMC cascade is obtained. The degree of product withdrawal is 87% and 98%, respectively. In the same case, without the enrichment section, the degree of product withdrawal does not exceed 2%. Thus, it was shown that this design of the membrane cascade apparatus has great potential for use in gases high purification applications and it does not require a large number of membrane elements and compressors to achieve a high degree of purity of the product in contrast to the cascade schemes proposed earlier.

Acknowledgements

This work was supported by the grant of the President of the Russian Federation (MD-5414.2016.8), the grant of the President of the Russian Federation (MK-2924.2017.8) and the Russian Foundation of Basic Research (16-38-60174 mol_a_dk).

References

1. *M.M. Trubyanov et al.* // Journal of Membrane Science 530 (2017) 53 – 64
2. *I.V. Vorotyntsev et al.* // Desalination and Water Treatment (2017) 1 – 9. doi: 10.5004/dwt.2017.20400
3. *V.M. Vorotyntsev et al.* // Desalination 147 (2002) 433 – 438
4. *V.M. Vorotyntsev et al.* // Separation and Purification Technology 22 (2001) 367 – 376

IONIC LIQUIDS AS CO₂ SOLVENTS FOR HIGH PRESSURE GAS-LIQUID PVTMS-MEMBRANE CONTACTORS

Stepan Bazhenov, Danila Bakhtin, Alexey Volkov

A.V.Topchiev Institute of Petrochemical Synthesis (TIPS RAS), Moscow, Russia

E-mail: sbazhenov@ips.ac.ru

Introduction

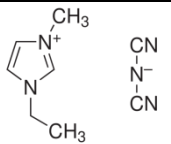
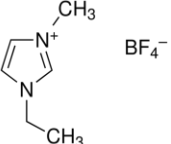
A very large number of studies dedicated to CO₂ capture via gas–liquid membrane contactors have been reported during last decades, but such an important field as high pressure membrane CO₂ absorption/stripping with non-aqueous physical solvents remains practically unexplored and amount of published data is very limited. This due to the fact, that process realization can face some challenges. Compared to water, physical solvents show higher viscosity and lower surface tension that prevents using of porous membranes due to liquid penetrating and rapid pore wetting. Taking into consideration that typical pressure of processes based on physical solvents is about 10-50 bar, it is highly required to use non-porous dense membranes that meet certain requirements: i) high CO₂ permeance, ii) chemical and mechanical stability in physical solvent, iii) absence of solvent leakage through the membrane at operated conditions. Wetting-resistant highly-permeable non-porous membranes based on glassy polymer poly(vinyl trimethylsilane) (PVTMS) meet the target and can be successfully implemented in CO₂ stripping from chemical and physical solvents [1,2].

In the present work, we provided insight into choosing and analyzing compatibility of PVTMS membranes and novel promising CO₂ physical sorbents – ionic liquids (ILs) – organic salts being in the liquid state under operation temperature and having saturated vapor pressure close to zero. The data are given for long-term ILs sorption in the PVTMS polymer and also for the polymer swelling degree in the ILs chosen.

Experiments

The literature data analysis allowed to choose the following ILs: two ILs based on the imidazolium cation – 1-ethyl-3-methylimidazolium dicyanamide ([Emim][DCA]) and 1-ethyl-3-methylimidazolium tetrafluoroborate ([Emim][BF₄]). These ILs are easy to obtain and therefore they are commonly used for solving various technological tasks, including CO₂ capture. The ILs properties are widely investigated in literature; CO₂ solubility in ILs is comparable to that in conventional physical sorbent Genosorb 300 (see Table 1). Chemical structures of the ILs chosen, their properties and data for CO₂ solubility are given in Table 1. We also chose alternative ILs based on novel phosphonium cation – trihexyltetradecylphosphonium bis(2,4,4-trimethylpentyl)phosphinate ([Thtdp][Phos]) and trihexyl(tetradecyl)phosphonium bromide ([Thtdp][Br]). As shown in recent works [3,4], these ILs have extra high CO₂ solubility values, at the same time being more thermo- and chemical stable compared to imidazolium-based analogues, which makes them promising CO₂ solvents.

Table 1 – Chemical structure and physicochemical properties of the ILs chosen*.

Name	Chemical structure	Viscosity, mPa·s	Mol. weight, g/mole	Density, g/sm ³	CO ₂ solubility at 10 bar and 50 °C, molar fraction
[Emim][DCA]		14.5	177.2	1.108	0.171
[Emim][BF ₄]		36.9	198.0	1.283	0.083

[Thtdp] [Phos]		1402.0	773.3	0.885	0.310
[Thtdp] [Br]		2988.0	563.8	0.959	0.114
Genosorb 300		7-8 mm ² /s	280	1.03	0.170

*the ILs properties were chosen from ILs properties database [5]

To determine PVTMS interaction with the ILs chosen, dense PVTMS films were prepared having thickness of 70–75 μm and diameter 5 cm. For this purpose, the commercial asymmetric PVTMS membrane was dissolved in toluene up to polymer content of 1.0% wt. The films were prepared by casting of polymer solution onto the cellophane support with following slow drying under room temperature. In order to remove residual solvent and to relax the tangential stress, the prepared films were exposed in 1-butanol for 2 days and then exposed in ethanol for 24 hours. Before using, the membranes were washed in aqueous ethanol solutions with gradual ethanol content decrease and further dried to constant weight. So, at least 20 membrane films were obtained.

To study equilibrium sorption of the chosen ILs in the PVTMS, a long-term experiment was performed concerning films immersed in the ILs. Before immersing, the PVTMS films were measured (thickness, weight, geometrical dimensions) and then placed into leak-proof, non-transparent tanks containing the ILs investigated (3 films per one IL). The films were immersed in ILs for 6900 hours (9.5 months). After that, the films were removed from ILs, residual ILs were removed from the films surface by blotting filter paper and the membranes properties were measured again.

Results and discussion

Based on the data obtained for measuring geometrical parameters and weight, the sorption and swelling degree values were calculated for PVTMS in the ILs chosen. Also, such parameters were determined as mass and volumetric IL fraction in PVTMS by the end of experiment. The experiments results are given in Table 2.

Table 2. PVTMS sorption and swelling degree in the ILs chosen.

Liquid	Sorption, mole/mole	Swelling degree, %	IL mass fraction, %	IL volumetric fraction, %
[Emim] [DCA]	0.0024	3.6	0.47	0.33
[Emim] [BF₄]	0.0037	3.3	0.65	0.54
[Thtdp] [Phos]	0.0031	5.9	1.70	1.61
[Thtdp] [Br]	0.0003	3.6	0.21	0.22

As can be seen from Table 2, every presented IL has low sorption properties towards PVTMS: for all ILs chosen, PVTMS sorption is within the range of 0.0003 – 0.0037 mole IL/mole PVTMS monomeric unit; the swelling degree (change in the film geometrical dimensions) of the polymer in the ILs chosen is also very low – 3.6-5.9%. It should be noted that the IL having maximum molecular weight [Thtdp][Phos] (773.3 g/mole) among other ILs chosen show high sorption properties. This fact indicates that high IL viscosity does not influence significantly the PVTMS sorption. Conversion of the values to the mass and volumetric IL fraction in the film shows that

these fractions are less than 1%. Furthermore, IL volumetric fraction in the PVTMS is within the range of 0.22 – 1.61% for different ILs. Taking into account that PVTMS free volume fraction is approx. 4%, it can be concluded that none of the ILs chosen occupies all material free volume. This indicates low ILs chosen affinity to the asymmetric PVTMS membranes material, which, in turn, allows to assume that ILs do not leak through the membranes, i.e. asymmetric PVTMS membranes have barrier properties towards the ILs chosen. So, the ILs chosen can be successfully employed as CO₂ solvents in high pressure membrane contactors based on asymmetric PVTMS membranes.

Acknowledgements

The reported study was funded by RFBR according to the research project No. 16-38-00873 МОЛ_a.

References

1. *Volkov A.V., Tsarkov S.E., Goetheer E.L.V., Volkov V.V.* Amine-based solvents regeneration in gas-liquid membrane contactor based on asymmetric PVTMS // *Petrol. Chem.* 2015 V. 55(9). P. 716-723.
2. *Bakhtin D., Bazhenov S., Volkov A.* High pressure gas-liquid membrane contactor for CO₂ stripping from physical solvent // *Proceedings of international conference “Ion transport in organic and inorganic membranes” Sochi, 2016.* P. 43-44. ISBN 978-5-9906777-3-9.
3. *Ramdin M., Olasagasti T.Z., Vlught T.J., de Loos T.W.* High pressure solubility of CO₂ in non-fluorinated phosphonium-based ionic liquids // *J. Supercritical Fluids.* 2013. V. 82. P. 41-49.
4. *Ramdin M., Amlianitis A., Bazhenov S., Volkov A., Volkov V., Vlught T.J., de Loos T.W.* Solubility of CO₂ and CH₄ in ionic liquids: ideal CO₂/CH₄ selectivity // *Ind. Eng. Chem. Res.* 2014. V. 53(40). P. 15427-15435.
5. <http://ilthermo.boulder.nist.gov/> (access date – 20.03.2017)

CHARACTERIZATION OF ION-EXCHANGE MEMBRANES USED IN FOOD INDUSTRY AND CONTRIBUTION TO THE CLEANING MEMBRANES USING CHEMICAL SOLUTIONS

^{1,2}Myriam Bdiri, ¹Lasâad Dammak, ¹Christian Larchet, ¹Lobna Chaabane, ²Fayçal Hellal

¹Institut de Chimie et des Matériaux Paris-Est (ICMPE), Thiais, France, *E-mail: dammak@u-pec.fr*

²Institut National de Sciences Appliquées et de Technologie, Tunisie, *E-mail: bdiri@icmpe.cnrs.fr*

The use of electro dialysis (ED) is widespread in the food industry for many applications such as whey and fruit juice filtration or tartaric stabilization of wine [1]. For all these applications, the fouling of ion-exchange membranes (IEM) due to organic matters represents one of the main problems encountered by industrials. In our work, four batches of IEM, new (n) and end-of-life (u) cation exchange membranes (CEM) and anion exchange membranes (AEM), from ED units used in Agri-Food industry – confidential subject – were characterized to study the effects of prolonged use and organic fouling on their performances.

Different methods of characterization were experimented on the samples, such as; exchange capacity (EC), thickness (Tm), conductivity (Km) [2], contact angle (θ), water content (te), table 1, traction tests, FTIR, structural et elementary SEM analysis and morphological analysis by optical microscopy.

Table 1: Characterization of IEM(s) results

	CEM (n)	CEM (u)	AEM (n)	AEM (u)
EC (mmol.g ⁻¹)	2.47 ± 0.13	1.40 ± 0.05	2.51 ± 0.10	1.23 ± 0.06
Tm (µm)	177 ± 4	270 ± 5	153 ± 2	169 ± 4
Km (S.cm ⁻¹)	13.4 ± 0.6	6.2 ± 0.4	12.6 ± 0.5	3.1 ± 0.2
θ (°)	47 ± 1.3	49.3 ± 1	63 ± 1.8	52.6 ± 1.3
te (%)	26.1 ± 0.7	40 ± 1.7	24.8 ± 1.1	23.7 ± 1

From table 1 it is seen that the prolonged use of the MEI and their organic fouling causes a strong alteration of the membranes physicochemical performances, which automatically leads to a significant drop in the processes efficiency, by the end of membranes life.

Non-aggressive cleaning strategies using chemical solutions were tested on end-of-life CEM and AEM, in *ex-situ* static mode, such as saline solutions [3] and water-ethanol mixture. The efficiency of the various cleaning procedures were evaluated by following EC, Km and θ for each sample of treated membrane as a function of the wash times in order to judge the recovery of some of their physicochemical properties as shown in figures 1-3.

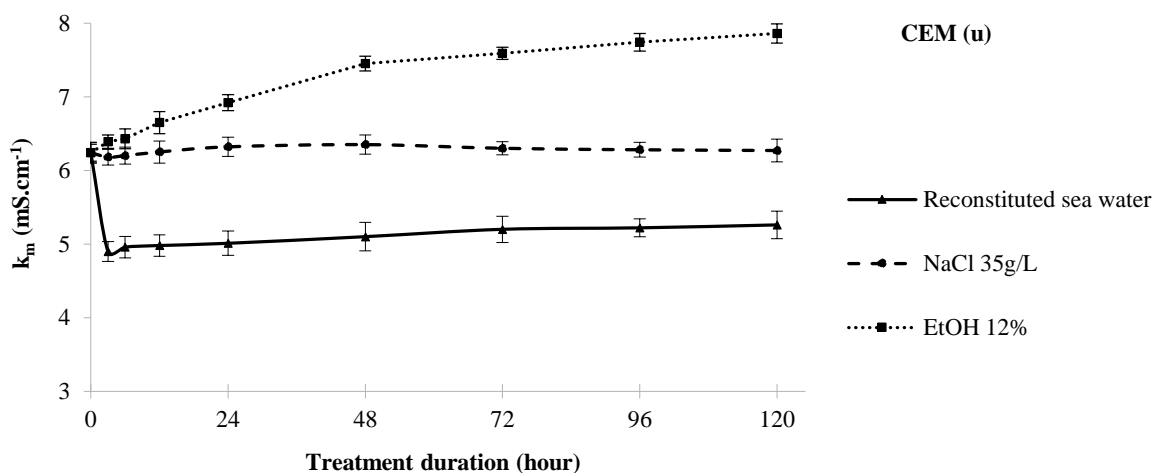


Figure 1. Evolution of conductivity (Km) during chemical treatments on CEM (u)

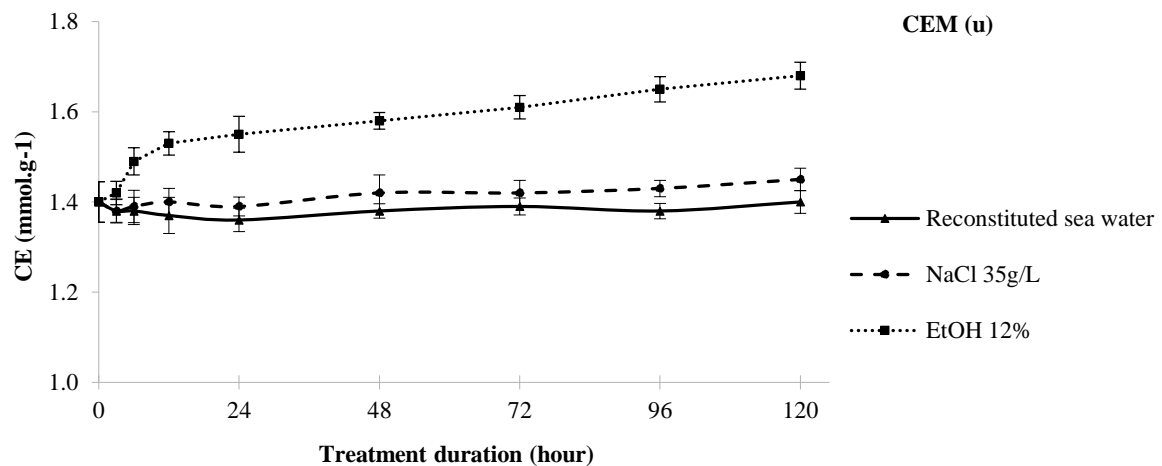


Figure 2. Evolution of exchange capacity (mmol.g^{-1}) during chemical treatments on CEM (u)

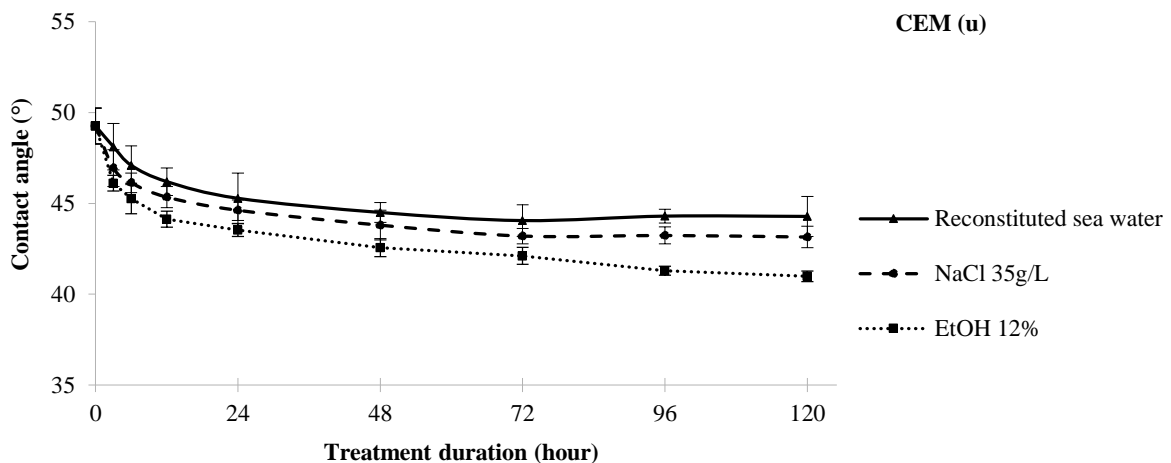


Figure 3. Evolution of contact angle (θ) during chemical treatments on CEM (u)

Figure 1 shows a significant increase of the membrane's electrical conductivity treated by water-ethanol mixture, which reaches 20% recovery after 48 hours cleaning and 26% after 120 hours. This cleaning efficiency is confirmed by the recovery of about 20% of exchange capacity (figure 2) and an important decrease of the surface hydrophobicity (figure 3) by the end of the treatment. As regards saline treatments, there are no significant changes in the evolution of the exchange capacity (figure 2). A significant drop in electrical conductivity at the beginning of the reconstituted seawater solution cleaning, caused by the interactions between the free functional sites of the membrane and the bivalent and monovalent ions in solution is noticed in figure 1. Only surface cleaning can be considered effective for saline treatments.

References

1. Nagarale R.K., Gohil G.S., Vinod K. Shahi. Recent developments on ion-exchange membranes and electro-membrane processes // *Advances in Colloid and Interface Science* 2006. V. 119. P. 97.
2. Ghalloussi R., Garcia-Vasquez W., Bellakhal N., Larchet C., Dammak L., Huguet P., Grande D. Ageing of ion-exchange membranes used in electrodialysis: Investigation of static parameters, electrolyte permeability and tensile strength // *Sep. and Pur. Tech.* 2011. V. 80. P. 270.
3. Corbaton-Baguena M.J., Alvarez-Blanco S., Vincent-Vela M.C. Cleaning of UF membranes fouled with BSA by means of saline solutions // *Separation and Purification Technology* 2014. V. 125. P. 1.

IMPACT OF MEMBRANE SCALING NATURE ON THE WATER SPLITTING AND ELECTROCONVECTION DEVELOPMENT AT THE SURFACE OF THE CATION EXCHANGE MEMBRANE

Ekaterina Belashova¹, Sergey Mikhaylin², Victor Nikonenko¹, Natalia Pismenskaya¹, Laurent Bazinet²

¹Membrane Institute, Kuban State University, Krasnodar, Russia

²Université Laval, Food sciences department, Laboratory of Food Processing and Electromembrane Processes, Quebec, Canada

E-mail: ekaterinabelashova23@gmail.com

Introduction

Electromembrane methods for separation and purification are increasingly used in industries (e.g. medicine, agriculture and food) dealing with solutions containing large amounts of dissolved components [1,2]. However, the large number of ionic and molecular components present in the treated solutions, including calcium or magnesium ions and particles entering the protolytic reactions (e.g., carbonate, phosphate ions) entails the formation of a fouling on ion-exchange membranes.

Previous works involving model salt solutions [3] and milk [4], investigated the nature of membrane scaling and its impact on electrodialysis (ED) performance. However, the mechanism of action of different scaling agents on electrochemical characteristics of the membrane systems remains poorly studied. In this context, the aim of this work was to elucidate the impact of the most abundant scaling agents such as compounds of Ca^{2+} and Mg^{2+} ions on the electrochemical characteristics of membrane system.

Experiments

The study was conducted in three stages. The first stage was aimed at the formation of scaling of different compositions on a cation-exchange membrane (CEM) surface by treating model salts solutions by ED. In the first case, the scale on a CMS-SB membrane contained a mixture of magnesium hydroxide and calcium carbonate (the membrane designated as CMX-SB-1); and in the second case, the scale on the same kind of membrane was mainly composed of magnesium hydroxide with traces of calcium hydroxide (designated as CMX-SB-2). In the second stage, the surfaces of original and fouled CEMs were analyzed using scanning electron microscopy (SEM), energy dispersive X-ray spectroscopy (EDS) and X-ray diffraction (XRD). Finally, in a third stage, the electrochemical behavior of the membrane systems, containing the original or fouled membranes, were studied by voltammetry techniques. Additionally, the pH of the depleted solution near the CEM surface was measured via extraction of a portion of solution with a capillary.

Results and Discussion

From obtained results, it appeared that the composition of mineral precipitate on the CEM surfaces affects the electrochemical behaviors of the membrane system (Fig. 1).

In the case of CMX-SB-1 membrane, where the scale was a two-layer deposit containing calcium carbonate in calcite form and a small amount of magnesium hydroxide in brucite form, the current-voltage characteristic (CVC) of the membrane system hardly differed from CVC of the system comprising original CMX-SB membrane. The systems containing CMX-SB and CMX-SB-1 membranes have the close values of limiting current, plateau lengths and pH of the solution near the CEM. In the overlimiting current mode, the solution acidification indicates the absence of intensive water splitting at the CMX-SB-1 interface. This could be explained by formation of CaCO_3 crystals on top of the $\text{Mg}(\text{OH})_2$ crystals. Since the gravitational convection under these conditions is poorly developed [5], overlimiting mass transfer mechanism in this case is the nonequilibrium electroconvection.

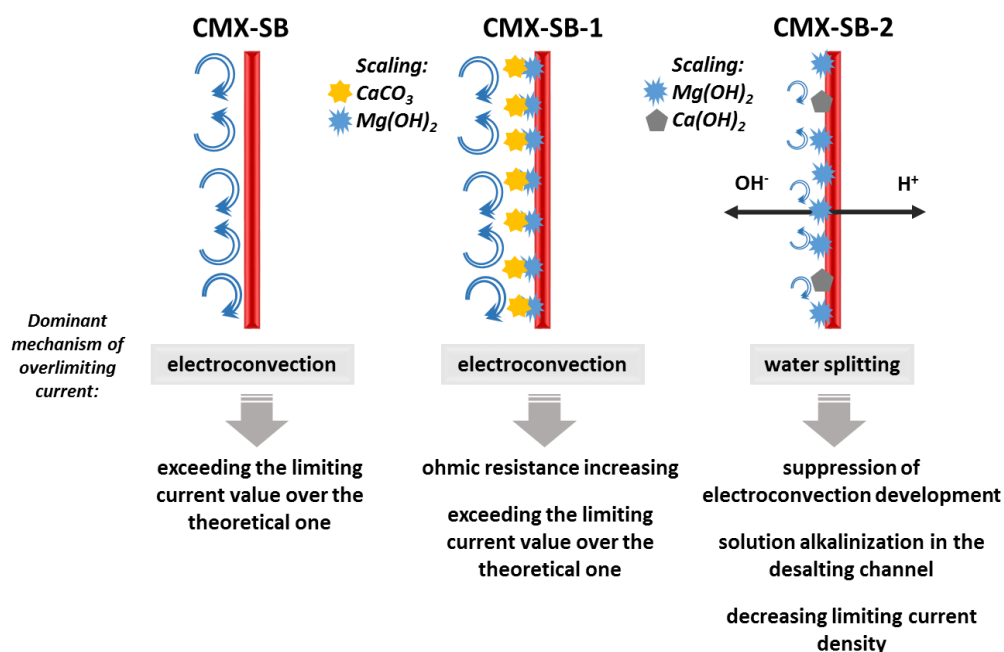


Figure 1. Scheme presentation of the effects near the CEM during ED treatment in the overlimiting current mode

In the case of CMX-SB-2 membrane, the situation is different. In the overlimiting current mode, the main effect is an intensive water splitting due to the presence of Mg(OH)_2 in brucite crystals and small amounts of Ca(OH)_2 in amorphous form. Magnesium and calcium hydroxides are known as effective catalyzers of water dissociation [6], which explains high alkalization of the depleted solution near the CMX-SB-2 membrane. As shown in [7], an intensive water splitting suppresses electroconvection due to the reduction of space charge at the depleted membrane surface: OH^- ions generated at the CEM depleted surface enter the space region of positive charge formed by the salt cations.

Conclusion

The composition and nature of the scaling formed on CEM surface has a great impact on the electrochemical behavior of the membrane system. Magnesium hydroxide precipitate led to an intensification of water splitting at the solution CEM interface, entailing suppression of electroconvection development. The presence of calcium carbonate in addition to magnesium hydroxide on the membrane surface, wherein calcium carbonate was the predominant component, led only to an increase in system electric resistance and did not influence neither the limiting current value nor the overlimiting mass transfer mechanism. This was due to the multilayer nature of the studied scaling: calcium carbonate crystallization occurred on the magnesium hydroxide crystals preventing their contact with water molecules, whereby catalysis of water splitting did not occur.

Acknowledgements

This investigation was carried out within French-Russian laboratory "Ion-exchange membranes and related processes". The authors are grateful to the Russian Foundation for Basic Research (grant 17-08-01442_a) for financial support.

References

1. Chen G., Song W., Qi B., Li J., Ghosh R., Wan Y. Separation of protein mixtures by an integrated electro-ultrafiltration-electrodialysis process // Separation and Purification Technology 2015. V. 147. P. 32-43.

2. Wang X., Zhang X., Wang Y., Du Y., Feng H., Xu T. Simultaneous recovery of ammonium and phosphorus via the integration of electrodialysis with struvite reactor // *Journal of Membrane Science* 2015. V. 490. P. 65-71.
3. Cifuentes-Araya N., Pourcelly G., Bazinet L. Multistep mineral fouling growth on a cation-exchange membrane ruled by gradual sieving effects of magnesium and carbonate ions and its delay by pulsed modes of electrodialysis // *Journal of Colloid and Interface Science* 2012. V. 372 P. 217-230.
4. Mikhaylin S., Nikonenko V., Pourcelly G., Bazinet L. Hybrid bipolar membrane electrodialysis / ultrafiltration technology assisted by a pulsed electric field for casein production // *Green Chemistry* 2016. V. 18. P. 307-314.
5. Pismenskaya N.D., Nikonenko V.V., Belova E.I., Lopatkova G.Yu, Sizat P., Pourcelly G., Larshe K. Coupled convection of solution near the surface of ion-exchange membranes in intensive current regimes // *Russian Journal of Electrochemistry* 2007. V. 43. P. 307-327.
6. Sheldeshov N.V., Zabolotskii V.I., Ganych V.V. Water dissociation rate at cation-exchange membrane - influence of insoluble metal-hydroxides // *Russian journal of electrochemistry* 1994. V. 30. P. 1333-1336.
7. Pismenskaya N.D., Belova E.I., Nikonenko V.V., Zabolotsky V.I., Lopatkova G.Y., Karzhavin Y.N., Larchet C. Lower rate of H⁺(OH⁻) ions generation at an anion-exchange membrane in electrodialysis // *Desalination and Water Treatment* 2010. V.21 P. 109-114.

STUDY OF ION DIFFUSION THROUGH ANODIC ALUMINA MEMBRANES

¹Mikhail Berekchiian, ^{1,2}Dmitrii Petukhov, ^{1,2}Andrei Eliseev

¹Department of Materials Science, Lomonosov Moscow State University, Moscow, Russia

²Department of Chemistry, Lomonosov Moscow State University, Moscow, Russia

E-mail: mikhail.berekchiyan@yandex.ru, di.petukhov@gmail.com, aaeliseev@inbox.ru

Introduction

The problem of mixture separation appeared long time ago and should be solved in different areas of human activity: from sifting of flour in village life to filtration of air by gas masks at war. Based on centuries-old experience, people came to the conclusion, that membranes solve these problems in the most successful way. For example, there are a large variety of membrane separation methods of liquid mixtures. However, some serious problems still remain unsolved, and a number of other needs to be improved. Water purification and desalination, filtration of solutions of proteins and inorganic salts are among them. Nowadays there is no common model for describing ion diffusion through porous media and predict membrane properties. So the main aim of this work was to study effective diffusion coefficients of anions and cations in nanoscale pores for development of the model of ion diffusion through the nanopores. For this aim, anodic alumina membranes with controlled pore diameters in the range from 10 to 200 nm were used as a perfect model object.

Experiments

In this work membranes were obtained by anodization of aluminum in 0.3M H₂C₂O₄ solution at 1–2°C and different voltages. After anodization we removed metal substrate and carried out barrier layer chemical etching with detection of pore opening point. Measurements of the effective diffusion coefficient D_e were carried out using a cell consist of two chambers separated with the membrane. Ion concentration was determined by mass spectrometry with inductively coupled plasma (ICP-MS). Membranes structure was characterized by scanning electron microscopy (SEM).

Results and Discussion

According to experimental data, the penetration rate of ions is strongly dependent on the solution pH (Fig. 1) and it leads to a change of effective diffusion coefficient. Apparently, there are two reasons of such ion behavior. The first of them is change of membrane potential with changing pH value of solution. The other reason is diffusion of hydrion at low pH. Due to their higher diffusivity they penetrate through the membrane faster than other cations. It leads both to decreasing of cation effective diffusion coefficient and increasing of anion effective diffusion coefficient (D_e) as a result of saving solution electroneutrality. Moreover, it was found that effective diffusion coefficient depends not only on pH, but also on the salt concentration in feed solution, D_e grows with increasing of the concentration and its value tends to the bulk diffusion coefficient D_0 . It should be noted, that effective diffusion coefficient of different cations decreases with increasing of their charge. It can be explained by increasing electrostatic interactions of ions with membrane surface and other particles, that is associated with a large surface charge. We also measured the membrane potential $\Delta\Phi_m$ and attempted to fit experimental data by the Teorell–Meyer–Sievers theory (TMS), which is the current model of ion diffusion through nanochannels.

Thus in this work we studied effective diffusion coefficient dependence on pH, salt concentration in feed solution and nature of ions, which penetrate through anodic alumina membranes with defined pore diameter (10 – 200 nm). Effective diffusion coefficient shows strong dependence on experimental conditions and membranes structure. Moreover, we measured the membrane potential $\Delta\Phi_m$ and attempted to fit it by the TMS-theory.

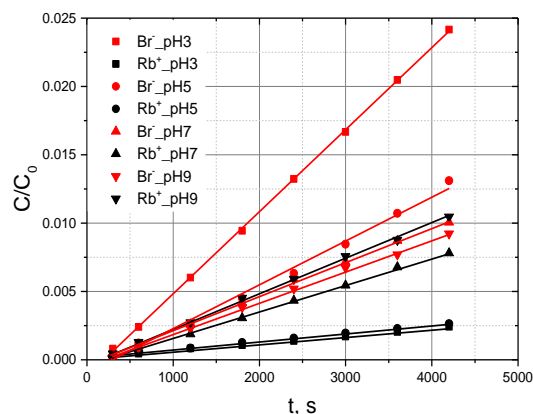


Figure 1. Concentration vs time for Rb⁺ and Br⁻ at different pH

JUSTIFICATION OF THE NANO-FILTRATION MEMBRANES APPLICATION AT SMALL RECREATIONAL FACILITIES UNDER CONDITIONS OF THE KRASNODAR TERRITORY CLIMATE

¹Sergey Bessarabov, ²Vita Borisova, ³Valeriya Plotnikova

¹LLS «Impuls», Russia, *E-mail: bessarabov001@yandex.ru*

²Platov South-Russian State Polytechnic University (NPI), Russia, *E-mail: vita-borisova@yandex.ru*

³Platov South-Russian State Polytechnic University (NPI), *E-mail: valeron19.96@mail.ru*

Introduction

In order to expand the recreational zone and provide recreation in the Krasnodar Territory, taking into account the reduction of the negative impact on the environment, it is necessary to build comfortable tent campuses, recreation centers with pontoon berths or shared yachting ports for yachting tourism, various types of motor aquatics, etc. [12]

Such areas should include ships parked on the water with their storage on the shore; an obligatory sanitary complex (toilet, shower, laundry), collection of waste and bilge water from yachts and boats; replenishment of water resources; small repair services; reception of other vessels, etc. [1-3].

Capital costs for seasonally-acting water supply systems are lower than for the permanent ones, and the following potential water users will be interested in them: located in hard-to-reach, remote areas, and also mobile fixed tourist bases that do not have a fixed link [2].

The recreational zone should be provided with drinking water that meets the requirements of SanPiN 2.1.4.1074-01. It is also essential that the construction and expansion of existing industrial, communal and storage facilities in the territories of recreational zones is not allowed. In this context, it is necessary to choose the methods of water conditioning and their adaptation for the conditions of the recreational zones of the Krasnodar Territory.

Recommended methods for water conditioning for small recreational facilities in the Krasnodar Territory

The problem of water preparation at small recreational facilities of the Krasnodar Territory remains unresolved to this day. At the sites, where the use of surface water is not possible for one reason or another, an alternative source may be the use of underground artesian waters.

One of the modern methods of demineralization and softening of water for domestic and drinking purposes is nanofiltration. The basis of this method, as well as in reverse osmosis, includes the use of membrane modules that are able to remove the ions present in the water from it and provide consumers with water for domestic and drinking purposes.

Nanofiltration (NF) is the process of separation of aqueous environments by means of a membrane having a less dense and more permeable selective layer than in reverse osmosis. Accordingly, nanofiltration membranes in comparison with reverse osmosis membranes have reduced selectivity, increased permeability and lower operating pressure for a given productivity.

Monovalent ions (cations and anions) are only slightly held by nanofiltration membranes, while their selectivity to multiply charged and large ions is high. This can be an advantage over reverse osmosis membranes, since it allows to obtain physiologically appropriate drinking water, i.e. water with salt content, corresponding to the biological needs of a man, thus the osmotic pressure is much less, which contributes to a reduction of electricity costs [4-7].

Their application can be justified by the need to minimize the negative impact on the environment, which is the main requirement in the construction and operation of water supply systems in the zones of seacoast sanitary protection [2].

In connection with these conditions, it is proposed to use mobile cleaning plants with nanofiltration membranes at the recreational facilities of the Krasnodar Territory. Fig. 1 shows a comparative analysis of the initial water parameters and energy consumption necessary for the preparation of 1 m³ of purified water.

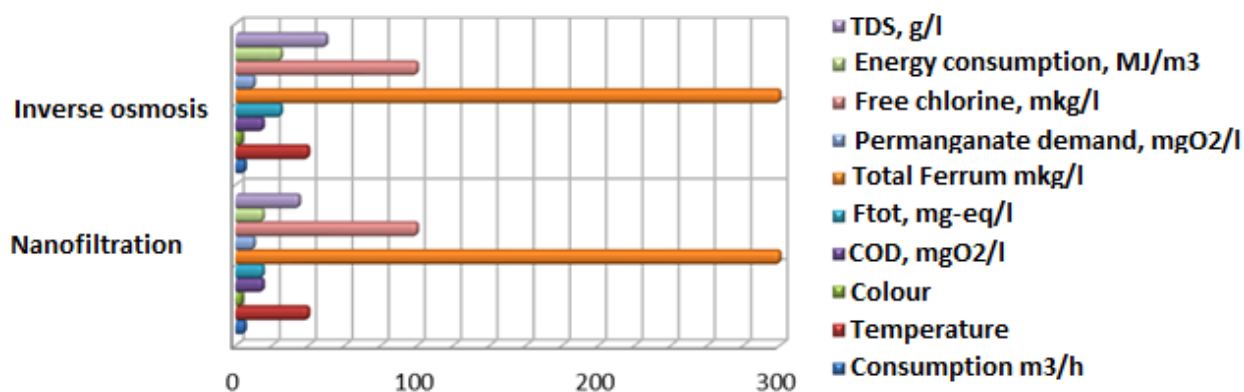


Figure 1. Hydrochemical indicators of the source water quality and energy consumption for the preparation of 1 m³ of purified water

The article was implemented in accordance with the state task No. 13.1236.2017 / IF (2017 - 2019) Development of energy-efficient and environmentally safe systems of decentralized water and energy supply for small recreational facilities in the Southern Region of the Russian Federation.

Conclusion

1. During steps of the analytical review it has been discovered that groundwater can be used as a source of water supply for recreational facilities, after appropriate preparation with the use of nanofiltration membranes.

2. According to the analysis of the diagram it is clear that the energy costs for nanofiltration are lower, and the efficiency of water purification is not inferior to reverse osmosis.

3. Despite the fact that the salt content of the concentrate in nanofiltration is less than that in reverse osmosis, the question of its processing remains open.

References

1. Kasharin, D.V.: Protective engineering structures made of composite materials in the water construction. South-Russian State Technical University (NPI). pp. 51 – 119 (2012)
2. Kasharin, D.V., Kasharina, T.P., Godin, P.A., Godin M.A.: Use of pipelines fabricated from composite materials for mobile diversion hydroelectric power plants. Power Technology and Engineering. T. 48. № 6. pp. 448 – 452, Springer (2015)
3. Kasharin, D.V., Kasharina, T.P., Godin M.A.: Mobile derivational micro-HPP for reserve water supply and standby power service of recreation facilities and harbour installations of Russky Island, Nashe More, vol. 62 № 4, pp. 272 – 277, Springer (2015).
4. Dzyubenko V.G., Dubyaga V.P., Svittsov A.A., Kagramanov G.G. Membrane technology today. Perspectives of the project "Russian membranes", Theses of the All-Russian NT conference "Membranes 2010" Moscow, 4-8.10.10, v. 2, Moscow: ISS RAS them. A.V. Topchieva, 2010.- P. 20-23.
5. Dzyubenko V.G., Kondrashev A.S. Membrane technology in the "Clean Water" program // Water supply and sewerage. - 2010. - №1-2. P. 416.
6. Ivanov M. On the market of membranes and membrane modules // Akva-Term. - 2010. - №5. - P. 15-18.
7. Methodical recommendations for ensuring compliance with the requirements of sanitary rules and norms SanPiN 2.1.4.559-96, Ed. V.L. Draginskogo, Moscow: VIMI, 2000, 92 p.
8. Mazaev V.T., Shelepina T.G., Mandrygin V.I. Drinking water quality control. - Moscow: Kolos. 1999. - 168 p.

CONDUCTIVE PROPERTIES OF MK-40 HETEROGENEOUS MEMBRANE IN DIFFERENT IONIC FORMS

Anastasia Bocharova, Irina Falina, Olga Demina

Physical Chemistry Department, Kuban State University, Krasnodar, Russia

E-mail: ab.bocharova@mail.ru

Introduction

Conductivity of ion-exchange membranes is an important characteristic for their application in electromembrane processes. Treatment of industrial wastewater needs the information about characteristics of ion-exchange materials in different ionic form, and their use in electro dialysis concentration of solutions makes it necessary to carry out the calculation of the conductivity of membranes in a wide range of solution concentrations. Therefore, the aim of this work was to investigate the conductivity of industrial heterogeneous membrane MK-40 in different ionic forms in a wide range of concentrations of electrolyte solutions.

Theory

Since the ion-exchange membrane is a heterogeneous material, its conductivity can be described from the standpoint of the generalized conductivity theory in which material properties can be expressed through the characteristics of the incoming phases. Quantitative evaluation of the internal characteristics is made on the base of structural-kinetic models of the generalized conductivity theory (Table 1): two phase conductivity model and extended three-wire model, which describe the membrane conductivity by exponential and power forms of Lichtenecker equation correspondingly.

Table 1. Structural-kinetic models of generalized conductivity theory

Generalized conductivity theory	
Two phase conductivity model [1]	Extended Three-wire model [2]
$\kappa_m = \kappa_{iso}^f \kappa^{1-f} \quad (1)$ $f + (1-f) = 1 \quad (2)$	$\kappa_m = a\kappa_{iso} + \frac{b\kappa\kappa_{iso}}{e\kappa + b\kappa_{iso}} + c\kappa \quad (3)$ $a + b + c = 1 \quad (4) \quad c = (1-f)^{1/\alpha} \quad (7)$ $e + d = 1 \quad (5) \quad e = (f-b)/a \quad (8)$ $b = f^{1/\alpha} \quad (6)$

where κ_{iso} , κ , κ_m - specific conductivity of membrane, gel phase and solution; f , $(1-f)$, α , a , b , c , d , e - geometric parameters of two-phase system. The parameters of the microheterogeneous model f , $(1-f)$ and α - are the structural parameters, since they characterize the volume fractions of gel phase and intergel solution and their spatial orientation towards the current direction respectively. The three-conductive model parameters a , b , c describe the fractions of current that path through three conductive channels: channel with serial arrangement of gel phase and intergel solution, channels of the gel phase and the intergel solution. Parameters e and d are equal to the fraction of current, that flows serially through the gel phase and the intergel solution of channel a .

The correct description the membrane conductivity in frames of the extended three-wire model requires the experimental conductivity concentration dependence of the material near the isoconductive point. In [1, 2] was performed the verification of extended three wire model in of NaCl solutions. This work presents the results of estimation the parameters of the extended three-wire model in a wide range of binary solutions concentrations.

Experimental

The object of investigation was commercial heterogeneous membrane MK-40 equilibrated with 0.05 – 2M solutions of HCl, LiCl, NaCl, KCl, CsCl. Conductivity of the membrane was determined by mercury-contact method on the base of active part of the cell impedance. Before measurement, the membranes were equilibrated with the specific solution.

Results and discussion

The obtained concentration dependencies are presented on Fig. 1. One can see, that membrane conductivity depends on the mobility the ion in solution, and concentration dependencies has increasing character in investigated range of concentrations.

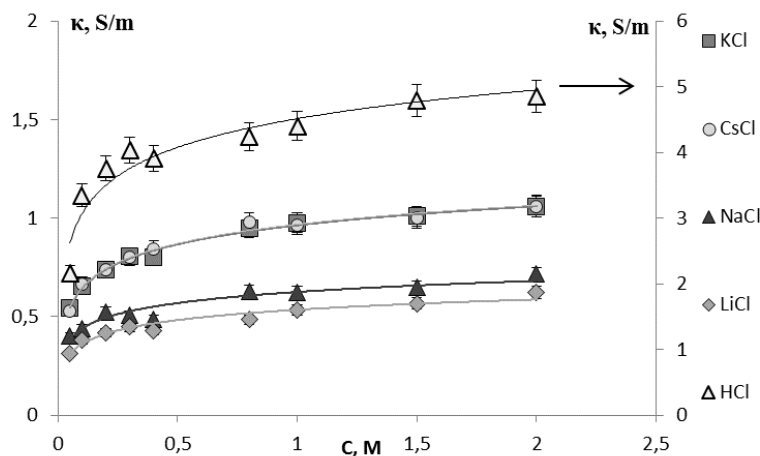


Figure 1. Conductivity concentration dependencies of MK-40 membrane in different electrolyte solutions

Obtained dependencies were used for calculation the parameters of two phase conductivity model and extended three-wire model. Table 2 shows the calculation results. One can see, that satisfactory agreement between calculation results in frames of two phase conductivity model and extended three-wire model is observed. Besides the range of solutions concentration does not essentially influence on value of the parameters.

Table 2: Parameters of MK-40 membrane in different solutions

Electrolyte	Extended three-wire model						Two phase conductivity model
	C = 0.05 - 0.4M		C = 0.05 - 1M		C = 0.05 - 2M		
	f	α	f	α	f	α	f
HCl	0.85	0.44	0.86	0.45	0.84	0.42	0.87
LiCl	0.83	0.57	0.83	0.48	0.77	0.37	0.82
NaCl	0.84	0.65	0.84	0.51	0.88	0.55	0.84
KCl	0.77	0.45	0.79	0.43	0.81	0.43	0.81
CsCl	0.811	0.47	0.795	0.43	0.80	0.45	0.80

Thus, the extended tree-wire model could be applied for conductivity description of ion exchange materials in a wide range of solutions concentration (0.1 – 2 mol/L), that has essential practical importance.

References

1. Zabolotsky V.I., Nikonenko V.V. // J. Membr. Sci. 1993. Vol. 79. P. 181.
2. Demina O., Kononenko N., Falina I. // Petroleum Chemistry. 2014. Vol. 4. № 2. P. 84-94.

THE RELATIONSHIP OF ENERGY CHARACTERISTICS OF SURFACES OF CONTINUOUS POLYMER MEMBRANES AND THEIR TRANSPORT PROPERTIES

Yuliya Bogdanova, Valentina Dolzhikova

Lomonosov Moscow State University, Moscow, Russia, E-mail: yulibogd@yandex.ru

Introduction

The possibilities of polymer application for the realization of the different practical tasks depend essentially on energy characteristics of polymer surface at the interfaces with gas (γ_{SV}) and liquids (γ_{SL}). Both these characteristics may be determined indirectly using contact angle measurements [1] in accordance to the Young equation for the equilibrium contact angle value (θ) of any liquid at the solid surface:

$$\gamma_{LV}\cos\theta = \gamma_{SV} - \gamma_{SL} \quad (1),$$

where γ_{LV} is the surface tension of liquid [1, 2] in context of molecular theory of wetting of Girifalco-Good-Fowkes [1, 2], which is based on the analysis if intermolecular interactions between the solid and liquid phases.

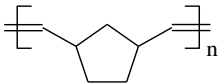
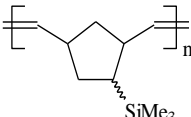
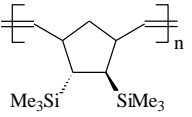
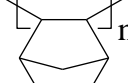
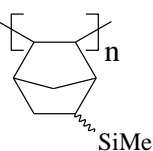
This paper shows new possibilities of the prediction and comparison of transport properties of continual membranes of amorphous polymers by means of its surface energy characteristics which were determined using contact angle measurements.

Experiments

The films of amorphous polymers with different chemical structure were studied. These were commercial Hyflons AD-60 and AD-80 (Solvay-Solexis), Teflons AF 1600 and AF 2400 (Du Pont) [3]. Polynorbornenes [4, 5] (Table 1), poly(4-methyl-2-pentine) (PMP) [6] and poly[1-(trimethylsilyl)-1-propine] (PTMSP) [7] were synthesized and characterized in Topchiev Institute of Petrochemical Synthesis, RAS; polynorbornene synthesis was realized by metathesis (MPNB) [4] and additive (APNB) [5] polymerization of corresponding monomers. Polymer films were prepared by coating from solutions at the surface of solid carriers (Alumina plates) with size 10x15x1 mm. 1 mass% of MPNB solution in toluene, 1 mass% of APNB solution in cyclohexane and 1 mass% of AD and AF in octafluorotoluene were used; then films were dried during 48 h at 20°C. PTMSP and PMP films were prepared in accordance to technique described in [8]. The films thickness was 300-500 nm.

Contact angles of probe liquids (H₂O and CH₂I₂) and aqueous ethanol solutions on the polymer surfaces were measured using sessile drop technique with accuracy 1°. The dispersive (γ_{SV}^d) and polar components (γ_{SV}^p) of polymer surface energy were calculated using Owens-Wendt-Kaelble approach [1]. The accuracy of determination of γ and its components was 1 mJ·m⁻². All measurements were performed at 20°C.

Table 1: Structural formulae of monomer links of polymers

Monomer link					
Polymer symbol	MPNB	(Me ₃ Si) –MPNB	(Me ₃ Si) ₂ –MPNB	APNB 2,3	Me ₃ Si –APNB 2,3

Results

Equations of molecular theory of wetting were obtained initially for smooth and homogeneous surface. But the properties of real surfaces must be taken into account. The calculation of the degree of heterogeneity of surfaces of polymer films has been performed in assumption of wetting in so-called Cassie-Baxter regime [2]:

$$\cos\theta = x\cos\theta_1 + (1-x)\cos\theta_2 \quad (2),$$

where x and $(1-x)$ are the fractions of the surface having contact angles θ_1 and θ_2 , respectively; θ is experimental contact angle of water at polymer film (Table 2), $\theta_1 = 0$ corresponds to wetting of pores filled with water at the polymer surface; θ_2 are contact angles of water at close-packing polymer surface.

Table 2: Contact angles of water

Polymer	θ , degree	θ_2 , degree	Functional groups at the close-packing polymer surface
MPNB	92	96	-CH ₂ -
APNB 2,3	91		
(Me ₃ Si) – MPNB	95	104	- CH ₃
(Me ₃ Si) ₂ – MPNB	100		
(Me ₃ Si) – APNB2,3	97		
PTMSP	85		
PMP	77	120	-CF ₂ -
AF 2400	114		
AF 1600	111		
AD 80	112		
AD 60	115		

The fractions of pores at the surfaces of polymer films x are comparable with fractional free volume of polymer FFV for all polynorbornenes (Figure 1). This means that the pores on the polymer surface really are filled with water: in case of AD and PTMSP $x < FFV$, for AF polymers $x \ll FFV$. This fact permits to believe that surface layers of polymer films have packing density more than inside. The results obtained prove the homogeneous regime of wetting and correctness of the approach to calculation of surface energy characteristics using experimental contact angles. The fact $x > FFV$ for PMP requires further consideration in spite of this polymer is included in the correlation of surface properties and transport properties of polymer films (Figure 2). The dependence $\ln P = f(\gamma_{sv}^d)$ is promising for the prediction and comparison of gas transport efficiency of different polymer membranes using its surface energy.

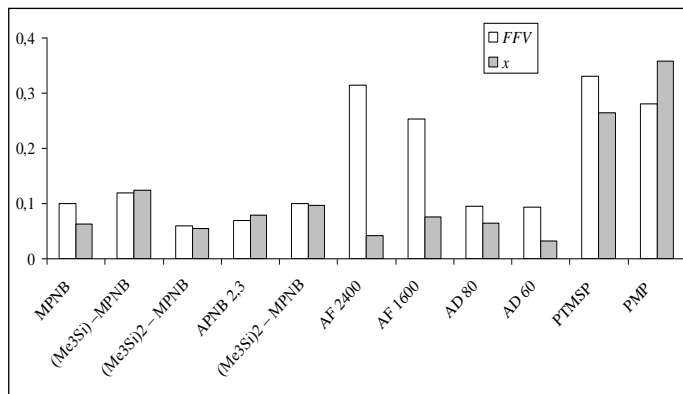


Figure 1. The relationship between the fractions of pores at the surfaces of polymer films x and fractional free volume of polymer FFV .

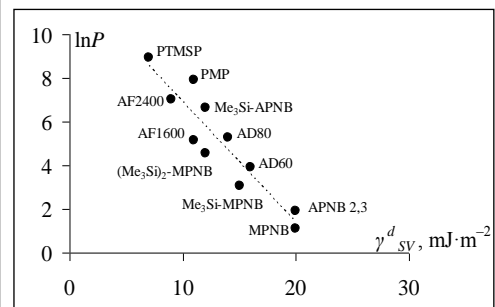


Figure 2. The dependence of gas permeability (P , Barrer) from dispersive component of surface energy of amorphous polymer films.

Films of PMP and PTMSP were investigated earlier in the context of nanofiltration of alcohol/water solutions. It was shown earlier that surface tension and contact angles of alcohol solutions at the polymer surfaces may be used for the determination of alcohol concentration providing the sorptive swelling of polymer film [9]. This process is controlled by γ_{SL} of the solution/film interface. The application of equation (1) for this analysis with fixed initial γ_{SV} values for PMP $\gamma_{SV} = (\gamma_{sv}^d + \gamma_{sv}^p) = (11+17) \text{ mJ}\cdot\text{m}^{-2}$ and PTMSP $\gamma_{SV} = (7+15) \text{ mJ}\cdot\text{m}^{-2}$ leads to the result devoid of physical meaning: $\gamma_{SL} < 0$. Hereby, the alteration of polymer surface energy after its contact in aqueous solutions must be taken into account. The surface energy characteristics of polymer films

after its contact with water during 30 min appeared to be $\gamma_{SV} = (6 + 36) \text{ mJ}\cdot\text{m}^{-2}$ for PTMSP and $\gamma_{SV} = (5 + 55) \text{ mJ}\cdot\text{m}^{-2}$ for PMP. The results obtained demonstrate a significant increase of the polar component of surface energy of polymer film caused by penetration of water in surface layer of PMP or PTMSP. Namely these γ_{SV} values were used for the calculation of γ_{SL} of the «alcohol solution/polymer film» interface. The $\gamma_{SL} = f(C)$ shows that γ_{SL} values corresponding to the beginning of sorptive swelling of polymer samples [10] appeared to be individual for each polymer: $\gamma_{SL} \in (5, 6) \text{ mJ}\cdot\text{m}^{-2}$ for PTMSP and $\gamma_{SL} \in (24, 26) \text{ mJ}\cdot\text{m}^{-2}$ for PMP (Figure 3). It is remarkable that γ_{SL} values are independent from nature of alcohol.

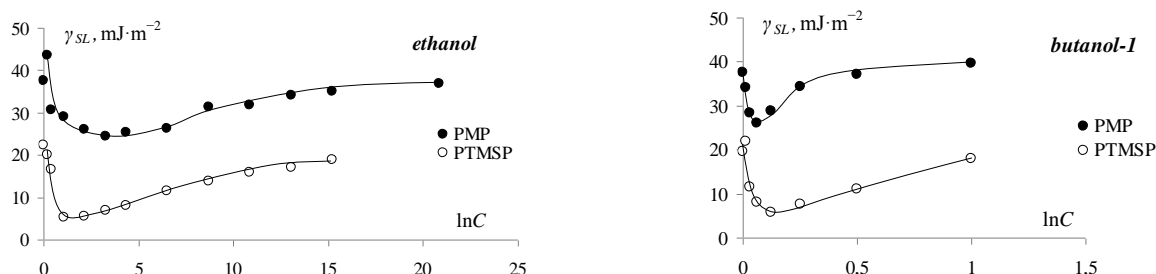


Figure 3. Isotherms of interfacial tension of aqueous alcohol solution/polymer»

Thus, the calculation of energy of «polymer/liquid» interface γ_{SL} and search of relationship of γ_{SL} value with polymer structure is a perspective approach for the express determination of alcohol concentration, corresponding to the sorptive swelling of the polymer during the nanofiltration of liquids through the continual polymer membranes.

References

1. *Vojtechovska J., Kvitek L.* Surface energy – effects of physical and chemical surface properties // *Acta Univ. Palaki. Olomuc. Fac. Perum Natur. Chemica* 44. 2005. P. 25-48.
2. *Golemme G., Nagy J.B., Fonseca A., Algieri C., Yampolskii Yu.* ^{129}Xe -NMR study of free volume in amorphous perfluorinated polymers: comparison with other methods // *Polymer*. 2003. Vol. 44. P. 5039-5045.
3. *Gringolts M.L., Bermeshev M.V., Starannikova L.E., Rogan Yu.V., Yampolskii Yu.P., Finkelstein E.Sh.* Synthesis and gas separation properties of metathesis polynorbornenes with different positions one and two SiMe_3 groups in the monomer unit // *Vysokomol. soed.* 2009. Vol. 51. № 11. P. 1970-1977. *in russian*
4. *Finkelshtein E.Sh., Makovetskii K.L., Gringolts M.L., Rogan Yu.V., Golenko T.G., Starannikova L.E., Yampolskii Yu.P., Shantarovich V.P., Suzuki T.* Addition-Type Polynorbornenes with $\text{Si}(\text{CH}_3)_3$ Side Groups: Synthesis, Gas Permeability, and Free Volume // *Macromolecules*. 2006. Vol. 39. P.7022-7029.
5. *Khotimskii V.S., Matson S.M., Litvinova E.G., Bondarenko G.N., Rebrov A.I.* Synthesis of poly-4-methyl-2-pentyne configuration different composition // *Vysokomol. soed. Ser. A.* 2003. Vol. 45. № 8. P. 1259-1267. *in russian*
6. *Khotimsky V.S., Tchirkova M.V., Litvinova E.G., Rebrov A.I., Bondarenko G.N.* Poly[1-(trimethylgermyl)-1-propyne] and Poly[1-(trimethylsilyl)-1-propyne] with various geometries: their synthesis and properties // *J. of Polym. Sci. Part A.* 2003. Vol. 41. P. 2133-2155.
7. *Volkov A.V., Volkov V.V., Khotimskii V.S.* Membranes based on poly-1-trimethylsilyl-1-propyne for separating liquids // *Vysokomol. Soed., Ser.A.* 2009. Vol. 51. №11. P. 2113-2128. *in russian*
8. *Bogdanova Y. G., Dolzhikova V. D., Yushkin A. A.* Wetting and adsorption modification in the system “highly permeable polymer film – aqueous solution of ethanol containing organic dyes” // *Chem. Bul. of Kazakh National Univ.* 2015. Vol. 79. № 3. P. 50–57.
9. *Yushkin A., Grekhov A., Matson S., Bermeshev M., Khotimsky V., Finkelstein E., Budd P.M., Volkov V., Vlugt T. J.H., Volkov A.* // *Reactive & Functional Polymers.* 2015. Vol. 86. P. 269-281.

DEVELOPMENT OF MATHEMATICAL MODEL OF WATER CAPACITIVE DEIONIZATION

Daniil Bograchev, Yurii Volkovich, Alexey Rychagov, Alexey Mikhailin, Valentin Sosenkin

A.N. Frumkin Institute of Physical Chemistry and Electrochemistry, Russian Academy of Science, Leninskii prospect 31, 119071 Moscow, Russia, E-mail: yuvolf40@mail.ru

Introduction

Capacitive deionization (CDI) is a new promising electrochemical method of water desalination. Economically, it is the most attractive technique in comparison with reverse osmosis, distillation and electromembrane separation [1]. CDI involves the passing of aqueous solution through the electrochemical cell between two highly dispersive carbon electrodes (HDCE) with a high specific surface area ($\approx 500 - 2500 \text{ m}^2 \text{ g}^{-1}$), between which a potential difference ($>1.2 \text{ V}$) is applied. Adsorption of anions and cations occurs on positively and negatively charged electrodes, respectively; the electric double layer (EDL) is charged similarly to that in supercapacitors. This results in deionization of the solution. When the circuit is closed or polarity is reversed, ions diffuse from the solid-liquid interface back to the solution. This causes an increase of the solution concentration and energy regeneration. Two products are obtained: pure water and a concentrated solution. The concentrate can be used further for different purposes. **The aim of the investigation** was to develop the mathematical model of CDI processes and to confirm it experimentally. Another purpose was to establish the effect of EDL characteristics on deionization.

Experiments

Materials: activated carbon textiles (ACT), such as CH900 (Curaray Co, Japan), VISKUMAK (Neorganica LTD, RF). The electrodes of the SAIT type (SAIT Co, Republic of Korea) were also used. These electrodes were manufactured by compaction of activated carbon powder in the presence of a binder (polytetrafluorethylene, PTFE).

Galvanostatic measurements of dependences of cell voltage on time were carried out in static cell (without hydrodynamic flow of solution) at 25°C under charging-discharging in order to determine the EDL capacitance. Single-component NaHCO_3 , CaCl_2 , and MgSO_4 solutions of different concentrations as well as a mixed solution were used. The capacitance of the electrodes ($C_{c,full}$) was determined as:

$$C_{c,full} = \frac{2I_{full}\Delta t}{\Delta U} \quad (1)$$

where U is the cell voltage, I_{full} is the current, t is the time.

Since adsorption capacity of the electrodes is proportional to the EDL capacitance ($C_{EDL,full}$), a change in solution concentration (Δc) during the process is expressed as:

$$\Delta c = \frac{C_{EDL,full}\Delta U}{2FV}, \quad (2)$$

where F is the Faraday constant, V is the solution volume. It is assumed that the adsorption efficiency is 100 % during the EDL charging. The expression (2) is also valid for electrodes of equal capacitance. In this work, the experimental method has been suggested that allows determining the EDL capacitance. The technique is based on measurements of electrochemical capacitance under various currents (i.e. under galvanostatic conditions) followed by calculations according to eq. (1). The typical curve of integral capacitance of the electrode vs current density is shown in Fig. 1. The capacitance grows at a decrease in current density and then manifests a plateau followed by a further decrease. The build-up of capacitance in the region of high current density is due to significant ohmic losses under these conditions. The plateau corresponds to very low ohmic losses; the capacitance is affected only by EDL. At low currents, pseudocapacitance of faradaic processes influences the value of C . It was suggested that the capacitance values of the plateau region corresponded to EDL capacitance per mass unit (C_{EDL}) in the first approximation.

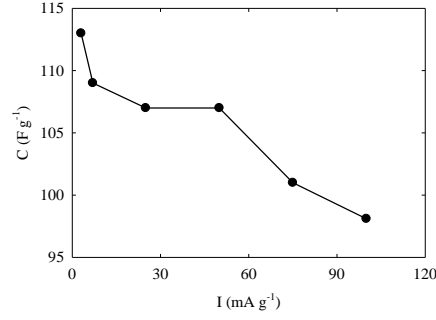


Figure 1. Dependence of capacitance of the CH900 electrode on current density in a 1 N CaCl₂ solution

Mathematical modeling for dynamic cell (with hydrodynamic flow of solution)

The equations for potential and concentration in the electrode region are:

$$C_S \frac{\partial \varphi - \varphi_C}{\partial t} = \frac{1}{r} \frac{\partial}{\partial r} \left(r \kappa_E \frac{\partial \varphi}{\partial r} \right) + \frac{\partial}{\partial z} \left(\kappa_E \frac{\partial \varphi}{\partial z} \right); \quad (3)$$

$$\varepsilon_E \frac{\partial c}{\partial t} + v_r \frac{\partial c}{\partial r} = D_E \left(\frac{1}{r} \frac{\partial}{\partial r} \left(r \frac{\partial c}{\partial r} \right) + \frac{\partial^2 c}{\partial z^2} \right) + \frac{C_S}{z_+ F} A_E \frac{\partial \varphi - \varphi_C}{\partial t}, \quad (4)$$

where C_S is the specific capacitance, φ_C is the electrode potential, φ is the electrolyte potential, t_+ and t_- are the cation and anion transfer numbers, ε_E is the porosity of the electrodes, $\kappa_E = \kappa_{E\lambda} c + \kappa_{surf}$ is the electrolyte conductivity in the electrodes, $\kappa_{E\lambda}$ is the reference electrolyte conductivity in electrode, κ_{surf} is the surface conductivity of the electrode [2], $D_E = D_0 \varepsilon_E^n$ is the effective diffusion coefficient of electrolyte in the electrode. As an example, Figs. 2 illustrate concentration fields for different time from the process beginning and for various thickness of the separator.

Theoretical and experimental data calculated for the cell with CH900 electrodes according to the dynamic CDI model are plotted in Fig. 3. As can be seen, the curves are close to each other. A certain divergence of these plots in the region of 0-15 s is evidently due to contact resistances in the cell. It is difficult to take them into consideration. A good agreement between the curves allows assuming correctness of the dynamic model, which can be used further for optimization of CDI processes.

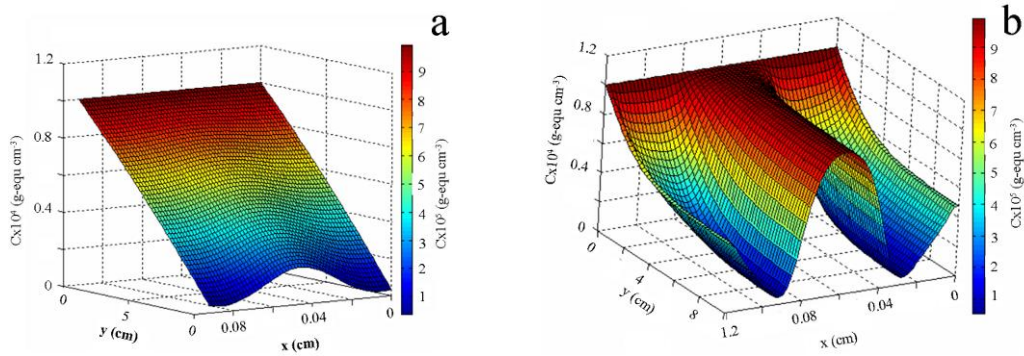


Figure 2. Concentration field calculated according to the dynamic model: a – flow velocity of the solutions $v=0.1 \text{ cm s}^{-1}$, separator thickness $L_s=0.0120 \text{ cm}$, time $t=100 \text{ s}$; b – $v=0.2 \text{ cm s}^{-1}$, $L_s=0.04 \text{ cm}$, $t=5 \text{ s}$. The calculations were performed for the CH900 electrodes in the mixed solution

Theoretical and experimental data calculated for the cell with CH900 electrodes according to the dynamic CDI model are plotted in Fig. 3. As can be seen, the curves are close to each other. A certain divergence of these plots in the region of 0-15 s is evidently due to contact resistances in

the cell. It is difficult to take them into consideration. A good agreement between the curves allows assuming correctness of the dynamic model, which can be used further for optimization of CDI processes.

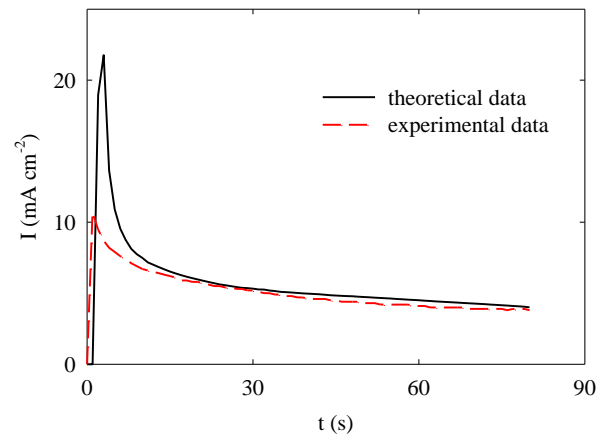


Figure 3. Comparison of the calculated and experimental dependences of current density on time. $U = 1.25$ V; the flow rate was $40 \text{ cm}^3 \text{ min}^{-1}$. The calculations were performed for the CH900 electrodes in the mixed solution

Conclusions

The 2D mathematical model of a dynamic CDI cell, which takes into consideration adsorption-desorption, ion transport, characteristics of porous structure of the electrodes and separator, surface conductivity of the electrodes as well as EDL capacitance (obtained in the static cell), has been developed. The experimental and theoretical data were found to be in a good agreement indicating correctness of the model. This means that the model can in future be applied to optimization of the CDI processes.

References

1. *Y. Oren* Capacitive deionization (CDI) for desalination and water treatment—past, present and future (a review)//Desalination. 228 (2008) 10.
2. *Yu. Volkovich, A.A. Mikhalin, A.Yu. Rychagov* Surface conductivity measurements for porous carbon electrodes //Russ. J. Electrochem. 49 (2013) 594.

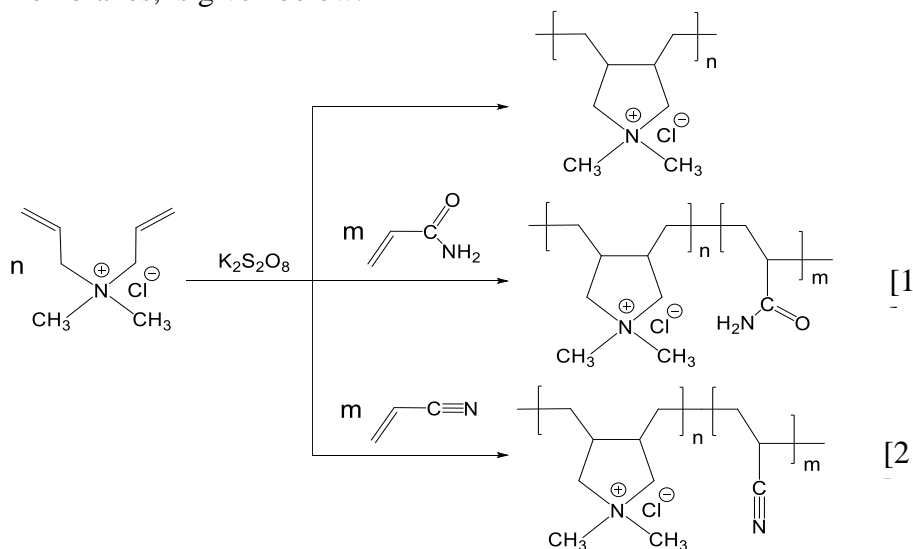
OPTIMAL CONDITIONS ADJUSTMENT FOR SYNTHESIS OF POLYMERIC MODIFIERS FOR ANION-EXCHANGE MEMBRANES

Denis Bondarev, Victor Zabolotsky, Alexander Bepalov, Anastasia But
Kuban State University, Krasnodar, Russia, E-mail: bondarew.denis1992@gmail.ru

Introduction

Modern tendencies of industry development and environmental standards increase determine new limits for energy efficiency of already existing technological processes. The use of extra-marginal current modes in the processes of electrolysis of low-concentrated solutions becomes economically feasible only while using sustainable membrane materials. It is known, that anion-exchange membranes have more elevated the catalytic effect in the reaction of dissociation of water, than cation-exchange ones have. This process is adverse, because of when new electric particles appear it causes the decrease of the space charge region and reduction of electroconvective [3]. The most common approach to overcome these limitations is the chemical modification of anion-exchange membranes, which results in their chemical stability.

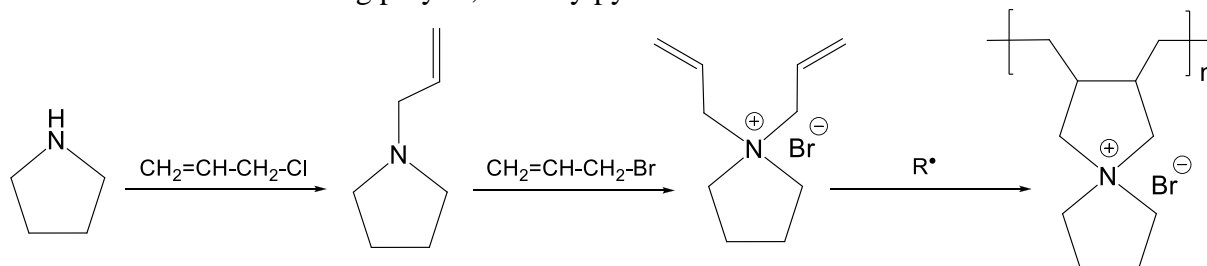
At the moment we know, that copolymers based on dimethyldiallylammonium chloride (DMDAAC) demonstrate the inhibitory activity when reacting of dissociation of water. In most cases such modification leads to increase of the limiting current on the membrane. The common scheme of obtaining of various copolymers, based on DMDAAC, which are used as modifiers for anion exchange membranes, is given below:



As we may see, the heterocyclic moiety, which contains quaternionic nitrogen atom, is a common structural element for all modifiers. The analysis of the chemical structure of already used modifiers allows us to suggest, that high-molecular compounds with quaternionic nitrogen atom, which belongs simultaneously to two cyclic systems and thereby forms a heterocyclic Spiro-fragment in the polymer, have a greater efficiency.

In this work we carried out the synthesis of polyelectrolytes with quaternionic nitrogen atom, which belongs simultaneously to two cyclic systems. The polymers, that we have obtained, was characterized by means of IR and NMR spectroscopy.

The scheme for obtaining poly-N,N-diallylpyrrolidinium bromide:



The polymers, that we have obtained, do not have spectral line 1680 cm^{-1} , which belongs to the double bond C=C. The Confirmation, that we obtained N-allylnormorphine and N-allylpyrrolidin we have carried out by using gas chromatography. The signals at the 5.7 and 6.1 M. D., which belong to vinyl protons, disappear in the $^1\text{H-NMR}$ spectrum of the polymer. The spectrum of the monomer does not have such the signals. At the same time, the signal of protons of methylene groups (1.5 m) appears in the $^1\text{H-NMR}$ spectrum of the polymer. Similarly, the ^{13}C NMR spectrum of the product obtained does not have the signals at 121 and 136 M. D., which belongs to carbon atom in the sp^2 -hybrid state.

The results of the examination of the influence of polymerization conditions on the yield of the obtained polymer are shown in Table 1.

Table 1: The effect of synthesis conditions on the yield of poly-N,N-diallylpyrrolidiniumbromide

Concentration of the monomer, %	Solvent	Initiator	Temperature, °C	Polymeryield, %
30	Water	$\text{K}_2\text{S}_2\text{O}_8$	70	22
60	Water	$\text{K}_2\text{S}_2\text{O}_8$	70	75
15	Butanol-1	Benzoyl peroxide	85	64
35	Butanol-1	Benzoyl peroxide	85	83

As we may notice, a higher yield of the target product at the same initial concentrations of the monomer was observed when using 1-butanol as solvent and benzoyl peroxide as the initiator.

Acknowledgements

The research is supported by RFBR (project № 16-48-230364 p_a).

References

1. Zabolotsky V.I., Bugakhov V.V., Sharafan M.V., Chermit R.H. // *Electrochemistry*. 2012. V.48, №6. P.721-731.
2. Zabolotskiy V.I., But A.Yu., Vasil`eva V.I., Akberova E.M., Melnikov S.S. // *J. Membr. Sci.* 2017. № 526. P. 60-72.
3. Andersen M.B., Soestbergen M. Van, Mani A., Bruus H., Biesheuvel P.M., Bazant M.Z. // *Phys. Rev. Lett.* V. 109. 2012. P. 108-112.

THERMOPERVAPORATION MEMBRANES BASED ON SYNDIOTACTIC POLYBUTADIENE AND POLYMETHYLSILOXANE FOR REMOVAL OF CHLORORGANIC FROM WATER

Ilya Borisov, Evgenia Grushevenko, Georgy Golubev, Danila Bakhtin, Vladimir Volkov
A.V. Topchiev Institute of Petrochemical Synthesis, Moscow, Russia, E-mail: boril@ips.ac.ru

Introduction

In the potable water of big cities, including Moscow, organochlorine compounds are often present. These compounds are principally formed under chlorine treatment of surface water. Also, the task concerning organochlorine compounds accumulation in ground water is challenging. In a number of wells providing potable water for Podolsk and Troitsk (Moscow region), water has elevated level of volatile organochlorine compounds (carbon tetrachloride, ethylene tetrachloride).

A promising non-waste technique for organochlorines removal from water is another membrane method – pervaporation [M. Peng, L. M. Vane, S. X. Liu, (2003). Recent advances in VOCs removal from water by pervaporation. *J. Hazard. Mater.* 98(1), 69-90.]. This technique has an advantage over nanofiltration, as it provides almost total purification of the treated water and organochlorine compounds are concentrated in permeate containing < 50% of water. Modern utilization technologies allow to combust or to ozonize these materials yielding in almost zero waste. For this reason, organic pollutants concentration under water purification is a substantial technique benefit. Utilization of water purification process waste certainly provides a means of reducing negative environment impact from hazardous solvents.

The most promising membrane materials for this task are polymers based on silicone (PDMS on the first place) and butadiene rubbers [1]. Silicone rubbers possess higher permeability due to higher chain mobility. However butadiene rubbers have higher selectivity to organics because their molecules are less polar and more hydrophobic.

In this work novel materials were synthesized which combine high permeability of silicone rubbers and high selectivity to organics of butadiene rubbers. New membrane materials promising for the separation of chlororganics from water were synthesized on the basis of syndiotactic polybutadiene (SPB), polydimethylsiloxane (PDMS) and polymethylhydrosiloxane (PMHS) by means hydrosilylation reaction. This approach allows varying the chemical structure of membrane material in a wide range to create material with optimal mass transport and separation features.

Experiments

Novel membrane materials were synthesized using the reaction of syndiotactic polybutadiene («JSR Corporation», Japan), vinyl-terminated PDMS (Sigma Aldrich) and PHMS (Sigma Aldrich) dissolved in toluene using homogeneous catalyst of Carsted (Sigma Aldrich, 2% Pt in xylol).

The membranes were prepared by casting reacting polymer solutions onto a cellophane support; then, the solvent was evaporated for 100–200 h under ambient conditions. Then membranes were conditioned in laboratory oven at 60 °C during 6 hours.

To study the permeability films were cast with thickness 100-110 μm. Permeability and diffusion coefficient of methane and butane through membranes were determined using Dynes-Barrer technique on the high precision apparatus of Helmholtz-Zentrum Geesthacht equipped with Baratron pressure sensor with accuracy 10⁻⁷ bar described elsewhere [2]. Sorption coefficient was calculated as a ratio of permeability to diffusion coefficient. The error in diffusion coefficient determination did not exceed 5% which corresponds well with [3].

Thermopervaporation experiments were conducted on the laboratory scale setup. The TPV module included liquid-carrying contours with different temperatures. In the first contour, a cooling agent thermostated with a thermostatic coolant was circulated. The second contour consists of the vessel containing the to-be-separated mixture, which was heated to a desired temperature with a heat exchanger, and a peristaltic pump. The accuracy of the maintained temperature was ±0.2°C. The temperatures of the feed mixture and the cooling agent at the

upstream and downstream sides of the TPV module were measured using the temperature detectors.

The module consisted of two mirror-symmetric flow chambers separated by a membrane and a cooling plate spaced by an air gap. The permeate was condensed against the cooling plate and removed from the module under the action of the force of gravity into a collector.

The working membrane area was 48 cm². Thermopervaporation process was conducted at a feed temperature of 40-70°C (± 0.2°C), and the downstream pressure was equal to the atmospheric pressure. The condensation temperature of the permeate was varied from 0 to 20°C.

Flux was estimated by weighting the collected permeate. Total permeate flux J [kg/m² h] was calculated as $J = m/(st)$ where m is the weight of the permeate [kg] passed through the membrane with area s [m²] within time t [h]. Separation factor for the binary mixture is calculated as

$$\alpha = \frac{Y/(1-Y)}{X/(1-X)}$$

where Y and X stand for the weight fractions of the target component (butanol) in the permeate and feed mixtures, respectively. Then, mass fluxes of butanol and water in the permeate are

$$J_b = J \cdot Y \text{ and } J_w = J - J_b.$$

Composition of the feed and permeate mixtures was analyzed by the method of gas chromatography on a Crystallux 4000 M gas chromatograph equipped with a TCD detector; the working parameters were the following: the injection temperature was 220°C, the column temperature was 180°C, and the detector temperature was 220°C. The probes were analyzed on a Porapak Q packed column. The water-butanol permeate (which is a two-phase system) was examined by adding water to homogenize the sample.

Results and Discussion

Permeability, diffusion and solubility coefficients of N₂, CH₄ and C₄H₁₀ through the PDMS/PMHS/SPB membrane different composition are shown in Table 1.

Table 1: Pure gas permeability, diffusion and solubility.

Membrane	Permeability coefficient, Barrer			Diffusion coefficient, 10 ⁻⁸ *cm ² /s			Solubility coefficient, 10 ⁻² *cm ³ (STP)/cm ³ cmHg		
	N ₂	CH ₄	C ₄ H ₁₀	N ₂	CH ₄	C ₄ H ₁₀	N ₂	CH ₄	C ₄ H ₁₀
PDMS/PMHS +40% wt SPB	172	550	9000	860	680	180	0.20	0.80	50
PDMS/PMHS +60% wt SPB	145	460	7500	800	640	160	0.18	0.71	46
PDMS/PMHS +90% wt SPB	22	60	730	200	143	20.5	0.11	0.42	36
PDMS	520	1650	18500	4500	2200	880	0.12	0.75	21

It is seen that with increasing of SPB content in the membrane material reduces its permeability. This apparently is due to a combination of PDMS and SPB transport properties: SPB has more than 2 orders of magnitude lower permeability coefficient compared to PDMS. Reduced permeability due to the decrease of penetrates diffusion coefficient that is caused by the difference in the segmental mobility of two polymers. SPB molecules are less flexible than the siloxane molecules, which increases the activation energy for molecule diffusion in membrane material. However, solubility coefficients values for all gases have maximum at SPB concentration in composition of 40% wt.

It should be noted that maximum solubility selectivity corresponds to SPB concentration of 90% wt, but the maximum permeability selectivity is observed for specimens 30 and 40% wt SPB,

which is accounted for by low diffusion selectivity. Furthermore, 30% wt SPB specimen has high permeability value compared to that of the PDMS, at the same time being 1.5 times more selective. So, these materials are promising for organochlorines removal from aqueous media.

Table 2: Pure gas permeability selectivity.

Membrane	Permeability Selectivity		Diffusion Selectivity		Solubility Selectivity	
	C ₄ H ₁₀ /CH ₄	C ₄ H ₁₀ /N ₂	C ₄ H ₁₀ /CH ₄	C ₄ H ₁₀ /N ₂	C ₄ H ₁₀ /CH ₄	C ₄ H ₁₀ /N ₂
PDMS/PMHS +30% wt SPB	52	16	0.21	0.26	250	63
PDMS/PMHS +40% wt SPB	52	16	0.20	0.25	255	65
PDMS/PMHS +70% wt SPB	33	12	0.10	0.14	330	86
PDMS	36	11	0.20	0.4	175	28

The report will be discussed the impact of the composition of the membrane material on its thermopervaporation properties in the allocation of butanol and organochlorine compounds from their aqueous solutions.

Acknowledgements

This work was supported by the Russian Foundation for Basic Research, project # 15-38-70041.

References

1. *M. Peng, L. M. Vane, S. X. Liu.* Recent advances in VOCs removal from water by pervaporation // *J. Hazard. Mater.* 2003. V. 98. N.1. P. 69-90.
2. *Macchione M., Jansen J. C., De Luca G., Tocci E., Longeri M., & Drioli E.* Experimental analysis and simulation of the gas transport in dense Hyflon® AD60X membranes: Influence of residual solvent // *Polymer.* 2007. V. 48. P. 2619-2635.
3. *Rogan Y., Starannikova L., Ryzhikh, V., Yampolskii Y., Bernardo P., Bazzarelli F., Jansen J. C., McKeown N. B.* Synthesis and gas permeation properties of novel spirobisindane-based polyimides of intrinsic microporosity // *Polymer Chemistry.* 2013. V. 4. N. 13. P. 3813-3820.

HIGHLY EFFICIENT COMPOSITE PTMSP MEMBRANES ON POLYSULFONE SUPPORTS FOR GAS-LIQUID MEMBRANE CONTACTORS

Ilya Borisov¹, Anna Ovcharova¹, Stepan Bazhenov¹, Rustem Ibragimov², Galina Bondarenko¹, Alexandr Bilyukevich³, Vladimir Volkov¹

¹A.V. Topchiev Institute of Petrochemical Synthesis, Moscow, Russia, *E-mail*: boril@ips.ac.ru

²Kazan National Research Technological University, Kazan, Russia

³Institute of Physical Organic Chemistry, National Academy of Sciences of Belarus, Minsk, Belarus

Introduction

Composite membranes have a number of advantages over asymmetric (Loeb-Sourirajan) ones. Thin-film composite (TFC) hollow fiber membranes are widely used due to the fact that they contain less than 1 g of selective polymer per square meter of the membrane; also, hollow fiber modules have high specific surface area which results in high productivity [1].

Deposition of fine defect-free selective layer requires highly efficient porous membrane support. Such membrane material as polysulfone (PSf) is widely used due to its mechanical, chemical and thermal stability [2]. Modified PSf membranes can be obtained in different ways including adding modifying macromolecules [3] or carbon nanotubes [4] to the polymer dope solution.

To achieve successful coating of the membrane, it is necessary to hydrophilize porous hydrophobic support [5]. Low-temperature plasma treatment allows to improve supports adhesion and wettability, as it activates upper surface molecular layers of the polymer. Another way of membrane modification is etching by Piranha – a mixture of H₂SO₄ and H₂O₂ (3:1). Piranha is highly oxidative and destroys organic contaminants on the polymer surface.

In the present work, the home-made porous asymmetric PSf hollow fiber supports were modified by means of low-temperature plasma treatment and Piranha etching. The membranes were analyzed using various techniques, such as scanning electron microscopy (SEM), gas permeance measurement, confocal scanning laser microscopy (CSLM), IR spectroscopy, contact angle measurement etc. The modified supports were used for deposition of fine poly[1-(trimethylsilyl)-1-propyne] (PTMSP) selective layer to obtain highly efficient composite membranes.

Experiments

The materials used to prepare spinning solutions were PSf pellets, Ultrason® S 6010 (BASF) and N-methylpyrrolidone (NMP 99% extra pure) supplied from Acros Organics, used as the base polymer and solvent, respectively. The pore-forming additive to the polymer solution was polyethylene glycol of average molecular weight 400 g/mole (PEG-400) supplied from Acros Organics. For membrane modification, 37% aqueous hydrogen peroxide solution and chemical pure concentrated sulfuric acid from Chimmed (Russia) were used.

The hollow fiber membranes were obtained via the dry-wet spinning technique, using water as both bore fluid and external coagulant. The hollow fibers prepared had selective layer on the lumen side. Experimental setup used for spinning is described elsewhere [6]. After spinning, the membranes were washed by water, exposed in ethanol and then in n-hexane to prevent capillary mesopores contraction.

Under membranes etching by Piranha mixture, process parameters (time, H₂SO₄ concentration, temperature) were varied. Low-temperature plasma treatment was carried out using the pilot-scale setup [5]. Air was used as plasma supporting gas (mass flux 0 – 0.24 g/s, pressure 110 Pa).

For preparation of composite membranes, PTMSP (Gelest, USA) solution in n-hexane was used; the polymer solution was forced into the fibers lumen. The PTMSP selective layer integrity was confirmed by gas permeance measurements.

The membranes prepared were characterized by means of gas permeance and contact angle measurement, SEM, CSLM, Fourier transform IR spectroscopy and X-ray Photoelectron Spectroscopy (XPS).

Results and Discussion

The cross section and outer surface SEM micrographs were obtained for both virgin and treated HF membranes. Outer surface of the virgin HF membrane, as well as air plasma and piranha mixture treated membranes images are shown in Figure 5 (a–c), respectively. It is clear that air plasma modified fiber has macroscopic defects on the outer surface and it proves that plasma does affect the membrane material. On the other hand, the fiber modified by piranha mixture does not seem to differ from the unmodified specimen. Figure 5 (c, d) shows cross section images of the virgin and treated hollow fibers. It can be observed that modification does not affect the membrane internal macrostructure. The fibers have similar geometrical parameters like outer and inner diameter values and wall thickness. The outer diameter value is 1.52–1.55 mm, the inner is 1.03–1.05 mm.

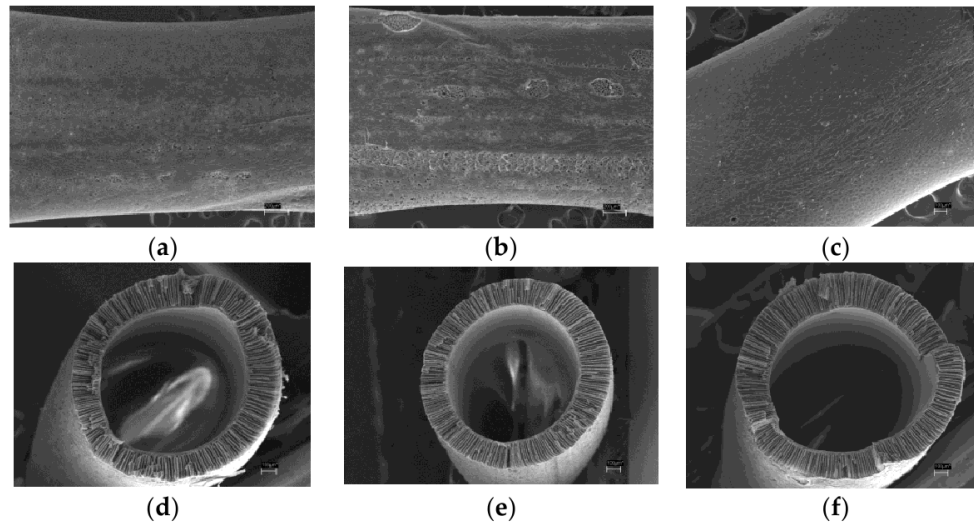


Figure 1. Image segment of the fiber outer surface, 100× magnification: (a) virgin membrane;

(b) air plasma treated membrane; (c) Piranha treated membrane; fiber cross section image, 130× magnification: (d) virgin membrane; (e) air plasma treated membrane; (f) Piranha treated membrane

After modification, contact angle and free surface energy values were obtained for both unmodified and modified fibers. The results are given in Table 1.

Table 1: Contact angle (θ) and free surface energy (γ_s) values for the unmodified and modified hollow fibers

Parameter	Unmodified membrane	Air plasma treated membrane	Piranha modified membrane
$\theta_{av}(\text{H}_2\text{O}), ^\circ$	81	59	63
$\theta_{av}(\text{ethylene glycol}),$	70	45	52
γ_{av}^s	24	42	39

The membrane treated by air plasma was chosen as a porous support for fabricating composite hollow fiber membranes with thin PTMSP dense layer, as it had the highest oxygen-containing functional groups concentration and also the highest free surface energy value (more phobic to hydrocarbons).

Si and S elemental profiles for selective top layer obtained by the electron probe microanalysis (EPMA) technique showed that silicon concentration is maximum on the membrane surface and decreases with probing depth increase. The calculated PTMSP layer thickness value was $4.5 \pm 0.5 \mu\text{m}$. Taking into account the method error, it can be concluded that PTMSP penetrates into support pores to the depth of $6.5 \pm 0.5 \mu\text{m}$.

Table 2 shows gas permeance and ideal selectivity values for the fabricated TFC membrane.

Table 2: Gas permeance of composite hollow fiber membranes with thin PTMSP dense layer on the inner surface of air plasma treated porous PSf support

Parameter	Composite membrane permeance and ideal selectivity
P/I (N ₂), GPU	320
P/I (CO ₂), GPU	1500
α (CO ₂ /N ₂)	4.7

Henis-Tripodi computation allowed to determine that 77.35% of gas transport resistance is driven by the PTMSP layer which penetrated into the support pores; the contribution of the support and the selective layer is 0.45% and 22.2%, respectively. For similar PSf membranes (not modified by air plasma), surface porosity is 0.4%. Composite PTMSP membranes on non-modified PSf supports have CO₂ permeance 96 GPU with 98.6% PTMSP layer in the support pores contribution in the overall mass transport resistance. Therefore, surface modification of the PSf membranes by air plasma allows for 2 order surface porosity increase, which, in turn, provides an opportunity to obtain composite membranes having the permeance order of magnitude greater than that of the membranes with non-modified support. It can be concluded that such membranes are promising for employing them in gas-liquid membrane contactors.

Acknowledgements

This work was performed at the Topchiev Institute of Petrochemical Synthesis and supported by the Russian Science Foundation, project no. 14-49-00101.

References

1. *Mansourizadeh A., Ismail A. F.* Hollow fiber gas-liquid membrane contactors for acid gas capture: a review // *J. Hazard. Mater.* 2009. V. 171. P. 38-53.
2. *Schott K.* Handbook of Industrial Membranes, 2nd ed., Elsevier NY., 1997.
3. *Korminouri F., Rahbari-Sisakht M., Matsuura T., Ismail A. F.* Surface modification of polysulfone hollow fiber membrane spun under different air-gap lengths for carbon dioxide absorption in membrane contactor system // *Chem. Eng. J.* 2015. V. 264. P. 453-461.
4. *Plisko T., Bilyukevich A., Volkov V., Osipov N.* Formation of hollow fiber membranes doped with multiwalled carbon nanotube dispersions // *Petr. Chem.* 2015. V. 55. P. 318-332.
5. *Borisov I., Ovcharova A., Bakhtin D., Bazhenov S., Volkov A., Ibragimov R., Gallyamov R., Bondarenko G., Mozhchil R., Bilyukevich A., Volkov V.* Development of Polysulfone Hollow Fiber Porous Supports for High Flux Composite Membranes: Air Plasma and Piranha Etching // *Fibers.* 2017. V. 5. P. 6.
6. *Bilyukevich, A., Plisko T., Liubimova A., Volkov V., Usosky V.* Hydrophilization of polysulfone hollow fiber membranes via addition of polyvinylpyrrolidone to the bore fluid // *J. Membr. Sci.* 2017. V. 524. P. 537-549.

POLYDIMETHYLSILALKYLENE-DIMETHYLSILOXANES - NEW MEMBRANE MATERIALS FOR SEPARATION BUTANOL FROM WATER VIA THERMOPERVAPORATION

Ilya Borisov, Nikolai Ushakov, Evgenia Grushevenko, Vladimir Volkov, Eugene Finkelshtein

A.V. Topchiev Institute of Petrochemical Synthesis, Moscow, Russia, *E-mail: boril@ips.ac.ru*

Introduction

Oxygen-containing additives for motor fuels (oxygenates) are high-performance commercial antiknock agents. According to the Technical Regulations of the Customs Union [1], the use of antiknock additives based on aromatic amines and/or oxygenates only is allowed.

At the same time, oxygenates are pollutants in wastewaters from the Fischer–Tropsch process and at refineries and petrochemical plants.

To solve the problem of recovery of oxygenates from aqueous reaction media, we for the first time offer using a version of pervaporation (evaporation through a membrane), namely, thermopervaporation (TPV), which has proved to be a promising method for the recovery of alcohols from aqueous media lately, together with extraction and adsorption [2].

Currently, pervaporation membranes (PMs) on the basis of silicon rubbers (first of all, PDMS), which do not provide selectivity that is sufficiently high to make pervaporative separation commercially viable when compared to the traditional separation of liquids by distillation [3], are used in industry for the recovery of oxygen-containing organic substances from aqueous media [3, 4]. In this work we create silicon materials based on polydimethylsildimethylene-dimethylsiloxane (PSDMS) and polydimethylsiltrimethylene-dimethylsiloxane (PSTMS) that possess enhanced selectivity in the thermopervaporative recovery of oxygenates from aqueous media and study their transport properties on a model water–butanol feed system [5].

Experiments

To obtain high-molecular-weight PSDMS and PSTMS (as well as polysiloxanes) via ring-opening polymerization, the corresponding high-purity cyclic monomers 2,2,5,5-tetramethyl-1-oxa-2,5-disilacyclopentane (1) and 2,2,6,6-tetramethyl-1-oxa-2,6-disilacyclohexane (2), respectively, are needed. We assessed three possible ways for the synthesis of 1, two of which are based on cyclization reactions with the formation of a siloxane bond.

To obtain PSDMS via ring-opening polymerization, solvent-free anionic polymerization of 1 initiated by tetrabutylammonium hydroxide at room temperature was used. Cationic polymerization mediated by trifluoromethanesulfonic acid turned out to be more efficient for the polymerization of monomer 2. The presence of terminal hydroxyl groups in PSDMS and PSTMS determined the method for PM fabrication from these materials, which is based on their controllable crosslinking via a reaction with tetraethoxysilane. Yields of polymers were from 76 till 93 %.

The membranes were prepared by casting polymer solutions in hexane onto a cellophane support; then, the solvent was evaporated for 100–200 h under ambient conditions, then membranes were conditioned in vacuum oven at 80°C during 5h. The ratio polymer: TEOS: catalyst was 10: 1: 0.2 wt. %. The film thickness was varied in the range of 40-44 microns. The diameter of the membranes was 7.5 cm. Membranes **MI** and **MII** were obtained on the basis of PSDMS and PSTMS polymers, respectively.

Thermopervaporation experiments were conducted on the laboratory scale setup. The TPV module included liquid-carrying contours with different temperatures. In the first contour, a cooling agent thermostated with a thermostatic coolant was circulated. The second contour consists of the vessel containing the to-be-separated mixture, which was heated to a desired temperature with a heat exchanger, and a peristaltic pump. The accuracy of the maintained temperature was $\pm 0.2^\circ\text{C}$. The temperatures of the feed mixture and the cooling agent at the upstream and downstream sides of the TPV module were measured using the temperature detectors.

The module consisted of two mirror-symmetric flow chambers separated by a membrane and a cooling plate spaced by an air gap. Permeate was condensed against the cooling plate and removed from the module under the action of the force of gravity into a collector.

The working membrane area was 48 cm². Thermopervaporation process was conducted at a feed temperature of 40-70°C (± 0.2°C), and the downstream pressure was equal to the atmospheric pressure. The condensation temperature of permeate was varied from 0 to 20°C.

Flux was estimated by weighting the collected permeate. Total permeate flux J [kg/m² h] was calculated as $J = m/(s \cdot t)$ where m is the weight of the permeate [kg] passed through the membrane with area s [m²] within time t [h]. Separation factor for the binary mixture is calculated as

$$\alpha = \frac{Y/(1-Y)}{X/(1-X)}$$

where Y and X stand for the weight fractions of the target component (butanol) in the permeate and feed mixtures, respectively. Then, mass fluxes of butanol and water in the permeate are

$$J_b = J \cdot Y \text{ and } J_w = J - J_b$$

Composition of the feed and permeate mixtures was analyzed by the method of gas chromatography on a Crystallux 4000 M gas chromatograph equipped with a TCD detector; the working parameters were the following: the injection temperature was 220°C, the column temperature was 180°C, and the detector temperature was 220°C. The probes were analyzed on a Porapak Q packed column. The water-butanol permeate (which is a two-phase system) was examined by adding water to homogenize the sample.

Results and Discussion

Data on the isolation of organic compounds from aqueous media via the TPV method are very limited. In order to compare the results obtained under different conditions including in the vacuum pervaporation, the data were presented in terms of permeability and permselectivity.

Table 2 shows the comparison of the permeability coefficients of the proposed membranes, a monolithic 400- μ m PDMS film, and the best samples of composite PDMS membranes presented in scientific literature [7]. As can be seen from Table 1, permeability coefficients for PDMS films in TPV and vacuum pervaporation are close, which suggests the applicability of this way

Table 1. A gas transport property of MI and MII membranes at 30 ° C and a partial pressure tends to 0

Membrane material	P_{BuOH} Barrer	P_w Barrer	Selectivity	Recalculated from
PSTMS 40 μ m	25700	7900	3,3	^a This work
PSDMS 40 μ m	31100	12800	2,5	^a This work
PDMS 40 μ m	42000	22600	1,9	^a This work
PDMS 400 μ m	49300	22300	2,0	^b [7]
PDMS 30 μ m on PVDF	61300	35600	1,7	^b [8]
PDMS 10 μ m on ceramics	92500	56500	1,6	^b [9]
PDMS 4 μ m on PAN	24600	29400	0,8	^b [10]
Pervatech PDMS	-	-	0,7	^a [11]

^aTPV ^bVPV

of presenting data. When applying a selective layer of PDMS onto porous supports, deviations from the values of permeability coefficients for the films are observed, both upwards [8, 9] and downwards [10]. According to the authors of [9], factors such as the viscosity of the solution of PDMS during application, pore size, and structure of the porous support play a crucial role for the

transport properties of a membrane. The permselectivity decreases with the decrease in the membrane thickness and becomes less than 1 for membranes with the layer of PDMS below 10 μm . For membranes with the thickness of the layer of PDMS above 10 μm , the selectivity varies within 1.6–2.0. It should be noted that the selectivity for PSDMS is 1.5-fold, while for PSTMS, almost twofold higher when compared to the selectivity of PDMS membranes at comparable values of permeability coefficients with respect to butanol. Therefore, by changing the length of the hydrocarbon fragment of polycyclocarbosiloxanes in the main chain, membranes with predetermined pervaporative characteristics can be created.

Thereby, by varying the length of the hydrocarbon fragment in the main chain of polycyclocarbosiloxanes sorption-selective materials with desired transport can be obtained.

Acknowledgements

This work was supported by the Russian Foundation for Basic Research, project # 15-08-06906.

References

1. *TR TS (Technical Regulations of the Customs Union) 013-2011: About Requirements to Motor and Aviation Gasoline, Diesel and Marine Fuel, Jet Fuel, and Fuel Oil.* 2.
2. H. J. Huang and S. Ramaswamy // *Sep. Purif. Technol.*, 2014, 132, 513.
3. L. M. Vane // *J. Chem. Technol. Biotechnol.*, 2005, V. 80, 603.
4. G. Liu, W. Wei, and W. Jin // *ACS Sustain. Chem. Eng.*, 2013, V. 2, 546.
5. I. L. Borisov, N. V. Ushakov, V. V. Volkov, and E. Sh., Finkel'shtein // *Izv. Akad. Nauk, Ser. Khim.*, 2016. No. 4, 1020.
6. I.L.Borisov, N.V.Ushakov, V.V.Volkov, E.Sh.Finkel'shtein. // *Petrol. Chem.*, 2016, V. 56, №9 798–804
7. M. H. V. Mulder, *Basic Principles of Membrane Technology* (Kluwer Academic, Dordrecht, 1990).
8. S. F. Li, F. Qin, P. Y. Qin, et al. // *Green Chem.*, 2013, V.15, 2180.
9. Z. Dong, G. Liu, S. Liu, et al. // *J. Membr. Sci.*, 2014, V. 450, 38.
10. J. Niemisto, W. Kujawski, and R. L. Keiski // *J. Membr. Sci.*, 2013, V. 434, 55.
11. A. Kujawska, J. Kujawski, M. Bryjak, and W. Kujawski // *Chem. Eng. Process.: Proc. Intens.* 2015, V. 94, 62.

POLYMERIC MEMBRANE FORMATION - INTERPLAY BETWEEN PROCESS CONDITIONS AND FINAL MORPHOLOGY. A COUPLING BETWEEN EXPERIMENTAL AND MODELING APPROACHES

Denis Bouyer

European Institute of Membranes, UM, Montpellier, France, *E-mail: denis.bouyer@umontpellier.fr*

Introduction

Polymeric membranes are usually fabricated by phase inversion methods: a thermodynamic instability is provoked from homogeneous polymeric system by temperature and/or composition change, thus inducing the formation of a lean polymer phase (the pores of the membrane after solvent extraction) and a rich polymer phase.

The final morphology of the membrane depends on the initial formulation, i.e. the system polymer/solvent/non-solvent and the mass and heat transfer mechanisms involved in the phase inversion process. Once the formulation is fixed, the structuration dynamics depends on the time scales of the material (liquid-liquid and liquid-solid demixing) and on the time scales of the transfers (diffusion, mass and heat exchanges) (Figure 1) [1, 2].

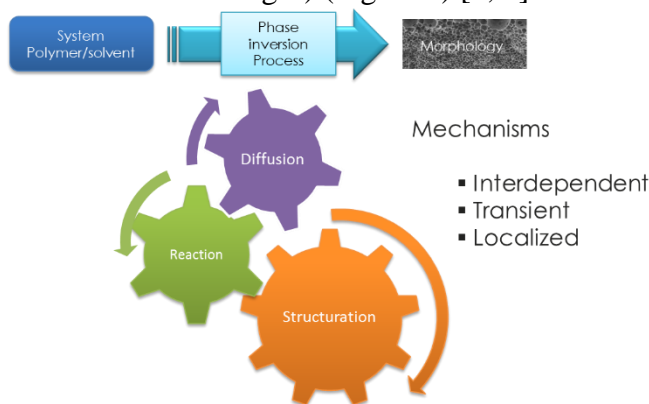


Figure 1. interplay between diffusion, phase inversion dynamics and reaction during membrane formation

Polymeric porous membranes characterized by macrovoids, cellular or nodular pore structure, lacy structure can be formed depending on the operating conditions. Nevertheless, the membrane formation is usually conducted by trial and error testing. Modeling the membrane formation mechanisms is therefore a crucial issue.

To bring new insights in the membrane modelling elaboration field, we developed an experimental method to obtain *in-situ* and *in-line* measurements of the solution composition during the VIPS process, prior to demixtion. In this respect, the numerical model could be validated using experimental composition profiles in the polymer solution rather than morphological properties of final membranes (Figure 2) [3]. The modeling approach was used to better understand the polymeric membrane formation mechanisms, for different kinds of applications [4, 5, 6].

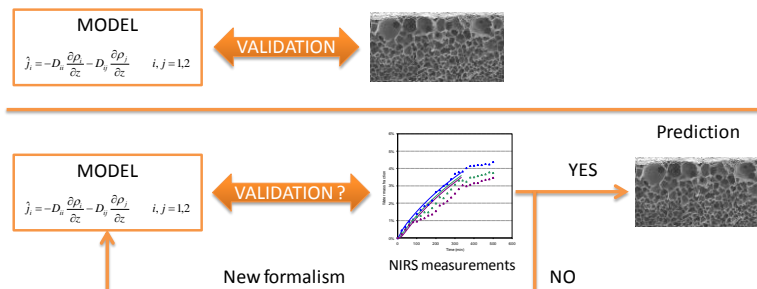


Figure 2. new procedure for validating the model before a comparison with membrane morphology

Methods

The numerical model involved a coupling between mass and heat transfer phenomena because of the exothermic water absorption involved in the process; cross diffusion equations were integrated in the continuity equation and classical diffusion formalism was used to correlate the self- and mutual-diffusion coefficients. The self-diffusion coefficients were estimated using the free volume theory of Vrentas and Duda and the external mass and heat transfer coefficients were determined using semi-empirical correlations. The thermodynamic was given by the Flory-Huggins theory (Table 1).

Table 1: main equations of the numerical model

Thermodynamic	$\frac{\Delta G_m}{RT} = \sum_{i=1}^3 n_i \ln \phi_i + g_{12} n_1 \phi_2 + \chi_{13} n_1 \phi_3 + \chi_{23} n_2 \phi_3$ and $\frac{\Delta \mu_i}{RT} = \frac{\partial}{\partial n_i} \left(\frac{\Delta G_m}{RT} \right)_{n_j, j \neq i}$
Continuity equation	$\frac{\partial \rho_i}{\partial t} = \frac{\partial}{\partial z} \left(- \sum_{j=1}^2 D_{ij} \frac{\partial \rho_j}{\partial z} \right) \quad i = 1, 2$
Diffusion formalism	$D_{ik} = \left[1 - \rho_j \hat{V}_i \left(1 - \frac{\alpha_i}{\alpha_3} \right) \right] \rho_i D_i \left(\frac{1}{RT} \frac{\partial \mu_i}{\partial \rho_k} \right) - \sum_{j=1}^2 \left(1 - \frac{\alpha_j}{\alpha_3} \right) \rho_j \hat{V}_j \rho_i D_j \left(\frac{1}{RT} \frac{\partial \mu_j}{\partial \rho_k} \right) \quad i, k = 1, 2$
Self-diffusion coefficient	$D_i = D_{0i} \exp \left(- \frac{w_i \hat{V}_i^* + w_j \hat{V}_j^* (\xi_{i3} / \xi_{j3}) + w_3 \hat{V}_3^* \xi_{i3}}{\hat{V}_{FH} / \gamma} \right) \quad i, j = 1, 2$
Mass and heat transfer	Mass transfer: $\frac{k_i L_c}{D_{ig}} Y_{air,lm} = 0.27 (Gr Sc_i)^{0.25}$ Heat transfer: $\frac{h_e L_c}{\lambda_g} = 0.27 (Gr Pr)^{0.25}$

The model was fully predictive and did not contain any adjustable parameter. The experimental validation was conducted using the Near Infrared Spectroscopy: the polymer solution was placed in a cell and exposed to humid vapours to induce the phase separation. The NIRS allowed (i) following the solution composition at three points during the VIPS process, until demixion (Figure 3), and therefore (ii) validating the model.

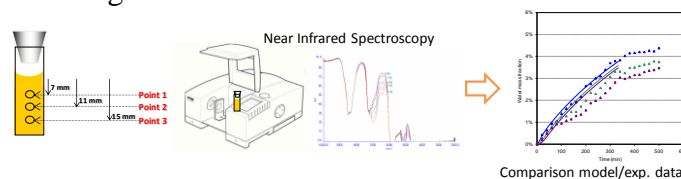


Figure 3. local measurements in the solution using Near Infrared Spectroscopy

Results

The system PEI/NMP/water was used in this work and the influence of both the formulation and the process parameters was investigated by this coupled experimental and modelling approach. At 12 wt-% of polymer, the model predictions were in good agreement with the experimental results, whatever the process conditions (Figure 4).

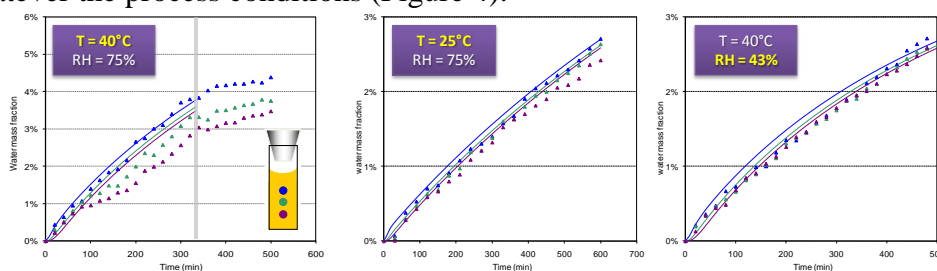


Figure 4. comparison between numerical predictions and experimental data

At higher polymer concentration (20 wt-%), the model overestimated the water transfer rate. Rheological measurements have been performed to understand this deviation and it was exhibited that a gelation phenomenon occurred at high polymer concentration, all the sooner since the water concentration increased, leading to reducing the mass transfer rate in the polymer matrix. So, the model was modified to take into account this phenomenon, leading to improving the agreement between the numerical and experimental results. The model predictions were then compared to

experimental data for other formulation (16 wt-%) and process (HR, T) conditions to prove its accuracy and reliability.

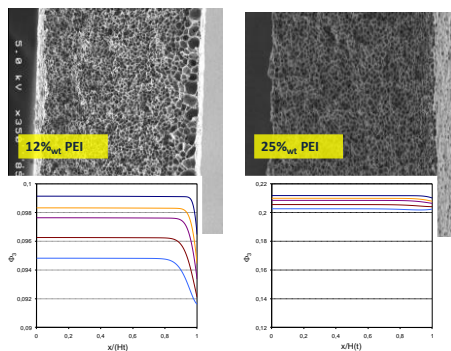


Figure 4: comparison between simulated concentration profiles and cell size gradient in membrane cross section at two polymer concentrations – PEI/NMP/water system

Figure 5. Comparison between simulated concentration profiles and cell size gradient in membrane cross section at two polymer concentrations - PEI/NMP/water system

Discussion

Once the model was validated using local measurements, it could be used to better understand the various membrane morphologies obtained in various operating conditions. The model was thus used in the thin film geometry (250 μm), i.e. the real conditions for membrane preparation. SEM images of membrane cross sections were made for the PEI/NMP/water system at low (12 wt-%) and high (20 wt-%) polymer concentration, and then they were compared to simulated polymer concentration profiles calculated at the demixtion time from the bottom ($x/H=0$) to the air/solution interface ($x/H=1$) (Figure 4). The membrane asymmetry observed at 12 wt-% was explained by the significant polymer concentration gradient near the air/solution interface induced by rapid water intake rate during VIPS process. Because of slower transfers, the concentration profiles were quite plate at 20 wt-% of polymer and therefore the membranes were symmetric with uniform cell size along the membrane thickness.

Lastly, the model was used as a predictive tool for choosing the appropriate operating conditions (formulation and/or process conditions) to control the membrane morphology, and especially the cell size profiles from the bottom to the top of the membrane.

References

- [1] Y.S. Su, C.Y. Kuo, D.M. Wang, J.Y. Lai, A. Deratani, C. Pochat, D. Bouyer, Interplay of Mass Transfer, Phase Separation, and Membrane Morphology in Vapor-Induced Phase Separation, *Journal of Membrane Science*, 338(1-2), 17-28 (2009)
- [2] A. Venault, A.J.J Leyba, F-C. Chou, D. Bouyer, I-J. Lin, T-C. Wei, Y. Chang, Design of near-superhydrophobic/superoleophilic PVDF and PP membranes for the gravity-driven breaking of water-in-oil emulsions, *JTICE*, 65, 459-471 (2016)
- [3] D. Bouyer, C. Pochat-Bohatier, Validation of mass transfer model for VIPS process using in-situ measurements performed by Near Infrared Spectroscopy, *AIChE Journal*, 59(2), 671-686 (2013)
- [4] A. Venault, D. Bouyer, C. Pochat, L. Vachoud, C. Faur, Modeling the mass transfer during the elaboration of chitosan-activated carbon composites for medical applications, *AIChE Journal*, 56(6), 1593-1609 (2010)
- [5] D. Bouyer, L. Vachoud, Y. Chakrabandhu, C. Pochat-Bohatier, Influence of mass transfer on gelation time using VIPS-gelation process for chitin dissolved in LiCl/NMP solvent – modelling and experimental study, *Chemical Engineering Journal*, 157, 605-619 (2010)
- [6] Denis Bouyer, Oualid M'Barki, Céline Pochat-Bohatier, Catherine Faur, Eddy Petit, Patrick Guenoun, Modeling the membrane formation of novel PVA membranes for predicting the composition path and their final morphology, *AIChE Journal* (2017)

WATER SPLITTING IN MB-2 BIPOLAR MEMBRANE, MODIFIED BY CHROMIUM(III) HYDROXIDE

Anastasya Boyarishcheva, Nikita Kovalev, Nikolay Sheldeshov, Victor Zabolotsky
Kuban State University, Krasnodar, Russia, E-mail: sheld_nv@mail.ru

Introduction

Using transition metal hydroxides to improve electrochemical characteristics of the bipolar membrane (BPM) was proposed firstly in [1]. In [2] methods of modification of MB-2 bipolar membrane analog (aMB-2) by d-metal hydroxides were compared, and it was shown that the best characteristics has membrane in which hydroxides were introduced by sequential treatment of cation exchange membrane by metal salt solution and alkali solution. However, stability of introduced chromium (III) hydroxide as catalytic additive in bipolar membrane in the processes of conversion of salt to acid and alkali, as well as stability of chromium (III) hydroxide to additional thermal treatment of membranes during hot pressing were not investigated.

Therefore, the aim of this work was to study the effect of temperature on the modification of cation exchange layer of bipolar membrane on its electrochemical characteristics and the stability of the introduced catalyst additive under the conditions of obtaining acid and alkali from the salt for 4-6 hours.

Experiments

The object of the study was modified bipolar MB-2 membrane analog, obtained by hot pressing of cation (Ralex CMH) and anion (Ralex AMH) exchange membranes. Bipolar membranes modified by chromium (III) hydroxide, were obtained by chemical precipitation of hydroxide in the cation-exchange membrane phase by sequential chemical treatment with solutions of the metal salt and alkali. Prior to pressing, the cation exchange membrane was heated in a thermo box at temperatures in the range of 120-190°C for 7 minutes. In addition, bipolar membranes were modified with chromium (III) sulfate and alkali at different time of treatment.

Electrochemical characteristics of bipolar membrane were measured by the electrochemical impedance method using a virtual impedance meter analyzer in 1 Hz – 1 MHz frequency range at 25°C in a flowing four-electrode cell, concentrations of sulfuric acid and sodium hydroxide were 0.1 mol-eq./l, the active area of the membrane was 2.27 cm². The amplitude of the alternating measuring voltage across the membrane was 50 mV. Relative error of impedance module was less than 5%. The dependence of resistance of the bipolar region R_b (where $R_b = R_0 - R_\infty$, R_0 is membrane resistance at "low" frequency, R_∞ is membrane resistance at "infinitely high" frequency) on electric current were calculated from the frequency spectra of the membrane impedance measured at different currents. Overvoltages of bipolar region of the membrane were calculated by Equation (1)

$$\eta_b = \int_0^{I^*} R_b dI \quad (1)$$

from dependence of the resistance of the bipolar region on electric current.

Stability of introduced chromium (III) hydroxide in bipolar membrane in the processes of conversion of salt to acid and alkali were studied at 2,46 A/dm² current density and circulation of 0,25 mol/l H₂SO₄ and 0,5 mol/l NaOH solutions through the measuring chambers of the cell. The potential difference on the bipolar membrane was measured for 4-6 hours.

Results and Discussion

Analysis of partial voltage-current characteristics of bipolar membranes modified by chromium (III) hydroxide (Figure 1) shows that heating in the range from 124°C to 164°C after cation exchange membrane modification reduces the overvoltage compare with the modified membrane without additional heating. However, heating in the range from 164°C to 190°C increases the overvoltage of the bipolar region of the membrane (Figure 2). It is can be caused by several

reasons: partial dehydration of chromium (III) hydroxide, change in the structure of chromium (III) hydroxide or penetration of polyethylene into bipolar region.

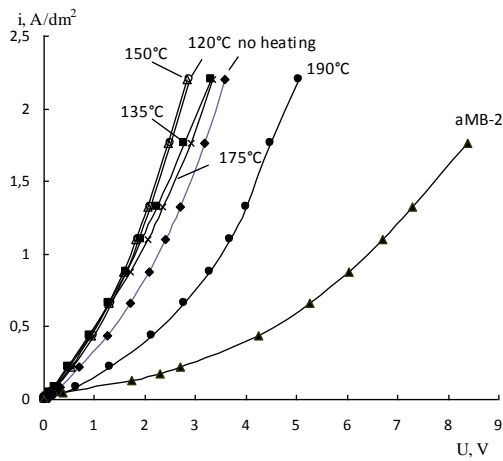


Figure 1. Partial voltage-current characteristics of bipolar region of the membranes modified by chromium (III) hydroxide at different temperatures of heating

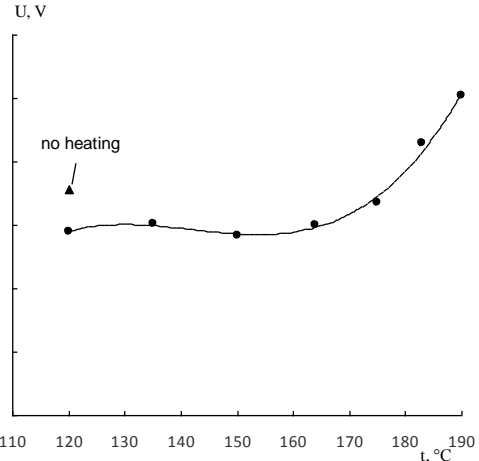


Figure 2. Dependence of the bipolar region overvoltage of membranes modified by chromium hydroxide (III) on temperature of heating

Comparison of partial voltage-current characteristics of bipolar membranes modified by chromium (III) chloride and chromium (III) sulfate shows that the values of the overvoltage of the resulting membranes do not depend on the type of the chromium(III) salt used for chemical deposition of chromium (III) hydroxide into the bipolar region (Figure 3). The catalytic addition of chromium (III) hydroxide significantly reduces the resistance of the bipolar region of the membrane (Figure 4) compared with initial aMB-2 membrane.

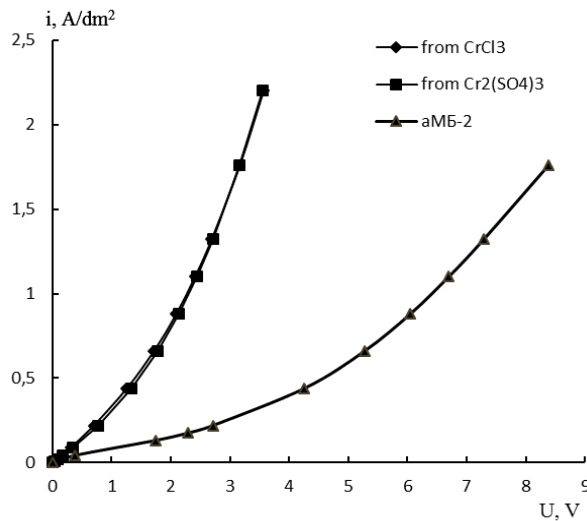


Figure 3. Partial voltage-current characteristics of bipolar region of the membranes modified by chromium (III) hydroxide obtained from chromium (III) chloride and chromium (III) sulfate

The resistance of the bipolar region of the membrane modified with chromium (III) hydroxide decreases with increasing current (Figure 4) due to increase in the electric field strength in the space charge region in the bipolar region of the membrane and, as a consequence due to increase of the rate of dissociation of water molecules at chromium (III) hydroxide as catalytic additive. The resistance of the bipolar region also depends on the time of treatment of cation layer by the chromium (III) salt and sodium hydroxide. The more treatment time of cation layer the less the overvoltage of the bipolar region of the membrane (Figure 5). The addition of chromium (III) hydroxide into the bipolar region of the membrane allows to decrease the resistance of the bipolar region of the membrane (Figure 5) by approximately 10-15 times compared to the initial aMB-2 membrane (Figure 1).

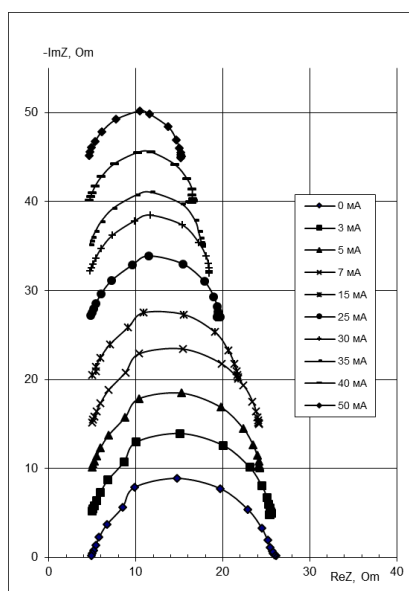


Figure 4. Frequency spectra of the electrochemical impedance of a bipolar membrane with chromium (III) hydroxide at 120 minutes treating time, measured at different currents

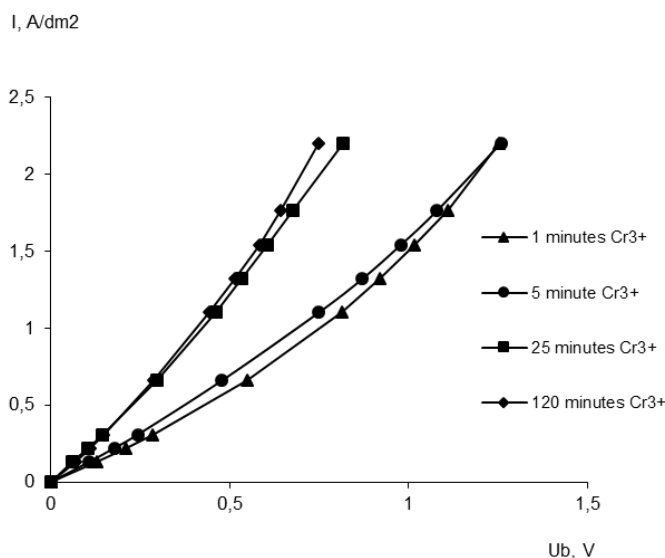


Figure 5. Partial voltage-current characteristics of the bipolar region of the membranes modified by chromium (III) hydroxide

The voltage drop at the modified bipolar membranes remains constant for at least 4-6 hours in the galvanostatic mode (Figure 6) during conversion of Na_2SO_4 into 0,25 mol/l H_2SO_4 and 0,5 mol/l NaOH solutions. This indicates the stability of chromium (III) hydroxide, introduced into the membrane, under the conditions of the process.

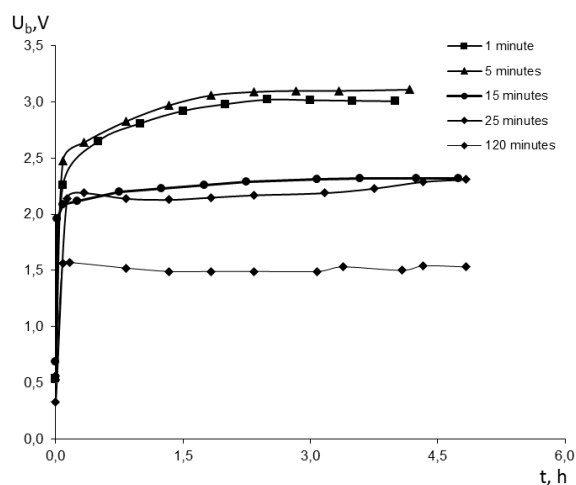


Figure 6. Dependence of the voltage drop on the bipolar membrane modified by chromium (III) hydroxide on time during conversion of Na_2SO_4 into 0,25 mol/l H_2SO_4 and 0,5 mol/l NaOH solutions. The numbers near lines are treatment time of cation layer by the chromium (III) salt and sodium hydroxide

The present work is supported by the State Task of the Ministry of Education and Science of the Russian Federation, project No. 10.3091.2017 / PP.

References

1. Simons R. Preparation of a high performance bipolar membrane // J. Membr. Sci. 1993. V. 78. P. 13-23.
2. Mel'nikov S.S., Shapovalova O.V., Shel'deshov N.V., Zabolotsky V.I. Effect of d-metal hydroxides in the water dissociation in bipolar membranes // Petroleum Chemistry. 2011. V. 51. No. 7. P. 573-580.

EXPERIMENTAL AND THEORETICAL INVESTIGATION OF SURFACE GEOMETRICAL HETEROGENEITY OF HOMOGENEOUS ION-EXCHANGE MEMBRANES USING SCANNING ELECTROCHEMICAL MICROSCOPY METHOD

¹Dmitrii Butylskii, ¹Semyon Mareev, ²Christian Larchet, ²Lasaad Dammak, ¹Natalia Pismenskaya, ¹Victor Nikonenko

¹Membrane Institute, Kuban State University, Krasnodar, Russia, *dmitrybutylsky@mail.ru*

²Institut de Chimie et des Matériaux Paris-Est, UMR 7182 CNRS – Université Paris-Est, 2 Rue Henri Dunant, 94320 Thiais, France

Introduction

It is known that the ion exchange membrane (IEM) surface can be undulated [1]. Traditional methods of determination of the membrane surface undulation are optical interferometry [1], scanning electron microscopy (SEM) [2] and atomic force microscopy (AFM) [3]. The conventional SEM and AFM techniques are applicable only to dry membrane samples. However, it is often of interest to know the undulation parameters of swollen membranes, which are thicker than the dry ones [4]. Therefore, the SEM and AFM methods will give distorted results.

Our work showcases the application of Scanning Electrochemical Microscopy (SECM) method [5] for investigation of surface undulation of homogeneous ion-exchange membranes in swollen state.

Experiments

A Neosepta CMX homogeneous cation-exchange membrane, produced by Astom Corp., Japan, was studied using the SECM setup described in our previous work [6]. This membrane is prepared by the so-called “paste method” and considered to be homogeneous.

We visualized the surface of CMX membrane with aid of SECM (Fig. 1a). All measurements were conducted in 0.02 M NaCl solution at current density of $0.4 j_{lim}$.

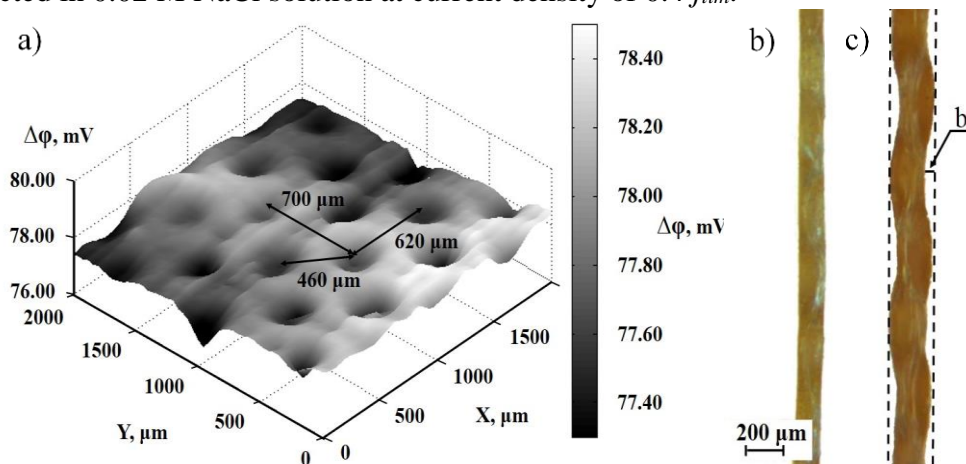


Figure 1 - Topography of potential drop distribution near the surface of the CMX membrane (a), optical cross section images of the dry (b) and swollen (c) CMX membrane

Results and Discussion

The results of investigation of the commercial CMX membrane surface using SECM method are given in Fig. 1a. Minima and maxima in the potential distribution maps correspond to the hills and valleys of the membrane surface, respectively. It was found that the surface of commercial CMX membrane is not smooth and flat, but it is undulated, as Fig. 1c shows.

Our SECM results (Fig. 1a) display that the surface of swollen CMX membrane possesses repeating hills and valleys with the distance between the tops of two hills about $620 \mu\text{m}$ in the X direction and $700 \mu\text{m}$ in the Y direction (Fig. 1a); the distance between the tops of two neighboring hills is $460 \mu\text{m}$. Optical micrographs of cross section of the membranes allow evaluating the amplitude of the curvature b , for the dry (Fig. 1b) and swollen membrane (Fig. 1c). The value of b was $5 \pm 5 \mu\text{m}$ for the dry membrane and $50 \pm 5 \mu\text{m}$ for the swollen one.

We attribute this undulation to unequal swelling of the membrane, which is caused by the presence of reinforcing grid and unequal distribution of ion-exchange material.

A two-dimensional stationary model of ion transport through the membrane and two adjacent diffusion boundary layers is proposed.

The real surface of homogeneous membrane is too complex to be described by mathematical means. In this case the transition to simplified representation of surface is needed (Fig. 2a). The unit cell of the membrane surface can be considered as a circle, which corresponds to the valley around a hill. Ion transport in the system is described by the Nernst-Planck and the material balance equations under the local electroneutrality assumption.

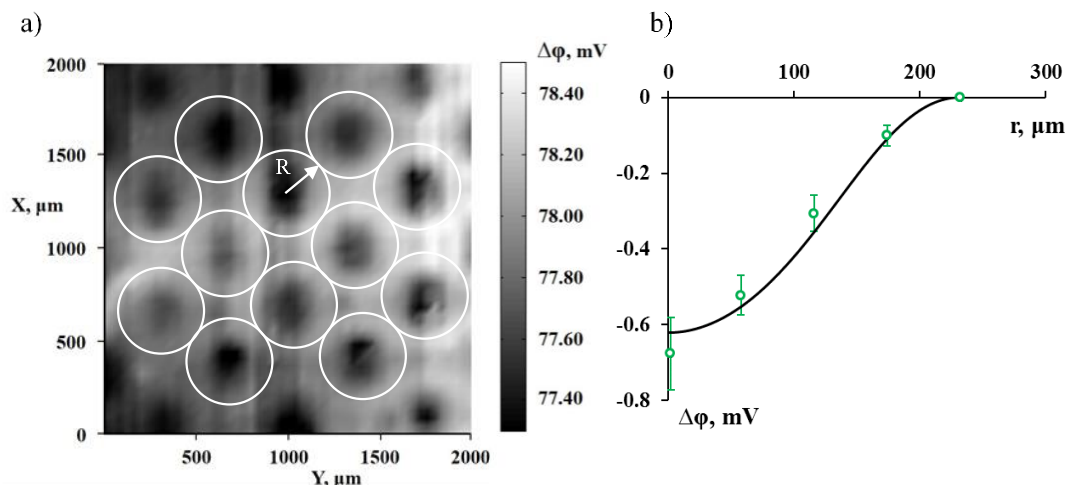


Figure 2 - Circles separate out the uniformly distributed areas of the same radius $R=230 \mu\text{m}$, which are simulated using the developed model (a). Comparison of experimental (points with confidence interval) and calculated (curves) distributions of potential near the surface of a CMX membrane in the plane spaced from the hilltop at a distance of 20 mm (b)

The results of potential distribution simulation are compared with experimental data (Fig. 2b). The fitting parameter b was estimated as $44 \pm 2 \mu\text{m}$ by matching experimental and theoretical potential drop distributions.

There is a significant correlation between the average value of b of swollen CMX membrane determined by SECM *in situ* ($44 \pm 2 \mu\text{m}$), and by optical microscopy ($50 \pm 5 \mu\text{m}$). However, the optical microscopy requires cutting the membrane.

Acknowledgments

The work is carried out in the French–Russian laboratory “Ion Exchange Membranes and Related Processes”. We are grateful to the Russian Foundation for Basic Research (Grant No. 17-08-01538_a) for financial support.

References

1. Güler E. et al. // Journal of Membrane Science. 2014. Vol. 455. P. 254-270.
2. Volodina E. et al. // Journal of colloid and interface science. 2005. Vol. 285. P. 247-258.
3. Krisilova E.V. et al. // Protection of Metals and Physical Chemistry of Surfaces. 2011. Vol. 47. № 1. P. 39-42.
4. Helfferich F. // McGraw-Hill. New York. 1962.
5. Bard A.J., Mirkin M.V. // CRC Press. 2012.
6. Butylskii D.Y. et al. //Petroleum Chemistry. 2016. Vol. 56. №. 11. P. 1006-1013.

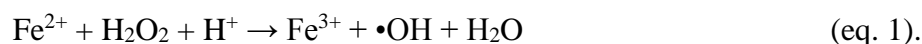
NANOMATERIALS FOR ELECTROCHEMICAL APPLICATIONS IN ENERGY CONVERSION AND WASTE WATER TREATMENT

Marc Cretin

Institut Européen des Membranes, IEM UMR-5635 CNRS, ENSCM, Université de Montpellier, Place Eugène Bataillon, 34095 Montpellier cedex 5, France, E-mail: marc.cretin@umontpellier.fr

Introduction

Scarcity of pure water worldwide is dramatically affecting the economic development of Third Countries but also the industrial growth of others. Towards the water recycling and reuse, Electrochemical Advanced Oxidation Processes (EAOPs) are of high interest since they are very efficient in the degradation of refractory pollutants that cannot be eliminated by conventional techniques. Amongst them, the electro-Fenton (EF) process allows the in situ generation of highly reactive and nonselective hydroxyl radicals indirectly by cathodic oxygen reduction, its subsequent H₂O₂ production and further Fenton reaction (eq. 1).



Experiments

Carbon felt is a good candidate to produce H₂O₂ from the reduction of dissolved oxygen [1] but it suffers from drawbacks like relatively low electronic conductivity and electrochemical active surface area. With the aim to increase carbon felt efficiency toward the electro-Fenton process, we develop in our research team, different modification routes to get microporous reactive carbon-based structures. It deals from basic thermal treatment under controlled atmosphere [2] to microporous carboneous coating prepared by combining Atomic Layer Deposition and solvothermal MOF growth on carbon felt (Fig. 1a) [3], going through graphene functionalization [4] and LDH deposition for heterogeneous catalysis [5].

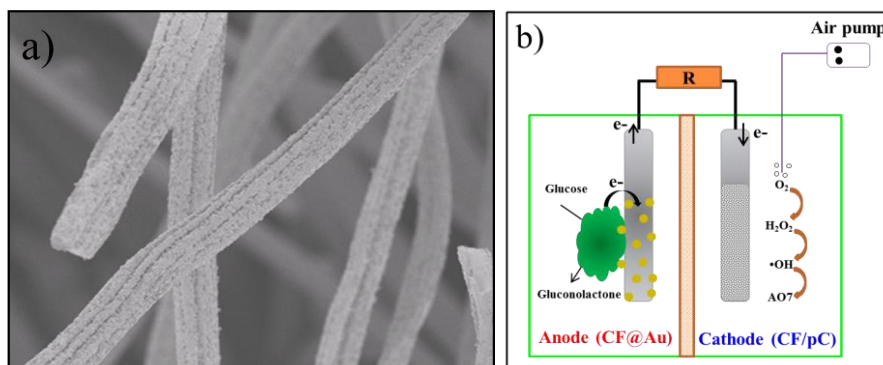


Figure 1: a) SEM image of a microporous carboneous coating on carbon felt
b) Schematic diagram of the Fuel Cell-Fenton based system.

Results and Discussion

We will discuss synthesis, characterization and electrocatalytic properties of the different structures. Carbon based nanomaterials will be then integrated in a electrolysis system for water treatment but also in a prospective fuel cell – Fenton system for zero-energy water depollution (Fig. 1b) [3]. Efficiency will be shown through the degradation and mineralization of pharmaceutical residues and organic dyes.

References

1. E. Brillas, I. Sire's, M.A. Oturan, (2009) Electro-Fenton Process and Related Electrochemical Technologies Based on Fenton's Reaction Chemistry Chem. Rev., 109, 6570–6631.
2. Thi Xuan Huong Le, Christophe Charmette, Mikhael Bechelany, Marc Cretin (2016) Facile Preparation of Porous Carbon Cathode to Eliminate Paracetamol in Aqueous Medium Using Electro-Fenton System, Electrochimica Acta, 188, 378–384.

3. *Thi Xuan Huong Le, Roseline Esmilaire, Martin Drobek, Mikhael Bechelany, Cyril Vallicari, Duy Linh Nguyen, Anne Julbe, Sophie Tingry, Marc Cretin (2016)* Design of novel Fuel Cell-Fenton system: a smart approach to zero energy depollution, *J. Mater. Chem. A*, 4, 17686–17693.
4. *Thi Xuan Huong Le, Mikhael Bechelany, Stella Lacour, Nihal Oturan, Mehmet A. Oturan, Marc Cretin (2015)* High removal efficiency of dye pollutants by electron-Fenton process using a graphene based cathode, *Carbon*, 94, 1003–1011.
5. *Soliu O. Ganiyu, Thi Xuan Huon Le, Mikhael Bechelany, Giovanni Esposito, Eric D. van Hullebusch, Mehmet A. Oturan, Marc Cretin (2016)* Hierarchical CoFe-Layered Double Hydroxide Modified Carbon-felt Cathode for Heterogeneous Electro-Fenton, *Journal of Materials Chemistry A*, DOI: 10.1039/C6TA09100H

THE NEUTRALIZATION DIALYSIS PROCESS: STATE OF THE ART AND PERSPECTIVES

¹Lasaad Dammak, ¹Mona Chérif, ²Anton Kozmai, ¹Lobna Chaabane, ¹Christian Larchet, ²Victor Nikonenko

¹Institut de Chimie et des Matériaux Paris-Est (ICMPE), Thiais, France, E-mail: dammak@u-pec.fr

²Membrane Institute, Kuban State University, Krasnodar, Russia, E-mail: kozmay@yandex.ru

Neutralization Dialysis (ND) is a membrane process based on the simultaneous use of two Donnan Dialysis operations [1, 2] where cation- and anion-exchange membranes separate a saline solution positioned between an acidic and an alkali solution respectively (fig. 1). The cation (anion) -exchange membrane allows the salt cations (anions) substitution of the treated solution by H^+ (OH^-) ions, leading to a mineral charge decrease in the solution.

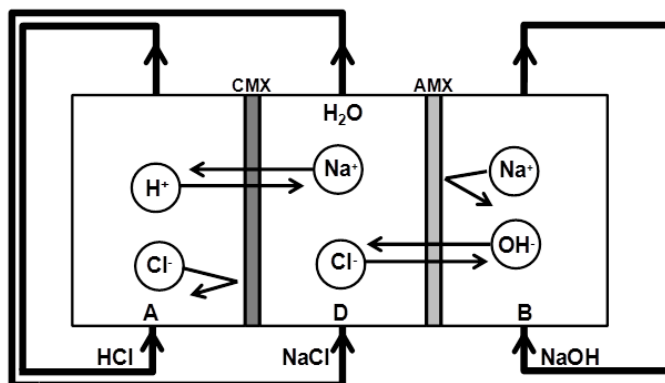


Figure 1. Schematic representation of ND with a three-compartment membrane stack

This method has certain advantages over existing methods such as Distillation, Nanofiltration, Reverse Osmosis and Electrodialysis. ND is not sophisticated technically, it demands low investment costs, it is characterized by low energy consumptions; its implantation is easy for isolated locations. Thus, ND can be considered as a promising membrane process convenient mainly to the developing countries, which suffer from the water lack but have access to ground and surface brackish waters.

Moreover, many studies [3-5] reveal the efficiency of ND process for desalination of solutions containing organic substances (mono- and oligosaccharides, polysaccharides, proteins). Different applications were envisaged such as separation of weak acids and bases [4], transport of glycine [5] and desalination of aqueous solutions of carbohydrates and milk whey [3].

In this process, multi-ionic solutions are treated. Lately, the interest for ion-exchange membrane processes allowing selective removal or selective substitution (fractionation) increased noticeably.

Even though numerous publications [6-8] describe ND applications, the ND process kinetics are poorly studied. One of the rare papers on the ND kinetics is that by Denisov *et al.* [9]. They developed a model based on the Nernst-Planck equations allowing the ion-exchange rate calculation (ion fluxes) across each of the membranes. However, Denisov *et al.* [9] did not investigate the influence of the operational conditions (the flow rate, the concentrations and pH in different compartments) on the ion-exchange kinetics. Furthermore, in the literature, no process optimization was attempted before the works of Chérif *et al.* [10].

The system can be theoretically studied with considering the following concentration profiles (fig. 2).

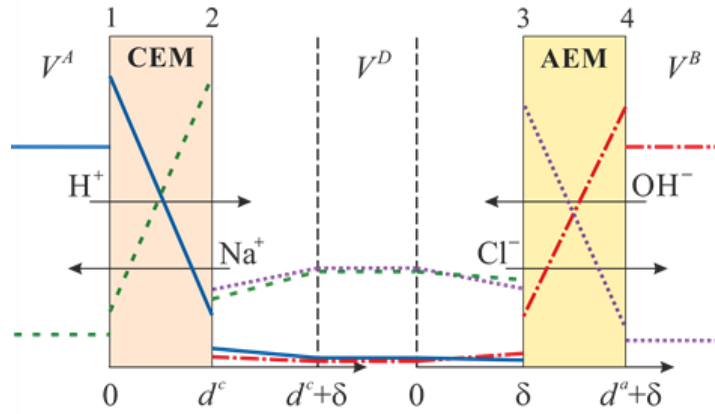


Figure 2. Scheme of the system under study. Concentration profiles are shown schematically for H^+ (solid line), Na^+ (dashed line), OH^- (dash-dot line) and Cl^- (points) ions

The following set of equations describes one-dimensional ion electro-diffusion transport in the membranes and in the diffusion layers occurring in the D compartment:
the Nernst-Planck (N-P) equations:

$$J_j = -D_j \left(\frac{\partial C_j}{\partial x} + z_j C_j \frac{F}{RT} \frac{\partial \varphi}{\partial x} \right) \quad (1)$$

the electro-neutrality condition:

$$\sum_j z_j C_j = \omega X \quad (2)$$

the condition of zero current flow:

$$\sum_j z_j J_j = 0 \quad (3)$$

the equation of material balance:

$$\frac{\partial C_j}{\partial t} = -\frac{\partial J_j}{\partial x} \quad (4)$$

The concentration changes in the acid (upper index A) compartment of volume V^A are associated with the H^+ ($J_H^{(1)}$) and the Na^+ ($J_{Na}^{(1)}$) fluxes through the left-hand boundary of the CEM:

$$-\frac{S}{V^A} J_H^{(1)} = \frac{\partial C_H^A}{\partial t} \quad (5)$$

and

$$-\frac{S}{V^A} J_{Na}^{(1)} = \frac{\partial C_{Na}^A}{\partial t} \quad (6)$$

The concentration changes in the **base** (upper index B) compartment of volume V^B are associated with the OH^- ($J_{OH}^{(4)}$) and the Cl^- ($J_{Cl}^{(4)}$) fluxes through the right-hand boundary of the AEM:

$$\frac{S}{V^B} J_{OH}^{(4)} = \frac{\partial C_{OH}^B}{\partial t} \quad (7)$$

and

$$\frac{S}{V^B} J_{Cl}^{(4)} = \frac{\partial C_{Cl}^B}{\partial t} \quad (8)$$

The ND can be coupled with the bipolar electro dialysis (EDBM) process and to photovoltaic energy production modulus to have an autonomous drinking water production system without the addition of a chemical reagent (fig. 3).

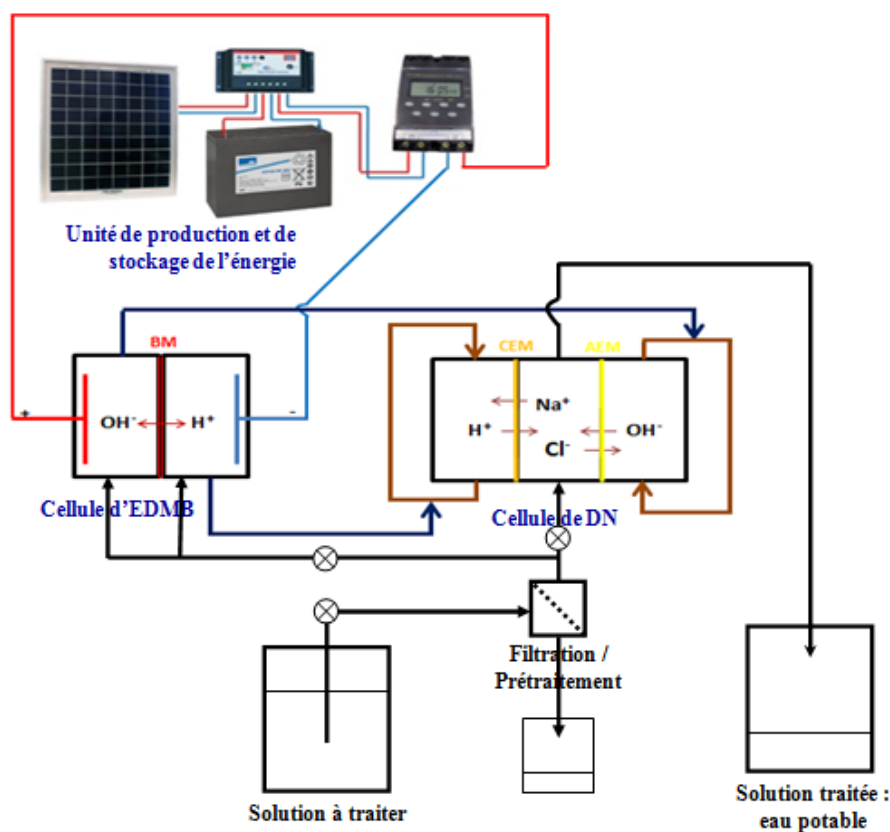


Figure 3. Device for autonomous drinking water production system

References

1. Igawa M., Echizenya K., Hayahsita T., Seno M. Donnan Dialysis Desalination // Chemistry Letters 1986. V. 11. P. 237.
2. Igawa M., Echizenya K., Hayahsita T., Seno M. Neutralization Dialysis for Deionization // Bulletin of the Chemical Society of Japan 1987. V. 60. P. 381.
3. Bleha M., Tishchenko G.A. Neutralization dialysis for desalination // J. Membr. Sci. 1992. V. 73. P. 305.
4. Igawa M., Tanabe H., Ida T., Yamamoto F., Okochi H. Separation of weak acids and bases by neutralization dialysis // Chem. Lett. 1993. V. 22. P. 1591.
5. Wang G., Tanabe H., Igawa M. Transport of glycine by neutralization dialysis // J. Membr. Sci. 1995. V. 106. P. 207.
6. Dieye A., Larchet C., Auclair B., Mar-Diop C. Elimination des Fluorures par la Dialyse Ionique Croisée // European Polymer Journal 1998. V. 34. P. 67.
7. Garmes H., Persin F., Sandeaux J., Pourcelly G., Mountadar M. Defluoridation of groundwater by a hybrid process combining adsorption and Donnan dialysis // Desalination 2002. V. 145. P. 287.
8. Çengelöglu Y., Tor A., Kir E., Ersözet M. Transport of hexavalent chromium through anion-exchange membranes // Desalination 2003. V. 154. P. 239.
9. Denisov G.A., Tishchenko G., Bleha M., Shataeva L. Theoretical analysis of neutralization dialysis in the three-compartment membrane cell // J. Membr. Sci. 1995. V. 98. P. 13.
10. Chérif M., Mkacher I., Dammak L., Ben Salah A., Walha K., Grande D., Nikonenko V. Water desalination by neutralization dialysis with ion-exchange membranes: flow rate and acid/alkali concentration effects // Desalination. 2015. V. 361. P. 13.

INVESTIGATION OF SELECTIVITY OF PERFLUORINATED MEMBRANES MODIFIED BY POLYANILINE

Ekaterina Dankovtseva, Svetlana Shkirskaya
Kuban State University, Krasnodar, Russia

Introduction

One of the most important properties of ion-exchange membranes, which determine their practical application, is their selectivity in relation to one or several types of ions. The experimental estimation of electromigration transport numbers of counter ions is associated with considerable difficulties so various theoretic approaches are used to evaluate them [1]. Nowadays, one of the approaches to obtain ion-exchange materials with improved characteristics is modification, so it is very important to evaluate selectivity for modified membranes. The purpose of this work is a comparative study of the selectivity of the perfluorinated membranes MF-4SK and MF-4SK/PANI.

Experiments

A perfluorinated membrane MF-4SK and a modified membrane MF-4SK/PANI were the objects of the study. The modification was carried out by the method of successive diffusion of polymerizing solutions through the MF-4SK membrane to water [2]. The definition of "apparent" transport number of counter ions through the membrane was carried out by potentiometric method and calculated by the equation

$$t_{+app} = \frac{1}{2} \left(1 + \frac{\Delta E_{mb}}{\Delta E_{id}} \right), \quad (1)$$

where ΔE_{mb} is the measured potential of a cell; ΔE_{id} is the membrane potential of an ideally selective membrane which was determined according to the equation:

$$E_{id} = \frac{RT}{F} \ln \frac{(m\gamma_{\pm})_2}{(m\gamma_{\pm})_1}, \quad (2)$$

where m is the molality of the solutions; γ_{\pm} is the average activity coefficients of the solution.

Results and Discussion

The estimation of electromigration transport numbers of counter ions in this work was carried out by two methods. In the first case, it was used the Scatchard equation:

$$t_{+}^* = t_{+app} + Mm_{\pm} 10^{-3} t_w \quad (3)$$

where M is the the molar mass of solvent, 18 g/mol; m_{\pm} is the average molality of external solution; t_w is the water transport numbers. For this purpose, the "apparent" transport numbers of counterions and water transport numbers of MF-4SK and MF-4SK/PANI membranes were determined experimentally (fig.1). It was experimental found that the intercalation of polyaniline into the MF-4SK membrane leads to an increase the selectivity of the modified samples.

Figure 2 shows the dependencies of the electromigration transport numbers of Na^+ ions in comparison with the "apparent" numbers for the initial (a) and modified membranes (b). It is shown that taking water transport into account leads to the preservation of high selectivity of membranes in the whole range of concentrations studied.

Another way to estimate the electromigration transport numbers includes the use of experimental data on the concentration dependences of the conductivity and diffusion permeability of membranes. The calculation is carried out using the equations:

$$t_{+(-)}(C) = \frac{L_{+(-)}^*(C)}{L_{+}^*(C) + L_{-}^*(C)} \quad (4)$$

where C is the equilibrium solution concentration; L_{+}^* and L_{-}^* are the concentration dependences of the counterion's and co-ion's electrodiffusion coefficients. The concentration dependences of the electrodiffusion coefficients were calculated:

$$L_+^*(C) = \frac{\kappa_m^d(C)}{zF^2} \left[1 + \sqrt{1 - \frac{2P^*(C)CF^2}{RT\kappa_m^d(C)\pi_{\pm}}} \right] \quad (5)$$

$$L_-^*(C) = \frac{\kappa_m^d(C)}{zF^2} \left[1 - \sqrt{1 - \frac{2P^*(C)CF^2}{RT\kappa_m^d(C)\pi_{\pm}}} \right] \quad (6)$$

were κ_m^d is the membrane conductivity measured by using direct current (DC); P^* is the differential coefficient of diffusion permeability; π_{\pm} is the correction factor.

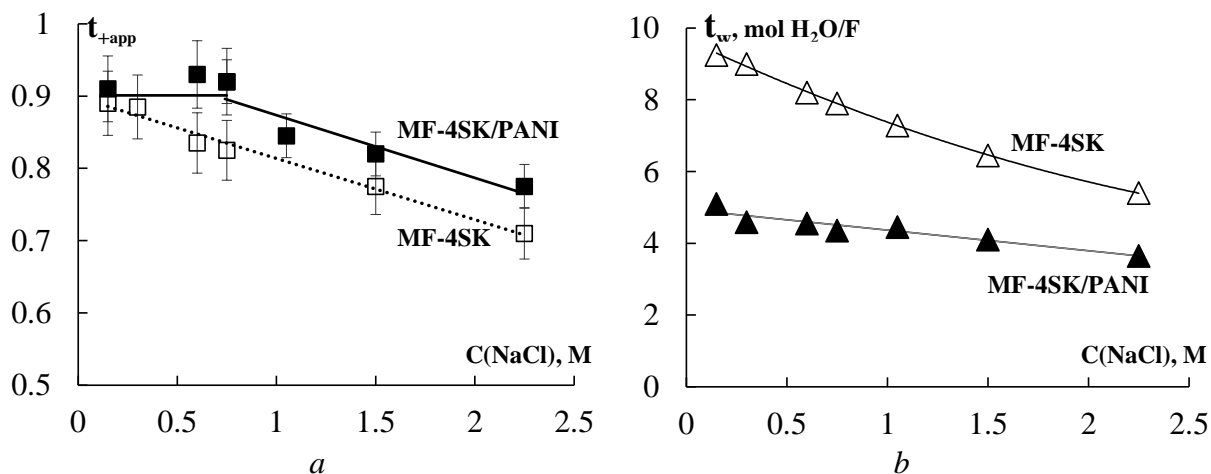


Figure 1. Dependencies of the transport numbers of counter-ions (a) and water transport numbers (b) of investigated membranes in NaCl solutions

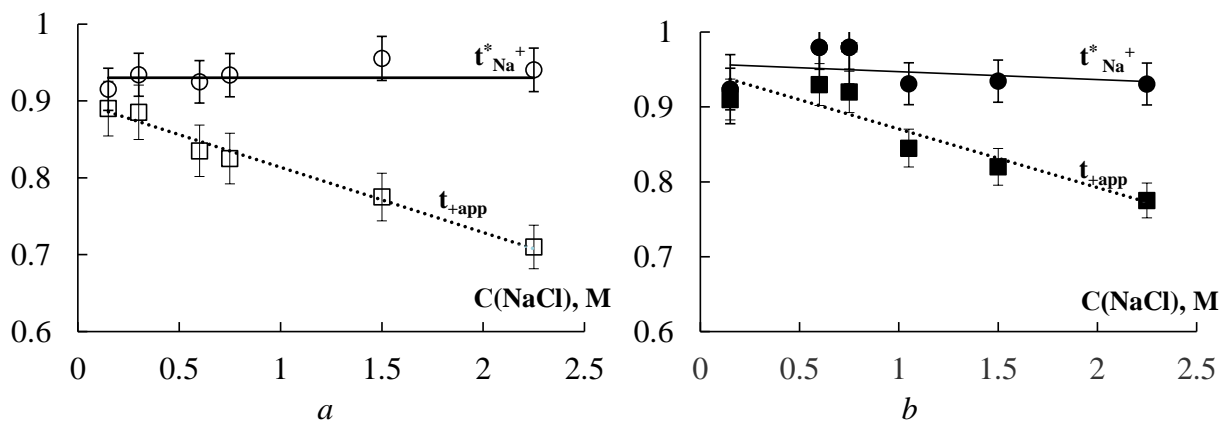


Figure 2. Dependencies of the transport numbers of counter ions for the MF-4SK (a) and MF-4SK/PANI (b) membranes in NaCl solutions

The electromigration transport numbers, calculated by the equation (4), are close to 1, which corresponds to an ideally selective membrane in the entire range of concentrations and close to electromigration transport numbers calculated by the Scatchard equation. So both approach can use to estimate electromigration transport numbers as in initial as in modified membranes

The present work was supported by the Russian Foundation for Basic Research (project № 16-08-01117-a).

References

1. Demina O.A., Shkirskaya S.A., Kononenko N.A., Nazyrova E.V. // Russ. J. of Electrochem. 2016. V. 52. No. 4. P. 291–298.
2. Berezina N.P., Shkirskaya S.A., Kolechko M.V., Popova O.V., Senchikhin I.N., Roldugin V.I. // Russ. J. Electrochem. 2011. V. 47. P. 995-1005.

BORON HYDRIDES FOR ENERGY: FOCUS ON MEMBRANES, AN UNDERINVESTIGATED FIELD

Umit Demirci

IEM (Institut Europeen des Membranes), UMR 5635 (CNRS-ENSCM-UM2), Universite de Montpellier, Place E. Bataillon, F-34095, Montpellier, France, *E-mail: umit.demirci@umontpellier.fr*

Introduction

Boron hydrides are potential energy carriers. A first example of application is chemical H storage. Many boron hydrides have been investigated; sodium borohydride NaBH₄ and ammonia borane NH₃BH₃ are typical examples [1,2]. A second example of application is low-temperature direct liquid-fed fuel cell; boron hydrides, which are soluble in water, are attractive fuels owing to a relative stability and high capacity of e⁻ release. NaBH₄ is a typical example [3]. Recent works have shown that polyboranes like sodium dodecaborate Na₂B₁₂H₁₂ could be used as well [4]. With all, the uses of membranes are crucial, but this is an underinvestigated field.

Discussion

The first application is chemical H storage. NaBH₄ is dehydrogenated by hydrolysis in the presence of a catalyst [1]: NaBH₄ + 4H₂O → NaB(OH)₄ + 4H₂. Up to 2016, it was claimed that the released H₂ is pure, but the H₂ stream is actually polluted by NaB(OH)₄ carried by H₂O vapor. This is an issue as this hinders implementation. Unfortunately, no filtration solution has been proposed to date. Besides, there is NH₃BH₃ which hydrolysis releases some ammonia NH₃ concomitant with H₂: NH₃BH₃ + 3H₂O → NH₃ + B(OH)₃ + 3H₂. In that case also, no filtration solution has been suggested [2]. With NH₃BH₃, dehydrogenation can also take place under heating. The pristine borane decomposes and besides H₂ high amounts of by-products (*e.g.* diborane B₂H₆, ammonia NH₃, borazine B₃N₃H₆) are generated: $a\text{NH}_3\text{BH}_3 \rightarrow b\text{NH}_2\text{BH}_2 + c\text{B}_2\text{H}_6 + 2c\text{NH}_3 + d\text{B}_3\text{N}_3\text{H}_6 + (b+4d)\text{H}_2$, with $a = b + 2c + 3d$. There are strategies that enable the decrease of the by-products, but the use of a membrane is still necessary.

The second application is liquid fuels of direct liquid-fed fuel cells. Aqueous alkaline NaBH₄ is one of these fuels. The BH₄⁻ anion can be oxidized: BH₄⁻ + 8 OH⁻ → BO₂⁻ + 6H₂O + 8e⁻ [3]. Anion exchange membranes are generally used but both BH₄⁻ and OH⁻ are able to cross-over to the cathodic compartment. One of the current challenges is thus the use of a selective membrane hindering the transport of BH₄⁻. Within the last few years, we have screened alternative fuels like, among others, sodium octahydrotriborate NaB₃H₈, hydrazine borane N₂H₄BH₃, and Na₂B₁₂H₁₂. The use of a selective membrane seems to be less critical for NaB₃H₈ and Na₂B₁₂H₁₂ because the B₃H₈⁻ and B₁₂H₁₂²⁻ anions are big. However, with N₂H₄BH₃, the BH₃ moiety transforms to BH₃OH⁻ in alkaline solution and its cross-over through the anionic membrane is as problematic as that of BH₄⁻. Alternative membranes are still necessary.

All of these aspects, with a focus on the underinvestigated membranes, will be presented during the meeting.

References

1. Schlesinger H. I., Brown H. C., Finholt A. E., Gilbreath J. R., Hoekstra H. R., Hyde E. K. Sodium borohydride, its hydrolysis and its use as a reducing agent and in the generation of hydrogen // J. Am. Chem. Soc. 1953. V. 75. P. 215-219.
2. Sanyal U., Demirci U. B., Jagirdar B. R., Miele P. Hydrolysis of ammonia borane as a hydrogen source: fundamental issues and potential solutions towards implementation // Chem. Sus. Chem. 2011. V. 4. P. 1731-1739.
3. Ma J., Choudhury N. A., Sahai Y. A comprehensive review of direct borohydride fuel cells // Renew. Sust. Energy Rev. 2010. V. 14. P. 183-199.
4. Unpublished results yet.

THE INFLUENCE OF PROTON-ACCEPTOR PROPERTIES AND CONCENTRATION OF DOPANTS INTRODUCED INTO MF-4SC MEMBRANES ON THE CROSS SENSITIVITY OF DP-SENSORS TO IONS IN ALKALINE SOLUTIONS OF GLUTAMIC AND ASPARTIC ACIDS

¹Tatyana Denisova, ²Ekaterina Safronova, ¹Anna Parshina, ¹Olga Bobreshova

¹Voronezh State University, Voronezh, Russia, *E-mail: tanyadenisova@list.ru*

²Kurnakov Institute of General and Inorganic Chemistry, RAS, Moscow, Russia

Introduction

The salts of glutamic and aspartic amino acids with alkali and alkaline earth metals are widely used in the food industry and in medicine as nutritional supplements and drugs [1]. In this connection, the development of rapid methods for the quantitative determination of ionic forms of these amino acids in aqueous solutions in the presence of alkaline and alkaline earth ions is actual. Aspartic and glutamic acids are aliphatic dicarboxylic amino acids. Therefore, it is proposed to use MF-4SC membranes containing silica, surface-modified by groups with proton-acceptor properties, to optimize the characteristics of potentiometric DP (Donnan potential)-sensors. The aim of this work is the investigation of proton-acceptor properties and concentrations effects of dopants incorporated into MF-4SC membranes on the DP-sensors characteristics in aqueous solutions of glutamic (Glu) and aspartic (Asp) amino acids, containing KOH.

Experiments

Aqueous solutions of glutamic (Glu) and aspartic (Asp) amino acids, containing KOH, were investigated. Concentrations of amino acids and KOH in test solutions were ranged from $1.0 \cdot 10^{-4}$ to $1.0 \cdot 10^{-2}$ M. The pH of Glu+KOH and Asp+KOH aqueous solutions was changed in the range from 2.61 ± 0.05 to 11.46 ± 0.05 and from 2.12 ± 0.05 to 11.25 ± 0.05 respectively. The hybrid materials based on MF-4SC membranes and silica nanoparticles modified by amine-containing hydrocarbon groups (3-aminopropyl-(R1), 3-(2-imidazol-1-yl) propyl- (R2)) were investigated as electrode active materials in DP-sensors. Concentration of silica nanoparticles was 3 wt.%, for amine-containing hydrocarbon groups – 5 and 10 mol.% from oxides concentration. The hybrid materials were prepared by casting procedure. The properties of membranes are described in [2].

Results and Discussion

The significant differences in the cross sensitivity of DP-sensors to K^+ cations and ions (anions and zwitterions) of amino acids in Glu+KOH and Asp+KOH solutions are revealed. The sensitivity of DP-sensors to Glu^- and Glu^\pm ions is lower than to K^+ ions, but to the Asp^- , Asp^\pm ions, on the contrary, is higher. This is due to a number of reasons. The concentration of zwitterions, which form cations as a result of the displacement of acid - base equilibrium in a membrane phase, in Asp + KOH solutions, is higher than in Glu + KOH solutions. The smaller size and the structural features cause the possibility for interaction of both carboxyl groups of aspartic acid with the amino-containing groups of dopant in membrane similar to the chelating effect. The highest accuracy of simultaneous determination of K^+ , Glu^- , Glu^\pm ions in aqueous solutions was obtained by using a pair of DP-sensors based on MF-4SC+3 wt.% SiO_2 membranes containing 10 mol.% of R1 and R2 on the oxide surface, for K^+ , Asp^- , Asp^\pm ions – by using a pair of DP-sensors based on MF-4SC and MF-4SC+3 wt.% SiO_2 + 5 mol.% R1 membranes.

This work was supported by the Russian Science Foundation (project no. 15-13-10036).

References

1. Yin J., Liu M., Ren W., Duan J., Yang G., Zhao Y., Fang R., Chen L., Li T., Yin Y. // PloS one. 2015. V. 10. №. 4. P. e0122893.
2. Mikheev A.G., Safronova E.Yu., Yaroslavtsev A.B. // Petroleum Chemistry. 2013. V. 53. № 7. P. 504-510 (original Russian text published in Membrany i Membrannye Tekhnologii. 2013. V. 3, №. 2, P. 93–99).

ELECTROCATALYTIC PROPERTIES OF EXTRACTS OBTAINED FROM *E. COLI* BB CULTURE AT MEDIATED GLUCOSE OXIDATION

Maria Dmitrieva, Ekaterina Zolotukhina, Ekaterina Gerasimova, Aleksey Terentyev, Yuriy Dobrovolsky

Institute of Problems of Chemical Physics of RAS, Chernogolovka, Russia

E-mail: angel.maria@mail.ru

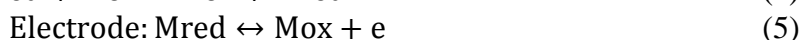
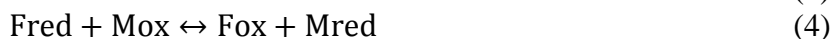
Introduction

Bioelectrocatalytic processes are intensively investigated recently. It is caused not only with singularity and complexity of the studied objects, but also with the big perspective of their practical application. Bioelectrocatalytic processes have already found their niche as portable power sources for the devices consuming low capacities of the electric power (mobile phones, the self-power biosensors, self-power implanted medical devices) [1]. All bioelectrocatalytic processes are based on the bioelectrocatalysis phenomenon. The bioelectrocatalysis is an acceleration of electrochemical process by the biological agent. Both electronic and ionic transfers occur in biofuel cells. The effective bioelectrocatalysis requires interaction of an enzymatic catalysis and electrochemical reaction on an electrode. There are two fundamentally different ways for achievement of this purpose – a direct bioelectrocatalysis and a mediated bioelectrocatalysis [2]. In the first case direct electron transfer from proteinaceous fragments on an electrode is realized:



S – substrate, P – product, F_{ox} , F_{red} - the oxidized and reduced enzyme forms.

In the second case protein isn't electroactive, and electrons to an electrode are transferred by the mediator system interacting with it



M_{ox} , M_{red} - the oxidized and reduced mediator forms.

The direct bioelectrocatalysis proceeds in two stages presented by the equations (1) and (2). However, only the limited number of redox-enzymes is capable to realization of a direct bioelectrocatalysis [3]. Therefore it is often necessary to apply the second way of interaction of enzymatic and electrochemical reactions (mediated bioelectrocatalysis). In this case low-molecular compounds (mediators) are used. Mediators carry out transfer of electrons between a substrate, the active center of enzyme and an electrode (the equations (3)-(5)).

Previous studies [4] have shown that «crude» proteinaceous *E. Coli* extract can be used as the catalyst of anode oxidation of organic fuels instead of pure enzymes. It should be mentioned that the technology for producing «crude» extracts is simpler and economic than technology for producing pure enzymes. The goal of this research is the investigation of the influence of the nature of a redox-mediator on electrocatalytic activity of the "crude" extracts in glucose oxidation reaction.

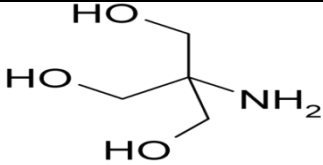
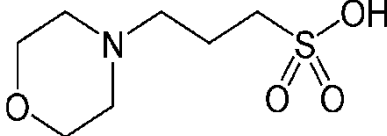
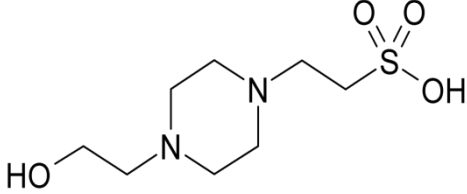
Experiments

Extracts have been obtained according to the technology described in article [4]. Electrochemical measurements were conducted using Autolab PGSTAT 101 potentiostat in a standard three electrode cell containing 15 ml of buffer solution as electrolyte and an Ag/AgCl reference electrode, a glassy carbon working electrode and a platinum foil counter electrode. All experiments were performed in the argon atmosphere by means of degassing on the Schlenk line. Active agents were added directly into the cell which was under pressure of argon (20mbar). Glucose was used as a substrate. All electrochemical measurements were performed in two modes of polarization: 1) potentiodynamic (cyclic voltammetry with scan rate of 20mV/s, 100mV/s); 2) potentiostatic. Current curves were measured with solution mixing by magnetic stirrer with a speed of 150 turns per min.

Results and Discussion

During the researches it has been proved that in the case of «crude» extracts only mediator electron transfer is possible. The nature of a mediator can have significant effect on electrochemical activity of proteinaceous extracts due to conformational and charging restrictions. To choose redox-mediator system which would allow to receive current responses on an electrode a number of the water-soluble mediators applied to biological enzymatic systems has been tested: methylene blue, neutral red, riboflavin, 2,4 – dinitrophenol, potassium ferricyanide, benzoquinone and nitrate of iron (III). Potassium ferricyanide, it appeared, was the most effective of them in this system. As it is inert to a substrate, doesn't enter interaction with air oxygen and the current responses in the system using potassium ferricyanide are steadily high. The conditions exerting impact on electrochemical activity of extracts in system with potassium ferricyanide as a mediator also have been studied (pH, temperature, concentration of reagents, structure and ionic force of the buffer solution). It will be noted that the nature of buffer solution has significant effect on the obtained current density (Table 1).

Table 1: Effect Of Buffer Nature On Current Density

Buffer solution, 0.1M (pH 7.6)	Structure	j, mkA/cm ²
TRIS		68
Potassium - phosphatic	K ₂ HPO ₄ +KH ₂ PO ₄	45
PBS	NaCl, KCl, Na ₂ HPO ₄ ,KH ₂ PO ₄	41
PB	KH ₂ PO ₄	41
MOPS		31
HEPES		25

Conclusion

The present paper shows that proteinaceous *E.Coli* extract can be used as the catalyst of anode mediated oxidation of organic fuels instead of pure enzymes.

References

1. *Cosnier S.* Recent advances on enzymatic glucose/oxygen and hydrogen/oxygen biofuel cells: Achievements and limitations // *J. Power Sources.* 2016. V. 325. P. 252.
2. *Leech D.* Enzymatic fuel cells: Recent progress // *Electrochim. Acta.* 2012. V. 84. P. 223.
3. *Stoica L.* Direct electron transfer – a favorite electron route for Cellobiose Dehydrogenase (CDH) from *Trametes Villosa*. Comparison with CDH from *Phanerochaete chrysosporium* // *Langmuir.* 2006. V. 22. P. 10801.
4. *Dmitrieva M.* Dehydrogenase and electrochemical activity of *Escherichia coli* extracts // *Appl. Biochem. Microbiol.* 2017. V. 53. № 4. P. 1.

ELECTROCHEMICAL OXIDATION OF ALCOHOLS ON Pd/C CATALYSTS SYNTHESIZED BY PULSE ALTERNATING CURRENT TECHNIQUE

Nikita Faddeev, Alexandra Kuriganova, Nina Smirnova

Platov South-Russian State Polytechnic University (NPI), Novocherkassk, Russia,

E-mail: nikita.faddeev@yandex.ru

Introduction

The use of variable pulse current in the processes of electrochemical dispersion of metals is a new promising direction in the production of nanosized materials. Earlier we have successfully used a pulse alternating current technique (PAC) for synthesis of metal-carbon, metal oxide-carbon nanostructured materials based on Pt nanoparticles [1], nickel oxide [2] and tin dioxide [3], which demonstrated good electrochemical properties in corresponding applications.

In this paper PAC technique was used to preparation of Pd/C catalytic systems. It is known that Pd has a high electrocatalytic activity comparable to Pt in the electrooxidation reaction of alcohols in an alkaline medium that makes him promising catalysts for the processes which takes place in fuel cells with direct oxidation of liquid fuel [4].

Experiments

The electrochemical cell has two Pd foil electrodes 0.25 mm thick immersed in an aqueous solution of KCl. The electrodes are connected to ac source operating at 50 Hz. Pd loading in the catalyst was controlled by the current amplitude and duration of the synthesis process. Finally, the freshly prepared catalyst was rinsed with H₂O and dried at 80 °C for 1 h.

Results and Discussion

X-ray diffraction studies of the synthesized composite material (Fig. 1) showed the presence of peaks in the range from 15 to 60 degrees typical for metallic palladium, the palladium nanoparticles have a narrow size distribution 6-10 nm

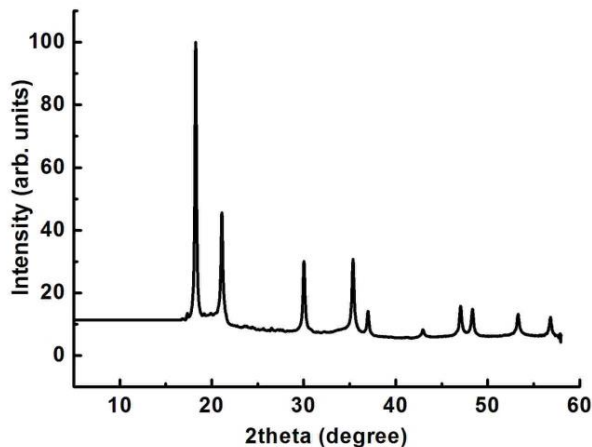


Figure 1 – The X-ray diffraction pattern of the Pd / C composite material obtained under the action of a variable pulse current

The catalytic properties of the resulting Pd / C composite material were investigated in the electrochemical oxidation of ethanol in an alkaline medium (Fig. 2).

Figure 1 shows the CVs oxidation of methanol and ethanol on a Pd/C catalyst. At the anode direction, in the range of potential 0.4 – 1.0 V peaks of alcohols oxidation were observed. A further decrease of the current at $E > 1.0$ V is due to the blocking of the active sites of the palladium surface by oxygen containing products that lead to decrease in the oxidation rate of alcohol. At the cathodic direction of the voltammogram, peaks due to the oxidation of alcohol are also observed, which are shifted to more cathodic potentials that can be due to the presence on the Pd surface a large number of adsorbed oxygen-containing species.

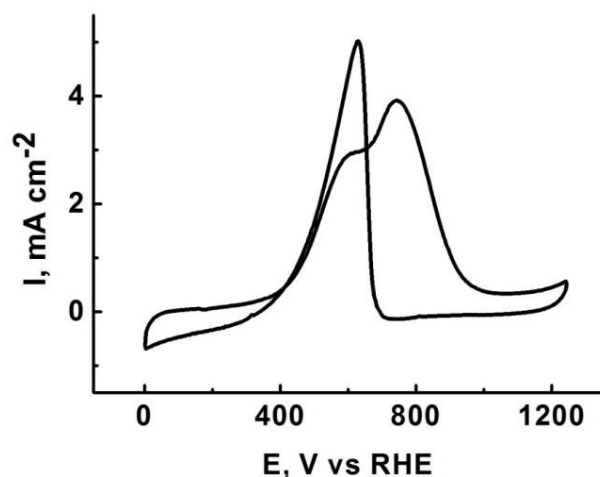


Figure. 2. CVs Pd/C catalyst in a solution of 1M NaOH + 0.5M EtOH. The scan rate of the potential is 50 mV/s.

Thus, nanoscale Pd/C composite materials were obtained via PAC technique; the materials are characterized by good electrocatalytic activity in the electrooxidation of alcohols in an alkaline medium.

References

1. Leontyev I., A. Kuriganova, Y. Kudryavtsev, B. Dkhil, N. Smirnova. New life of a forgotten method: Electrochemical route toward highly efficient Pt/C catalysts for low-temperature fuel cells // *Appl. Catal. A: Gen.* 2012. V. 431–432. P. 120
2. D. Leontyeva, I. Leontyev, M. Avramenko, Yu. Yuzjuk, Yu. Kukushkina, N. Smirnova. Electrochemical dispersion as a simple and effective technique toward preparation of NiO based nanocomposite for supercapacitor application // *Electrochim Acta.* 2013. Vol. 114. P. 356–362.
3. A. Kuriganova, C. Vlaic, S. Ivanov, D. Leontyeva, A. Bund, N. Smirnova. Electrochemical dispersion method for the synthesis of SnO₂ as anode material for lithium ion batteries // *J. Appl. Electrochem.* 2016. DOI: 10.1007/s10800-016-0936-2
4. C. Xu, L. Cheng, P. Shen, Y. Liu, *Electrochem. Commun.* 9 (2007) 997–1001.

VERIFICATION OF CAPILLARY MODEL OF FREE SOLVENT ELECTROSMOTIC TRANSFER IN ION-EXCHANGE MEMBRANES

Irina Falina, Olga Demina, Victor Zabolotsky

Department of Physical Chemistry, Kuban State University, Krasnodar, Russia

E-mail: irina_falina@mail.ru

Introduction

The electroosmotic permeability of the ion-exchange membrane is the basic characteristic of the material for its application in the electrodialysis concentrating of electrolyte solutions. The capillary model permits to evaluate the electroosmotic transport of the free solvent through ion-exchange membranes on the base of its physic-chemical properties and conductivity concentration dependence. Nevertheless, the verification of this approach with help of experimental data was not still carried out.

Theory

According to capillary model, transport number of the free solvent through the ion-exchange membrane could be described by Helmholtz-Smoluchowski equation in form [1]

$$\beta_w = \pi \frac{1}{V_m} F \frac{\theta \varepsilon \varepsilon_0}{\eta} \zeta \frac{mr^2}{\kappa}, \quad (1)$$

where ε is the relative dielectric constant of the solution; ε_0 is the dielectric constant of vacuum; η is the dynamic viscosity of the solution; m is the number of pores per 1 m² of the membrane area; r is the pore radius in the membrane, corresponding to maximum on differential porosimetric curve; F is the Faraday constant; V_m is the water molar volume, ζ is the electrokinetic potential, κ is conductivity of the membrane, and θ is parameter, taking into account portion of through mesopores and their tortuosity.

Electrokinetic potential is determined as the potential in the point placed in diffusive part of electrical double layer, which is distant (d) from the Helmholtz plane on radius of hydrated ion equal to the sum of the diameter of the water molecule and the radius of the counterion.

$$\xi = \ln \frac{e^{y_1/2} - 1}{e^{y_1/2} + 1} - \ln \frac{e^{y/2} - 1}{e^{y/2} + 1}, \quad (2)$$

where

$$\xi = \frac{d}{\sqrt{\frac{RT\varepsilon\varepsilon_0}{2F^2z^2C}}}, \quad y = \frac{F\xi}{RT}, \quad y_0 = \frac{F\varphi_1}{RT}.$$

and z is the charge of the transferred ions.

In the mesopores of the ion-exchange membrane where the electroosmotic transport of the free solvent mainly occurs, the thickness of the electric double layer is much smaller than its radius of curvature; therefore, the electrostatic potential (φ_1) is determined by the equation of the Stern theory for the planar electric double layer [1]:

$$q = 4dCF \operatorname{sh}\left(\frac{\varphi_1 F}{RT}\right) + 2A\sqrt{c} \operatorname{sh}\left(\frac{\varphi_1 F}{2RT}\right), \quad (3)$$

where q is surface density of the electric charges; C is the electrolyte concentration deep in solution; R is the gas constant; T is the absolute temperature; $A = \sqrt{2\varepsilon\varepsilon_0 RT}$.

The surface density of the electric charges of ionic groups uniformly distributed in the ion-exchange material is calculated from the ion-exchange capacity of the membrane (Q , mol/g_m) and the specific surface area of pores (S , m²/g_m):

$$q = \frac{FQ}{S}. \quad (4)$$

Results and Discussion

The water electroosmotic flux in the membrane system consists of two parts: free water and water, transferred in ion's hydration shells. Hence, the transport number of free solvent equals

$$\beta_w = t_w - t_{wh}. \quad (5)$$

where t_w , β_w and t_{wh} are transport numbers of total electroosmotic, free and hydration water, correspondingly.

Capillary model was experimentally verified for the samples of experimental perfluorinated sulfocationic MF-4SK membrane with different specific water capacity. The experimental data on ion-exchange capacity, pore radii distribution and concentration dependence of membrane conductivity in NaCl solution were used to calculate the β_w using set of equations 1-4. In case when $\theta = 1$ calculation results essentially exceeds the experimental data. Experimental t_w concentration dependencies were used for adjustment of calculation results to experimental data by θ varying. Figure 1 presents the results of β_w calculations according to capillary model and on the base of experimental data (equation 5), taking into account that t_{wh} equals to 4 mol H₂O/F.

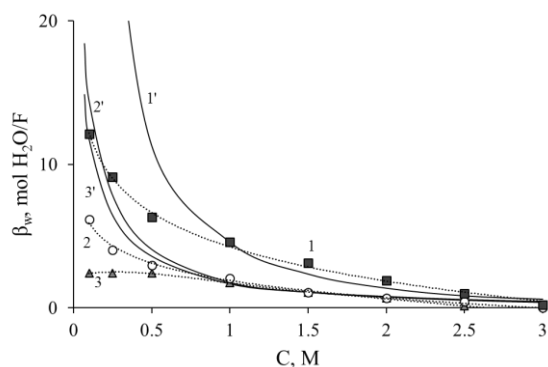


Figure 1. Concentration dependences of free water transport numbers through MF-4SK membranes for after adjustment of the θ value.

1, 2, 3 – experimental data, 1', 2', 3' – calculation results. 1, 1' – $n = 11.3$ mol H₂O/mol SO₃⁻; 2, 2' – $n = 20.2$ mol H₂O/mol SO₃⁻; 3, 3' – $n = 36.6$ mol H₂O/mol SO₃⁻.

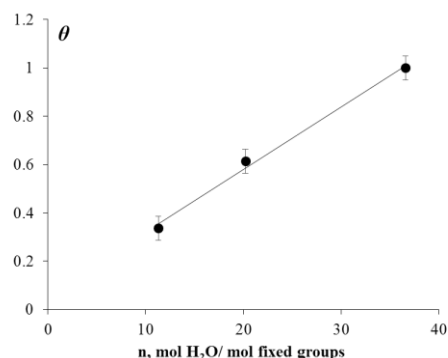


Figure 2. Dependence of through pore portion on specific water content of MF-4SK membranes

One can see from figure 1 that in range of concentrated solutions ($C > 1$ M) there is a good agreement between theoretical and experimental curves. Since electroosmotic transfer through the membrane decreases the efficiency of the processes of solution concentrating by electro dialysis, prediction of the electroosmotic permeability in concentrated solutions is more important problem. Figure 2 shows the dependence of the through pore portion on the specific water content of the perfluorinated membranes which has the linear character and permits to predict the θ value on the basis of hydrophilic characteristics of the membrane. Thus, the equation obtained on the basis of the capillary model using the Stern theory of electric double layer allows one to calculate the transport number of the free solvent through the ion-exchange membrane from its physicochemical and structural characteristics.

Acknowledgements

The work was carried out with the financial support of the state task of the Ministry of Education and Science of the Russian Federation (project No. 10.3091.2017/PP).

References

1. Zabolotskii V.I., Demina O. A., Protasov K.V. // Rus. J. Electrochem. 2014. V. 50. No. 5. P. 412–418.
2. Berezina N.P., Gnusin N.P., Dyomina O.A., Timofeyev S.V. // J. Membr. Sci. 1994. V. 86. P. 207-229.

STUDY OF THE PROTON TRANSFER PROCESSES IN NON-AQUEOUS SOLUTIONS OF BRØNSTED ACID

Irina Fedorova, Lyubov Safonova

G. A. Krestov Institute of Solution Chemistry of Russian Academy of Sciences, Ivanovo, Russia

E-mail: fiv@isc-ras.ru

Introduction

Lately, phosphorus acids with the formula H_3PO_{n+1} for $n=1\div 3$ are considered suitable candidates as ionomers because of their efficient proton transport properties. They are amphoteric, i.e. can act as both proton acceptors (through $O(=P)$) and proton donors (sharing hydroxyl protons) and have a relatively high dielectric constant. The combination of these properties leads to a high degree of auto dissociation which favors the formation of a hydrogen-bonding network. This work is a continuation of our previous computational studies relating to the processes of proton transfer in the H-bonded complexes of phosphoric and phosphonic acids (H_3PO_4 and H_3PO_3) with DMF [1, 2]. To extend our study, in the present work, we investigate the last member of this family, phosphinic acid (H_3PO_2), also called hypophosphorous acid. In addition, structural data for the H_3PO_2 -DMF complex were obtained for the first time. Since proton transfer occurs mostly in solution, the effects of solvation on the potential energy surface (PES) for proton transfer were studied.

Computational methods

Geometry optimizations of the solvated complexes were carried out with the B3LYP/6-31++G(d,p) level of theory as implemented in the Gaussian 09 program. All calculations in solvent were performed using the CPCM approach to model the condensed phase. The minimum-energy states of the complexes were confirmed by calculating the harmonic frequencies.

The potential energy profiles for proton transfer from phosphinic acid to proton acceptor atoms in H_3PO_2 and DMF molecules (oxygen atoms in $P=O$ and $C=O$ groups), respectively, as a function of the proton coordinate ($\delta=r_1-r_2$, where r_1 and r_2 are the distances from hydrogen atom to oxygen atoms in $O_1-H\dots O_2$ fragment) were evaluated using the potential energy surface (PES) scan method. A hydrogen atom was transferred between oxygen atoms in a hydrogen bond with an increment of 0.05 \AA , and the transition state at each point of the scan was optimized under different conditions: (i) fixed $O\dots O$ distance for the H-bond, where the acidic proton is transferred only and (ii) relaxed $O\dots O$ distance. The former situation is associated with the significant rates of proton transfer, especially in the systems with very strong H-bonds wherein the structural rearrangement (H-bond breaking and forming) is rate-limiting step of this process [3].

The energy values (ΔE) for proton transfer in considered complexes were calculated from the difference of the energies of the partially optimized geometries with R_i and δ_i parameters and the fully optimized structure ($E(R, \delta)$).

Results and Discussion

Figure 1 shows the most stable $(H_3PO_2)_2$ and H_3PO_2 -DMF structures in DMF environment modeled by the CPCM.

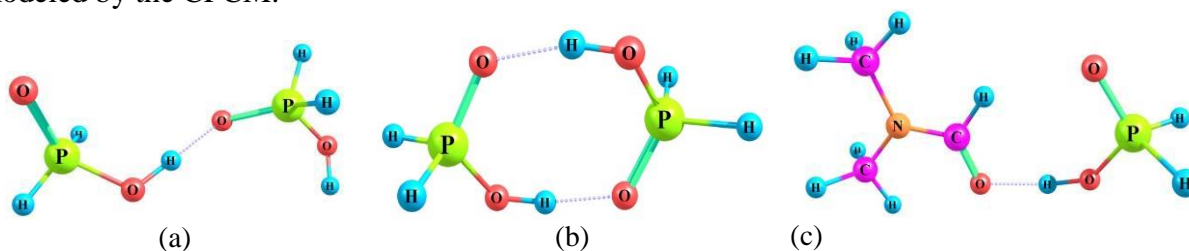


Figure 1. Optimized structures of two different kinds of H_3PO_2 dimers (a, b) and H_3PO_2 -DMF complex (c) under CPCM solvent conditions

In the structure 1a, the H_3PO_2 dimer contains only one hydrogen bond with $O\dots O$ distance of 2.604 \AA and H-bond angle of 177.6° . Configuration 1b is a clear ring-like structure where the two

H_3PO_2 molecules are held together by two H-bonds. The O...O distance of 2.602 Å and respective angle of 172.8° in the cyclic (H_3PO_2)₂ are equal for both hydrogen bonds. The calculated values of the binding energies of acid monomers in dimers show that the formation of both acid dimers in DMF environment is an energetically favorable process. The binding energy (E_{bind}) of the linear H_3PO_2 dimer was calculated to be -35.52 kJ/mol, while the E_{bind} value of cyclic configuration is -63.16 kJ/mol (31.58 kJ/mol per one H-bond).

The hydrogen bond between H_3PO_2 and DMF molecules in the complex is quasisymmetric, i.e. the hydrogen atom is closer to the oxygen atom in the O-H group of acid than to the oxygen atom of the C=O group of DMF. The O...O distance in the H_3PO_2 -DMF is 2.563 Å, indicating a much stronger hydrogen bond compared to the H_3PO_2 dimers. The supplement angle value (178.3°) shows an insignificant deviation from linearity of the three atoms. For H_3PO_2 -DMF the E_{bind} value is -51.98 kJ/mol.

Proton transfer in the fully relaxed structures of H-bonded complexes. As can be seen in Figure 2, the PES for proton transfer in the cyclic H_3PO_2 dimer has symmetric energy profile with respect to the center of the hydrogen bond ($\delta \sim 0$). In this case, the proton transfer along one of the H-bonds promotes the back transfer of the other proton in the second hydrogen bond (the double proton transfer); and the structure transforms itself into the initial configurations.

For the linear H_3PO_2 dimer and H_3PO_2 -DMF the potential curves show similar shapes. The PES for each of these complexes has single minimum. The transferred proton is localized near the oxygen atom in the hydroxyl group of phosphinic acid. The energy of these systems rapidly increases with the proton transfer. Although these complexes have strong H-bonds, the proton transfer is not observed either.

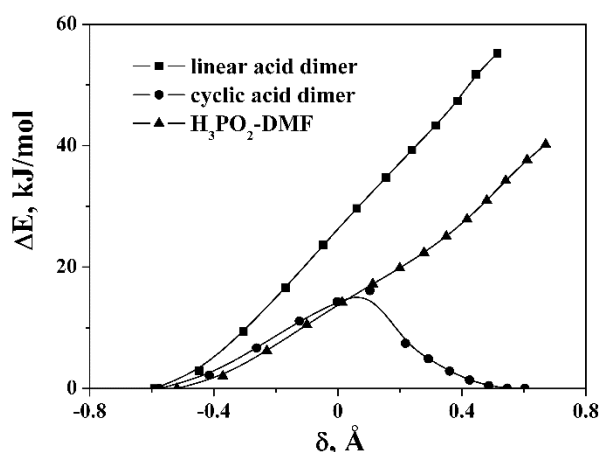


Figure 2. Potential energy profiles for proton transfer in the solvated H_3PO_2 dimers and H_3PO_2 -DMF complex. The curves for each case are assigned in the legend

Proton transfer in H-bonded complexes at fixed O...O distances (r_{OO}). The energy curves for proton transfer in the H_3PO_2 -DMF are plotted in Figure 3. Similar results are observed for linear structure of the H_3PO_2 dimer. The PES has a single distinct minimum for sufficiently small O...O distances whereas a double-well curve appears along the proton transfer coordinates at $r_{\text{OO}} > 2.5$ Å. In the latter cases, the proton can pass through the energy barrier, if this process will take place. This suggests that a hydrogen atom will be bonded to either the oxygen of acid or the DMF oxygen atom, but will not stay in the transition state. With increasing intermolecular O...O distance the energy barrier increases. It is worth noting that the proton transfer process in the solvated complex of H_3PO_2 with DMF at fixed distances is more favored than the ones between acid molecules themselves. For comparison, the energy barrier heights for, e.g., $r_{\text{OO}} = 2.7$ Å are 68.59 and 51.97 kJ/mol for the linear H_3PO_4 dimer and H_3PO_2 -DMF, respectively.

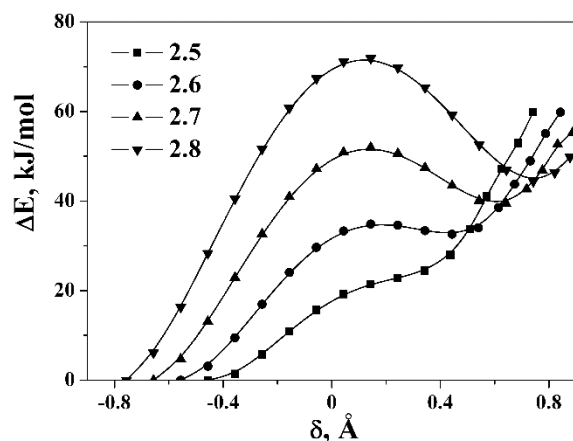


Figure 3. Potential energy profiles for proton transfer in the solvated H_3PO_2 -DMF complex at various fixed O...O distances. The curves for each distance (Å) are assigned in the legend

In order to compare the three acids of phosphorus (phosphoric, phosphonic and phosphinic acids), the energy profiles for proton transfer in acid-DMF complexes at $r_{\text{OO}}=2.7$ Å are collected together in Figure 4. All curves show qualitatively similar shapes when passing from H_3PO_2 to H_3PO_3 and H_3PO_4 . The PES for each of the complexes has a double-well form (but not symmetric). The height of the energy barrier for proton transfer in complexes of these acids with DMF becomes lower with increasing number of OH groups of acid.

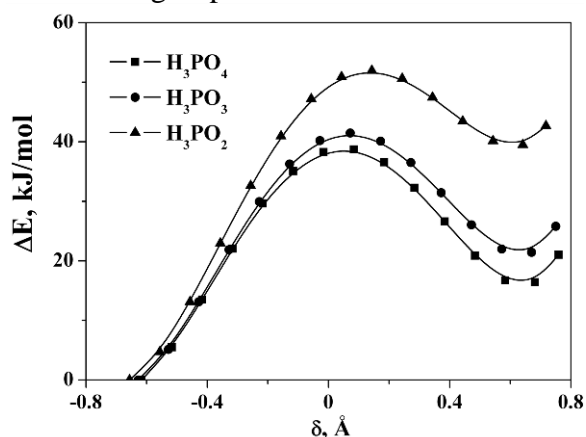


Figure 4. Comparison of the potential energy curves for proton transfer in the solvated complexes of phosphorus acids with DMF at $r_{\text{OO}}=2.7$ Å. The curves for each case are assigned in the legend

This work was partially financially supported by the Russian Foundation for Basic Research (Project No. 15-43-03088).

References

1. Fedorova I. V., Khatuntseva E. A., Krest'yaninov M. A., Safonova L. P. C-PCM based calculation of energy profiles for proton transfer in phosphorus-containing acid-*N,N*-dimethylformamide complexes // Russ. J. Phys. Chem. A. 2016. V. 90. № 2. P. 293-299.
2. Fedorova I. V., Krestyaninov M. A., Kiselev M. G., Safonova L. P. Solvent effect on proton transfer in the complexes of *N,N*-dimethylformamide with sulfuric and phosphoric acid: A DFT investigation // J. Mol. Struct. 2016. V. 1106. P. 424-429.
3. Kreuer K. D. On the complexity of proton conduction phenomena // Solid State Ionics. 2000. V. 136-137. P. 149-160.

THEORETICAL AND EXPERIMENTAL TOOLS FOR INVESTIGATING TRANSPORT PROPERTIES THROUGH NF MEMBRANES

¹Patrick Fievet, ²Anthony Szymczyk, ¹Sébastien Déon

¹Institut UTINAM, Besançon, France, *E-mail: patrick.fievet@univ-fcomte.fr*

²Institut des Sciences Chimiques de Rennes, Rennes, France,
E-mail: anthony.szymczyk@univ-rennes1.fr

Nanofiltration (NF) uses membranes with charged pores of nano-scale dimensions. Due to its real potentialities for the separation or purification of liquid mixtures, this technique has found applications in various industrial sectors like industrial effluent treatment, water softening, drinking water production... Consequently, researchers have engaged in the development of transport models and characterization techniques with the aim of identifying and understanding the physical phenomena involved in the solute separation by NF membranes. The most widely adopted NF models are based on the extended Nernst-Planck equation to describe the mass transfer and an equilibrium partitioning relation to describe the distribution of ions at the pore inlet and outlet. Among the continuous models, the SEDE (Steric, Electric and Dielectric Exclusion) model is one of the latest developed [1]. It includes the dielectric exclusion mechanism, in terms of both Born dielectric effect and image forces contribution, in partitioning equations at membrane/solution interfaces. In this presentation, the coupling between the various mechanisms involved in the retention phenomenon will be pointed out and discussed. It will be shown that both dielectric effects (i.e. image forces and Born dielectric effect) make the Donnan exclusion stronger whereas the presence of a fixed charge on the pore walls as well as the ionic atmosphere surrounding an ion screens the interaction of this ion with the pore wall via image forces.

The SEDE model can also be used to analyse the electrical potential difference, called membrane potential, arising through NF membranes separating two solutions of the same electrolyte at the same temperature and hydrostatic pressure but different concentrations. Up to now, theoretical studies on the membrane potential phenomenon have been performed from either the Teorell-Meyer-Sievers model or the space charge model. The common feature of these studies is that ions were treated as point charges and dielectric effects were neglected. The membrane potential of charged membranes is always bounded between the Nernst potential (at low concentrations) and the diffusion potential (at high concentrations). It will be shown that pore size can be deduced from the high-concentration limit of the membrane potential (which depends on neither the dielectric constant inside the pores nor the membrane fixed charge but is only affected by the pore size) measured with binary electrolytes whereas the membrane potential measured at high salt concentration with ternary mixtures (i.e. three different ions coming from two binary electrolytes with a common ion) can be used to compute the dielectric constant inside pores provided that the pore size is known [2,3,4]. The membrane potential constitutes an alternative way for membrane characterization with the advantage of avoiding the need of additional rejection rate measurements. However, this approach has the disadvantage of using all or part of model equations to determine the desired magnitude.

Among the magnitudes of interest, the dielectric constant of the solution inside nanopores has rarely been estimated independently from NF measurements. Yet, such an independent measurement is crucial in validating the lowering of the dielectric constant of a solution inside nanodimensional pores and in reducing the number of fitting parameters for a better understanding and description of the separation properties of NF membranes. The measurement of the dielectric constant of the solution inside the active-layer pores is particularly made difficult by the presence of one or several supporting-layers much thicker than the active layer, which is responsible for separations. Literature shows that the separation of the individual properties of both active and support layers of NF membranes by Electrochemical Impedance Spectroscopy (EIS) is not possible or differences in the EIS spectra obtained with and without membrane, in a configuration solution/membrane/solution, are interpreted as being characteristic of support layer/active layer separation [5]. A different approach was recently adopted, whereby the membrane support layer

was removed by dissolution and measurements were performed directly with the free active layer [6]. Moreover, a mercury/active layer/mercury configuration was used in order to eliminate the contribution of external solution layer to the impedance. The comparison of impedance spectra obtained for the whole membrane and active layer alone revealed very low contribution of the active layer to the overall membrane impedance. The dielectric constant (ϵ_p) and conductivity inside the pores of the active layer were evaluated from capacity and resistance measurements. The dielectric constant inside the pores was found to be smaller than its bulk value, irrespective of the electrolyte used, and pore conductivity exceeded the bulk conductivity.

The membrane charge also plays an important role in ion rejection. However, in the case of membranes composed of several layers or membranes with ion-rejection capability, tangential streaming potential measurements are preferred because it is difficult to get a meaningful and reliable interpretation of data from transversal measurements. However, the contribution of the underlying support layer(s) to the cell electric conductance but also, in some cases, to the measured streaming current gives rise to complications in the interpretation of tangential streaming potential data [7,8,9]. That is why, it has been proposed to measure the streaming current along composite membrane skin-layers since its interpretation is not complicated by the electric conduction through the porous sublayer(s). The dependence of streaming current coefficient on the channel cross-section (for flat membranes, the channel is obtained by putting two identical membranes face to face) enables to determine separately the contributions of external and internal (pore surface) membrane surfaces to the streaming current and to deduce the zeta potential of external membrane surface. This potential can then be converted into effective charge density.

Many studies have shown that the rejection of neutral solutes by NF decreases in the presence of a salt. This phenomenon could be explained by a partial dehydration of neutral solutes in the presence of ions because water would preferentially solvate ions (“salting-out” effect) and/or an increase in the mean pore size due to repulsive forces between counter-ions inside the pores (“pore swelling” effect). In order to investigate the significance of these effects, rejection properties of NF ceramic and organic membranes were studied with single polyethyleneglycol (PEG) solution and mixed PEG/salt solutions [10,11,12]. For the ceramic membrane, the decrease in the rejection rate was imputed to the sole partial dehydration of PEG molecules induced by the surrounding ions (the pore swelling cannot be invoked since pores are rigid). This assumption was confirmed by the lowering of the PEG rejection rates which followed the Hofmeister series. For the organic membrane, it was found that the salting-out effect cannot solely explain the rejection lowering of a neutral solute in the presence of salt. The contribution of both phenomena to the rejection decrease could be quantified. It was found that the contribution of the salting-out effect also follows the Hofmeister series. The pore swelling phenomenon due to accumulation of counterions inside pores resulting from an increase in the membrane charge was supported by electrokinetic charge density measurements.

It is crucial that transport models and characterization tools continue to be developed in order to better understand the physical phenomena involved in the solute separation by NF membranes, thus increasing the development of this membrane process.

References

1. *Szymczyk A., Fievet P.* Investigating transport properties of nanofiltration membranes by means of a steric, electric and dielectric exclusion model // *J. Membr. Sci.* 2005. V. 252. P. 77-88.
2. *Lanteri Y., Szymczyk A., Fievet P.* Influence of steric, electric and dielectric effects on membrane potential // *Langmuir*, 2008. V. 24. P. 7955–7962.
3. *Lanteri Y., Szymczyk A., Fievet P.* Membrane potential in multi-ionic mixtures // *J. Phys. Chem. B*, 2009. V. 113. P. 9197–9204.
4. *Escoda A., Lanteri Y., Fievet P., Déon S., Szymczyk A.* Determining the dielectric constant inside pores of nanofiltration membranes from membrane potential measurements // *Langmuir* 2010. V. 26. P. 14628–14635.

5. *Montalvillo M., Silva V., Palacio L., Calvo J. I., Carmona F. J., Hernández A., Prádanos P.* Charge and dielectric characterization of nanofiltration membranes by impedance spectroscopy, *J. Membr. Sci.* 2014. V. 454. P. 163-173.
6. *Efligenir A., Fievet P., Déon S., Salut R.* Characterization of the isolated active layer of a NF membrane by electrochemical impedance spectroscopy // *J. Membr. Sci.* 2015. V. 477. P. 172-182.
7. *Yaroshchuk A. E., Luxbacher T.* Interpretation of electrokinetic measurements with porous films: role of electric conductance and streaming current within porous structure // *Langmuir* 2010. V. 26. P. 10882–10889.
8. *Déon S., Fievet P., Osman Doubad C.* Tangential streaming potential/current measurements for the characterization of composite membranes // *J. Colloid Int. Sci.*, 2012. V. 423–424. P. 413–421.
9. *Efligenir A., Fievet P., Déon S., Sauvade P.* Tangential electrokinetic characterization of hollow fiber membranes: effects of external solution on cell electric conductance and streaming current // *J. Membr. Sci.* 2015. V. 496. P. 293-300.
10. *Bouranene S., Szymczyk A., Fievet P., Vidonne A.* Influence of inorganic electrolytes on the retention of polyethyleneglycol by a nanofiltration ceramic membrane // *J. Membr. Sci.* 2007. V. 290. P. 216-221.
11. *Escoda A., Fievet P., Lakard S., Szymczyk A., Déon S.* Influence of salts on the rejection of polyethyleneglycol by an NF organic membrane: pore swelling and salting-out effects // *J. Membr. Sci.* 2010. V. 347. P. 174-182.
12. *Escoda A., Bouranene S., Fievet P., Déon S., Szymczyk A.* Dehydration and pore swelling effects on the transfer of PEG through NF membranes // *Membrane Water Treatment* 2013. V. 4. P. 127-142.

SYNTHESIS AND PREDICTION OF TRANSPORT PROPERTIES OF HYBRID BILAYER ION-EXCHANGE MEMBRANES ON THE BASE OF MF-4SC, HALLOYSITE AND PLATINUM

Anatoly Filippov

Gubkin University, Moscow, Russia, *E-mail: filippov.a@gubkin.ru*

Introduction

It is well-known that American cation-exchange perfluorinated membrane Nafion-117[®] (DuPont de Nemours, USA) and its Russian analogue MF-4SC (LTD Plastpolymer, Russia) are among the most widely used as separators in various devices like fuel cells, electrolyzers, electrolysers, sensors and investigated ion-exchange materials. Surface and spatial modification of ion-exchange membranes by incorporation of different inorganic dopants allows to change their stability and structural properties as well as ion and molecular transport. Polyaniline, nanoparticles of noble metals, oxides of zirconium and silicon [1], carbon and halloysite nanotubes [2] and other materials that can transform transport properties of the membranes in the preferred direction are frequently used as such dopants. This poses the priority problem of a reliable characterization of the newly created hybrid nanocomposites membranes. Here we propose an attempt to solve this problem for bilayer hybrid membranes, based on a theoretical examination of the electrodiffusion transport and our own experimental data for monolayer membranes. As a dopant, halloysite and platinum nanoparticles were used. Halloysite nanotubes of 2% by weight were added to one of the membrane layers during its synthesis by casting method. Halloysite clay is a natural tubule material formed by rolled kaolin sheets. Halloysite is aluminosilicate which is chemically identical to kaolin but typically contains minor amount (less than 1 wt%) of iron ions. Prior to synthesis, nanoparticles of platinum were deposited on the external surface of halloysite nanotubes [3]. A similar attempt to membrane characterization was made in our recent work [4] for the surface-modified MF-4SC membranes in low-temperature plasma. Thus, halloysite nanotubes are used not only as a container for the delivery of metallic nanoparticles inside the membrane matrix, but also as a hydrophilic object, which increases the moisture content of the membrane. Ion-exchange membranes with enhanced water uptake are interesting for fuel cells applications because make it possible to improve the properties of fuel cells.

Experiment

Composite (hybrid) bilayer membranes based on the perfluorinated matrix MF-4SC, halloysite nanotubes and platinum nanoparticles were synthesized by a two-stage casting process: first a thicker layer of unmodified polymer, then a thin layer of polymer with the added halloysite nanotubes and platinum nanoparticles embedded on their outer surface (membrane No 1). A bilayer composite was also synthesized in a different order - a thinner, halloysite-modified layer was first cast, followed by a layer of pure polymer without dopant (membrane No. 2). When casting the membrane No. 1, a solution of polymer LF-4SC (manufactured by JSC "Plastpolymer", St. Petersburg, Russia) and a solvent of dimethylformamide were used. Initially, the first layer was cast from a pure polymer solution (thickness of 160 μm). The membrane was dried according to a standard procedure developed and described in detail in our work [3]. Then, after the first layer completely dried out, the second layer (thickness of 40 μm) was cast from a modified polymer solution of LF-4SC (using dimethylformamide as a solvent) with the addition of 2% wt. of halloysite nanotubes with platinum nanoparticles encapsulated on the outer surface of nanotubes. When casting membrane No. 2 we used a solution of polymer LF-4SC and two solvents: dimethylformamide and isopropyl alcohol. Primarily, the first layer was cast from a modified polymer solution of LF-4SC (isopropyl alcohol solvent) with the addition of 2% wt. of halloysite nanotubes functionalized by platinum nanoparticles on their outer surface (the thickness of the modified layer was 40 μm). The membrane was dried according to the standard procedure described in [3]. Then, after complete drying of the first layer, the second layer (160 μm thick) was cast from a pure polymer solution of LF-4SC (a solvent was dimethylformamide). Thus,

reproducible homogeneous and resistant to aggressive media double-layer membranes without microdefects (microcracks), having a constant thickness were synthesized. The obtained hybrid nanocomposites No. 1 and No. 2 were studied by electron microscopy (Figs 1, 2) and characterized.

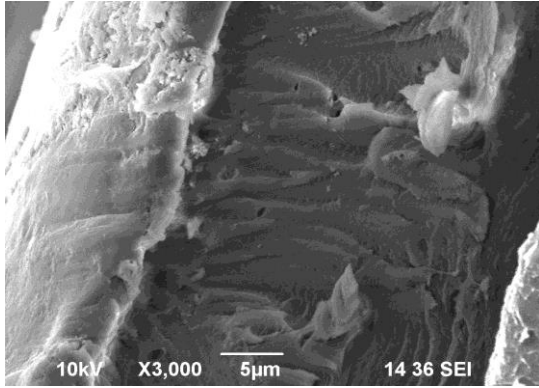


Figure 1. Microphotography of the cross section of bilayer hybrid membrane No. 2.

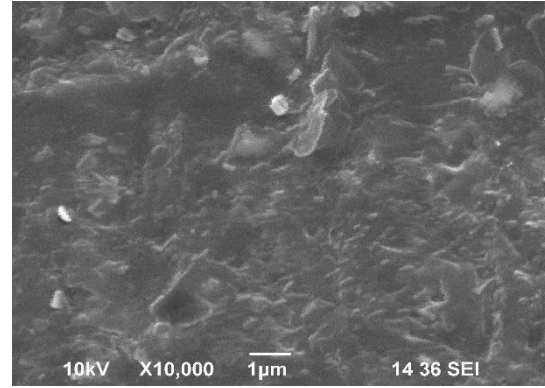


Figure 2. Microphotography of the modified surface of bilayer hybrid membrane No. 2.

Theoretical prediction of diffusion permeability and comparison with experiment

Earlier in [3], we obtained data on the magnitude of physico-chemical parameters (diffusion coefficients of ions $D_{m\pm}$ and the equilibrium ion-pair distribution coefficient γ_m , Table 1) of a single-layer membrane MF-4SC cast from a solution of a pure polymer and a membrane spatially modified by halloysite nanotubes (2% wt.) with platinum nanoparticles. On their basis, a priori to the experiment, the weak asymmetry of the diffusion permeability of the two-layer membrane No. 2 was quantitatively predicted. The calculation based on the model of the bilayer membrane developed earlier by us [5] showed a good agreement between the theoretical and experimental values of the diffusion permeability of the bilayer membrane over a solution of hydrochloric acid. This makes it possible to create bilayer hybrids with a predetermined diffusion permeability.

Table 1. Parameters of pure and hybrid single-layer membranes MF-4SC [3].

Membrane	γ_m	$D_{m+}, \mu\text{m}^2/\text{s}$	$D_{m-}, \mu\text{m}^2/\text{s}$	$D_m, \mu\text{m}^2/\text{s}$
initial MF-4SC, $i=2$	0.481	1417	15.4	30.1
MF-4SC/Hall+Pt, $i=1$	0.442	990	6.2	12.3

To find the theoretical values of diffusion permeability coefficients, the following formulas obtained in the above-mentioned work [5] were used:

$$P_s = \frac{(\bar{D}_{m1}/\gamma_1)(1+h_2/h_1)}{\sqrt{(|\bar{\sigma}_2| + \sqrt{\bar{\sigma}_1^2 + 4})^2 + 4(\bar{v}^2 - 1) + (|\bar{\sigma}_2|\bar{v} + \sqrt{\bar{\sigma}_1^2 + 4})}}, \quad (1)$$

$$P_w = \frac{(\bar{D}_{m1}/\gamma_1)(1+h_2/h_1)}{\sqrt{(|\bar{\sigma}_2| + \bar{v}\sqrt{\bar{\sigma}_1^2 + 4})^2 - 4(\bar{v}^2 - 1) + (|\bar{\sigma}_1| + \bar{v}\sqrt{\bar{\sigma}_2^2 + 4})}}, \quad (2)$$

where $\bar{\sigma}_i = \gamma_i \left| \frac{\bar{\rho}_i}{C_0} \right| > 0$, $\bar{D}_{mi} = \frac{2D_{mi+}D_{mi-}}{D_{mi+} + D_{mi-}}$, $\gamma_i = \sqrt{\gamma_{i+}\gamma_{i-}}$, $i = 1, 2$, $\bar{v} = \frac{\bar{D}_{m1}h_2\gamma_2}{\bar{D}_{m2}h_1\gamma_1}$, i – number of the membrane layer (1- modified, 2- unmodified layer), ρ_i – layer exchange capacity, \bar{D}_i , $D_{mi\pm}$, γ_i , $\gamma_{i\pm}$ – diffusion and equilibrium distribution coefficients of the electrolyte molecule and ions in the membrane, C_0 – electrolyte concentration, h_i – thickness of the i -layer. Exchange capacities of both layers were considered equal to 0.98 M, and the ratio of the layer thicknesses $h_2/h_1 = 4$. The remaining parameters used are shown in Table 1. A comparison of the predicted

theoretical concentration dependences (curves) of the diffusion permeability coefficients of the bilayer membrane and their measured values (circles) is shown in Fig. 3 and 4. We note that the curves are drawn without any fitting of the physicochemical parameters of the membrane. The agreement between experiment and theory for a membrane facing the modified side to water is slightly better than when this side is turned to an acid solution.

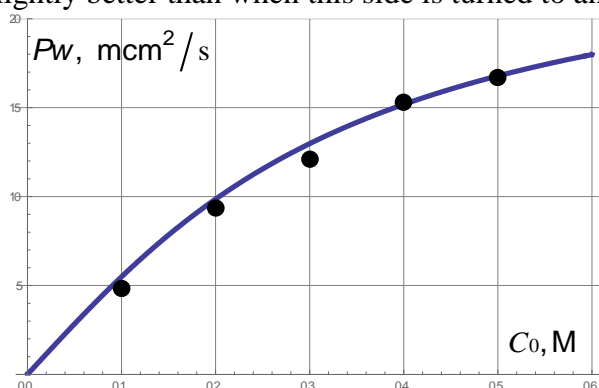


Figure 3. Dependence of the coefficient P_w on the concentration of HCl.

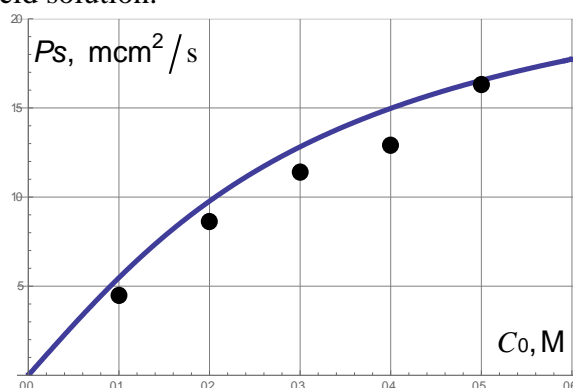


Figure 4. Dependence of the coefficient P_s on the concentration of HCl.

Conclusion

The study of the transport characteristics of perfluorinated membranes after their spatial modification with halloysite nanotubes and platinum nanoparticles showed that the diffusion permeability of hybrid membranes is somewhat lower in comparison with the initial (pure) membrane. In this case, the integral coefficient of diffusion permeability of the membrane modified by halloysite nanotubes covered with platinum nanoparticles decreases by 50-55%. This suggests that under the operating conditions of the fuel cell the crossover through the modified membranes will be lower. The electric conductivity of membranes increases after modification. The greatest effect of increasing the electric conductivity (by about 30%) was noted again for a sample modified with halloysite and Pt. Since the observed changes in the structural characteristics cannot cause such an increase in the conductivity of the samples, the possible cause of this effect can be the contribution of the electronic conductivity of the metal. Thus, the modification of the perfluorinated membrane by the halloysite nanotubes with metal nanoparticles deposited on their outer surface does not lead to a noticeable change in the structure of the membranes and does not worsen their transport properties. This makes it possible to predict the effective use of hybrid membranes based on MF-4SC and halloysite nanotubes with platinum nanoparticles, not only as separating diaphragms in fuel cells and electromembrane devices, but also as promising catalytic systems.

This study was supported by the Ministry of Education and Science of the Russian Federation (Grant No 14.Z50.31.0035).

References

1. Filippov A.N., Safronova E.Yu. Yaroslavtsev A.B. // *J. Memb. Sci.* 2014. V.471. P.110–117.
2. Filippov A., Khanukaeva Daria, Afonin D., Skorikova G., Ivanov E., Vinokurov V., Lvov Yu. // *J. Mater. Sci. & Chem. Eng.* 2015. V.3. P.58-65.
3. Filippov A., Afonin D., Kononenko N., Lvov Yu., Vinokurov V. // *Colloids Surf. A.* 2017. V.521. P.251-259.
4. Filippov A., Afonin D., Kononenko N., Shkirskaya S. // *AIP Conference Proceedings.* 2015. V.1684. P.030004-1–030004-9.
5. Filippov A.N., Starov V.M., Kononenko N.A., Berezina N.P. Asymmetry of diffusion permeability of bi-layer membranes // *Adv. Colloid Interface Sci.* 2008. V.139. P.29–44.

CELL METHOD TO CALCULATION OF ELECTRIC CONDUCTIVITY OF ION-EXCHANGE MEMBRANES

Anatoly Filippov, Tamara Philippova

Gubkin University, Moscow, Russia, E-mail: filippov.a@gubkin.ru

Introduction

The cell method is one among significant effective methods to investigate dense dispersion systems such as, for example, porous ion-exchange membranes. A formation of the cell model for the dense swarm particles may be based on replacement of real system of randomly spatially located particles by a periodic structure of identical spheres to be arranged in spherical cells. The influence of neighboring particles is taken into account by choosing boundary conditions in a special way. Attempts to systemize the variety of electrokinetic, electrodiffusive and diffusiokinetic processes were undertaken recently elsewhere using thermodynamics of irreversible processes. An advantage of a such approach leads to measure directly in experiments all thermodynamic variables, fluxes and forces, involved in governing equations.

Theory

Let us choose the following thermodynamic forces as independent variables to be given during experimental observation: pressure drop $p_{10} - p_{20} = -\Phi_1 h$, electric potential $\varphi_{10} - \varphi_{20} = -\Phi_2 h$ and chemical potential $(c_{10} - c_{20})RT = -\Phi_3 h$ drops be arisen on a porous film (membrane) with the thickness h immersed within measuring device which is filled by binary electrolyte solution.

As dependent experimentally determined variables we can take thermodynamic fluxes: I_1 – fluid flux; I_2 – charge flux (electric current); I_3 – diffusion flux. Then the phenomenological transport equations may be written in the following way:

$$I_i = -\sum_{k=1}^3 L_{ik} \Phi_k, \quad i = 1, 2, 3, \quad (1)$$

where kinetic coefficients L_{ik} can be determined using the cell model. It is known that the matrix consisted of kinetic coefficients should be symmetrical one in accordance with Onsager's theorem, i.e. $L_{ik} = L_{ki}$. The main point of the present consideration is to calculate specific electric conductivity of the membrane L_{22} :

$$L_{22} = -\left. \frac{I_2}{\Phi_2} \right|_{\Phi_1=0, \Phi_3=0}. \quad (2)$$

Relation (2) indicates that correct measuring of L_{22} is possible only upon an absence of the cell diffusion potential as well as external pressure drop and under condition $\Phi_2 = \text{const}$. These boundary conditions lead to independent determination of the velocity field, concentration and electric potential profiles within the unique cell. We should mention here that the hydrodynamic permeability L_{11} in case of uncharged membrane consisting of cylindrical and spherical partly porous particles was calculated in our works [1, 2].

As it was mentioned above, the ion-exchange membrane can be assumed as a periodic array of porous charged spheres with the same radius a to be immersed into fluid spherical shells of radius b . The value of b has to be chosen in such a way that the ratio of the particle volume to that of the cell is equal to a volume fraction α in regard to the dispersion system:

$$\alpha = \gamma^3 = (a/b)^3 = 1 - \varepsilon, \quad (3)$$

where ε is porosity.

The fluid motion in an outer region ($a < r < b$) will be described by Stokes' equations under low Reynolds numbers ("creeping flow") with additional electromassive force:

$$\nabla p^o = \mu^o \Delta \mathbf{v}^o - \rho^o \nabla \varphi^o, \quad (4)$$

where $\rho^o = (z_+ c_+^o - z_- c_-^o) F$ presents the volume electric charge; z_{\pm} – valences of the electrolyte ions without sign; c_{\pm}^o – concentrations of cations and anions; F – the Faraday constant; and the incompressibility condition:

$$\nabla \cdot \mathbf{v}^o = 0. \quad (5)$$

The following notations are used here: p^o – local pressure; \mathbf{v}^o – vector of the fluid velocity; μ^o – dynamic viscosity of that fluid; φ^o – local electric potential to be found from Poisson's equation:

$$\Delta \varphi^o = -4\pi \rho^o / \varepsilon^o, \quad (6)$$

with ε^o as dielectric constant of the outer solution.

In a common case of the steady-state electro-hydrodynamic problem, the system of governing equations (4)-(6) must be completed with equations of the concentrations conservation:

$$\nabla \cdot \mathbf{J}^{o\pm} = 0, \quad (7)$$

where $\mathbf{J}^{o\pm}$ are the densities of the ions' fluxes:

$$\mathbf{J}^{o\pm} = \mathbf{v}^o c_{\pm}^o - D_{\pm} \left(\nabla c_{\pm}^o \pm z_{\pm} c_{\pm}^o \nabla \varphi^o \frac{F}{RT} \right). \quad (8)$$

Here D_{\pm} are ions diffusivities, R is the universal gas constant and T is the absolute temperature. The fluid motion in an inner region ($0 \leq r < a$) is governed by the modified Brinkman equation taken with volumetric electric force:

$$\nabla p^i = \mu^i \Delta \mathbf{v}^i - k \mathbf{v}^i - \rho^i \nabla \varphi^i, \quad (9)$$

where $\rho^i = (z_+ c_+^i - z_- c_-^i) F$ and μ^i – dynamic viscosity of the "Brinkman fluid"; k is the Brinkman constant to be in an reverse proportionality with respect to the permeability of the porous medium. We suppose also that the "Brinkman fluid" is incompressible:

$$\nabla \cdot \mathbf{v}^i = 0 \quad (10)$$

and electric potential satisfies the Poisson equation:

$$\Delta \varphi^i = -4\pi (\rho^i - \rho_v) / \varepsilon^i \quad (11)$$

where ε^i is dielectric permittivity of the Brinkman medium and ρ_v is the bulk density of a fixed electric charge of the porous skeleton. Further, it is necessary to complete the system of (9)-(11) equations with the equation of conservation of concentrations:

$$\nabla \cdot \mathbf{J}^{i\pm} = 0, \quad (12)$$

where densities of the fluxes of positive and negative ions within porous particle are given as follows:

$$\mathbf{J}^{i\pm} = \mathbf{v}^i c_{\pm}^i - D_{\pm}^m \left(\nabla c_{\pm}^i \pm z_{\pm} c_{\pm}^i \nabla \varphi^i \frac{F}{RT} \right) \quad (13)$$

and D_{\pm}^m are the ions diffusivities within the porous medium.

Results and discussion

The system of governing equations (4)-(13) should be completed by appropriate boundary conditions: continuity of stresses, velocities and normal components of ion fluxes at interface

$r = a$, Mehta and Morse (Cunningham) condition at the cell surface $r = b$. Assuming the outer and inner Debye's lengths to be small compared with particle's radius a , we can effectively remove double electric layers by the electric potential and ions' concentrations jumps through the interface $r = a$:

$$c_{\pm}^i = \frac{c_{\pm}^o}{\gamma_{\pm}} \exp\left(\mp z_{\pm} \left(\varphi^i - \varphi^o\right) \frac{F}{RT}\right) \quad (14)$$

with γ_{\pm} as equilibrium distribution coefficients for cations and anions inside porous particle. We apply the method of perturbation of equilibrium solution and assume that all deviations from the equilibrium are small. As a result, using the solution found together with formulae (2), we have got exact value of the electric conductivity. The general formula is sufficiently cumbersome one so we restricted ourselves here by the limiting case of excluded co-ions (ideal selective membrane) and neglected the difference between ions' diffusivities (i.e. $D_{\pm} = D_{\pm}^m = D_0$) for simplicity of an analysis:

$$L_{22} / \left(\frac{2D_0 F^2}{RT} \right) = \left(1 + \frac{3(1-\varepsilon)}{2} \left(\frac{\rho_V - c_0}{\varepsilon \rho_V + (3-\varepsilon)c_0} - \frac{1}{3-\varepsilon} \right) \right) c_0, \quad (z_{\pm} = 1). \quad (15)$$

Figure 1 shows 3D-dependence of electric conductivity of the cation-exchange membrane as function of electrolyte concentration c_0 and porosity $\varepsilon = 1 - \alpha$ under high ion-exchange capacity $\rho_V = 10 M$.

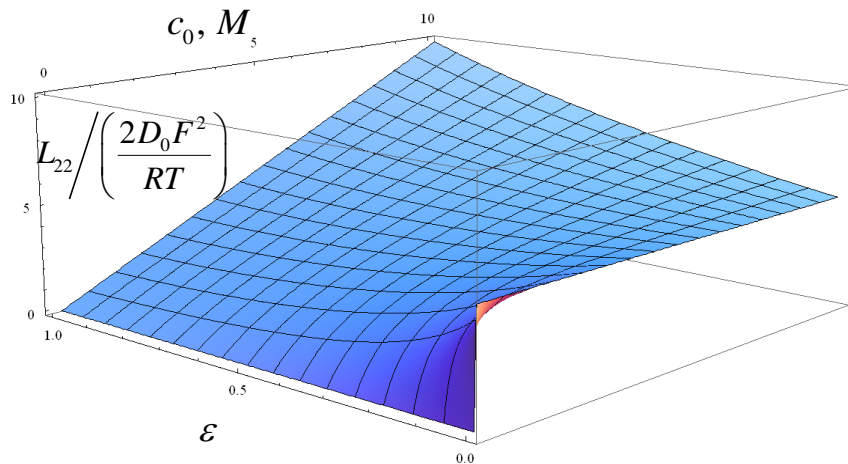


Fig. 1. Dependence of electric conductivity L_{22} on electrolyte concentration c_0 and porosity ε

From figure it is clear that all dependencies on concentration are presented by convex curves when porosity is not very high that corresponds to the experimental behavior of electric conductivity. If porosity is higher then conductivity can be higher or lower in dependence of the concentration value. Next our step will be a comparison between theoretical and experimental values of the membrane conductivity.

This study was supported by the Russian Foundation for Basic Research (Grant No 17-08-01287).

References

1. Deo Satya, Filippov Anatoly, Tiwari Ashish, Vasin Sergey, Starov Victor. Hydrodynamic permeability of aggregates of porous particles with an impermeable core // *Adv. Colloid Interface Sci.* 2011. V.164. P.21–37.
2. Yadav Pramod Kumar, Tiwari Ashish, Deo Satya, Filippov Anatoly, Vasin Sergey. Hydrodynamic permeability of membranes built up by spherical particles covered by porous shells: effect of stress jump condition // *Acta Mechanica.* 2010. V.215, P.193–209.

ASYMPTOTIC AND NUMERICAL INVESTIGATION OF ELECTROPHORESIS IN A WEAK ELECTRIC FIELD

^{1,2}Elizaveta Frants, ³Georgy Ganchenko, ³Vladimir Shelistov, ^{3,4}Evgeny Demekhin

¹Department of mathematics and computer science, Financial University, Krasnodar, Russia
E-mail: eafrants@gmail.com

²Department of applied mathematics, Kuban State University, Krasnodar, Russia

³Laboratory of micro- and nanoscale electro- and hydrodynamics, Financial University, Krasnodar, Russia, *E-mail: ganchenko.ru@gmail.com, VShelistov@fa.ru*

⁴Research Institute of Mechanics, Moscow State University, Moscow, Russia,
E-mail: edemekhi@gmail.com

Introduction

In this paper, we study the motion of an ion-exchange particle in an electrolyte solution under a weak external electric field. Analytic estimates for the particle's velocity have been obtained using an asymptotic method. In addition, a numerical solution has been obtained, including the concentrations' and electric potential profiles and flow streamlines. A comparison of analytical results with the results of numerical simulation has been made.

Mathematical model

We consider the motion of a conducting micro-particle with an ion-selective surface permeable only for positive ions in a diluted solution of a binary electrolyte under an electric field of strength E_∞ . Under the following assumptions: diffusion coefficients and valences of cations and anions are equal, Reynolds number is small (which corresponds to micro- and nanosize particles), and the particle's surface is semipermeable, this motion is described with the Nernst–Planck–Poisson–Stokes system of equations. Since the particle under consideration is spherical, the solution is sought in the spherical coordinate system moving with the particle's velocity and with the origin at the center of the particle. The fluid motion is considered in the Stokes approximation. The problem is symmetric, so it is sufficient to consider the dependence on one angle and to take the system of equations in a two-dimensional formulation:

$$\frac{\partial c^\pm}{\partial t} + \mathbf{U} \cdot \nabla c^\pm = \pm \nabla (c^\pm \nabla \Phi) + \nabla^2 c^\pm; \quad (1)$$

$$\nu^2 \nabla^2 \Phi = c^- - c^+; \quad (2)$$

$$-\nabla P + \nabla^2 \mathbf{U} = (c^+ - c^-) \frac{\kappa}{\nu^2} \nabla \Phi = 0, \quad \nabla \cdot \mathbf{U} = 0. \quad (3)$$

Here c^\pm are the molar concentration of cations and anions, \mathbf{U} is the velocity vector, Φ is the electrostatic potential, P is the pressure, ν is the Debye number, κ is a coupling coefficient between the hydrodynamic and electrostatic parts of the problem.

We impose the following boundary conditions on the particle's surface: the concentration of positive ions is fixed; the flow of negative ions through the surface is absent; the potential of the conducting particle is constant and, without loss of generality, may be set to zero; the velocity components satisfy the impermeability and no-slip conditions:

$$r = 1: c^+ = p, \quad c^- \frac{\partial \Phi}{\partial r} - \frac{\partial c^-}{\partial r} = 0, \quad \Phi = 0, \quad \mathbf{U} = 0. \quad (4)$$

Far from the microparticle, the concentration tends to equilibrium and the electric strength and velocity vectors are assumed to be parallel to the x -axis of the Cartesian coordinate system:

$$r \rightarrow \infty: c^+ \rightarrow 1, \quad c^- \rightarrow 1, \quad \mathbf{U} \rightarrow (-U_\infty \sin \theta, U_\infty \cos \theta), \quad \Phi \rightarrow -E_\infty r \cos \theta. \quad (5)$$

The problem is closed by imposing the initial conditions: the concentrations of cations and anions are assumed equal to the equilibrium concentration: $t = 0: c^\pm = 1$.

Results and Discussion

In order to obtain an asymptotic solution of a system in partial derivatives, we used the general expansion of the functions of the system with respect to only linear terms:

$$c^\pm = c_0^\pm + c_1^\pm \cdot E_\infty + O(E_\infty^2), \quad \Phi = \Phi_0 + \Phi_1 \cdot E_\infty + O(E_\infty^2), \quad U = U_0 + U_1 \cdot E_\infty + O(E_\infty^2). \quad (6)$$

The zero-order terms have been found from the assumption that $\nu \rightarrow 0$. As a result, analytical expressions have been obtained for the functions $K = c^- + c^+$ and Φ . In addition, a formula expressing the dependence of the particle velocity U_∞ on the field strength E_∞ has been obtained. This dependence has turned out to be linear.

Fig. 1 shows the comparison of the total ion concentration K calculated from analytical formulas (continuous lines) with the results of numerical simulation. The analytical expression for the function $\rho = c^+ - c^-$ coincides with the calculated expression with graphical accuracy.

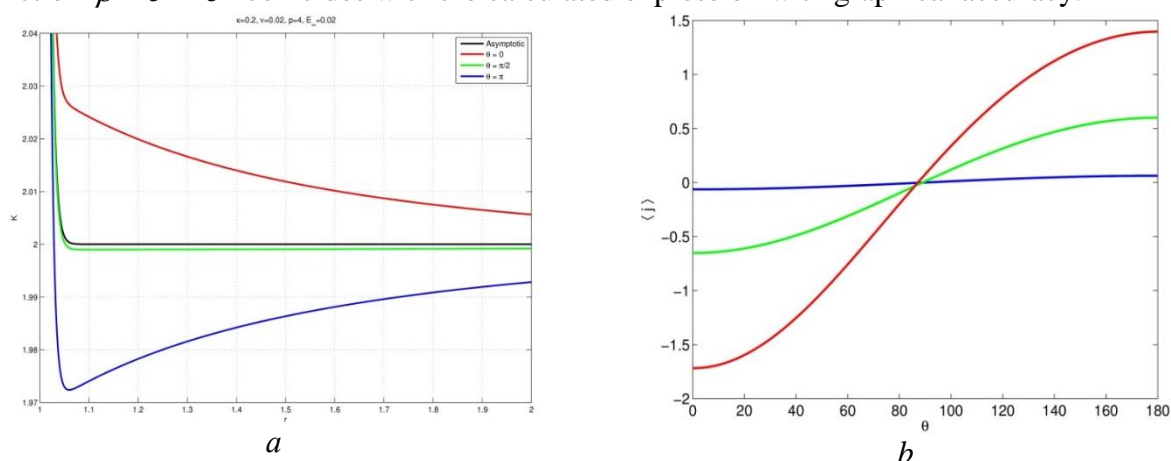


Fig. 1. (a) Comparison of the analytical results with numerical simulation for the total ion concentration K and (b) the average current on the particle's surface as a function of the angle.

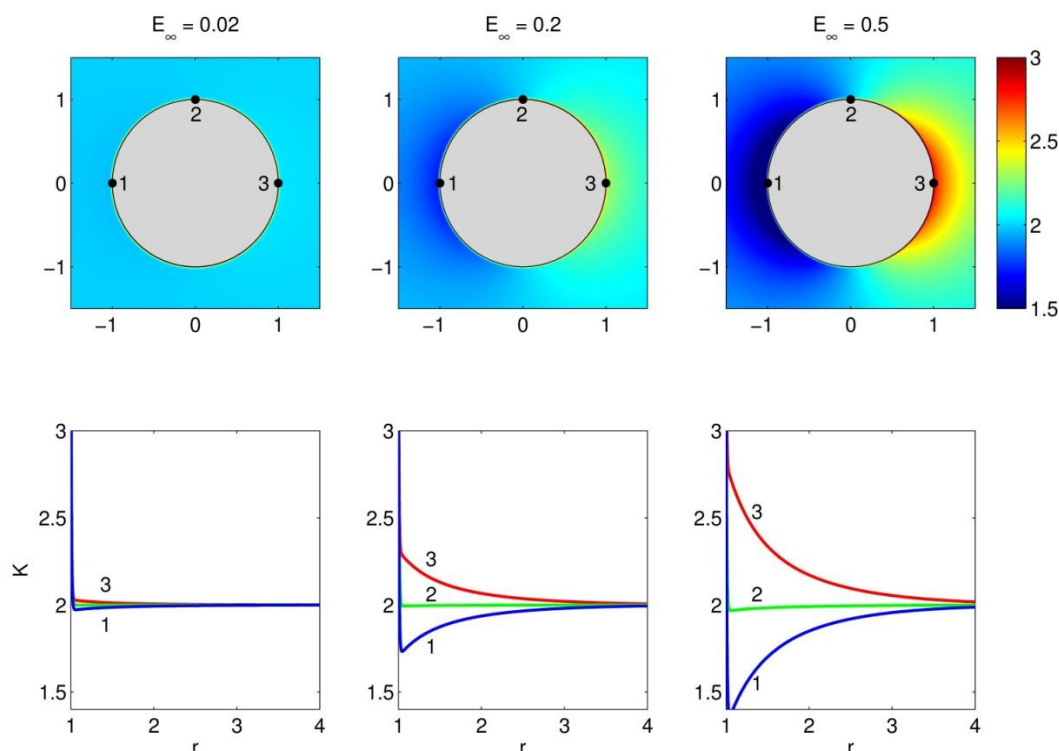


Fig. 2. The distribution of the potential near the particle's surface at different field strengths (upper row) and charge density curves K (bottom row) for the same field strengths for the angle values: $\theta = 0^\circ$, 90° and 180° (curves 1, 2 and 3, respectively).

The work is supported by the Russian Foundation for Basic Research (project No 16-08-00643).

PHASE COMPOSITION, THERMAL AND TRANSPORT PROPERTIES OF RUBIDIUM MONO AND DIHYDROGEN PHOSPHATES SYSTEM

Anna Gaidamaka^{1,2}, Irina Bagryantseva^{1,2}, Valentina Ponomareva^{1,2}

¹Novosibirsk State University, 630090 Novosibirsk, Russia, E-mail: a.gaidamaka@g.nsu.ru

²Institute of Solid State Chemistry and Mechanochemistry SB RAS, 630128 Novosibirsk, Russia

Introduction

Solid acids $M_nH_m(AO_4)_p$ ($M = \text{alkali metal, } A = \text{P, S, Se}$) present an important class of proton conductors. These compounds have high proton conductivity at the intermediate temperature range (130-250°C). Solid acids can be used as perspective electrolytes for membranes of the intermediate temperature fuel cells. They are of interest from both practical and fundamental points of view. Investigations of systems based on solid acids allow improving knowledge about hydrogen bond and proton transport mechanisms.

The investigation of $(1-x)\text{CsH}_2\text{PO}_4 - x\text{Cs}_2\text{HPO}_4 \cdot 2\text{H}_2\text{O}$ gave interesting results: compositions showed high conductivity, a new $\text{Cs}_3(\text{HPO}_4)(\text{H}_2\text{PO}_4) \cdot 2\text{H}_2\text{O}$ phase was found [1]. Due to isotypical crystal structure of cesium and rubidium dihydrogen phosphates one can suggest an existence of highly conductive phases in similar system based on rubidium salts. RbH_2PO_4 is known to exhibit a superprotonic phase transition with conductivity increase by several orders of magnitude. The aim of the present study is to investigate phase composition, thermal and transport properties of $(1-x)\text{RbH}_2\text{PO}_4 - x\text{Rb}_2\text{HPO}_4$ system ($x = 0-1$).

Experiments

$\text{Rb}_2\text{HPO}_4 \cdot 2\text{H}_2\text{O}$ and RbH_2PO_4 were prepared by slow evaporation of aqueous solution containing Rb_2CO_3 and H_3PO_4 in 1:1 and 1:2 molar ratio, respectively. The samples $(1-x)\text{RbH}_2\text{PO}_4 - x\text{Rb}_2\text{HPO}_4$ ($x = 0.1, 0.2, 0.25, 0.33, 0.5, 0.67$) were prepared by solid state synthesis. The properties of $(1-x)\text{RbH}_2\text{PO}_4 - x\text{Rb}_2\text{HPO}_4$ have been investigated with the help of thermal analysis methods (DSC, TG), X-ray powder diffraction (XRD), IR-spectroscopy and ac-impedance spectroscopy.

Results and Discussion

XRD show a mixture of two phases in all samples except $x=0.25$. XRD for $x=0.25$ corresponds to single $\text{Rb}_5\text{H}_7(\text{PO}_4)_4$ phase. The other samples represent a mixture of $\text{Rb}_5\text{H}_7(\text{PO}_4)_4$ and one of the starting compounds (RbH_2PO_4 for $x = 0.1, 0.2$ or $\text{Rb}_2\text{HPO}_4 \cdot 2\text{H}_2\text{O}$ for $x = 0.33, 0.5, 0.67$, respectively). The properties of $\text{Rb}_5\text{H}_7(\text{PO}_4)_4$ except of some details of crystalline structure haven't been studied yet [2]. Thermal and electrotransport properties of $\text{Rb}_5\text{H}_7(\text{PO}_4)_4$ were investigated via thermogravimetry, differential thermal analysis and ac-impedance spectroscopy for the first time.

IR-spectra of all samples represent a superposition of bands from two phases. Appearance of some specific bands in $3000-1600 \text{ cm}^{-1}$ range is an evidence for existence of strong hydrogen bond network. One can predict the low conductivity for all samples at low temperatures. Multiple bands in $500-1300 \text{ cm}^{-1}$ range in $\text{Rb}_5\text{H}_7(\text{PO}_4)_4$ can say about appearance of strong deformation of phosphate tetrahedra in crystal structure.

Temperature dependences of conductivity were measured and analyzed for all compositions. The low conductivity values were observed at the temperature range $\sim 50-200^\circ\text{C}$. Proton conductivity of $\text{Rb}_2\text{HPO}_4 \cdot 2\text{H}_2\text{O}$ and $\text{Rb}_5\text{H}_7(\text{PO}_4)_4$ have been investigated for the first time.

Obtained results are strongly different from those for $(1-x)\text{CsH}_2\text{PO}_4 - x\text{Cs}_2\text{HPO}_4 \cdot 2\text{H}_2\text{O}$ system. The additional measurements of conductivity under humidified conditions should be carried out to investigate transport properties of the title system in details.

References

1. V. Ponomareva, G. Lavrova, I. Bagryantseva // Conf. proc. of Int. conf. «Ion transport in organic and inorganic membranes»(23-28 May 2016, Krasnodar-Sochi) P. 226.
2. M.T. Averbuch-Pouchot, A. Durif // Acta Cryst. 1985. V. C41. P.1555-1556

EVALUATION OF MODIFICATION OF MATERIALS "POLYKON A" BY POROUS SILICON NANOPARTICLES

Igor Galushka¹, Denis Terin^{1,2}, Marina Kardash², Larisa Karpenko-Jereb³, Denis Ambarnov², Artem Morozov², Sergey Tsyplyaev²

¹Saratov State University. E-mail: terinden@mail.ru

²Yuri Gagarin State Technical University of Saratov

³Graz University of Technology

Introduction

Polymer composite materials which have prospective ion-exchange properties (for example, water preparation and water purification) are attracting increasing attention. Among such materials, a special place is occupied by the group of compounds "Polikon". Materials "Polykon" have been manufactured by polycondensation method. This method has been widely and thoroughly described earlier in [1,2] and continues to develop and modify because of its simplicity and economy. This work is the continuation of a comprehensive detailed study. Our research is focused on the scientific justification, development and implementation of polycondensation filling technology for the production of multifunctional polymeric composite materials.

Computing Experiments

The object of the study is the model structure of «Polykon A» on novolac phenol-formaldehyde (NPF) fabric and polyacrylonitrile fiber (PAN). The structures are modified by porous silicon nanoparticles. Modeling of the properties of a fragment of a layer of porous silicon (NPS) was carried out (the method is described in [3]). In the model layer, the broken bonds were stabilized by hydrogen. Stabilization with hydrogen maximally approximates the calculated models to real structures. The configurations of the sample structures are shown in Fig. 1.

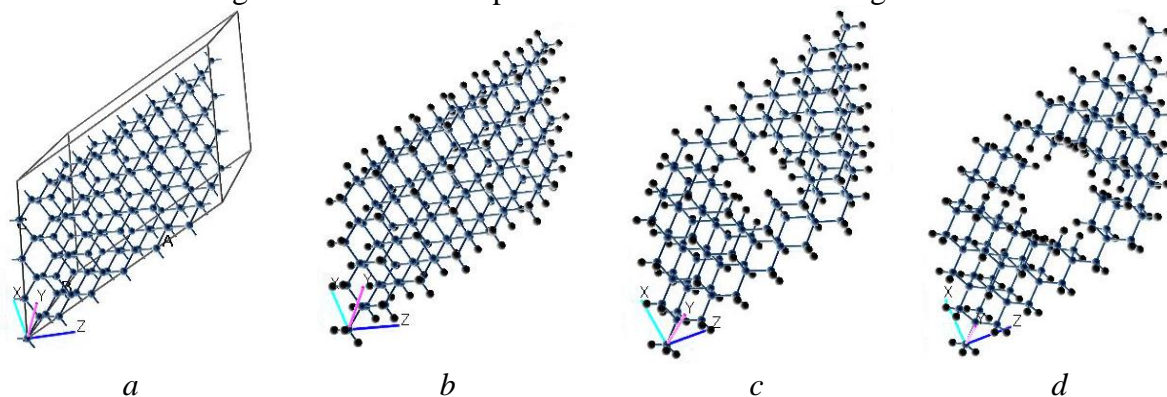


Figure 1. Configurations of fragments of NPS

The elemental composition is given in the table. Geometry optimization was carried out in the Atomistix Toolkit program using the quasi-Newton method. Next, using the local density approximation (LDA) method for calculating the electronic structure of the density functional theory (DFT) using the PZ function, computational grid for the density of states with maximum approximation corresponds to k-point 2x2x2 parameters, and calculates parameters of the structures placed in a vacuum (with a temperature of 300 K). External forces (acting on the structure) are absent.

Table: Element composition and position of the zones.

Sample	Number of atoms in the sample		Valence band level, eV	Conduction band level, eV
	Si	H		
1	143	-	-0.75	0.65
2	143	108	-0.82	0.62
3	125	120	-1.35	0.5
4	109	128	-1.53	0.47

The density of the state is calculated for the samples: No.1 - single-crystal silicon with broken surface bonds (fig.1a), No. 2 - monocrystalline silicon with hydrogen saturated external bounds

(fig.1b), No. 3 - porous silicon with 50% porosity with hydrogen saturated external bounds (fig.1c), No. 4 - porous silicon with a porosity of 70% with broken bonds saturated with hydrogen (fig.1d).

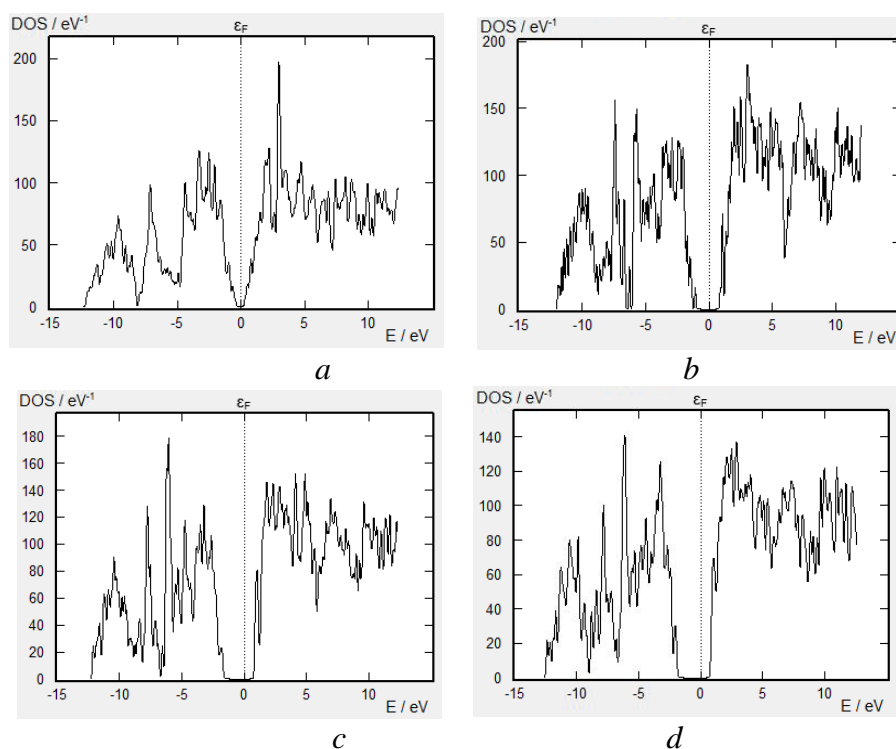


Figure 2. The calculated density of the state of NPS

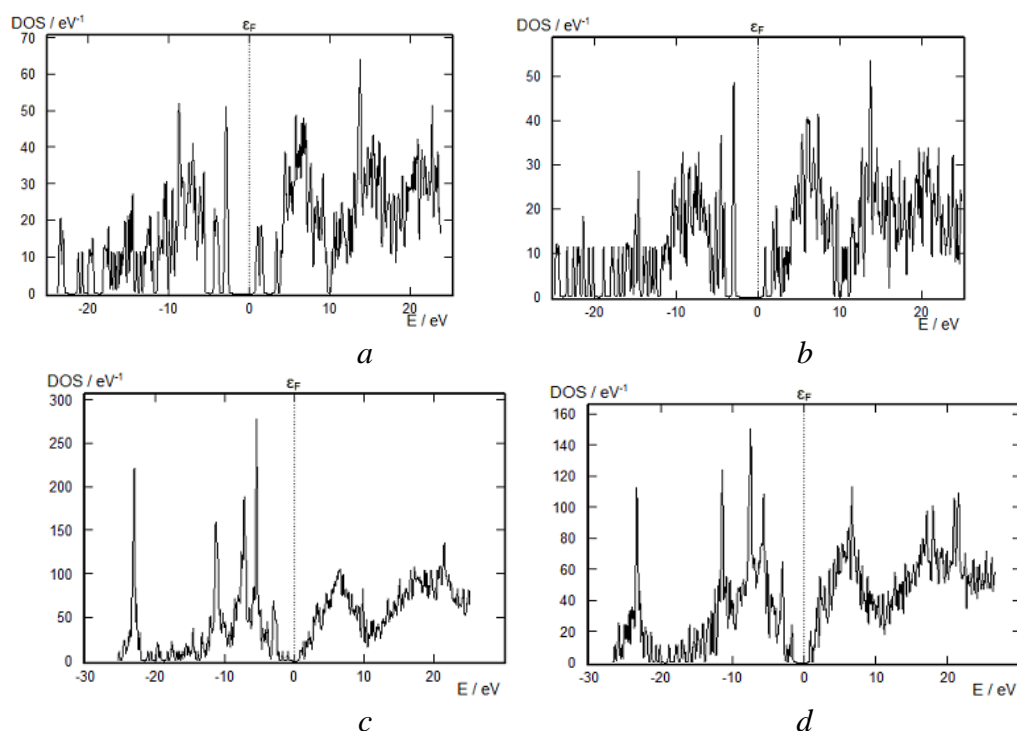


Figure 3. Polykon A NPF (a) and PAN (b) with stabilized silicon in aqueous medium at NPF (c) and PAN (d)

Results of Computing Experiments and Discussion

In this paper, an information system (database) has been developed that allows to store, visualize, structure the data obtained by molecular modeling, quantum chemical calculations and accumulated as a result of experiments [4]. From the analysis of the density of states, we can see

the displacement of the allowed bands relative to the Fermi level with increasing porosity of the structures and saturation of broken silicon bonds.

The results of calculating the density of states of systems of various combinations of fiber matrices of NPF and PAN with functional groups of the monomerization composition of weakly basic anion exchanger in an aqueous suspension with NPS particles are shown in Fig. 3. Analysis of the presented results makes it possible to unambiguously estimate the contribution of NPS to the density of states of structures.

Thus, the density of a state without particles has an explicit band gap with distinct boundaries and without intrazone local levels. When the silicon particles are introduced into the aqueous suspension, localized energy levels are formed in the region of the band gap and the band width significantly changes. We can also distinguish the increase in the filling density of allowed bands, in particular the valence band.

References

1. Conformational analysis of chemically reactive groups in Polikon K. Part 1/*Terin D.V., M.M.Kardash, Tyurin I.A., Ainetdinov D.V., Revzina E.M.* //Fibre Chemistry. 2015. Vol. 46, № 5. P. 304-308.
2. *Kardash, M.M.* Search for a Technological Invariant and Evolution of the Structure-Property Relation for Polikon Materials/*Kardash M.M., Terin D.V.*//Petroleum Chemistry. 2016. Vol. 56, № 5. P. 413-422.
3. In situ methods and control device of processes and structures/*Bilenko D.I, Belobrovaya O.Ya., Terin D.V.* [et al.] Saratov: Saratov state university, 2014. Part 1. 200 p. (in Russian).
4. *Morozov A.I.* Database "Elements of molecular modeling of materials"Polikon"/ Technological foresight: design, implementation, monitoring, analysis: a collection of scientific papers on the materials of the All-Russian School of Conf. "Business-engineering technologies". Saratov: Techno-Decor, 2016. P. 88-93 (in Russian).

TWO-LAYER FLOW OF THE ELECTROLYTE-DIELECTIC SYSTEM UNDER AC ELECTRIC FIELD

¹Georgy Ganchenko, ²Ekaterina Gorbacheva ^{1,3}Evgeny Demekhin

¹Laboratory of electro-hydrodynamics of micro- and nanoscales, Financial University, Krasnodar, Russia, *E-mail: ganchenko.ru@gmail.com*

²Kuban State University, Krasnodar, Russia, *E-mail: katya1911@list.ru*

³Department of mathematics and computer science, Financial University, Krasnodar, Russia, *E-mail: edemekhi@gmail.com*

Introduction

The electroosmosis microflow of two layers dielectric-electrolyte system in AC external electric field is scrutinized. Such a system is commonly used for transportation of dielectric liquids in microscales. The electroosmotic motion of the electrolyte, induced by an external electric field, imply the motion of the liquid dielectric through the interface [1]. For the practical issues, application of AC electric field is more profitable, because it allows to avoid the undesirable chemical reactions [2].

Mathematical model

The two-phase microflow of conductive (electrolyte) and nonconductive (dielectric) viscous liquids bounded by two charged solid walls in external AC electric field is scrutinized. An interface between two liquids is assumed to be a free surface. The electrolyte behavior is described by the Nernst-Planck-Poisson-Stokes system of equations for the ions concentrations, electric field and velocity field; the behavior of dielectric field is given by the Poisson-Stokes system of equations for electric potential and velocity field. The stress-balance boundary condition is applied on the interface. The solid surfaces are assumed to be impermeable to cations and anions, and the electric potential is fixed here. An external electric field directed along the channel.

Results and Discussion

The one-dimensional solution, which corresponds to the flow with unperturbed interface, is founded out. Its linear stability is investigated. This study based on the Floquet theory for discretization of the system in time, and on the Galerkin method – for discretization in space. The dependences of the critical absolute value of the electric field intension on frequency and other parameters of the system are obtained. It is found that the one-dimensional flow is stabilized with frequency magnification.

The work is supported, in part, by the Russian Foundation for Basic Research (project No 15-08-02483-a).

References

1. Demekhin E. A., Ganchenko G.S., Navarkar A., Amiroudine S. The stability of two layer dielectric-electrolyte micro-flow sub-jected to an external electric field // *Physics of Fluids*. 2016. Vol. 28. N. 9. P. 092003.
2. Mayur M., Amiroudine S., Lasseux D., Chakraborty S. Effect of interfacial Maxwell stress on time periodic electro-osmotic flow in a thin liquid film with a flat interface // *Electrophoresis*. 2014. Vol. 35. N. 5. P. 670–680.

INVESTIGATION OF ELECTROLYTE NEAR NONIDEAL IONSELECTIVE SURFACES

¹Nataly Ganchenko, ²Georgy Ganchenko, ^{2,3}Evgeny Demekhin

¹Kuban State university, Krasnodar, Russia, *E-mail: nataly.ganchenko@gmail.com*

²Laboratory of electro-hydrodynamics of micro- and nanoscales, Financial University, Krasnodar, Russia, *E-mail: ganchenko.ru@gmail.com*

³Department of mathematics and computer science, Financial University, Krasnodar, Russia
E-mail: edemekhi@gmail.com

Introduction

The work is dedicated to investigation of electrolyte behavior near and inside the imperfect membranes. As it has been shown in the latest research [1, 2], the consideration of imperfectly selective membranes is what allows to discover the new types of instability, such as equilibrium instability and instability within the Ohmic current regimes.

Mathematical model

The three-layer system electrolyte-membrane-electrolyte is scrutinized, and the behavior in all the areas is described by the Nernst-Planck-Poisson-Stokes system of equations. The distinction for the membrane area consists in existence of the space charge of membrane and absence of electrolyte movement. Also, the chemical reactions of water dissociation can take place inside the membrane. The latter plays a crucial role for the investigation of the bipolar membranes [3], because of high intensity of electric field in the junction between two oppositely charged membranes, which intensifies the water dissociation processes due to the second Wien effect.

Results and Discussion

The consideration of imperfect monopolar membranes allowed to detect a new type of instability – oscillatory instability for the membranes with a small charge or for the electrolytes with a high concentration of salt [4]. For the bipolar membranes, the one dimensional solution was found numerically and the presence of overlimiting current regime was detected. Such a regime arises due to the second Wien effect, water dissociation processes and the catalytic reactions with the ionic groups of membrane.

The work is supported, in part, by the Russian Foundation for Basic Research and the Administration of the Krasnodar region (project No 16-48-230107-r_a)

References

1. *I. Rubinstein, B. Zaltzman* Equilibrium Electroconvective Instability // *Physical Review Letters*. 2015, V. 114, 114502.
2. *K.A. Nebavskaya, V.V. Sarapulova, K.G. Sabbatovskiy, V.D. Sobolev, N.D. Pismenskaya, P. Sistat, M. Cretin, V.V. Nikonenko* Impact of ion exchange membrane surface charge and hydrophobicity on electroconvection at underlimiting and overlimiting currents // *Journal of Membrane Science*. 2017, V. 523, 36.
3. *V.I. Zabolocky, V.V. Nikonenko* Perenos ionov v membranah, Nauka, Moscow, 1996. [in Russian]
4. *G.S. Ganchenko, E.N. Kalaydin, J. Schiffbauer, E.A. Demekhin* Modes of electrokinetic instability for imperfect electric membranes // *Physical Review E*. 2016. V. 94, 063106.

THE INFLUENCE OF THE CURRENT DENSITY ON THE DIFFUSION BOUNDARY LAYER STRUCTURE IN SODIUM, CALCIUM AND MAGNESIUM CHLORIDE SOLUTIONS

Violetta Gil, Victor Nikonenko, Natalia Pismenskaya

Institute of Membranes, Kuban State University, Krasnodar, Russia, E-mail: violetta_gil@mail.ru

Introduction

At present, it is established that the main mechanism of the overlimiting current through ion-exchange membranes in electro dialysis of dilute solutions is electroconvection (EC) [1, 2]. The EC can reduce the diffusion boundary layer (DBL) thickness in several times.

The nature of the counterion, in particular its ability to the structuring of water, plays an important role in the development of EC. The purpose of this work is the investigation of the dependence of the DBL structure near the membrane surface on the current density in the binary electrolyte solutions containing singly- or doubly-charged counterions.

The prediction of behavior of membrane systems in different electrolytes can help to evaluate the risk of scaling on the surface and in the bulk of the membrane during treatment of solutions containing hardness ions (Ca^{2+} , Mg^{2+} , etc.).

Experiments

The experimental current-voltage curves were obtained for the systems with three different solutions (NaCl, CaCl_2 , and MgCl_2) of the same concentration (0.02 M). The heterogeneous cation-exchange MK-40 membrane (Shchekinoazot, Russia) was used. The experimental methods and the experimental data are described in [3].

Theory

The DBL of thickness δ is divided in three regions: an electroneutral region of thickness δ_1 ; the electromigration zone of the extended space charge region (SCR) of thickness δ_2 , where the contribution of diffusion in the ion flux is negligible; and the quasi-equilibrium zone of the SCR near the membrane surface (quasi-equilibrium electric double layer (EDL)) of thickness δ_3 .

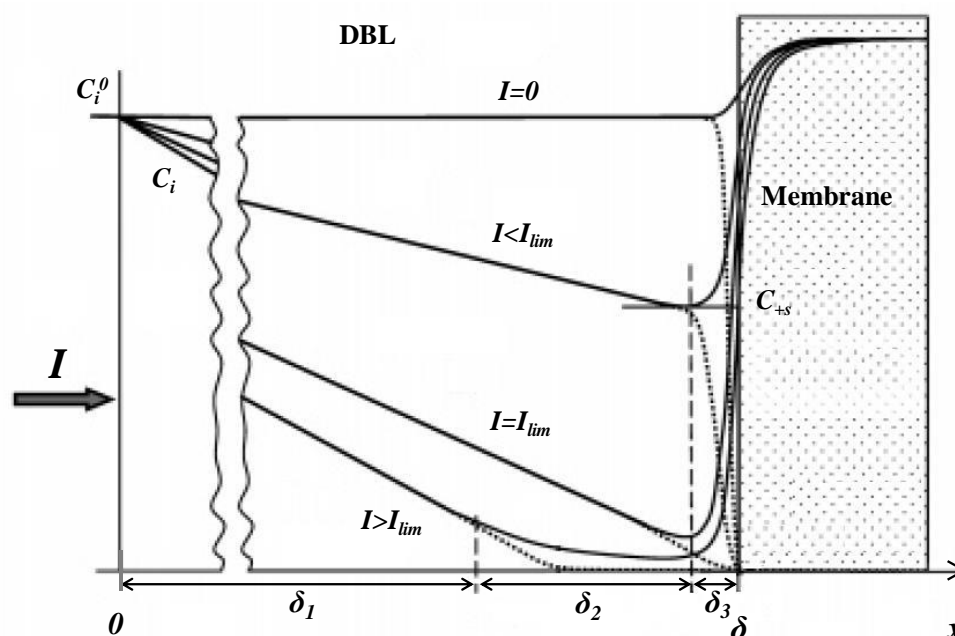


Figure 1. Scheme of the DBL structure near a cation-exchange membrane; salt counterion (solid line) and co-ion (dashed line) concentration profiles at different current densities I . I_{lim} is the limiting current density

When approaching the membrane, the concentration of salt counterion decreases almost linearly in the electroneutral zone, then it decreases slowly in the electromigration zone and

increases very rapidly in the quasi-equilibrium zone. The electromigration and quasi-equilibrium zones are separated by a point where $dC_+/dx=0$ and the concentration of the salt counterions reaches its minimum (noted as C_{+s}) (Fig. 1).

The ion transport is described by the Nernst-Planck and Poisson equations:

$$J_+ = -D_+ \left(\frac{dC_+}{dX} - z_+ C_+ \frac{FE}{RT} \right) \quad (1)$$

$$J_- = -D_- \left(\frac{dC_-}{dX} - z_- C_- \frac{FE}{RT} \right) \quad (2)$$

$$\varepsilon_0 \varepsilon \frac{dE}{dX} = F(z_+ C_+ + z_- C_-) \quad (3)$$

where J_i , D_i , z_i are the flux density, diffusion coefficient, and charge number of ions i ($i=+,-$), respectively; E is the electric field, ε_0 is the permittivity of the vacuum, ε is the relative dielectric permittivity of the medium.

The solution of Eqs. (1)-(3) allows obtaining the following equation, that can be used to calculate C_{+s} in the case of multiply-charged counterions:

$$(C_+^0 - C_{+s}) \left(1 - \frac{z_+}{z_-} \right) \frac{z_+ F D_+}{I} + \frac{\varepsilon \varepsilon_0 R T I}{2 F^3 D_+ z_+^3 C_{+s}^2} + \sqrt{\frac{\varepsilon \varepsilon_0 R T}{2 F^2 z_+^2 C_{+s}}} = \delta \quad (4)$$

The three terms in the left-hand side of Eq. (4) are the thicknesses of the DBL three zones: δ_1 , δ_2 and δ_3 , respectively.

The following algorithm is proposed for calculation of δ_1 , δ_2 and δ_3 for a given current density. For this purpose, experimental current-voltage characteristics (CVC) (Fig. 2) and the model equations are used. When a tentative value of δ is chosen, C_{+s} is calculated using Eq. (4). The obtained value of C_{+s} is used to calculate the potential drop (PD) across different zones of the DBL using the equation $\Delta\varphi_{calc} = f(C_{+s}, C_+^0, z_+, z_-, \delta, I)$ deduced from Eqs. (1)-(3). The calculated PD is compared with the experimental value for the given current density. The sought value of δ is found when the difference between the calculated and experimental values of PD is lower than 1 mV.

Results and Discussion

The dependences of the total DBL thickness and the thicknesses of its components on the I/I_{lim} ratio for three electrolytes studied (NaCl, CaCl₂, and MgCl₂) are shown in Figs. 3 and 4.

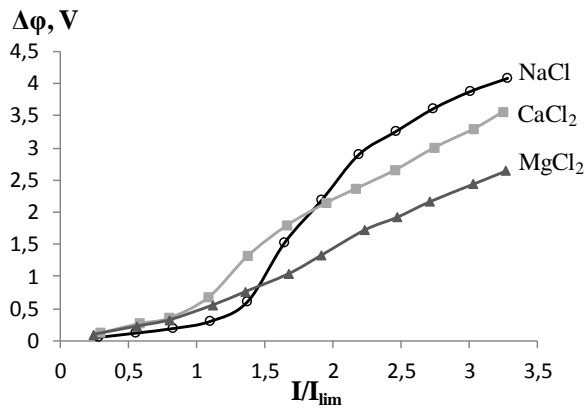


Figure 2. Experimental CVC. Limiting current densities were calculated using the Lévêque equation

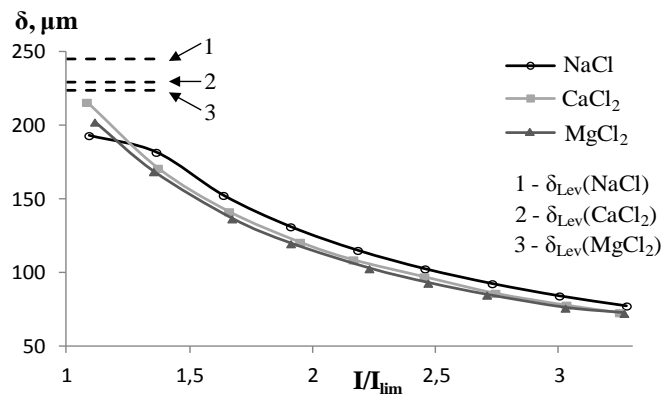


Figure 3. Dependence of δ value on the current density normalized to the limiting current density

The calculated values of δ vary in the order $\text{Na}^+ > \text{Ca}^{2+} > \text{Mg}^{2+}$ (Fig. 3). The values of δ_2 and δ_3 are in the same order (Fig. 4). The higher the experimental PD for a given I/I_{lim} ratio, the smaller $C_{+,s}$, and the higher are the calculated values of δ , δ_2 and δ_3 .

Fig. 3 shows also the values of δ_{Lev} calculated using the L ev eque equation [4]:

$$\delta_{\text{Lev}} = 0,68h \left(\frac{LD}{h^2V_0} \right)^{1/3} \quad (5)$$

where h is the intermembrane distance, L is the channel length, V_0 is the linear rate of solution flow, D is the electrolyte diffusion coefficient.

For all electrolytes, the values of δ_{Lev} approximately agree with the results of extrapolation of $\delta - I/I_{\text{lim}}$ curves to $I/I_{\text{lim}} = 1$.

When $I < I_{\text{lim}}$, the extended part of the SCR is absent, and all space charge is located in the quasi-equilibrium EDL. When the current exceeds its limiting value, δ_2 takes macroscopic values comparable with the DBL thickness δ (Fig. 4a).

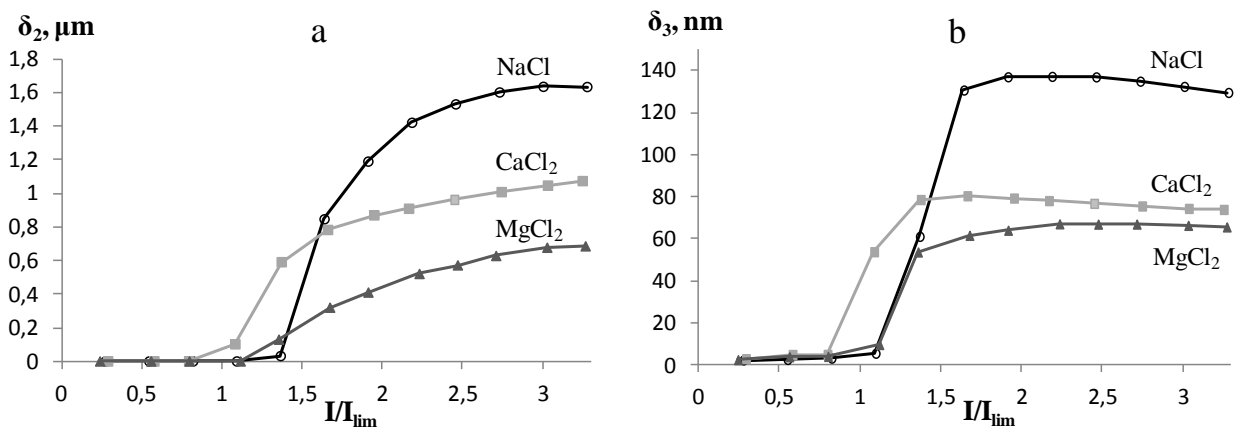


Figure 4. Dependences of δ_2 (a) and δ_3 (b) values on the current density normalized to the limiting current density.

As Fig. 4b shows, the quasi-equilibrium EDL thickness for Na^+ ion is essentially higher than that for doubly-charged ions. In addition to the reason given above, note that δ_3 is inversely proportional to the counterion charge number (the third term in the left-hand side of Eq. (4)).

Acknowledgment

This investigation was realized within French-Russian International Associated Laboratory "Ion-exchange membranes and related processes". The authors are grateful to the RFBR, Russia (grant 17-08-01442).

References

1. Rubinstein I., Zaltzman B. Electro-osmotically induced convection at a permselective membrane // *Phys. Rev. E* 2000. V. 62. P. 2238.
2. Kwak R., Guan G., Peng W.K., Han J. Microscale electro dialysis: concentration profiling and vortex visualization // *Desalination* 2013. V. 308. P. 138.
3. Gil V.V., Andreeva M.A., Pismenskaya N.D., Nikonenko V.V., Larchet C., Dammak L. Effect of counterion hydration numbers on the development of electroconvection at the surface of heterogeneous cation-exchange membrane modified with an MF-4SK film // *Petroleum Chem.* 2016. V. 56. P. 440.
4. Gnusin N.P., Zabolotsky V.I., Nikonenko V.V., Urtenov M.K. Convective-diffusion model of electro dialytic desalination - limiting current and diffusion layer // *Sov. Electrochem.* 1986. V. 22. P. 273 (in Russian).

TRANSPORT OF SODIUM CHLORIDE AND PHENYLALANINE THROUGH ION-EXCHANGE MEMBRANES IN NEUTRALIZATION DIALYSIS

Elena Goleva, Vera Vasil'eva

Voronezh State University, Voronezh, Russia, E-mail: vorobjeva_ea@mail.ru

Introduction

Neutralizing dialysis is a continuous membrane desalination process, first described in papers by Igawa et al [1, 2], consists in that salt ions from the feed solution, which circulates between a cation-exchange and an anion-exchange membrane, are selectively exchanged for equivalent quantities of H^+ and OH^- ions supplied through the respective membranes from stripping solutions of acid and alkali, which circulate, respectively, on the other side of the cation- and anion-exchange membranes. Neutralizing dialysis is a low investment, low operational and maintenance cost process, low energy consuming (only the pumps) and relatively easy to implement. By combining transport processes with the chemical reaction taking place in Neutralizing dialysis, it is possible to accelerate process by an additional mechanism, which so far has not been sufficiently investigated from both the experimental and theoretical point of view. The Neutralizing dialysis process has been used for the separation of non-electrolytes of organic solutes from ions [1], deionization [3], weak acid and base separation [4], glycine transport [5] as well as industrial aqueous solution desalination [6].

The aim of our study was an experimental investigation of the effect of various physicochemical parameters of the process on the rate and extent of desalination of salt solutions of phenylalanine.

Experiments

Neutralization dialysis of solutions was carried out using three-compartment flowing dialyzer of continuous action (Fig. 1). The acidic (3), alkali (1) and desalination (2) compartments were fed respectively with HCl, NaOH and NaCl or NaCl(Phe) solutions. The circulating volumes were respectively 2.0 L, 2.0 L and 1.0 L for acidic, alkali and desalination solutions maintained at 25 °C.

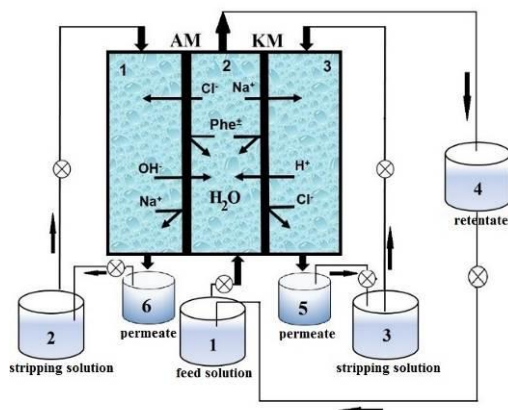


Figure 1. Schematic representation of ND with a three-compartment membrane stack.

At a dialysis used a heterogeneous cation-exchange MK-40pr and anion-exchange MA-40pr membranes in the hydrogen and hydroxyl forms respectively in with geometrical-nonuniform (profiled) surface. Zabolotsky V. I. et al. developed the technique of ion-exchange membranes profiling by wet hot pressing, which is patented in RF [7], and defined conditions which are not degrading physical, chemical, transporting and structure characteristics of membranes. Examined solution was fed to the middle section of the device at a rate of $4.5 \cdot 10^{-4}$ m/s, and in counter-flow regime acid was passed and alkali at a rate of $5.8 \cdot 10^{-4}$ m/s.

Solutions of alkylaromatic nonpolar amino acid phenylalanine and mineral salt sodium chloride were studied. Since the pH of the examined solutions were 5.20-5.60, the amino acid that was an ampholyte ($pJ=5.91$), was in the form of bipolar ion. The range of concentrations of sodium chloride and phenylalanine in their equimolar mixture solutions was 0.0010-0.1500 M. Concentrations of hydrochloric acid and sodium hydroxide solutions were 0.3 M.

Results and Discussion

The difference in the fluxes of the mutual diffusion of H^+/Na^+ ions across the cation-exchange membrane and OH^-/Cl^- ions across the anion-exchange membrane causes the pH oscillation in the demineralized solution (Fig.2a) in the case of demineralization of sodium chloride solutions by neutralization dialysis. This was revealed earlier in works on the kinetics of neutralization dialysis [8, 9].

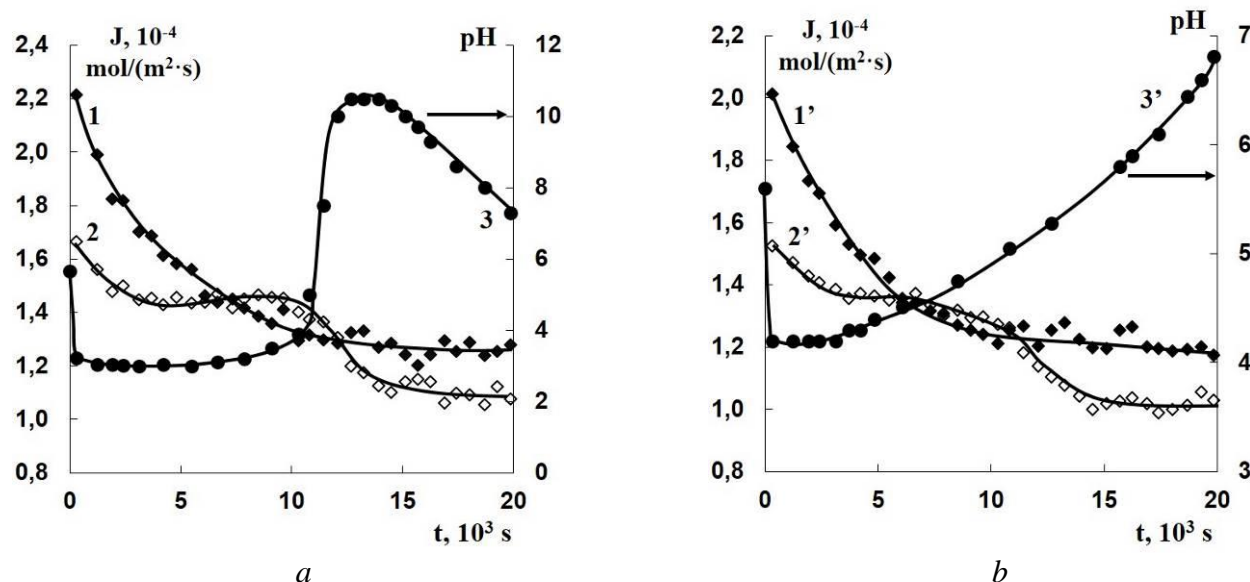
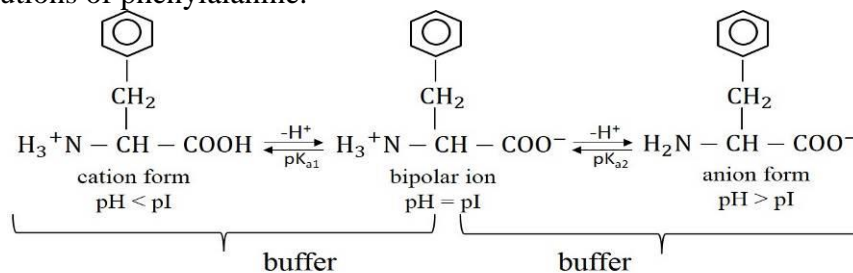


Figure 1. Time dependence of the fluxes of Na^+ across the MK-40pr (H^+) (1, 1'), Cl^- across the MA-40pr (OH^-) (2, 2') and pH in the solution of retentate (3, 3') in neutralization dialysis of individual (a) and mixed equimolar (b) solution of the sodium chloride and phenylalanine $C_0(NaCl)=C_0(Phe)=2,5 \cdot 10^{-2}$ mol/L

The pH of the demineralized solution changed insignificantly and in the stationary state the process passed at pH = 6.80 as a result of the buffer action of the amino acid in the demineralization of water-salt solutions of phenylalanine.



While solving problems of membrane separation it should be proceeded that the degree of mineral ions recovery must be high, and the losses of the cleaned product (amino acid) minimal (Table 1.).

Table 1: The degree of mineral ions recovery and loss of amino acid during Donnan and neutralization dialyses

Concentration of equimolar solution, 10^{-2} M	The degree of recovery R, %				Loss of amino acid L (Phe), %	
	Donnan dialysis		Neutralisation dialysis		Donnan dialysis	Neutralisation dialysis
	Na	Cl	Na	Cl		
1,0	46,3	31,4	83,2	66,4	8,5	0,32
2,5	34,4	24,2	61,8	49,3	6,0	0,26
5,0	20,3	16,1	37,1	29,6	5,5	0,22
10,0	9,4	7,0	20,5	16,9	4,8	0,16
15,0	6,0	4,4	14,7	12,2	4,0	0,12

Neutralizing dialysis is characterized by large values of the mineral ions and amino acid separation factor, by the degree of mineral ions recovery, and small losses of phenylalanine due to the presence of an amino acid in bipolar form in a demineralized solution.

Despite high separation factors at neutralization dialysis it failed to clean amino acid from mineral components completely in one stage of laboratory dialysis variant. The aim set was achieved using a system with recirculation flow. For equimolar mixed solution almost complete degree of mineral ions recovery was achieved within 5-6 cycles.

With the decrease of electrolyte content in the feed mixture solution with amino acid number of cycles to achieve virtually complete ($R = 99,9\%$) recovery of mineral ions is reduced.

Total losses of amino acids in seven cycles due to diffusion and osmotic transfer while recirculated neutralization dialysis equimolar mixtures through the ion exchange membranes do not exceed 8-10%.

Acknowledgments

The present work is supported by the Russian Science Foundation (project № 17-19-01486)

We are grateful prof. V.I. Zabolotsky (Kuban State University) for the provided samples of a profiled ion-exchange membranes.

References

1. *Igawa M. et al.* Donnan dialysis deionization // *Chem. Lett.* 1986. V. 11. P. 237–238.
2. *Igawa M. et al.* Neutralization dialysis for deionization // *Bull. Chem. Soc. Jpn.* 1987. V. 60. P. 381–383.
3. *German M. et al.* Hydrogen ion (H⁺) in waste acid as a driver for environmentally sustainable processes: opportunities and challenges // *Environ. Sci. Technol.* 2013. V. 47. P. 2145–2150.
4. *Tanabe H. et al.* Separation of weak acids and bases by neutralization dialysis // *Ind. Eng. Chem. Res.* 1995. V. 34. P. 2450–2454.
5. *Wang G. et al.* Transport of glycine by neutralization dialysis // *J. Membr. Sci.* 1995. V. 106. P. 207–211.
6. *Bleha M. et al.* Neutralization dialysis for desalination // *J. Membr. Sci.* 1992. V. 73. P. 305–311.
7. *Zabolotskii V. I., Loza C. A., Sharafan M. V.* Method of profiling of ion-exchange membrane. Pat. RF 2284851, BO1D 61/52, 10.10.2006.
8. *Denisov G.A. et al.* Theoretical analysis of neutralization dialysis in the three-compartment membrane cell // *J. Membr. Sci.* 1995. V. 98, № 1-2. P. 13-25.
9. *Cherif M. et al.* Water desalination by neutralization dialysis with ion-exchange membranes: Flow rate and acid/alkali concentration effects // *Desalination.* 2015. V. 361. P. 13–24.

POLYMETHYLPENTENE: THE OPTIMUM MATERIAL FOR ION EXCHANGE MEMBRANES FABRICATION BY UV POST-GRAFTING

¹Daniel Golubenko, ^{1,2}Andrey Yaroslavtsev

¹Kurnakov IGIC RAS, Moscow, Russia, 119991 E-mail: yaroslav@igic.ras.ru

²Tophiev IPS RAS, Moscow, Russia, 119991

Introduction

Radiation-induced graft polymerization of the polar functional monomers with a non-polar polymer film is one of the effective methods for ion-exchange membranes preparation [2]. The using to UV-activation instead of radiation would make the process much easier and safer. It is known that the tertiary carbon atoms of polypropylene (PP) and undergo photochemical oxidation under UV-radiation [3]. Since oxidation is accompanied by the accumulation of peroxides in the polymer, it can be used as the initiator for the radical grafting of polystyrene, which one can be converted into ion exchange material with the help of functionalization. However, PP has a low gas permeability, which upon the irradiation leads to heterogeneity of film oxidation and the course of competing processes, for example, crosslinking. As a result, this negatively affects on the properties of ion-exchange membranes. This disadvantage is devoid of polymethylpentene (PMP), which has high gas permeability ($20 \cdot 10^{-13}$ vs. $1.7 \cdot 10^{-13}$ $\text{cm}^3 \text{cm cm}^{-2} \text{s}^{-1} \text{Pa}^{-1}$ for PP) and two tertiary carbon atoms per monomer unit (Fig.1). In this work, we consider the kinetics of styrene polymerization on UV-irradiated polymethylpentene films with different crystallinity and the influence of the synthesis conditions and the properties of the initial films on the properties of the resulting ion-exchange membranes.

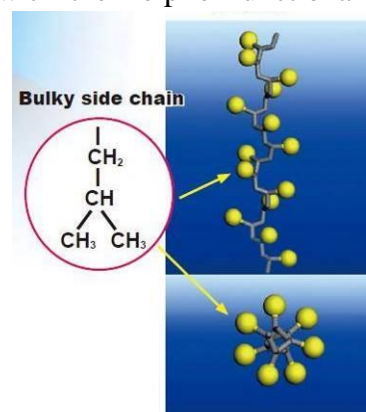


Figure 1. The chemical formula of PMP side groups and their arrangement in a crystal (adapted from [1])

Experiments

We used an extruded PMP films 50 microns thick (Grade MX004 and MX002, Mitsui Chemicals, Japan). Irradiation was carried out under the mercury lamp. Radical polymerization was performed in a boiling styrene solution in methanol. Sulfonation was performed with 1.5% chlorosulfonic acid solution in organochlorine solvents. After sulfonating the membrane was activated by boiling in distilled water. Grafting degree of styrene was calculated as:

$$\text{GD} = \frac{m_p - m_o}{m_o} 100, \%$$

where m_o and m_p - film masses before and after polymerization.

Results and Discussion

After grafting the significant increase in weight of samples (by 11-119%) due to the polymerization of styrene on the PMP matrix is observed, as evidence it is accompanied by the appearance of characteristic peaks of polystyrene at the IR spectra in the region of 700 cm^{-1} . The styrene polymerization kinetics significantly depends on the nature of the polymer (Fig. 2) and in 2-3 times faster for polymethylpentene than for polypropylene. Furthermore, polymerization reaction for the more crystalline grade MX002 at the beginning of the process (0.5-1.5 h) is much slower, however, the reaction rate for a less crystalline MX004 grade quickly slows down and the grafting degree (GD) reaches of saturation. This behavior of the process is explained by the parallel flow of several reactions (initiation, chain growth, chain termination) and the dependence of their constants on the nature of the polymers. Apparently, chain termination considerably slowed down in more crystalline PMP films, which can be interpreted as a low probability of the growing chains meeting due to their low mobility in high crystalline phase, what is in good accordance with [4]

and swelling data (Fig.2). This allows achieving high values of the GD in compare with less crystalline samples, but the polymerization kinetics during the initial stages significantly loses.

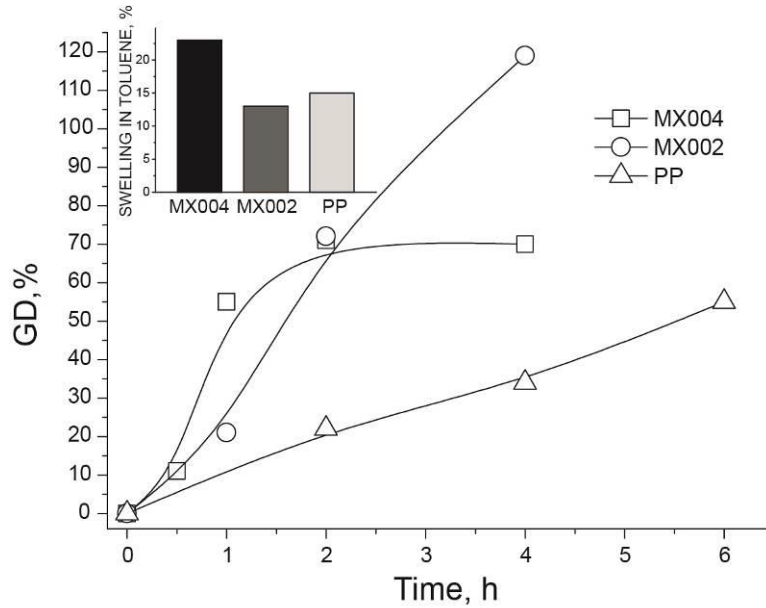


Figure 2. Polymerization kinetics for various grades of polymethylpentene (MX004 and MX002) and PP

Varying of the synthesis time (degree of grafting) results in the obtaining of the membranes with different conductivity and mechanical properties (Fig. 3). The increasing of the grafting degree makes membrane more elastic and reduces the membrane resistance. The observed effects are results of the increasing in the swelling degree of the ion exchange phase that are known and well described phenomena.

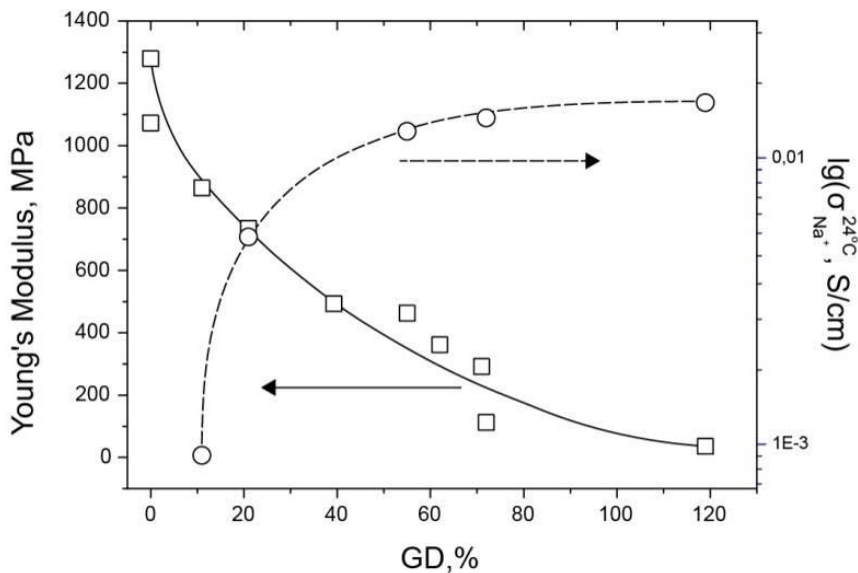


Figure 3. Young's Modulus and Na^+ conductivity of ion-exchange membranes based on PMP vs. grafting degree (GD, %)

Thus, grafted cation-exchange membranes based on polymethylpentene and sulfonated polystyrene have been obtained. Interrelations between the properties of finite membranes and the conditions of their synthesis are shown and interpreted. Membranes with a small content of sulfonated polystyrene have excellent mechanical properties and are recommended for use in electrodialysis, while materials containing a lot of sulfonated polystyrene and having a low ion resistance can be used in reverse electrodialysis.

Acknowledgment

This work was supported by Russian Science Foundation (project № 16-13-00127).

References

1. *A. Mitsui Chemicals* TPX Technical brochure 2010.
2. *Nasef M.M., Güven O.* Radiation-grafted copolymers for separation and purification purposes: Status, challenges and future directions // *Prog. Polym. Sci.* 2012. V. 37. P. 1597-1656. doi:10.1016/j.progpolymsci.2012.07.004.
3. *Gijsman P., Hennekens J., Vincent J.* The mechanism of the low-temperature oxidation of polypropylene // *Polym. Degrad. Stab.* 1993. V. 42. P. 95-105. doi:10.1016/0141-3910(93)90031-D.
4. *Wilson J.E.* Radiolytic Grafting of Styrene on Polymethylpentene Film // *J. Macromol. Sci. Part A - Chem.* 1971. V. 5. P. 777-792. doi:10.1080/00222337108061058.

THERMOPERVAPORATION PROCESS WITH SEMI-AUTOMATIC ADSORPTION METHOD FOR BIO-BUTANOL RECOVERY FROM FERMENTATION BROTH

Georgy Golubev, Ilya Borisov, Vladimir Vasilevsky, Vladimir Volkov

A.V. Topchiev Institute of Petrochemical Synthesis, Moscow, Russia, *E-mail: GolubevGS@ips.ac.ru*

Introduction

Butanol is an important component of chemical industry. Approximately half of the currently produced butanol and its derivatives (glycol esters, acrylate esters and methacrylate, butyl acetate) is used as solvents in the coatings industry. The advantage here is that butanol prevents blushing of certain coatings when they dry under humid conditions.

Butanol can be produced by fermentation from renewable feedstocks, referred to as biobutanol. A major problem in the production of biobutanol is the inhibitory effect on the microorganisms, which leads to lower productivity of the target component, and high energy discharge. One of the solutions of the problem is to provide a bioreactor with continuous removal of solvents in the fermentation process itself, the use of which allows to obtain the concentrated product at the output and also reduce the inhibitory effect of the solvent for a deep processing.

Pervaporation and, in particular, thermopervaporation (TPV) have attracted attention as a perspective method of recovery of biobutanol from fermentation broth along with the extraction and adsorption [1].

At present time, TPV is used only at the laboratory level scale. One of the causes is that permeate traditional TPV configuration module can block the gap to form a liquid film between the membrane and the condensation surface. This phenomenon is observed for small values of the air gap thickness (<2.5 mm) in a classical configuration modules where permeate is removed from under gravity condensation surface [2]. The membrane material used for butanol removal from fermentation broth was highly permeable glassy polymer poly(1-trimethylsilyl-1-propyne) (PTMSP). Pervaporation characteristics of PTMSP decrease under change from binary solutions to multi-component model mixtures and further to real fermentation broths [3]. This is related to the sorption occurring in PTMSP free volume for low-volatile and almost non-permeable fermentation by-products (e.g., diols). It was shown that regeneration of PTMSP membranes properties takes place under batch low-volatile compounds extraction from the membrane using enriched by organic components permeate [3]. In conventional TPV process, membrane regeneration by permeate is technically complex. In the novel hybrid TPV technique [4], a porous porous condenser surface is used instead of a solid condensation surface and the condensed permeate is used as coolant. In the present work, butanol removal from fermentation broths was investigated, with batch membrane regeneration by means of filling an air gap with permeate. Also, the novel approach proposed allows to reduce the air gap between the membrane and the condensation surface up to 1 mm, resulting in enhanced mass transfer in air gap.

Experiments

Membranes

The PTMSP membranes for pilot test were prepared by casting polymer solutions in chloroform onto a rectangular shape with Teflon coating. The solvent was evaporated for 50–100 h. The size of initial films was 8 x 28 cm, thickness – 42 μm .

All solutions were prepared from high-grade organic solvents by weighing.

Thermopervaporation concept assisted by phase separation

Thermopervaporation pilot scale with a porous metal surface permeate condensation is shown schematically in Figure 1. The module is equipped with 2 membranes, total active area of which amounts to 33,6 x 10⁻³ m².

TPV process proceeds as follows: feed was continuously circulated between hot part of the membrane module (4) and feed tank (1). The membrane selective layer was in direct and continuous contact with the feed. The permeate passes through the membrane (5), evaporates in the air gap 2 mm (6) and then condensed on the porous cooling plate (7). The condensate wets the

condensation surface, penetrates the pores and flows into with coolant chamber. It should be noted that the pressure in coolant chamber is lower than in the condensation chamber, by the fact that the pump (10) providing a coolant circulation system is located after the module TPV. Held in the coolant chamber permeate is used as refrigerant. Accumulated during the experiment condensed permeate is discharged from the coolant tank (11) and analyzed. Thermopervaporation experiments were performed in contact with binary aqueous mixtures of butanol, four-component mixture model and the fermentation broth.

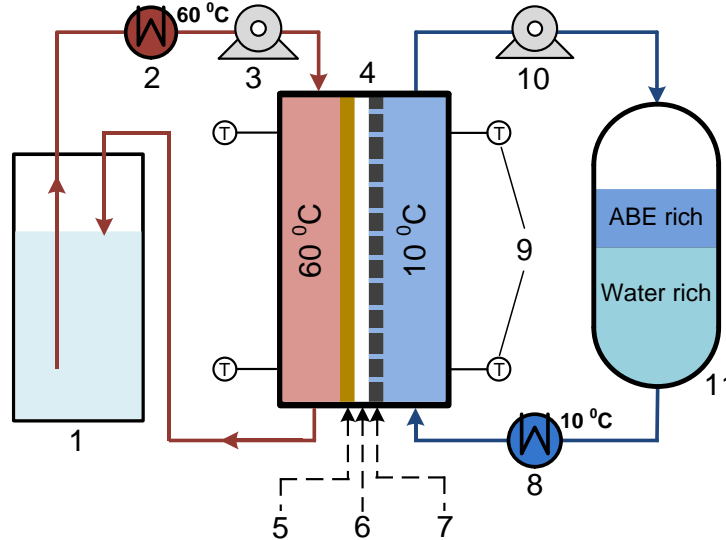


Figure 1. Scheme of pilot thermopervaporation rig with porous cooling plate used in experiments

Batch membranes regeneration was carried out as follows: under the continuous thermopervaporation, the pump providing refrigerant circulation in condensation loop was switched off for 1 minute. The coolant penetrated through the porous condensation surface into an air chamber where it wetted the membrane surface; then the pump was switched on again, the coolant exited the air gap, and the separation process continued.

Results and Discussion

Figure 2 shows the results of TPV research for PTMSP membranes under separation of 1% wt aqueous butanol solution. It was shown that for 50 hours, TPV characteristics (total permeate flux, butanol flux and separation factor) decrease in a range of 10%. It was found that under membrane regeneration by aqueous permeate phase containing 7.6% wt butanol in water, PTMSP TPV characteristics fully recover to initial values.

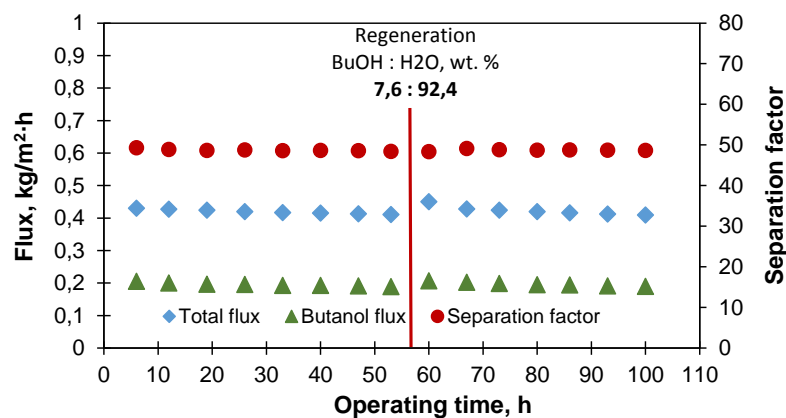


Figure 2. PTMSP membrane regeneration by aqueous permeate phase under thermopervaporative separation of 1% wt aqueous butanol solution, $T_p = 60^\circ\text{C}$, $T_K = 10^\circ\text{C}$.

Data given at Fig. 3 show that membrane permeance for butanol decreases with time. This is related to the sorption occurring in PTMSP free volume for low-volatile components (diols) which accumulate in the membrane and do not transfer in permeate, resulting in fractional blocking of the membrane transport channels of nanoporous PTMSP and also in mass transfer decrease for target components (butanol). It was found that regeneration by organic permeate phase containing 0.6 : 69.1 : 0.27% wt acetone : butanol : ethanol, respectively, fully recover membrane properties to the initial values. This indicates that concentrated by butanol permeate fully extracts pollutants from the PTMSP membrane surface.

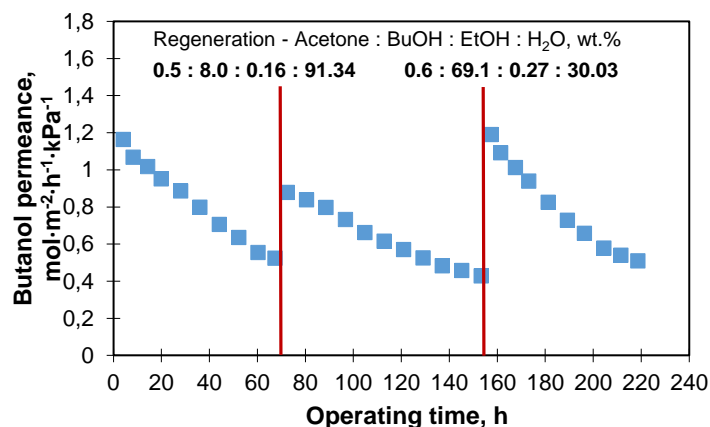


Figure 3. Butanol permeance as a function of experiment duration, $T_f = 60^\circ\text{C}$, $T_c = 10^\circ\text{C}$

Acknowledgements

This work was supported by the Presidium of the Russian Academy of Sciences (PRAN) (project PRAN18).

References

1. Huang H.L., Ramaswamy S. Separation and purification of biobutanol during bioconversion of biomass // Sep. Pur. Tech. 2014. V.132 P.513.
2. Borisov I.L., Volkov V.V. Thermopervaporation concept for biobutanol recovery: The effect of process parameters // Sep. Pur. Tech. 2015. V.146. P.33.
3. Volkov A.V., Volkov V.V., Khotimskii V.S. Membranes based on poly [(1-trimethylsilyl)-1-propyne] for liquid-liquid separation // Polym. Sci. Ser. A. 2009. V. 51. P. 1367.
4. Borisov, I.L., Golubev G.S., Vasilevsky V.P., Volkov A.V., Volkov, V.V. Novel hybrid process for bio-butanol recovery: Thermopervaporation with porous condenser assisted by phase separation. // J. Membr. Sci. 2017. V. 523. P. 291.

SIMULATION OF LIQUID FLOW IN THE CHANNEL OF A LABORATORY ELECTRODIALYSIS CELL

Andrey Gorobchenko, Semyon Mareev, Andrey Kononov

Kuban State University, Krasnodar, Russia, gorobchenkoandrey@mail.ru

Introduction

Hydrodynamic conditions play major role in electro dialysis process [1]. The distribution of solution velocity in lab-scale cell should be strictly controlled in studies of electrochemical characteristics of ion exchange membrane. For this end the lab-scale flow-through electro dialysis cell, which ensures the laminarity of solution passing between the membranes, was developed at the Physical Chemistry Department of Kuban State University [2, 3].

Theoretical

The studied system is presented in Fig. 1. The arrows show the principal direction of solution flow between the membranes. Geometrical parameters of the model (Fig.1b,c) correspond to real dimensions of operating zone of electro dialysis cell (Fig.1a).

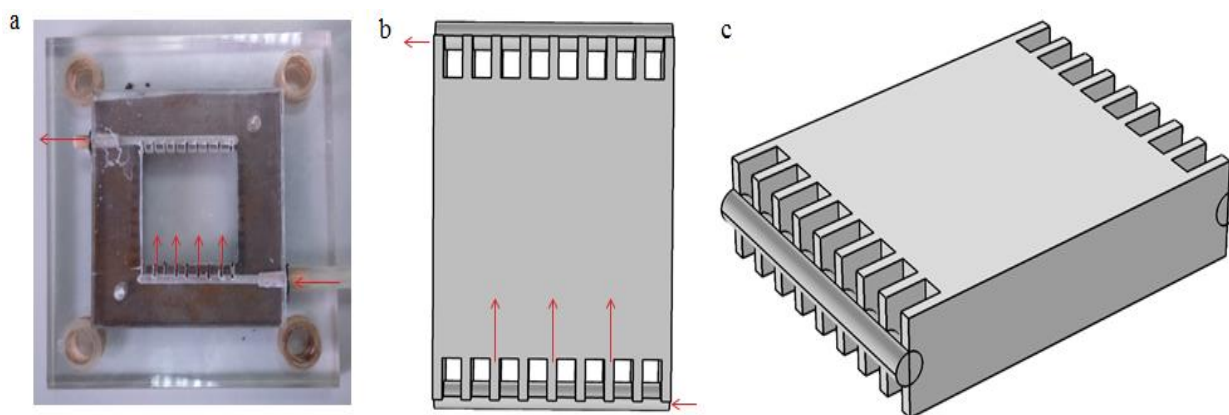


Figure 1. Photo of chamber of experimental cell (a) and geometry of zones containing the solution (b,c) of studied system

A three dimensional stationary mathematical model was formulated for the flow of incompressible liquid, based on the Navier-Stokes equations. The boundary conditions were as follows: uniform distribution of solution velocity was set on the solution inlet and outlet and the no-slip condition was placed on all other boundaries (meaning that the flow velocity would be zero on that interfaces). The average linear solution flow velocity in operating zone of the channel was 0.004 m/s at normal pressure. The problem was solved numerically using Comsol Multiphysics 5.0 package.

Results and discussions

The distribution of solution velocity in studied channel is asymmetric, and the hydrodynamic mode is laminar as it is shown in Fig. 2.

The velocity profile in cross section is not symmetric (Fig. 3). Two maximums are observed slightly off center and closer to channel walls. It is explained by inertial component of the flow: when entering the system, liquid flows by cylindrical channel with strictly determined speed, then part of liquid changes the direction and passes into main chamber through the flanges closer to solution inlet, but the main portion of liquid does not change the direction and enters the main chamber only at the dead end of the cylinder. However, the parabolic flow distribution dominates in the middle of the chamber.

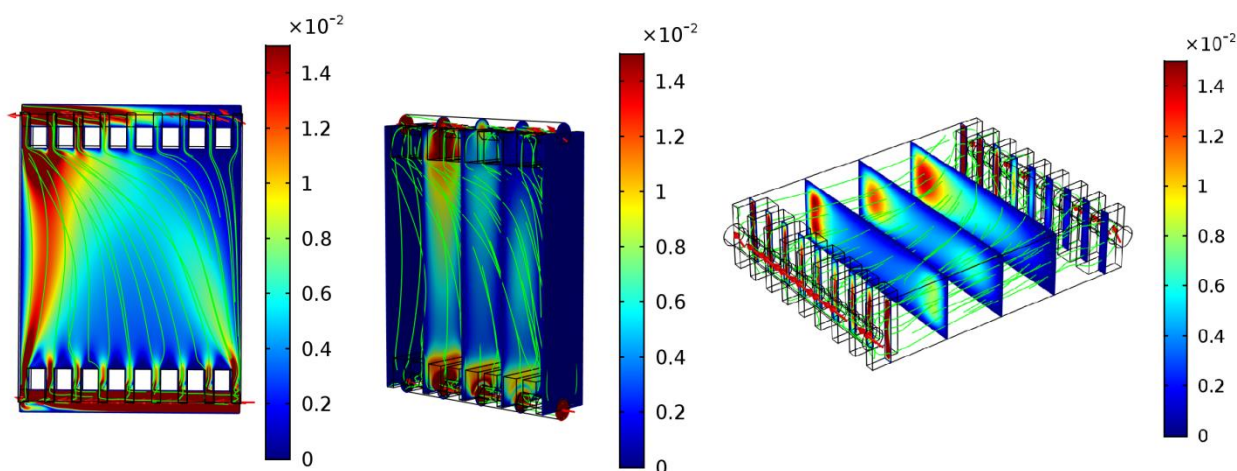


Figure 2. Distribution of flow velocities in cross sections normal to general direction of flow. Local linear flow velocity measured in meters per second is given in color scale

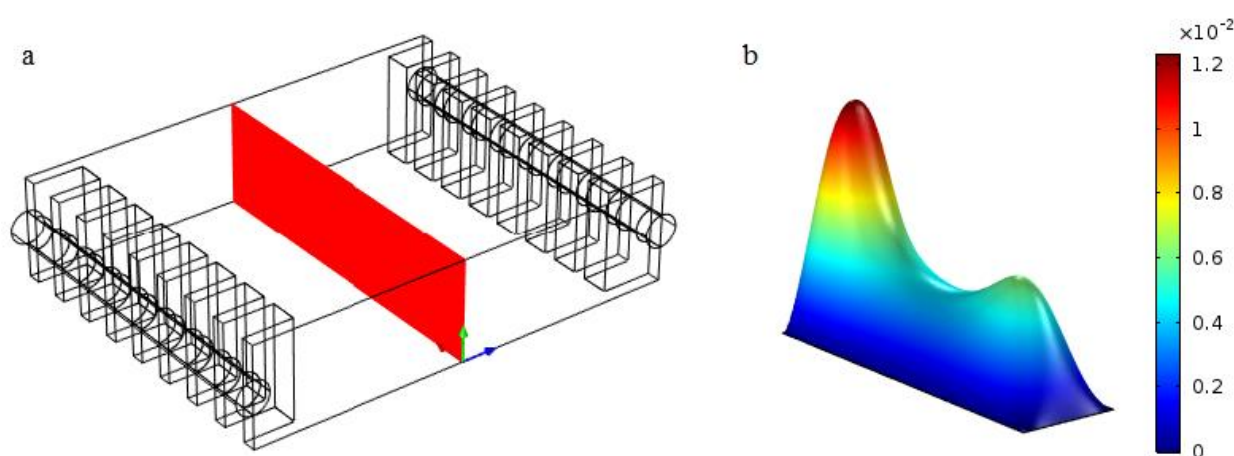


Figure 3. Distribution of flow velocity (b) in YZ cross section situated in the middle of the chamber (a)

Acknowledgements

This investigation was realized within French-Russian laboratory "Ion-exchange membranes and related processes". The authors are grateful to RFBR, Russia (grant 17-08-015-38) for financial support.

References

1. Strathmann H. Electrodialysis, a mature technology with a multitude of new applications // Desalination 264 (2010) 268;
2. Volodina E., Pismenskaya N., Nikonenko V. et all. // J. Colloid Interface Sci. 2005. Vol. 285. P. 247.
3. Pismenskaya N.D., Nikonenko V.V., Melnik N.A., Belova E.I. Patent 100276 Russian Federation, MPK G01N27/40 (2006.01). Device for the integrated study of mass transfer and electrochemical characteristics of ion-exchange membrane. Kuban state university, Krasnodar, Russia, No. 2010129861/28; priority 16.07. 2010; publication 10.12. 2010

SILICONE RUBBERS WITH ALKYL AND SILICON-CONTAINING SIDE CHAINS SUBSTITUENTS FOR HYDROCARBONS SEPARATION

Evgenia Grushevenko, Ilya Borisov, Danila Bahtin, George Shandryuk, Galina Bondarenko, Alexey Volkov

A.V. Topchiev Institute of Petrochemical Synthesis, Moscow, Russia

E-mail: evgrushevenko@ips.ac.ru

Introduction

In the world, global demand for natural gas will increase by 50-70% compared to 2010 level by 2040 [1]. Wherein the coverage such significant growth in demand for gas will be implemented by using shale and multicomponent gas containing significant amounts of C_{3+} hydrocarbons, as well as traditional natural gas [1]. In this regard, task of conditioning natural gas take on special importance. Light hydrocarbons such as methane, ethane, propane and butane are not only energy sources but also valuable raw materials for obtaining a variety of different industrial materials [2]. Absorption, adsorption, separation, cryogenic and membrane technologies is used nowadays for gas treatment and separation, depending on the task [3]. Membrane technologies are well proven in gas separation processes, including in petrochemical processes, because: that separation process are carried out without a phase transition, it is possible to create compact, modular installations, low power consumption for the separation process (separation under atmospheric conditions is possible) [4]. One of the most complicated separations is condensable gases, particularly propane and butane, removal from natural gas. When choosing membrane material and separation conditions, it is important that C_{3+} hydrocarbons concentration in dry natural gas may be up to 15%. This implies necessity for choosing the material capable of selective hydrocarbons separation from methane mixtures.

In contrast to the polymers with intrinsic microporosity characterized by a high fraction of non-equilibrium free volume (more than 20% [5]) and a significant reduction of membrane performance in time [6], rubber material possesses long-term stable membrane transport properties. This allowed them to find a real industrial application as separation membrane materials. Despite all the benefits of existing silicone rubbers based membranes, their selectivity values are quite low for C_{3+} hydrocarbons removal from natural and associated petroleum gas. Thus, the problem of finding new silicone rubbers possessing high C_4/C_1 selectivity in comparison with the existing silicone rubbers is relevant.

The goal of this work is finding novel membrane materials based on silicone rubbers substituted on side chain and is to determine the substituent influence on the transport properties of the membrane material.

Experimental

Membrane materials with high selectivity to organic vapors and with stability of separation characteristics over time was created from crosslinkable polymers based on polymethylsiloxane modified by alkyl and silicone containing hydrocarbon radicals. In this research membrane polymers were synthesized based on poly(methylhydrosiloxane) modified hydrocarbons substituents in the side (M-PMS). Technique was developed for the preparation of membranes based on poly(octylmethylsiloxane) (POMS), poly(decylmethylsiloxane) (PDecMS), poly(hexylmethylsiloxane) (PHexMS), poly(4,4-dimethyl-4-silpentylmethylsiloxane) (PDMSPMS), poly(3,3-dimethyl-3-silbutylmethylsiloxane) (PDMSBMS), poly(ethylcyclohexanemethylsiloxane) (PECHMS) and poly(3,3-dimethylbutylmethylsiloxane) (PDMBMS). Gas transport properties of these membranes were investigated. To study gas separation membranes properties was chosen the following gases: permanent gases (nitrogen, methane) and condensable gas (carbon dioxide, propane, butane) - as a model system. The membranes gas permeability and diffusion coefficients for nitrogen, methane and propane were measured at 30°C according to Daynes-Barrer technique using precise unit "Helmholtz-Zentrum Geesthacht" mounted with pressure sensor ("Baratron"), accuracy 10^{-7} bar. Permeability

coefficient (P) is given in barrers. The ideal selectivity (a_p) was calculated as the ratio between the corresponding gas permeability coefficients.

IR spectra registration was carried in the films surface reflection mode using IR microscope HYPERION-2000 conjugated with IR Fourier spectrometer IFS 66 v/s Bruker (Ge crystal, scan.-50, resolution 2 cm^{-1} , range $600\text{-}4000\text{cm}^{-1}$).

Calorimetric studies were performed on a DSC823 differential scanning calorimeter of the company "Mettler" at a rate of temperature change of 10 deg/min in an argon atmosphere in the temperature range from -140 to 100°C .

Results and Discussion

To obtain M-PMS in this work, for the first time, such modifying agents as: 1-hexene, 1-decene, allyltrimethylsilane, vinyltrimethylsilane, vinylcyclohexane, 3,3-dimethylbutene-1. To compare obtained M-PMS with the materials presented in the literature, samples of POMS membranes were also obtained. The ratio of the cross-linking agent to the modifying agent - 5/95 - was chosen based on the author's work [7].

In Table 1 are presented main characteristic of obtained membrane materials: glass transition temperature, shear modulus, substitution degree and density. In figure 1 are presented gas permeation properties of obtained membrane materials.

Table 1. Main characteristic of M-PMS membrane materials.

Membrane	Glass transition temperature, $^\circ\text{C}$	Substitution degree, %	Density, g/cm^3
PHexMS	-105.1	82	1.09
POMS	-93.0	87	0.99
PDecMS	-68.3	89	1.04
PDMSPPMS	-68.3	85	1.03
PDMSBMS	-44.7	80	1.01
PDMBMS	-44.7	70	0.99
PECHMS	-41.4	75	1.04

As we can see from Table 1, this method of obtaining membrane materials makes it possible to obtain high substitution degrees for all the represented side chain substituents.

In case of gas permeability coefficients values for n-butane, obtained M-PMS membranes are arranged as follows (to decrease P, barrer):

PHexMS (8000) > POMS (7400) > PDecMS (6400) > PDMSPPMS (6100) > PDMSBMS (2440) > PDMBMS (1360) > PECHMS (700)

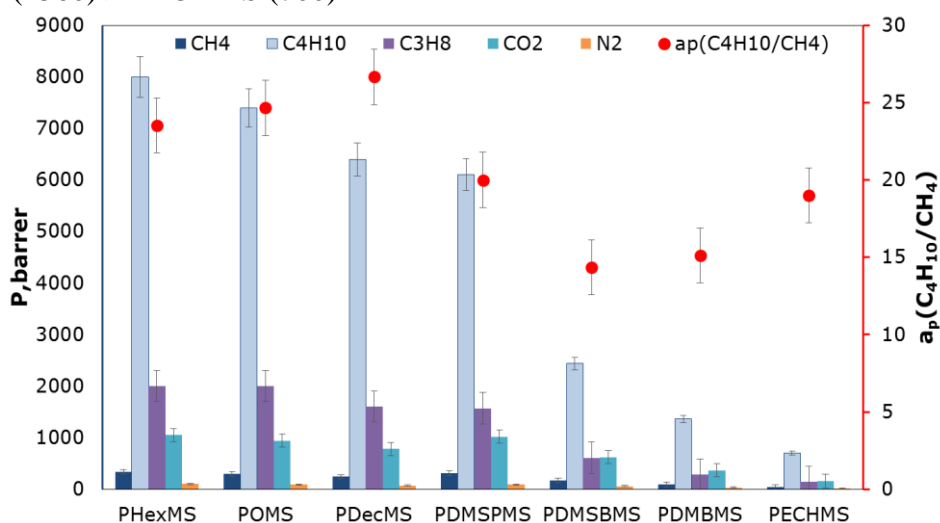


Fig. 1. Gas permeability coefficients and ideal selectivity of M-PMS membranes

The decrease in the permeability coefficient in this row of membranes is associated with an increase in the rigidity of the polymer chain, which is also indicated by an increase in the glass transition temperature in the same row.

The picture of the ideal selectivity for n-butane/methane differs somewhat:

PDecMS (27.0) > POMS (24.7) > PHexMS (23.5) > PDMSPMS (20.0) > PECHMS (19) > PDMBMS (15.1) > PDMSBMS (14.4)

All M-PMS have lower permeability coefficient than that of PDMS but exceed its separation selectivity. As separation selectivity is essential for removal of organic vapors and C₃₊ hydrocarbons target fraction from natural gas, it can be concluded that the M-PMS obtained have an advantage over PDMS. Also, the PDecMS obtained is a more selective material than POMS known in literature.

Acknowledgements

This work was supported by the Russian Foundation for Basic Research, project no. 16-08-00830.

References

1. *Administration, U.S. Energy Information*. International Energy Outlook 2016 With Projections to 2040. Washington : б.н., 2016. DOE/EIA-0484(2016).
2. *Sikdar N. et al.* Dynamic Entangled Porous Framework for Hydrocarbon (C₂–C₃) Storage, CO₂ Capture, and Separation // *Chemistry–A European Journal*. 2016. V. 22. N.17. P. 6059-6070.
3. *Freeman B. et al.* Materials science of membranes for gas and vapor separation. John Wiley & Sons, 2006. P. 444.
4. *Ravanchi M. T. et al.* Application of membrane separation processes in petrochemical industry: a review // *Desalination*. 2009. V. 235. N. 1. P. 199-244.
5. *Yu. Yampolskii.* Polymeric Gas separation membranes // *Macromol.* 2012. V. 45 P. 3298-3311.
6. *A.Yushkin et al.* Study of glassy polymers fractional accessible volume (FAV) by extended method of hydrostatic weighing: Effect of porous structure on liquid transport // *React.Funct. Polym.* 2015. V. 86. P. 269-281.
7. *E.A.Grushevenko et al.* Membrane material based on octyl-substituted polymethylsiloxane for separation of C₃/C₁ hydrocarbons // *Petroleum Chemistry*. 2017. V. 57. N. 4. P. 334-340.

SYNTHESIS OF Fe_3O_4 NANOSTRUCTURES BY SONO-CHEMICAL METHOD AND ITS APPLICATION IN CELLULOSE ACETATE POLYMERIC NANOCOMPOSITE MEMBRANE

Farhad Heidary

Department of Chemistry, Faculty of Science, Arak University, Arak 38156-8-8349, Iran

E-mail: F-heidary@araku.ac.ir

Introduction

Sono-chemical is a fast procedure for fabricating mono-disperse nanoparticles. Magnetic nanoparticles and nano-additives have gained much attention in composite industries due to the fact that adding of a small amount of nanostructure to a composite can lead to a great improvement in physical and chemical properties of the composite [1-4]. In this work we have used the sono-chemical process to successfully synthesize Fe_3O_4 nanoparticles. Then, cellulose acetate / Fe_3O_4 nanocomposite membrane was prepared to obtain a new mixed matrix membrane. Nanostructures were characterized scanning electron microscopy (SEM). The results showed that presence of Fe_3O_4 nanoparticles in the membrane structure enhanced the ions rejection.

Experiments

In a typical synthesis, 0.002 mol of $\text{FeCl}_3 \cdot 6\text{H}_2\text{O}$ and 0.001 mol of $\text{FeCl}_2 \cdot 4\text{H}_2\text{O}$ were dissolved in 100 ml distilled water. Under ultrasonic irradiation (100W) sodium hydroxide (1M) was added to the solvent. The magnetite product was centrifuged, washed with alcohol and distilled water for several times, and dried in oven at 60 °C for 8 h. 1.6 gr of cellulose acetate and 1.5 gr of PVP (as pore former) are dissolved in 10 ml acetone. 0.3 gr of Fe_3O_4 is dispersed in 10 ml acetone solution with ultrasonic waves (20 min, 60W). The magnetite dispersion is then slowly added to the polymer solution. The new solution is then mixed and stirred for 5 hours. In order to evaporate the solvent, the product is casted on a piece of glass template (Figure 1). This is immediately immersed in the non-solvent bath (pure water) at room temperature without any evaporation. The composite cellulose acetate / Fe_3O_4 membrane was finally dried at 50°C for three hours.

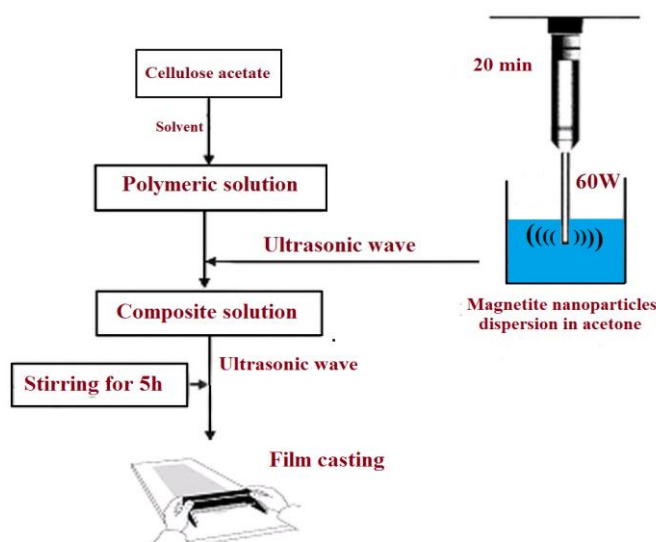


Figure 1. Preparation of cellulose acetate/ Fe_3O_4 nanocomposite

Results and Discussion

Scanning electron microscopy image of magnetite nanoparticles prepared by sodium hydroxide addition is shown in Figure 2. In experimental condition nanoparticles with average diameter size less than 100 nm were obtained. The prepared nanocomposite membrane was utilized for removal of nickel ions from water. The performances of virgin and modified membranes were examined using a dead end filtration cell under 2 bars at room temperature. Experimental setup composed of nitrogen gas cylinder, pressure regulator, membrane stirred cell and permeate tube. Membrane

performance was evaluated by rejection determination. The rejections of the nickel ions were estimated by measuring the ions concentration in the feed and permeate using atomic absorption. The rejection of prepared membranes is depicted in Figure 3. The acceptable ion rejection of virgin membrane is because of the presence of functional groups in cellulose acetate structure. The rejection improvement in modified membrane is due to the adsorption characteristic of Fe_3O_4 nanoparticles.



Figure 2. SEM images of prepared magnetite nanoparticles

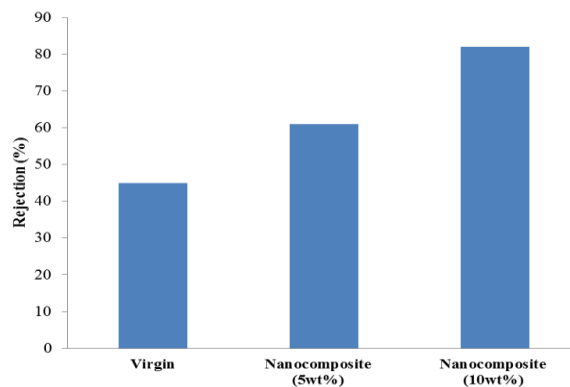


Figure 3. Rejection of prepared membranes

References

1. Mitra A., Mahapatra A. S., Mallick A., Chakrabarti P. K. Enhanced microwave absorption and magnetic phase transitions of nanoparticles of multiferroic LaFeO_3 incorporated in multiwalled carbon nanotubes (MWCNTs) // *J. Magn. Magn. Mater.* 2017. V. 435. P. 117–125.
2. Sharifalhoseini Z., Entezari M. H., Jalal R. Evaluation of antibacterial activity of anticorrosive electroless Ni–P coating against *Escherichia coli* and its enhancement by deposition of sonosynthesized ZnO nanoparticles // *Surf. Coat. Technol.* 2015. V. 266. P. 160–166.
3. Heidary F., Khodabakhshi A. R., Ghanbari D. A novel sulfonated poly phenylene oxide-poly vinylchloride/ZnO cation-exchange membrane applicable in refining of saline liquids // *J. Clust. Sci.* 2017. DOI: 10.1007/s10876-017-1156-6.
4. Vignesh K., Kang M. Facile synthesis, characterization and recyclable photocatalytic activity of $\text{Ag}_2\text{WO}_4@g\text{-C}_3\text{N}_4$ // *Mater. Sci. Eng., B* 2015. V. 199. P. 30–36.

PREPARATION OF NANOCOMPOSITE MEMBRANE CONTAINING MAGNETITE NANOPARTICLES FOR REMOVAL OF METAL IONS

¹Farhad Heidary*, ²Behrouz Heidari, ¹Siavash Heidary, ¹Elahe Naseri, ¹Maryam Ansari

¹Young Researchers and Elite Club, Arak Branch, Islamic Azad University, Arak, Iran

²Department of Electrical Engineering, Arak-Branch, Islamic Azad University, Arak, Iran

*E-mail: Heidary.farhad@yahoo.com

Introduction

Heavy metals are commonly associated with introducing pollution and toxicity into the atmosphere and environments [1]. There are numerous physical and chemical treatments, including adsorption and chemical precipitation, for removal of heavy metals from wastewater [2, 3]. The techniques are mainly expensive with low selectivity. Another option for separation of heavy metals from wastewater is membrane technology [4]. High performance may be obtained by integration of membranes with the existing plants [5] or membrane modification [6]. In current work, PES+PVDF/PVA/Fe₃O₄ nanocomposite membrane containing 8-Hydroxyquinoline (as a chelating agent) was prepared to obtain a new mixed matrix membrane with the enhanced affinity for lead ions.

Experiments

The nanocomposites solution was prepared by dissolving polymer and in-situ formation of Fe₃O₄ nanoparticles in the polymeric matrix. Typical synthesis process is as follows: The fabricated PES/PVDF membrane was treated with prepared aqueous solution of PVA/Fe₃O₄. For this purpose, the PES/PVDF membrane was immersed in the aqueous solution of PVA/Fe₃O₄ for 5min. The excess solution was drained off and the composite PES+PVDF/PVA/Fe₃O₄ membrane was finally dried at 40°C for three hours.

The prepared nanocomposite membrane was utilized for removal of lead ions from water. The SEM image of the membrane is presented in Figure 1. The membranes showed a characteristic morphology of asymmetric membrane, consisting of a dense skin-layer and a porous sub-layer with finger-like structure. The performances of virgin and modified membranes were examined using a dead end filtration cell under 2 bars at room temperature. Experimental setup composed of nitrogen gas cylinder, pressure regulator, membrane stirred cell and permeate tube. The detail of the experimental setup is shown in Figure 2.

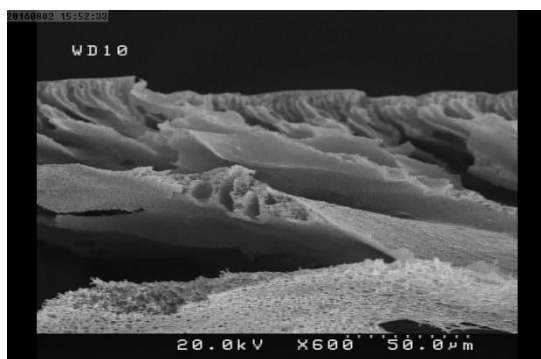


Figure 1. SEM images of prepared membranes

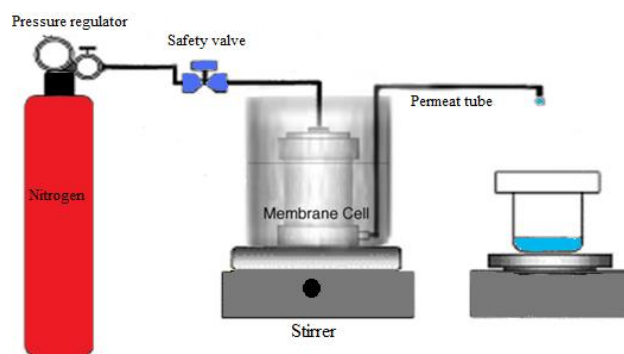


Figure 2. Dead end filtration system

Results and Discussion

Membrane performance was evaluated by flux and rejection determination. The flux shows the amount of permeates or product and the rejection indicates the selectivity of the membrane. The rejections of the lead ions were estimated by measuring the ions concentration in the feed and permeate using atomic absorption. The rejection and flux of prepared membranes are depicted in Figure 3 and 4 respectively. The rejection improvement in modified membranes is due to the significant presence of covalently attached ligands and adsorption characteristic of Fe₃O₄

nanoparticles. Virgin membrane possesses much lower functional groups compared to the coated membranes. Also, partially pore blockage of the modified membranes (compared to virgin sample) leads to lower flux.

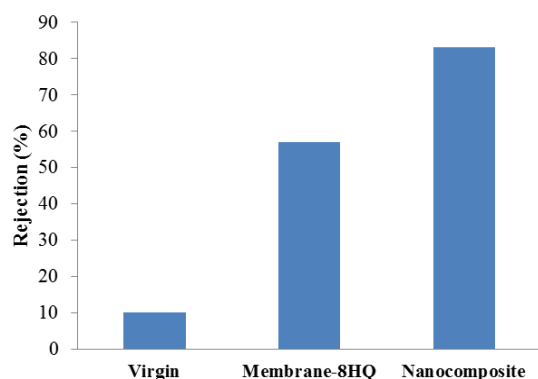


Figure 3. Lead rejection of prepared membranes

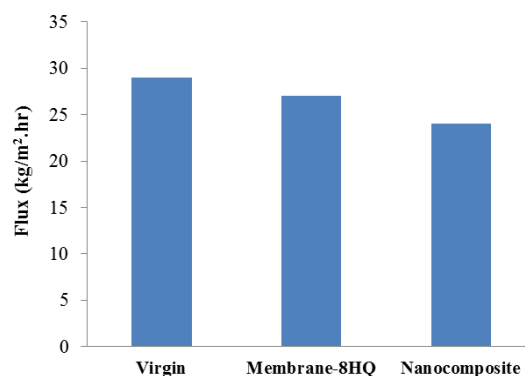


Figure 4. Flux of prepared membranes

References

1. O'Connell D. W., Birkinshaw C., O'Dwyer T. F. Heavy metal adsorbents prepared from the modification of cellulose: a review // *Bioresour. Technol.* 2008. V. 99. P. 6709-6724.
2. Basha S., Murthy Z. V. P., Jha B. Biosorption of hexavalent chromium by chemically modified seaweed // *Chem. Eng. J.* 2008. V. 137. P. 480-488.
3. Oubagaranadin J. U. K., Sathyamurthy N., Murthy Z. V. P. Evaluation of Fuller's earth for the adsorption of mercury from aqueous solutions: a comparative study with activated carbon // *J. Hazard. Mater.* 2007. V. 142. P. 165-174.
4. Murthy Z. V. P., Chaudhari L. B. Separation of binary heavy metals from aqueous solutions by nanofiltration and characterization of the membrane using Spiegler–Kedem model // *Chem. Eng. J.* 2009. V. 150. P. 181-187.
5. Baek K., Kim B. K., Cho H. J., Yang J.W. Removal characteristics of anionic metals by micellar enhanced ultrafiltration // *J. Hazard. Mater.* 2003. V. 99. P. 303-311.
6. Madaeni S. S. Effect of surface roughness on retention of reverse osmosis membranes // *J. Porous Mater.* 2004. V. 11. P. 255-263.

PREPARATION OF COBALT (II) POLYPORPHINE FILMS BY ELECTROCHEMICAL METHOD AND THEIR CATALYTIC PROPERTIES

^{1,2}Olga Istakova, ^{1,2}Dmitry Konev, ^{1,2,3}Mikhail Vorotyntsev

¹Institute for Problems of Chemical Physics of the Russian Academy of Sciences, Chernogolovka, Russia

²D. I. Mendeleev University of Chemical Technology of Russia, Moscow, Russia

³M. V. Lomonosov Moscow State University, Moscow, Russia

E-mail: oistakova@gmail.com

Introduction

Electroactive materials produced by introduction of porphyrin macrocycle into conjugated polymer film are of great practical interest. Basing on a new recently developed high-efficiency method of Mg(II) porphine (**MgP**) synthesis [1], homopolymers of Mg(II) porphine (**pMgP**) with original optical and electrical properties were obtained [2] by means of direct electropolymerization of MgP. It opens the route towards other representatives of this new electroactive polymer family [2, 3], via the replacement of coordinated Mg(II) ions inside already formed **pMgP** film at the electrode surface leading to **pMP** (M = Zn, Co, Fe, Mn...). Such transition-metal containing polyporphine materials might be prospective as catalysts of various processes, in particular for the oxygen reduction, owing to the presence of MeN₄ active centers, as it has been found for corresponding molecular porphyrins. Polyporphines possess an important advantage, compared to other porphyrin-based polymers, as having the maximal possible content of this macrocycle due to the absence of polymer chains of a different nature or linking/substituent groups.

Use of the routine metalation method of the tetrapyrrole heterocycles, i.e. the treatment of the free base polyporphine with a metal ion salt, had allowed us to prepare for the first time polyporphines of cobalt and zinc [3]. However, this method suffers from potential contamination of the polymer by salt hydrolysis products, as well as from poor adhesion and poor stability of the electroactive layer, extended duration of the procedure and high temperature (requiring a sufficiently high thermal stability of the polymer and the support).

The goal of this work has been to develop an alternative method of the metalation of polyporphine films, with substitution of thermal treatment by electrochemical polarization of the film in solution of the corresponding metal salt (cobalt salt in this study) and test these polyporphine films in oxygen electroreduction reaction in aqueous solutions.

Experiments

First, magnesium(II) polyporphine of type I, **pMgP**, have been prepared by electrooxidative polymerization of MgP in acetonitrile-based (AN) electrolyte solution. This procedure results in polymeric film formation at the electrode/electrolyte interface. Then, the film was demetalated by ion exchange of Mg(II) by protons from solution of CF₃COOH, according to the method described in Ref. [3]. The subsequent metalation step was performed via electrochemical treatment (fig. 1) in solution of cobalt perchlorate (AN) by application of several cycles of linear potential sweep between certain limits. CV experiments with polymer-coated electrode transferred to background electrolyte in the wide potential intervals were used for metalated films characterization.

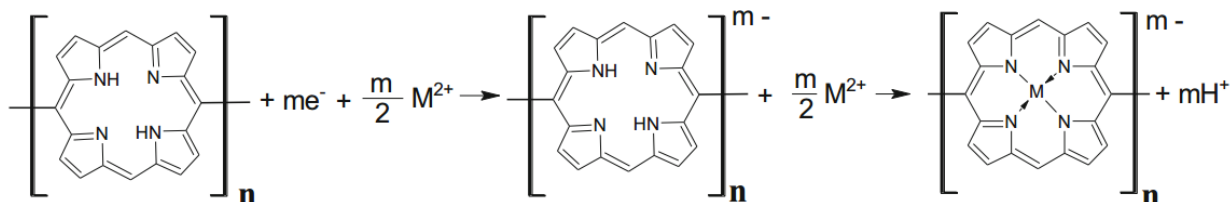


Figure 1. Scheme for introducing a metal cation into the free base polyporphine film with the use of the electrochemical procedure

Additionally resulting films were characterized by means of UV-Vis and IR spectroscopic techniques.

Results and Discussion

Freshly polymerized pMgP film on Pt electrode demonstrates following electrochemical behavior (fig.2a, black line): it may be in a neutral (insulating) or in a positively or negatively charged (conducting) state, depending on the electrode potential. Replacement of Mg by 2H shifts the potential intervals of these redox-transitions to positive direction on about 0.3V (fig.2a, grey line). It was found that being placed to 0.5mM $\text{Co}(\text{ClO}_4)_2$ in AN (with 0.1 M TBAPF₆ as background electrolyte) and treated electrochemically in the CV regime (between -1.1V and +0.4V), free base polyporphine film reveals the progressive growth of positive and negative currents at the potential range of Co(I)/Co(II) and Co(II)/Co(III) redox-transitions (fig.2b). After the saturation of this growth (about 30 cycles later) and transfer of the electrode to cobalt-free background electrolyte these redox-transitions still present (fig.2a, dashed line). This fact testifies in favor of almost complete replacement of 2H by Co(II) ions according the scheme on fig.1 [4].

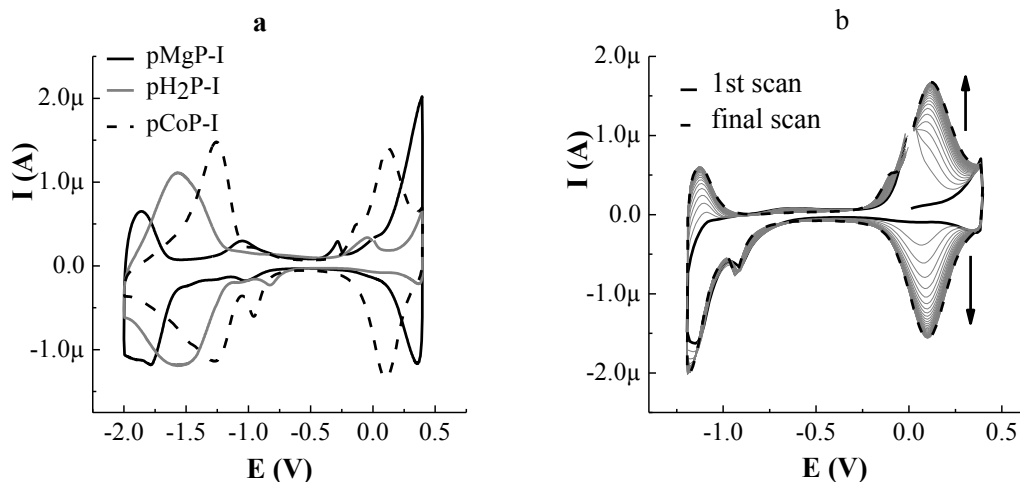


Figure 2. (a) - CV-responses of pMP ($M = \text{Mg}, 2\text{H}, \text{Co}$) film-coated Pt electrode in contact with 0.1M TBAPF₆ + AN solution (potential range: between -2.0 V and 0.4 V). (b) - multi-cycle CV response of of pH₂P film-coated Pt electrode in 0.5mM $\text{Co}(\text{ClO}_4)_2$ + 0.1M TBAPF₆ + 1.5mM Lutidine+AN. Cathodic limit: -1.2 V. All potential values are given vs. Ag/0.01M AgNO₃ + AN. Scan rate: 0.1 V/s

We have also studied oxidative transformation of thus obtained cobalt polyporphine films, which results in condensed structure materials (transition of polymer of type I into polymer of type II, **pCoP-II**), characterized by combination of electrochemical and spectroscopic methods. The behavior of pCoP-II polymer films in oxygen electroreduction reaction was studied by means of CV and stationary voltammetry in alkaline medium (fig.3a, b).

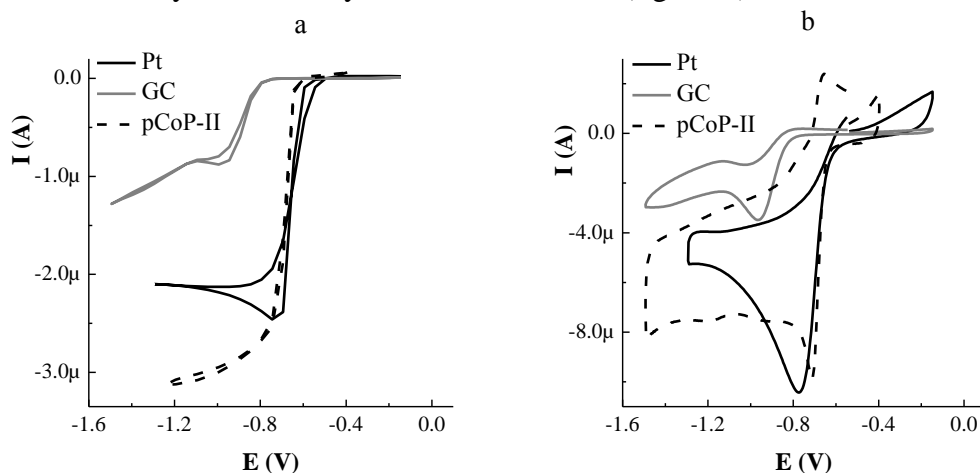


Figure 3. (a) – Stationary curves (Scan rate: 0.1 V/s) and (b) cyclic voltammograms of the Pt and glassy carbon electrodes without a film and glassy carbon electrode coated with a pCoP-II film, 0.1 M NaOH in H₂O. All potential values are given vs. RHE.

As one can see from these plots, the pCoP-II films possess catalytic activity with respect to oxygen and are of interest as platinum-free catalysts of oxygen electroreduction. Comparison of these results with recent literature data for similar materials published in top electrochemical journals has allowed to make favorable conclusions on attractive prospects of synthesized polymeric materials for a broad range of applications.

Acknowledgements

This work was supported by the Presidium of the Russian Academy of Sciences (program OHNM-03).

References

1. *Dogutan D.K., Ptaszek M., Lindsey J.S.* Direct synthesis of magnesium porphine via 1-formyldipyrrromethane // *J. Org. Chem.* 2007. V. 72. P. 5008 – 5011.
2. *Vorotyntsev M.A., Konev D.V., Devillers C.H., et al.* Magnesium (II) polyporphine: The first electron-conducting polymer with directly linked unsubstituted porphyrin units obtained by electrooxidation at a very low potential // *Electrochim. Acta.* 2010. V. 55. P. 6703 – 6714.
3. *Konev D.V., Devillers C.H., Lizgina K.V., et al.* Synthesis of new electroactive polymers by ion-exchange replacement of Mg (II) by 2H⁺ or Zn (II) cations inside Mg (II) polyporphine film, with their subsequent electrochemical transformation to condensed-structure materials // *Electrochim. Acta.* 2014. V. 122. P. 3 - 10.
4. *Istakova O.I., Konev D.V., Zyubin A.S., et al.* Electrochemical route to Co (II) polyporphine // *Journal of Solid State Electrochemistry.* 2016. V. 20. P. 3189 - 3197.

EFFECT OF POLYMER AND COUNTER-ION NATURE ON THE STRUCTURAL FEATURES OF THE POLYMER ELECTROLYTE MEMBRANES

Larisa Karpenko-Jereb

Institute of Electronic Sensor Systems, Graz University of Technology, Graz, Austria

E-mail: larisa.karpenko-jereb@tugraz.at

Introduction

The ion-exchange membranes are widely applied in electro-membrane processes as well in the separation and purification [1]. The transport characteristic and membrane selectivity depends on the thermodynamic properties of the water, which are determined by nature of the polymer and the counter-ion. The goal of the work is to analyze the water binding energy and the dissociation of functional groups in the polymer electrolyte membranes having different chemical structure at various solvation (water or methanol) levels using quantum chemical methods.

Computational Methods

The studied membranes Nafion, IonClad and M3 (Fig.1) possess the perfluorinated backbone, however various side chains terminated with the functional groups of distinctly different ionic strength. The calculations have been performed by the Program ORCA [2]. The geometries had been optimized by the Restricted Hartree Fock (RHF) method with the 6-31G (d,p) basis set and tight optimization criteria. The quality of minima has been checked via frequency analysis. The calculation of the binding energy of the membrane-solvent complexes have been carried out using the local pair natural orbital - coupled-electron pair approximation (LPNO-CEPA/1). From the values of the electrons energy of dry (E_{dry}) and hydrated membranes ($E_{cluster}$) the specific binding energy (E_B) of the water molecules was computed by the following expression:

$$E_B = \frac{E_{cluster} - E_{dry}}{X} - E_{solv} \quad (1)$$

where E_{solv} is the electrons energy of one solvent molecule, X is the number of solvent molecules in the membrane. The specific binding energy indicates the binding energy per solvent molecule.

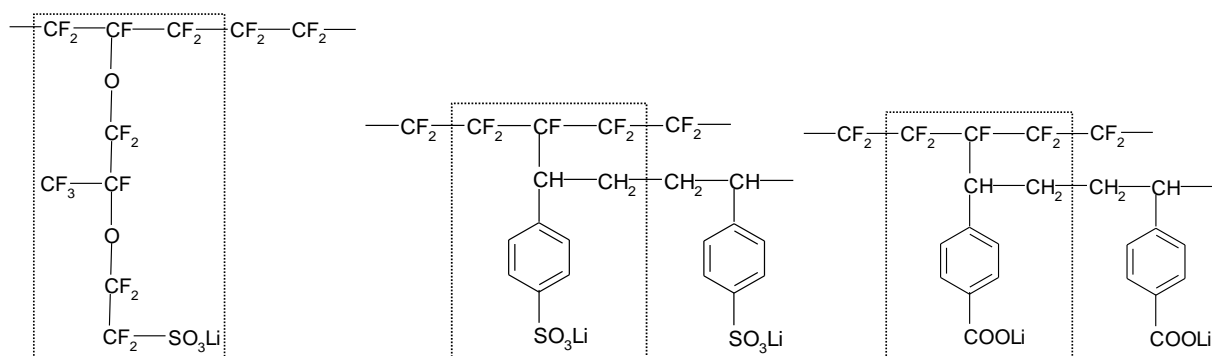


Figure 1. Chemical structure of the membranes: Nafion (left), IonClad (middle), M3 (right). The membrane models used in the quantum calculations are marked by the squares.

Results and Discussion

The optimized structures of the membranes MK-40 and Nafion with the hydration levels $X=0$; 1; 3; 6 and 8 are shown in Figure 2. As seen from the figure in membrane MK-40 the sulfonic acid groups are in a non-dissociated state in the whole studied range of the hydration level, while in the perfluorinated membrane Nafion the dissociation of the ion-exchange group is observed for $X \geq 3$. Moreover, the water molecules in the polystyrene membrane MK-40 are dislocated around the end-group, while the water molecules in the Nafion membrane locate under the end-group and form a cluster [3].

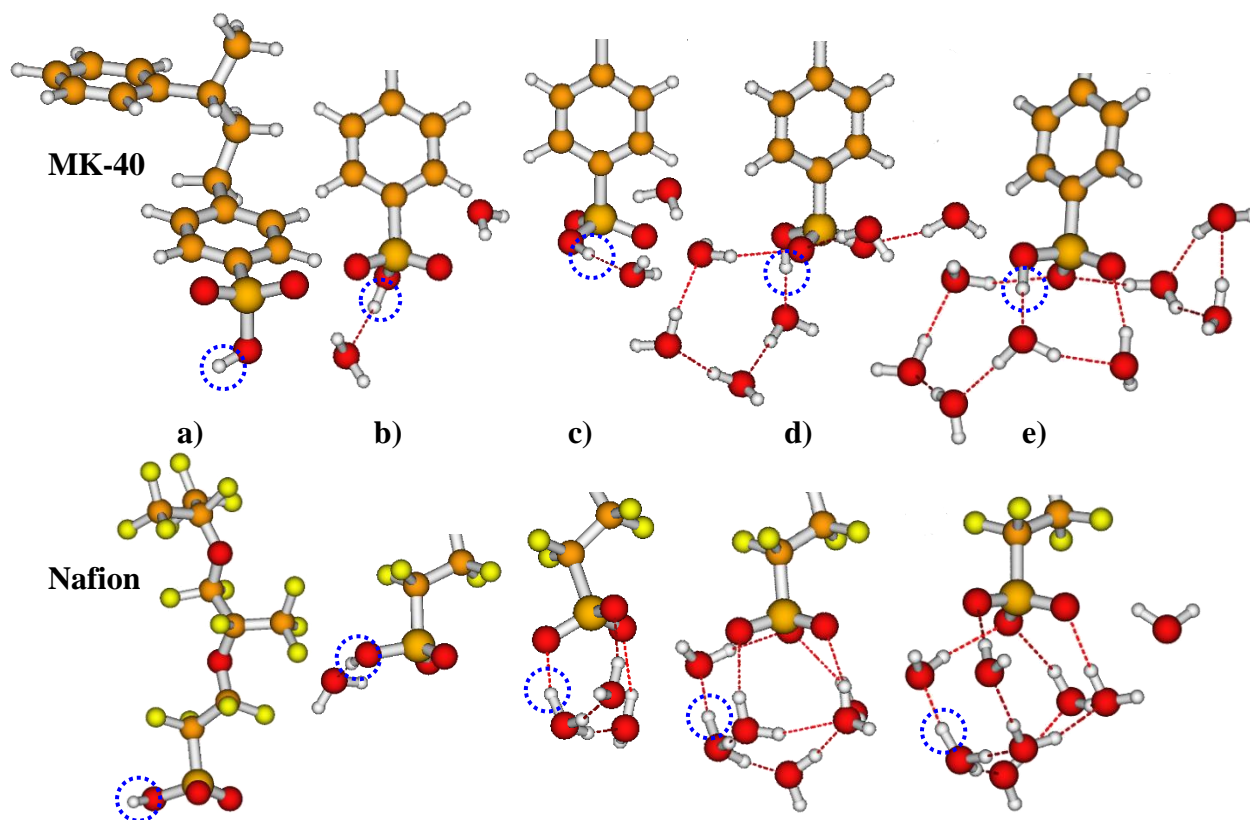


Figure 2. Calculated geometries of dry membranes (a) and membrane fragments (b-e) at various hydration levels: $X=1$ (b); $X=3$ (c); $X=6$ (d); $X=8$ (e). Protons are marked with a dotted circle.

Figure 3 (left) depicts the closest distances between the fixed group of Nafion membrane and counter ions ($-\text{SO}_3^- \dots \text{Cat}^+$) as a function of the hydration level. In the dry Nafion, the distance $-\text{SO}_3^- \dots \text{Cat}^+$ increases with the atomic radius of the counter ion in the following sequence $\text{H}^+ < \text{Li}^+ < \text{Na}^+$. In Li^+ and Na^+ -forms of the Nafion membrane the dissociation of the functional groups occurs, when the functional group is surrounded by seven water molecules. The distances $-\text{SO}_3^- \dots \text{Li}^+$ and $-\text{SO}_3^- \dots \text{Na}^+$ reach comparable values, 3.70 Å and 3.77 Å respectively. At higher hydration level $X > 7$, Li^+ and Na^+ ions are located further away from the sulfonic groups than the protons are. The mean distance $-\text{SO}_3^- \dots \text{H}^+$ equals 3.46 Å at this hydration range ($X > 7$). It should be mentioned that prior to the dissociation, the hydrogen is connected to the sulfonic group by a covalent bond, while the alkali metal ions Li^+ and Na^+ create ionic bonds. After the dissociation, the proton builds the hydronium ion, which has a significantly larger radius than the proton and also than lithium and sodium cations. Since the hydronium ion has larger size and lower surface charge density than the studied alkali cations, the hydronium ion is less distanced from the sulfonic group at the higher hydration level ($X \geq 7$).

The water binding energy in Nafion membrane is presented in Fig. 3 (right). The diagram demonstrates the water binding energy per water molecule in Nafion membrane of the three ionic forms investigated, as a function of the hydration level. In the whole investigated range of the hydration level, the binding energy per water molecules is stronger for Nafion containing the alkali ions as the counter ions, because the alkali ions possess quite large surface charge density, which strengthens the electrostatic attraction of the water molecules. The static ab initio calculations are consistent with experimental observations demonstrating that the water diffusion coefficient is higher in H^+ -form Nafion than in Na^+ or Li^+ forms [4].

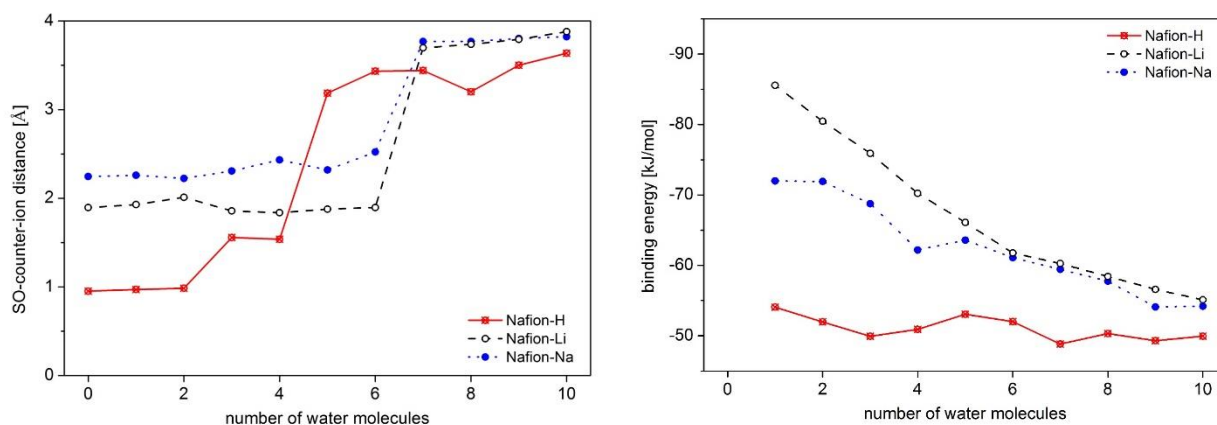


Figure 3. Minimal distance between sulfo-group and counter-ions (left) and the binding energy per water molecule (right) in Nafion membrane of different ionic forms: H^+ , Li^+ and Na^+ [4].

Conclusion

It has been shown that the ability of the functional group to dissociate becomes more pronounced with: 1) growing electron density of the polymer side chains, especially when the electronegative group is directly connected to the functional group; 2) increasing polarity of the absorbed solvent; 3) acidity of the fixed group.

The binding energy of the solvent molecules with the membrane generally decreases with increasing solvation level. In the Nafion membrane, the binding energy of water and methanol is slightly higher than in the aromatic membranes IonClad and M3.

References

1. *Strathmann H.* Ion-exchange membrane separation processes / Membrane Science and Technology Series, 9. Elsevier 2004. 348 pp.
2. *Neese F.* ORCA Version 2.8, An ab initio, density functional and semi-empirical program package, University Bonn, September 2010.
3. *Karpenko-Jereb L.V., Kelterer A.-M., Berezina N.P., Pimenov, A.V.* Conductometric and computational study of cationic polymer membranes in H^+ and Na^+ -forms at various hydration levels // *J. Membr. Sci.* 2013. V. 444. P. 127-138.
4. *Karpenko-Jereb L., Rynkowska E., Kujawski W., Lunghammer S., Kujawa J., Marais S., Fatyeyeva K., Chappey C., Kelterer A.-M.* Ab initio study of cationic polymeric membranes in water and methanol // *Ionics.* 2016. V. 22. P. 357–367.

IMPACT OF IONOMER IN CATALYST LAYER ON PERFORMANCE OF A POLYMER ELECTROLYTE FUEL CELL

¹Larisa Karpenko-Jereb, ¹Eduard Schatt, ²Clemens Fink, ²Peter Urthaler, ¹Alexander Bergmann, ²Reinhard Tatschl

¹Institute of Electronic Sensor Systems, Graz University of Technology, Austria

E-mail: larisa.karpenko-jereb@tugraz.at

²Advanced Simulation Technologies, AVL List GmbH, Graz, Austria

The paper presents a systematic investigation of the influence of alterations in the values of the model characteristics of the cathode catalyst layer [1] on the performance of a PEMFC. The individual influences of seven geometric and transport parameters have been tested on a single channel fuel cell using the CFD code AVL FIRE simulation.

The calculations of PEMFC performance have been conducted by increasing and decreasing the values of each tested parameter, and comparing the results to a reference case. The following parameters have been tested: 1) ionomer volume fraction; 2) porosity; 3) agglomerate radius; 4) ionomer film thickness; 5) catalyst thickness; 6) ionic conductivity; 7) electrical conductivity.

The dependencies of the current density on the following quantities were analyzed in detail:

a) the cell potential, b) volumetric reaction current c) surface O₂ concentration, d) oxygen crossover flux, e) average O₂ concentration, f) H₂ crossover flux, g) membrane water concentration, h) membrane water flux, i) mean H₂O mass fraction in gas phase, j) total volume fraction in liquid phase, k) mean H₂O mole fraction in gas phase, l) mean H₂O volume fraction in gas phase, m) mean H₂O volume fraction in liquid phase, n) mean temperature in gas phase, o) mean temperature of liquid phase, p) mean temperature of solid phase, q) temperature at the cathode catalyst layer and r) temperature at the anode catalyst layer.

The results showed that the variations in the volume fractions of the carbon and ionomer phases caused up to 80% changes in the current density of the fuel cell. The variations in the thickness, ionic and electronic conductivities of the cathode catalyst layer led to around 10% alteration in the cell performance. The changes in the geometric model parameters of the catalyst layer such as in the agglomerate radius and ionomer film thickness insignificantly affected the cell current density.

Acknowledgment

The study has been financially supported by the Austrian Research Promotion Agency (FFG), the Austrian Ministry for Transport, Innovation and Technology (BMVIT) and the company AVL List GmbH: Program “Mobilität der Zukunft”, Project “FC-DIAMOND” (No. 850328, 2015-2018) - PEM Fuel Cell Degradation Analysis and Minimization Methodology Based on Joint Experimental and Simulation Techniques.

References

- [1] C. Fink, N. Kosir, R. Tatschl. PEFC Catalyst Layer Modeling in CFD Simulations: From Interface to Agglomerate Models / 6th EUROPEAN PEFC & Electrolyser Forum. 4–7 July 2017, Lucerne/Switzerland. Oral presentation, accepted.

MASS TRANSFER CHARACTERISTICS OF ANION EXCHANGE MEMBRANES IN NaCl AND NaH₂PO₄ SOLUTIONS

Olesya Kharchenko, Ekaterina Belashova, Natalia Pismenskaya

Membrane Institute, Kuban State University, Krasnodar, Russia, E-mail: olesia93rus@mail.ru

Introduction

The extraction of phosphate ions from municipal and waste water of galvanic production and food industry has a certain complexity. Monosodium phosphate is used in medicine, acts as food additive E339, which is recommended for the production of bakery, meat, fish products. Therefore, there is a problem of monosodium phosphate extracting from sewage and natural waters by electrodialysis. The problem in the electrodialysis of this solution is in the fact that phosphate ions are ampholytes that enters the protonation-deprotonation reaction. The consequence of these reactions is the transformation of phosphate ions from one form to another, depending on the pH of the solution. Calculations carried out using the three-layer 1D model [1] show that in the case of NaH₂PO₄ solution, the transport number of double charged phosphate ions is not zero even in the under-limiting current mode. With the current increase, contribution of these ions to mass transfer increases, and at $i/i_{lim} \approx 2$, the electric charge in the membrane is transferred mainly by double-charged phosphate anions. This paper is aimed at experimental verification of these theoretical results.

Experiment

The object of the study is the heterogeneous anion-exchange membrane MA-41. The current-voltage characteristics (CVCs) were obtained in a four-chamber laboratory cell [2]. The membranes were studied in 0.02 M solutions of NaCl and NaH₂PO₄. Concentration dependences of transport numbers were obtained in the same cell by the method described in [5]. The investigations were carried out at a temperature of 25 ± 1 °C. In the NaCl solution, the transport numbers are calculated for Cl⁻ and OH⁻ ions. In the case of the NaH₂PO₄ solution, it was assumed that the flux of double-charged phosphate ions transported through the anion-exchange membrane is equal to the flux of protons coming from this membrane into the desalting channel. Double-charged anions HPO₄²⁻ are formed in the membrane due to the deprotonation of single-charged anions H₂PO₄⁻. Limiting current i_{lim} was calculated using Leveque equation.

Results and Discussion

Figure 1 shows the total and partial CVC of the MA-41 membrane in NaCl (a) and NaH₂PO₄ (b) solutions. Figure 2 shows the transport numbers of counter-ions in the membrane for given ratios of i/i_{lim} . As was to be expected, the CVC measured in a NaCl solution has one limiting current (Fig. 1a). Their values approximately coincide with those calculated by the Leveque equation. In the under-limiting current mode, the main charge carriers are Cl⁻ anions. For example, their share in the total transfer for $i/i_{lim}=0.85$ is equal to 0.93. Accordingly, the share of hydroxyl ions does not exceed value 0.07. The water splitting starts before i_{lim} , because of the fact that the fraction of the conducting surface of this heterogeneous membrane does not exceed 0.2 [3]. Therefore, the potential drop, which corresponds to the starting of water splitting ($\Delta\phi'=0.3V$ [4]), is achieved much earlier than in the case of a homogeneous membrane. At the currents close to the limiting value and exceeding it, the proton partial current exponentially increases with the increase in potential drop. However, the measured values of T_{OH^-} for $i/i_{lim}=1.3$ ($\Delta\phi'=3V$) do not exceed 0.225.

In the case of NaH₂PO₄ solution (Fig. 1b) at a current under i_{lim} , the curvature of the linear section is observed on the CVC. This curvature can be related to the appearance of the first limiting current i_{lim}^{exp1} , which is most pronounced in the case of the homogeneous membrane [1]. In the range between i_{lim}^{exp1} and i_{lim}^{exp2} , the electric charge through the membrane is transferred by single-charged and double-charged phosphate ions. The transport numbers of these ions are 0.42 (H₂PO₄⁻) and 0.48 (HPO₄²⁻). An increase in the current density leads to a further growth in the partial current (Fig. 1b) and transport numbers (Fig. 2b) of double-charged phosphate ions.

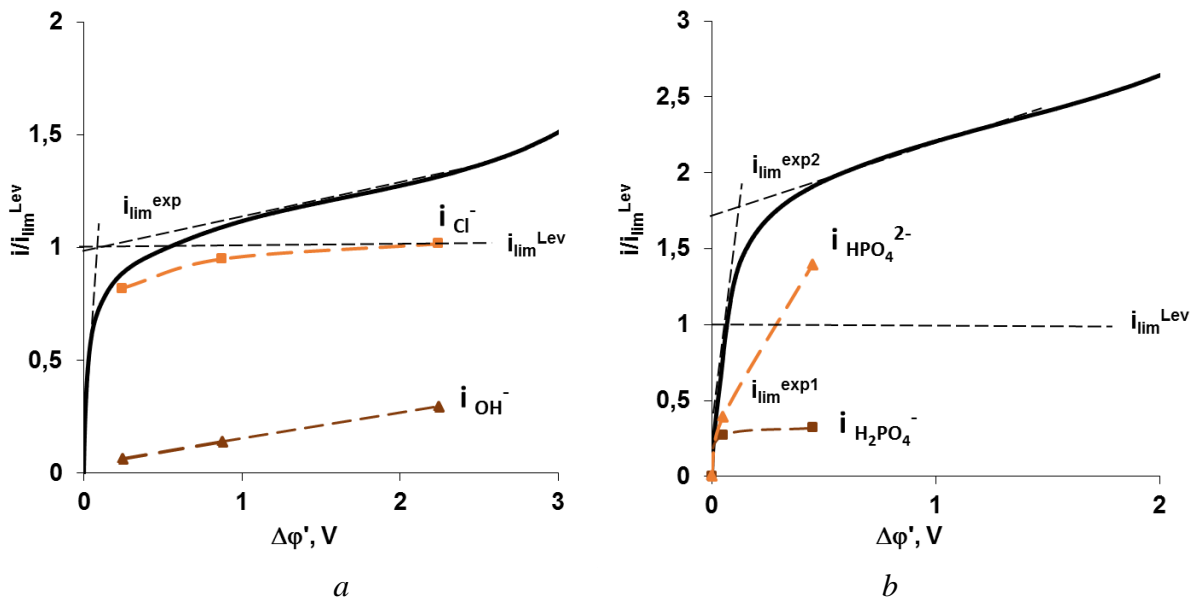


Figure 1. The total and partial CVC of the MA-41 membrane in NaCl (a) and NaH₂PO₄ (b) solutions

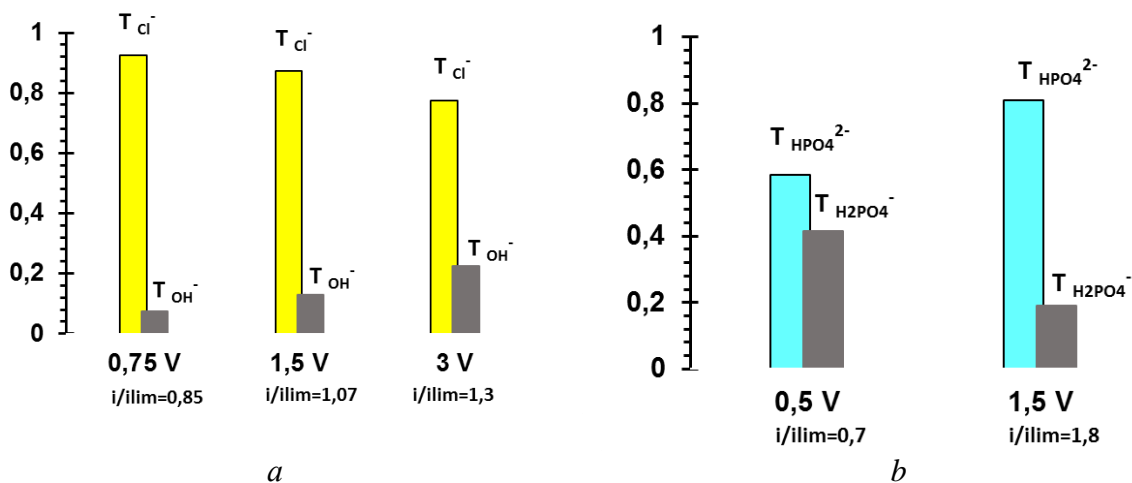


Figure 2. Transport numbers in the membrane for NaH₂PO₄ (a) and NaCl (b) solutions

Thus, as was shown by the mathematical modeling, the transfer through the anion-exchange membrane in monosodium phosphate solution is carried out by single-charged and double-charged phosphate ions. The higher the current value, the greater the share of the double-charged ions in the current transfer.

Acknowledgements

This investigation was carried out within French-Russian laboratory "Ion-exchange membranes and related processes". The authors are grateful to RFBR, Russia and administration of Krasnodar region (grant 16-48-230852 reg) for financial support.

References

1. Belashova E., Pismenskaya N., Pourcelly G., Sista P., Lacour S. Phenomenon of two limiting currents in a system containing an anion exchange membrane and hydrophosphate ions // Ion Transport in Inorg. and Org. Membranes 2016. P. 50-51
2. Belova E., Lopatkova G., Pismenskaya N., Nikonenko V., Larchet C., Pourcelly G. The effect of anion-exchange membrane surface properties on mechanisms of overlimiting mass transfer // J. Phys. Chem. B. 2006. V.110. P. 13458-13469.

3. *Volodina E., Pismenskaya N., Nikonenko V., Larchet C., Pourcelly G.* Ion transfer across ion-exchange membranes with homogeneous and heterogeneous surfaces // *J. of colloid and interface science* 2005. V. 285. P. 247-258.
4. *Pismenskaya N.D., Nikonenko V.V., Belova E.I., Lopatkova G.Yu., Sista Ph., Pourcelly G., Larchet K.* Coupled convection of a solution near the surface of ion-exchange membranes in intense current regimes // *Electrochemistry* 2007. V.43 №3. P. 307-327.
5. *Belashova E.D., Melnik N.A., Pismenskaya N.D., Shevtsova K.A., Nebavsky A.V., Lebedev K.A., Nikonenko V.V.* Overlimiting mass transfer through cation-exchange membranes modified by Nafion film and carbon nanotubes//*Electrochimica Acta* 2012. V. 59. P. 412-423

SYNTHESIS AND INVESTIGATION OF THE CATALYTIC PROPERTIES OF NOVEL PT-CO NANOPARTICLES WITH GRADIENT STRUCTURE

¹Serezha Kirakosyan, ¹Sergey Belenov, ¹Vladimir Guterman

Southern Federal University, Rostov-on-Don, Zorge st.7, Russia

E-mail: serezha.kirakosyan.92@mail.ru

Introduction

In the modern world, the rapid development of technology leads to an increase in the already enormous needs of humanity for energy. However, the resources that now cover most of the energy consumption are exhaustible and by the end of the century will run out. Thus, alternative sources of energy are becoming increasingly important. One of them are low-temperature fuel cells, which include electrocatalysts based on platinum [1]. Catalysts for low-temperature fuel cells are nanoparticles of platinum and its alloys PtM (M = Co, Ag, Cu) deposited on a carbon support. Variations in the method of sequential synthesis of such catalysts are of great interest.

Experiments

The aim of this work is the synthesis of platinum-cobalt materials with a gradient structure (Fig.1) and their comparison with materials with the alloy structure in the oxygen reduction reaction (ORR). Pt-Co/C electrocatalysts were obtained by chemical reduction methods.

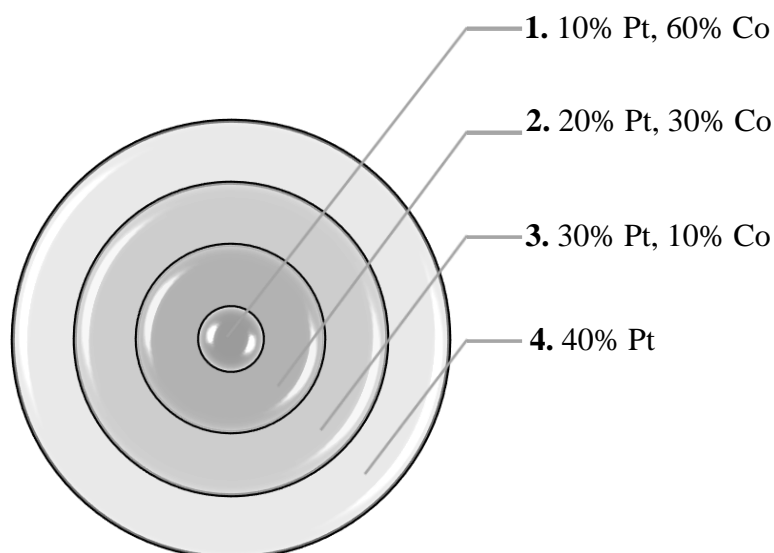


Figure 1. Schematic model of a nanoparticle with the gradient structure. The percentages are relative to the total load of metals

The mass fraction of Pt in the samples was determined by thermogravimetric analysis of the mass of the residue after burning (800 ° C, 40 minutes).

The average crystallite size was calculated from the results of X-ray diffraction for the characteristic reflection (111) using the Scherrer`s equation [2].

The ESA of platinum in the catalyst was determined from the amount of electricity expended on the electrochemical desorption of atomic hydrogen adsorbed during the recording of the 2-nd cyclic voltammogram at a potential sweep rate of 20 mV / s.

Results and discussion

The preparation of nanoparticles with a gradient structure was carried out in 4 stages (Fig. 1), on each of which the platinum content increased, which is confirmed by the results of elemental analysis and thermogravimetry - Table 1. The crystallite size for the material at each stage also regularly increased from 1.5 to 2.3 nm.

It was found that the Pt-Co / C nanoparticles obtained with the gradient synthesis method showed a high ESA (Table 1), relative to the materials obtained by simultaneous reduction. And also, high values of catalytic activity in the ORR.

Table 1: Composition, structure and ESA for PtCox catalysts obtained

№ stage	Composition	Pt loading (%)	ESA, (m²/g(Pt))	Average crystallite size (nm)
1	PtCo _{11,5}	2,3	-	1,5
2	PtCo _{2,7}	3,5	-	2,1
3	PtCo _{1,4}	7,4	-	2,2
4	PtCo _{1,1}	12,7	105	2,3
alloy	PtCo _{0,8}	19,5	43	4,1

Thus, materials with a gradient structure of nanoparticles are promising for use as cathode catalysts for low-temperature fuel cells and require further research and synthesis optimization to increase their specific characteristics.

The work was carried out within the framework of the Ministry of Education and Science of Russian Federation (assignment No. 13.3005.2017 / PCh).

References

1. *Guterman V.E., Lastovina T.A., Belenov S.V. et al. // Journal of Solid State Electrochemistry. – 2014. – №18. – p. 1307-1317.*
2. *Bagotsky V.S. // Rus. J. of Electrochemistry. (rus) – 2003. – №.9. – P. 1027-1045.*

INVESTIGATION OF THE INTERACTIONS OF ANTHOCYANINS WITH SOME ION-EXCHANGE MATERIALS USING COLOR INDICATION TECHNIQUE

Anastasia Klevtsova, Veronika Sarapulova, Natalia Pismenskaya

Kuban State University, Stavropolskaya 149, 350040 Krasnodar, Russia

E-mail: nastya_k1314@yandex.ru

Introduction

Fouling is the main problem of modern membrane technology. One of the mechanisms of fouling is the sorption of charged particles in the pores and on the surface of ion-exchange materials [1, 2] having a chemical affinity to material of membrane. The aim of this work was to study the sorption of ion-exchange materials of anthocyanins, which are ampholytes and change electrical charge depending on pH of the solution.

Experiment

The objects of the investigation were cation exchange (KU-2-8) or anion exchange (AV-17-2, AV-17-8, EDE-10-P) resin. Samples (0.5 g) of each ion exchange resin were placed into ten tubes. An aqueous solution of anthocyanins ($C_{Ant} = 11 \pm 1 \text{ mg/dm}^3$, $\text{pH} = 3.7$, $V = 10 \text{ cm}^3$) was added to each of them. After a defined period of time (from 5 to 150 min) 2 samples (1 cm^3) were taken from each tube and diluted to 10 cm^3 by buffer solution ($\text{pH} = 1$ or $\text{pH} = 4.5$). The coefficient of optical density of the solution was identified at the wavelengths of 520 and 700 cm^{-1} . The concentration of anthocyanins in solution (C_{Ant}) was calculated by the method [3]. The content of anthocyanins in the resin was determined from the difference in the concentrations of these substances at the beginning and end of the experiment. The experiment was repeated by placing a sample of the resin in the solution of anthocyanins with $\text{pH} = 6.0$ and $\text{pH} = 9.0$. The chemical structure of anthocyanins in the solution and in the resin was determined using dependence of color on pH [4], which was obtained using buffer solutions.

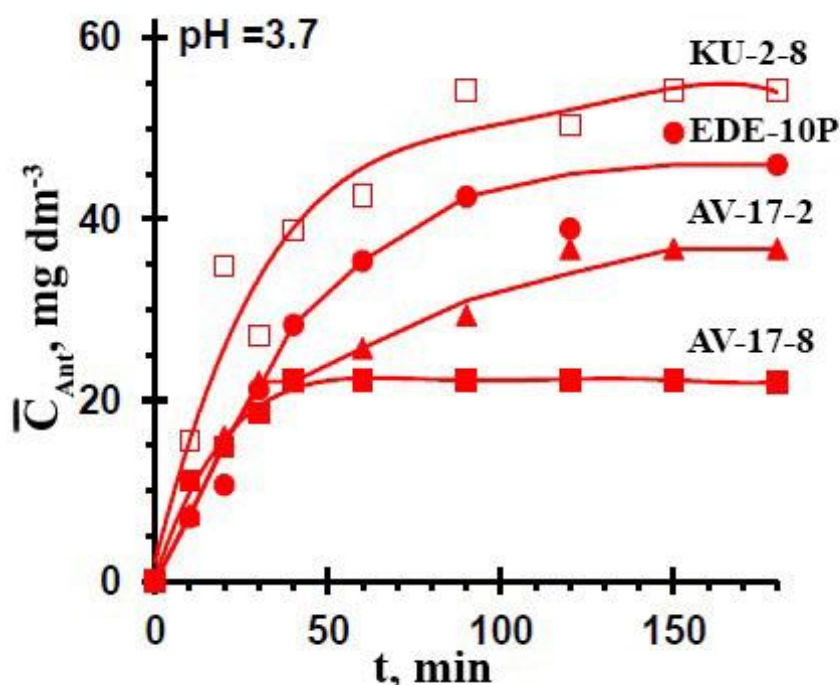


Figure 1. The kinetic dependence of the sorption of anthocyanins by ion exchange resins from aqueous solution

Results and Discussion

It has been established (Figure 1) that the cation exchange resin adsorbs more intensively anthocyanins from acidic solutions in comparison with anion exchange resins. Resins KU-2-8 and

AB-17-8 have the same matrix based on polystyrene crosslinked with divinylbenzene. The difference in their behavior with respect to anthocyanins is the charge of fixed groups. The negative charge of the resin KU-2-8 fixed sulfonic groups involves the electrostatic interaction with cations of anthocyanins. The color indication of resin AB-17-8 after its equilibration with anthocyanin solution indicates that the pH of its internal solution is within of 5-6. At these values, the anthocyanin transforms into a purple phenolate of the quinoid form (3), which has not electric charge. Most likely, the presence of anthocyanin in AB-17-8 is mainly provided by π - π (stacking) interactions with the aromatic matrix of the resin. The aliphatic matrix EDE-10-P does not imply π - π (stacking) interactions with anthocyanins.

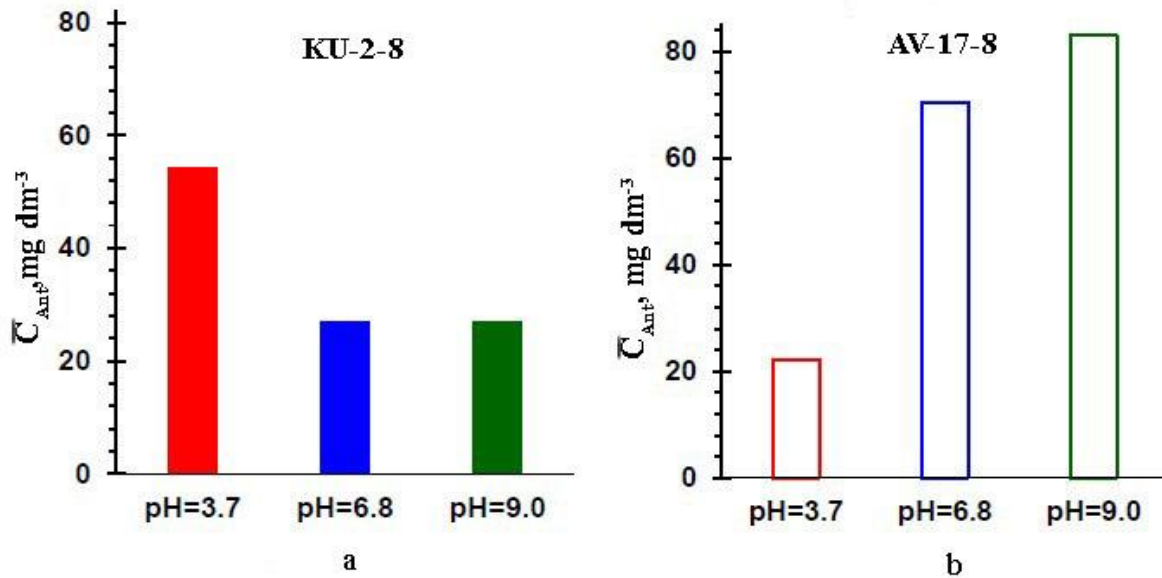


Figure 2. The anthocyanins concentration in KU-2-8 (a) and AV-17-8 (b) resins after equilibration with solutions that have different pH values

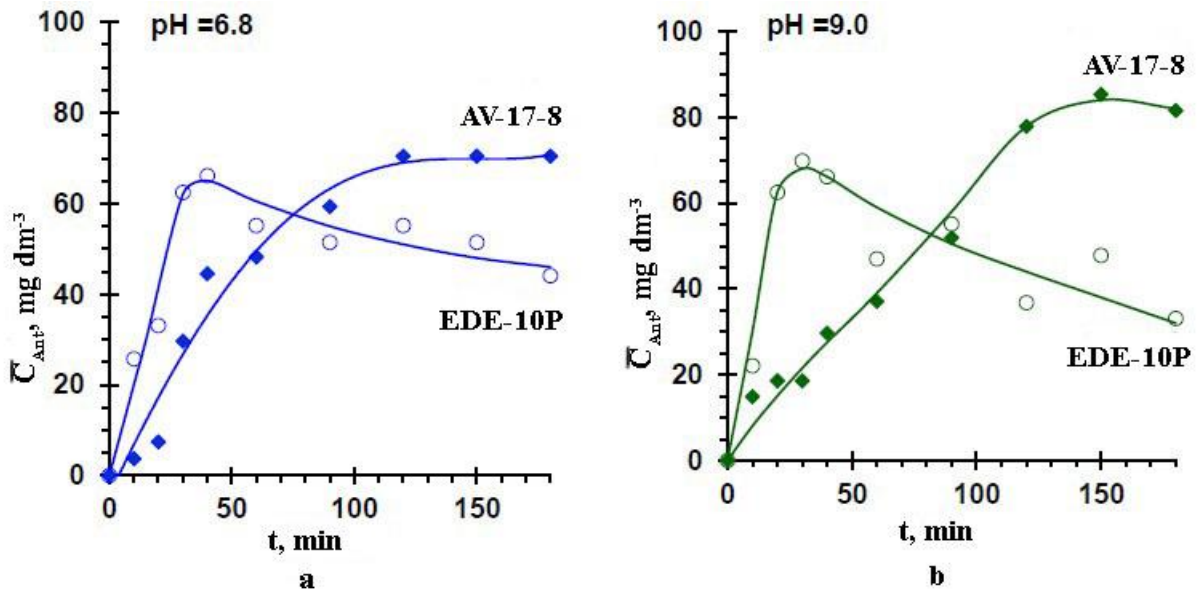


Figure 3. Kinetic dependence of the anthocyanins concentration in KU-2-8 (a) and AV-17-8 (b) resins immersed in solutions that have different pH values

The color indication of this resin shows that the pH of the internal solution is in the range of 9-11. A stronger shift of pH to the alkaline values is due to a more intense Donnan exclusion of protons from the resin. The reason is an increase in the ion exchange capacity of EDE-10P by 2 times in comparison with AB-17-8. At such pH values, the anthocyanin acquires a negative charge,

and reacts in an electrostatic interaction with fixed groups of the resin. The formation of hydrogen bonds between secondary, tertiary amino groups and deprotonated polar groups of anthocyanins is also possible. The presence of these interactions provides a noticeable increase in the concentration of anthocyanins in the EDE-10P resin compared to AB-17-8. Resin AB-17-2 has a lower degree of cross-linking (and thus it has larger pores) compared to AB-17-8. The presence of larger pores in AV-17-2 in comparison with AB-17-8 partially removes steric difficulties associated with the diffusion of sufficiently large anthocyanin molecules into the ion-exchange matrix. As a result, the concentration of anthocyanins in this slightly-cross-linked resin increases compared to the AB-17-8 resin.

At neutral (pH = 6.8) and alkaline (pH = 9.0) pH values of the external solution at the pH of the internal solution KU-2-8, judging from the color indication scale, is in the range 4-6. At these pH values, anthocyanins are mainly in the form of colorless pseudo base or purple quinoid phenolate form, which haven't electric charge. Apparently, the main mechanism of sorption of anthocyanins in this case is π - π (stacking) interactions with the resin matrix. Therefore, for solutions with a pH of 6.8 - 9.0, the amount of sorbed anthocyanins remains practically constant (Fig. 2a). At the pH of the external solution of 6.8 - 9.0, the pH of the internal solution in the resin AB-17-8 increases correspondingly to 9 and 12, when the anthocyanins acquire a negative charge, transforming into a singly charged blue quinoid form and a doubly charged blue-green form. As the internal solution is enriched with the double-charged anthocyanine anions, their electrostatic interactions with the positively charged fixed AB-17-8 groups are enhanced and the sorption of these substances by the anion exchange resin increases (Fig. 2b).

The kinetic curve of sorption for EDE-10P resin passes through a maximum, which can be observed both in the case of neutral solutions (Fig. 3a), and in the case of alkaline solutions (Fig. 3b) of anthocyanins. The complex form of the kinetic dependencies of sorption of anthocyanins with EDE-10P resin (Fig. 3) is explained by the fact that after a sufficiently long period of time (about 100 min), an appreciable number of protons accumulate in the solution adjacent to EDE-10P resin. As a result, some of the anthocyanins in the near-surface layer of the resin apparently transform into a positively charged pyrylic form and are desorbed from the resin because of electrostatic repulsion from the same charged fixed groups.

Acknowledgements

This investigation was carried out within French-Russian laboratory "Ion-exchange membranes and related processes". We are grateful for financial support to the Russian Scientific Foundation (grant No 17-19-01486).

References

1. *Aimar P., Bacchin P.* Slow colloidal aggregation and membrane fouling // *J. Membr. Sci.*. 2010. V. 360, No. 1. P. 70-76.
2. *Boissier B., Lutin F., Moutounet M., Vernhet A., Boissier B.* Particles deposition during the cross-flow microfiltration of red wines—incidence of the hydrodynamic conditions and of the yeast to fines ratio // *Chem. Eng. Process.* 2008. V. 47, No.3. P. 276-286.
3. Juice products. Methods for the determination of anthocyanins: MGS GOST ISO 32709-2014.
4. *Ribéreau - Gayon P., Glories Y., Maujean A., Dubourdieu D.* Handbook of Enology: The Chemistry of Wine, Stabilization and Treatments, 2nd ed. Dunod: Paris, 2006. V. 2.

CHANGES IN TRANSPORT-STRUCTURAL CHARACTERISTICS OF HETEROGENEOUS ION-EXCHANGE MEMBRANES AFTER CONTACT WITH SOLUTIONS CONTAINING ANIONS OF CARBOXYLIC ACIDS

Denis Kolot, Stanislav Melnikov, Elena Nosova

Kuban State University, Krasnodar, Russia

Introduction

Ion exchange membranes and processes with their use are widely used: in water treatment (drinking water production, highly purified water for power generation and chemical industries); in the food industry (processing of dairy products, juices, beers, wines); in energy production (fuel cells, reverse electrodialysis); in new directions of "green chemistry" - separation of fermentation products of biomass (amino acids, biofuels, molecules for the production of plastics, including biodegradable ones); in analytical chemistry (preconcentration of solutions, membrane sensors), in medicine, etc. [1].

The most promising membranes for specific electromembrane technologies are selected by studying their fundamental physicochemical properties. One of the most important characteristics of ion-exchange membranes is their specific electrical conductivity. The study of the concentration dependence of electrical conductivity makes it possible to obtain necessary information for the calculation of the transport-structural properties of membranes [2].

The aim of this work was to study the concentration dependence of the electrical conductivity of ion-exchange membranes in solutions of certain carboxylic acids and their salts, as well as the calculation of the transport-structural parameters of membranes, based on this dependence.

Experiments

Serial heterogeneous ion-exchange membranes of Russian and foreign production were chosen for the study. The choice of membranes is justified by several factors. First is the mechanical and chemical robustness of heterogeneous membranes compared to homogeneous. The second one is their lower price and availability on the market. Comparison of physicochemical properties of studied membranes is presented in Table 1.

Table 1. Physicochemical properties of heterogeneous ion-exchange membranes.

Membrane	Ralex CM-Pes	Ralex AMH-Pes	MK-40	MA-41
Fixed groups	-SO ₃ H	-N ⁺ (CH ₃) ₃	-SO ₃ H	-N ⁺ (CH ₃) ₃
Ionite	-	-	KU-2-8	AV-17-8
Inert binder	PE	PE	PE	PE
Ion-exchange capacity, mmol/g-wet	1.12	0.86	1.08	0.91
Water uptake W, %	44	45	33	36
Thickness in wet state, microns	520	550	540	530

All samples underwent standard pretreatment procedure, after which each sample was equilibrated with working solution. To study how the presence of carboxylic acids affect membranes properties membranes electrical conductivity was studied in solutions of sodium chloride, sodium acetate, acetic and citric acids.

Concentration dependences of membranes electrical conductivity were studied by mercury contact method [3].

Results and Discussion

The results of measuring the electrical conductivity of the membranes under study in solutions of sodium chloride are shown in Fig. 1.

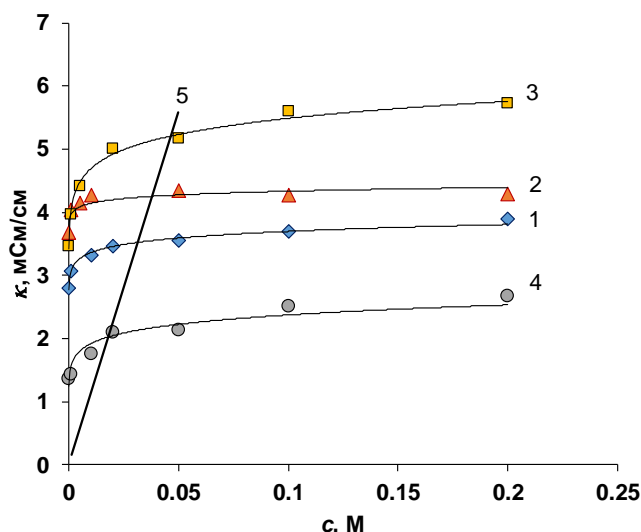


Figure 1. Concentration dependence of electrical conductivity of heterogeneous membranes in a sodium chloride solution: 1 – Ralex CM-Pes, 2 – Ralex AMH-Pes, 3 – MK-40, 4 – MA-41 and equilibrium solution (5).

From the concentration dependence of the electrical conductivity of membranes in a sodium chloride solution, it is seen that in each pair of membranes (MK-40, MA-41 and Ralex CM, Ralex AMH), anion-exchange membranes show better electrical conductivity. This is due to the greater mobility of the chloride ion, compared to the sodium ion (the diffusion coefficients are $2.034 \cdot 10^{-5}$ and $1.334 \cdot 10^{-5}$ cm^2/s , respectively). The underestimated values of the electrical conductivity of the membrane MA-41, in comparison with the data known in the literature [4], are apparently related to the specificity of a particular batch of membranes. It is also seen that the dependence of electrical conductivity for membranes MK-40 and MA-41 is more pronounced, while for Ralex membranes the electrical conductivity practically does not change with increasing concentration. This effect is caused by the more homogeneous structure of Ralex membranes, as the authors of [5] have already pointed out. Transport-structural parameters, found from the concentration dependence of the electrical conductivity of membranes, support this assumption in the framework of the extended three-wire model (Table 2).

Table 2. The parameters of the extended three-wire model found from the concentration dependence of the electrical conductivity of ion-exchange membranes in a sodium chloride solution.

Parameters of the extended three-wire model	Ralex CM	Ralex AMH	MK-40	MA-41
a	0.15	0.10	0.30	0.29
b	0.85	0.90	0.68	0.69
c	0.00	0.00	0.02	0.02
d	0.34	0.25	0.48	0.15
e	0.66	0.75	0.52	0.85
f	0.95	0.97	0.84	0.86
α	0.321	0.239	0.461	0.126

In the transition to solutions containing organic cation ion conductivity of membranes becomes higher compared with the anion. This is particularly evident in solutions of organic acids (Fig. 2).

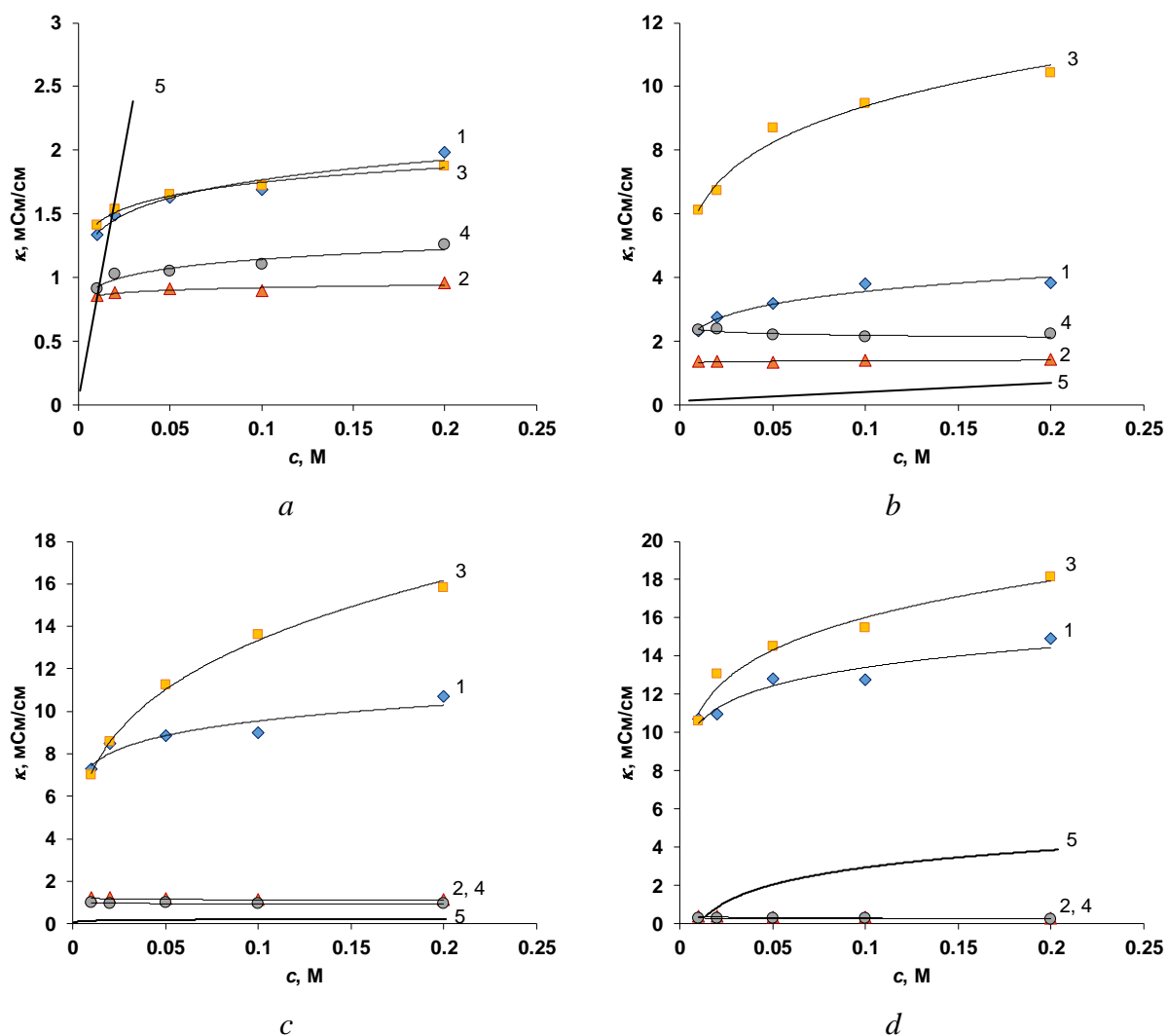


Figure 2. Concentration dependence of the electrical conductivity of ion-exchange membranes in a solution of sodium acetate (a), acetic acid (b), succinic acid (c), citric acid (d). 1 – Ralex CM, 2 – Ralex AMH, 3 – MK-40, 4 – MA-41, 5 – equilibrium solution.

To find the structural parameters of ion-exchange membranes when they come into contact with solutions of organic acids within the framework of known models (microheterogeneous or extended three-wire) is not possible at the moment since calculations for these models require knowing the coordinates of the point of "isoelectric conductivity." However, as can be seen from Fig. 2, in the case of weak electrolytes, such a point can not be found.

Acknowledgments

This work was supported by Russian Foundation for Basic Research, grant № 16-08-01177-a.

References

1. Strathmann H. // *Desalination*, 2010, vol. 264, p. 268.
2. Gnusin N.P., Berezina N.P., Kononenko N.A., Dyomina O.A. // *J. Memb. Sci.*, 2004, vol. 243, p. 301.
3. Karpenko L.V., Demina O.A., Dvorkina G.A., Parshikov S.B., Larshe K., Berezina N.P. // *Elektrokhimija*, 2001, T. 37, p. 328.
4. Demina O.A., Demin A.V., Zabolotskii V.I., Berezina N.P. // *Rus. J. Electrochem.*, 2011, vol. 47, p. 759.
5. Melnikov S., Loza S., Sharafan M., Zabolotskiy V. // *Separ. Purif. Technol.*, 2015, vol. 157, p. 179.

EXPERIMENTAL AND THEORETICAL INVESTIGATIONS OF DIFFUSION AND ELECTROSMOTIC PERMEABILITY OF ION-EXCHANGE MEMBRANES

¹Natalia Kononenko, ¹Olga Demina, ¹Irina Falina, ¹Svetlana Shkirkaya, ²Anatoly Filippov

¹Kuban State University, Krasnodar, Russia, *E-mail: kononenk@chem.kubsu.ru*

²Gubkin University, Moscow, Russia, *E-mail: a.filippov@mtu-net.ru*

Introduction

Diffusion and electroosmotic permeability of ion-exchange membranes are important transport properties influencing the efficiency of electromembrane desalination and concentrating of electrolyte solutions. Nowadays we accumulated a variety of experimental data on diffusion and electroosmotic characteristics of ion-exchange membranes of different structural types in solutions of various nature and concentration. An actual task is the theoretical description of these phenomena within the framework of various modeling approaches. The problem is that the differential coefficient of diffusion permeability should be used to estimate the electromembrane process efficiency but its value could not be determined experimentally. The possibility of theoretical estimation of diffusion characteristics becomes especially relevant with the preparation of new membrane modifications. The need of the theoretical estimation of electroosmotic permeability is caused by the fact that its experimental measuring is associated with serious difficulties. The most general experimental volumetric method allows obtaining the membrane electroosmotic characteristics only in chloride solutions. Therefore, the aim of this paper was to use various known model approaches to describe the diffusion and electroosmotic characteristics of ion-exchange membranes.

Experiments and Theoretical approaches

Sulfocationic heterogeneous MK-40 and perfluorinated Nafion type membranes were the objects under consideration. The concentration dependences of the membrane diffusion permeability were obtained for simple binary as well as asymmetrical electrolytes. All experiments on diffusion of the electrolyte solution into pure water were carried out in the two-chamber cell with platinum electrodes. The water transport numbers were calculated from electroosmotic permeability of the membranes measured by the volumetric method in the two-chamber cell with reversible silver chloride electrodes. The membrane conductivity was determined from the value of membrane resistance measured as active portion of the membrane impedance with the use of the mercury-contact technique [1]. The measurement errors for all characteristics did not exceed 3-5%.

To theoretically calculation of membrane diffusion characteristics we used the two-phase model of inhomogeneous membrane; the approach without model representation of the membrane structure taking into account correlation between the differential coefficient of diffusion permeability [2] and diffusion flux; and the model for transport of ions through a fine-porous ion-exchange membrane [3]. The extended three-wire model was used to estimate approximately the transport number of water through the membrane in a process of electroosmosis [4].

Results and Discussion

Theoretical calculation of the differential coefficient of diffusion permeability (P_m^*) was carried out by two methods. The first one is based on the use of the two-phase model of an inhomogeneous membrane with the help of the transport-structure parameters which were determined from the concentration dependencies of conductivity and diffusion flux measured experimentally. The second method is based using correlation between P_m^* and the diffusion flux. In last case, the membrane is regarded as a quasi-homogeneous system without model representation. Estimation of the P_m^* value was carried out using concentration dependences of the electrolyte solution diffusion flux through the membrane. Comparative analysis of results obtained using two-phase conducting model and independent method showed that the difference between the P_m^* values does

not exceed 5% for all studied systems in the range of solution concentrations from 0.1 M to 1.0 M [2].

We extended previously proposed model of the ion transport through a fine-porous ion-exchange membrane to the case of diffusion of 2:1 and 1:2 electrolytes [3]. The mathematical model takes into account the different mechanisms of diffusion and electro-migration transport of electrolytes with singly and doubly charged co- and counter-ions, as well as the individual diffusion and equilibrium distribution coefficients of ions inside the membrane and phenomenon of concentration polarization in the vicinity of its surfaces. The results obtained allow estimating the influence of the nature of the counter- and co-ion on the membrane diffusion permeability. This approach can be used to evaluate the diffusion characteristics of modified membranes that allow revealing the role of the modifying component in the formation of the membrane transport channels.

The opportunity to estimate theoretically the transport number of water with the help of the extended three-wire model based on the dependence of the membrane conductivity upon the solution concentration, was shown [4]. This approach makes it possible to find not only parameters which characterize the part of current flow through the structural fragments of the swollen membrane, the volume fractions of conducting phases and their orientation with respect to the electric current, but also to calculate the electro-migration transport numbers of counter-ions (\bar{t}_+). The transport numbers of water (t_w , mol H₂O/F) can be calculated according to the Scatchard equation

$$\bar{t}_+ = t_{+app} + m_{\pm} M_w t_w,$$

where m_{\pm} is the average molality of the solution, M_w is the molar weight of water and t_{+app} is apparent transport numbers of the counter-ions, measured by the potentiometric method. The value of t_{+app} needed for calculation of t_w , can be taken from catalogs of ion-exchange materials.

In present work we calculated the water transport number for MK-40 membrane. The value of $\bar{t}_+ = 0.99$ was found from the concentration dependence of the membrane conductivity based on the extended three-wire model. We took the magnitude of $t_{+app} = 0.98$ from [5]. The transport number of water calculated on the base of these values was equal to 7.1 mol H₂O/F. The transport number of water for MK-40 membrane in NaCl solution (0.1 M) found in our independent experiment was 6.5 mol H₂O/F. The similar estimation for Nafion 115 membrane showed that calculated t_w value is 14.4 mol H₂O/F but experimental t_w value is 10 mol H₂O/F in the same solution. When concentration of solution increases, the calculated and experimental t_w values for perfluorinated membrane become closer and in 3 M NaCl solution are 5.2 mol H₂O/F and 4.7 mol H₂O/F, respectively.

The satisfactory agreement between calculated and experimental values suggests that the electroosmotic permeability of the membranes can be approximately estimated within the framework of the extended three-wire model utilizing only the concentration dependence of the membrane conductivity.

The present work was supported by the Russian Foundation for Basic Research (project № 15-08-03285-a).

References

1. Gnusin N.P., Berezina N.P., Kononenko N.A., Demina O.A. // J. Membr. Sci. 2004. V.243. P.301.
2. Demina O.A., Kononenko N.A., Falina I.V., Demin A.V. // Colloid J. 2017. V.79. No.3. P.317.
3. Filippov A.N., Kononenko N.A., Demina O.A. // Colloid J. 2017. V. 79. No. 4.
4. Demina O.A., Kononenko N.A., Falina I.V. // Petroleum Chemistry. 2014. V.54. No.7. P.515.
5. Ion-Exchnage Membranes, Granulates, and Powders: Catalog. Moscow: 1977. 32 p.

INVESTIGATION OF CORRELATION BETWEEN STRUCTURAL AND ELECTROTRANSPORT PROPERTIES OF MODIFIED ION-EXCHANGE MEMBRANES

¹Natalia Kononenko, ²Daniel Grande, ¹Victor Nikonenko

¹Kuban State University, Krasnodar, Russia, *E-mail: kononenk@chem.kubsu.ru*

²Institut de Chimie et des Matériaux Paris-Est, CNRS – Université Paris-Est, Thiais, France

In the present work the results of investigation of correlation between structural and electrotransport characteristics of ion-exchange membranes are summarized. The methods of differential scanning calorimetry (DSC)-based thermoporosimetry [1] and standard contact porosimetry (SCP) [2] were used to determining pore volume distribution versus pore radius or water binding energy in ion-exchange membranes. Comparative analysis showed that the great advantage of the DSC is its rapidity; a quite small amount of material is needed for the test. However, the range of pore sizes detectable by this method is not very large. If the pore radius is lower than about 6 nm, the heat flow is too low to be correctly measured. The pores with radius higher than 300 nm are not seen as well, because of small difference in water binding energy in these pores and in bulk water. Besides, the correct application of this method requires the knowledge of the pore shape; the calculated size of pore radii differs by almost twice when assuming pores cylindrical or spherical.

The SCP method is more informative for evaluation of material structural characteristics. This method allows the investigation of the structure and the water state in all kinds of porous materials, and is quite effective when applying to ion-exchange membranes. This method is relatively simple and nondestructive, it can be applied for measurements in a wide range of pore sizes from about 1 to 10⁵ nm. As it is based on the comparison of water binding energy in the sample under study and in the standards where the pore size distribution is known, it can be applied for any pore shapes. After the treatment of porosimetric curves, it is possible to obtain the water volume distribution on binding energy and the pore size. The maximum value of porosity (V_0), the specific internal surface area, the distance between the neighboring fixed groups at the internal interface, the degree of membrane heterogeneity as volume of macropores (V_{macro}) and ionic selectivity as fraction of the practically ideal selective micro and mesopores volume in total volume of water in the membrane ($\frac{V_{micro}}{V_0}$) can be calculate from porosimetric curves (Fig. 1).

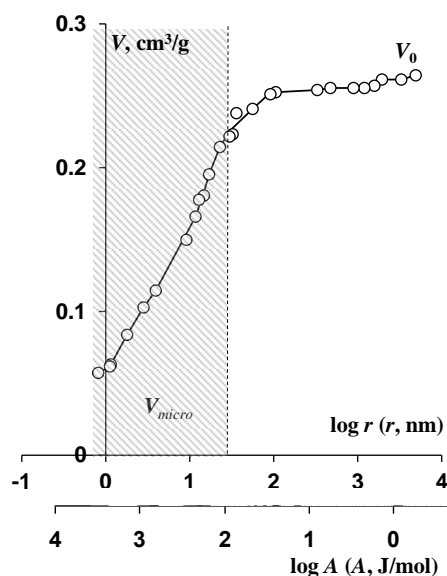


Figure 1. Integral functions of water distribution on the binding energy and the effective pore radii for the Nafion 115 membrane

Membrane conductivity, diffusion permeability and transport number of counter-ions and water were measured to find the correlation between structural and electrotransport characteristics of ion-exchange membranes. Perfluorinated MF-4SK (Russia) and Nafion 115 (USA) membranes modified by the organic and mineral additions were used as subjects of research. Polyaniline, silica, hydrogen zirconium phosphate and platinum dispersion were used as modifiers.

The results of a comparative analysis of structural characteristics found from porosimetric curves and electrotransport properties are presented in Fig. 2.

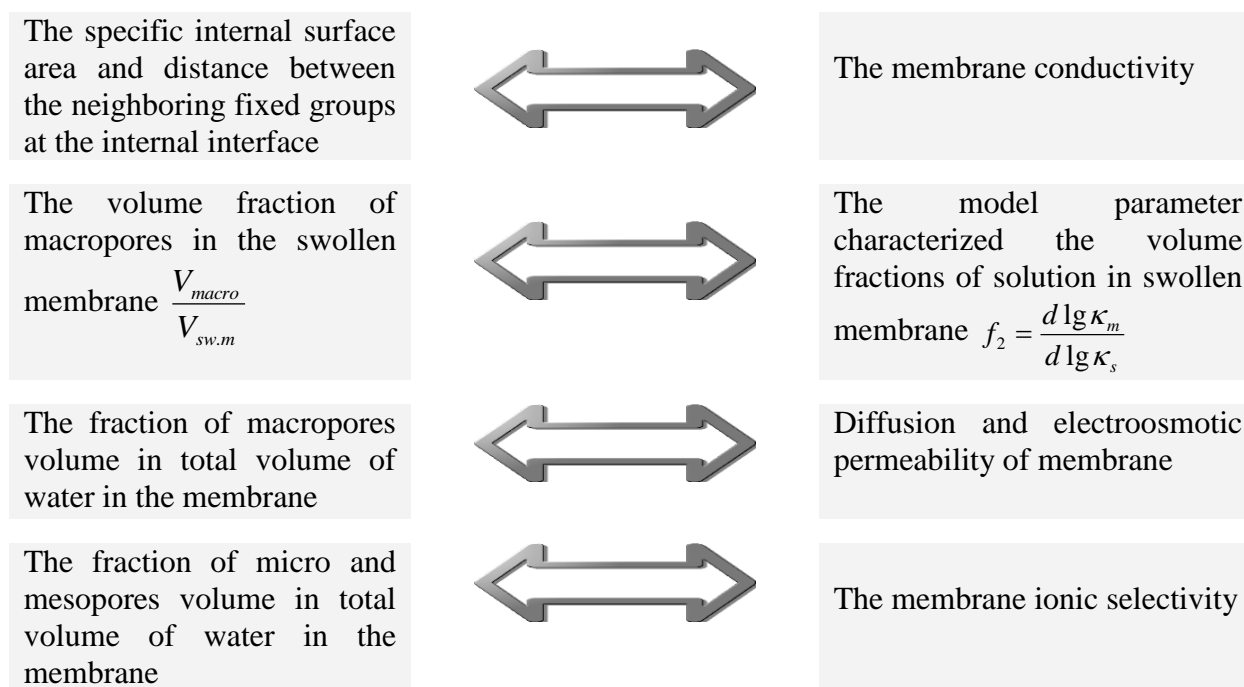


Figure 2. Correlation between characteristics of pore structure and electrotransport properties of ion-exchange membranes

In particular, such kind of analysis allows evaluation of the effect of modifier introduction into membrane structure. It is possible to establish that the presence of hydrogen zirconium phosphate gives rise to water content, while the incorporation of silica results in both reducing and increasing water content depending on conditions of modification. If modification is accompanied by grow of total water volume it leads to increase as conductivity and water transport numbers. Such effects are typical for perfluorinated membranes after modification by hydrogen zirconium phosphate and silica nanoparticles without heat treatment. Reduction of conductivity and electroosmotic permeability is usually associated with decreasing in membrane hydrate characteristics. Similar effects take place in the case of additional heat treatment of perfluorinated membranes modified by silica. It was shown that the varying of the polyaniline synthesis conditions allows to prepare the material with different set of the characteristics.

Thus, the correlation between structural characteristics and electrotransport properties of the modified perfluorinated membranes was established and the role of nature of modifying components and method of membrane modification was revealed. It allows one to make an idea about the localization of the modifier in membrane structure.

The present work was supported by the Russian Foundation for Basic Research (project RFBR 15-58-16002).

References

1. Brun M., Lallemand A., Quinson J.-F., Eyraud C. // *Thermochim. Acta* 1977, 21, 59-88.
2. Volfkovich Yu.M., Filippov A.N., Bagotsky V.S. *Structural properties of porous materials and powders used in different fields of science and technology*. Springer-Verlag; 2014.

1D GALVANOSTATIC MODEL OF ION TRANSPORT IN MEMBRANE SYSTEM AT OVERLIMITING CURRENT MODES

Andrey Kononov, Semyon Mareev, Andrey Gorobchenko, Victor Nikonenko
Kuban State University, Krasnodar, Russia, E-mail: v_nikonenko@mail.ru

Introduction

Application of intensive current regimes makes it possible to increase significantly the mass transfer rate and, consequently, to reduce the area of expensive ion-exchange membranes used in electro dialysis apparatus, which gives a noticeable economic effect [1]. Such regimes are also used in microfluidic devices [2], in capacitive deionization [3] *etc.* In this study we aim to review 1D model of ion transport in membrane system at overlimiting current density.

Theory

The system under study is considered as a plane five-layer system involving a membrane, two DBLs adjacent to the membrane and two bulk solutions. 1D electrodiffusion of a binary electrolyte is studied. The ion transport in the system under study is described by the Nernst-Planck-Poisson (NPP) and material balance equations. The following assumptions were used: the concentration in bulk solution is constant, electroosmotic transfer of ions and coupled effects of internal concentration polarization are not considered. The membrane is considered as homogeneous layer with fixed charge. Only one adjacent parameter is used – diffusion layer thickness. The model allows to calculate time-dependent concentration profiles in membrane system at direct current density.

Numerical solution of the problem was obtained using Comsol Multiphysics software package.

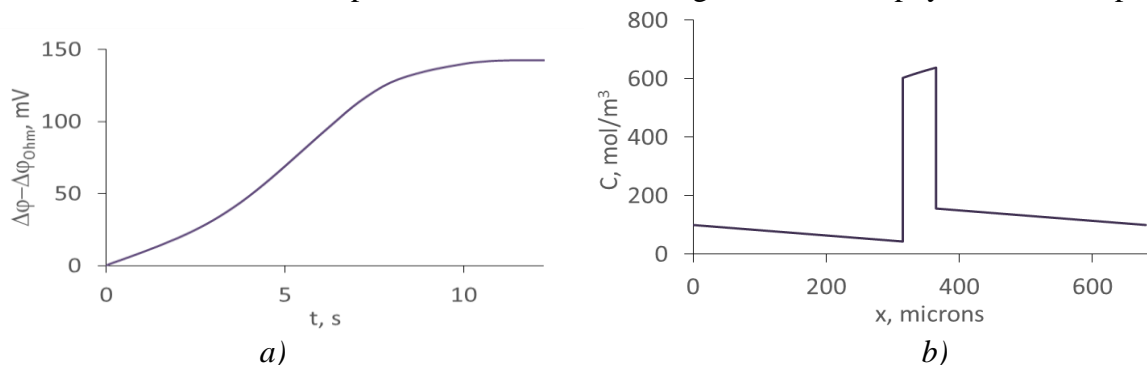


Figure. Chronopotentiometric curve (a) and concentration profile in the membrane system (b), calculated using the 1D model.

Acknowledgements

The study was realized in frame of French-Russian laboratory "Ion-exchange membranes and related processes" with the financial support of RFBR (grant N° 16-38-60135), Russia.

References

1. Nikonenko V.V. *et al.* Desalination at overlimiting currents: State-of-the-art and perspectives // Desalination 342 (2014) 85.
2. Kim S.J. *et al.* Concentration polarization and nonlinear electrokinetic flow near a nanofluidic channel // Phys. Rev. Lett. 99 (2007) 44501.
3. Biesheuvel P.M. *et al.* Membrane capacity deionization // J. Membr. Sci. 346 (2010) 256.

TRANSPORT THROUGH NUCLEAR FILTERS OF THE NANOPARTICLES OF SILVER SYNTHESIZED IN WATER-ALCOHOLIC SOLUTIONS *MURRAYA PANICULATA*

¹Olga Koshkina, ¹Irina Antropova, ¹Dariya Nebaikina, ¹Phyo Myint O, ¹Eldar Magomedbekov, ^{1,2}Aleksandr Smolyanskii

¹D.Mendeleev University of Chemical Technology of Russia, Moscow

E-mail: olga_koshkina_94@mail.ru

²Branch of JSC "Karpov Institute of Physical Chemistry", Moscow, Russia.

E-mail: fizhimiya-2010@mail.ru

Introduction

High toxicity of nanoparticles (NPs) of metals, synthesized by traditional methods, limits the application of these materials in medicine. Current research in the area of development of methods of "green" synthesis of metal NPs based on the interaction of water solutions of metal salts with extracts of various medicinal plants [1] are relevant. In particular, a promising direction for green synthesis of silver NP (Ag-NP) may be the interaction between water solutions of AgNO₃ with water-ethanol extract of leaves of *Murraya paniculata*. This plant grows in Southeast Asia. Extracts for its pharmacological characteristics is not inferior to extracts of known medicinal plants.

The present report describes about the discovery of the photosensibilization effect of the formation of nanoparticles and fractal aggregates of Ag-NP in the result of photoreduction ions Ag⁺ in the interaction with organic compounds of different classes extracted from the leaves of *Murraya paniculata*, as well as the catalytic effect of the additives of ethanol on photosynthesis, grow and aggregation of Ag-NP.

Experiments

In the experiments used the leaves of *Murraya paniculata* collected in Myanmar. After grinding the sample powder of the leaves of *Murraya paniculata* (0.5 – 2.5 g) was dissolved at room temperature in distilled water or in water-ethanol mixture (ethanol 40% (vol.)), and kept in the dark for two weeks. Synthesis of Ag-NP was carried out by adding 47.5 ml water solution of 1mM AgNO₃ to 2.5 ml of water-ethanol extract of *Murraya paniculata*, and subsequent storage of the obtained solutions in the absence and in the presence of daylight. In the first case, the duration of the experiment was 16 days, the second – 2-3 days.

Formation process Ag-NP by optical spectroscopy and transmission electron microscopy (TEM) was monitored. TEM-analysis is the study of the structure of Ag-NP and fractal aggregates formed on the surface of a copper grid covered with carbon by evaporation of micro-drops of the colloidal solution of Ag-NP. TEM-analysis was carried out using the instrument FEI Tecnai G2 F20 S-Twin TMP (FEI production Company (USA)) at an accelerating voltage of 200 kV in bright field. The device resolution of 0.14 nm (line resolution). Processing and analysis of electron microscopic images was performed using software ImageJ 1.49 [2], using the Fraclac plug-in [3], publicly available on the Internet.

Result and discussion

The Change colour of the mixture of AgNO₃ and an extract of *Murraya paniculata* from light green to yellow-brown after exposure to daylight was detected. The Change colour was accompanied by the appearance of intense bands of optical absorption maximum from 430 to 470 nm depending on the composition of the mixture. The introduction of ethanol in the reaction mixture led to a short-wave shift of the maximum absorption band. The intensity of optical absorption band with a maximum in the wavelength range of 430 – 470 nm increased with increasing sample *Murraya paniculata*, as a result of the addition of ethanol, was detected. When performing a similar experiment in the dark was not recorded significant changes of the colour mixture and the occurrence of intense optical absorption in the 430 – 470 nm.

Method TEM, photobleaching in mixtures of AgNO₃ and an extract of *Murraya paniculata* numerous of silver nanoparticles of spherical, elliptical, and irregular shape from 10 to 40 nm, which form fractal aggregates with the dimension D of 1.85 to 1.87. The calculated value of D corresponds to the formation of a fractal cluster as the result of Brownian motion Ag-NP in the volume of solution within the model three-dimensional "cluster – cluster Association". The presence of silver in the composition of NP was confirmed by X-rays fluorescence elemental analysis (EDAX). When performing TEM analysis by electron diffraction observed diffraction rings, indicating the formation of crystallites in the Ag-NP.

Thus, the result of the present study obtained the foundation study of the creation methods photobiosynthesis non-toxic nanoparticles and fractal aggregates of silver for the development of pharmacological agents of new generation.

The present study was undertaken with the financial support of the Russian Foundation for basic research (project No. 17-07-00524).

References

1. *F. Cataldo, O. Ursin, G. Angelini.* Synthesis of silver nanoparticles by radiolysis, photolysis and chemical Reduction of AgNO₃ in Hibiscus sabdariffa infusion (karkade) // J. Radiation Nucl. Chem, 2016. – Vol. 307. PP. 447-455
2. *T. Ferreira, W. Rasband.* ImageJ User Guide/Ij 1.46r, <http://rsb.info.nih.gov/ij/docs/guide/user-guide>
3. *A.L. Karperien.* Fraclac for ImageJ, 2013 (Australia: Charles Sturt University) DOI: 10.13140/2.1.4775.8402

PREPARATION OF THE BIMETALLIC CATALYSTS ON POLYMERIC SUPPORT FOR THE PROCESS OF NITRATE REMOVAL FROM WATER

Margarita Kostyanaya, Inna Petrova, Vladimir Volkov, Andrey Yaroslavtsev

Topchiev Institute of Petrochemical Synthesis RAS, Moscow, Russia

E-mail: *ivpetrova@ips.ac.ru*

Introduction

Nitrates and nitrites are becoming one of the most pervasive groundwater pollutants in many countries due to the high solubility in water and to rapid growth in agricultural and industrial activities. High concentrations of these ions in the water constitute a serious threat to health. The sources of contamination include agricultural and urban wastewater, unsafe disposal of untreated sanitary and industrial waste, leakage of wastewater treatment systems, landfills, manure, NO_x waste from air pollution control devices [1]. The threshold limit value of nitrates and nitrites in drinking water is 10 and 0.1 mg/l, respectively.

At current, catalytic hydrogenation on the bimetallic catalysts is one of the most promising ways of nitrate and nitrite removal from wastewater. For this process, it was demonstrated the necessity for the bimetallic system, consisting of a precious metal (Pt or Pd) and promoter (Cu, Ni, Fe, Sn, In, Ag) [2]. At first, nitrates are reduced to nitrites on the promoter and then nitrites are reduced to nitrogen or turn into ammonium on Pd.

However, previously developed schemes of catalytic nitrate removal from water have a number of disadvantages associated with the necessity for feeding hydrogen into the system at high pressure or hydrogen presaturation of water.

In this work, the nitrate and nitrite removal from water in a single step have been studied in a catalytic membrane reactor without additional expensive equipment, under normal conditions, and without hydrogen bubbling.

Experiments

In this work, we used Celgard X50 hydrophobic porous polypropylene hollow fiber membranes (lumen diameter is 220 μm, wall thickness is 40 μm, porosity is 40%, pore size is 0.03 μm).

Preliminary preparation of the outer surface of the initial membranes was carried out prior to the application of the catalyst. Membranes were washed successively in acetone and ethanol and then etched with an aqueous solution of NaOH.

At the moment, a sequential application of the catalyst was carried out (first Pd, then Cu). Different methods were used for depositing of metals on the outer surface of the membranes:

- reduction of metallic salts by aliphatic alcohols;
- reduction of metallic salts by hydrazine-hydrate.

A series of Pd/Cu-loaded catalytic membranes was obtained. The time of palladium deposition varied from 10 to 25 hours, copper deposition was carried out for both 30 and 60 seconds. The surface of the initial and modified membranes was analyzed by SEM, EDAX and XPA.

Figure 1 shows SEM image of Pd/Cu-loaded polypropylene membrane. There can be seen large agglomerates of Pd particles with a size of 1 μm or more and agglomerates of copper particles that are noticeably smaller. At the same time, the arrangement of copper particles on the surface of the membrane is sufficiently dispersed, so that it can be said that the metals will exhibit sufficient catalytic activity.

The principle of the proposed method of nitrate removal from water in one stage is as follows: polypropylene porous hollow fiber membrane containing the catalyst on the outer surface acts as a highly efficient gas-liquid contactor as well as a reactor, so that the process of nitrate removal is carried out in one step. The water containing nitrate sweeps the membrane, and hydrogen is supplied to the hollow fiber membrane lumen side as reducing agent and diffuses through the membrane pores to the bimetallic catalyst on its outer surface where catalytic hydrogenation reactions proceed at room temperature.

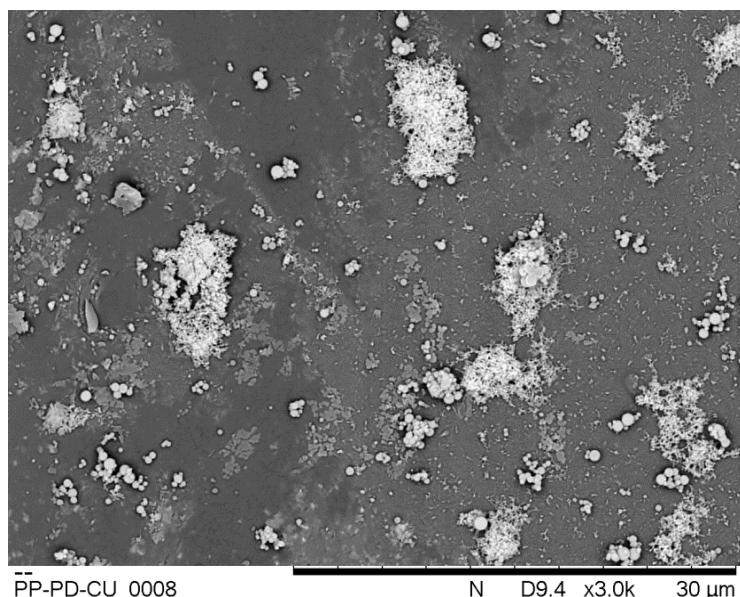


Figure 1. SEM image of Pd/Cu-loaded polypropylene membrane

The ion chromatography was used for quantitative analysis of the reaction of nitrate and nitrite removal from water.

Results and Discussion

Pd/Cu-loaded porous polypropylene membranes with different Pd and Cu loading on the outer surface were prepared. The results of SEM and EDAX analysis indicate the presence of metallic copper and palladium on the membrane surface. Palladium particles form conglomerates of particles of 1 μm or more, while copper is located on the membrane surface more disperse, and conglomerates of the particles formed do not exceed 3 μm .

Pd/Cu-loaded porous polypropylene hollow fiber membranes obtained were used to create a batch-mode catalytic membrane reactor for the removal of nitrates from water.

As expected, changes in nitrate concentration in the water were not observed during the process of nitrate removal on monometallic Pd-catalyst, confirming the necessity to apply second metal-promoter for the reduction of nitrates to nitrites. When using the membrane contactor without the catalyst, changes in nitrate and nitrite concentration are not observed.

As expected, when working with membranes containing only palladium, changes in nitrate concentration were not observed, that is, nitrates can not be removed by gas stripping and a second metallic catalyst is required for the nitrate reduction reaction. The experiments were also carried out to remove nitrites on Pd-loaded membranes. When helium was supplied to the hollow fiber membrane lumen side, no changes in the nitrite concentration were observed; while working with hydrogen, the nitrite concentration in water decreased.

Figure 2 presents the dependence of nitrate concentration in water on the time of the experiment on the obtained Pd/Cu-loaded membranes. Similarly, in the case of helium, changes in the concentration were not observed, but when H_2 is used, it is evident that membranes with different contents of Pd and Cu are catalytically active in the reaction. A different Pd:Cu ratio affects the residual concentration of nitrates, i.e. if Pd content is too small, this catalyst is completely inefficient, because Pd is needed to activate hydrogen. Likewise, when Cu content is small, the decrease is also inconspicuous. With an increase in the amount of Pd and Cu on the surface, the membranes exhibit greater catalytic activity.

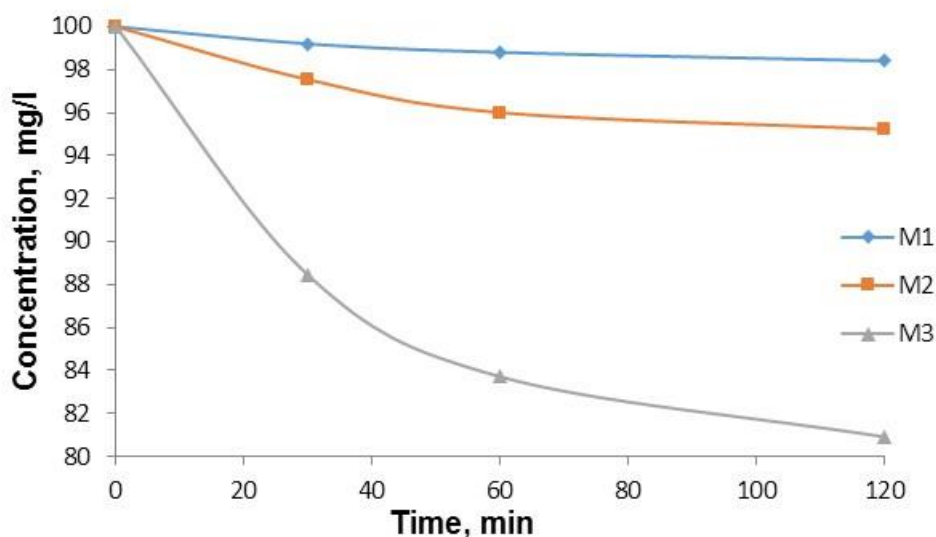


Figure 2. Concentration profiles of nitrates in the experiment with the stack of alternating Pd/Cu-loaded membranes. M1 (Pd:Cu 1:6), M2 (Pd:Cu 2:1), M3 (Pd:Cu 1:1.1)

Conclusions

Thus, the possibility of nitrate removal from water by the proposed method on hollow fiber membranes with bicatalyst on their surface has been demonstrated. Catalytic membrane reactors based on Pd/Cu-loaded porous polypropylene hollow fiber membranes show catalytic activity in the process of nitrate and nitrite removal from water. Catalytic activity does not change during 20 hours or more.

Acknowledgment

The authors would like to acknowledge the Russian Foundation for Basic Research (Grant №16-08-012521).

References

1. Bhatnagara A., Sillanpaa M. A review of emerging adsorbents for nitrate removal from water // Chem. Eng. J. 2011. V. 168. P. 493-504.
2. Vorlop K.D., Tacke T. Erste Schritte auf dem Weg zur edelmetallkatalysierten Nitrat- und Nitrit-Entfernung aus Trinkwasser // Chem. Ing. Tech. 1989. V. 61. P. 836-837.

EVALUATION OF THE POSSIBILITY OF THE EMERGENCE OF GRAVITATIONAL CONVECTION DUE TO THE RECOMBINATION OF HYDROGEN IONS AND HYDROXYL

Anna Kovalenko, Makhmet Urtenov, Alexander Pismenskiy

Kuban State University, Krasnodar, Russia, E-mail: savanna-05@mail.ru

Introduction

This study is devoted to the assessment of the possibility of the appearance of gravitational convection due to the recombination of ions H^+ and OH^- . The solution of the boundary value problem of the mathematical model of electrodiffusion of four types of ions (two salt ions, and also H^+ and OH^- ions) in a diffusion layer in electromembrane systems with an ideally selective membrane [1], the thermal conduction equation, and the Navier-Stokes equation was used.

Experiments

The recombination of ions H^+ and OH^- occurs in the depth of the solution, while heat is released in a narrow reaction layer. This can lead to a noticeable uneven heating of the solution, and as a consequence to gravitational convection. To test this hypothesis, the heat released during recombination H^+ and OH^- ions is calculated, and then the solution flow is calculated using the equations of thermal conductivity and Navier-Stokes.

1. The amount of heat emitted during the formation of 1 mole of water is equal to 56,6 kJ / mol. Therefore, the amount of heat Q_w that is released in the reaction layer with a unit cross section per unit time is $Q_w = 56,6 \cdot 10^3 \cdot I_w / F$.

2. Suppose that a stationary state is maintained in the depth of the solution and at the interphase boundary. In this case the temperature distribution will become stationary in some time. Suppose that all heat is released in the reaction layer. Since the reaction layer is much smaller than the diffusion layer, it contracts to the point x_1 , and a constant temperature is maintained outside the diffusion layer.

From Fig. 1 it is shown that gravitational convection, starting near the exit from the channel, spreads quite quickly to the entire channel.

3. Near the interphase boundary, the Joule heating of the solution occurs due to the passage of the current. At the same time, an endothermic reaction of dissociation of water molecules takes place in the membrane, at which the same amount of heat is absorbed. It is released during recombination. The amount of heat released during Joule heating of the solution is equal to $Q_j = I \cdot \Delta = 10^{-2} \text{ J} / \text{cm}^2 \cdot \text{s}$ and it is two orders of magnitude greater than that absorbed by the dissociation reaction of the water molecules. Therefore, we can assume that there is a point source of heat at the boundary. This can also be modeled as above in the form of a point source.

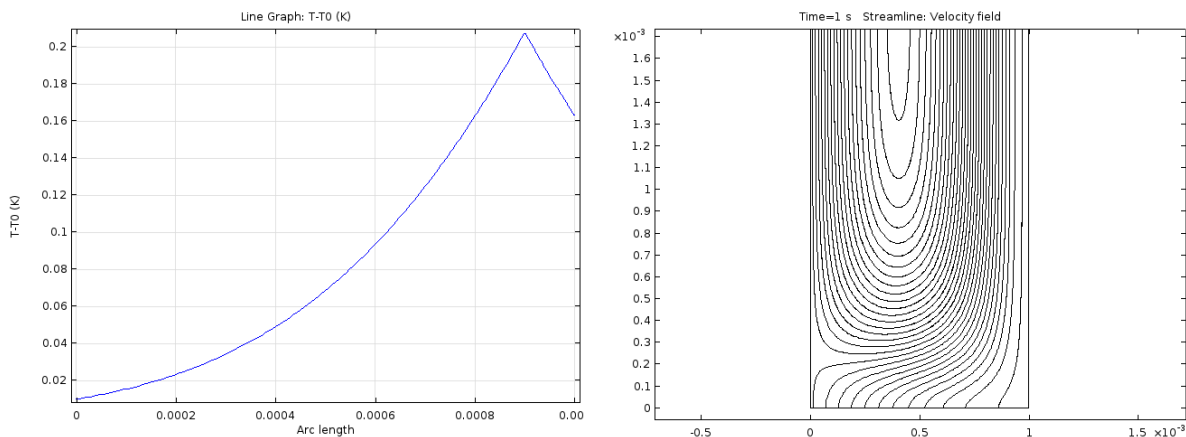


Figure 1. Temperature distribution in the cross section of the channel and the flow lines of the solution at an average flow velocity of 10^{-6} m/s at $t=1 \text{ sec}$.

Results and Discussion

At the initial instants of time, gravitational convection is mainly determined by the Joule heating of the solution. Further, because of gravitational convection, the concentration polarization is smoothed out, and, accordingly, the resistance of the solution decreases. Therefore, the role of Joule heating of the solution in gravitational convection is reduced. Thus, the role of gravitational convection, which arises from the exothermic recombination of water molecules in the depth of the solution, increases.

Acknowledgments

This work was supported by Russian Science Foundation, grants № 16-08-00128 A and 16-48-230856 r_a.

References

1. *Kovalenko A.V., Urtenov M.Kh., et al*, Influence of the dissociation / recombination reaction of water molecules on the transfer of 1: 1 electrolyte in membrane systems in the diffusion layer. Part 1. Mathematical model // Scientific journal KubSAU 2016. V. 7 (121). P. 1929 – 1941

INFLUENCE OF DISSOCIATION / RECOMBINATION OF WATER MOLECULES ON THE TRANSPORT OF BINARY SALT IONS IN MEMBRANE SYSTEMS

Anna Kovalenko, Makhamet Urtenov, Natalia Seidova, Alexander Pismenskiy
Kuban State University, Krasnodar, Russia, E-mail: savanna-05@mail.ru

Introduction

The object of the study is the electrodiffusion of four types of ions simultaneously (two ions of salt, and also H^+ and OH^- ions) in the diffusion layer in the electromembrane systems with an ideally selective membrane, taking into account the violation of the electroneutrality and the reaction dissociation / recombination of water molecules, as well as the development of mathematical models of these processes, the construction of effective algorithms for an asymptotic and a numerical analysis for various types of electrolytes.

Experiments

A new mathematical model of the salt ion transport process is proposed in the paper, taking into account the space charge and the water dissociation / recombination reaction in the form of a boundary value problem for the system of ordinary differential equations. This system is reduced to the form convenient for numerical solution. The necessary boundary conditions for the electric field strength are calculated. The numerical and asymptotic solution of this boundary-value problem and a physico-chemical analysis of the effect of the dissociation / recombination reaction on the transport of salt ions are carried out.

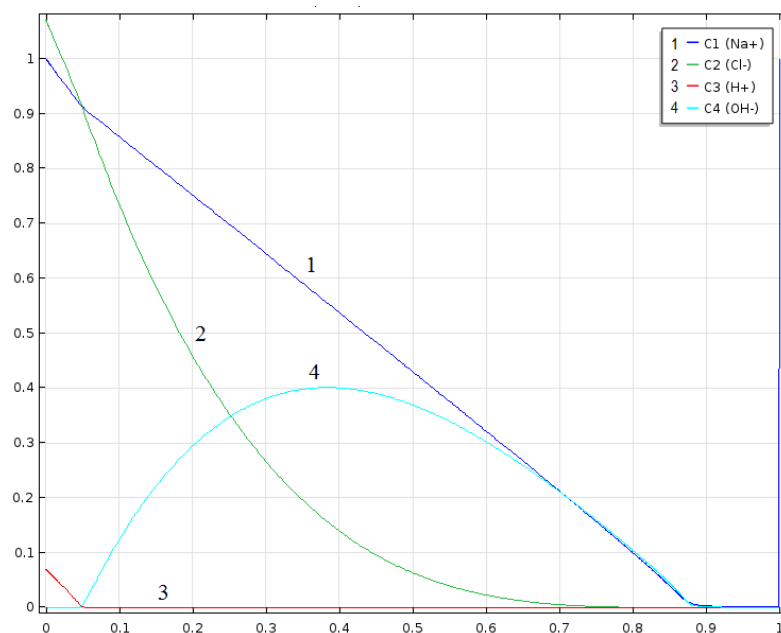


Figure 1. Structure of the diffusion layer under the intense current conditions. Variables are given in a dimensionless form.

Results and Discussion

The structure of the Nernst diffusion layer at currents above the Harkác current is revealed (fig.1). It is shown that there are two types of boundary layers in the diffusion layer: the inner (reaction) boundary layer and the boundary layer at the interface between the solution and the membrane. The reaction layer is an internal boundary layer along the hydrogen and hydroxyl ion streams. The reaction layer occupies about one hundred and fiftieth part of the diffusion layer, and therefore, in many cases it can be considered a point. In the reaction layer, there is also an internal boundary layer for electric field intensity, i.e. there will be a sharp change ("burst") of the electric field intensity. The dimensions of the boundary layers along the streams and in the reaction layer

are different. The boundary layer at the interphase boundary of the solution / membrane arises from the electric field intensity and the concentration of counter-ions.

Acknowledgments

This work was supported by Russian Science Foundation, grant № 16-08-00128 A.

References

1. *Kovalenko A.V., Urtenov M.Kh., et al*, Influence of the dissociation / recombination reaction of water molecules on the transfer of 1: 1 electrolyte in membrane systems in the diffusion layer. Part 1. Mathematical model // Scientific journal KubSAU 2016. V. 7 (121). P. 1929 – 1941
2. *Kovalenko A.V., Urtenov M.Kh., et al*, Influence of the dissociation / recombination reaction of water molecules on the transfer of 1: 1 electrolyte in membrane systems in the diffusion layer. Part 2. Asymptotic Analysis // Scientific journal KubSAU 2016. V. 8 (122). P. 241 – 254

DISSOCIATION OF ALCOHOLS AND WATER IN ORGANIC SOLUTIONS

Nikita Kovalev, Anna Akimova, Nuriyet Hapacheva, Anton Serdiuk, Nikolay Sheldeshov, Victor Zabolotsky

Kuban State University, Krasnodar, Russia

Introduction

The bipolar electro dialysis is one of the membrane processes using bipolar membranes, which has recently become more widely used. Bipolar heterogeneous membranes are a system consisting of a cation exchange, anion exchange layer and a bipolar region in which a space charge region is formed. Water molecules dissociate in this layer when electric current is passed through the membrane. This process in membrane systems containing aqueous solutions has been well studied now. In [1-3] the mechanism of water molecules dissociation with participation of ionogenic groups of membranes and compounds introduced into the solution was proposed. To date, numerous studies have been published in which the effect of catalytic additives of organic and inorganic nature introduced into the bipolar region of the membrane has been investigated [4].

However, even in the early 1970s, the volt-ampere characteristics of bipolar membranes swelled in alcohols were investigated [5], and it was shown that these dependences are described by the equations derived for the *p-n* junction of semiconductors. Recently, interest in this area has been renewed and dissociation of methanol, ethanol in the bipolar membrane [6-8] and synthesis of methyl methoxyacetate [9] were studied. Nevertheless, the dissociation of water molecules in water-organic solutions and the dissociation of alcohol molecules in anhydrous alcohols in bipolar membranes, as well as the influence of various catalytic additives on these mechanism, have not been practically investigated.

Therefore, the aim of the work is to study the dissociation of alcohols, as well dissociation of water in the presence of organic compounds in modified bipolar membranes.

Experiments

The object of research was analog MB-2, modified by phosphoric acid cation exchange resin KF-1, carboxyl cation exchange resin KB-4, anionite EDE-10P and chromium hydroxide(III). Dissociation of alcohols was studied in anhydrous methanol, ethanol, propanol-1, ethylene glycol, propylene glycol, glycerol. Sodium iodide with concentration of 0.1 M was introduced into these alcohols to reduce the resistance of the membrane system.

To study the process of dissociation of water molecules and alcohol molecules, the electrochemical impedance method was chosen, which allows discrimination the resistance of the space-charge region from the total resistance of the bipolar membrane. Measurements of the frequency spectra of the impedance of membranes were carried out in the frequency range from 1 mHz to 1 MHz in a four-electrode electrochemical sealed cell with an active membrane area of 3.87 cm² and platinum electrodes at a temperature of 25°C. The assembly of the electrochemical cell was carried out in high purity nitrogen atmosphere.

The frequency spectrum of the impedance allows to calculate the resistance of the bipolar region. Its dependence on current allows to calculate overvoltage of the bipolar region (Equation (1)) and calculate the dependence of current density on overvoltage of the bipolar region.

$$\eta_b = \int_0^{I^*} R_b dI, \quad (1) \quad i = k_\Sigma \frac{\varepsilon \varepsilon_0}{\beta} [\exp(\beta E_m(\eta_b)) - \exp(\beta E_m(0))]. \quad (2)$$

The Equation (2) proposed in [10] includes the sum of the rate constants of the limiting dissociation stages $k_{20} + k_{40}$ and the parameter β , which are the main characteristics of dissociation of molecules in the bipolar membrane.

The total constant k_Σ and parameter β were calculated with approximating current-voltage characteristics of the bipolar regions of the membranes. The sum of the rate constants of the limiting stages of dissociation $k_{20} + k_{40}$ was calculated by equation (3)

$$k_{20+40} = \frac{k_\Sigma}{c_{alc}}. \quad (3)$$

The dissociation of alcohols at large overvoltages was studied with general volt-ampere characteristics of the electrochemical cell at power supplied on the cell not more than 0.1 W.

Results and Discussion

Analog of MB-2 membrane containing KF-1 in anhydrous alcohols was studied by the impedance method and it was shown that distorted semicircle is observed in the high frequency region, which belongs to the monopolar region of the bipolar membrane. The resistance of monopolar regions depends on the nature of the alcohols, in particular their viscosity (Figure 1). Small distorted semicircle is observed at low frequencies for methanol and glycerin, which increases with small overvoltages, and then decreases with an increase in overvoltage. This is due to removal of salt ions from the bipolar region and the subsequent dissociation of alcohol (Figure 1). Only one semicircle corresponding to the resistance of the monopolar regions of the membrane is visible in the case of ethylene glycol and propanol-1 in the entire frequency range and for all values of overvoltages in 0-9 V range. These data indicate that there is no dissociation of ethylene glycol and propanol-1 under these conditions.

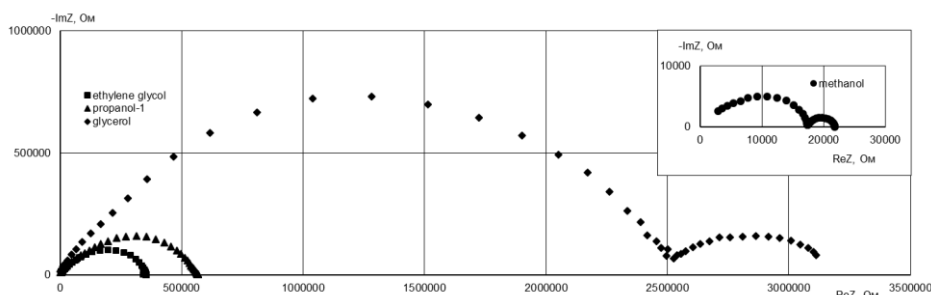


Figure 1. Frequency spectra of the electrochemical impedance of the analog MB-2 bipolar membrane with KF-1 catalytic additive in anhydrous alcohols with addition of 0.1 M NaI·H₂O at 1 V overvoltage on the bipolar region of the membrane

The rate of dissociation of methanol is higher than in the case of glycerin in analog MB-2 bipolar membrane with KF-1 catalytic additive since the current densities in the case of methanol are higher than in the case of glycerin at the same overvoltages of bipolar region (Figure 2). This is may be a consequence of a lower viscosity of methanol in spite of the fact that acidity of methanol is less than of glycerin. The same regularities are consistent with the dependence of the resistance of the bipolar region on the current through the membranes (Figure 3) and with the general volt-ampere characteristics of the electrochemical cell at high values of the applied voltages (Figure 4).

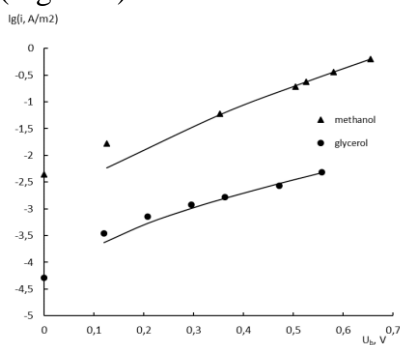


Figure 2. Dependence of the logarithm of the current density on the overvoltage of the bipolar region of the membrane aMB-2 with KF-1 catalytic additive in methanol and glycerol with the addition of 0.1 M NaI H₂O. Lines are calculated with Equation (2)

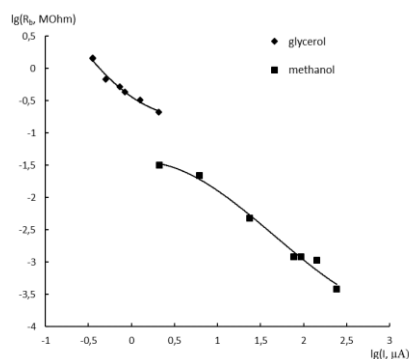


Figure 3. Dependence of the logarithm of the resistance of the bipolar region of aMB-2 membrane with KF-1 catalytic additive in methanol and glycerol with the addition of 0.1 M NaI H₂O from the logarithm of the current

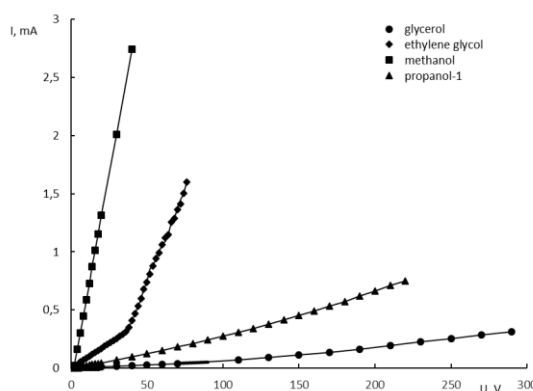


Figure 4. Current-voltage characteristics of electrochemical cell containing cation-exchange membrane, anion exchange membrane, and aMB-2 with KF-1 catalytic additive in alcohols with the addition of 0.1 M NaI H₂O

The obtained experimental data allow to calculate the dissociation reaction parameters $k_{20}+k_{40}$ and β for alcohols according to equations (2) and (3) (Table 1). The dissociation of alcohols in the bipolar membrane proceeds many times slower than the dissociation of water molecules in aqueous solutions, while the $k_{20}+k_{40}$ and β parameters for glycerol are higher than for methanol.

Table: Characteristics of water and alcohols molecules dissociation in the space charge region of aMB-2 membrane modified with KF-1

The environment of bipolar membrane	ϵ	$k_{20}+k_{40}$, l/(mole·s)	$\beta \cdot 10^9$, mV
0,05 M H ₂ SO ₄ and 0,1 M NaOH water solutions, aMB-1	78.5	0.36	3.4
Glycerol, aMB-2	43	0.209	26.5
Methanol, aMB-1	30	0.0544	20

Study was supported by Russian Foundation for Basic Research, research project № 14-08-00897.

References

1. Greben' V. P., Pivovarov N. I., Kovarsky N. I. Nefedova G. Z. // J. Phys. Chem. 1978. Vol. 52, No. 10. P. 2641-2645. (in Russian)
2. Simons R. // Nature. 1979. Vol. 280. P. 824-826.
3. Timashev, S.F., Kirganova E.V. // Rus. J. Electrochem. 1981. T. 17. P. 440-443. (in Russian)
4. Shel'deshov N. V., Zabolotsky V. I. // Membranes and membrane technologies. Collective of authors. Responsible Editor Yaroslavtsev A. B. The Scientific World, 2013. 612 p. (in Russian)
5. Maslov V.N. Zotov U.A. Chernova A.I. Melchuk I.A. // Dokl. USSR Academy of Sciences (in Russian), 1968. B. 183. № 6. P. 1371 – 1374.
6. Tzu-Jen Chou, Akihiko Tanioka. // J. Colloid Interface Sci. 1999. B. 212, P. 576-584.
7. Qihua Li, Chuanhui Huang, Tongwen Xu. // J. Membr. Sci., 2008. P. 20-22.
8. Nobuyuki Onishi, Toshihisa Osaki, Mie Minagawa, Akihiko Tanioka. // J. Electroanal. Chem., 2001. P. 34-41.
9. Qihua Li, Chuanhui Huang, Tongwen Xu. // J. Membr. Sci. 2009. Vol. 325. P. 28-32.
10. Umnov V.V., Shel'deshov N.V., Zabolotskii V.I. // Rus. J. Electrochem. 1999. Vol. 35. № 8. P. 871-878.

THE STUDY OF WATER AND ETHANOL VAPORS DIFFUSION IN POLYMERIC MEMBRANES

Alina Kozlova, Maxim Shalygin, Vladimir Teplaykov

A.V.Topchiev Institute of Petrochemical Synthesis RAS, Moscow, Russia

E-mail: a_a_kozlova@ips.ac.ru

Introduction

Currently membrane separation of vapors is one of the developing directions in the field of membrane separation. In comparison with gas separation, the area of selective vapor transfer in non-porous polymeric membranes and membrane materials is much less studied. The transfer of vapors in polymeric membranes follows dissolution-diffusion mechanism as gases. According to proposed correlation approach for gas transfer [1] in case of availability of data for some components, it is possible to predict gas transport properties of membrane in relation to components which experimental data are absent for or to predict properties of other membranes. The availability of information on the diffusion coefficients and solubility significantly improve prediction accuracy. Since very few data on vapors diffusion in polymeric membrane materials can be found in literature, and taking into account probability of a complex behavior of vapor transfer, current study is focused on the determination of water and ethanol vapors diffusion coefficients under various conditions.

Experiments

A technique for the experimental determination of the diffusion coefficients of vapors in polymeric membrane materials has been developed, it allows also to vary the activity of vapors. The experimental setup is shown in Fig. 1.

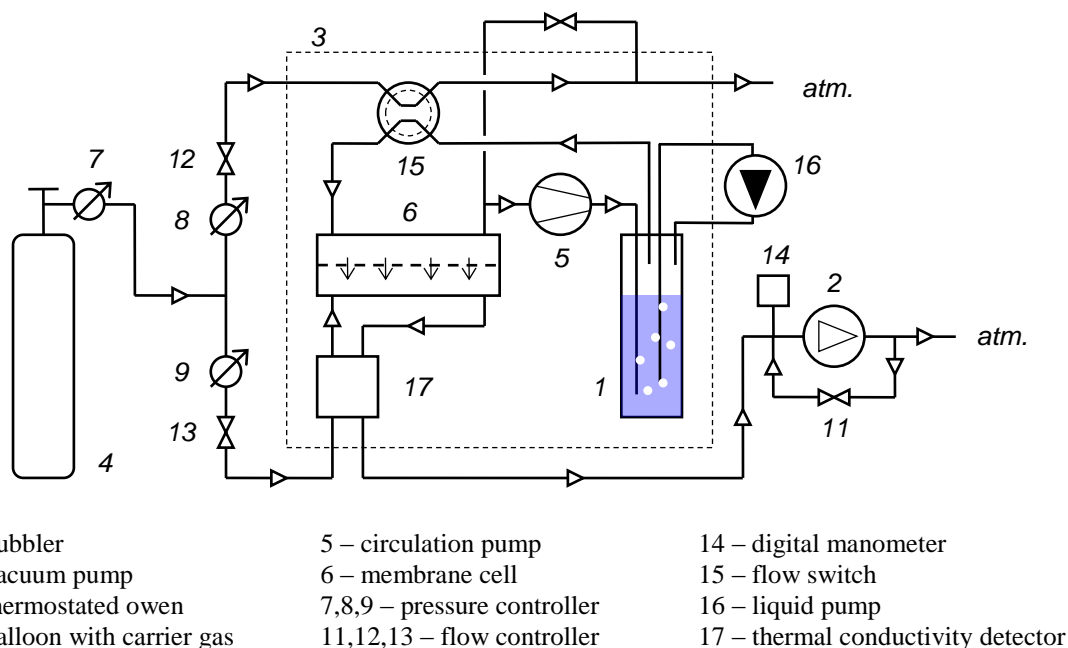


Figure 1. Scheme of the diffusion coefficients measuring setup

Results and Discussion

The dependences of the diffusion coefficients of water and ethanol vapors in polyvinyltrimethylsilane (PVTMS) on the temperature were obtained in the range 40-70 °C (Fig. 2). The diffusion activation energies were determined from the temperature dependences. In addition, the dependence of the diffusion coefficients on the activity of vapors was investigated.

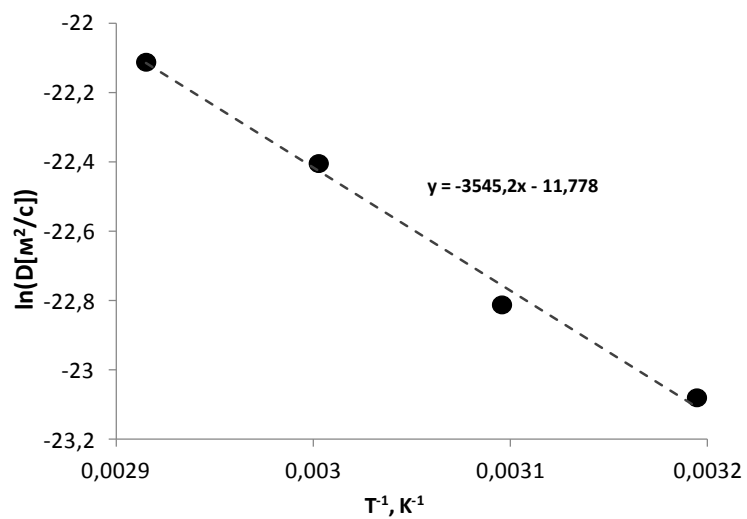


Figure 2. Arrhenius plot of the diffusion coefficients of water vapor on temperature for PVTMS.

Acknowledgements

This work is supported by RFBR Grant No. 16-08-01187.

References

1. *Teplyakov V.V, Meares P.* Correlation aspects of the selective gas permeabilities of polymeric materials and membranes // *Gas Sep. Purif.* 1990. V. 4. P. 68-72.

STATIONARY AND NON-STATIONARY MODELS OF ION TRANSFER IN NEUTRALIZATION DIALYSIS

²Anton Kozmai, ¹Mona Chérif, ¹Lasaad Dammak, ¹Myriam Bdiri, ²Victor Nikonenko, ¹Christian Larchet, ²Ul'ia Aniskina

¹Institut de Chimie et des Matériaux Paris-Est (ICMPE), Thiais, France, E-mail: larchet@u-pec.fr

²Membrane Institute, Kuban State University, Krasnodar, Russia, E-mail: kozmay@yandex.ru

Introduction

The Neutralization Dialysis (ND) process is based on the simultaneous use of two Donnan dialysis operations: one using acidic solution and a cation-exchange membrane (CEM) and the other one using alkaline solution and an anion-exchange membrane (AEM). The H^+ ions penetrate across the CEM and the OH^- ions penetrate across the AEM into the desalination compartment in exchange for the mineral ions initially present there, thus allowing the demineralization of the feed solution. ND is not technically sophisticated, it demands low investment costs, it is characterized by low energy consumptions; its implantation is easy for isolated locations. Different applications were considered such as separation of weak acids and bases [1], transport of glycine [2] and desalination of aqueous solutions of carbohydrates and milk whey [3]. However, this process is poorly studied both experimentally and theoretically. It is particularly difficult to maintain a predetermined value of pH of the product, while the applications require a specified value of pH [4-7]. Namely, for drinking water, the pH must be from 6.5 to 8.5; for organic solutions, the desired value of pH depends on the form of the resulting product to be obtained. Moreover, low or high pH reduces the ion-exchange rate of desalination [7]. As for the theory, there are some quasi-steady state models, which were developed for stationary [5] or/and circulation [4, 5] regimes of ND processes. The main quasi-steady state assumption is that the rates of the concentration profile formation in the solution and membranes are substantially greater than the rate of change in the inlet concentration.

Theory

A system, consisted of three compartments filled with different solutions (HCl, NaOH and NaCl) separated by a cation- and an anion-exchange membrane, is studied (fig. 1).

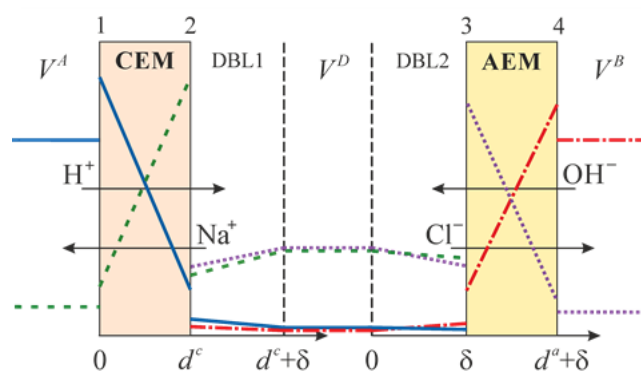


Figure 1. Scheme of the system under study. Concentration profiles are shown schematically for H^+ (solid line), Na^+ (dashed line), OH^- (dash-dot line) and Cl^- (points) ions

V^A , V^B and V^D are the volumes of acid, alkali (base) and saline (under desalination) solutions, respectively, circulating through the corresponding compartments and intermediate tanks. δ is the diffusion boundary layer (DBL) thickness assumed the same near the CEM and AEM. CEM (of thickness d^c) and AEM (of thickness d^a) are supposed to be ideally selective (the co-ion transport is neglected), which is justified [8] in relatively diluted solutions as used in this study. Convective transport within the diffusion layers is neglected; it is taken into account implicitly by adjusting the

DBL thickness. Longitudinal concentration changes along the channel are not taken into account. It is assumed that the ion concentrations in the bulk of compartment D and in the corresponding intermediate tank are the same. The material balance equations are applied to the circulating solution of volume V^D as a whole. The diffusion layers in the A and B compartments are neglected. At the membrane/solution interfaces, the local thermodynamic equilibrium between exchangeable ions is assumed. Additionally, the local equilibrium of the water self-ionization reaction: $H^+ + OH^- \rightleftharpoons H_2O$ is assumed.

The non-steady state model developed is based on the Nernst-Planck equations, the electroneutrality condition, the condition of zero current flow and the equation of material balance.

Results and Discussion

A good agreement is found between the simulated and experimental curves representing the pH and electric conductivity vs. time in the saline solution (fig. 2). We have compared the model developed with the quasi-steady state model. We have found that the difference between these two models occurs at the beginning of ND process where the effect of initial membrane state is important.

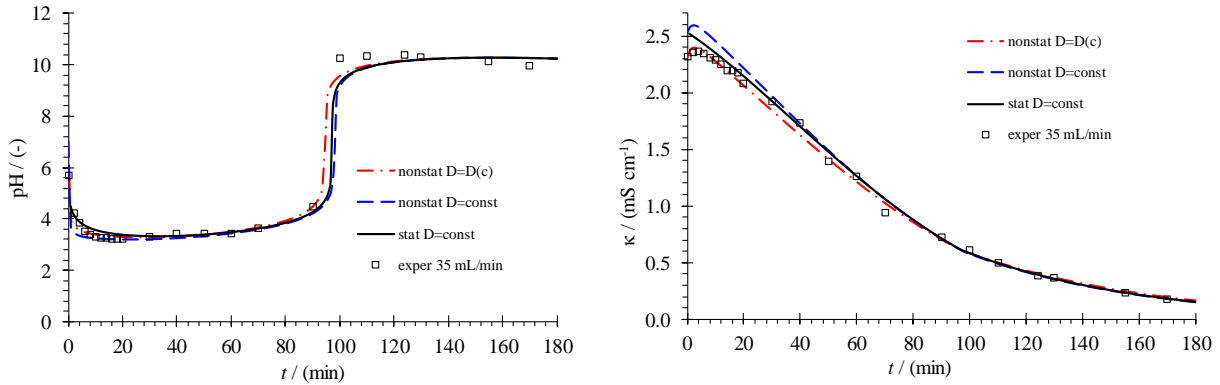


Figure 2. Calculated (using non-steady state (“nonstat”) and quasi-steady state (“stat”) models) and experimental time-dependences of the saline solution pH (a) and conductivity (b) in the desalination compartment as well as flux densities (c) across the CEM (J^c) and AEM (J^a). The values of parameters used in both models are the same

Four different cases of initial concentration distributions in the membranes are considered. It is found that in the case where the CEM is in the H^+ form and the AEM is in the OH^- form, high exchange rates across the surface layers of these membranes bathing the saline solution result in a few pH fluctuations of the saline solution (fig. 3).

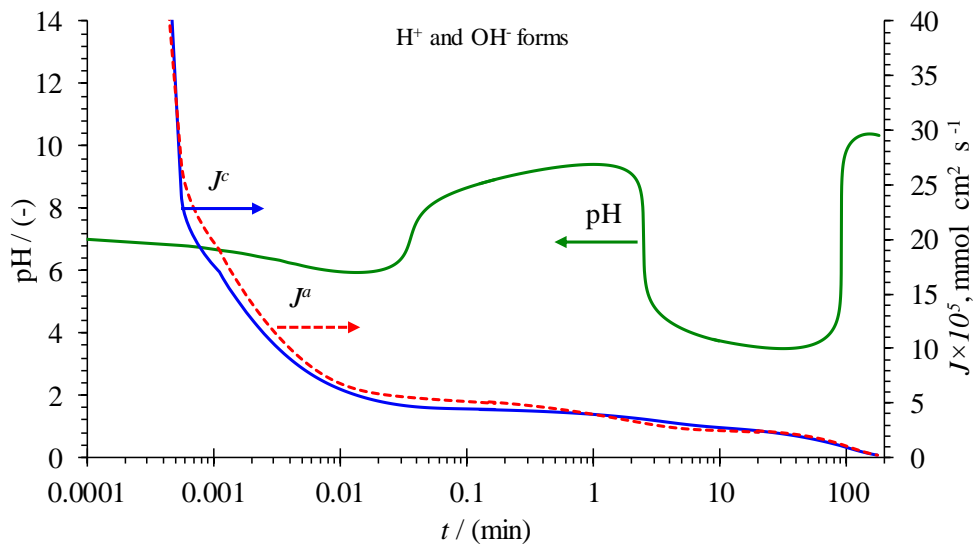


Figure 3. Calculated (using the non-steady state model) time-dependences of the saline solution pH (a), pH and fluxes through the CEM (J^c) and the AEM (J^a), and conductivity of solution (c) in the D compartment for various initial states of the CEM and the AEM

These fluctuations cannot be described by the quasi-steady state model. However, the two models describe well the pH fluctuations occurring in the saline solution after the concentration profiles in the membrane approach a linear form (about 20 minutes after starting the operation).

The oscillations in the pH saline solution are linked with the delay in variations of the concentration profiles in the membranes after changing saline solution composition. When ion exchange across one of the membranes is dominant, this generates strong pH variations in the

solution, which accelerates the ion exchange through the other membrane. However, the passage of the “leadership” from one membrane to the other requires some time during which the pH continues to vary. Finally, the increasing rate of ion exchange across the other membrane results in the change in the direction of pH variation.

Note that the electrodiffusion processes governing the neutralization dialysis are similar to those occurring in reverse electrodialysis [9, 10]: in both cases, the driving force is the concentration gradient across a membrane. Thus, the theory developed in this paper can be also applied in this novel technique of clean energy generation.

Acknowledgements

We are grateful for financial support to the Russian Scientific Foundation (grant 17-19-0186).

References

1. *Igawa M., Tanabe H., Ida T., Yamamoto F., Okochi H.* Separation of weak acids and bases by neutralization dialysis // *Chem. Lett.* 1993. V. 22. P. 1591.
2. *Wang G., Tanabe H., Igawa M.* Transport of glycine by neutralization dialysis // *J. Membr. Sci.* 1995. V. 106. P. 207.
3. *Bleha M., Tishchenko G.A.* Neutralization dialysis for desalination // *J. Membr. Sci.* 1992. V. 73. P. 305.
4. *Denisov G.A., Tishchenko G., Bleha M., Shataeva L.* Theoretical analysis of neutralization dialysis in the three-compartment membrane cell // *J. Membr. Sci.* 1995. V. 98. P. 13.
5. *Sato K., Yonemoto T., Tadaki T.* Modeling of ionic transport in neutralization dialysis deionization // *J. Chem. Eng. Jpn.* 1993. V. 26. P. 68.
6. *Chérif M., Mkacher I., Ghalloussi R., Chaabane L., Ben Salah A., Walha K., Dammak L., Grande D.* Experimental investigation of neutralization dialysis in three-compartment membrane stack // *Desalin. Water. Treat.* 2014. V. 56. P. 1.
7. *Chérif M., Mkacher I., Dammak L., Ben Salah A., Walha K., Grande D., Nikonenko V.* Water desalination by neutralization dialysis with ion-exchange membranes: flow rate and acid/ alkali concentration effects // *Desalination.* 2015. V. 361. P. 13.
8. *Larchet C., Auclair B., Nikonenko V.* Approximate evaluation of water transport number in ion-exchange membranes // *Electrochim. Acta.* 2004. V. 49. P. 1711.
9. *Logan B.E., Elimelech M.* Membrane-based processes for sustainable power generation using water // *Nature.* 2012. V. 488. P. 313.
10. *Vermaas D.A., Saakes M., Nijmeijer K.* Power generation using profiled membranes in reverse electrodialysis // *J. Membr. Sci.* 2011. V. 385-386. P. 234.

CATALYTICAL, CHEMICAL AND ELECTROCHEMICAL ACTIVITY OF METAL (Ag, Cu) NANOPARTICLES IN ION-EXCHANGE MATRIXES

Tamara Kravchenko

Voronezh State University, Voronezh, Russia, E-mail: krav280937@yandex.ru

Introduction

Stabilized in the ion-exchange polymer matrixes a metal nanoparticles show increase the catalytical, chemical and electrochemical activity by using developed and defective surface. At the same time pores of the ion-exchange matrix able to execute a transport and a sorption functions by using the canal system and the fix charging centers as sources and drains for ionic reagents [1]. The aim of the present investigation contens in characterization of the catalytical, chemical and electrochemical activity of metal – ion exchange materials as bifunctional nanocomposite structur.

Catalytical activity

Quantitative marks was made by the current exchange density i_0 of the model oxygen reaction



that by reaction rate at equilibrium.

The molecular oxygen reduction was investigated on the nanocomposite metal/ion-exchange membrane/active carbon Me(Ag,Cu)/MF-4SK/AC by voltamperometrical method. Accodiny Levichs' equation for limiting diffusion current was calculated the effective electron number which shows increase of fourelectron mechanism deposition. Two Tafel shift $0.057 \div 0.073 B$ and $0.103 \div 0.131 B$ probably connect with adsorption and charge shift.

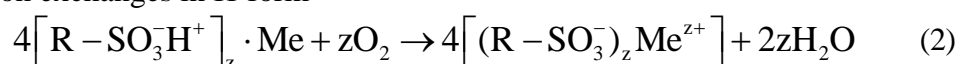
Table 1. Electrochemical active surface S_{ela} , limiting current density in composite film i_{lim}^{film} and exchange current density i_0 of oxygen reaction on Me/MΦ-4CK/AC in 0,1 M H₂SO₄

Material of nanocomposite	Reducer of metal	Weight part of metal W, %	S_{ela}/S_{geom}	$-i_{lim}^{ext}, A/M^2$	$-i_{lim}^{film}, A/M^2$	$-i_0, A/M^2$
Ag/MF-4SK/Norit 30	N ₂ H ₄	0.25 ± 0.02	75.9	25.9 ± 1.3	1.94	1.1 · 10 ⁻⁶
Ag/ MF-4SK /Norit 30	NaBH ₄	0.30 ± 0.02	81.3	29.6 ± 1.5	0.93	2.0 · 10 ⁻⁶
Ag/ MF-4SK /UM-76 (soot)	N ₂ H ₄	0.40 ± 0.02	83.9	40.0 ± 1.0	2.13	2.8 · 10 ⁻⁷
Ag				40.0 ± 1.0		4.8 · 10 ⁻⁹

Dependence of the limiting current density i_{lim} on a root square from rotation velocity don't extrapolated in coordinate begining, that gives evidence about a process complexity. It were used the criterial Kouteskii-Levich coordinates. Calculating value of the limiting current density in a composite film shows deposition of the inter diffusion (table 1). High value of the current exchange density calculating on the electrochemical active surface indicates about a catalytical activity synthetic composites.

Chemical activity

Chemical activity of the metal nanoparticles contributes a chemical reaction with oxygen in the macroporous sulfocation exchanges in H-form



Here **R** - granul polymeric matrix (KU-23), $-\text{SO}_3^-$ - ion-exchange center, H^+ - counter-ion, z - metal ion charge, Me – metal (Ag, Cu). Repitition cycle of metal precipitation allows to receive a nanocomposite with high content of metal particles $[\text{R} - \text{SO}_3\text{H}^+]_{zn} \cdot \text{Me}_n$, where n – a metal atom number at zn mol-eqv of ion exchanger.

Interaction of a metal nanoparticles with oxygen reduces to the metal ions formation (Ag^+ , Cu^{2+}) and their localization as counter ions on the sulfogroups in contrast to chemical stability

compact argentum. When a metal component capacity and a counter ions commensurable a degree and a rate of oxygen sorption high, that it is clear from the dynamic exit curves on high chemical active coppercontaining sulfocation exchanger in H-form. With a metal capacity increase it was limited the time of oxygen slip rises. Maximum was determinated probably a percolation electron conductivity and a distribution unteventless of the ionic and the oxide products about a grain layer left [2].

Ordinary differential system describing the distribution of layer fronts $\xi_1(\text{Cu}/\text{Cu}_2\text{O})$ and $\xi_2(\text{Cu}_2\text{O}/\text{CuO})$ may be given equations [3]

$$\frac{d\xi_1}{d\tau} = -\frac{d_{12}\xi_2}{Z_c}, \quad (3)$$

$$\frac{d\xi_2}{d\tau} = -\frac{\xi_1(\xi_2 - \xi_1) + d_{11}\xi_2}{Z_c}, \quad (4)$$

where $Z_c = \left(1 - \xi_2 \left(1 - \frac{1}{Bi}\right)\right) \left(\xi_1 \xi_2 (\xi_2 - \xi_1) + d_{11}\xi_2^2 + d_{12}\xi_1^2\right) - d_{22}(\xi_1^2 - \xi_1 \xi_2 - d_{11}\xi_2)$, Bi – Biots' criterion, d_{ij} - constat.

Calculation and experimental data are found in within permissible errors (figure). In result it was described kinetics of oxygen redox sorption of oxygen with different factors (ionic form matrixes, oxygen concentration, solution velocity) and conditions (static, dynamics).

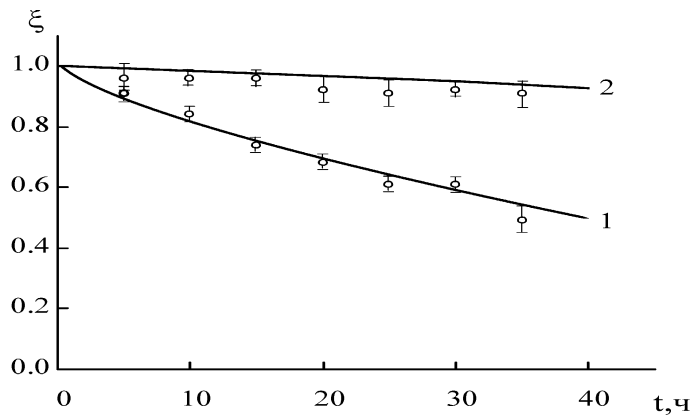
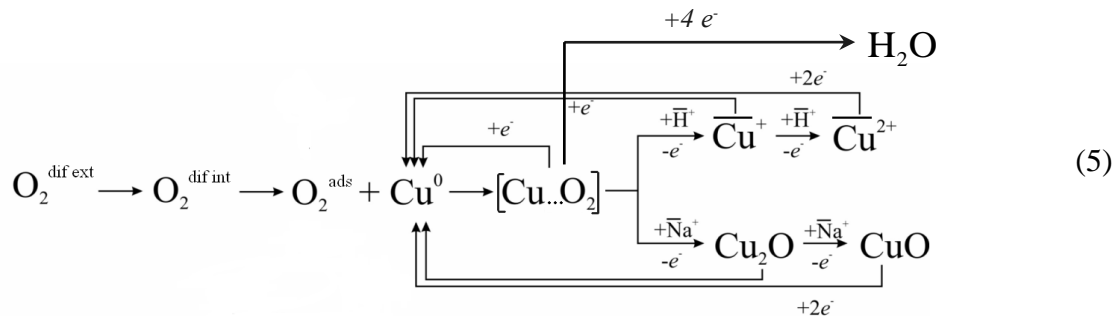


Figure. Kinetic curves for coordinates of chemical reactions between dissolved water oxygen and nanocomposite Cu-KU-23 in H^+ -form. Points – a experimental data, curves – a calculation on the equations (3) and (4). Curve: 1 – ξ_1 , 2 – ξ_2 . Thin layer method.

Electrochemical activity

The cathodic polarization contributes changes in succession of a oxygen reduction stages. Besides enter and inter oxygen diffusion, chemisorption complex formation and his oxydation as without polarization, in this schema it was considered the electrochemical reduction stages of the adsorption oxygen and the oxidated copper nanoparticles.



where $\overline{H^+}$ and $\overline{Na^+}$ - counter ions.

It was building a mathematical model of redox electrosorption. At electrochemical polarization system of equations (3) and (4) expand multiplier $(1 - i/i_{lim})$, where i_{lim} – oxygen the limit external diffusion current density. Note that when an electric current is applied, the growth of a chemical component slowed sharply and approached values of less than 0.4 at the fixed duration of the process [3]. At the same time, an increase in the density of electric current led to a substantial increase in the total amount of oxygen removed from liquid phase (table 2).

Table 2: Amount of oxygen ($Q \times 10^3$, mol) reduced during the redox sorption of molecular oxygen in a granular layer of Cu·KU-23 (Na⁺) upon cathode polarization with electric current $i/i_{lim} = 0.7$

t, h	Q_{elch}	Q_{ch}	$Q_{theor} = Q_{elch} + Q_{ch}$	$Q_{experiment}$
15	0.70	0.11	0.81	1.32
50	2.33	0.16	2.49	2.60
150	7.00	0.40	7.40	7.71

Q_{elch} and Q_{ch} were determined for electrochemical and chemical processes, respectively.

Part of nanocomposite grain slice from a thin layer (about 20%) shows a satisfactory correlation with theory. The other part shows that the electroregeneration stage of the forming oxide metal must be considered in a mathematical discription.

Acknowledgments

This work was supported by the Russian Foundation for Basic Research (grant № 17-08-00426a) and by the Russian Ministry of Education and Science (grant № 675, 2014-2016, Voronezh State University).

References

1. V.V. Volkov, T.A. Kravchenko, V.I. Roldughin Metal nanoparticles in catalytic polymer membranes and ion-exchange system for advanced purification of water from molecular oxygen // Rus. Chem. Rev. 82 (5). 2013. P. 465-482.
2. S.V. Khorolskaya, L.N. Polyanskii, T.A. Kravchenko, D.V. Konev, V.A. Krusanov. Percolation effect in dynamics of oxygen redox sorption with metal – ion exchanger nanocomposites // Rus. Nanotechnology. 2015. V. 10. P. 69-74.
3. L.N. Polyanskii, E.N. Korshov, D.D. Vachnin, T.A. Kravchenko. Redox sorption on metal - ion exchanger nanocomposites at electrochemical polarization // Rus. J. Phys. Chem. 2016. V. 9. P. 1414-1420.

COMPOSITE TRACK-ETCHED MEMBRANES WITH SILVER NANOPARTICLES

Olga Kristavchuk^{1,2,*}, Ilya Nikiforov^{1,2}, Vladimir Kukushkin³, Alexander Nechaev^{1,2}, Pavel Apel^{1,2}

¹Joint Institute for Nuclear Research, Dubna, Russia, *artoshina@jinr.ru

²Dubna State University, Dubna, Russia

³Institute of Solid State Physics Russian Academy of Sciences, Chernogolovka, Russia

Introduction

Research in the field of membrane materials and technologies is vigorously advancing in many directions. For example, porous materials modified with nanoparticles of silver are considered as substrates for highly sensitive analysis based on the phenomenon of the surface-enhanced Raman scattering (SERS) of light [1-2]. Flow-through SERS-active sensors perform at the same time two functions – selective separation and amplification of light scattering [1]. In order to obtain a stable colloidal silver suspension, the electric arc method is successfully applied, during which an electric discharge between silver electrodes immersed in deionized water takes place [3].

The purpose of this work was to immobilize silver nanoparticles from a suspension onto the surface of a polyethylene terephthalate (PET) track-etched membrane (TM) using polyethyleneimine (PEI) as a link molecule and to study the properties of the silver-modified TM surface. We chose PEI because of its ability to efficiently attach to the PET TM due to the formation of a strong bond between its amino groups and the PET carboxyl groups. Nitrogen in a protonated form gives the TM surface a positive charge, which allows us to utilize the electrostatic mechanism of attraction of the negatively charged nanoparticles to achieve the desired immobilization.

Experiments

PET TM of 23 μm thickness and pore density $5 \times 10^8 \text{ cm}^{-2}$ were used. The pores were cigar-shaped with inlet holes of 0.15 μm . The TM were manufactured at the Laboratory of Nuclear Reactions, Joint Institute for Nuclear Research, Dubna.

In order to immobilize silver nanoparticles (NP Ag) on the TM surface, the TM surface was previously modified with PEI. TM was cleaned with acetone and ultrapure water and then placed in a 0.1% PEI solution for 3 hours. The samples were then repeatedly washed with water and immersed for 1 hour in a 0.01 M HCl solution in order to protonate the amino group. All operations were performed at room temperature. Samples with thus modified surfaces were placed in beakers containing 100 ml of a suspension of silver nanoparticles for each sample.

The composition and surface morphology of thus modified membranes, including measures of nanoparticles aggregation, were characterized using X-ray photoelectron spectroscopy and scanning electron microscopy. The SERS enhancement factor for Rhodamine 6G molecules adsorbed on the membranes was determined.

Results and discussion

As shown in [3], a silver nanoparticle in the suspension has a negative charge due to the formation of an ionic shell around it. Also, the authors of [3] showed the presence of silver in a cationic form as well. It should be noted that the ionic composition of the suspension is an important factor for understanding the processes that influencing the deposition of nanoparticles on various surfaces.

The process of manufacturing of PET TM results in the appearance of carboxylic groups on their surface, which upon dissociation give the surface a negative charge. Subsequent modification of the TM surface by PEI leads to a change in the charge of the TM surface, ensuring the electrostatic attraction of the negatively charged Ag NP to the surface.

Images of the surface of TM with the immobilized silver nanoparticles obtained by scanning electron microscopy are shown in Fig. 1. The average diameter of Ag NP was found to be 22.4 nm. Particles are evenly distributed on the surface of the membrane, covering approximately 20%

of the free from pores area. Single particles are prevailing (about 11% of the total number of NP), while double (8%) and triple (7%) clusters are also common.

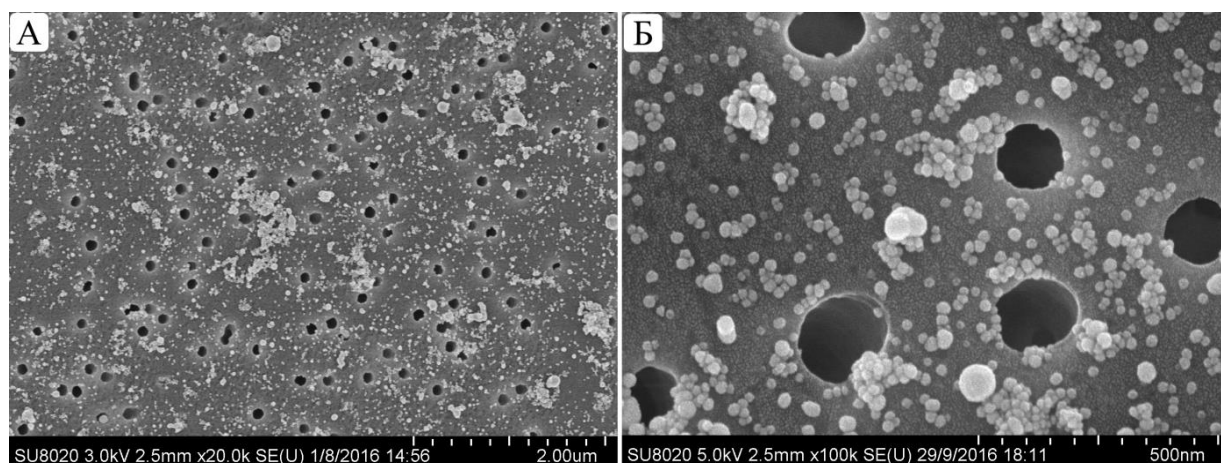


Figure 1. SEM photographs of TM with immobilized Np Ag. A thin conducting layer of gold was deposited on the samples

Increasing the holding time of the TM samples in the silver NP suspension led to an increase in the number of NPs on the surface, as evidenced by the results of X-ray photoelectron spectroscopy (XPS) which demonstrate a concomitant increase in the intensity of silver peaks (367 and 373 eV) with increasing time of the membrane samples in the Ag NP suspension (Fig. 3). The nitrogen peak at 399 eV on curves 2-4 relates to the amino groups of PEI. The peaks of oxygen and carbon are mainly related to the membrane material - PET.

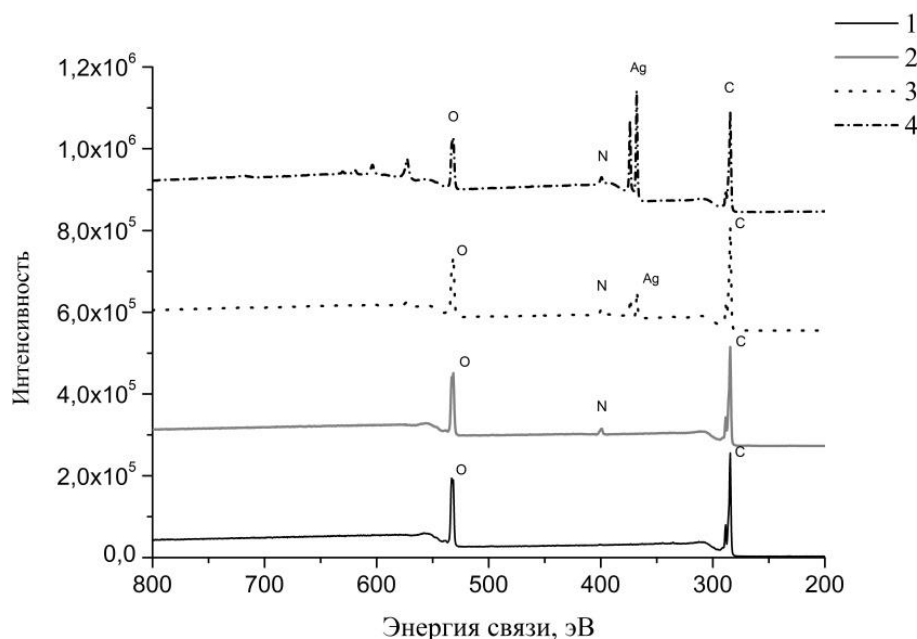


Figure 2. Results of XPS: 1 - original TM, 2 - TM-PEI, 3 - TM-PEI-Ag 12 hours, 4 - TM-PEI-Ag 48 hours

The Ag NP enriched track-etched membranes were used in SERS studies. Spectroscopy was carried out near the plasmon resonance of silver nanoparticles and the resonant photoexcitation of the test dye Rhodamine 6G. Laser radiation with a wavelength of 532 nm was used (Fig. 3). The maximum increase in the Raman scattering of light (2×10^6) was obtained with a sample held in the Ag suspension for 48 hours.

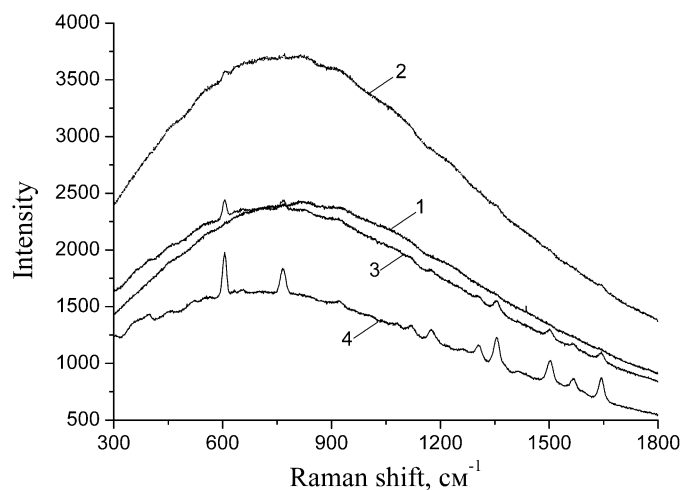


Figure 3 - Raman spectra of rhodamine 6G on the surface of TM with immobilized NP Ag: 1 - 12 h, 2 - 24 h, 3 - 36 h, 4 - 48 h. Laser excitation with a wavelength of 532 nm.

The research work has been supported by the Russian Scientific Foundation, Project №16-15-10332.

References

1. Taurozzi J.S., Tarabara V.V. // Environmental Engineering Sci. 2007. V. 24. № 1. P. 122.
2. Wigginton K.R., Vikesland P.J. // Analyst. 2010. V. 135. P. 1320.
3. Tien D., Chen L., Thai N.V., Ashraf S. // J. of Nanomaterials. 2010. V. 2010. 634757.

WATER AND WATER SATURATED VAPOR TRANSFER RATE THROUGH PROTON EXCHANGE POLYMER MEMBRANES

Dina Kritskaya¹, Emil Abdrashitov¹, Veslav Bokun¹, Ardalion Ponomarev¹, Eugeny Sanginov², Yuri Dobrovolsky²

¹Branch of Talose Institute for Energy Problems of Chemical Physics of RAS, Chernogolovka, Russia
E-mail: dinak@binep.ac.ru

²Institute of Problems of Chemical Physics of RAS, Chernogolovka, Russia

Introduction

Transport properties of proton exchange membranes contained SO_3^- groups are significantly determined by the water uptake. It was shown that at high humidity conditions reducing of the membrane thickness does not result to increasing of water flux through Nafion-115 [1, 2]. For this unusual result explanation some has to admit that a resistance of the inner part of membrane is lower essentially than a resistance of its interfaces. The dependence of water transfer rate on the membrane thickness appears only when the humidity is reduced essentially and resistance of the inner membrane layers increases on the order of magnitude.

This work aim was a comparative study of water and water saturated vapor transfer rates through a commercial membranes (Nafion-115, MF-4SK) and the composite proton exchange membranes based on industrial polymer (polyvinylidene fluoride (PVDF), polypropylene (PP), ultra-high-molecular weight polyethylene (UHMPE), stretched polytetrafluoroethylene (str-PTFE)) films modified by a sulfonated polystyrene (sPS) [3, 4].

Experiments

Water and water vapor transfer rates (W_w , W_v) through commercial (Nafion-115, MF-4SK) and the synthesized (PVDF-sPS, PP-sPS, UHMPE-sPS and str-PTFE-sPS) membranes was measured by the method of an liquid evaporation from the weighted cell through the studied membranes. The evaporated surface of the membranes was always subjected by the forced air blowing. Two ways of water evaporation through the samples were used. First is the water evaporation through the membrane on the normal position of the cell – membrane is disposed «above» vapor (W_v). Second is the water evaporation from the turned upside-down cell– water is disposed «on» the membrane (W_w).

The control experiments on the water evaporation through the membranes without the forced air blowing and from the open water surface (W_0) were realized also.

Results and Discussion

During control experiments the relation $W_w/W_0 \approx 0.5$ was obtained by the comparative measures of water evaporation through the Nafion-115 (W_w) and from the open water surface (W_0). This relationship is maintained both in the absence of forced air blowing as well as at its realization, in spite of significant increasing of W_w and W_0 of about 15 times. One can value the hydrophilic (evaporating) part of Nafion-115 surface (f_w) using the advancing and receding angles of this wet membrane moistening [5] as $0.8 > f_w > 0.4$. As can be seen the «specific» rates of the water evaporation from the open water surface and from the hydrophilic part of Nafion-115 surface (water is disposed «on» the membrane) are close enough.

These results confirm that the water evaporation rate (W_w) through Nafion-115 is limited by the rate of water removal from the surface (W_{w-s}) regardless of the way of water evaporation. The relations $W_w = W_{w-s}$ and $W_{w-s} \sim \Delta p$ are valid when the evaporating surfaces are blown by a stream of air ($\Delta p = p_s - p_{\text{air}}$; p_s and p_{air} – a saturated water vapor pressure on a surface and water vapor pressure in air flux, respectively).

The dependence of a water and water saturated vapor transfer rates through cation exchange membranes on the value Δp and on the membrane thicknesses was studied. The evaporation rates of a water $W_w(I)$ and its saturated vapor $W_v(2)$ through PVDF-sPS, PP-sPS, UHMPE-sPS, str-PTFE-sPS, Nafion-115, MF-4SK membranes are compared with the experimental values Δp on the figure. The evaporation rates $W_w(I)$ and $W_v(2)$ were measured under forced air blowing of the

cell. The experimental points for the «thin» membranes ($60 \div 80 \mu\text{m}$) are selected on figure by the dark colour. The light points are the values of the water transfer rates through «tick» membranes ($110 \div 260 \mu\text{m}$).

It is seen that the linear dependences of $W_w(1)$ and $W_v(2)$ on Δp are observed for all studied membranes independently of their structure and thickness. The efficient permeation values of the water P_w and its saturated vapor P_v calculated from the linear dependences 1 and 2 by use of the relations $P_w = W_w / \Delta p$ and $P_v = W_v / \Delta p$ are equal to 25 and $2.5 \text{ mg}(\text{h mm Hg})^{-1}$ accordingly.

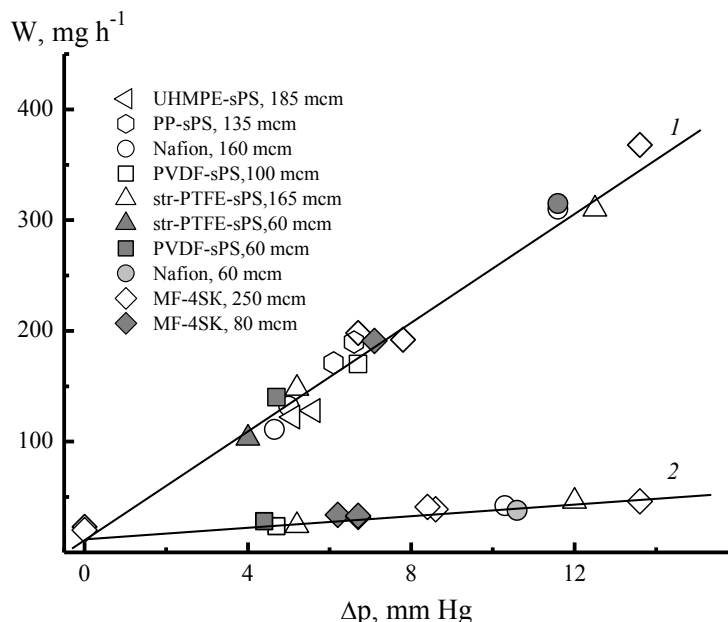


Figure. Dependences of the water (1) and water saturated vapor (2) transfer rates through the PVDF-sPS, PP-sPS, UHMPE-sPS, str-PTFE-sPS, Nafion-115, MF-4SK membranes ($60 - 250 \mu\text{m}$) on Δp . Relative humidity of air stream is $30 \div 75\%$. Samples area is 3 cm^2 .

Presented data indicate that at room temperature the water and water saturated vapor transfer rates through proton exchange membranes do not depend on the type and thickness (within $60 - 250 \mu\text{m}$) of the membranes, and the water saturated vapor transfer rates are on order of magnitude less than the liquid water transfer rates. The independence of the water and water vapor flow on the membrane thickness and their chemical nature allows us to conclude that at high hydration level the transfer of water is limited by the sorption and desorption processes. In the case of the liquid water the transfer rate is limited by the rate of water removing from the membrane surface. In the case of the water vapor the transfer rate is limited by the rate of water sorption from the gas phase inside of membrane.

The obtained results are of practical interest for optimizing the operation of fuel cells based on proton exchange polymer membranes.

References

1. P.Majsztrik, A. Bocarsly, J. Benziger // J. Phys. Chem. B. 2008. V. 112. №5. P. 16280.
2. J. Peron, Ana Mani, X. Zhao, D. Edwards, M. Adachi, T. Soboleva, Zh. Shi, Zh. Xie, T. Navessin, St. Holdcroft // Journal of Membrane Science. 2010. V. 356. P. 44.
3. Abdrashitov Emil F., Bokun Veslav Ch., Kritskaya Dina A., Sanginov Evgeny A., Ponomarev Ardalion N., Dobrovolsky Yury A. // Solid State Ionics. 2013. V. 251. P. 9.
4. Emil F. Abdrashitov, Dina A. Kritskaya, Veslav C. Bokun, Ardalion N. Ponomarev, Ksenia S. Novikova, Evgeny A. Sanginov, Yury A. Dobrovolsky // Solid State Ionics. 2016. V. 286. P. 135.
5. T.A. Zawodzinski, S.Gottesfeld // J. Appl. Electrochemistry. Short Communication. 1993. Vol. 23. P. 86.

APPLICATION OF SORPTION AND EXTRACTION PROCESSES IN THE FLOWSHEETS OF HYDROMETALLURGICAL PROCESSING OF ORES OF DEPOSITS OF KAZAKHSTAN

Larissa Kushakova, Anna Reznichenko, Natalia Sizikova, Olesya Brailko

The Eastern Mining and Metallurgical Research Institute for Non-ferrous Metals, Ust-Kamenogorsk, the Republic of Kazakhstan, *E-mail: tims.vcm@mail.ru*

Introduction

The world trend of a gradual increase of the share of hydrometallurgical production in the total volume of non-ferrous metals production takes place in Kazakhstan. To the greatest extent it is reflected in the metallurgy of copper during implementation of heap leaching of oxide copper ores and extraction technology, as well as during hydrometallurgical processing of gold-bearing ores with the use of gold sorption by specialized activated coals or ion-exchange resins. Research on the sorption and extraction recovery of target components from solutions also take a significant place in the development of technologies for hydrometallurgical processing of oxide nickel ores and various types of technogenic raw materials.

Experimental part

Since 1997, the Institute has carried out the research on the use of extraction technology for the processing of copper-containing raw materials of Kazakhstan. Oxide and mixed copper ores of the Kounrad, Shatyrcul, Bencala, Aktogay, Ay, Ayak-Kodzhan, Karchiga, Beschoku, Nurkazgan, Taskora, Borly, Baytemir, Vavilonskoe, Zhezkazganskoe, Koksai and other deposits were tested. One of the parts of the research work for the development of the optimal ores processing technology is specialized research on extraction recovery of copper using various specialized extractants based on aldoximes, ketoximes and a number of their modifiers in various ratios.

The research on study of the possibility of sorption extraction of copper from product leach solutions of oxide copper ores using ion-exchange resins were carried out for a number of deposits, but advantages over extractive technologies were not found.

According to the developments of VNIItsvetmet, various options for oxide copper ores processing have already been implemented and are being prepared for implementation:

- leaching of generated dumps of off-balance ores (Kounrad deposit),
- heap leaching of ores of pit size (Aktogay deposit),
- heap leaching of crushed ore (Ayak-Kodzhan, Ay, etc.).

Marketable product of hydrometallurgical processing of oxide copper ores is cathode copper of high grades (copper grade 99.99%) with recovery from 75 to 90% depending on the copper content in ore and the features of its material composition. In contrast to copper, when gold is recovered from solutions of cyanide leaching of gold-bearing ores, sorption technologies with the use of specialized grades of activated carbon or ion-exchange resins are the most widespread. Dozens of gold recovery plants are successfully operating in Kazakhstan. Technologies of sorption leaching of gold are sufficiently proved out, however, in the case of processing of gold-copper ores, a number of specific problems that require specialized research and development of special solutions arise. Up to date, about 40 deposits of silicate oxide nickel ores of industrial interest were found in the Republic of Kazakhstan. The recovery degree of nickel in the solution varies from 75 to 95%, depending on the chosen method of processing and the ore properties. Various options of leach solutions processing were tested, including the use of sorption and extraction processes. However, due to the complex and multicomponent composition of solutions, their processing requires the use of multi-stage complex schemes, which is one of the reasons for the lack of development of the explored deposits.

Conclusion

The application of extraction technologies in the metallurgy of copper and sorption processes in the metallurgy of gold is widespread in Kazakhstan. The development of nickel ore deposits is constrained by the lack of efficient technologies for recovery of nickel from leach solutions. The research in this field remains relevant, including consideration of the possibility to use electrodialysis and/or other ion-exchange processes.

EVALUATION OF STRUCTURAL CHANGES FOR NANOFILTRATION MEMBRANES BY THE DIFFRACTOMETRY METHOD

¹Sergey Lazarev, ¹Urii Golovin, ¹Olga Kovaleva, ¹Valerii Polikarpov, ¹Irina Khorokhorina
¹Tambov State Technical University, Tambov, Russia, *E-mail*: geometry@mail.nnn.tstu.ru

Introduction

In the work, studies for samples of semipermeable composite nanofiltration membranes, both virgin and working, by X-ray scattering methods were performed. It was found, that the mechanical load, caused by an excess pressure equal to 1.5 MPa, for the OFAM-K membrane, causes conformational changes of Phenolone C-4 macromolecules in the crystalline and amorphous intercrystalline phases, while the calculated degrees of crystallinity decreases from 49% to 36%. It is noted, that in the working sample of the porous composite nanofiltration material OPMN-P a polymorphous rearrangement of the crystalline phase takes place, and changes the size in the crystal cell in the direction of the crystalline axis.

Experiments

X-ray diffraction studies of nanofiltration membranes samples, such as OFAM-K and OPMN-P, were performed on a Dron-3 diffractometer in an automated mode, supported by the software package Lgraf-2 and Difwin, in the region of large angles 2θ from 50 to 500. The X-ray diffraction was recorded from the substrate and the active layer of the virgin and working sample of the membrane (within 24 hours) in reflection geometry in increments of 0.010. We used the radiation $\lambda = 1.542 \text{ \AA}$). Monochromatization was provided by a Ni-filter. The current and voltage on the X-ray tube were 20 mA and 35 kV. The obtained experimental data for further processing and identification of the phase composition of the membrane were transferred to the software package Origin 7.5 on a PC.

Results and Discussion

The degree of crystallinity (CK) was determined by the method, described in [1]. For this purpose, the distribution of the scattering intensity was divided into two parts: crystal peaks and scattering of the amorphous component. According to [2], CK% was calculated from the ratio of the integrated intensity of crystalline peaks to the total intensity under the scattering curve minus background scattering

$$CK\% = \frac{I_0 - I_a}{I_0} \cdot 100\%, \quad (1)$$

where I_0 - the integral scattering intensity under the entire scattering curve, I_a - the integrated scattering intensity under the selected amorphous component.

The calculation of the regions of coherent scattering (OKP) was carried out according to the Selyakov-Scherrer relation [1]:

$$L_{okp} = \frac{k \cdot \lambda}{\beta \cdot \cos 2\theta}, \quad (2)$$

where β - the half-width of the peak, radian; $\lambda = 1.542$ - X-ray wavelength, \AA ; $k = 0,94$ - dimensionless coefficient (Scherrer's constant); 2θ - the diffraction angle.

It is noted, that the selective and transport properties of composite membranes are largely determined by the joint structure of the substrate and the active layer [2]. Therefore, at the first stages of the study it was necessary to reveal the individual structure of the substrate and the active layer. In Fig. 1 shows the X-ray diffraction patterns of the substrate and the active layer for OFAM-K and OPMN-P membranes.

We note, that on the X-ray diffraction pattern of the OFAM-K membrane substrate from Phenylon C-4, three intense reflexes are recorded at $2\theta = 17.66^\circ$; 22.8° ; 25.61° , low intensity at $2\theta = 20^\circ$ against the background of an amorphous halo. The x-ray degree of crystallinity is 57%.

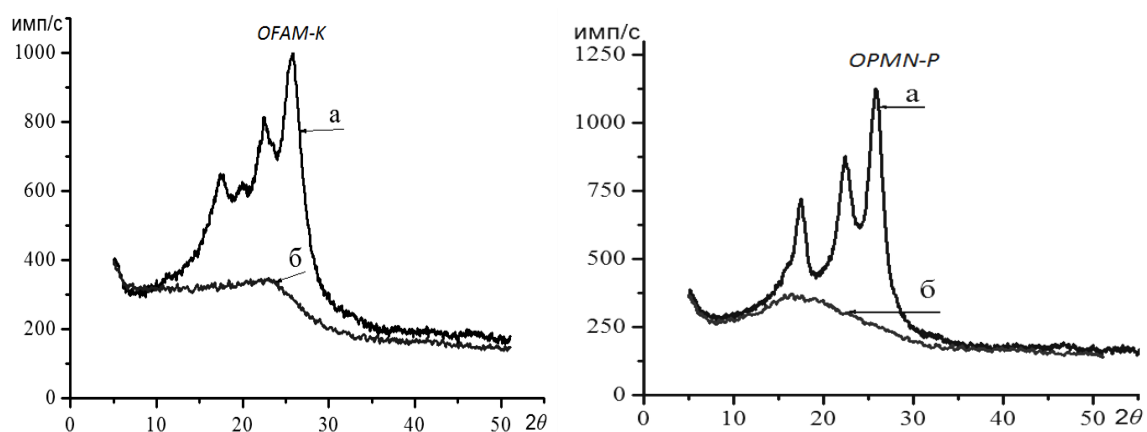


Figure 1. X-ray diffraction patterns of the substrate and active layer for OFAM-K and OPMN-P membranes: a - substrate; б - active layer

The active layer of the OFAM-K membrane, made of non-woven lавсан, is completely amorphous with the center of gravity of the halo-reflex at an angle of $2\theta = 22^\circ$ [2] and coincides with the amorphous halo of the substrate (Figure 1).

The X-ray diffraction pattern of the polyamide substrate of the OPMN-P membrane has three intense peaks at angles $2\theta = 17.9^\circ$; 22.6° ; 25.95° (Figure 1). The x-ray degree of crystallinity is 70%. The active layer from polypropylene for this membrane has an amorphous halo with a center of gravity at an angle of $2\theta = 14.8^\circ$ [3]. The data from a full-profile analysis of the samples of the OPMN-P and OFAM-K membranes are given in Table 1, which indicate significant structural rearrangements in the membrane polymer.

Table 1: Microstructural parameters for the OPMN-P and OPAM-K membranes

OPMN-P										
Virgin sample						Working sample				
EXP. for 2θ		17,9	22,6		25,95		14,72		22,2	25,63
Angle FPA 2θ	17,22	17,72	22,62	13,33	26,04	11,24	14,79	21,88	21,95	25,3
$d_{(abc)}$ Å	5,72	5,51	4,38	4,24	3,82	8,71	6,7	4,49	4,41	4,0
	6,08	0,86	2,82	12,6	1,67	3,59	3	7,56	1,93	1,47
$L_{(OKP)}$ Å	14,68	103,84	32,99	7,13	54,31	24,97	29,86	12,04	47,4	60,7
$I/I_{25,95}$	1,4	0,1	1,26	2,8	1	1,5	4,5	6,8	3	1
Cryst.			44%					55%		
OFAM-K										
Virgin sample						Working sample				
EXP. for 2θ	17,66	20	22,8		25,61	17,8	22,89		25,58	
Angle FPA 2θ	17,62	20,46	22,56	22,96	25,55	17,52	22,38	25,3	25,81	36,81
$d_{(abc)}$ Å	5,59	4,94	4,33	4,3	3,86	5,55	4,31	3,9	3,86	2,78
	1,75	1,12	1,13	6,89	1,38	3,95	2,97	8,95	1,84	11,9
$L_{(OKP)}$ Å	51,9	82,2	79,5	13,07	65,6	25,9	30,14	10,11	47,7	7,77
$I/I_{25,95}$	0,54		0,6	2,5	1	1,9	1,3	4,4	1	3
Cryst.			49%					36%		

EXP – experimental data; FPA – full-profile analysis

References

1. Azarov V.I., Burov A.V., Obolenskaya A.V. Chemistry of wood and synthetic polymers. Textbook for high schools. SPb.: SPbLTA, 1999. 628 p.
2. Fedotov Yu.A., Smirnova N.N. Aromatic polyamides with ionogenic groups: synthesis, properties, field of application. // Plastic masses. 2008. № 14. P. 18-21.
3. Arisova V.N. Structure and properties of CM. Tutorial. Volgograd: Volgograd State Technical University. 2008. 94 p.

INVESTIGATION OF THE PROCESS OF ULTRAFILTRATION SEPARATION OF TECHNOLOGICAL SOLUTIONS IN THE PRODUCTION OF ALCOHOL FROM MOLASSES

¹Sergey Lazarev, ¹Olga Kovaleva, ¹Roman Popov, ¹Sergey Kovalev

¹Tambov State Technical University, Tambov, Russia, E-mail: geometry@mail.nnn.tstu.ru

Introduction

Wide application of promising membrane methods for separation and concentration of biological solutions at biochemical enterprises is hindered by the lack of effective and up-to-date apparatus designs and the specific treatment of liquids containing polysaccharides and active cells (yeast).

Experiments

Flat-chamber, roll-type and tubular type apparatus are used for concentration of substances dissolved in solution. The existing methods do not take into account such an important component of separation of biological fluids as the formation of a dynamic membrane. Calculation based on the known papers [1] is incorrect since the additional cooling of the flow is not taken into account at a small flow rate of the concentrated liquid above the surface of the membrane. One of the ways of processing these wastes [2] can be the application of the ultrafiltration method using porous polymer partitions.

The above-mentioned features of the formation of a dynamic membrane are pushing researchers to develop modern designs of apparatuses that provide a large area of membrane separation for wide intermembrane channels; the example of such implementation is the apparatus described in the works of AG. Pervov et al. [3].

Results and Discussion

Based on the literary analysis of the designs of membrane roll-type apparatus, the design of the apparatus shown in Figure 1, 2 was developed.

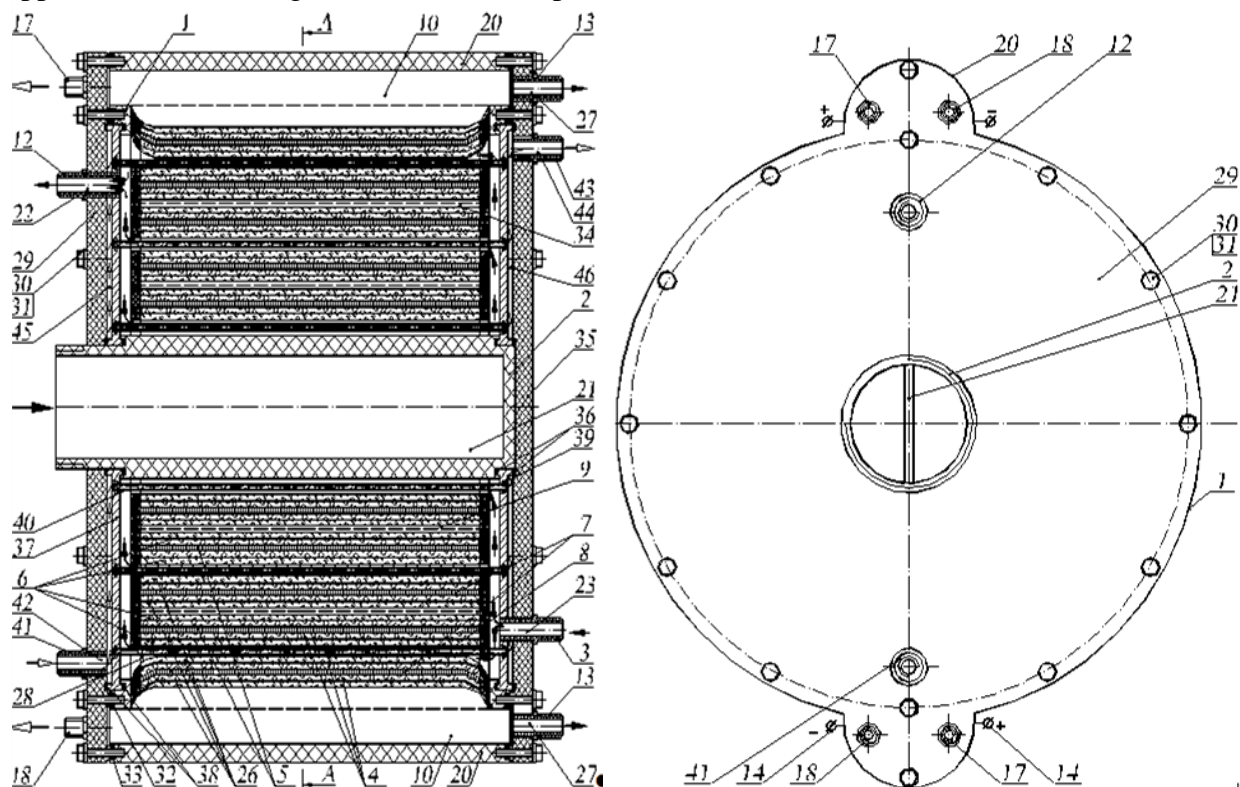


Figure 1. Electrobaromembrane apparatus of roll type

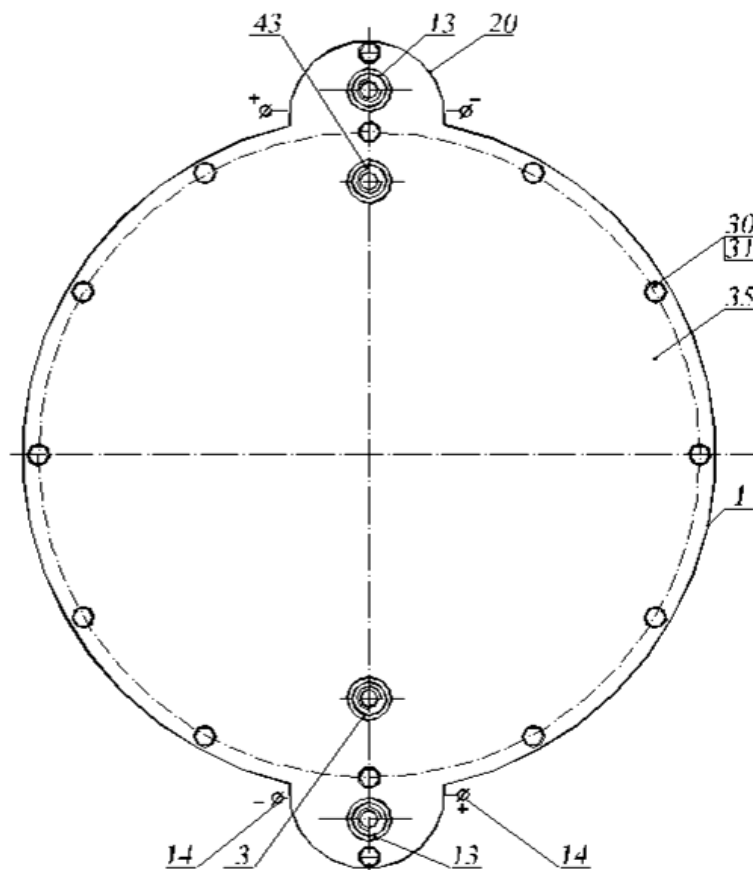


Figure 2. Electrobaromembrane apparatus of roll type

The apparent advantage of the designed structure is the possibility of cooling the solution.

The device functions as follows: the solution is fed into the perforated tube 2 and the solution fitting 3, which form two separation circuits (Figure 1). In the first circuit, the stock solution is supplied through the tube 2 divided into two sections along the entire length by a vertical partition 21. Then the solution enters the channel 34 in which the grid turbulizer 9 is located. From two sides of the grid turbulizer 9, the channel is formed by cathode membranes, anode membranes 26, 6, membrane substrates 4, drainage nets - cathode 7 and anode 5 and membrane substrates 4, cathode and anode membranes 26, 6, all of which are glued together from the end surfaces.

In the second circuit, the solution is fed through the fitting which is used for the supply of the stock solution 3 and enters the space formed between the body of the apparatus 1, the cathode and anode membranes 26, 6 and the perforated tube 2 (Figure 1). The latter serves to supply the stock solution and divided into two sections of the same volume along the entire length by a vertical partition 21, creating a manifold for the flow of the stock solution 28. It contains the grid turbulizers 8, into which the tubes 40 are interlaced. The tubes 40 do not touch the surfaces of the neighboring cathode and anode membranes 26 and 6.

The circuit with the supply to the apparatus of electric current is needed only in the case when it is necessary to extract cations and anions of substances from the solution in different ways (it is used in separation of potassium, phosphorus, sulfates, phosphates). When moving, the solution in the first separation circuit is turbulized by means of the grid turbulizer 9 (Figure 1) and reaches the cathode and anode membranes 26 and 6.

Simultaneously with the supply of the stock solution (Figure 1, 2), through the opening 42 and the connection 41, the cooling water is fed to the lid 29 and supplied to the distributing channel 45, where it is dispersed through the tubes 40. Then it flows into the collecting channel 46, and then it is removed from the apparatus through the opening 44 and the outlet of the cooling water 43 located on the lid 35.

The solution, flowing through the channel 34 (Figure 1) gets concentrated and enters the retentate manifolds 10, and then it is discharged through the opening 27 on the lid 35, into which the retentate discharge fitting 13 is screwed.

The solution supplied through the openings 23 into the lid 35 and the latch 37 gets concentrated in the manifold for the solution flow 28 (Figure 1) and then it is discharged through the opening 22 in the latch 37 and the lid 29, into which the retentate fitting 12 is screwed.

The stock solution, flowing through the channel 34 and the manifold for the solution flow 28 (Figure 1), is consecutively concentrated.

The area of the membrane for the first circuit is calculated as follows:

$$S_{\text{apparatus } 1} = k_1 \cdot l \cdot b, \quad (2)$$

The area of the membrane for the second circuit is calculated as follows

$$S_{\text{apparatus } 2} = k_2 \cdot l \cdot b, \quad (3)$$

The total area of the membrane for the first and second circuits is calculated by the formula (4)

$$S_{\text{apparatus}} = l \cdot b \cdot (k_1 + k_2), \quad (4)$$

where l , b is the membrane length and width, respectively; $k_{1,2}$ are the number of the membrane tapes in the first and second circuits, located as the active layer to the solution to be separated.

Thus, the total specific flux for the device presented in the design is calculated by the formula (5):

$$J = \frac{V}{l \cdot b \cdot (k_1 + k_2) \cdot \tau}. \quad (5)$$

The developed membrane device (Figure 1) can be used for concentration of biological solutions, for example, in the separation and concentration of solutions manufactured at JSC BIOCHEM in Rasskazovo.

References

1. *Dytneriskij Ju.I.* Reverse osmosis and ultrafiltration. M.: Himija, 1978. 352 p.
2. *Kornienko L.V.* The study of membrane methods for processing distillery grains wastes. Avtoref. dissert... k.t.n. Kiev. 2015. 22 p.
3. *Pervov A.G., Andrianov A.P., Jurchevskij E.B.* Improving the design of membrane devices // Water supply and sanitary engineering. 2009. № 7. P. 62-68.

ION-SELECTIVE AND ELECTROCHEMICAL PROPERTIES OF CARBON COATED ALUMINA NANOFIBER MEMBRANES

¹Denis Lebedev, ¹Alexey Shiverskiy, ^{1,2}Mikhail Simunin, ¹Victoria Bykanova, ¹Vera Solodovnichenko, ¹Ilya Ryzhkov

¹Institute of Computational Modeling SB RAS, Krasnoyarsk, Russia, *E-mail: lebedev@icm.krasn.ru*

²Molecular Electronics Department KSC SB RAS, Krasnoyarsk, Russia

Introduction

In recent years, there has been a growing interest in studying the separation of ionic solutions with a help of various types of membranes. In this work, we have proposed a new type of ceramic membranes based on a unique Nafen™ material. This material is represented by highly aligned alumina nanofibers of 10–15 nm in diameter. The membranes are prepared by filtration of nanofiber suspension through a porous support followed by drying and sintering [1]. The selectivity is achieved by depositing carbon on the nanofibrous structure in the CVD reactor. The main aim of this work is to investigate ionic selectivity and electrochemical properties of the prepared membranes (C-Nafen membrane).

Experimental

The ion permselectivity of prepared membranes was studied by measuring the potential difference between two electrolyte solutions with different concentrations separated by a membrane. Measurements were carried out in the laboratory made electrochemical cell consisting of two compartments (half-cells), between which the membrane is clamped with the help of connection rods and nuts. The scheme of experimental setup is shown in Fig. 1.

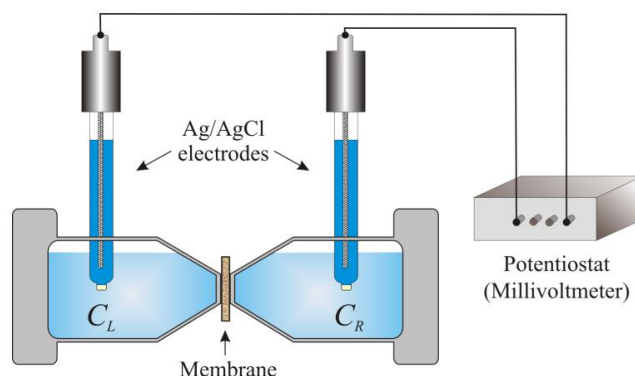


Figure 1. The scheme of electrochemical cell and experimental setup.

The measurements were performed in KCl aqueous solution. First, the solution with fixed concentration was placed in both half-cells. The system was kept at room temperature of 25 °C during 12 hours. The measurements were performed by increasing the concentration of KCl in the left half-cell by consecutive addition of the KCl concentrate (1M or 4.2M). The Nernst equation with transference is used for interpretation of experimental data and calculation the transfer numbers [2]. Moreover, the model of Teorell, Meyer and Sievers (TMS) [3] is employed to determine the surface and volume density of fixed charge.

The electrochemical stability of C-Nafen membranes was studied by cyclic voltammetry (CVA) in a three-electrode electrochemical cell. The working as well as counter electrodes were represented by fragments of C-Nafen membranes due to their large specific surface area. The potential was applied to the cell by Potentiostat PI-50Pro (ELINS Ltd., Russia).

Result and discussion

A typical cyclic voltammogram for C-Nafen membrane in 0.1 M KCl aqueous solution is shown in Fig. 2a. The value corresponds to the ‘broken circuit’ potential. In the range of applied voltages from –0.5 V to +0.8 V, no waves corresponding to redox reactions was observed. This behavior is typical for carbon materials [4]. Note that the preliminary blowing of inert gas through the electrolyte can extend the electrochemical stability range to –0.8 ... +1.0 V due to removal of adsorbed oxygen. Measurements confirm that the C-Nafen membrane behaves like an ideally

polarized electrode, which opens the principle possibility of using it for switchable ion-transport selectivity. In our work, the specific electrical capacitance of C-Nafen membranes was studied by various electrochemical methods. It was shown that the specific capacitance value is in the range of 6–10 $\mu\text{F}/\text{cm}^2$, which is quite typical for surfaces with a specific area of 100–150 m^2/g .

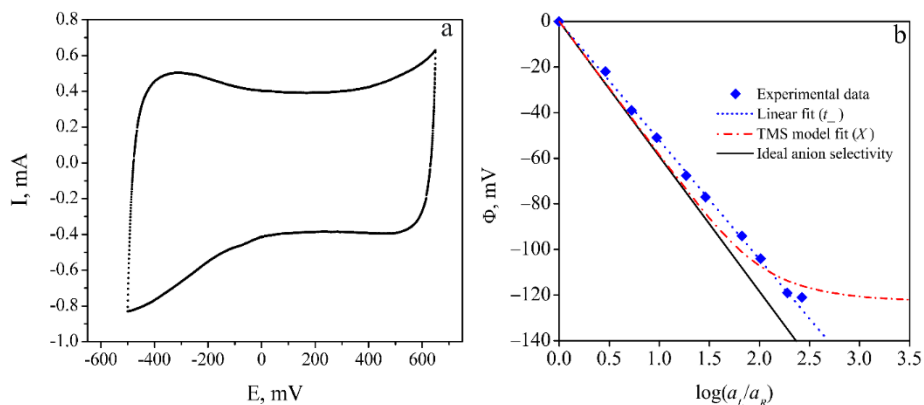


Figure 2. a – Cyclic voltammogram of C-Nafen membrane in 0.1 M KCl aqueous solution. Scan rate is 1 mV s^{-1} ; b – The dependence of membrane potential Φ on the logarithm of activities ratio for C-Nafen membrane.

We have studied the ionic selectivity of C-Nafen membranes by measuring the EMF of electrochemical cell consisting of two half-cells with different KCl concentrations. The concentration in the right half-cell (C_R) was fixed, while the concentration in the left half-cell (C_L) was varied from C_R up to 4.2 M. The experimentally determined membrane potential for the C-Nafen membrane shown in Fig. 2b gives evidence of high anion selectivity with transference numbers $t^+=0.05$, $t^-=0.95$. In Fig. 2b, the horizontal axis is represented by the decimal logarithm of activities ratio in the left and right half-cells. Activities were calculated from activity coefficients reported in [5]. The density of membrane fixed charge was determined from one-parameter fits of TMS model. The volume and surface charge density for constant concentration $C_R = 10 \text{ mM}$ were 1021.1 mM and $394.0 \cdot 10^{-3} \text{ C m}^{-2}$, respectively. The deposition of carbon layer changes the interaction of membrane surface with the electrolyte solution. The ions preferably bind on the structural defects of carbon layer. Modelling of Na^+ и Cl^- adsorption on the carbon surface reveals that the preferable adsorption of alkali metal is observed in this case. Thus, we conclude that the adsorption of alkaline metal ions leads to the increase of membrane charge, and, consequently, improves the selective properties of membrane.

The ion-selective and electrochemical properties of the produced membranes make them potential candidates for applications in nano- and ultrafiltration. Another important application is related to switchable ion-transport selectivity. Preliminary experiments have shown that the ionic conductivity of membrane can be varied by applying a potential to the conductive membrane surface.

This work is supported the Russian Science Foundation, Project 15–19–10017.

References

1. Lebedev D.V., Shiverskiy A.V., Simunin M.M., Solodovnichenko V.S., Parfenov V.A., Bykanova V.V., Khartov S.V., Ryzhkov I.I. Preparation and Ionic Selectivity of Carbon-Coated Alumina Nanofiber Membranes *Petroleum Chemistry*, 2017, Vol. 57, P. 306–317.
2. H. Strathmann. Introduction to membrane science. Germany: Wiley–VCH, Weinheim. 2011. 524 p.
3. Y. Tanaka. Ion exchange membranes: fundamentals and applications. Amsterdam: Elsevier. 2015. 522 p.
4. A. Yu, V. Chabot, J. Zhang. Electrochemical supercapacitors for energy storage and delivery: Fundamentals and Applications. Boca Raton: CRC Press. 2013. 373 p.
5. Lide D.R. Handbook of Chemistry and Physics 84th Edition, CRC press, Boca Raton, 2003 – 2004.

MATHEMATICAL MODEL OF ION TRANSPORT THROUGH THE INTERFACE: THE ION EXCHANGE MEMBRANE / STRONG ELECTROLYTE

¹Konstantin Lebedev, ¹Victor Zabolotsky, ¹Nikolay Sheldeshov, ²Vera Vasil'eva, ¹Michail Kasparov

¹Kuban State University, Krasnodar, Russia, E-mail: klebedev.ya@yandex.ru

²Voronezh State University, Voronezh, Russia

Introduction

The article presents a mathematical model of the ion transport across exchange membrane/solution phase boundary. The border is considered as extended in space object with all the properties which are inherent in the physico-chemical phases. It is regarded as a special physico-chemical environment having a distributed exchange capacity, which causes the spatial charge and, dissociation of water molecules. The size of this object is estimated in the range of 1-300 nm. The surface morphology of industrial membrane type MK-40, MA-41 and MA-41P was investigated experimentally by scanning electron microscopy. The amplitude of average surface roughness was analyzed. In this work, the reaction layer is modeled as a region formed by the topography and morphology of the membrane. The properties of the membrane are dictated by the properties of the solution and the properties of the membrane in contact. To determine the dependence of $Q(x)$ the procedure is proposed for estimating the proportion of hard phase in the total volume, which can be judged by surface membrane microprofile. In the model the height of the micro inhomogeneities determines the zone of the reaction layer. Influence of surface morphology on the V-A characteristics and the sizes of the convective instability of cation-exchange membrane evaluated numerically simulating the hydrodynamic flow conditions using a solution of the Navier – Stokes equations. The transfer of a strong electrolyte such as NaCl ions through the thin layer of the reaction layer is considered. The place of nanomodel in the structure of a three-layer membrane system is showed.

Theory

Figure 1 shows the system consisting of diffusion layer, membrane and thin reaction layer placed in the membrane where the decomposition of molecules of water occur. In the system the ions are present: 1 – Na^+ , 2 – Cl^- , 3 – H^+ , 4 – OH^- .

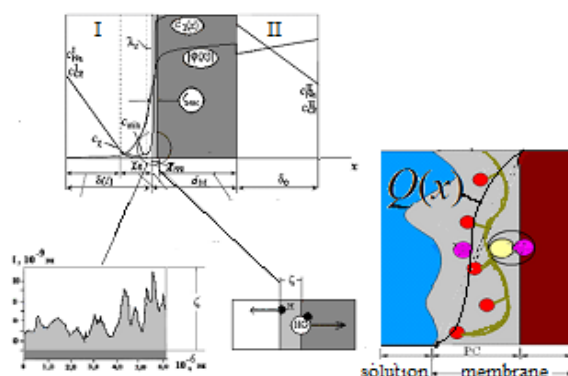


Figure 1. Schematic drawing of a three-layer ion exchange membrane system, consisting of diffusion layers and membranes: diffusion layer I has quasielectrostatic region and the region of spatial charge χ_s ; a diffusion layer II is electroneutral

Model can be represented as a system of 10 differential equations [1, 2]. Ten boundary conditions were defined in terms of Dirichlet.

Experiments

In this work, the reaction layer (RL) of the membrane surface is modeled as the area formed by the topography and morphology of the membrane. Properties of the RL are determined by the properties of the solution and the properties of the membrane which is in contact with the solution. In the swollen state the macropores and the structure defects are filled with a solution. Elementary

volume of the RL contains water, ion exchange and inert material. When moving across RL from solution phase to the membrane phase content of the solution decreases, and the effective exchange capacity increases.

The height of the microheterogeneities of the membrane surface (Figure 2) defines in the framework of the model the zone of the reaction layer.

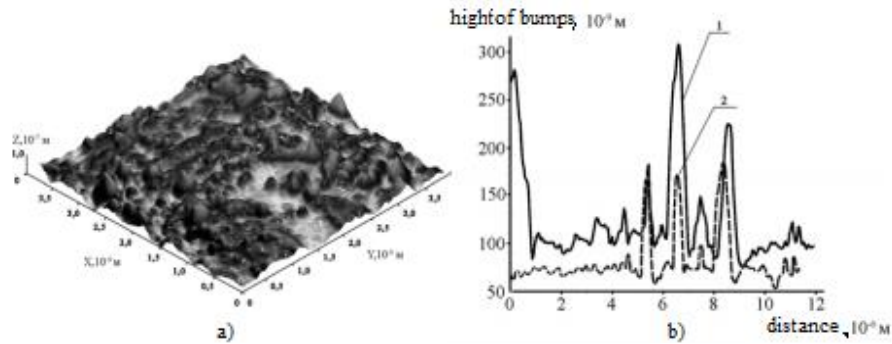


Figure 2. Surface 3D image (a) and the microprofile of cation exchange membrane MK-40 surface (b), measured by atomic force microscopy. The scanned field is $4 \mu\text{m} \times 4 \mu\text{m}$ (a) and $10 \mu\text{m} \times 10 \mu\text{m}$ (b). Dashed line is microprofile of the sample after conditioning, the solid line is microprofile of the sample after high-intensity current operation modes

For determining the dependence of $Q(x)$ the procedure for estimating the fraction of hard phase in the total volume is proposed. Solid phase fraction can be estimated by the vertical micro-profile line of the cross section of the membrane surface Figure 3.

Results and Discussion

The concentration of cations of Na^+ is comparable to the exchange capacity of the membrane, whereas the ion concentration products of decomposition of water molecules by four orders smaller.

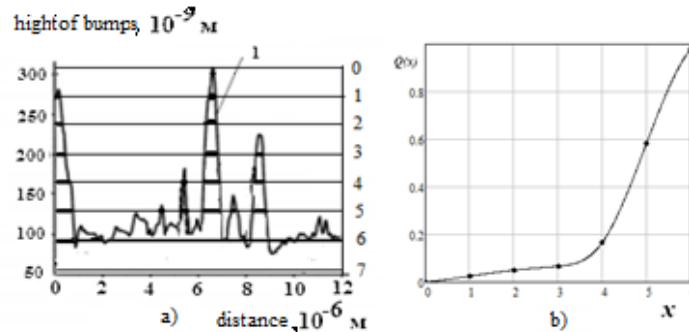


Figure 3. Sections (0-7) of the membrane microprofile in which the fractional volume of the solid phase is calculated (a). The volume fraction of the solid phase depending on the layer number (b). Layers divide the whole length (from 0 to 300 nm) of the layer on 7 segments (built according to the Table 1)

Table 1: Dependence of the volume fraction of the solid phase on the layer number

Layer number	1	2	3	4	5	6	7
Volume fraction of the solid phase	0.025	0.050	0.067	0.167	0.583	0.980	1.000

Comparison of distributions of concentrations, ion exchange capacity, and space charge leads to conclusion that positively charged ions bring the main contribution in formation of the space electric charge being the algebraic sum of cations', anions' and fixed charges.

Regularities in the behavior of space have been investigated. Numerical calculations are performed for the thickness of the nanolayer in the range from 1 to 40 nm.

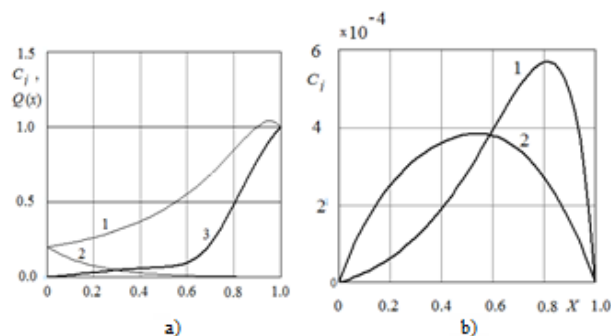


Figure 4. The dimensionless concentration profiles of Na^+ (1), Cl^- (2), Q (3) (a) and H^+ (1), OH^- (2) (b) in nanolayer

The shape of the space charge and its integral value were studied. The distribution of the space charge ρ is determined by the membrane potential and ion concentration distribution and can be varied depending on the distribution capacity ion exchange of material, surface morphology. The numerical calculations represented in Figure 5.

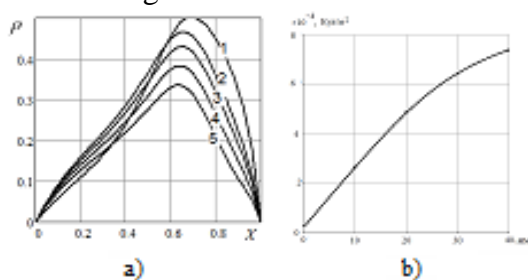


Figure 5. The distribution of the dimensionless density of space charge at different thickness of the nanolayer, nm: 1 - 1, 2 - 10, 3 - 20, 4 - 30, 5 - 40 (a). The dependence of the integral surface charge density on the thickness of the nanolayer (b)

The figure shows that the shape of the space charge distribution is slightly differed on the thickness of the nanolayer, the maximum value is reduced, almost not moving, remaining in a neighborhood of the point $X = 0.65$. However, the integral value $\bar{\rho} = \int_0^L \rho dx$ increases as the layer thickness increases. At the distances about 40 nm, the charge density does not exceed 10^{-3} C/m^2 .

The model also allows to investigate the dependence of the fluxes of ions through the layer; current-voltage curves for the given input parameters of the model. The fluxes of ions being generated due to water dissociation change their values with the thickness of the layer, however, the current density in every point of the layer remains constant.

Acknowledgments

The present work is supported by Russian Foundation for Basic Research and the Administration of the Krasnodar region (project № 16-48-230433).

References

1. Lebedev K., Zabolotsky V., Sheldeshov N., Vasileva V., Vasilenko P., Kasparov M. Mathematical modeling of overlimiting current regime of electro dialysis cell. Diffusion and reaction layer // International conference "Ion transport in organic and inorganic membranes" Krasnodar-Sochi / Russia, 23-28 May 2016. P. 173-176.
2. Zabolotskii V.I., Lebedev K.A., Sheldeshov N.V., Vasileva V.I., Kasparov M.A. Mathematical model of ion transport through the interface: the ion exchange membrane / strong electrolyte // Polythematic online scientific journal of Kuban State Agrarian University (Scientific Journal of KubSAU) [Electronic resource]. – Krasnodar: KubSAU, 2016. – № 124 (10). <http://ej.kubagro.ru/archive.asp?n=124>

COMPETITIVE ELECTROMASS TRANSFER OF CATIONS OF HYDROGEN AND PHENYLAMMONIUM THROUGH THE PERFLUORATED MEMBRANE MF-4SK

Natalia Loza, Nazar Romanyuk, Sergey Loza

Kuban State University, Krasnodar, Russia, E-mail: nata_loza@mail.ru

Preparation of composites based on perfluorinated membranes and polyaniline with predetermined properties requires intercalation of an optimum amount of the modifier [1]. To develop an approach to the quantitative determination of the content of polyaniline in the composites obtained under external electric field [2] that is necessary to study the transfer of aniline and background acid through the membrane. Therefore, the aim of this paper is to study the competitive electromass transfer of cations of hydrogen and phenylammonium through the perfluorinated membrane MF-4SK.

Competitive transfer was studied in a laboratory electrolysers (Figure 1), which consists of 8 alternating membranes MA-41 and 7 membranes MF-4SK. The size of the working area of the membranes was $5 \times 20 \text{ cm}^2$, the distance between the membranes was 0.1 cm. The experiment was carried out in galvanostatic mode at a current density of 1 A/dm^2 , the flow rate through each chamber was 12 l/h. Initially, the aniline was only in the desalting chamber (DC), in an amount of 0.01 mol/l with the presence of 0.025 mol/l of background sulfuric acid. The electrode chamber and the concentration chamber (CC) contained 0.025 mol/l sulfuric acid solution. The volume of solutions circulating through DC and CC was 20 l.

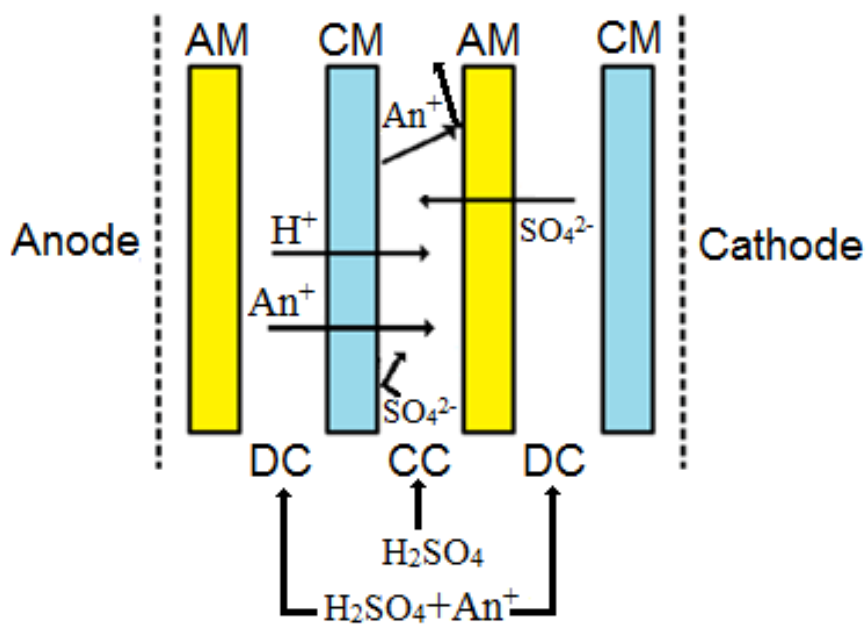


Figure 1. Scheme of competitive electromass transfer of hydrogen cations and phenylammonium: AM – anion-exchange membrane; CM – cation-exchange membrane; An^+ – phenyl ammonium cation

Sampling was carried out at the inlet and outlet of DC and CC, while the pH of the solution was determined, as well as the concentration of aniline, which was determined by the photometric method.

Analysis of the data of change in concentration of the aniline in the electrolysers chambers showed that aniline in the concentration chamber does not appear immediately, but approximately 30 min after the start of the experiment (Fig. 2).

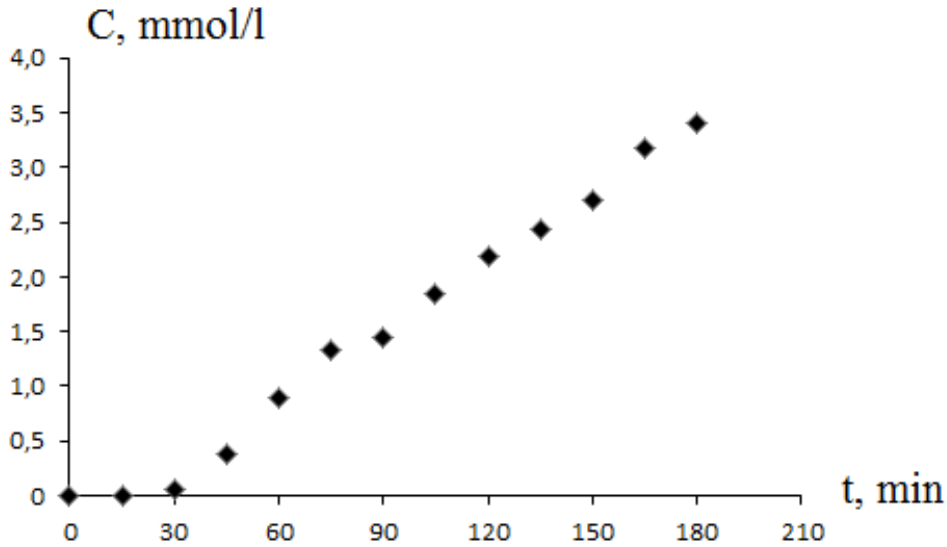


Figure 2. Time dependence of aniline concentration at CC outlet

This may be due to the sorption of aniline by a cation-exchange membrane during the initial stage of the experiment. Analyzing the difference of concentrations at the inlet and outlet of DC and CC by equation (1), it was determined that the aniline was sorbed in the membrane in an amount of 1.4 mmol/dm²:

$$q = \frac{V \cdot (C_s^{DC} - C_f^{DC} - C_f^{CC})}{b \cdot S} \quad (1)$$

where q – amount of sorbed aniline in the membrane (mmol/dm²); V – volume (l); C_s^{DC} – initial concentration of aniline in DC (mmol/l); C_f^{DC} – final concentration of aniline in DC (mmol/l); C_f^{CC} – final concentration of aniline in CC (mmol/l); b – number of membranes MF-4SK; S – area of the membrane (dm²).

According to the received data, the mass transfer coefficient and current efficiency were calculated by the equations:

$$K = \frac{(C_0 - C) \cdot w}{C_0 \cdot S \cdot n} \quad (2)$$

$$\eta = \frac{(C_0 - C) \cdot F \cdot w \cdot z}{I \cdot n} \quad (3)$$

where C_0 – concentration at the entrance to the chamber (mol/l); C – concentration at the outlet of the chamber (mol/l); w – flow rate (dm³/h); S – area of the membrane (dm²); n – number of desalting chambers; F – Faraday number (A·h/mol); I – current (A); z – is the valence number of substance ions.

The dependence of the current efficiency and the mass transfer coefficient of the cation of phenylammonium and sulfuric acid on time, with the condition of the ideally selective membrane is shown at Fig. 3.

Analysis of the dependence of the current efficiency from time shows that the transport numbers for hydrogen cations are 4-6 times greater than for phenylammonium during competitive mass transfer (Fig. 3, a). Analyzing the data of the mass transfer coefficient from time, it can be seen that the hydrogen cations are transported through the investigated membrane 1.5-2 times more intensively than the phenylammonium cations in the organic-mineral mixture (Fig. 3, b).

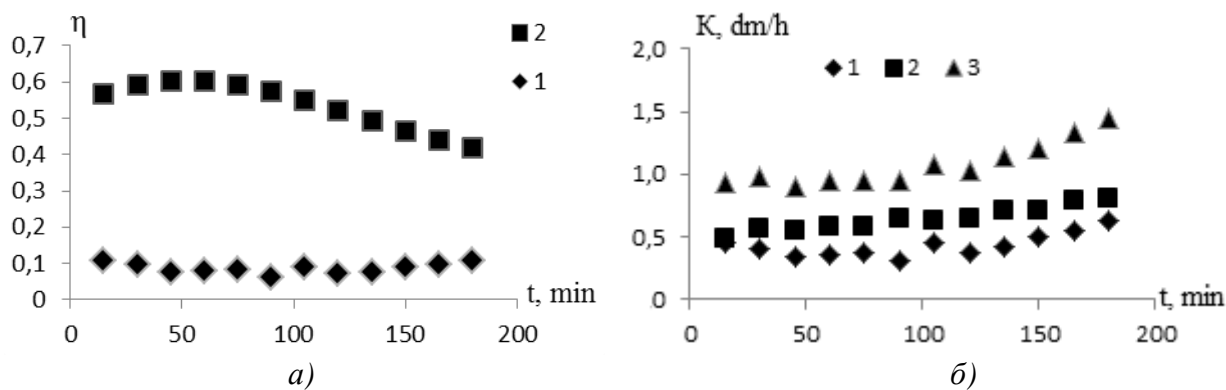


Figure 3. Dependence of current efficiency (a) and mass transfer coefficient (b) for DC from time of electro dialysis desalination of a mixture of 0.025 M sulfuric acid solution and 0.01 M aniline: 1 - data for aniline; 2 - data for sulfuric acid; 3 - summary data for the organic-mineral mixture

Conclusions

A study of the competitive electro-mass transfer of cations of hydrogen and phenylammonium through the perfluorinated membrane MF-4SK at a current density of 1 A/dm² was investigated. It was found that the phenylammonium cation, in contrast to hydrogen, is transported through the membrane less intensively and appears in the CC not immediately, but after some time, while the transfer numbers for the phenyl ammonium cations are 4-6 times lower than for the hydrogen cations during the electro dialysis of the organic-mineral mixture.

This work was supported by Russian Foundation for Basic Research, grant № 16-08-01125 A.

References

1. Yaroslavtsev A.B., Nikonenko V.V. // Nanotechnologies in Russia. 2009. Vol. 4. № 3. P. 33–53.
2. Kononenko N.A., Loza S.A., Loza N.V. // Pat. RU № 2566415, № 2014129703/05, 18.07.2014; publ. 27.10.2015.

ENERGY GENERATION BY REVERSE ELECTRODIALYSIS

Sergey Loza, Kristina Dmitrieva, Alexander Korzhov, Natalia Loza, Victor Zabolotsky
Kuban State University, Krasnodar, Russia, E-mail: s_loza@mail.ru

Introduction

Recently, there has been a sharp increase in interest in the problem of direct conversion of the salt concentration gradient between salt and fresh water into electricity using reverse electrodialysis (RED), which is associated with an increased demand for alternative and autonomous energy sources. The gradient of salt concentration in the sea and river water separated by an ion-selective membrane leads to the formation of a potential difference. In a cell consisting of alternating cation and anion exchange membranes, between which salt and fresh water flows, the potential difference arising on the membranes is summed and can be used as an energy source.

The first work devoted the production of electricity by RED was published more than half a century ago [1], but there are still no industrial installations for reverse electrodialysis. Thermodynamic calculation shows that when mixing 1 m³ of river water with 1 m³ of sea water, 1.4 MJ of energy (0.4 kW·h) can be obtained. Theoretically, when mixing all the river water on the Earth from the sea, it is possible to obtain 2400 GW of electric power from which 1000 GW can technically be used [2, 3]. In Russia in 2012, the total capacity of power plants was 223 GW.

The wide practical application of the EDR process is hindered by the low specific power of the process, high capital costs and high cost of electricity received [4, 5].

The efficiency of obtaining electricity by reverse electrodialysis can be improved by using membranes with a profiled surface. The use of such membranes allows to exclude the inert spacer between the membranes and to reduce the costs of pumping the solution by several times, which positively affects the overall efficiency of the process [6]. Also, the increased surface area has a positive effect on the process efficiency. Therefore, it is necessary to use highly efficient and inexpensive membrane materials for EDR. Such a materials can be heterogeneous ion-exchange Russian membrane, which are cheap, non-toxic, and technologically advanced. Also promising is the use of profiled membranes with a homogenized surface [7]. Such membranes have a higher active surface and low hydrophilicity of the surface, which is very important under conditions of reverse electrodialysis.

The aim of the work is to develop the scientific basis for obtaining electrical energy from a renewable source using the reverse electrodialysis method using ion-exchange materials consisting of polyelectrolyte surface films and matrixes from profiled heterogeneous membranes.

Experiments

To obtain the electric power, an experimental setup containing an electrochemical power generator was assembled. The electrochemical generator contained 5 pairs of alternating cation- and anion-exchange membranes. Commercial membranes MC-40 and MA-41 were used as well as profiled membranes based on them. Work area of each membrane was 5x20 cm². The electrodes was made from titanium and covered by platinum. When pumping the salt and fresh water through the cell the Donnan potential appears. Such a voltage can be used to get the electric energy when a reversible redox reaction goes on electrodes with are introduced at both ends of the membrane stack. This reaction need to convert the ionic current into electrical current As the RedOx system, an equimolar mixture of potassium ferro- and ferricyanide was used. The reaction on the electrodes: $Fe(CN_6)^{3-} + e \leftrightarrow Fe(CN_6)^{4-}$. The working solution were:

1. Model solution of river water – 1 g/l NaCl.
2. Model solution of salt water - saturated NaCl solution.
3. Electrode chamber solution – 0.025 M K₃Fe(CN)₆, 0.025 M K₄Fe(CN)₆ and 0.25 M NaCl

When no load applied to the cell the maximum voltage can be observed (open circuit voltage). On the contrary, in case of a short circuit, the maximum current flows through the cell with an extremely low potential. In the medium current load the maximum power can be obtained.

Results and Discussion

With a high load resistance, the current generated is small enough, and conversely, with a small load resistance, the current increases, but a significant drop in the generated potential difference is observed. Thus, the curves of the generated power pass through a maximum. Analysis of the curves in Figure 1 allows us to conclude that the use of profiled membranes allows to increase the power of the electrochemical generator by 30%.

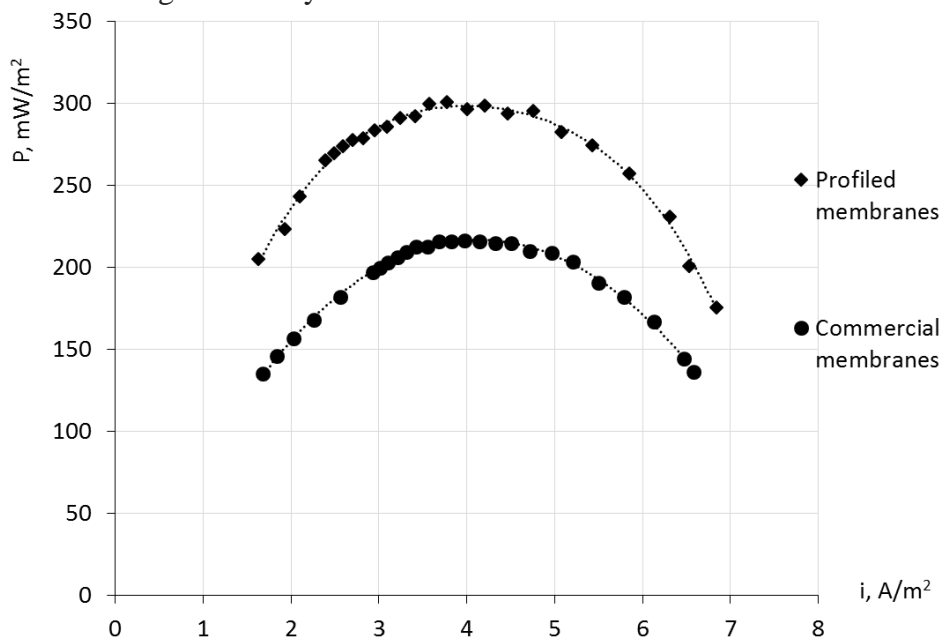


Figure 1 Dependence of specific electric power of load current

Conclusions

Within the framework of this work a laboratory installation was created, which allows obtaining power characteristics of reverse electro dialysis units. Preliminary results of the study of reverse electro dialysis using commercial ion-exchange membranes and profiled bilayer membranes based on them were obtained. It is shown that the use of profiled bilayer membranes makes it possible to increase the specific power of a laboratory electrochemical energy generator by 30%. Due to the increased hydrophobicity of the surface of profiled bilayer membranes, the biofouling of their surface should decrease in case of working on natural river water.

Acknowledgment

The present work is supported by the Ministry of Education and Science of Russia within the framework of the base part project №10.9572.2017/BP.

References

1. *Pattle R.E.* // Nature 1954, 174, (4431), 660-660.
2. *Kuleszo J., Kroeze C., Post J. W., Fekete B. M.* // Journal of Integrative Environmental Sciences 2010, 7, (S1), 89-96.
3. *Kuleszo J.* // MSc thesis Wageningen University, 2008.
4. *Veerman J., Jong R.M.D., Saakes M., Metz S.J., Harmsen G.J.* // Journal of Membrane Science, 2009, 343, (1-2), 7-15.
5. *Post J.W., Goeting C.H., Valk J., Goinga S., Veerman J., Hack P.J.F.M.* // Desalination and water treatment, 2010, 16, 182-193.
6. *Vermaas D., Saakes M., Nijmeijer K.* // Journal of Membrane Science, 2011, 385-386, 234-242.
7. *Loza S.A., Zabolotsky V.I., Loza N.V., Fomenko M.A.* // Petroleum Chemistry 2016, Vol. 56, Iss. 11, pp 1027-1033.

HYDROGEN PRODUCTION VIA METANOL STEAM REFORMING WITH THE USE OF MEMBRANE CATALYSIS

Aleksandra Lytkina¹, Natalia Orekhova¹, Margarita Ermilova¹, Ilya Petriev², Mikhail Baryshev², Andrey Yaroslavtsev¹

¹Topchiev Institute of Petrochemical Synthesis RAS, Moscow, Russia, *lytkina@ips.ac.ru*

²Kuban State University, Krasnodar, Russia

Introduction

Continuous production of ultra-pure hydrogen for utilizing in downstream Polymer Electrolyte Membrane Fuel Cells (PEMFC) for small or medium scale applications has grown increasing interest, in recent decade. Methanol may be the appropriate feedstock for mentioned applications. It is known that the methanol steam reforming (MSR) reaction proceeds with high efficiency under mild conditions at a temperature of 250-320 C and atmospheric pressure [1].

The used catalytic systems for the most part are presented by a metal catalyst and a support. Metals from the VIIB-group are often used as the catalysts, characterized by the high activity and the selectivity towards hydrogen. One of the ways to improve the stability and to reduce the cost of such catalysts is an addition of a second metal [2,3]. An importance of a support choice is highlighted by an essential dependence of the products yields and the process selectivity on its nature and even structure. New fine carbon materials are of great interest. The unique properties of these materials make them appropriate for the use as the catalyst supports [4].

Nevertheless, the main drawback of this reaction system is represented by the CO formation, because it can poison the PEMFCs anodic catalyst. The problem of high purity hydrogen production can be successfully solved in the case of using of membrane catalysis by selective removal of hydrogen.

The goal of the work was to develop new active and selective zirconia and carbon-based nanostructured bimetallic catalysts for MSR and to test obtained catalyst in a conventional (CR) and membrane (MR) reactors.

Experimental

New bimetallic (Ru-Rh, Cu-Ni) nanostructured catalysts were obtained on different carbon (detonation nanodiamond (DND), carbon black “Vulcan”, IR pyrolysed polyacrylonitrile, carbon black Ketjenblack EC-600JD, carbon SIBUNIT) supports by electrolyses deposition methods and tested in conventional tubular flow reactor and membrane reactor for H₂ production by MSR (fig.1). MR represented a flow system with a plane Pd-containing membrane. Dense Pd-Ru (6%) membrane and Pd-Ag (23%) were used owing to its full hydrogen permselectivity. The Pd-Ag (23%) membrane was modified by finely-divided palladium coating, formed by magnetron sputtering method. Obtained catalysts were characterized by BET, XRD, TEM methods. TEM image of Ru-Rh/SIBUNIT catalyst (fig.2) shows that an average size of metal particle is of ~ 5 nm.

Table 1: Supports surface area

Support	BET surface area, m ² /g
DND	286±3
Vulcan	200±3
IR PAN	1880±3
Ketjenblack EC-600JD	1300±3
SIBUNIT	495±3

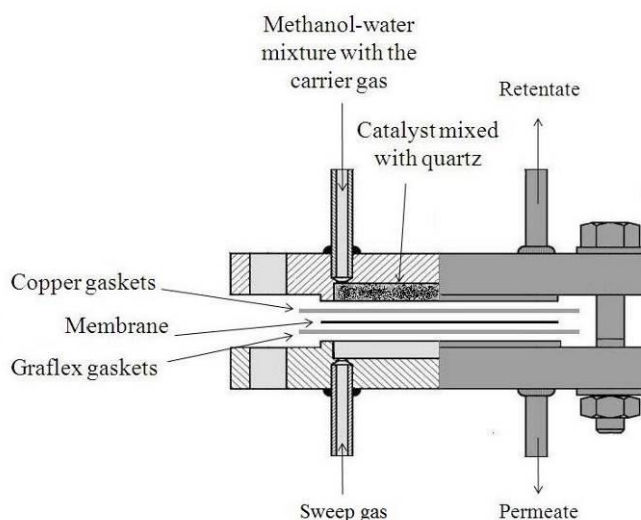


Figure 1. Scheme of the membrane reactor used during the work

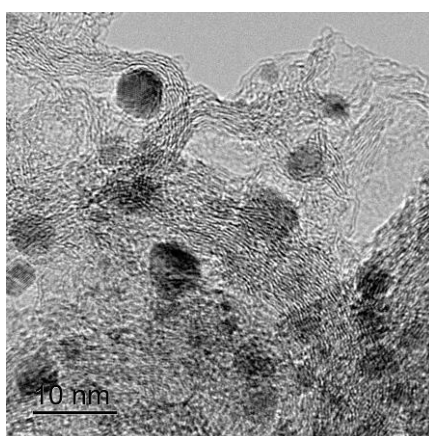


Figure 2. TEM image of Ru-Rh/SIBUNIT catalyst (the arrows shows a metal particle)

Results and discussion

All obtained catalysts are active in MSR reaction. It was shown also, that activity of catalysts and products distribution depends on metal type, support structure and surface area. Effect of a support was investigated for Ru-Rh system. It was shown that DND displays higher hydrogen productivity. Maximum amount of hydrogen at 300 - 310 °C was obtained on the DND supported catalyst, which is 2.3 moles from 3 theoretically possible. Ru-Rh system is more active than Cu-Ni as it is shown on the example of catalysts supported on DND.

Comparative study of the CR and MR with two different membranes was occurred. The effect of investigated catalysts on the MR performances as well as a general comparison of the experimental results was considered. Obtained results demonstrate the ability of the membrane to promote the MSR reaction. Selective hydrogen recovery from the reaction zone shifts the position of equilibrium to the product side and improves conversion of methanol (table 2). The use of the Pd-Ag modified membrane allows to increase hydrogen recovery in 10%.

In case of all catalysts the decrease of CO quantity takes place in MR (fig 3). The hydrogen stream produced from the membrane reactor is ultra pure: especially, it is CO-free and then suitable to be directly fed to a polymer electrolyte membrane fuel cell.

Table 2: Methanol conversion in conventional and membrane reactors

T=350°C	CR	MR (Pd-Ru)	MR (Pd-Ag)
Ru-Rh/DND	82	94	95
Ru-Rh/PAN	75	80	84
Ru-Rh/Vulcan	48	66	70

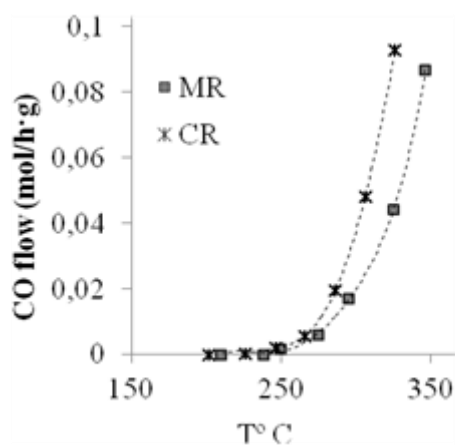


Figure 3. Carbon monoxide yield on Ru-Rh/DND in the CR and MR

This investigation was financial supported by the Russian Ministry of Education and Science (Ref. N°RFMEFI58617X0053), Russia, and CNRS, France (project N° 38200SF).

References

1. Iulianelli A., Ribeirinha P., Mendes A., Basile A. Methanol steam reforming for hydrogen generation via conventional and membrane reactors: A review / Renewable and Sustainable Energy Reviews. 2014, 29, 355-368.
2. Sa S., Silva H., Brandao L., Sousa J.M., Mendes A. Catalysts for methanol steam reforming – A review / Appl. Catal. B: Environmental. 2010, 99, 43-57.
3. Lytkina A.A., Zhilyaeva N.A., Ermilova M.M., Orekhova N.V., Yaroslavtsev A.B. Influence of the support structure and composition of Ni–Cu-based catalysts on hydrogen production by methanol steam reforming./ Int.J.Hydrogen energy. 2015, 40, 9677–9684
4. Deng W., Liu M., Tan X., Zhang Q., Wang Y. Conversion of cellobiose into sorbitol in neutral water medium over carbon nanotube-supported ruthenium catalysts. Original Research Article / J. Catal. 2010, 271, 22-32.

IONIC CONDUCTIVITY OF POLYNAPHTHALENEIMID MEMBRANES MODIFIED WITH SILICA

¹Sofia Makulova, ¹Yulia Karavanova, ¹Andrey Yaroslavtsev, ²Igor Ponomarev

¹Kurnakov Institute of General and Inorganic Chemistry of the Russian Academy of Sciences (IGIC RAS), Moscow, Russia, E-mail: akula149@rambler.ru, yuka86@mail.ru, yaroslav@igic.ras.ru

²A.N.Nesmeyanov Institute of Organoelement Compounds of Russian Academy of Sciences (INEOS RAS), Moscow, Russia

Introduction

The development of hydrogen fuel cell is one of the most advanced areas of focus in the modern science. This fuel cell works effective only at a high temperature, because the catalyst become poisoned at a low one. But the high temperature and low humidity lead to degradation of ionic conduction of exist membranes. So creation and research the membrane materials which are stable under such conditions is a relevant objective of the modern science. One of the most effective ways of membrane modification is synthesis of inorganic nanoparticles into pores of the membrane material.

Experiments

Objectives: polynaphthaleneimid membrane doped with nanoparticles of silica with sulphurized surface (in situ, with surface modification under different acidity – pH0, pH2 and by casting with modified nanoparticles). The measurements were made at the temperature 30 — 200°C, in water at the temperature 30 — 90°C and under different humidity at the temperature 30 — 90°C.

Results and Discussion

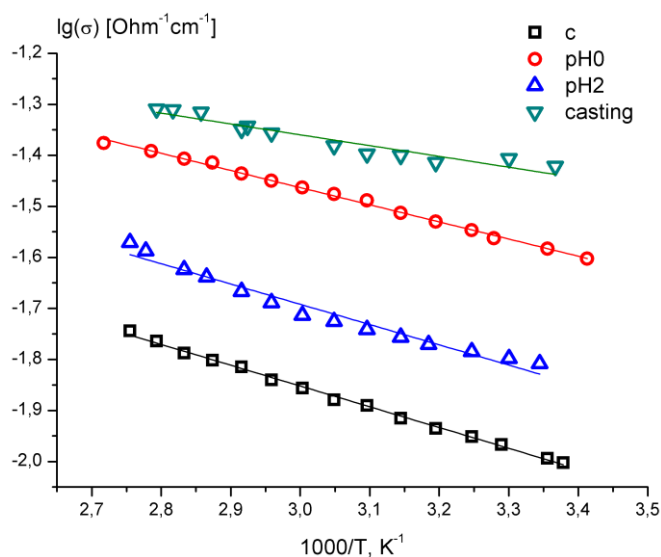


Figure 1. Ionic conductivity of polynaphthaleneimid membrane doped with silica in water medium.

Doping of polynaphthaleneimid membrane material by casting with nanoparticles of silica maximize the transport ability of the membrane in water medium (Fig.1). It should be also noted that surface modifying with high concentration of acid is more effective as opposed to high-temperature measuring.

Doping of the polynaphthaleneimid membrane material with nanoparticles of silica increase ionic conductivity of the material under low humidity (Fig. 2). It should be noted that surface modifying with low concentration of acid is more effective than with the higher one. The material made by casting doesn't increase the ionic conductivity under such conditions but decrease the activation energy of ion transfer. Inference should be drawn that *in situ* modifying increases the water content of the material.

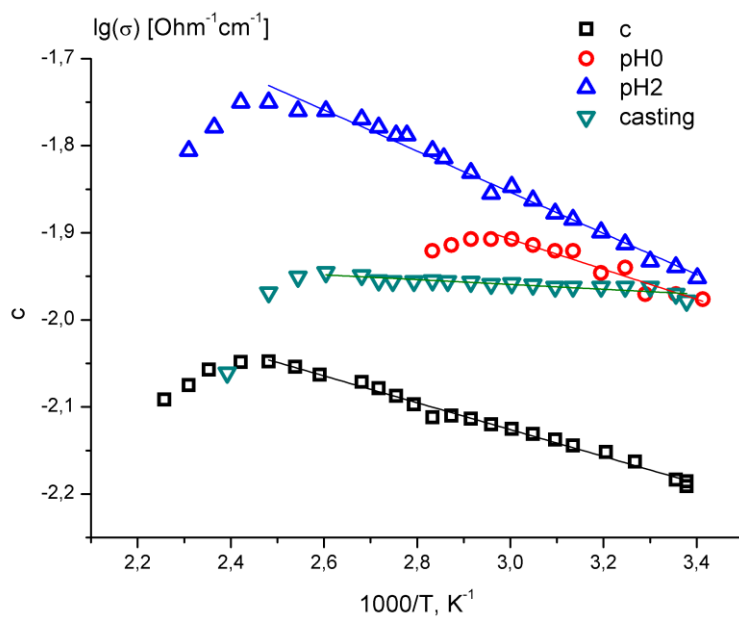


Figure 2. Ionic conductivity of polynaphthaleneimid membrane doped with silica at high-temperature.

Ionic conductivity and other diffusion properties of composite membranes were studied. The high ionic conductivity and low gas permeability make them promising materials for using in a hydrogen fuel cell.

The reported study was supported by Russian Science Foundation grant (project № 16-13-00127).

CO₂ STRIPPING FROM THE IONIC LIQUID USING A DENSE MEMBRANE CONTACTOR

Alexander Malakhov, Stepan Bazhenov, Alexey Volkov

A.V.Topchiev Institute of Petrochemical Synthesis, RAS, Moscow, Russia

E-mail: sbazhenov@ips.ac.ru

Introduction

Gas–liquid membrane contactors can be used for regeneration of liquid absorbents via direct CO₂ stripping, i.e. transferring of CO₂ from the feed liquid phase to the permeate gas phase through a membrane.

A commonly used membrane contactors for gas absorption/stripping are the systems in which the porous membranes (pore size 0.1-0.3 μm) act as nonselective barriers to separate two phases. The main problem in the operation of these contactors is the membrane wetting which leads to substantial increase of mass transfer resistance. There are two ways to eliminate membrane wetting and stop any penetration of the solvent into the membrane. One way of doing this is to use a composite hollow fiber or an asymmetric skinned membrane. The alternative is to use a dense, self-standing polymeric membrane, highly permeable to CO₂ and impermeable to the solvent [1-4].

In addition, the liquid absorbent type is an important factor in membrane CO₂ absorption/desorption. In this work, room temperature ionic liquids (RTILs) were chosen as virtually non-volatile solvents for their potential use in CO₂ stripping.

The first objective of this study is sorption tests among several available RTILs in order to identify the RTIL with lowest thermodynamic affinity to poly(trimethylsilylpropyne) (PTMSP). Among potential candidates imidazolium-based ionic liquid [Emim][BF₄] was chosen, in which the polymer swelling does not exceed 2 % wt. The other and main objective is to investigate the CO₂ stripping flux and efficiency in flat sheet contactor based on dense PTMSP membrane and the relative contribution of the membrane resistance.

Experimental

Regeneration of ionic liquid [Emim][BF₄] in membrane contactor based on PTMSP dense membranes (20 μm) was carried out at the lab-scale high pressure/temperature membrane gas desorption set-up described elsewhere [5].

Carbon dioxide desorption from the solvent [Emim][BF₄] was carried out in the flat sheet membrane contactor. The dense membrane separates the two phases: feed solution of CO₂ in the ionic liquid at 10 bar and permeate gas phase under atmospheric pressure. CO₂-saturated [Emim][BF₄] is convected parallel to the membrane surface through rectangular channel, diffuse through the membrane phase and then desorbed to the permeate cell. Inlet concentration of the gas in [Emim][BF₄] is equal the equilibrium one at CO₂ pressure 10 bar and temperature 303 K (0.54 mol/L).

Results and Discussion

Principal characteristics of gas mass transfer in the contactor are the stripping flux and the stripping efficiency. The last parameter is defined as

$$\eta = 1 - C_L^{\text{out}} / C_L^{\text{in}} \quad (1)$$

where C_L^{out} and C_L^{in} are the feed liquid phase CO₂ concentrations at outlet and inlet of flat sheet contactor, respectively. The CO₂ stripping flux J is equals the mass loss of the gas at liquid flow through slit channel per membrane area A , per unit time:

$$J = \frac{Q_L}{A} (C_L^{\text{in}} - C_L^{\text{out}}) = \frac{Q_L}{A} C_L^{\text{in}} \eta \quad (2)$$

where Q_L (m³/s) is the liquid flow rate. This flux was measured in the experiment at different liquid flow rates; the stripping efficiency далее определялась from Eq. (1).

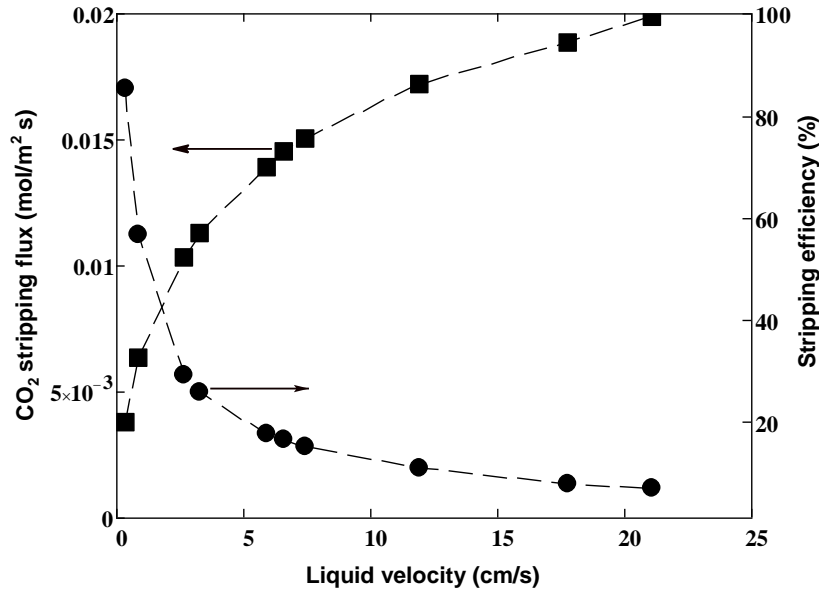


Figure 1. The stripping efficiency and CO₂ flux vs. the liquid velocity $u = Q_L / A$ where A is the cross-sectional area of rectangular channel; $T = 303$ K.

Stripping characteristics are shown on fig. 1. As can be seen, CO₂ flux increased with the liquid velocity, while the efficiency decreases. Trade-off between the flux and the efficiency suggest that the function $J \times \eta$ passes through a maximum. A simple estimate shows that the maximum of the product of J and η is attained at the liquid velocity of about 1.2 cm/s. In this regard, it is the optimal flow rate of the liquid solution for the system studied. At this flow rate, $\eta \approx 48\%$ and $J = 0.0074$ mol/m² s (1.2 kg/m² h).

For the overall mass transfer coefficient (MCT) based on liquid phase we obtain the expression:

$$k_{ov} = -\frac{Q_L}{A} \cdot \ln(1 - \eta) \quad (3)$$

It has been found that the overall MCT increased with the liquid velocity from $1.6 \cdot 10^{-3}$ cm/s to $3.8 \cdot 10^{-3}$ cm/s. Considering that solubility coefficient of CO₂ in [Emim][BF₄] is equal $S = 0.054$ mmol/(cm³·bar) at 303 K, the overall MCT based on gas phase $k_{ov}^{(g)} = S k_{ov}$ varies within the range of 25-61 GPU (gas permeation unit, 10^{-6} cm³(STP)/(cm²·s·cm Hg)).

According to resistance in series approach, the overall resistance to gas transfer through the membrane can be expressed as the sum of the resistances associated with each phase: feed, membrane, and permeate. Using the assumption that the gas-phase resistance is much smaller than the total resistance and can be neglected, we get the overall resistance based on gas phase

$$R^{(g)} \equiv \frac{1}{k_{ov}^{(g)}} = \frac{\delta}{P} + \frac{l_m}{P_m}, \quad (4)$$

where $P = DS$ and $P_m = D_m S_m$ are the permeability coefficients of CO₂ in feed boundary layer and the membrane, respectively; D is the gas diffusivity across the boundary layer with thickness δ , D_m is the diffusion coefficient of the gas through the membrane with thickness l_m , S_m denotes the solubility coefficient of the gas in the membrane.

The question arises, which of the contributions to overall resistance is dominant: the membrane resistance or liquid layer resistance? Membrane inevitably contains some amount of the sorbed liquid, therefore the membrane permeability P_m different to the smaller side from the permeability of pure PTMSP membrane P_p . At the same time, the thickness of swollen membrane l_m exceeds the thickness of dry membrane l . Taking these two factors into account, we obtained the following expression for the total resistance:

$$R^{(g)} = R_L + R_m = \frac{\delta}{P} + \frac{l}{P_p} \beta, \quad (5)$$

where $\beta = 1 + \frac{\phi}{1-\phi} \frac{P_p}{P}$ is the factor describing the increase in membrane resistance due to the liquid sorption in the polymer, ϕ is the volume fraction of ionic liquid in the polymer. The equation (5) states that the overall resistance to gas transfer is sum of the liquid film resistance and the pure polymer membrane resistance multiplied by “sorption factor” β . Numerical evaluation of the membrane resistance contribution showed that it is less than 7% in the entire range of liquid velocities investigated. Consequently, the liquid phase mass transfer resistance is the dominating contribution in the overall resistance.

The work also addresses the following issues: the evaluation of boundary liquid layer thickness as a function of flow rate, intensification of CO₂ desorption by raising the temperature etc.

Acknowledgments

The research was supported by the Russian Foundation for Basic Research (project no. 17-08-00619).

References

1. *Nguyen P.T., Lasseguette E., Medina-Gonzalez Y. et al.* A dense membrane contactor for intensified CO₂ gas/liquid absorption in post-combustion capture, // *J. Membr. Sci.* 2011. V. 377. P. 261–272.
2. *Trusov A., Legkov S., van den Broeke L.J.P. et al.* Gas/liquid membrane contactors based on disubstituted polyacetylene for CO₂ absorption liquid regeneration at high pressure and temperature // *J. Membr. Sci.* 2011. V. 383. P. 241–249.
3. *Dibrov G.A., Volkov V.V., Vasilevsky V.P. et al.* Robust high-permeance PTMSP composite membranes for CO₂ membrane gas desorption at elevated temperatures and pressures // *J. Membr. Sci.* 2014. V. 470. P. 439–450.
4. *Kerber J., Repke J.-U.* Mass transfer and selectivity analysis of a dense membrane contactor for upgrading biogas // *J. Membr. Sci.* 2016. V. 520. P. 450–464.
5. *Shutova A.A., Trusov A.N., Bermeshev M.V. et al.* Regeneration of alkanolamine solutions in membrane contactor based on novel polynorbornene // *Oil & Gas Sci. Technol.–Revue d'IFP Energies nouvelles.* 2014. V. 69(6). P. 1059-1068.

THREE-DIMENSIONAL MODEL OF IMPEDANCE OF THE ION EXCHANGE MEMBRANE WITH ELECTRICALLY INHOMOGENEOUS SURFACE

Semyon Mareev, Anton Kozmai, Vladlen Nichka, Victor Nikonenko

Membrane Institute, Kuban State University, Krasnodar, Russia, E-mail: nichkavs@mail.ru

Introduction

Electrochemical responses of materials with heterogeneous surface essentially depend on the parameters of surface heterogeneity: on the size and the shape, as well as the surface fraction of conductive and nonconductive areas. Understanding of the effect of membrane/electrode surface heterogeneity on the electrochemical behavior of membrane/electrode systems in conditions of concentration polarization is an actual problem of modern electrochemistry. These effects can be efficiently studied by electrochemical impedance spectroscopy (EIS) [1, 2].

Theory

We propose a three-dimensional model of ion transport through the membrane and two adjacent diffusion boundary layers (DBLs). Ion transport in the depleted DBL adjacent to the membrane is described by the Nernst-Planck equation, the mass conservation law, the equation of current flow and the local electroneutrality condition. Using cylindrical symmetry, the system under study is considered in two coordinates r and z .

Results and discussions

A three-dimensional problem of ion transport in system with heterogeneous membrane is solved in the case of a zero current density. Impedance spectra were calculated for different conductive surface portion ε (Fig.). As it can be seen from figure, in the case of small ε , the impedance spectra of the system with electrically heterogeneous membrane consist of two arcs. When $\varepsilon=1$ spectra has only one arc.

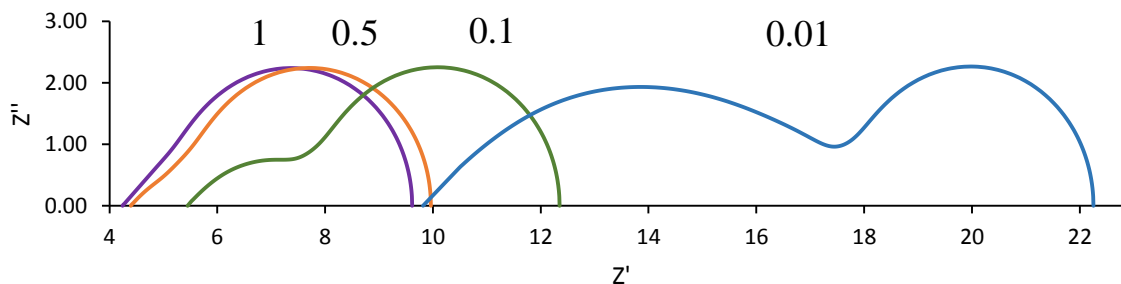


Figure. Numerical calculations of impedance spectra at various conductive surface portion ε (shown on the plot near the corresponding curve) and fixed value of the DBL thickness $\delta = 260\mu\text{m}$

Acknowledgements

This investigation was realized within French-Russian laboratory "Ion-exchange membranes and related processes". The authors are grateful to RFBR, Russia (grants No. 15-58-16005 NCNI, 16-38-60135-mol_a_dk) for financial support.

References

1. Deslouis C. et al. Impedance techniques at partially blocked electrodes by scale deposition. *Electrochimica Acta*. 1997. V. 42(8). P. 1219-1233.
2. Kozmai A.E. et al. 2D modelling of impedance of heterogeneous ion-exchange membranes // *Ecological Bulletin of Research Centers of the Black Sea Economic Cooperation*. 2014. V. 4. P 38-43.

SELECTIVE GAS PERMEABILITY OF POLY(4-METHYL-1-PENTENE) MODIFIED BY GAS PHASE FLUORINATION

Svetlana Markova¹, Alexander Kharitonov², Vladimir Teplyakov¹

¹A.V.Topchiev Institute of Petrochemical Synthesis RAS, Moscow, Russia, E-mail: markova@ips.ac.ru

²Institute of Energy Problems of Chemical Physics (Branch) RAS, Chernogolovka, Moscow Region, Russia

Introduction

Polymer fluorination is an object of intensive researches as a surface properties modification method of polymer products. The practical application of direct fluorination in membrane gas separation allows improving the separation properties of the polymer membranes and increasing their chemical stability [1]. In addition, direct gas phase fluorination can be used to modify the polymer films and membranes of any shape (flat sheet membranes, hollow fibers) as well as membrane modules.

Experiments

Polymer films based on poly(4-methyl-1-pentene) (PMP) modified by gas phase fluorination have been used to investigate the gas transport parameters. One-side gas phase fluorination has been carried out with N₂-F₂ (10 vol% of F₂) mixture in a closed reactor at a temperature of 26 °C and a fluorination time of 1 and 4 hours. The permeability of He, CH₄, and CO₂ has been measured by the permeability differential method with the gas chromatography analysis. The partial pressure drop was equal to 1 bar and helium and argon have been used as the gas carriers. The diffusion coefficients have been calculated from the experimental differential permeability curves. The gas transfer parameters have been studied from the modified and unmodified sides of the films in order to take into account the possible appearance of gas transfer anisotropy.

Results and Discussion

The permeability and diffusion coefficients of the gases under investigation have been experimentally determined. The results are shown in Table 1.

Table 1: The permeability and diffusion coefficients of gases through the fluorinated PMP.

a) fluorination time – 1 hour

	Gas	P, Barrer	D, cm ² /s, 10 ⁷
PMP ↑*	CO ₂	59.5	2.8
PMP ↓**	CO ₂	55.4	2.8
PMP ↑	CH ₄	13.2	1.3
PMP ↓	CH ₄	10.9	1.5
PMP ↑	He	163	-

b) fluorination time – 4 hour

	Gas	P, Barrer	D, cm ² /s, 10 ⁷
PMP ↑	CO ₂	33.0	2.3
PMP ↓	CO ₂	29.7	1.7
PMP ↑	CH ₄	2.1	~0.2
PMP ↓	CH ₄	3.5	
PMP ↑	He	141	-
PMP ↓	He	140	-

Table 2: The permeability and diffusion coefficients of gases for the initial PMP.

Gas	P, Barrer	D, cm ² /s, 10 ⁷
CO ₂	84.0	3.3
CH ₄	16.6	2.4
He	111	-

The Table 1 shows that the gas phase fluorination in this case brings about to an increasing in the permeability of He, a significant decreasing in the CH₄ permeability (which is particularly noticeable with long fluorination time) and to a less intensive decreasing in CO₂ permeability as compared with the initial data (Table 2).

Based on the values of the gas permeability coefficients ideal separation factors of CO₂/CH₄ and He/CH₄ pairs for the fluorinated PMP films has been calculated. The results are shown in Table 3.

Table 3: Ideal separation factors for the fluorinated PMP films.

a) fluorination time – 1 hour

	CO ₂ /CH ₄	He/CH ₄
PMP ↑	4.5	12.3
PMP ↓	5.1	13.2

b) fluorination time – 4 hour

	CO ₂ /CH ₄	He/CH ₄
PMP ↑	15.9	67.6
PMP ↓	8.5	40.0

* PMP ↑ - from an unmodified side; ** PMP ↓ - from modified side.

The Table 3 shows that, in general, gas phase fluorination leads to a significant improvement in the gas separating properties of PMP as compared with the initial films. Thus, the ideal separation factors for the initial PMP films were 5.1 and 6.7 for CO₂/ CH₄ and He/CH₄ pairs, respectively, and for the fluorinated film (for 4 hours) 15.9 and 67.6, respectively. At the same time, the anisotropy effect of the permeability have been fixed (see selectivity data in Table 3). To explain this effect the IR spectroscopy method is used.

The study was carried out in the frames of RFBR grant № 15-03-03033.

References

1. A.P. Kharitonov. Direct fluorination of polymers – From fundamental research to industrial applications // Progress in Organic Coatings. 2008. V. 61. P. 192-204.

BIMETALLIC PT-BASED CATALYSTS: STRUCTURE, ACTIVITY IN THE OXYGEN REDUCTION REACTION AND METHANOL ELECTROOXIDATION

¹Vladislav Menshchikov, ¹Sergey Belenov, ¹Anastasia Alekseenko, ¹Vadim Volochaev

¹Southern Federal University, Rostov-on-Don, Zorge st.,7, Russia, E-mail: men.vlad@mail.ru

Introduction

Low-temperature fuel cells are promising power source for a wide range of devices. In recent years, interest in methanol fuel cells has significantly increased. Methanol is less dangerous in handling, storage and transportation in compare with hydrogen. One of the methanol possibilities using as fuel is direct anodic oxidation in Direct Methanol Fuel Cells (DMFC). However, the widespread commercial use of such devices make it difficult high cost of produced electricity and low stability [1]. One of the areas increasing efficiency is of the alloying of platinum catalysts with different d-metals, such as: Co, Cu, Ni, Cr, Fe [2, 3].

Experiments

The aim of this study was to comparative study of the structure and activity of Pt/C and PtM/C (M = Ni, Co, Cu) materials in oxygen reduction reaction (ORR) and methanol electrooxidation.

Catalysts were studied by X-ray diffraction to determine of the average crystallite size (Table 1); cyclic voltammetry on a disk electrode for measuring of the electrochemically active surface area (ESA), and activity in ORR and methanol electrooxidation reaction [4].

Results and discussion

Comparison of Pt/C and PtM/C catalyst shows a large value for (ESA) Pt/C catalyst compared with PtM/C (Fig. 1a). The measurement of the ESA value for all catalysts was carried out by two independent methods: adsorption/desorption of hydrogen and CO-stripping (Table 1). At the same time, activity in the electrochemical reaction of methanol (Fig. 1b) showed greater activity PtM/C materials in comparison with the commercial Pt/C catalyst.

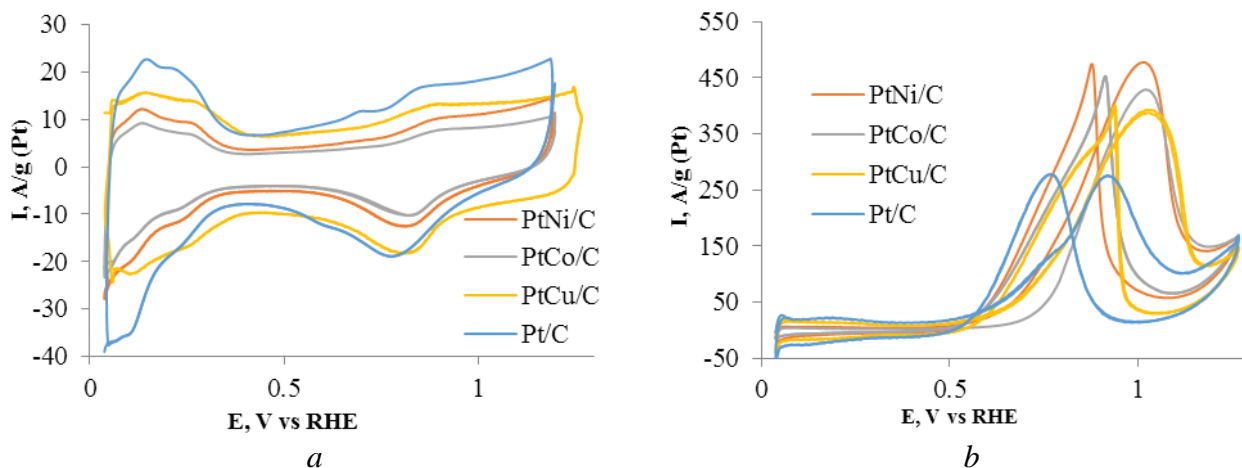


Figure 1. Cyclic voltammograms to Pt/C and PtM/C catalysts. (a) Electrolyte 0.1M HClO₄, saturated with argon, at atmospheric pressure; potential sweep rate 20 mV/s. (b) Electrolyte 0.1M HClO₄ + 0.5M CH₃OH, saturated with argon, at atmospheric pressure; potential sweep rate 20 mV/s.

It was found that the PtNi/C catalyst show higher activity in the methanol electrooxidation reaction, because this material was demonstrated highest value of currents of methanol oxidation in compare with different studied materials.

Thus, a comparative study of Pt/C and PtM/C (M = Cu, Ni, Co) catalysts showed a large activity of bimetallic PtM/C materials in the methanol electrooxidation reaction, in despite of the smaller electrochemically active surface area.

Table 1: Comparison of the structure and electrochemically active surface area (ESA) of Pt/C and PtM (M = Ni, Co, Cu)/C catalysts.

Materials	Pt loading (%)	Average crystallite size (nm)	ESA, by H_{ads} ($m^2/g(Pt)$)	ESA, by CO-stripping ($m^2/g Pt$)
Pt/C	20,0	2,6	94	132
PtCu/C	20,8	2,0	55	56
PtNi/C	16,3	2,5	51	52
PtCo/C	20,3	2,7	67	68

The work was carried out within the framework of the Ministry of Education and Science of the Russian Federation (assignment No. 13.3005.2017 / PCh).

References

1. *Guterman V.E., Belenov S.V., Pakharev A.Yu., Min M., Tabachkova N.Yu., Mikheykina E.B., Vysochina L.L., Lastovina T.A.* Pt-M/C (M = Cu, Ag) electrocatalysts with an inhomogeneous distribution of metals in the nanoparticles // *Int. J. Hydrogen Energy*, 2016, 41 (3), 1609 - 1626.
2. *Srabiomyan V.V., Pryadchenko V.V, Kurzin A.A., Belenov S.V., Avakyan L.A., Guterman V.E., Bugaev L.A.* Atomic Structure of PtCu Nanoparticles in PtCu/C Catalysts from EXAFS Spectroscopy Data // *Int. J. Fizika Tverdogo Tela*, 2016, 58 (4), 730–739
3. *Alekseenko A.A., Guterman V.E., Volochaev V.A., Belenov S.V.* Effect of wet synthesis conditions on the microstructure and active surface area of Pt/C catalysts // *Int. J. Inorganic Materials*, 2015, 51 (12), 1258-1263.
4. *Menshchikov V. S., Belenov S. V., Guterman V. E., Volochaev V. A.* PtM (M = Ni, Co, Cu)/C catalysts: synthesis, structure, activity in oxygen redaction and methanol oxidation reaction // *Kondensirovannye sredy i mezhfaznye granitsy*, 2017, 19 (1), 87–97.

DIFFUSION PERMEABILITY OF RALEX ANION EXCHANGE MEMBRANES, MODIFIED BY MF-4SC AND POLYANILINE

Olga Mikhaleva, Svetlana Shkirskaya, Stanislav Melnikov, Sergey Dolgoplov
Kuban State University, Krasnodar, Russia

Introduction

Nowadays, electro dialysis separation and concentration of electrolyte solutions is one of the most important fields of heterogeneous ion-exchange membranes application. In recent years, the modification of membranes to improve their transport and physicochemical characteristics is a promising direction. A large number of works are devoted to the study and improvement of the properties of cation-exchange membranes [1, 2], but anion-exchange membranes are essential for the electro dialysis cells as well [3]. Diffusion permeability is one of the main transport characteristics of ion-exchange membranes. The purpose of this work is to study the diffusion permeability of modified anion-exchange membranes in electrolytes solutions of various nature.

Experiments

The heterogeneous anion-exchange membranes Ralex AMH-Pes (MEGA a.s., Czech Republic) were the objects of the study. The composite Ralex/MF-4SK was obtained by the method used in [4]: the MF-4SK film was applied on the surface of a heterogeneous anionexchange membrane which was pretreated with acetic acid. The composite Ralex/PANI was obtained by chemical synthesis of polyaniline by the method of successive diffusion of polymerizing solutions through the anion-exchange membrane to water [5]. The composite Ralex/MF-4SK/PANI was obtained by a successive combination of the two methods mentioned above.

The values of the diffusion flux and the integral coefficient of diffusion permeability were determined by diffusion of the electrolyte solution through the membrane into pure water. The intensity of the increase in the concentration of the electrolyte in the chamber with water was monitored by a conductometric method. The specific electrical conductivity of membranes (κ_m) was calculated from data on the resistance of samples measured by the mercury-contact method at an alternating current frequency of 50-500 kHz. The surface and sections of the initial and modified membranes were investigated by the MBS-10 microscope with magnifying 40 times.

Results and Discussion

The samples Ralex/MF-4SK, Ralex/PANI, and Ralex/MF-4SK/PANI with the physicochemical characteristics shown in Table 1 were obtained in present work. It can be seen that modification the anion-exchange membrane by a thin layer of the cation exchanger results in an insignificant decrease of ion-exchange capacity, but modification by polyaniline containing positive nitrogen-containing centers, to an increase of this characteristic. The electrical conductivity of the Ralex/MF-4SK composite is 7% higher than that of the original membrane, and for Ralex/PANI and Ralex/MF-4SK/PANI composites, the electrical conductivity decreases by 8%, due to the blocking effect of the polyaniline layer.

Table 1: The physico-chemical characteristics of investigated membranes

Membrane	l , cm	Q , mmol/g _{sw}	κ^* , S/m
Ralex	0,052	1,25	0,52
Ralex/MF-4SK	0,056	1,16	0,56
Ralex/PANI	0,058	1,36	0,48
Ralex/MF-4SK/PANI	0,057	1,27	0,49

**Electroconductivity was obtained in 0,1 M NaCl*

Due to the modification of the membrane surface only from one side, all samples have an anisotropic structure, which is observed when studying the sections of modified samples under a microscope. The thickness of modified layers for all composite samples were estimated and presented in fig.1.

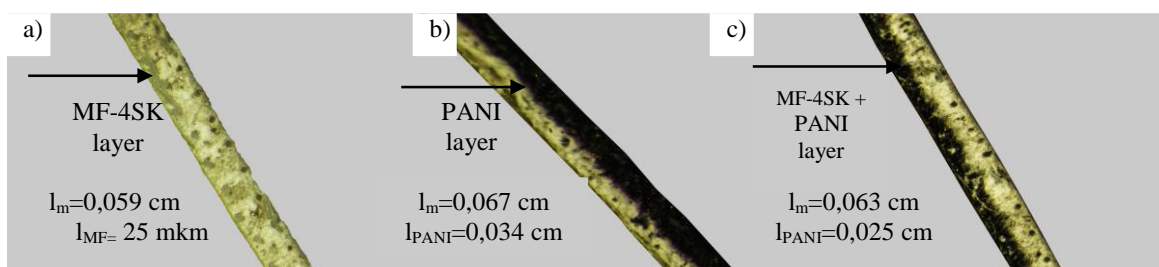


Figure 1. Microimages of sections of the obtained samples: a) Ralex/MF-4SK, b) Ralex/PANI; c) Ralex/MF-4SK/PANI

Concentration dependences of diffusion permeability in NaCl and HCl solutions were obtained for the samples under study (fig. 2). As can be seen from the fig. 2 the diffusion permeability in NaCl solutions is lower 10 times than in HCl. It is known that the limiting stage of the diffusion permeability of ion-exchange membranes is the transfer of the coion. For the Ralex composite membranes, Na^+ and H^+ were co-ions. The mobility of the H^+ ion is much higher than the mobility of the Na^+ ion, which explains the higher diffusion permeability in HCl solutions for all samples compared to NaCl.

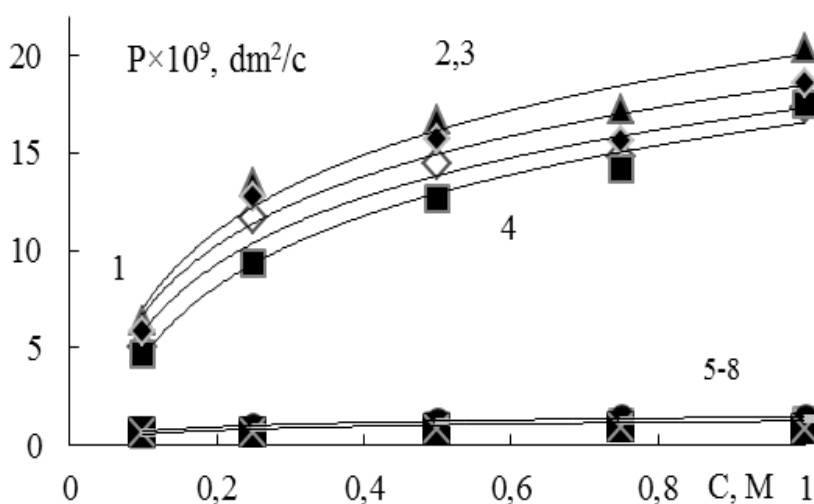


Figure 2. Concentration dependences of the diffusion permeability coefficient in HCl solutions: 1, 5 - Ralex; 2, 6 - Ralex/MF-4SK/PANI; 3, 7 - Ralex/MF-4SK; 4, 8 - Ralex/PANI, 1-4 in solutions of HCl and 5-8 in solutions of NaCl

The all investigated composite membranes have an anisotropic structure (Fig. 1), so it was interesting to investigate the asymmetry of diffusion permeability for a various orientation of the modified layer to the flux of electrolyte solution. The effect of diffusion permeability asymmetry for all the modified samples was not found in the whole range of concentration of HCl and NaCl solutions (Fig. 3). It can be assumed that this is due to the structure of heterogeneous membranes, which little change when applying thin layers of the modifier, and this may be because polyaniline contains the same-charged amino groups, similar to fixed groups in the anion-exchange membrane. It can be seen from the fig.3 that modifying with the layer of MF-4SK leads to an increase in the diffusion permeability of the composite by an average on 15% in NaCl and HCl solutions in the concentration range under study. The most significant effect on the diffusion permeability of the Ralex anion-exchange membrane is modifying by polyaniline, which leads to a 10-30% decrease in this characteristic in the concentration range above 0.5 mol/l NaCl.

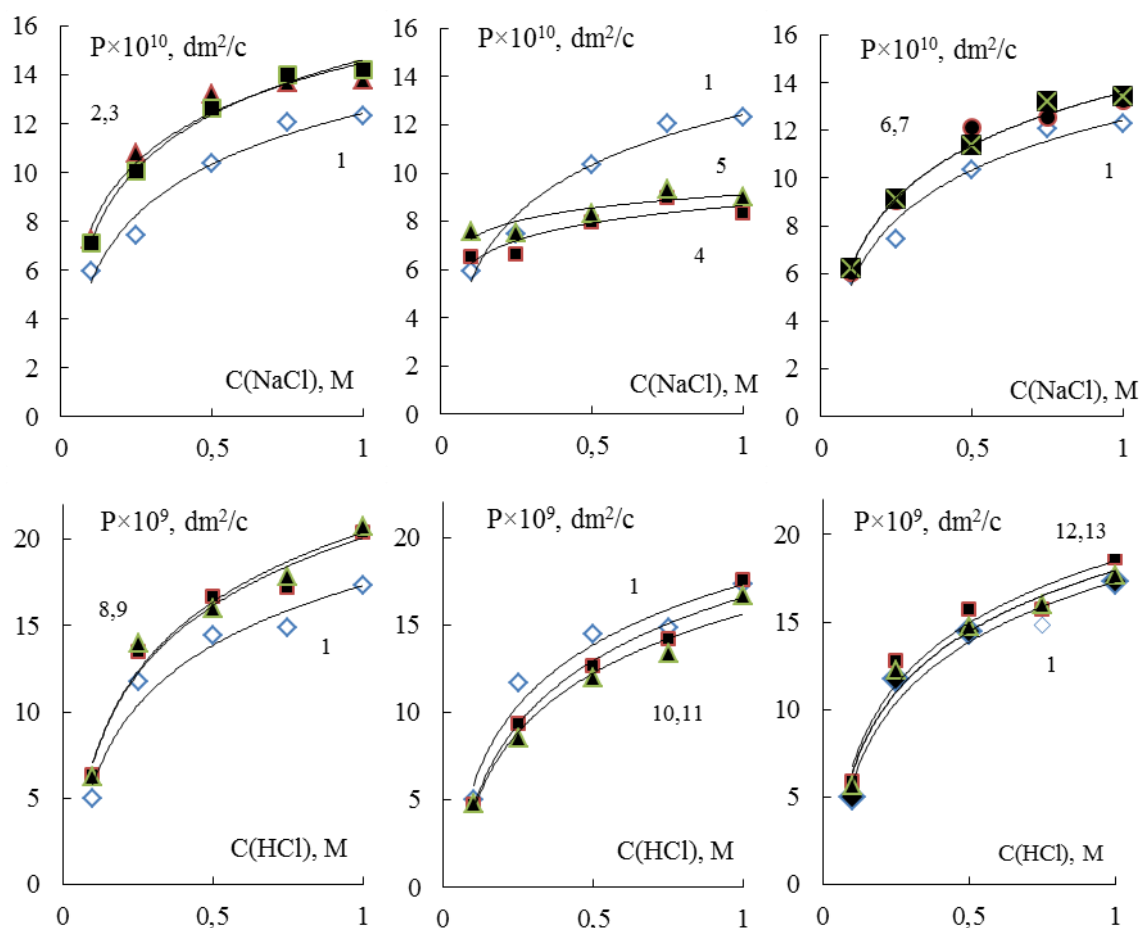


Figure 3. Concentration dependences of the diffusion permeability coefficient in NaCl solutions: 1 - Ralex; 2, 3, 8, 9 - Ralex / MF-4SC with the orientation of the unmodified and modified side to the electrolyte solution; 4, 5, 10, 11 - Ralex / PANI with orientation, modified and unmodified side to electrolyte solution; 6, 7, 12, 13 - Ralex / MF-4SC / PANI under orientation, modified and unmodified side to the electrolyte solution

Such decrease of diffusion permeability is a positive effect of the work of electro dialysis devices and will contribute to a higher concentration of electrolyte solutions, and will prevent the passage of ions from the concentration chamber into the desalting chamber.

The present work was supported by the Russian Foundation for Basic Research (project № 15-08-03285-a).

References

1. Kononenko N.A., Loza N.V., Shkirskaya S.A., Falina I.V., Khanukaeva D.Yu. // J. Solid State Electrochem. 2015. Vol. 19. P. 2623–2631.
2. Yaroslavtsev A.B., Stenina I.A., Voropaeva E.Y., Ilyina A.A. // Polym. Adv. Technol. 2009. V.20. P. 566–570.
3. Demina O.A., Berezina N.P., Demin A.V., Sata T. // Russ. J. of Electrochem. 2002. V.38. № 8. P. 896-902.
4. Zabolotskii V., Sheldeshov N., Melnikov S. // J. Appl. Electrochem. 2013. V. 43. P. 1117–1129.
5. Shkirskaya S.A., Kononenko N.A., Loza N.V., Falina I.V. Patent RF, No 2612269 (24.11.2015).

INFLUENCE OF THE MODIFICATION OF THE ANION-EXCHANGE LAYER OF THE BIPOLAR MEMBRANE ON THE DISSOCIATION RATE OF WATER MOLECULES IN THE BIPOLAR REGION

Tatyana Mochalova, Alexander Beshpalov, Nikolay Sheldeshov, Victor Zabolotsky
Kuban State University, Krasnodar, Russia, E-mail: sheld_nv@mail.ru

Introduction

The processes using bipolar ion-exchange membranes (BPM) are finding more and more applications in the industry in recent years. Due to the unique property of generating hydrogen and hydroxyl ions in the space charge region when the current is applied to the system, BPM is used in various processes: in the preparation of organic and inorganic acids and alkalis, for pH correction of juices and milk serum, in production of deionized water, in removing flue gases from the air.

In order to reduce the energy costs of such processes, bipolar membranes with a low operating voltage are necessary. Currently, the most effective and common method of reducing voltage on the bipolar membrane is the introduction of catalytic additives of various nature in its bipolar region [1].

As studies show, additives introduced into the bipolar region in the form of highly disperse powders have a high catalytic activity. However, uniform application of powders at the membrane surface is difficult, in addition, the powders are weakly held on the surface of the original cation and anion-exchange membranes. The use of water-soluble polyelectrolytes is a simple way of fixing powders on the surface of membranes. Therefore, the purpose of this work is to study the influence of hybrid additives introduced into the bipolar region in the form of suspensions of powder in solutions of polyelectrolytes.

Experiments

The objects of the study were analogues of the MB-2 bipolar membrane. The initial anion exchange membrane Ralex AMH was modified with suspensions of the EDE-10P anion exchange resin powder, and also the powder of copper(II) ions complex with EDE-10P amino groups in a solution of polyacrylic acid and the suspensions of the same powders in a solution of polyhexamethyleneguanidine. Further, the modified anion-exchange membrane was compressed with a cation exchange membrane Ralex CMH at a temperature of 120°C and a pressure of 15 atmospheres.

The frequency spectra of the electrochemical impedance were measured by a virtual impedance meter at a temperature of 25°C. The measurements were carried out in the 1 Hz – 1 MHz frequency range of alternating current in a flowing four-electrode cell with a working membrane area of 2.27 cm². The cell was washed with 0.05 M sulfuric acid solution at the cation exchange side of the bipolar membrane and 0.1 M sodium hydroxide solution at the anion exchange side of the bipolar membrane.

The differential resistance of the bipolar region was found from the frequency spectra of the electrochemical impedance of the membrane. The overvoltage of the bipolar region of the membrane was calculated from its dependence on the electric current (Equation 1) [2].

$$\eta_b = \int_0^{I^*} R_b dI \quad (1)$$

Results and Discussion

It is seen from the dependences of the resistance on current density and partial current-voltage characteristics of bipolar membranes that hybrid additives containing powder particles introduced into the membrane together with polyelectrolytes have a higher catalytic effect than the corresponding solutions of polyelectrolytes (Figures 1-4). However, hybrid additives have less pronounced catalytic effect than additives of EDE-10P powders and copper ions complex with EDE-10P.

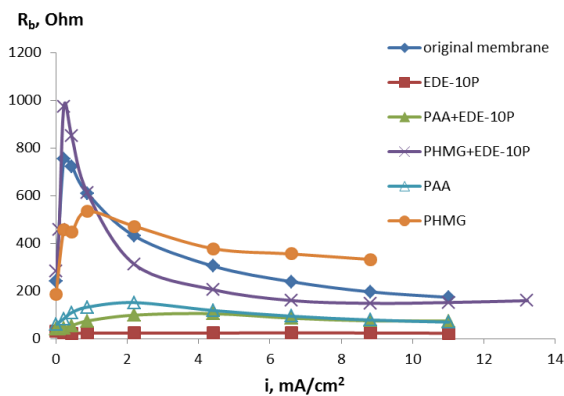


Figure 1. Dependence of resistance of membrane bipolar region on the current density

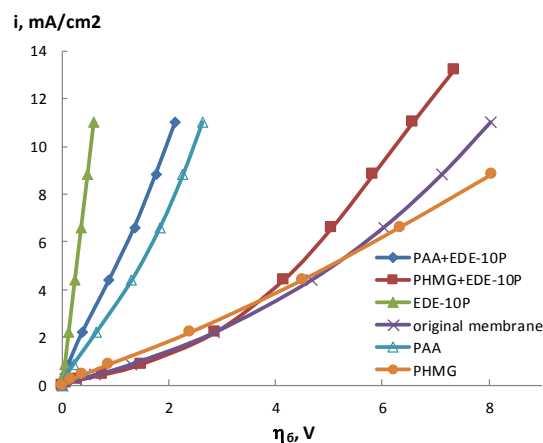


Figure 2. Partial current-voltage characteristics of bipolar region of the membranes

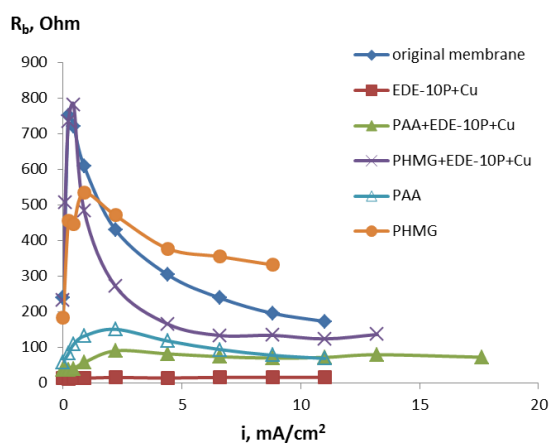


Figure 3. Dependence of resistance of membrane bipolar region on the current density

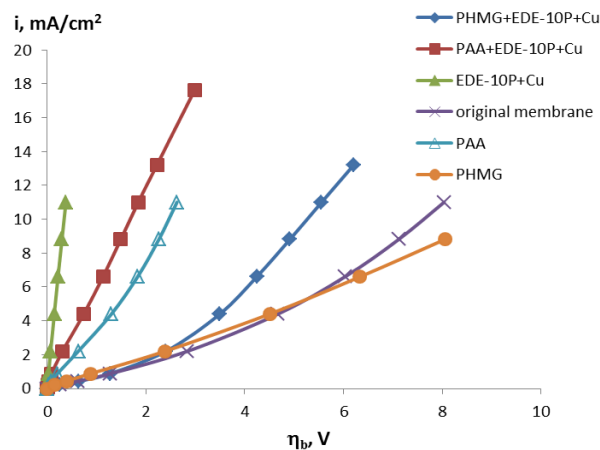


Figure 4. Partial current-voltage characteristics of bipolar region of the membranes

This may be due to adsorption of polyacrylic acid molecules on the surface of an anion exchange membrane or due to adsorption of polyhexamethyleneguanidine molecules on the surface of a cation-exchange membrane. In this case, the powder particles containing catalytic centers are displaced from the space charge region and do not show catalytic effect in the dissociation reaction of water molecules.

As the complex compound of copper ions with the EDE-10P anionite can break down in the bipolar membrane at the production of acids and alkalis, its stability was investigated in an apparatus containing an electrochemical cell in which there were 0.25 mol/l sulfuric acid solution and 0.5 mol/l sodium hydroxide solution on both sides of the membrane.

Researches were carried out in galvanostatic mode. The potential difference at the bipolar membrane was measured for 7 days periodically in 30-60 minutes. The total time during which the bipolar membrane was under current was 45 hours.

It was found that the voltage drop across the membrane, the resistance and overvoltage of the bipolar region increased about two times during the researches (Figures 5-7).

This indicates the instability of the complex compound of copper ions with EDE-10P anionite, introduced into the membrane, under conditions of obtaining acid and alkali from the salt. A possible reason of voltage increase in the bipolar region of the membrane is the slow destruction

of the complex containing copper (II) ions during its alkalization, which leads to a decrease in the concentration of active centers in the bipolar region.

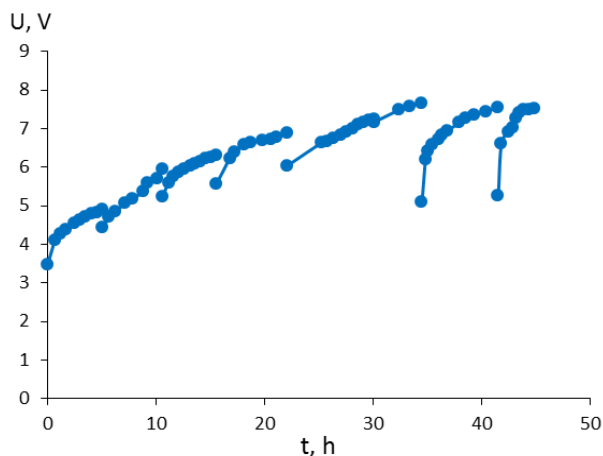


Figure 5. Dependence of voltage drop at the bipolar membrane on time

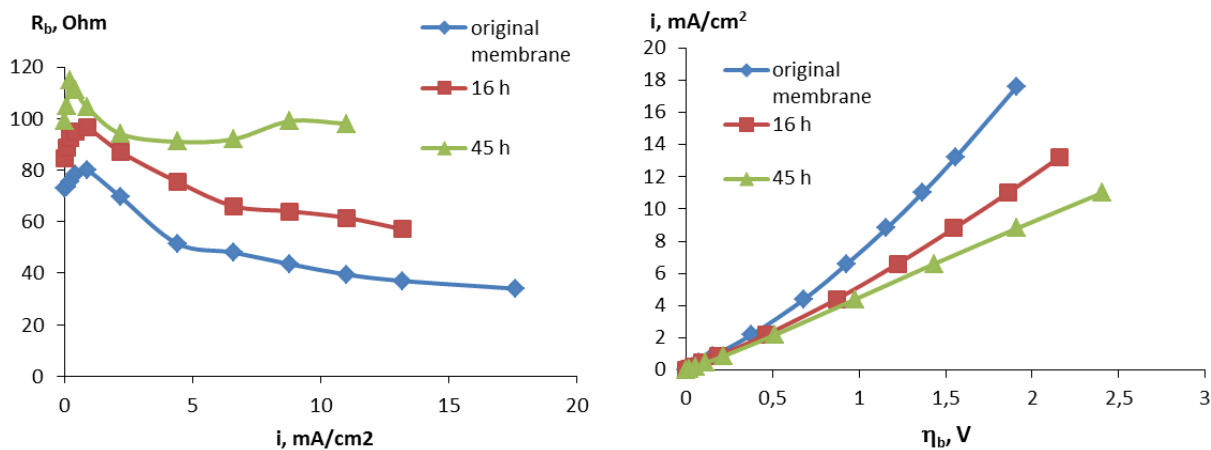


Figure 6. Dependence of resistance of bipolar membrane on the current

Figure 7. Partial current-voltage characteristics of bipolar region of the membranes

Therefore, it is advisable to use a powder of EDE-10P anionite as a catalytic additive, which is stable under conditions of obtaining acids and alkalis using bipolar membranes.

The present work is supported by the State Task of the Ministry of Education and Science of the Russian Federation, project No. 10.3091.2017 / PP.

References

1. Shel'deshov N. V., Krupenko O. N., Shadrina M. V., and V. I. Zabolotskii. Electrochemical parameters of heterogeneous bipolar membranes: dependence on the structure and nature of monopolar layers // *Rus. J. Electrochem.* V. 38. № 8. 2002. P. 884–887. Translated from *Elektrokhimiya*. V. 38. № 8. 2002. P. 989-993.
2. Shel'deshov N. V., Zabolotsky V. I. Bipolar ion-exchange membranes. Receiving. Properties. Application // *Membranes and membrane technologies. Collective of authors. Responsible Editor Yaroslavtsev A. B. The Scientific World*, 2013. 612 p. (in Russian)

IONIC TRANSPORT IN SOLID ELECTROLYTES $\text{Li}_{1+x}\text{Al}_x\text{Ge}_{2-x}(\text{PO}_4)_3$ WITH NASICON STRUCTURE

¹Mariya Moshareva,² Svetlana Novikova, ³Andrey Yaroslavtsev

Kurnakov Institute of General and Inorganic Chemistry, RAS, Russia

¹E-mail: moshareva.m@gmail.com

²E-mail: svetlana_novi@mail.ru

³E-mail: yaroslav@igic.ras.ru

Introduction

Lithium ion batteries (LIBs) are widely used portable energy source now. The possibility of substitution of liquid electrolyte by solid electrolyte attracts an attention because it would make LIBs more safe, reduce level of degradation of electrode materials and minimize the solubility of transition metal in electrolyte. Solid electrolyte must exhibit high enough ionic conductivity, in particular lithium one.

NASICON complex phosphates are among the attractive solid electrolytes [1]. One of the most conductive compositions among NASICON-type lithium ion conductors previously obtained was $\text{Li}_{1+x}\text{Al}_x\text{Ge}_{2-x}(\text{PO}_4)_3$ [2]. The heterovalent substitution of germanium by aluminium leads to the formation of charged point defects and conductivity increases consequently and considerably reduce of the material cost. The problem of incomplete embedding of Al^{3+} into crystal cell with $x > 0.5$ appears when solid-state synthesis is used [3]. Liquid-state methods are described also but they are based on germanium and aluminium alkoxides which are expensive and susceptible to hydrolysis [4] or utilize dissolution of germanium oxide in oxalic acid which requires a long time [5]. So, the development of simple ways of $\text{Li}_{1+x}\text{Al}_x\text{Ge}_{2-x}(\text{PO}_4)_3$ synthesis with high degree of substitution of germanium for aluminum and ionic conductivity study of the obtained materials is of great interest.

Experiments

New liquid-state synthesis of $\text{Li}_{1+x}\text{Al}_x\text{Ge}_{2-x}(\text{PO}_4)_3$ were offered. It is based on obtaining of GeO_2 alkaline solution and use of water-soluble salts $\text{Al}(\text{NO}_3)_3 \cdot 9\text{H}_2\text{O}$, LiNO_3 , $(\text{NH}_4)_2\text{HPO}_4$. GeO_2 was dissolved in aqueous solution of ammonia (1.2 wt.%) and salts were dissolved in water acidified by HNO_3 (pH ~ 3). Sol was obtained (pH ~ 7) when solutions were mixed together. Sol was evaporated at 80°C under stirring and then gel obtained was calcined at 300°C for 4 hours. Powder obtained was ground and calcined at 600-850°C for 12 hours. Powder was pressed into pellets and pellets were annealed at 850-1000 °C for 12 hours.

Results and Discussion

XRD patterns show that the formation of crystalline rhombohedral NASICON structure begins at 750°C, but admixture of GeO_2 is present. Almost single-phase samples are formed at 850-900°C. The destruction of crystalline structure begins at 1000°C. The proposed synthesis allows to achieve the embedding of Al^{3+} into crystal cell of $\text{Li}_{1+x}\text{Al}_x\text{Ge}_{2-x}(\text{PO}_4)_3$ when $x=0.5, 0.6$. Admixture of aluminium phosphate is present when $x=0.65$. It may indicate that limit of embedding of Al^{3+} into $\text{LiGe}_2(\text{PO}_4)_3$ crystalline structure is achieved.

The cell volume increases with increasing of x as a consequence of the larger Al^{3+} size then Ge^{4+} size (0.535 Å and 0.530 Å respectively [6]).

Electrical conductivity measurements were carried out by impedance spectroscopy from room temperature up to 300°C. Conductivity of $\text{Li}_{1.5}\text{Al}_{0.5}\text{Ge}_{1.5}(\text{PO}_4)_3$ obtained at 850 and 900°C is 1.0×10^{-4} и $2.2 \times 10^{-4} \text{ Ohm}^{-1}\text{cm}^{-1}$ respectively at 25°C. The increasing of conductivity correlates with the increasing of the relative density of the pellets which is 62 and 72% respectively. The optimal temperature of the ceramic formation is 900°C.

$\text{Li}_{1.6}\text{Al}_{0.6}\text{Ge}_{1.4}(\text{PO}_4)_3$ obtained at 900°C (density 86%) exhibits the best conductivity and the lowest activation energy in the low-temperature range among samples obtained. Its conductivity is $3.8 \times 10^{-4} \text{ Ohm}^{-1}\text{cm}^{-1}$ at 25°C and activation energy of conductivity from 25°C up to 250°C is $30.5 \pm 0.4 \text{ KJ/mol}$.

This work was financially supported by the Russian Foundation for Basic Research and Moscow Government (project no. 15-38-70042).

References

1. *Yaroslavtsev A. B., Stenina I. A.* Complex Phosphates with the NASICON Structure ($M_xA_2(PO_4)_3$) // Russian Journal of Inorganic Chemistry, 2006, V. 51, 1, P. 97.
2. *Fergus J. W.* Ceramic and polymeric solid electrolytes for lithium-ion batteries // J. Power Sources, 2010, V. 195, P. 4554.
3. *Yamamoto H., Tabuchi M., Takeuchi T., Kageyama H., Nakamura O.* Ionic conductivity enhancement in $LiGe_2(PO_4)_3$ // J. of Power Sources, 1997, V.68, P.397.
4. *Kotobuki M., Koishi M.* Sol-gel synthesis of $Li_{1.5}Al_{0.5}Ge_{1.5}(PO_4)_3$ solid electrolyte // Ceramics International, 2015, V. 41, P. 8562.
5. *Kunshina G. B., Bocharova I. V., Lokshin E. P.* Synthesis and Conductivity Studies of $Li_{1.5}Al_{0.5}Ge_{1.5}(PO_4)_3$ Solid Electrolyte // Inorganic Materials, 2016, V. 52, № 3, P. 279.
6. *Shanon R. D.* Revised effective ionic radii and systematic studies of interatomic distances in halides and chalcogenides // Acta Cryst., 1976, V. A32, P. 751.

INFLUENCE OF MODIFIERS IN ION-EXCHANGE MEMBRANES ON STRUCTURE OF HYDRATE COMPLEX FIXED ION – COUNTER ION

Ekaterina Nazyrova, Svetlana Shkirskaia, Viktoria Soloshko

Kuban State University, Krasnodar, Russia, E-mail: katerina.nazyrova@mail.ru

Introduction

Selectivity is the most important characteristic of membranes that has great influence on their applying in electromembrane processes as well as in fuel cells. The effects of hydration including the structure of the hydrated complex fixed ion-counter ion is also important for using membranes in various electromembrane devices [1].

Experiments

The perfluorinated membrane Nafion 115 (Du Pont, USA) and the modified membrane Nafion 115/SiO₂ were the objects of study. Modification was carried out by intercalation of the hydrated silica into the matrix of the membrane (*in situ* method) [2]. The modifier content was about 3%. The water content in the ion-exchange membranes was determined by gravimetric method.

Results and Discussion

Concentration dependences of potentiometric transport numbers of counter ions and water transport numbers in NaCl and HCl solutions were obtained in [3] and used to calculate the electromigration transport numbers of counter ions of the Nafion and Nafion/SiO₂ membranes by the Scachard equation:

$$t_{+}^{*} = t_{+app} + Mm_{\pm} 10^{-3} t_w \quad (2)$$

where M is the the molar mass of solvent, 18 g/mol; m_{\pm} is the average molality of external solution. As can be seen from the obtained results (fig. 1), the selectivity of investigated membranes is higher in HCl solutions than in NaCl because of the specific selectivity of perfluorinated membrane to H⁺.

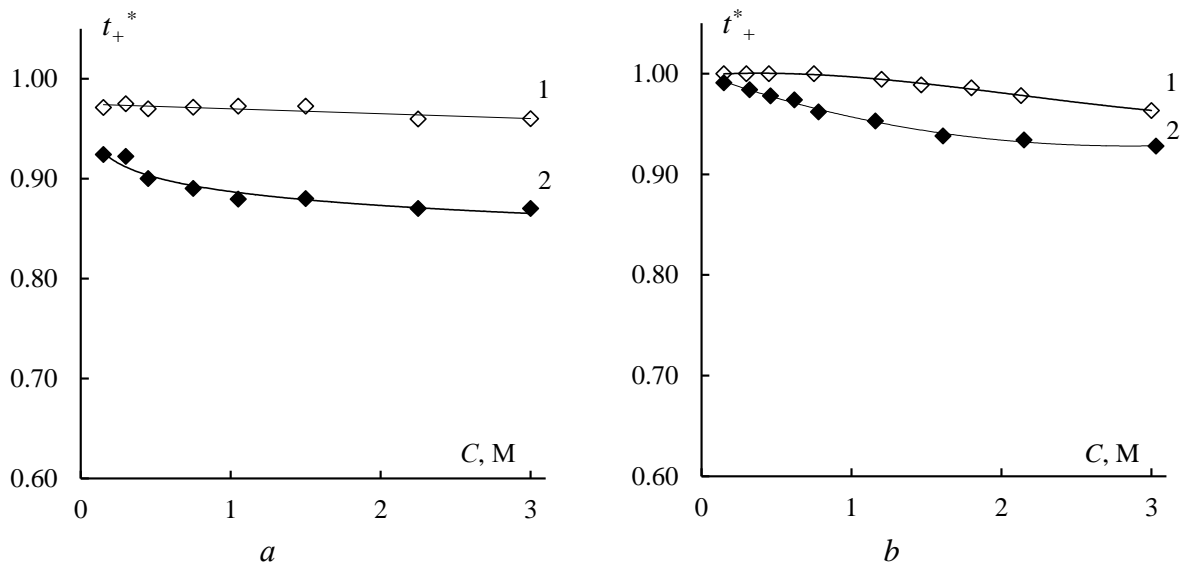


Figure 1. Concentration dependencies of electromigration transport numbers of counter ions in NaCl (a) and HCl (b) solutions: 1 – Nafion, 2 – Nafion/SiO₂

The model describing the electroosmotic properties of ion-exchange membranes as two-phase systems was used to estimate the distribution of water in the hydrated complex fixed ion-counter ion in modified Nafion membranes. The division of structural elements of the swollen membrane into two pseudophases (gel and intergel solution) is carried out by the mechanism of conductivity and allows to estimate the total flow of water as flows through the phases of membrane:

$$t_w = \frac{\gamma}{(1-A)} \cdot \frac{\left[W - (1-f) \frac{\rho_w}{\rho_m} \right]}{QM_w} + (1-\gamma)(t_+ - Bt_-)h_+, \quad (3)$$

where $A = \frac{\bar{h}_-}{\bar{h}_+}$ – the parameter equal to the ratio of hydration numbers of fixed ion \bar{h}_- and counter

ion \bar{h}_+ in the gel phase of the sulfocationic membrane; $B = \frac{h_-}{h_+}$ – the parameter equal to the ratio

of the hydration numbers of the anion h_- to the cation h_+ in the electrolyte solution in contact with the membrane; t_+, t_- – ion transport numbers in solution; ρ_m and ρ_w – density of swollen membrane and water respectively; W – water content in membrane; Q – ion-exchange capacity; $(1-f)$ – the volume fraction of the solution in the swollen membrane; γ – the fraction of current passing across the gel phase. The parameters f and γ are calculated using the extended three-wire model [3]. The first part of equation (3) includes physicochemical characteristics of membrane which can be combined into a parameter \bar{n} that has the meaning of the hydrate capacity of the gel phase:

$$\bar{n} = \frac{\left[W - (1-f) \frac{\rho_w}{\rho_m} \right]}{QM_w}. \quad (4)$$

The representation of the experimental results in the coordinates $t_w - \bar{n}$ allows to find the parameter A . The values of hydration numbers of the fixed ion \bar{h}_- and counter ion \bar{h}_+ were determined from the comparison of the parameter A and the value of the hydrate capacity of the gel phase \bar{n} (table 1). The obtained results are consistent with the NMR data: the hydration number of the sulfo group is in the range of 1 to 3.

Table 1: Equilibrium hydrate characteristics of the gel phase in 0.1 M NaCl and HCl

Solution	Membrane	$\bar{n},$ $\frac{molH_2O}{molSO_3^-}$	$A = \frac{\bar{h}_{SO_3^-}}{\bar{h}_+}$	$\bar{h}_{SO_3^-},$ $\frac{molH_2O}{molSO_3^-}$	$\bar{h}_+,$ $\frac{molH_2O}{mol}$
NaCl	Nafion	15	2/5	2	5
	Nafion/SiO ₂	16	3/5	3	5
HCl	Nafion	10	1/2	1	2
	Nafion/SiO ₂	12	1/1	2	2

As can be seen from the table, the intercalation of hydrated silica into the Nafion membrane leads to a more equivalent distribution of water near the fixed ion and counter ion both in NaCl and HCl solutions.

The present work was supported by the Russian Foundation for Basic Research (project № 16-08-01117-a).

References

1. Shkirkaya S., Nazyrova E., Kononenko N., Dyomina O. // J. Sorption and chromatographic processes 2016. V.16, № 5. P. 711-718.
2. Novikova S., Safronova E., Lysova A., Yaroslavtsev A. // Mendeleev Communications 2010. V. 20. P. 156–157.
3. Shkirkaya S., Nazyrova E., Kononenko N., Dyomina O. // Membranes and Membrane Technologies 2016. V. 6, № 3. P. 262-267.

ACCOUNTING FOR MEMBRANE CONDUCTIVITY IN DETERMINATION OF SURFACE CHARGE VIA STREAMING POTENTIAL MEASUREMENTS

¹Ksenia Nebavskaya, ¹Natalia Pismenskaya, ²Konstantin Sabbatovskiy, ²Vladimir Sobolev, ²Victor Nikonenko

¹Institute of Membranes, Kuban State University, Krasnodar, Russia

E-mail: *littlegreenchemist@yandex.ru*

²Frumkin Institute of Physical Chemistry and Electrochemistry RAS, Moscow, Russia

Introduction

The values of zeta potential and surface charge of ion exchange membranes determine the intensity of development of equilibrium electroconvection [1] and serve as indicator of fouling [2]. The zeta potential of the membranes is most frequently calculated from the data of streaming potential measurements. However, unlike the classical samples studied by electrokinetic, ion exchange membranes possess electrical conductivity and rough surface, so the special approaches should be used for more valid calculations of their zeta potential and surface charge.

Theory

Classical Helmholtz-Smoluchowski equation is widely used to calculate zeta potential of membranes. It is written as follows:

$$\zeta = \frac{\Delta E}{\Delta P} \frac{\eta \kappa_0}{\varepsilon \varepsilon_0} \quad (1)$$

where ΔE and ΔP are data from streaming potential measurements (ratio of registered potential to applied pressure drop), η , κ_0 and $\varepsilon \varepsilon_0$ are respectively dynamic viscosity, conductivity and permittivity of solution feeding the gap.

Yaroshchuk and Ribitsch generalized the classical equation to take into account the conductivity of walls forming the slit channel [2]. It includes the membrane conductivity κ_m , its thickness d_m and the intermembrane distance h :

$$\zeta = \frac{\Delta E}{\Delta P} \frac{\eta \kappa_0}{\varepsilon \varepsilon_0} \left(1 + 2 \frac{\kappa_m d_m}{\kappa_0 h} \right) \quad (2)$$

To take into account the relief of real membranes, we repeated the considerations made by Yaroshchuk and Ribitsch while including the roughness factor γ . The deduced equation is as follows:

$$\zeta = \frac{\Delta E}{\Delta P} \frac{\eta \kappa_0}{\varepsilon \varepsilon_0 \gamma} \left(1 + 2 \frac{\kappa_m d_m}{\kappa_0 h} \right) \quad (3)$$

All calculated zeta potentials were substituted into Grahame equation to obtain the surface charge:

$$\sigma = \sqrt{8 \varepsilon \varepsilon_0 C R T} \times \sinh \left(\frac{\zeta F}{2 R T} \right) \quad (4)$$

where C is electrolyte concentration, R is the gas constant and F is the Faraday constant.

Alternatively the zeta potential can be evaluated with Donnan potential:

$$\Delta \varphi_D = \frac{R T}{F} \ln \frac{Q}{C} \quad (5)$$

where Q is ion exchange capacity.

The surface charge can be evaluated from the known ion exchange capacity, if it is assumed that the ions are situated in the nodes of cubic lattice which is uniform throughout the membrane:

$$\sigma_Q = e \sqrt[3]{\frac{e F}{Q}} \quad (6)$$

where e is the charge of electron, 1.6×10^{-19} C.

Experiments

The streaming potential measurements were made using the gap cell developed in IPCE RAS (Figure 1) [2]. Two samples formed a slit rectangular channel of 25 mm length, 2 mm width, and 70 μm height. The experiments were conducted at 20°C, using a 0.02 M NaCl solution with conductivity 0.1309 S/m.

Four samples of homogeneous anion exchange AMX-Sb membrane (Astom, Japan) were studied equilibrated with 0.02 M NaCl solution. The first sample was commercial membrane (AMX-Sb), the second sample operated under current of 6 mA/cm² ($\sim 2 i_{lim}$) for 30 hours, and the third and the fourth samples were coated with one (AMX-Sb_{mod1}) or two (AMX-Sb_{mod2}) thin layers of MF-4SK cation exchange material.

As was determined from optical and atomic force microscopy data, the surface of original membrane possesses the wavy pattern, which results in roughness factor of 1.15. The membrane conductivity was 0.32 S/m while its thickness was 134 μm . Neither membrane conductivity nor its thickness changed during the modifications described above.

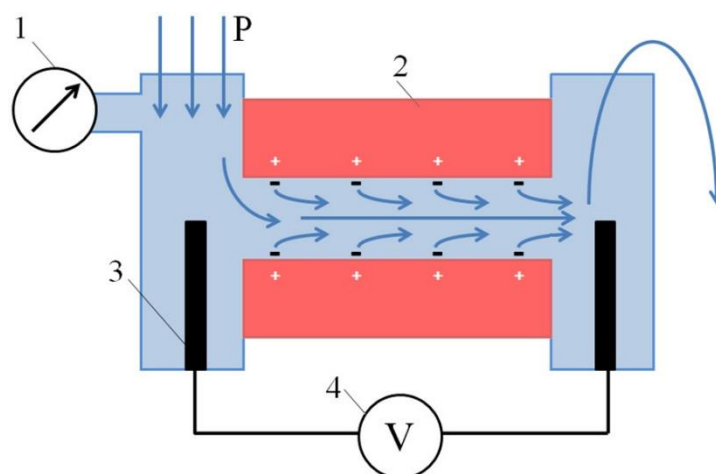


Figure 1. Scheme of gap cell for streaming potential measurements. 1 is pressure gauge, 2 is studied membrane, 3 is the Ag/AgCl electrode and 4 is voltmeter

Results and Discussion

The measured streaming potentials, zeta potentials calculated using equations 1-3 and corresponding surface charges are given in Table 1.

Table 1: Streaming potential measurement data and calculated electrokinetic characteristics

Sample	AMX-Sb	AMX-Sb _{used}	AMX-Sb _{mod1}	AMX-Sb _{mod2}
Streaming potential, mV/bar	15.1	4.1	-0.4	-0.8
Zeta potential, mV, by Eq. 1	27.5	7.4	-0.7	-1.5
Corresponding surface charge, $\mu\text{C}/\text{cm}^2$	0.95	0.24	-0.02	-0.05
Zeta potential, mV, by Eq. 1	284.6	77.5	-7.6	-15.1
Corresponding surface charge, $\mu\text{C}/\text{cm}^2$	232.90	3.67	-0.25	-0.50
Zeta potential, mV, by Eq. 1	247.5	66.7	-6.1	-13.9
Corresponding surface charge, $\mu\text{C}/\text{cm}^2$	111.66	2.93	-0.22	-0.44

The Donnan potential drop at the surface of this membrane is estimated as 110 mV. The surface charge calculated basing on known ion exchange capacity is 14 $\mu\text{C}/\text{cm}^2$. These evaluations are essentially higher than the values found using equations 1 and 4; hence the wall conductivity should be taken into account when calculating the zeta potential of ion exchange membranes. However, the values found when using the equations 2 and 4 are unrealistically high. Accounting the surface roughness allows obtaining more reasonable values of surface charge (equations 3 and 4); nevertheless, both zeta potential and surface charge remain high. This may be explained by the underestimated roughness factor. The evidence exists [4] that AMX-Sb surface possesses, aside

from wavy pattern with amplitude of tens of microns, a relief in micrometer scale, which is harder to evaluate.

Acknowledgements

We are grateful to the RFBR for financial support (grant no. 15-58-16005_NCNIL_a).

References

1. *Nebavskaya K., Sarapulova V., Sabbatovskiy K., Sobolev V., Pismenskaya N., Sistas P., Cretin M., Nikonenko V.* Impact of ion exchange membrane surface charge and hydrophobicity on electroconvection at underlimiting and overlimiting currents // *J. Membr. Sci.* 2017. V. 523. P. 36-44.
2. *Yaroshchuk A., Ribitsch V.* Role of channel wall conductance in the determination of zeta potential from electrokinetic measurements // *Langmuir.* 2002. V. 18. P. 2036-2038.
3. *Guler E., van Baak W., Saakes M., Nijmeijer K.* Monovalent ion-selective membranes for reverse electrodialysis // *J. Membr. Sci.* 2014. V. 455. P. 254-270.

COMPARISON OF CHRONOPOTENTIOMETRIC CURVES OF HETEROGENEOUS ION-EXCHANGE MEMBRANES WITH HYDROPHOBIC OR HYDROPHILIC NON-CONDUCTIVE SURFACE AREAS. 2D SIMULATION

Andrey Nebavskiy, Semyon Mareev, Vladlen Nichka, Ksenia Nebavskaya

Kuban State University, Krasnodar, Russia, E-mail: nearhim@gmail.com

Introduction

Due to their lower cost, heterogeneous ion exchange membranes are widely used in electrodialysis. It was recently shown [1] via mathematical modeling that, depending on the fraction of insulating surface, the heterogeneous membranes can possess mass transport characteristics exceeding the homogeneous membranes. The questions of precise fraction of insulating surface required for such improvements, and also of simultaneous optimization of heterogeneity and other parameters affecting the mass transport, such as hydrophobicity of membrane surface, is still open, though.

Modelling

The modeling was implemented for galvanostatic mode for easier comparison with experimental studies of electrochemical characteristics of ion exchange membranes (chronopotentiometry, voltammetry). The equations of basic mathematical model [2] were used together with the electric current stream function to simulate the mass transport through heterogeneous membrane:

$$\begin{aligned} \vec{J}_i &= -\frac{F}{RT} z_i D_i c_i \nabla \varphi - D_i \nabla c_i + c_i \vec{V}, & \frac{\partial c_i}{\partial t} &= -\nabla \cdot \vec{J}_i, & \Delta \varphi &= -\frac{F}{\varepsilon \varepsilon_0} \sum_i z_i c_i \\ \Delta \eta &= -\frac{F^2}{RT} \left(\left(\sum_i z_i^2 D_i \frac{\partial c_i}{\partial y} \right) \frac{\partial \varphi}{\partial x} - \left(\sum_i z_i^2 D_i \frac{\partial c_i}{\partial x} \right) \frac{\partial \varphi}{\partial y} \right) + F \left(\left(\sum_i z_i \frac{\partial c_i}{\partial y} \right) V_x - \left(\sum_i z_i \frac{\partial c_i}{\partial x} \right) V_y + \left(\sum_i z_i c_i \right) \left(\frac{\partial V_x}{\partial y} - \frac{\partial V_y}{\partial x} \right) \right) \\ i_x &= \frac{\partial \eta}{\partial y}, & i_y &= -\frac{\partial \eta}{\partial x}, & \frac{\partial \vec{V}}{\partial t} + (\vec{V} \nabla) \vec{V} &= -\frac{1}{\rho_0} \nabla P + \nu \Delta \vec{V} + \frac{1}{\rho_0} \Delta \varphi \nabla \varphi, & \nabla \cdot \vec{V} &= 0 \end{aligned}$$

The model is two dimensional and nonstationary. The simulated region is a rectangle, framed with flat membrane surface on one side and solution bulk on the other. The distance between them is set equal to Nernst diffusion layer thickness calculated using Leveque equation [2]. These equations were also used to calculate the theoretical limiting current i_{lim} . In simulations, the current density was $1.5 i_{lim}$ and the electrolyte was 0.02 M NaCl.

$$\delta_{Lev} = 0.71h \left(\frac{LD}{h^2 V_0} \right)^{1/3} \quad i_{avlim}^0 = \frac{FDc_0}{h(T_i - t_i)} \left[1.47 \left(\frac{h^2 V_0}{LD} \right)^{1/3} - 0.2 \right]$$

The anion exchange membrane with surface consisting of interchanging conductive and insulating stripes was modeled. The lengths of conductive and insulating stripes were 10 μm and 40 μm , respectively. Here we report the calculation results for the membrane composed from three repeating bi-stripes, as shown in Fig. 1.

Two terminal cases were studied. In first one (further denoted as “hydrophobic membrane”) the

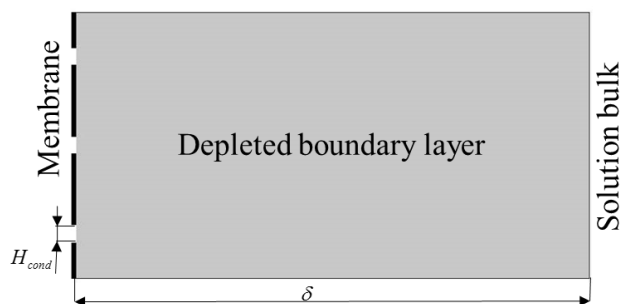


Figure 1. Simulated region

insulated stripes were considered as hydrophobic and did not hinder the stream of liquid. In second one (further denoted as “hydrophilic membrane”) the insulating surface was considered as hydrophilic and it completely stopped the slip of liquid near-surface layer over the surface.

The boundary conditions are identical to those used in [2,3], except that at conductive stripes:

$$\bar{J}_i \Big|_{x=0} = \frac{T_i}{z_i F \varepsilon_c} \frac{\partial \eta}{\partial y} \Big|_{x=0}, \quad c_i \Big|_{x=0} = C_m, \quad \varphi \Big|_{x=0} = 0, \quad \bar{V} \Big|_{x=0} = 0, \quad \frac{\partial \eta}{\partial x} \Big|_{x=0} = 0$$

At hydrophobic insulating stripes:

At hydrophilic insulating stripes:

$$(V_x) \Big|_{x=0} = 0, \quad \frac{\partial V_x}{\partial x} \Big|_{x=0} = 0, \quad \frac{\partial \eta}{\partial y} \Big|_{x=0} = 0 \quad (V_x) \Big|_{x=0} = 0, \quad \frac{\partial V_x}{\partial x} \Big|_{x=0} = 0, \quad \frac{\partial \eta}{\partial y} \Big|_{x=0} = 0$$

Results and Discussion

The calculated chronopotentiograms (ChP) are given in Fig. 2, and the calculated ion concentration profiles near the membrane surface at different times shown in the ChP (Fig. 2) are given in Fig. 3.

It can be seen from Fig. 2 that the potential drop in diffusion layer is sufficiently higher in case of hydrophilic membrane. The counterion concentration (Fig. 3) is always higher near the surface of hydrophobic membrane.

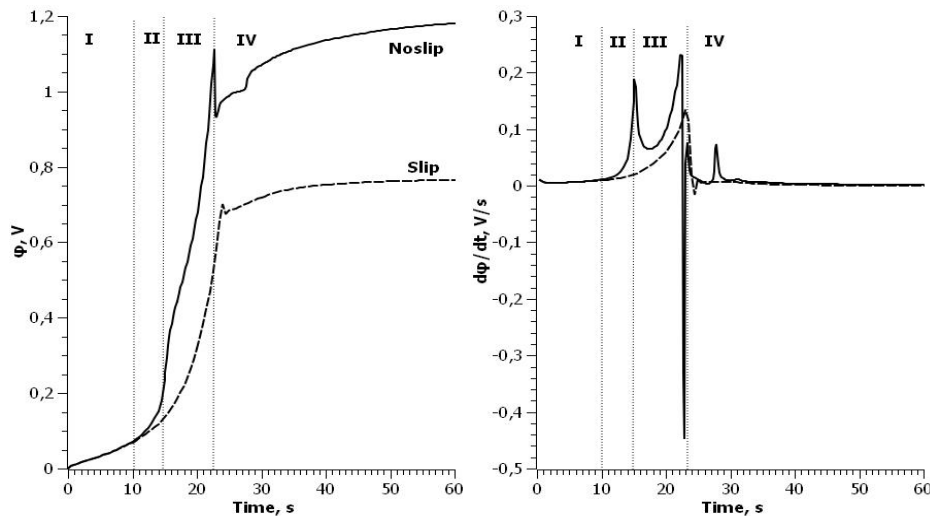


Figure 2. Calculated ChPs in “potential drop vs. time” (to the left) and “derivative of potential drop vs. time” (to the right) coordinates. Dashed lines correspond to hydrophobic membrane and the solid line – to hydrophilic one

Four regions can be found in ChPs, differing in the mode of ion delivery to membrane surface. During the first one, lasting for first 10 s, practically no difference can be observed in ChPs and in concentration profiles of hydrophobic and hydrophilic membranes. The potential drop here is low, meaning the low Ohmic and diffusional resistance of the system. The dominant mechanism of ion delivery is electrodiffusion.

The second region (10-15 s) is characterised by steep increase of potential drop caused by continuing desalination of solution near the membrane surface. The ChPs of modelled membranes differ here due to modes of delivery of ions to membrane surface. The profile of counterion concentration near the hydrophilic membrane is almost linear, meaning that, due to absence of slip of near-surface solution the main mechanism of ion delivery is still electrodiffusion. Decreasing potential drop in ChP and strongly nonlinear concentration profile near the hydrophobic membrane show that the mechanism of ion delivery becomes mixed. The easy change in mechanism of mass transport is explained by absence of resistance to convective transport from the hydrophobic membrane surface. The convective mixing here has low intensity and occurs only close to membrane surface near the conductive stripes. For hydrophilic membrane such change happens later, at transition time $t=15.2$ s ($0.79 \tau_{sand}$).

In the third region (15-23 s) smooth but quite significant growth of potential drop appears in both systems due to continuing desalination of solution near the conductive stripes. After that, the potential drop steeply decreases, its later increase significantly slows down and, after some time, the potential reaches stationary value. The concentration profiles near both membranes bend, and

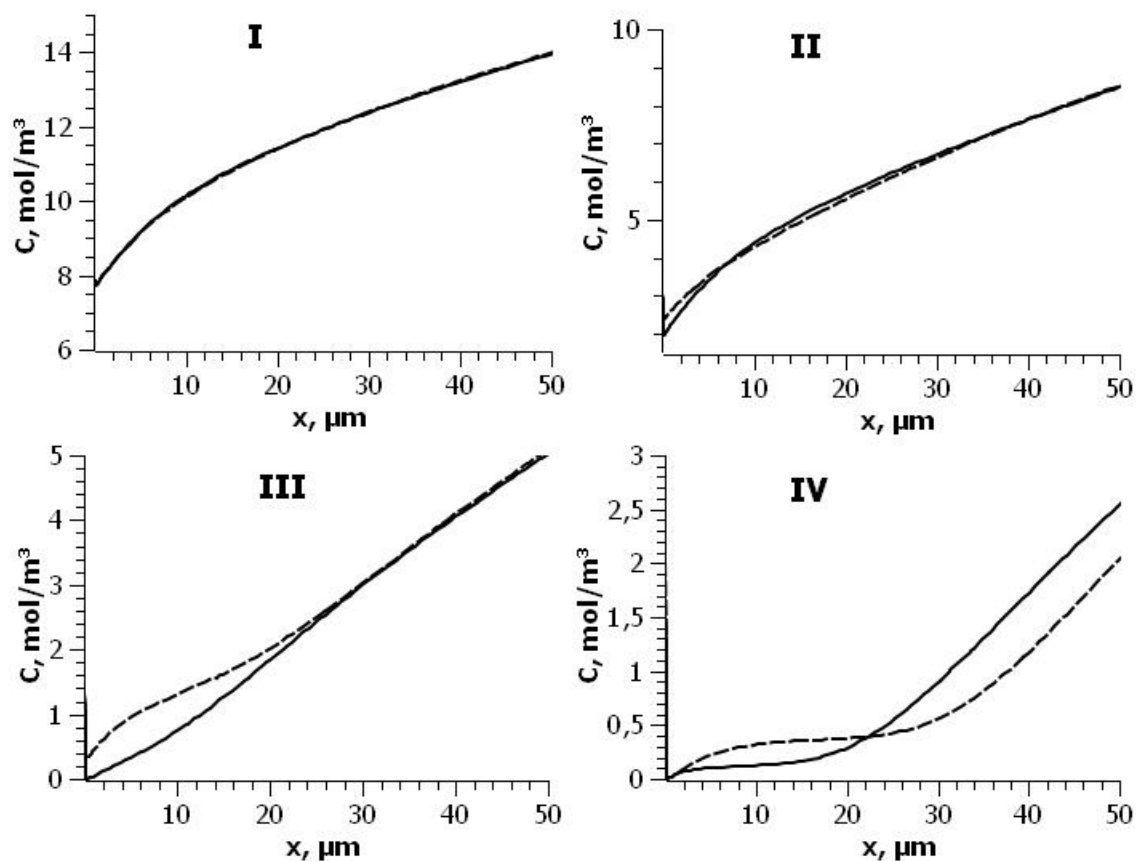


Figure 3. Counterion concentration profiles. Roman numbers correspond to moments marked in Fig. 2. Dashed lines denote the values for hydrophobic membrane and solid – for hydrophilic one

the second transition time appear (at $t=22$ s for hydrophilic and $t=23$ s for hydrophobic membrane, which correspond to $1,15 \tau_{Sand}$)) due to change of mass transport mechanism in entire studied area.

In fourth region (from 25 s) the concentration profiles become further deformed. Bends in ChPs depend on many factors, such as the number of repeating bi-stripes.

Acknowledgements

We are grateful to the RFBR for financial support (grant no. 16-38-00794_mol_a).

References

1. Davidson S.M., Wessling M., Mani A. On the Dynamical Regimes of Pattern-Accelerated Electroconvection// Scientific Reports, 2016, V. 6, Art. no: 22505
2. Urtenov M.K., Uzdenova A.M., Kovalenko A.V., Nikonenko V.V., Pismenskaya N.D., Vasil'eva V.I., Sistat P., Pourcelly G. Basic mathematical model of overlimiting transfer enhanced by electroconvection in flow-through electro dialysis membrane cells //J. Mem. Sci., 2013, V. 447, P. 190-202
3. Mareev S.A., Nichka V.S., Butylskii D.Yu., Urtenov M.Kh., Pismenskaya N.D., Apel P.Yu., Nikonenko V.V. Chronopotentiometric Response of an Electrically Heterogeneous Permselective Surface: 3D Modeling of Transition Time and Experiment// J. Phys. Chem. C, 2016, V. 120 (24), P. 13113–13119

THE PHENOMENON OF TWO TRANSITION TIMES IN CHRONOPOTENTIOMETRY OF SYSTEMS WITH ELECTRICALLY INHOMOGENEOUS ION EXCHANGE MEMBRANES. EXPERIMENT AND MODEL

Vladlen Nichka, Semyon Mareev, Andrey Nebavskiy, Dmitrii Butylskii, Natalia Pismenskaya, Victor Nikonenko

Membrane Institute, Kuban State University, Krasnodar, Russia, mareev-semyon@bk.ru

Introduction

The transition time is an important kinetic characteristic of ion transport [1, 2, 3]. This time corresponds to the moment during chronopotentiometric measurements under a given direct current density $i > i_{lim}$ when the electrolyte concentration at membrane (or electrode) surface attains such a low value that additional mechanisms of ion transfer arise. This paper describes a phenomenon of two transition times, which occurs in systems with heterogeneous membranes.

Experiment

A specially designed membrane with tailored surface structure was investigated. A polyethylene terephthalate track-etched membrane of thickness 10 μm (Fig. 1) produced at the Joint Institute for Nuclear Research, Dubna, Russia is used as the substrate. The membrane has cylindrical (from 25.4 to 26.3 microns in diameter) pores, randomly distributed with the density $1.47 \cdot 10^4$ pores/ cm^2 . We coated the membrane on one side with a Nafion® perfluorinated dispersion, producing the surficial layer with thickness $\sim 3 \mu\text{m}$; the Nafion® dispersion also filled the pores. Hence we obtained a membrane with a smooth homogeneous permselective surface on one side and a heterogeneous surface on the other. Thus, most of the surface of modified membrane is nonconductive, while it involves circular conductive areas filled with the Nafion® material occupying about $\approx 7.7\%$ of the surface.

Chronopotentiograms were obtained according to the procedure described in [3], a flow-through cell and a 0.02 M NaCl solution were used.

Results and discussions

The investigation of properties of model membrane has shown that the presence of electrical heterogeneity on its surface leads to appearance of two transition times in chronopotentiograms obtained at current densities from 1.2 to 1.7 i_{lim} , where i_{lim} is the theoretical limiting current. The first transition time is lower than the value calculated using the Sand equation (in 2.5-10 times, depending on the current density) and the second one is slightly higher (in ~ 1.1 times). The determination of the first transition time is impossible at current densities higher than 1.7 limiting currents, since the potential increases very steeply so the transition time should be less than one second; hence only one transition time remains, which was previously the second one.

We report an approach to 3D modelling (with cylindrical symmetry) of kinetic dependence of ion transfer through a surface composed from the conductive and nonconductive areas. We use the electrical current stream function for formulation and solution of the model. The theoretical chronopotentiograms were compared with experimental ones, and it was shown that at initial stage they are in good match. The differences increase when approaching the transition time. Nevertheless, the theoretical and experimental transition times are in good agreement until the current density reaches the 1.7 limiting currents. Only the second transition time remains at higher current density, and the supposed reason for this is the smoothening of concentration profile due to occurrence of phenomena coupled with passage of current, which are not accounted for in this model.

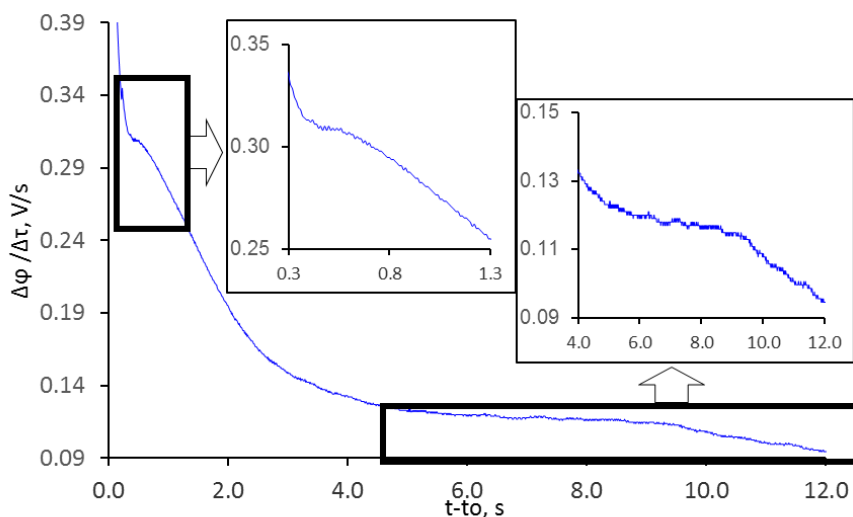


Figure 1. Determination of transition time for the model membrane by the inflection point of plot in coordinates “derivative of potential drop – time”

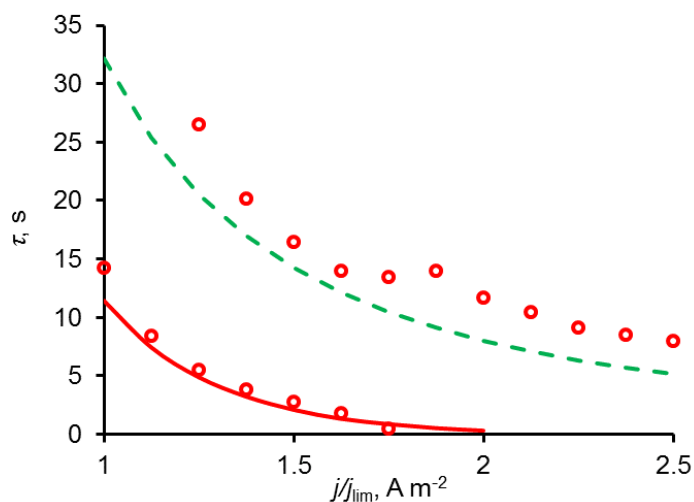


Figure 2. Experimental (points) and theoretical (lines) transition times for model membrane. The dashed line denotes the times calculated using Sand equation, and the solid line denotes the times calculated using 3D model

Acknowledgments

The work was carried out within the framework of joint French-Russian laboratory “Ion-Exchange Membranes and Related Processes”. The authors are grateful to the RFBR for the financial support (grant No. 16-38-60135mol_dk).

References

1. Krol J.J., Wessling M., Strathmann H. // *J. Membr. Sci.* 1999. Vol. 162. P.155.
2. Choi J.-H., Moon S.-H. // *J. Membr. Sci.* 2001. Vol. 191. P. 225.
3. Volodina E., Pismenskaya N., Nikonenko V. et all. // *J. Colloid Interface Sci.* 2005. Vol. 285. P. 247.
4. Mareev S. A., Butylskii D. Yu., Pismenskaya N. D., Nikonenko V. V. // *J. Membr. Sci.* 2016. Vol. 500. P. 171.

THE STUDY OF ION TRANSPORT IN THE SYSTEM "HETEROGENEOUS ION-EXCHANGE MEMBRANE - AMMONIUM NITRATE SOLUTION"

Sabukhi Niftaliev, Olga Kozaderova, Kseniya Kim

Voronezh State University of Engineering Technologies, Voronezh, Russia

E-mail: kmkseniya@mail.ru

Electrodialysis of nitrogen-containing salt solutions is a promising method of cleaning of waste generated in the production of mineral fertilizers. However, transport properties of ion-exchange membranes during the electrodialysis of ammonium nitrate solutions have not been studied in a proper way. Therefore, the purpose of this paper was to study transport characteristics of the heterogeneous ion-exchange membranes MK-40 and MA-41 in the ammonium nitrate solutions for intense current modes of electrodialysis.

The electrodialysis was carried out in a seven-section apparatus separated by the cation-exchange (MK-40) and anion-exchange (MA-41) membranes (Fig. 1).

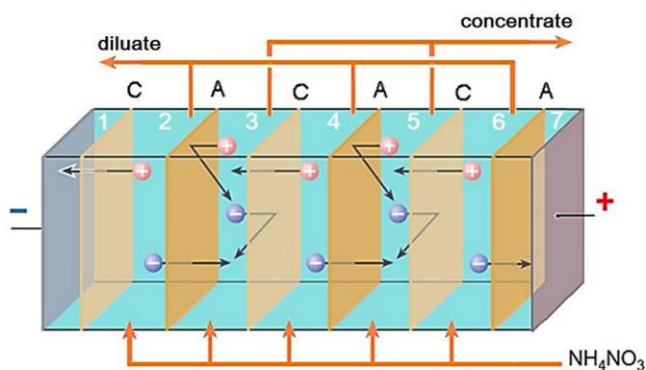


Figure 1. Electrodialysis cell with the alternating cation-exchange (K) and anion-exchange (A) membranes.

Intensity of the generation of medium ions on the membrane-solution interphase boundary was determined by the method of selective polarization of membranes [1]: the ammonium nitrate solution with the concentration of 0,012 mole / dm³ was fed to the desalting section 4, and in the desalting sections 2 and 6 – 0,12 mole / dm³. Under these conditions, the limiting current density was reached only on the membranes of the desalting section 4, the determination of pH of the solutions in the sections 3 and 5 made it possible to estimate intensity of the generation of medium ions by the membranes of the section 4.

Dependence of the flux value of the ions NH₄⁺ and NO₃⁻ during electrodialysis of the model solution with the membrane pair MK-40 / MA-41 on the current density is shown in Fig. 2.

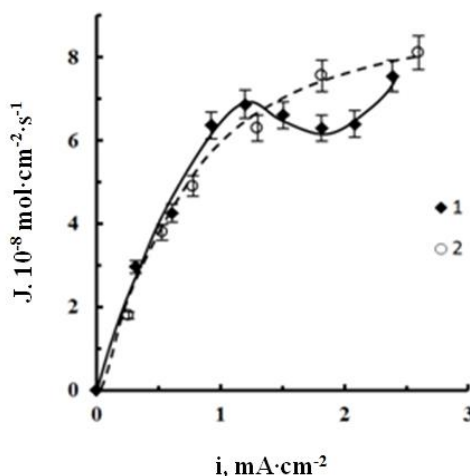
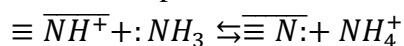


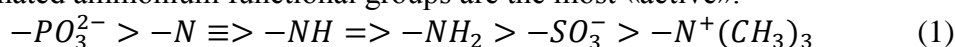
Figure 2. Dependence of the ion fluxes of NH₄⁺ (1) through MK-40 and NO₃⁻ (2) through MA-41 on the current density during electrodialysis of the solution NH₄NO₃ (0,012 mole / dm³)

Decrease in the flux of ammonium ions when there is excess of the limiting current density can be explained by the «barrier effect» [2]. In our system the decrease in the flux of NH_4^+ - ions is connected with the fact that they interacting with OH^- -ions formed on the «cation-exchange membrane-solution» boundary during the dissociation of water molecules in the desalting section lose the ability to pass through the cation-exchange membrane. Further when the limiting current exceeds twice the convective instability, leading to active mixing of the solution, the consequence of which is increase in the ion flux, develops in the system.

Decrease in the flux of nitrate ions is connected with the influence of ammonium ions in the alkaline medium on the anion exchange membranes with quaternary and tertiary ammonium groups, which leads to the change in the composition of the functional groups:



Reactions of this type contribute to increase in the generation of the ions H^+/OH^- during the electro dialysis process in over-limiting current conditions, since in accordance with the row of catalytic activity of ionogenic membrane groups with respect to the dissociation reaction of water molecules [3], deprotonated ammonium functional groups are the most «active».



To confirm the influence of ammonium ions on the transport of nitrate ions through anion-exchange membranes the experiment on the electro dialysis of NH_4NO_3 and KNO_3 was carried out. The results of the experiment are shown in Fig. 6, from which it can be seen that during the electro dialysis of the KNO_3 solution under conditions of exceeding the limiting current density, the decrease of the NO_3^- - ions flux does not happen (Fig. 2).

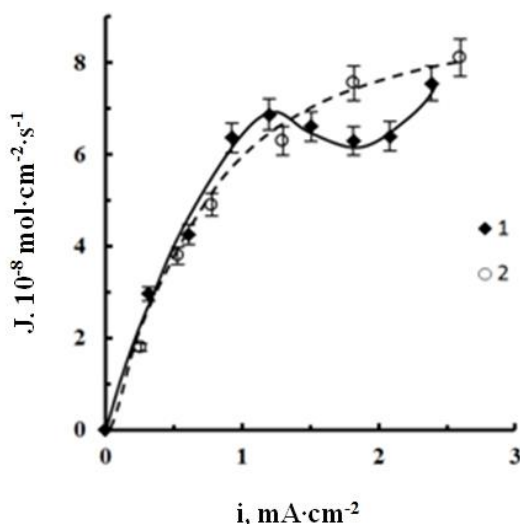


Figure 3. Dependence of the NO_3^- - ions fluxes through the anion-exchange membrane MA-41 on the current density during the electro dialysis of the solutions $0,012 \text{ mole} / \text{dm}^3$: 1 - NH_4NO_3 , 2 - KNO_3

To estimate the generation intensity of medium ions by the anion exchange membrane during electro dialysis of NH_4NO_3 and KNO_3 the method of the selective polarization of ion-exchange membranes was used. In Fig. 3 and 4 the transport numbers of the anions of the electrolyte and hydroxyl ions, as well as fluxes of OH^- -ions through the anion-exchange membrane, as a function of the dimensionless current density $-i/i_{\text{lim}}$ are shown.

It can be seen from the data that in the case of the ammonium nitrate solution the generation of OH^- - ions by the MA-41 membrane is indeed more active.

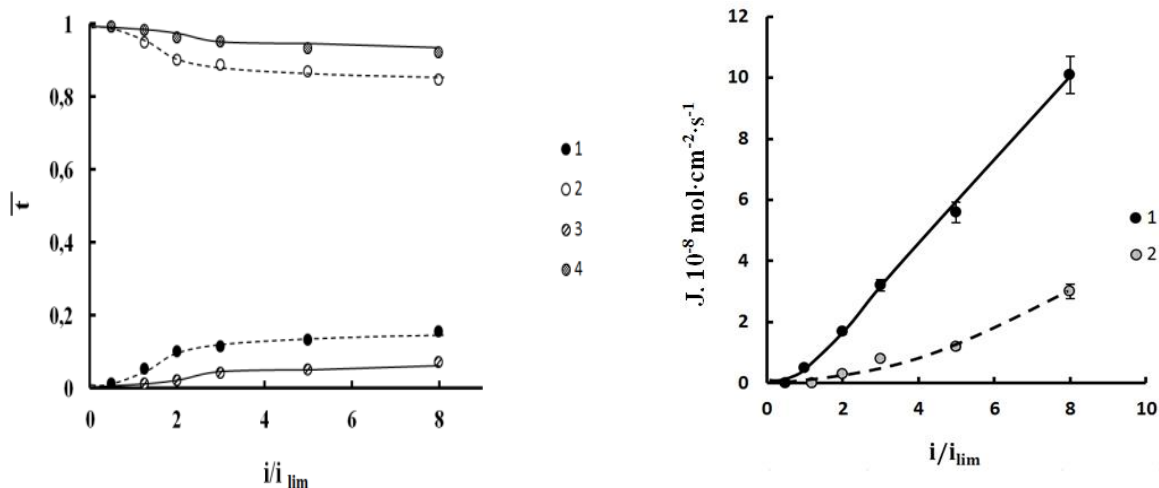


Figure 4 (left). Dependence of the ion transport numbers for the anion-exchange membrane MA-41 on the dimensionless current density during electro dialysis of NH_4NO_3 and KNO_3 :

1 – OH^- (NH_4NO_3), 2 – NO_3^- (NH_4NO_3), 3 – OH^- (KNO_3), 4 – NO_3^- (KNO_3)

Fig.4 (right). Dependence of the OH^- -ion fluxes through the anion-exchange membrane MA-41 on the dimensionless current density during electro dialysis of: 1 – NH_4NO_3 , 2 – KNO_3

Thus, the decrease in nitrate ion fluxes in the presence of ammonium ions is connected with the influence of NH_4^+ on the functional groups of the anion exchange membrane. It manifests itself in increase in the catalytic activity of these groups with respect to the water dissociation reaction and, as a result, in a higher competitive flux of medium ions.

References

1. Isaev N.I. Dissolution of sparingly soluble electrolytes by electro dialysis with ion-exchange membranes, Synthesis and properties of ion-exchange materials, Nauka, 1968.
2. Shaposhnik V.A., Selemenev V.F., Terent'eva N.P. et al. Barrier effect during electromigration of proline and valine across ion exchange membranes by electro dialysis // Russian. J. of Appl. Chem., 1988, V. 61, No. 5, pp. 1183-1185.
3. Zabolotskiy V.I. Dissociation of water molecules in systems with ion-exchange membranes// Uspehi himii. 1988. V. 57. P. 1403.

IMPACT OF CURRENT DENSITY, SOLUTION CONCENTRATION AND SURFACE CHARGE DENSITY ON THE MECHANISM OF ELECTROCONVECTION IN MEMBRANE SYSTEMS. PERSPECTIVES IN FIGHTING SCALING

¹Victor Nikonenko, ¹Aminat Uzdenova, ¹Ksenia Nebavskaya, ¹Marina Andreeva,

²Lasaad Dammak

¹Membrane Institute, Kuban State University, Krasnodar, Russia, *E-mail: v_nikonenko@mail.ru*

²Institute de Chimie et des Matériaux de Paris Est, UMR 7182 CNRS-Université Paris-Est, Thiais, France

Electroconvection (EC) is recognized as the main effect, which provides overlimiting mass transfer in electrodialysis and microfluidic systems. Besides, this phenomenon is found effective in fighting scaling occurring on ion-exchange membranes in desalination compartments [1]. Understanding the mechanisms of EC and the possibilities of use of this effect for diminishing the deposit of poorly soluble salts and hydroxides present an important issue for the theory and practice of electrodialysis.

In this study, we show that the mechanism of EC depends on the some governing parameters of electrodialysis as well as on the membrane properties. An important fact for understanding the phenomenon of EC is that the thickness and structure of the double electrical layer (DEL) at the membrane / solution depend on the polarizing electric current. This fact was first noticed by Levich, who as early as in 1949 showed [2] that the flow of small currents shifts the electrolyte concentration c_s at the electrode surface. Decreasing c_s results in increasing the DEL thickness, which remains quasiequilibrium. However, when the current density is higher than the limiting one, i_{lim} , an essentially non-equilibrium extended space charge region (SCR) forms. Its thickness may attain a few microns, while the maximum thickness of the quasiequilibrium DEL is of the order of 100 nm. Note, that the charge of the quasiequilibrium part of SCR strongly depends on the charge of the ion-selective surface, q_s , while the charge of its extended part is almost independent of q_s . In accordance to the state of SCR, at $i < i_{lim}$, only equilibrium EC (which is also known as the electroosmosis (EO) of the first kind [3] can occur, while at $i > i_{lim}$, non-equilibrium EC (or EO of the second kind) arises [3]. The both kinds of EC may be stable or unstable; the latter occurs if the voltage/current surpasses a certain threshold.

For the development of EO of both the first and second kind, a tangential electric field is required, whose action on the SCR leads to EO slip. The tangential field can be due to the electrical inhomogeneity and / or curvature of the surface, as well as to the inhomogeneity in the distribution of concentration.

An unstable EC causes current/voltage oscillations, which can be seen on the voltammograms and chronopotentiograms. Usually, these oscillations start at a voltage of about 1 V. However, in some cases (high charge and surface heterogeneity, multiply-charged counterion), such oscillations can begin at a corrected potential drop of 30-50 mV [4]. In this case, an anomalous region in the stationary current-voltage characteristic appears: with increasing current density, the potential drop does not increase, as usual, but decreases (Fig. 1).

Curve I relates to the AMX-SB membrane, which is characterized by a high (positive) surface charge and moderate degree of hydrophobicity. EC arising at this membrane is high both at low and high voltages, the PD is the lowest among all studied membranes. Membrane II has a lower surface charge and nearly the same degree of hydrophobicity. Hence, EC is less intensive than in the case of AMX-SB membrane. The surface charge of membrane III is negative, and its absolute value is nearly zero, however, the degree of hydrophobicity is quite high. Fig. 1 shows that the equilibrium EC is very low or absent near this membrane, while non-equilibrium EC is quite high. The result is explained by the fact that the equilibrium EC highly depends of the absolute surface charge, while the non-equilibrium EC is mainly determined by the degree of hydrophobicity. This rule is confirmed by the shape of the chronopotentiogram for membrane IV, which negative surface charge is slightly higher in absolute value than that of membrane III, but the degree of hydrophobicity is lower.

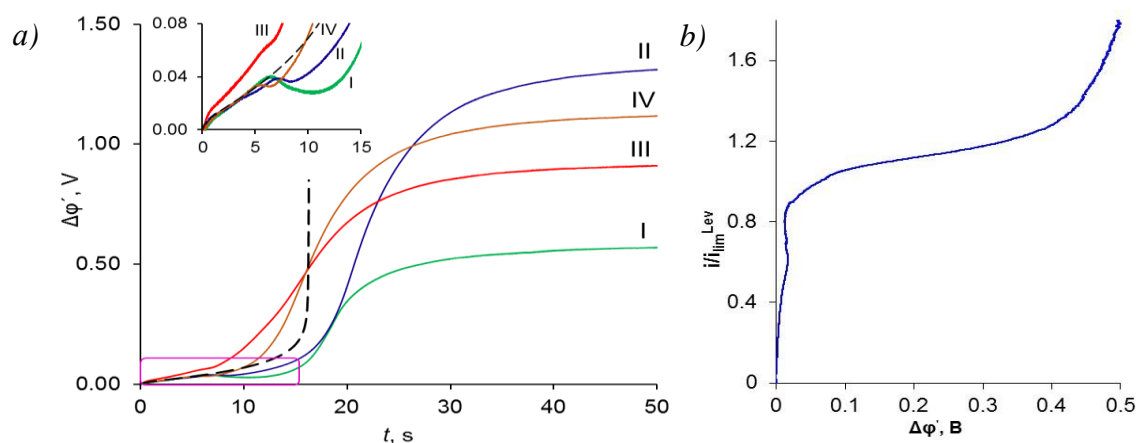


Figure 1. a – Chronopotentiograms of an AMX-SB anion exchange membrane and its three modifications differing in the surface charge and degree of hydrophobicity at a current density of $i = 1.4 i_{lim}$. The dotted line shows the theoretical curve calculated using a 1D model without taken into account EC (adapted from [4]); b – voltammogram of AMX-SB

As for the effect of solution concentration, the situation is rather complicated. On the one hand, more the concentration, less the equilibrium DEL thickness; the thickness of the expanded SCR being nearly independent of the concentration (when the ratio i/i_{lim} is fixed). On the other hand, with increasing concentration, electric current density increases, and, consequently, the electric force applied to the space charge increases also. As a result, as experiment and simulations [5] show, increasing concentration would lead to a decrease in EC. The decrease in intensity of EC should be less pronounced at high voltages, where Rubinstein-Zaltzman EC instability occurs.

The experimental data by Mikhaylin [1] and our recent results show that EC can be an effective means of fighting precipitation of Ca^{2+} and Mg^{2+} together with OH^- and CO_3^{2-} ions, which occurs in desalination compartments when treating solutions modeling milk mineral composition. It is of interest that in 0.04 M $MgCl_2$ solution, no precipitate forms at $i < 1.1 i_{lim}$, and at $i > 1.5 i_{lim}$, while in the interval $1.1 i_{lim} < i < 1.5 i_{lim}$ there is formation of scaling.

Acknowledgments

This investigation was realized in the frame of a joint French-Russian PHC Kolmogorov 2017 project of the French-Russian International Associated Laboratory "Ion-exchange membranes and related processes" with the financial support of Minobrnauki (Ref. N° RFMEFI58617X0053), Russia, and CNRS, France (project N° 38200SF).

References

1. Mikhaylin S., Nikonenko V., Pismenskaya N., Pourcelly G., Choi S., Kwon H. J., Han J., Bazinet L. How physico-chemical and surface properties of cation-exchange membrane affect membrane scaling and electroconvective vortices: Influence on performance of electrodialysis with pulsed electric field // *Desalination* 2016. V. 393. P. 102–114.
2. Levich V.G. The theory of non-equilibrium double layer // *Proc. USSR Acad. Sci.* 1949. V. 67. P. 309-312.
3. Dukhin S.S. Electrokinetic phenomena of the second kind and their applications // *Adv. Colloid Interface Sci.* 1991. V. 35. P. 173-196.
4. Nebavskaya K. A., Sarapulova V. V., Sabbatovskiy K. G., Sobolev V. D., Pismenskaya N. D., Sistat P., Cretin M., Nikonenko V. V. Impact of ion exchange membrane surface charge and hydrophobicity on electroconvection at underlimiting and overlimiting currents // *J. Membr. Sci.* 2017. V. 523. P. 36–44.
5. Uzdenova A. M., Kovalenko A. V., Urtenov M. Kh, Nikonenko V. V. Theoretical analysis of the effect of ion concentration in solution and at membrane surface on mass transfer at overlimiting currents // *Russ. J. Electrochem.* 2017. in press

CONCENTRATION OF MINERAL SALTS IN A MEMBRANE DISTILLER WITH THE POROUS CONDENSER

Eduard Novitsky, Ilya Borisov, Georgy Golubev, Dmitry Matveev, Alexey Volkov

A.V. Topchiev Institute of Petrochemical Synthesis, Moscow, Russia, E-mail: ednov@ips.ac.ru

Introduction

The new concept of a membrane distillation based on the porous condenser in the air gap developed earlier is effective in the fresh water production from seawaters of various salinity [1, 2]. However, also the problem of processing of the low-concentrated solutions (50-70 g/kg) which are formed in processes of membrane desalination of seawater, first by the method of the reverse osmosis is currently important. The essence of a problem is in what such waters usually dump to the seawater area that involves negative ecological consequences, including increase in salinity of water in the place of operation of the desalination plants and change of flora and fauna of the seawater area. In connection, therewith development of technology of concentrating of such weak brines is of interest to create economically acceptable technology of their drying with receiving useful products. The real research sets as the purpose to adapt membrane distillation with application of earlier developed designs of membrane distillation as intermediate stage increase in salinity of concentrates of reverse osmosis processes for the subsequent drying and production of dry salts.

Experiments

For behavior of researches, experimental stand which scheme submitted in the drawing was created. The membrane distillation module of this scheme was described in [1, 2].

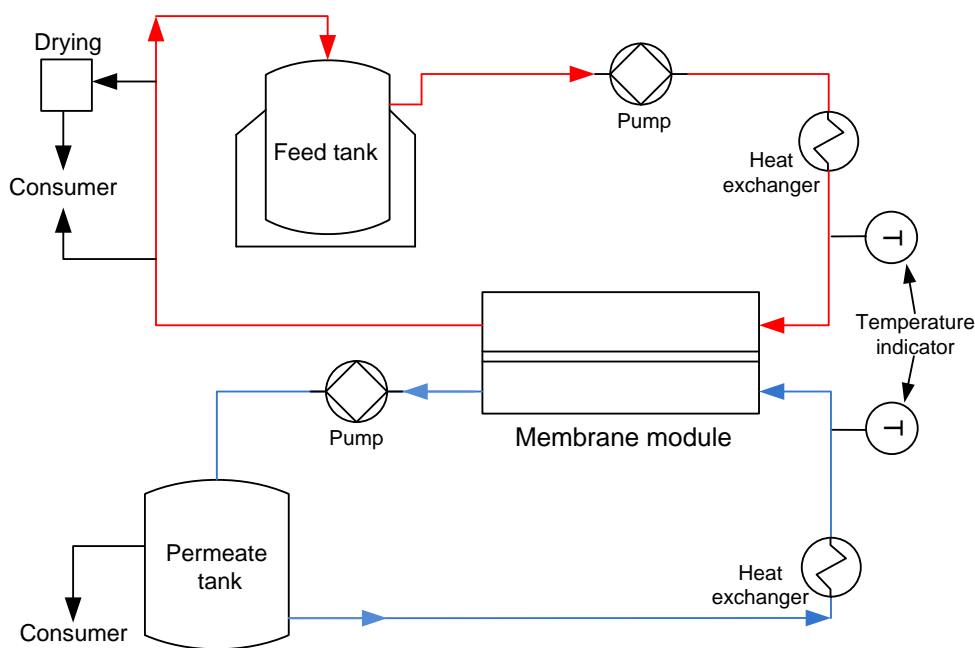


Figure. Scheme of membrane distillation module

The module belongs to type of a membrane distiller with an air gap; its device is a distinctive detail existence of the porous condenser in over membrane space. The apparatus is equipped with a hydrophobic poly(tetrafluoroethylene) membrane, thickness – 57 μm , porosity – 80%, the area of a membrane – 96 cm^2 .

Stand operating procedure. Before work, tanks are filled: tank of initial solution a sodium chloride brine with concentration not less than 40 g/l. Tank of condensate is filled with the distilled water. Experiments are made at temperatures of 50 and 80 $^{\circ}\text{C}$. Temperature of a cold contour – 22 ± 2 $^{\circ}\text{C}$. After a thermostating of hot and cold contours include supply of initial solution and the distilled water in a distiller, speed of pumping of 0.6 l/min. After an hour of continuous work process is stopped. Determine the mass of a concentrate and condensate and their salinity.

Results and Discussion

The process of two model solutions 40 and 60 g/l which imitate seawater (The Red Sea) and a concentrates of reverse osmoses desalters is investigated. Results of experiments at 50 and 80 °C in the Table.

Table: Experimental results

Feed concentration g/kg	Feed temperature °C	Experiment's time, h	Water flux kg/m ² ·h	Concentrate salinity, g/kg
40.0	50	1.0	5.8	47.7
	80	1.0	17.2	77.0
60.0	50	1.0	6.0	72.0
	80	1.0	17.0	113.7

The received results show that under the chosen experimental conditions in the developed model of a membrane distiller receiving concentrates with almost double increase in content of salt is possible. On the other hand, it is obvious that the chosen operating mode of a distiller is not optimum. It is possible that for increase in extent of concentration of the received brines it is necessary to increase the speed of the freshened stream at simultaneous reduction of frequency rate of circulation.

Acknowledgements

This work was supported by the Russian Foundation for Basic Research, project no. 17-08-00040.

References

1. *I.Borisov, V.Vasilevskii, O. Shorcheva, G.Golubev, E.Novitsky, A.Volkov, V.Volkov.* Thermomembrane process for separation low volatile compounds and volatile organic components from water. // "Ion transport in organic and inorganic membranes". Conference Proceeding, Sochi. 2016. P. 66-68. ISBN 978-5-9906777-3-9.
2. *A.V. Volkov, E.G. Novitsky, I.L. Borisov, V.P. Vasilevsky, V.V. Volkov.* Porous condenser for thermally driven membrane processes: Gravity independent operation//Separation and Purification Technology. 2016. V. 171. P. 191–196.

COMPOSITE SnO₂/C CARRIER, OBTAINED BY ELECTROCHEMICAL METHOD, AND SUPPORTED PLATINUM CATALYSTS

¹Ivan Novomlinskiy, ¹Irina Gerasimova, ¹Vladimir Guterman

¹Southern Federal University, Rostov-on-Don, Russia, *E-mail: novomlinskij@rambler.ru*

Introduction

The functional characteristics of platinum-containing electrocatalysts for low-temperature fuel cells are determined by their composition and structure. The most common carrier for catalysts still remain a variety of carbon materials. Degradation of inflicted platinum-carbon catalysts during operation low-temperature fuel cell, accompanied by decrease in mass activity, more pronounced on the oxygen electrode. It is due to different reasons. Firstly, gradually there is an Ostwald ripening of nanoparticles of platinum, due to the preferential dissolution of metal from the surface of small nanoparticles and reprecipitation on large. The second reason is oxidation of the carbon support predominantly near the interface platinum/carbon. The consequence of this is both a complete loss of contact of a portion of the nanoparticles with the carrier and facilitating their movement along the surface of the carbon, followed by connection in agglomerates. Also, there is the corrosion of platinum, which may be accompanied by subsequent restoration of its ions to the metal inside the polymer membrane. The smaller the size of the platinum nanoparticles, the lower their thermodynamic stability.

As one of the factors that increases the corrosion-morphological stability of the electrocatalyst, being considered the modification of the carbon support. The best from the point of view of resistance to oxidation are represented oxides. In addition, modification of the carbon support can increase the activity of the catalyst in the methanol oxidation reaction. [1]

The aim of our work was the obtain of composite SnO₂-C materials for the subsequent application of platinum.

Experiments

To obtain SnO₂-C electrocatalysts electrolysis conducted in galvanostatic conditions with stirring the carbon suspension (Vulcan XC-72), in a tin electrolyte (SnCl₂ solution, 0.1-1 M). The technique is described in detail in the article [2]. As the background electrolyte was used a 2M H₂SO₄. Current strength 9 A. Thus, a series of SnO₂-C materials with different mass fraction of SnO₂ was obtained. Further, the reduction of platinum with formaldehyde [3] in the liquid phase received a series of Pt/ SnO₂-C materials.

The resulting materials were investigated by gravimetry, x-ray diffraction, x-ray fluorescence analysis and cyclic voltammetry.

Results and Discussion

To study the microstructure of Pt/SnO₂-C materials and their electrochemical behaviors were selected samples with similar loading of platinum, while the mass fraction of tin oxide was varied from 2 to 10 %. Data analysis x-ray fluorescence studies confirmed the theoretical ratio of Sn:Pt.

On diffractograms (figure 1) for the obtained samples exhibit peaks of platinum and oxides of tin. Before the deposition of platinum (material SnO_x-C), there is reflections of tin oxide (II). Apparently, during the preparation of the catalyst and its drying, tin oxide is oxidized to tin oxide (IV), as evidenced by the disappearance of the reflections characteristic of tin oxide (II). The average diameter of the crystallites of platinum, calculated according to the Scherrer formula, is about 2-3 nm.

An electrochemical study of materials showed that the materials are characterized by a surface area of 120-170 m²/g (Pt) (ECSA is determined by the area of the peaks of adsorption and desorption of hydrogen). In addition, the samples are characterized by high activity in the oxygen reduction reaction. With increasing mass fraction of tin oxide in the material, there is a slight decrease in ECSA and activity in ORR, that can be explained by the increase in the share of platinum nanoparticles that are attached to the tin oxide, as a result of which they lose electric contact and do not participate in the reaction.

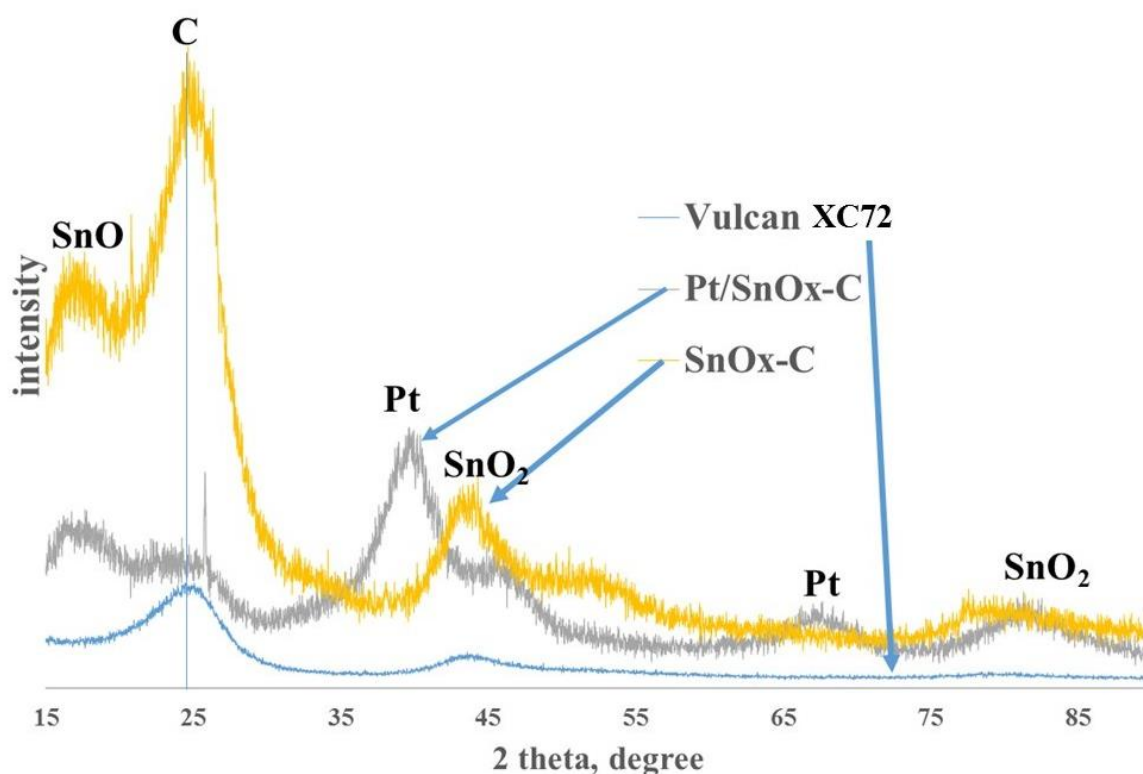


Figure 1. Diffractograms of the obtained samples

Thus, we received several materials, the characteristics of which are to some extent better than commercial analogs. Such materials, with further study, may have increased stability with respect to Pt/C materials.

The work is executed at support of the Ministry of education and science of the Russian Federation (grant №13.3005.2017/PCh)

References

1. Kuriganova A.B., Leontyeva D.V., Smirnova N.V., Ivanov S., Bund A. Electrochemical dispersion technique for preparation of hybrid MO_x-C supports and Pt/MO_x-C electrocatalysts for low-temperature fuel cells. *Journal of Applied Electrochemistry*. 2016. T. 46. № 12. С. 1245-1260.
2. Novomlinskij I.N., Volochaev V.A., Tsvetkova G.G., Guterman V.E., New electrochemical method for the preparation of Pt/C nanostructured materials // *Kondensirovannye sredy i mezhfaznye granitsy.*, 2017. T.19, №1, с.112-119
3. Alekseenko A.A., Guterman V.E., Volochaev V.A., Belenov S.V. Effect of wet synthesis conditions on the microstructure and active surface area of Pt/C catalysts. *Inorganic Materials*, 2015. 51. с.1258-1263

TRANSPORT PROPERTIES OF ASYMMETRIC AND COMPOSITE MEMBRANES BASED ON CHITOSAN COPOLYMERS WITH VINYL MONOMERS

¹Kseniia Otvagina, ²Alla Mochalova, ¹Tatyana Sazanova, ¹Artem Atlaskin, ¹Ilya Vorotyntsev

¹Nizhny Novgorod State Technical University n.a. R.E. Alekseev, 603950, Nizhny Novgorod, 24 Minina str., Russia, *E-mail: k.v.otvagina@gmail.com*

²Lobachevsky State University of Nizhny Novgorod, 603950, Nizhny Novgorod, 23 Gagarin av., Russia

Introduction

In the past decades, membrane separation of contaminations and impurities from gases and liquids has been attracting a rising interest due to their advantages over conventional separation processes such as reduced environmental impact, lower energy consumption, and operating costs. A variety of polymeric materials and the possibility to modify them enables the design of a membrane with desired separation performance for a particular task. Among polymers for “green” membrane design, amino polysaccharide chitosan (CS) stands out due to remarkable thermal stability and biodegradability. Chitosan is derived from chitin, an abundant natural polymer constituting the crustacean’s exoskeleton. Due to the presence of the amino group in its repeating unit, it shows an efficient binding of acid gases, such as carbon dioxide, negatively charged dispersions and microbial contaminations. High crystallinity of CS causes low physical-mechanical properties and low permeability through pure CS films. Previously it was shown that mechanical stability and permeability of gases through the CS membrane could be improved by obtaining copolymers with vinyl monomers and ionic liquid doping [1]. However, operational properties of the material also depend on the membrane morphology and the method of production. There are different approaches for the membrane production according to desirable morphology: sintering, stretching, track-etching, phase inversion and coating. Most commercially available membranes are produced by phase inversion technique. This is a very versatile technique allowing all kinds of morphology to be obtained. Phase inversion is well studied for acetate cellulose, polysulfones, polyamides and etc.

The scope of the present work is focused on preparation and characterization of asymmetric and composite membranes based on CS copolymers with poly(acrylonitrile) (PAN) and poly(styrene).

Experiments

CS copolymers with acrylonitrile (CS-PAN) and styrene (CS-PS) were obtained according to the previously published technique [2]. Composite membranes were prepared by copolymer solution casting onto porous support (polysulfonamide) followed by solvent evaporation. Asymmetric membranes of pure CS and CS copolymers were obtained by phase inversion technique. The 2% solution of sodium hydroxide in water was used as a nonsolvent. In order to control the formation of asymmetric and composite membranes microscopy method were used. Scanning electron microscopy (SEM) micrographs of the surfaces fractured perpendicular to the membrane plane (cross-section) were obtained with a Zeiss Merlin SEM (Carl Zeiss, Germany) at 10 kV. Atomic force microscopy was conducted using SPM-9700 (Shimadzu, Japan) with the silicon vibration cantilevers Pointprobe FMR-20 (Nano World Innovative Technologies, Switzerland) with a typical tip curvature radius of no greater than 8 nm with 15 μm length of the tip. Measurements were all carried out under ambient conditions using the tapping mode of imaging. The arithmetic average roughness height (R_a) and the mean roughness depth (R_z) were obtained by a program in the AFM image processing toolbox SPM Online, Version 4.02, (Shimadzu, Japan). Transport properties of the membranes were investigated in pervaporation and gas separation. Pervaporation was tested on water – tetrahydrofuran (THF) mixture in azeotropic composition (water content = 6%, THF content = 94%) using a laboratory cell with an effective membrane area of 9,6 cm^2 at abundant temperature. Permeate composition was identified using a refractometry. The fluxes, J ($\text{kg}/\text{m}^2 \text{h}$), were determined as an amount of liquid transported through

the unit of the membrane area per hour. The single gas permeability coefficients of nitrogen, carbon dioxide, and methane through the obtained membranes were measured. Ideal selectivity (α) for pairs of gases was calculated as a ratio of its permeability coefficients.

Results and Discussion

SEM cross-sections micrographs of the obtained composite membranes allowed confirming the excellent adhesion of the selective top layer onto the porous support (polysulfonamide) with the thickness of 750 and 1200 nm for CS-PAN and CS-PS, correspondingly. SEM micrographs are presented at figure 1.

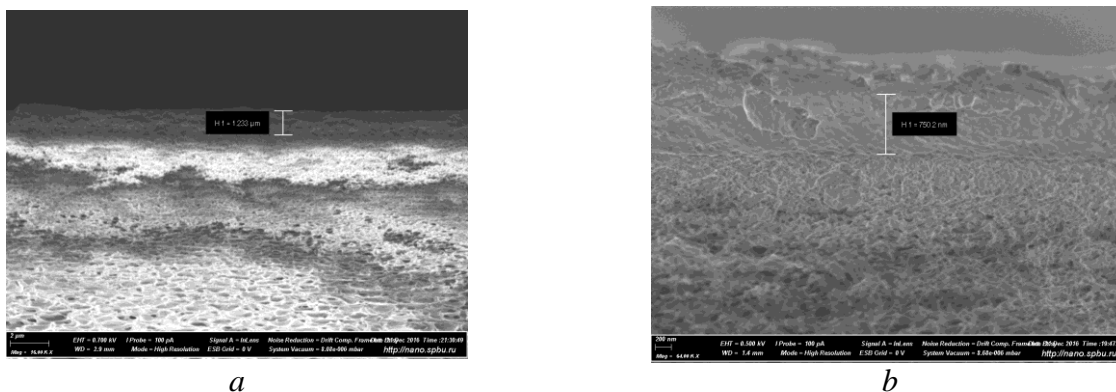


Figure 1. The SEM micrographs of composite membranes: a) CS-PS top layer; b) CS-PAN top layer

It demonstrated that copolymers formed continuous nonporous coat without any defects. AFM images reveals nodular microstructure of the surface, which is typical for homogeneous films based on obtained copolymers. The roughness parameters Ra and the Rz increased 2-fold in comparison to the preliminary surface of the support. Transport properties of the developed membranes was tested during separation of azeotropic water – tetrahydrofuran (THF) mixture (water content = 6%, THF content = 94%) by pervaporation. Pervaporation data is presented in table 1.

Table 1: Pervaporation data

Membrane selective layer	Water content in tested binary mixture, wt. %	Water content in permeate, wt. %	J, (kg/m ² h)
CS-PAN	6	94,8	0,145
CA-PS	6	6	0,143

Prepared membranes were tested for gas permeation using N₂, CH₄ and CO₂ as test gases. The values of permeability coefficients are presented in table 2.

Table 2. Pervaporation data

Gas	Permeability coefficient, Barrer		
	support	Support + CS-PS	Support + CS-PAN
He	1640,13	266,52	55,01
N ₂	786,66	124,30	21,75
Ar	625,36	113,10	18,45
H ₂	2115,02	352,10	69,14
CH ₄	943,65	160,70	42,04
CO ₂	683,75	110,02	29,00
N ₂ O	627,50	100,53	25,22
NH ₃	79714,06	172,70	23,67
H ₂ S	974,96	117,62	42,17

New CS based membranes were prepared by phase inversion method using “wet” and “dry” technique. The AFM of the materials based on pure CS shows a difference in the surface topography of the two sides of the membrane "to the substrate" or "to the air".

This is confirmed by the difference in the parameters of the roughness Ra and Rz for both sides more than twice. On the surface of membranes, depressions are visualized, which may be dead-end pores of complex configuration. The results of SEM confirm the formation of an asymmetric structure of membranes obtained by the "wet" method, with the formation of a denser and more friable layers of different thicknesses. In the case of membranes obtained by the "dry" method, the formation of an asymmetric structure was not confirmed.

There we can conclude that obtained membrane despite low separation ability might be useful for special applications, and also the approach shown there might be distribute for wide range of CS copolymers.

References

1. *Otvagina, Ksenia V., et al.* Preparation and Characterization of Facilitated Transport Membranes Composed of Chitosan-Styrene and Chitosan-Acrylonitrile Copolymers Modified by Methylimidazolium Based Ionic Liquids for CO₂ Separation from CH₄ and N₂//Membranes 6.2. 2016. 31.

HYDROPHOBIZATION OF POROUS POLYSULFONE HOLLOW FIBER MEMBRANES: LOW TEMPERATURE PLASMA TREATMENT

Anna Ovcharova¹, Ilya Borisov¹, Stepan Bazhenov¹, Rustem Ibragimov², Vladimir Vasilevsky¹, Alexandr Bilydukevich³, Vladimir Volkov¹

¹A.V. Topchiev Institute of Petrochemical Synthesis, Moscow, Russia, *E-mail*: ovcharoff@ips.ac.ru

²Kazan National Research Technological University, Kazan, Russia

³Institute of Physical Organic Chemistry, National Academy of Sciences of Belarus, Minsk, Belarus

Introduction

Porous polysulfone hollow fiber membranes are widely used in a number of applications due to their relative low cost and a number of advantages such as simplicity of fabrication and high specific surface area of membrane modules based on them. Fabrication of porous hydrophilic membranes is quite mature, and hydrophilic materials generally have higher thermal resistance than hydrophobic ones [1]. Hence, surface hydrophobic modification of hydrophilic membranes has been proposed for gas-liquid membrane contactor (MC) processes.

Basically, surface hydrophobic modification can be realized by a number of ways. Plasma treatment is an exemplary method for surface modification, as plasmas only modify the top 1-10 nm of the material [2]. Furthermore, plasma treatment has been proved to be useful for the formation of a hydrophobic layer on a hydrophilic base membrane.

The low-temperature plasma treatment entails a number of physicochemical processes, depending of the discharge type (plasma frequency) and the nature of the plasma gas, which makes it possible to control the targeted mode of the structure and the chemical composition of the surface of polymer membranes [3].

In the present work, the home-made porous asymmetric polysulfone hollow fiber membranes were treated by various types of low-temperature plasma, using plasma supporting gases such as carbon tetrafluoride (CF₄), methane (CH₄) and gas mixtures: argon and carbon tetrafluoride (Ar + CF₄), argon and methane (Ar + CH₄). The treatment time was also varied. Both unmodified and low-temperature plasma treated hollow fiber membranes were analyzed using contact angle measurement, determination of physical mechanical properties, X-ray analysis, scanning electron microscopy (SEM) and confocal scanning laser microscopy (CSLM).

Experiments

The materials used to prepare spinning solutions were PSf pellets, Ultrason® S 6010 (BASF) and N-methylpyrrolidone (NMP 99% extra pure) supplied from Acros Organics, used as the base polymer and solvent, respectively. The pore-forming additive to the polymer solution was polyethylene glycol of average molecular weight 400 g/mole (PEG-400) supplied from Acros Organics.

The hollow fiber membranes were obtained via the dry-wet spinning technique, using water as both bore fluid and external coagulant. The hollow fibers prepared had selective layer on the lumen side. Experimental setup used for spinning is described elsewhere [4]. After spinning, the membranes were washed by water, exposed in ethanol and then in n-hexane to prevent capillary mesopores contraction.

Under membranes treatment by low-temperature plasma, process parameters (treatment time, type of plasma-supporting gas) were varied. Low-temperature plasma treatment was carried out using the pilot-scale setup described elsewhere [5].

Both unmodified and plasma treated membranes were characterized by means of contact angle measurement, determination of physical mechanical properties, X-ray analysis, scanning electron microscopy (SEM) and confocal scanning laser microscopy (CSLM).

Results and Discussion

To analyze change in the membranes hydrophobicity, water contact angle measurement was carried out using the conventional sessile drop technique. The results for both unmodified and plasma treated membranes are given in Table 1.

Table 1: Water contact angle (θ) for the unmodified and plasma treated hollow fibers

Type of the membrane	$\theta_{av} (H_2O), ^\circ$
Unmodified	76
Treated by CF_4 plasma	84
Treated by CH_4 plasma	82
Treated by Ar + CF_4 plasma	89
Treated by Ar + CH_4 plasma	98

As can be seen from Table 1, the most successful hydrophobic modification occurred for treatment using a mixture of argon and methane as plasma supporting gas. Water contact angle increased from 76° to 98° , thus making the surface of the membranes more resistant to wetting by aqueous media which may be very important for employing such membranes in gas-liquid membrane contactor processes.

After modification, we carried out measurement of the physical mechanical properties such as maximum strength, tensile strength and deformation. The analysis was performed using precise simulation machine AGS-X.

For the plasma treated membranes, the maximum strength decreased from 4.1 to 3.5 N, the tensile strength – from 1.7 to 1.5 MPa and the deformation decreased from 38.3 to 27.5 %. However, such decrease is close to negligible and indicates that plasma affects the membrane material due to the generation of active species.

The results of analysis by confocal scanning laser microscopy are depicted at Fig. 1.

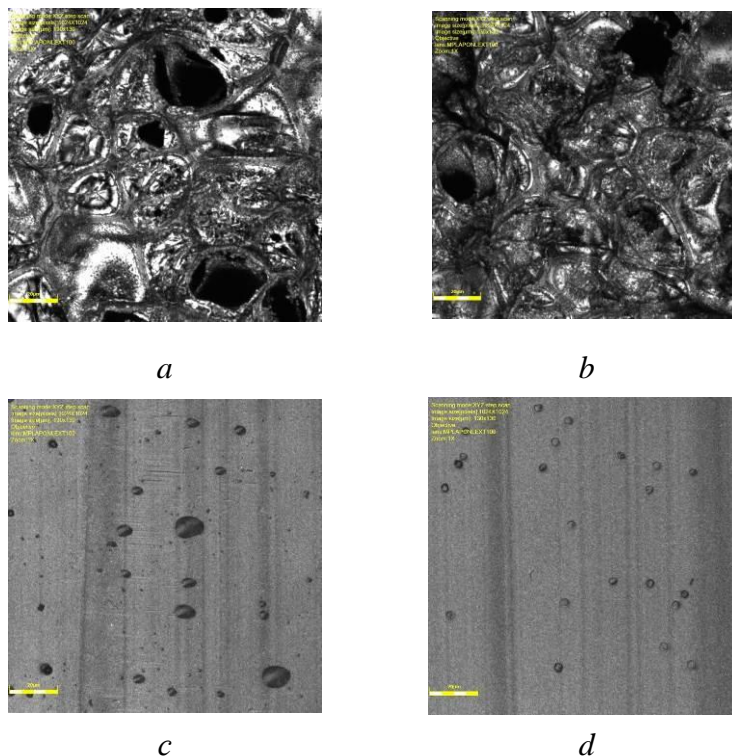


Figure 1. Outer surface of the unmodified (a) and plasma treated membrane (b); inner surface of the unmodified (c) and plasma treated membrane (d), magnification 2000x

After the plasma treatment, no visible changes in the membrane surface morphology is observed; only slight increase is observed for roughness height (R_z). It can also be seen from Fig. 1 that plasma treatment leads to smoothing of the membrane inner surface. This phenomena is related to the fact that ionic bombardment of the specimens surface and recombination of charged

plasma particles in the membrane selective layer causes energy release, which, in turn, leads to extra specimen surface texturing. All these phenomena indicate that low temperature plasma penetrates into the membrane bulk up to the selective layer.

After modification, the roughness height (R_z) increased from 0.399 to 0.425 μm and average roughness profile decreased from 0.064 to 0.060 μm .

It can be concluded that low-temperature plasma treatment using a mixture of argon and methane as a plasma supporting gas provides a reliable way to obtain hydrophobic polysulfone hollow fiber membranes without decrease in physical mechanical properties. Such membranes may be promising for employing them in gas-liquid membrane contactors with aqueous absorbents.

Acknowledgements

This work was performed at the Topchiev Institute of Petrochemical Synthesis and supported by the Russian Science Foundation, project no. 14-49-00101.

References

1. Liu L., Shen F., Xiangrong C., Jianquan L., Su Y., Huanhuan W., Wan Y. A novel plasma-induced surface hydrophobization strategy for membrane distillation: etching, dipping and grafting. *J. Membr. Sci.* 2016. V. 499. P. 544.
2. Grace J., Gerenser L. Plasma treatment of polymers // *J. Disper. Sci. Technol.* 2003. V. 24. P. 305.
3. Volkov V., Ibragimov R., Abdullin I., Gallyamov R., Ovcharova A., Bildyukevich A. Modification of polysulfone porous hollow fiber membranes by air plasma treatment // *J. Phys. Conf. Ser.* 2016. V. 751. P. 012028.
4. Bildyukevich A., Plisko T., Liubimova A., Volkov V., Usosky V. Hydrophilization of polysulfone hollow fiber membranes via addition of polyvinylpyrrolidone to the bore fluid // *J. Membr. Sci.* 2017. V. 524. P. 537-549.
5. Borisov I., Ovcharova A., Bakhtin D., Bazhenov S., Volkov A., Ibragimov R., Gallyamov R., Bondarenko G., Mozhchil R., Bildyukevich A., Volkov V. Development of Polysulfone Hollow Fiber Porous Supports for High Flux Composite Membranes: Air Plasma and Piranha Etching // *Fibers.* 2017. V. 5. P. 6.

POLYSULFONE POROUS HOLLOW FIBER MEMBRANES FOR ETHYLENE-ETHANE SEPARATION IN A GAS-LIQUID MEMBRANE CONTACTOR

¹Anna Ovcharova, ¹Vladimir Vasilevsky, ¹Ilya Borisov, ¹Stepan Bazhenov, ¹Alexey Volkov, ²Alexandr Bilydukevich, ¹Vladimir Volkov

¹A.V.Topchiev Institute of Petrochemical Synthesis (TIPS RAS), Moscow, Russia

²Institute of Physical Organic Chemistry (IPOC NASB), Minsk, Belarus

E-mail: sbazhenov@ips.ac.ru

Introduction

Olefin/paraffin separation is one of the most important processes in the petrochemical industry. Light olefins such as ethylene and propylene are produced in volume: in 2011, ethylene worldwide overall production was 141 MT, propylene – 70 MT [1]. The main difficulty in separation of olefin from paraffin having same carbon number is low difference in components boiling temperatures, e.g. for ethylene and ethane mixture, $\Delta T_B = 14.7^\circ$. A perspective option for such separation is using gas-liquid membrane contactor where gas and liquid phases are divided by membrane and liquid solvent (transition metals salts solution) is able to complex with olefin [2]. The membrane contactor benefit is high area per unit volume (up to 3000 m²/m³ [3]). Furthermore, it provides an opportunity for independent gas and liquid flow rate control which is impossible in conventional columns. In this work, home-made asymmetric porous hollow fiber polysulfone (PSf) membranes having mesoporous ($d_{av} = 2$ nm) skin layer structure and modified surface and membrane contactors based on them are used for ethylene/ethane separation [4]. Such porous structure was chosen based on the expectation that decreased average pore size value compared to that of the UF-grade membranes will provide an opportunity to escape liquid absorbent penetration into the porous structure still keeping high olefin permeance values (being orders of magnitude higher than those of composite membranes). The latter benefit of such membranes structure is to be achieved not only by pore size tailoring, but also by increasing the skin layer surface hydrophobic properties.

Experiments

Hollow fiber membranes were prepared via a dry-wet phase inversion technique in the free spinning mode in air when bore fluid (distilled water) was brought into liquid polymer solution (23.9 % t. of PSf in N-methylpyrrolidone with polyethylene glycol (PEG 400) additive) orifice, resulting in the selective layer appearance on the fibers lumen side [5]. Under this mode, the spun fiber gets into coagulation bath by gravity and coils of its own accord. For enhancing of membrane surface hydrophobicity, aqueous phase perfluorinated acrylic copolymer (PAC) ProtectGuard[®] Pro was used. The as-prepared membranes and used after contactor tests were characterized with: scanning electron microscopy (SEM, Hitachi Table top Microscope TM 3030), energy-dispersive X-ray spectroscopy (EDX, Bruker Quantax 70 EDS system), X-Ray diffraction analysis (Rigaku D/max-RC), gas permeance measurements with further pore size processing using Dusty Gas model (DGM), contact angle measurements (LK-1 goniometer). The ethylene/ethane separation experiments were done with a membrane contactor which was a stainless steel tube containing three hollow fiber membranes with overall surface area fixed by epoxy resin. Feed gas mixture (ethylene (20%)/ethane (80%)) was brought into fibers shell side, overall gas mixture pressure was close to atmospheric. Aqueous silver nitrate (AgNO₃) solutions with different concentrations (1, 3 and 4M) was used as a solvent and was brought into fibers lumen by peristaltic pump in a closed loop mode. Gas and liquid flow rates were varied and controlled. Gas mixture composition was analyzed by Crystallux-4000M gas chromatograph (GC) with a TCD detector. All experiments were carried out at room temperature.

Results and discussion

Cross section images were captured for the prepared and PAC-modified membranes (see Fig.1a). As is seen, membranes have asymmetric structure consisting of thick drainage layer with finger-like macrovoids, transition layer having spongelike structure and thin (20-30 μ m) skin layer from the lumen side.

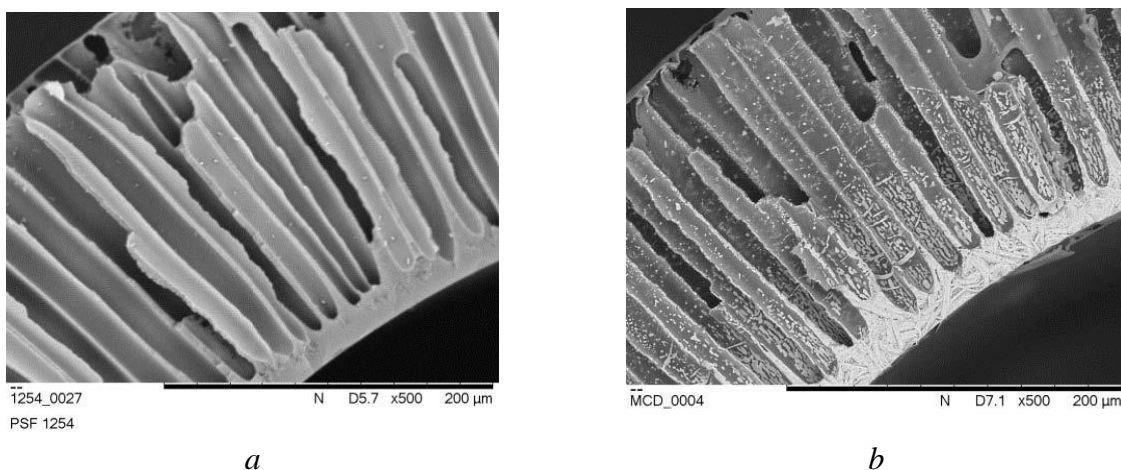


Figure 1. SEM images of the PAC-modified PSf membranes top view before (a) and after (b) membrane contactor experiment. Magnification 500x

Gas permeance measurements showed that developed membranes have relatively high gas permeances for carbon dioxide and helium: $5 \text{ m}^3/(\text{m}^2 \cdot \text{h} \cdot \text{bar})$ for CO_2 and $10.5 \text{ m}^3/(\text{m}^2 \cdot \text{h} \cdot \text{bar})$ for He. Ideal separation factor value indicates (2.1) that mixed Knudsen-Poiseuille flow regime is present. Calculated by DGM average selective layer pore size was 2 nm which corresponds to mesoporous structure type. Contact angle measurements showed that PAC-modified membranes have relatively high hydrophobic properties: 90° (water) and 79° (ethylene glycol) compared to 78° (water) and 70° (ethylene glycol) for as-prepared unmodified membranes.

Within membrane contactor tests, ethylene permeance values, P/l (C_2H_4), were obtained under 1, 3 and 4M concentrations of solvent. Fig. 2 depicts the effect of the silver nitrate solution concentration on the maximum ethylene permeance values. As is seen, ethylene permeance vs silver nitrate concentration curve shows a distinct maximum. Ethylene absorption flux increases when using the more concentrated salt solution, but as shown in [6], solution molar absorptivity (moles of olefin absorbed by 1 mole of Ag^+) decreases when salt concentration increases due to the enhanced $\text{Ag}^+/\text{NO}_3^-$ interactions in concentrated solutions. These interactions restrict silver-olefin complexation.

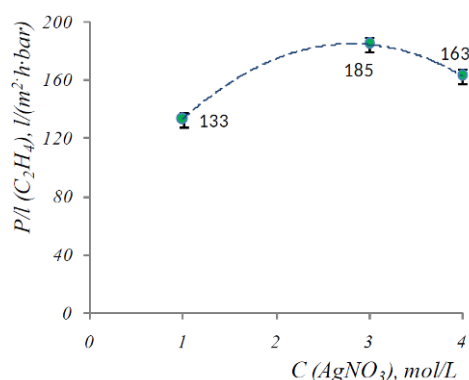


Figure 2. Maximum ethylene permeance dependence on the AgNO_3 concentration

The highest ethylene permeance value – $0.185 \text{ m}^3/(\text{m}^2 \cdot \text{h} \cdot \text{bar})$, which is at the level of the best results available in literature for porous membranes, at ethylene recovery up to 39%, which is three times higher than that in literature, corresponds to the following operating parameters: $C(\text{AgNO}_3) = 3\text{M}$, solvent linear velocity in the fibers lumen is 5 cm/s (estimated Reynolds number $\text{Re} = 160$), gas mixture linear velocity in the membranes shell side is 3 m/s. In all experiments inverse relation between ethylene permeance and solvent flow rate was observed. Maximum ethylene from ethylene-ethane mixture recovery rate (39%) was also obtained under minimal liquid velocity studied, but gas mixture flow rate increase led to the recovery rate value decrease.

It can be seen from Fig.1b, where the SEM images of PAC-modified membranes after 2 months of membrane contactor experiments (when silver nitrate solution was supplied into hollow fibers

lumen) are presented, PAC layer on the skin layer surface is still present but pores space is partially clogged by silver compound depositions (penetration depth ~ 750 μm). Nevertheless, silver traces amount from the hollow fiber shell side is small to negligible which indicates that no solvent leakage into the shell side occurred during all membrane contactor operating period. Probably, salt deposition into the membranes pore space is due to the solvent pressure rise when its velocity in the fibers lumen is increased and also to the fact that deposition of silver compounds increases membrane wettability.

Table 1 gives gas permeance and contact angle values of the membranes after membrane contactor experiment.

Table 1. Gas permeance and contact angle values for the membranes after contactor tests.

CO ₂ permeance, m ³ /(m ² ·h·bar)	He permeance, m ³ /(m ² ·h·bar)	Ideal He/CO ₂ separation factor	Water contact angle, °	Ethylene glycol contact angle, °
0.4±0.01	0.9±0.02	2.1	89±2	84±2

It can be seen that gas permeance of the membranes after membrane contactor experiments decreased by an order of magnitude compared to initial values. Such decrease is probably due to the silver nitrate crystals deposition on the membranes pore walls which leads to the blocking of a transport pores fraction. However, it should be noted that after membrane contactor experiments, the membranes gas permeance values for both helium and carbon dioxide remained significantly higher than maximum (185 l/(m²·h·bar)) ethylene permeance in the contactor, which is accounted for by extra liquid phase resistance in the membrane module. EDX tests showed that layer containing perfluorinated groups of PAC remains on the hollow fibers inner surface even after membrane contactor tests.

Acknowledgements

This work was performed at the A.V. Topchiev Institute of Petrochemical Synthesis and supported by the Russian Science Foundation, project no. 14-49-00101. A.A. Ovcharova, V.P. Vasilevsky, I.L. Borisov, S.D. Bazhenov, A.V. Bilyukevich and V.V. Volkov acknowledge the financial support of RSF. Authors thank K.A. Kutuzov for carrying out the membrane contactor experiments, S.P. Molchanov and S.N. Polyakov for providing X-ray diffraction analysis data and D.S. Bakhtin for providing SEM and EDX images.

References

1. True W.R. Global ethylene capacity continues advance in 2011 // Oil Gas J. 2012. V. 110. P. 78–84.
2. Ghasem N., Al-Marzouqi M., Ismail Z. Gas–liquid membrane contactor for ethylene/ethane separation by aqueous silver nitrate solution // Sep. Purif. Technol. 2014. V. 127. P.140–148.
3. Bazhenov S.D., Lyubimova E.S. Gas-Liquid Membrane Contactors for Carbon Dioxide Capture from Gaseous Streams // Petr. Chem. 2016. V.56. P. 893–919.
4. Ovcharova A., Vasilevsky V., Borisov I., Bazhenov S., Volkov A., Bilyukevich A., Volkov V. Polysulfone porous hollow fiber membranes for ethylene-ethane separation in gas-liquid membrane contactor // Sep. Pur. Technol. 2017. DOI: 10.1016/j.seppur.2017.03.023
5. Ovcharova A. A., Vasilevsky V. P., Borisov I. L., Usosky V. V., Volkov V. V. Porous hollow fiber membranes with varying hydrophobic–hydrophilic surface properties for gas–liquid membrane contactors // Petr. Chem. 2016. V. 56(11). P. 1066-1073.
6. Cho I.H., Yasuda H.K., Marrero T.R. Solubility of ethylene in aqueous silver nitrate // J. Chem. Eng. Data. 1995. V. 40. P. 107–111

THE INFLUENCE OF MOISTURE CONTENT AND TRANSPORT PROPERTIES OF PERFLUORATED MEMBRANES ON THE DP-SENSORS CHARACTERISTICS DEPENDING ON THE ANALITES NATURE AND SOLUTION pH

¹Anna Parshina, ²Ekaterina Safronova, ¹Olga Bobreshova

¹Voronezh State University, Voronezh, Russia, *E-mail: parshina_ann@mail.ru*

²Kurnakov Institute of General and Inorganic Chemistry, RAS, Moscow, Russia

Introduction

The development of simple to manage, rapid, inexpensive but reliable instrumental methods for the solving of off-laboratory analysis tasks is actual. A need to expand of the analytes range (primarily of organic ions) and the complexity of test media compositions causes the need of improvement in principles for processing of multidimensional sensory responses (the multisensory approach) and the obtaining of new electrode-active materials. The obtaining of new materials for sensors by processing and /or modifying the commercially available membranes, the number of which is limited, is the most promising [1]. It allows to influence on the ion exchange processes, sorption processes and acid-base equilibrium in membranes without the use of ionophores. The aim of this work was a detection of interconnection between the composition, structure, properties of perfluorosulfonic cation-exchange membranes subjected to the treatment and/or containing of dopants nanoparticles, and the characteristics of multisensory systems based on them depending on the analytes nature and solution pH.

Experiments

The aqueous solutions of amino acids (Met, Val, His), vitamins (Thiamin, Pyridoxin), drugs (pyruvic acid, Taurine) and inorganic electrolytes (HCl, KCl, KOH) were investigated. The components concentrations in test solutions were ranged from $1.0 \cdot 10^{-4}$ to $1.0 \cdot 10^{-2}$ M. Nafion and MF-4SC membranes subjected to a heat treatment and mechanical deformation at the different relative humidity, and hybrid materials based on them, containing of zirconia and silica with a modified surface and acid salts of heteropolyacids were used.

Results and Discussion

The correlation between the sensitivity of DP-sensors to cations in acidic solution of Val, His, Thiamin and Pyridoxin and the moisture content and the diffusion permeability of membranes is identified. It is shown that the reduction of moisture content and increase of membranes selectivity to cations leads to an increase in DP-sensors sensitivity to organic cations and its reduction to interfering H_3O^+ ions. It is achieved if the transition of organic cations in membrane is not limited by steric. In this case, the interaction of bulky organic cations with the fixed groups of membrane (and dopant) excludes of protons part from the ion exchange. The interrelation between the size of dopants, their proton-donor ability, diffusion permeability of hybrid membranes and the DP-sensors sensitivity to anions (and zwitterions) of Met, pyruvic acid and Taurine in the alkaline solutions is revealed. The sensitivity of DP-sensors to analytes in the anionic form depends on the dopant volume and reaches of maximum at the minimum volume inside the pore, which is sufficient for their passage. The sensitivity of DP-sensors to analytes in the anionic and zwitterionic form increases with an increase in diffusion permeability of membranes and the number of acid groups of membrane (and dopant) available for interaction with analyte. The determination of amino acids cations (Val, His) and vitamins cations (Thiamin, Pyridoxin) at the $pH < 7$ and the simultaneous determination of potassium cations and ions (Met, pyruvic acid, Taurine) at the $pH > 7$ was performed using DP-sensors based on membranes with optimized properties.

This present work was supported by the Russian Science Foundation (project no. 15-13-10036).

References

1. Safronova E.Yu., Yaroslavtsev A.B. // Petroleum chemistry. 2016. T.56. №4. P.281 (original Russian text published in Membrany i Membrannye Tekhnologii. 2016. V.6, №1, P.3).

ANOMALOUS CURRENT-VOLTAGE AND CHRONOPOTENTIOMETRIC CURVES OF HOMOGENEOUS ANION-EXCHANGE MEMBRANE IN MONOSODIUM PHOSPHATE SOLUTION

Natalia Pismenskaya, Ekaterina Belashova, Olesya Kharchenko, Victor Nikonenko

Membrane Institute, Kuban State University, Krasnodar, Russia

E-mail: ekaterinabelashova23@gmail.com

Introduction

Electromembrane processes of purification, separation and concentration in combination with other membrane methods are widely introduced in food and pharmaceutical industry [1], as well as in production of nutrients for the livestock industry [2]. This direction is based on the treatment of ampholyte containing solutions, whose source is the products of biochemical processing of biomass and organic waste [3]. The main feature of ampholytes is their ability to be present in the form of anions, cations, bipolar (zwitterion) ions or neutral molecules depending on the pH of the solution. These forms are involved in protonation-deprotonation reactions with a solvent (water) or with each other.

In this context, the aim of this work was to elucidate the impact of ampholyte transformation on current-voltage characteristic (CVC) and chronopotentiometric (ChP) characteristics of a homogeneous anion-exchange membrane.

Experiments

The CVC and ChP characteristics of a homogeneous anion-exchange AX membrane were obtained in a laboratory scale four-chamber electrochemical cell, described in [4]. The AX membrane, paired with a heterogeneous cation-exchange membrane MK-40 (Shchekinoazot Ltd, Russia), formed a desalting channel. The active surface area of each membrane was $2 \times 2 \text{ cm}^2$. Two Luggin-Haber capillaries connected with Ag/AgCl electrodes were used to measure the potential drop across the AX membrane. The flow cell had special solution input and output devices allowing the formation of a laminar flow regime in each channel. Thereby, the theoretical value of a limiting current (i_{lim}^{Lev}) can be calculated by the L ev eque equation [5].

The chronopotentiometric characteristics were obtained in the double-pulse mode, at which the interval between the 1st and 2nd pulses was 60 s. This time is sufficient for the dissipation of concentration profiles in the diffusion boundary layers (DBLs).

All experiments were conducted at a constant temperature $25 \pm 1 \text{ }^\circ\text{C}$. The studies were carried out using 0.02 mol/L solutions of NaH_2PO_4 .

Results and Discussion

Figure 1a shows the ChP characteristics of the AX membrane in NaH_2PO_4 solution for the currents $i > i_{lim}^{Lev}$. The value of i_{lim}^{Lev} is close to the first limiting current i_{lim}^I observed on the steady-state current-voltage curve (Fig. 1b). As can be seen from Figure 1a, when the limiting current i_{lim}^{Lev} is exceeded twice, the time required by the system to achieve a quasi-steady state is about 15 min. This value is much longer than that for the system AEM / NaCl [6].

After switching off the current for 60 s, the form of ChP curves becomes close to the classical one, observed for electrolytes, which do not participate in the protonation / deprotonation reactions. This suggests that an unusual form of the ChP curves is weakly related to processes occurring in the diffusion layers. Therefore, the forms of the ChP curves can be associated with processes occurring inside the AEM. The form of ChP curves is associated with additional stages preceding the establishment of a quasi-stationary state (Fig. 2). Figure 2 shows initial sections of the chronopotentiometric curves reduced by the ohmic section (I). The appearance of additional stages is caused by the transformation of singly-charged H_2PO_4^- anions into doubly-charged HPO_4^{2-} ones inside the membrane.

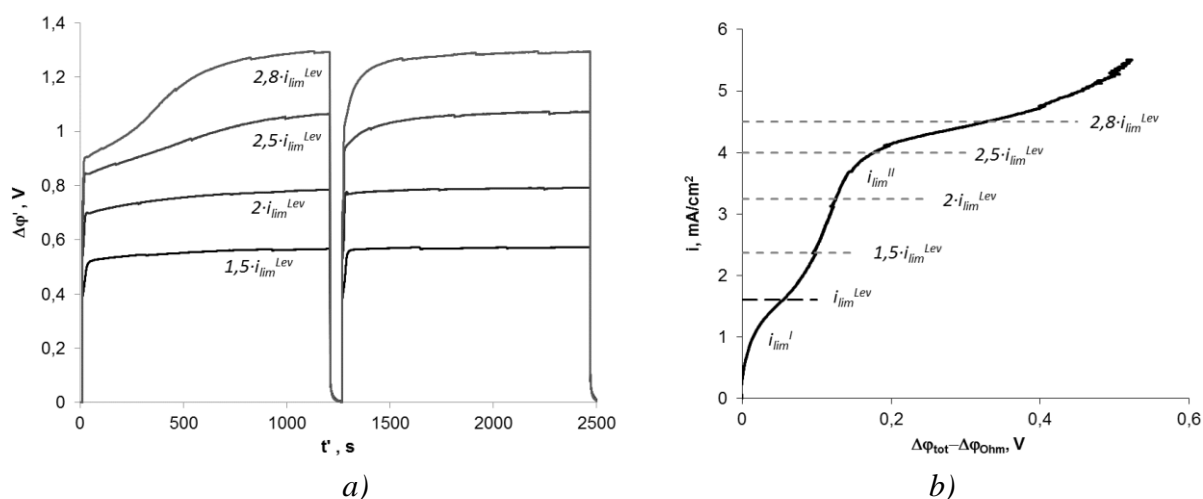


Figure 1. Two-pulse chronopotentiometric (a) and current-voltage (b) curves of AX membrane in 0,02 M solution of NaH_2PO_4

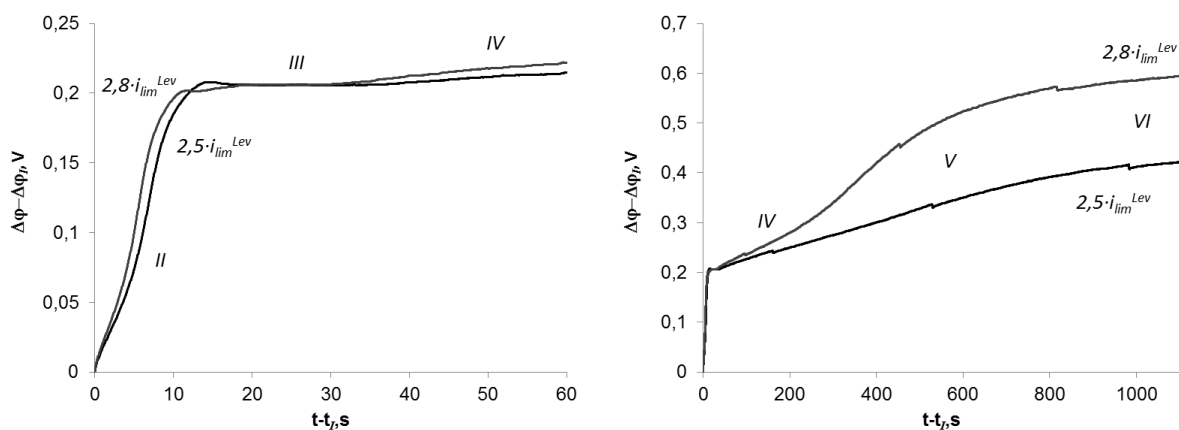


Figure 2. Initial sections (a) and total corrected chronopotentiometric curves (b) of the AX membrane in a 0.02 M solution of NaH_2PO_4

On stage *II* the charge is mainly carried by H_2PO_4^- anions. It is limited by the diffusion of electrolyte from the bulk solution to the membrane surface, i.e. determined by external diffusion. The decrease of the electrolyte concentration at the membrane surface causes the Donnan exclusion of protons from the membrane and an increase in internal solution pH at the depleted interface. When the H_2PO_4^- anions enter the interface, a part of them transform into the HPO_4^{2-} anions and the liberated protons are generated into the depleted DBL. When the rate of this transformation becomes sufficiently high, the system reaches a quasi-steady-state (stage *III* in Fig. 2). In this stage, initially only a near-surface layer of the membrane passes from mainly H_2PO_4^- to principally HPO_4^{2-} form. The concentration gradient of these anions in the membrane causes a concentration gradient of H^+ ions. Due to this gradient and electromigration, protons are transferred from the membrane bulk to its depleted interface. Simultaneously, the boundary between the HPO_4^{2-} zone and the H_2PO_4^- zone in the membrane passes from its depleted interface towards its concentrated side. During this process, which is essentially longer than the establishment of concentration profile in the DBL, the concentration gradient of H^+ ions near the depleted interface decreases in time. The latter reduces the flux of these ions, which causes a further decrease of electrolyte concentration in the near-surface depleted solution and, as a consequence, a growth of overall potential drop (stage *IV*). If the current density is lower than the second limiting current, $i_{\text{lim}}^{\text{II}}$, there is no inflection point on the chronopotentiogram (Fig. 2b). However, if $i > i_{\text{lim}}^{\text{II}}$, there is an inflection point, which is caused by saturation of the near-surface layer of the membrane with HPO_4^{2-} and the onset of another mechanism of current transfer, which

may be transformation of HPO_4^{2-} into PO_4^{3-} ions or water splitting at the membrane/depleted solution interface.

The observed phenomena are not only of theoretical but also of practical interest. In particular, they should be taken into account during the electrodialysis process of ampholyte treatment in nonequilibrium conditions.

Acknowledgements

This investigation was carried out within French-Russian laboratory "Ion-exchange membranes and related processes". The authors are grateful to the Russian Foundation for Basic Research (grant 15-08- 04522) for financial support.

References

1. *He R., Girgih A.T., Rozoy E., Bazinet L., Ju X.-R., Aluko R. E.* Selective separation and concentration of antihypertensive peptides from rapeseed protein hydrolysate by electrodialysis with ultrafiltration membranes // *Food Chemistry* 2016. V. 197. P. 1008-1014.
2. *Chen G., Song W., Qi B., Li J., Ghosh R., Wan Y.* Separation of protein mixtures by an integrated electro-ultrafiltration-electrodialysis process // *Separation and Purification Technology* 2015. V. 147, P. 32-43.
3. *Xu J., Su X.-F., Bao J.-W., Chen Y.-Q., Zhang H.-J., Tang L., Wang K., Zhang J.-H., Chen X.-Sh., Mao Zh.-G.* Cleaner production of citric acid by recycling its extraction wastewater treated with anaerobic digestion and electrodialysis in an integrated citric acid–methane production process // *Bioresource Technology* 2015. V. 189. P. 186-194.
4. *Belova E., Lopatkova G., Pismenskaya N., Nikonenko V., Larchet C., Pourcelly G.* The effect of anion-exchange membrane surface properties on mechanisms of overlimiting mass transfer // *Journal of Physical Chemistry B* 2006. V. 110. P. 13458-13469.
5. *Newman, J. S.* *Electrochemical Systems.* New York: Prentice Hall, Englewood Cliffs, 1973.
6. *Nebavskaya K.A., Sarapulova V.V., Sabbatovskiy K.G., Sobolev V.D., Pismenskaya N.D., Sistas P., Cretin M., Nikonenko V.V.* Impact of ion exchange membrane surface charge and hydrophobicity on electroconvection at underlimiting and overlimiting currents // *Journal of Membrane Science* 2017. V. 523. P. 36-44.

MODELING OF MASS TRANSFER PROCESSES IN ELECTRODIALYSIS OF AMPHOLITES WITH THE ACCOUNT OF NONISOTHERMAL DEPROTONING-PROTONING REACTIONS

Alexander Pismenskiy, Mahamet Urtenov, Anna Kovalenko, Ekaterina Belashova

Kuban State University, Stavropolskaya 149, 350040 Krasnodar, Russia, E-mail: pism@kubsu.ru

Introduction

It is known that ampholytes can exhibit both acidic and basic properties depending on the pH of the solution and enter into deprotoning-protoning reactions with the solvent (water) or with each other. These reactions in ampholyte-containing solutions are accompanied by thermal effects, and they can occur at pre-limiting electric currents, unlike dissociation-recombination reactions of water molecules [1].

The experimental current-voltage characteristics of the anion-exchange membrane (AEM), obtained [2] in ampholyte-containing sodium dihydrogen phosphate (NaH_2PO_4) solution, indicate a significant increase of the limiting current in a vertical position of the desalination channel (DC) of an electrodialyzer, compared to a horizontal one with the DC located under the membrane. This is explained by the influence of gravitational convection, which develops in a vertical position of the DC. At the same time, this effect is observed to a much lesser extent during electrodialysis under the same conditions of solutions that do not contain ampholytes, for example, $NaCl$ solution. One of the reasons for the observed gravitational convection in ampholyte-containing systems is presumably the thermal effects arising from deprotoning-protoning reactions.

Theory

Besides the Joule heating in the NaH_2PO_4 solution, the absorption of heat Q_1 at the solution/AEM interface occurs as a result of the dissociation (deprotoning) of the ampholyte anion $H_2PO_4^-$:



and the absorption of heat Q_2 at a certain distance from the interface as a result of the recombination reaction (protoning) to the molecular form – orthophosphoric acid:



These two reactions are spatially separated, as indicated by calculations made with the 1D three-layer model [3], which considers the transfer of carbonate ions through AEM. According to this model, protons appear in the depleted diffusion layer as a result of their Donnan exclusion from the membrane and the dissociation of HCO_3^- at the membrane/solution interface and recombine with HCO_3^- at some distance from the membrane within the diffusion layer. Calculations performed by the authors with the similar model allow suggesting that under conditions of concentration polarization, the distance from the membrane to the point at which the maximum of the molecular form (H_3PO_4) is formed is 100-200 μm .

In mathematical modeling of the electrodialysis process of heat and mass transfer, in many cases it is possible to confine ourselves to considering just the DC, considering the concentration in the concentration chambers to be constant and taking into account the influence of cation exchange and anion exchange membranes via boundary conditions. The 2D mathematical model of nonstationary transfer of ampholyte-containing solutions (NaH_2PO_4) in a half of a smooth rectangular DC adjacent to the AEM. The model assumes a potentiodynamic current mode (the electric potential drop varies with time). Membranes are supposed to be homogeneous and ideally selective, and their surfaces are equipotential. The solution is pumped with an average velocity V_0 .

Let C_i , j_i , D_i , z_i are concentrations, fluxes, diffusion coefficients and charge numbers, respectively, for sodium Na^+ ($i=1$), dihydrogen phosphate $H_2PO_4^-$ ($i=2$), hydrogen H^+ ($i=3$) and orthophosphoric acid H_3PO_4 ($i=4$); \vec{E} , φ are the electric field intensity and potential. The fluxes of the ions and the scheme of their interaction in the transverse section of the DC are

simplified in Fig. 1, where $x = 0$ corresponds to the AEM/solution interface, $x = h$ is the middle of the channel (the half of the intermembrane space), $x = \Theta$ is the middle of the reaction layer.

The system of equations. Let R_i are chemical reactions taking place with the i -th component of the solution. Then, from the condition of material balance, we obtain

$$\frac{\partial C_i}{\partial t} = -\text{div} \vec{j}_i + R_i, \quad (3)$$

$$i = 1, \dots, 4$$

Na^+ ions do not participate in chemical reactions. H^+ and HPO_4^{2-} ions are formed by deprotoning reaction of the

$H_2PO_4^-$ ion at the AEM/solution interface (1). This reaction is taken into account in the boundary conditions. In addition, the HPO_4^{2-} ions are completely removed from the solution through the membrane into the concentration chamber and, hence, they can be excluded from consideration. The $H_2PO_4^-$ and H^+ ions react with the formation of H_3PO_4 (2), which can also dissociate. Thus,

$$R_1 = 0, \quad R_2 = R_3 = -R_4 = K_d C_4 - K_r C_2 C_3, \quad (4)$$

where K_d is the dissociation (deprotoning) rate constant of the orthophosphoric acid, K_r is the recombination (protoning) rate constant of the acid. The calculations show that $K_d = 21.75 \cdot 10^7 \text{ s}^{-1}$, $K_r = 3 \cdot 10^7 \text{ m}^3/(\text{mole} \cdot \text{s})$.

Ions Na^+ , $H_2PO_4^-$, H^+ are transported via electromigration, diffusion and convective transfer, while molecules of H_3PO_4 – via diffusion and convective transport only, hence:

$$\vec{j}_i = \frac{F}{RT_0} z_i D_i C_i \vec{E} - D_i \nabla C_i + C_i \vec{V}, \quad i = 1, \dots, 3; \quad \vec{j}_4 = -D_4 \nabla C_4 + C_4 \vec{V} \quad (5)$$

The equations (3)–(5) are supplemented with the electroneutrality condition (6), the electric current flow condition (7), the heat equation (8), taking into account the Joule heating of the solution and heat absorption Q_2 under the endothermic reaction (2), the Navier-Stokes equation (9) taking into account Archimedean buoyancy forces:

$$z_1 C_1 + z_2 C_2 + z_3 C_3 = 0, \quad \vec{I} = F(z_1 \vec{j}_1 + z_2 \vec{j}_2 + z_3 \vec{j}_3) \quad (6), (7)$$

$$\frac{\partial T}{\partial t} + (\vec{V}, \nabla T) = \alpha \Delta T + \frac{1}{\rho_0 c_p} G - \frac{1}{\rho_0 c_p} Q_2, \quad (8)$$

$$\frac{\partial \vec{V}}{\partial t} + (\vec{V} \nabla) \vec{V} = -\frac{1}{\rho_0} \nabla P + \nu \Delta \vec{V} + \frac{1}{\rho_0} \vec{f}, \quad \text{div}(\vec{V}) = 0. \quad (9)$$

Here, α , ρ_0 , c_p are the coefficient of thermal diffusivity of the solution, the initial density and specific heat of the solution, respectively, $G = (\vec{E}, \vec{I})$ is the density of heat sources at time t as a result of the electric current flow through the solution (Joule heating), $Q_2 = k(K_d C_4 - K_r C_2 C_3)$ is the heat outflow density at time t associated with the formation of orthophosphoric acid, where

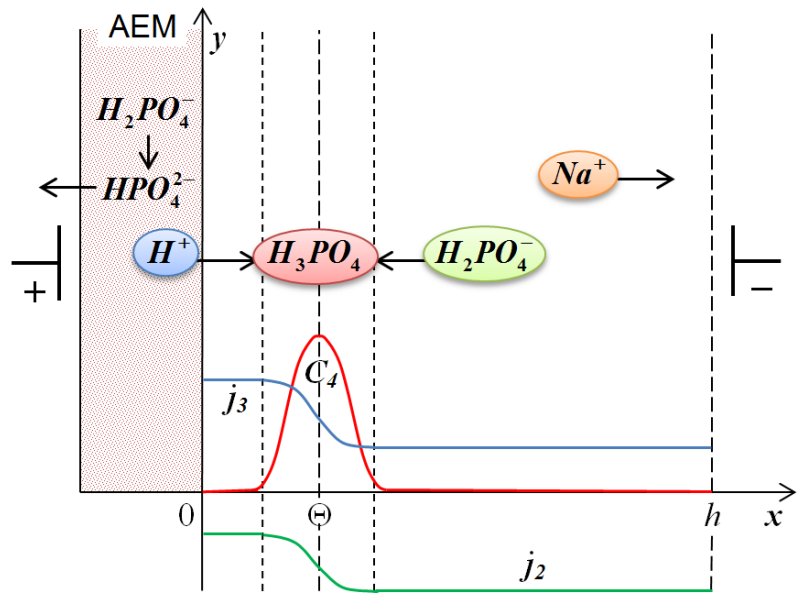


Figure 1. Schematic structure of the diffusion layer according to the model in the transverse section of the semi-channel.

Index values: 2 – $H_2PO_4^-$, 3 – H^+ , 4 – H_3PO_4

k is the amount of heat absorbed by the formation of one mole of acid per unit time. Since the preliminarily current mode and the gravitational convection are studied primarily, the lifting (Archimedian) forces $\vec{f} = -\bar{g}\bar{\Delta}\rho$ are considered, and using the Boussinesq approximation we derive:

$$\bar{\Delta}\rho = \rho - \rho_0 = \frac{\partial\rho}{\partial C_1}(C_1 - C_{01}) + \frac{\partial\rho}{\partial C_2}(C_2 - C_{02}) + \frac{\partial\rho}{\partial C_3}(C_3 - C_{03}) + \frac{\partial\rho}{\partial C_4}(C_4 - C_{04}) + \frac{\partial\rho}{\partial T}(T - T_0)$$

Note that in the system of equations (3)–(9) the unknown functions are: $C_i, \vec{j}_i, i = 1, 2, 3, 4, \vec{I}, \vec{E} = -\nabla\varphi, T, \vec{V}$.

Boundary conditions:

$$C_4(t, 0, y) = C_{4m} = 0, \quad \vec{n} \cdot \vec{j}_1(t, 0, y) = 0, \quad \text{where } \vec{n} \text{ is the outer normal vector;}$$

$$-\frac{\partial}{\partial x} \mathbf{j}_{3,x}(t, 0, y) + K_{d,2} C_2(t, 0, y) = 0, \quad \mathbf{j}_{3,y}(t, 0, y) = 0,$$

$$\vec{V}(t, 0, y) = \vec{V}_m = 0, \quad \varphi(t, 0, y) = 0, \quad T(t, 0, y) = T_0.$$

$$C_i(t, h, y) = C_{i0}, \quad i = 1, \dots, 4, \quad T(t, h, y) = T_0, \quad \vec{V}(t, h, y) = (0; 1.5 \cdot V_0)^T, \quad \varphi(t, h, y) = \varphi_0 + \alpha \cdot t,$$

where φ_0 is the specified initial value of the electric potential drop, a is the specified rate of change in the potential drop. At that $a = 0, \varphi_0 < 0$ for the potentiostatic mode, and $\varphi_0 = 0, a \neq 0$ for the potentiodynamic case.

$$C_1(t, x, 0) = C_0, \quad C_2(t, x, 0) = C_0, \quad C_3(t, x, 0) = 0, \quad C_4(t, x, 0) = 0, \quad T(t, x, 0) = T_0,$$

$$V_x(t, x, 0) = V_x(t, x, L) = 0, \quad V_y(t, x, 0) = V_y(t, x, L) = 1.5 \cdot V_0 x(2h - x) / h^2.$$

$$-\vec{n} \cdot \vec{j}_i(t, x, L) = V_y(t, x, L) \cdot C_i(t, x, L), \quad i = 1, \dots, 4, \quad \vec{n} \cdot \nabla T(t, x, L) = 0.$$

Initial conditions:

$$C_1(0, x, y) = C_0, \quad C_2(0, x, y) = C_0, \quad C_3(0, x, y) = 0, \quad C_4(0, x, y) = 0,$$

$$\varphi(0, x, y) = \varphi_0 x / h, \quad T(0, x, y) = T_0, \quad V_y(0, x, y) = 1.5 \cdot V_0 x(2h - x) / h^2.$$

Results

The new mathematical model is proposed that allows theoretically studying of the interaction of forced and gravitational convections, when the latter is conditioned not only by concentration gradients but also by nonisothermal nonequilibrium deprotonation-protonation reactions, as well as by the Joule heating of the solution and the heat transfer through the membranes. The results of the numerical and asymptotic solution of this problem will be presented in subsequent papers.

Acknowledgements

The study is sponsored by RFBR and the administration of Krasnodar region (grant no. 16-48-230856 r_a).

References

1. Nikonenko V., Kovalenko A., Urtenov M., Pismenskaya N., Han J., Sizat P., Pourcelly G. Desalination at overlimiting currents: State-of-the-art and perspectives // Desalination. 2014. N. 342. P. 85–106.
2. Pismenskiy A.V., Belashova E.D., Urtenov M.Kh., Kovalenko A.V. Non-stationary 2D model of the gravitational convection in electrodialysis of ampholytecontaining solutions // Polythematic online scientific journal of Kuban State Agrarian University. 2016. V. 123, N. 09. URL: <http://ej.kubagro.ru/2016/09/pdf/116.pdf>.
3. Nikonenko, V., Lebedev K., Manzanares J.A., Pourcelly G. // Electrochim. Acta. 2003. V. 48, N. 24. P.3639-3650.

EFFECT OF ACIDITY ON THE REGENERATION PROCESS IN BROMATE FUEL CELLS

¹Roman Pichugov, ¹Mikhail Petrov, ^{2,3}Dmitry Konev, ^{1,2}Anatoly Antipov, ¹⁻⁴Mikhail Vorotyntsev

¹M. V. Lomonosov Moscow State University, Moscow, Russia, *E-mail: rompich90@gmail.com*

²D. I. Mendeleev University of Chemical Technology, Moscow, Russia

³Institute of Problems of Chemical Physics, Russian Academy of Sciences, Chernogolovka, Russia

⁴ICMUB, UMR 6302 CNRS-Université de Bourgogne, Dijon, France

World's demand in power sources for stationary and portable applications is estimated to be in the order of tens of billions units per year and therefore the task of finding and using high-energy sources is becoming an important issue. Contemporary fuel cell (FC) wherein the air oxygen is used as an oxidizer (hydrogen-air, methanol-air) are characterized by high energy intensity. However, in a quite number of application areas the use of air as an oxidizer is hindered or impossible (underwater objects, mines, spacecrafts, satellites, etc.). Additionally, the application of FC is often limited by the need to use expensive platinum catalysts, mainly used to provide the required characteristics of air cathode.

In recent years genuine efforts have been undertaken to replace the inefficient air cathode by more promising oxidants [1]. One such oxidizing agents is an acidic bromate solution, for instance, lithium bromate. The energy intensity of a hydrogen-bromate battery is commensurable to that of modern lithium-ion systems and the discharge capacity of the battery can reach several watts per square centimeter.

Large-scale application of such fuel cells requires serious developments in the solution of regeneration problem of a spent oxidizer, i.e. conversion of the acid solution of bromide formed after electroreduction back to bromate.

The present work aims at verifying the possibility of obtaining bromate anion as a result of bromine disproportionation reaction generated on the electrode by the oxidation of bromide in an alkaline solution. It is known that rate of such disproportionation increases with the pH of the medium whereas in order to maintain the overall energy efficiency of the discharge-regeneration cycle (bromated-bromide-bromate) regeneration is beneficial to conduct in a neutral or slightly alkaline medium thus minimizing the current consumption on the neutralization of the spent oxidizer in a special reactor.

The studies were carried out using rotating ring-disk electrode (RRDE) comparing the catching coefficients on the ring for bromine generated by the disk in solutions with different pH values. It was found that oxidation of bromide on the disk in a concentrated solution of sodium carbonate leads to the reduction of the catching coefficient of bromine formed on the ring by 12 % compared with the acidic solution. On the basis of the work conducted one has made the conclusion that slightly alkaline medium could be used for carrying out electrochemical regeneration of the hydrogen-bromate battery oxidizer.

Acknowledgements

The study was financially supported by The Ministry of Education and Science grant № 14.607.21.0143 UIC: RFMEFI60716X0143

References

1. Tolmachev Y.V., Piatkivskiy A., Ryzhov V.V., Konev D.V., Vorotyntsev M.A., Energy cycle based on a high specific energy aqueous flow battery and its potential use for fully electric vehicles and for direct solar-to-chemical energy conversion // *Journal of Solid State Electrochemistry*, 2015, Vol. 19, P. 2711–2722.

SPECTROPHOTOMETRIC ANALYSIS OF BROMINE SPECIES IN CONCENTRATED AQUEOUS SOLUTIONS AT DIFFERENT PH

¹Roman Pichugov, ¹Mikhail Petrov, ^{2,3}Dmitry Konev, ^{1,2}Anatoly Antipov, ¹⁻⁴Mikhail Vorotyntsev

¹M. V. Lomonosov Moscow State University, Moscow, Russia, *E-mail: rompich90@gmail.com*

²D. I. Mendeleev University of Chemical Technology, Moscow, Russia

³Institute of Problems of Chemical Physics, Russian Academy of Sciences, Chernogolovka, Russia

⁴ICMUB, UMR 6302 CNRS-Université de Bourgogne, Dijon, France

The problem of determining the composition of bromine-containing medium has recently become particularly relevant due to the appearance of redox flow batteries (RFB) using bromate reduction at the cathode [1]. Direct (discharge) and reverse (charge) operating mode of such RFB acid-base, redox and complexing transitions between different bromine species (from bromate (+5) to bromide (-1)) completely determine the most important characteristics: Faraday and energy efficiency of redox cycle as well as rate and capacity.

Despite the fact that a considerable amount of research is dedicated to thermodynamics and kinetics of the oxidation of various substrates by bromate anion [2] [3] their findings are relevant to sufficiently dilute solutions while in FRB concentrated media are used providing required values for the density of stored energy and capacity.

The purpose of present work was to develop a methodology for analyzing the composition of concentrated bromine-containing media, allowing rapid and accurate monitoring concentration change of main components. At the same time it should be possible to widely replicate of hardware design of the method in order to equip each FRB with it.

To achieve this goal a flow cell was constructed, equipped with fiber optic spectrophotometer, a glass electrode and microelectrode specially arranged for simultaneous registration of pH, UV-VIS spectra and total oxidation capacity of the medium. Based on the literature data and calibration results of the test compositions a program was developed that allows analyzing the output data of the flow cell and calculating the content of the medium components.

Acknowledgements.

The study was financially supported by The Ministry of Education and Science grant № 14.607.21.0143 UIC: RFMEFI60716X0143

References

1. Vorotyntsev M. A., Konev D. V., Tolmachev Y. V. , *Electrochim. Acta.* 2015. Vol. 173. P. 779–795.
2. Beckwith R.C., Magnerum D.W., *Inorg. Chem.* 1997, Vol. 36, P. 3754-3760
3. KShirsagar G., Field R.J, *J. Chem. Phys.*, 1988, Vol. 92, P. 7074-7079.

MODIFICATION OF ULTRAFILTRATION MEMBRANES BY ADDITION OF POLYELECTROLYTES TO THE COAGULATION BATH

Tatiana Plisko¹, Alexandr Bilydukevich¹, Svetlana Aponovich¹, Stepan Bazhenov²

¹Institute of Physical Organic Chemistry, National Academy of Sciences of Belarus, Minsk, Belarus

²A.V. Topchiev Institute of Petrochemical Synthesis, Moscow, Russia

E-mail: plisko.v.tatiana@gmail.com

Introduction

Nowadays, the main challenge in designing ultrafiltration membranes is increasing membrane fouling resistance without sacrificing membrane transport properties [1]. The most effective approaches to increase the fouling resistance of membranes is considered to be increasing the hydrophilicity of membrane skin layer, the reduction of surface roughness, the improvement of charge property and the utilization of steric repulsion effect [2]. Hydrophilic membranes are considered to be less viable to biofouling and show lower sorption capacity towards proteins and natural organic matter in micro-, ultra- and nanofiltration processes [3]. Novel method of modification of ultrafiltration membranes using aqueous solutions of commercially available cationic and anionic polyelectrolytes based on acrylamide copolymers is proposed.

Polyelectrolytes based on acrylamide copolymers are utilized as flocculants for drinking water treatment. The main idea of this study is that using aqueous solutions of polyelectrolytes as coagulation medium upon membrane preparation via phase inversion technique leads to the modification of the skin layer due to immobilization of the charged macromolecules of polyelectrolytes. Due to the extremely high molecular weight of commercially available flocculants ($M \geq 5 \cdot 10^6$ Da), their introduction to the coagulation bath is expected to change the viscosity of the coagulation medium which results in the changes of the kinetics of the phase inversion process. The influence of the chemical nature of the polyelectrolytes and their concentration in the coagulation bath on the physico-chemical properties, charge, hydrophilic/hydrophobic balance of the skin layer, structure, transport properties and antifouling resistance of the membrane was studied.

Experiments

Polysulfone (PSF, Ultrason S 6010), N,N-dimethylacetamide (DMAc) and polyethylene glycol (PEG-400, $M_n=400$ g·mole⁻¹) were purchased from BASF (Germany).

Flat-sheet PSF ultrafiltration membranes were prepared via non-solvent induced phase separation technique. Distilled water, and 0.05%, 0.1% and 0.2% aqueous solutions of commercially available high molecular weight cationic and anionic polyelectrolytes based on acrylamide Praestol 859 BS and Praestol 2540 (Ashland) were used as coagulation bath. Coagulation bath temperature was kept at 25°C, 40°C, 60°C and 70°C. Human serum albumin (HSA, MW = 67000 Da, isoelectric point of pH 4.7, Sigma-Aldrich) feed solution was prepared in the phosphate buffer at pH=7.0 at HSA concentration 0.05% and used for permeation and rejection tests. The protein contents were analyzed with UV-Vis spectrophotometer (Metertech UV-VIS SP 8001) at a wavelength of 280 nm. Membrane rejection coefficient was also assessed using 0.3 g·L⁻¹ aqueous solution of polyvinylpyrrolidone PVP K-30 ($M_n=40\ 000$ g·mole⁻¹) as a model solution. PVP concentration was measured using an LIR-2 interferometer (Zagorsk Optical and Mechanical Plant, Russia). To study antifouling stability of modified membranes surface water from the Slepianski Chanel (Minsk, Republic of Belarus) was filtered in dead-end ultrafiltration mode at P= 0.1 MPa and flux was measured at intervals of every 30 s. Turbidity of feed water and permeate was determined using a turbidimeter 2100 AN (Hach, Germany), calibrated with a formazin standard. Total Fe content in feed water and permeate was determined using atomic emission spectrometer with inductively coupled plasma (Vista PRO, Varian, USA).

Results and Discussion

Chemical nature and charge of the polyelectrolyte was shown to influence the structure, transport properties and antifouling stability of the polysulfone ultrafiltration membranes (Table,

Fig. 1, 2). Modification of polysulfone membranes by anionic flocculant Praestol 2540 was found to increase pure water flux from 710 to 1170 L·m⁻²·h⁻¹, increase PVP K-30 solution flux from 320 to 660 L·m⁻²·h⁻¹ and decrease rejection coefficients of PVP K-30 and HSA significantly (Table). Modification of the membrane by cationic polyelectrolyte Praestol 859 BS yields in the three-fold decrease of the pure water flux and two-fold decrease of PVP K-30 solution flux. It was revealed, that modification of polysulfone membranes by cationic polyelectrolyte results in the increase of the fouling recovery ratio after HSA solution filtration (at pH=7.0) (Table). These changes are attributed to different kinetics of phase inversion process which depends on the viscosity and chemical nature of coagulation medium. Addition of anionic polyelectrolyte to the coagulation bath was found to yield in the formation of more porous and open structure of the skin layer, while addition of cationic polyelectrolyte results in formation of denser structure of the skin layer compared to the initial membrane (Figure 1). Contact angle of the inner surface of the membrane skin layer was revealed to decrease from 49° to 39-40° upon modification by polyelectrolytes (Table 1).

Comparison of normalized flux of surface water allows concluding that membranes modified using polyelectrolytes are more stable to fouling by natural organic matter compared to the initial membrane due to the formation of charged and more hydrophilic surface of the skin layer (Fig. 2).

Table 1: Performance of polysulfone flat sheet membranes

Membrane performance	Coagulation bath		
	water	0,1% Praestol 2540 solution	0,1% Praestol 859 BS solution
Pure water flux, L·m ⁻² ·h ⁻¹	710	1170	240
PVP K-30 aqueous solution flux, L·m ⁻² ·h ⁻¹	320	660	180
Rejection (PVP K-30), %	18	5	15
HSA solution flux, L·m ⁻² ·h ⁻¹	140	240	180
Fouling recovery ratio after HSA solution filtration, %	16	16	48
Rejection (HSA), %	>99	58	>99
Contact angle of the skin layer, °	49±2	40±2	39±2

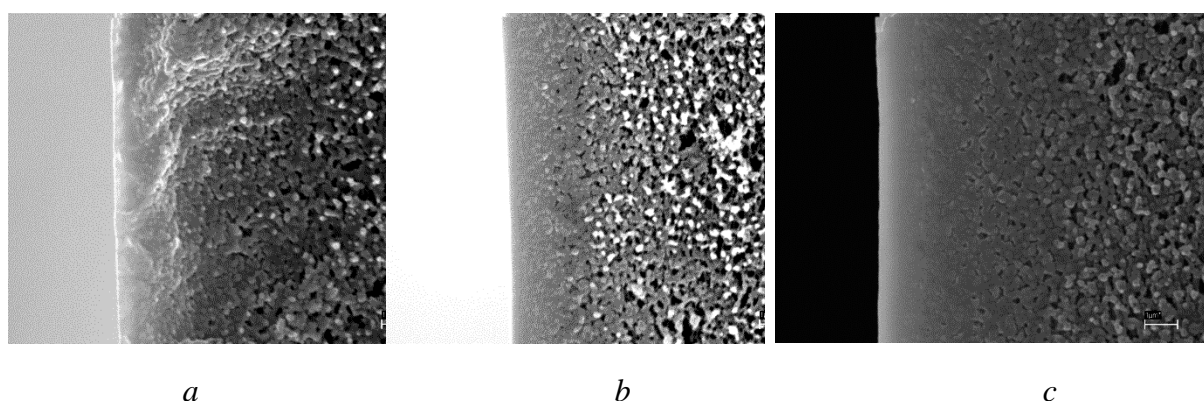


Figure 1. SEM-images of the skin layer of flat sheet polysulfone membranes, coagulation bath: 1 – distilled water; 2 - 0,1% aqueous solution of Praestol 859 BS; 3 – 0,1% aqueous of Praestol 2540

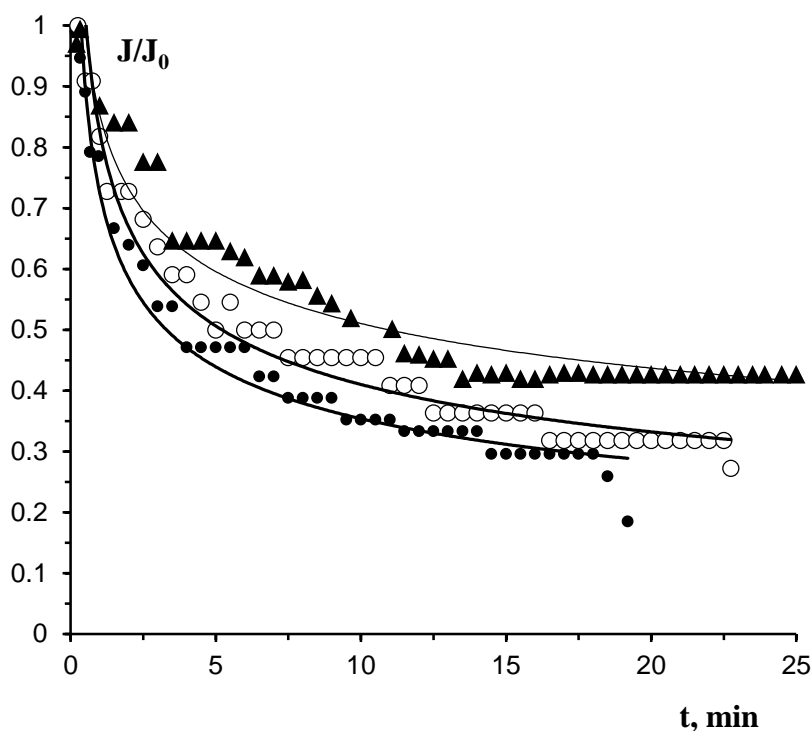


Figure 2. Time-dependent normalized flux of surface water for polysulfone flat sheet membranes, coagulation bath: 1 – distilled water, 2 – 0,1% Praestol 2540 aqueous solution, 3 – 0,1% Praestol 859 BS aqueous solution

Modification of polymer membranes via addition of polyelectrolytes to the coagulation bath was found to be an effective approach to increase membrane antifouling stability toward natural organic matter in the process of the filtration of surface water and significantly increase the flux of ultrafiltration membranes (via modification by anionic polyelectrolyte).

Acknowledgements

This work was performed at the Topchiev Institute of Petrochemical Synthesis and supported by the Russian Science Foundation, project no. 14-49-00101.

References

1. Ng L., Mohammad A., Ng C. A review on nanofiltration membrane fabrication and modification using polyelectrolytes: Effective ways to develop membrane selective barriers and rejection capability // *Adv. Colloid Interface Sci.* 2013. V. 197-198. P. 85-107.
2. Menne D., Kamp J., Wong J., Wessling M. Precise tuning of salt retention of back washable polyelectrolyte multilayer hollow fiber nanofiltration membranes // *J. Membr. Sci.* 2016. V. 499. P. 396-405.
3. Bilyukevich A., Plisko T., Liubimova A., Volkov V., Usosky V. Hydrophilization of polysulfone hollow fiber membranes via addition of polyvinylpyrrolidone to the bore fluid // *J. Membr. Sci.* 2017. V. 524. P. 537-549.

PREPARATION OF HIGH FLUX POLYPHENYLSULFONE MEMBRANES USING UPPER AND LOWER CRITICAL SOLUTION TEMPERATURE SYSTEMS: EFFECT OF COAGULATION BATH TEMPERATURE

Tatiana Plisko¹, Alexandr Bilydukevich¹, Yana Isaichykava¹, Anna Ovcharova²

¹Institute of Physical Organic Chemistry, National Academy of Sciences of Belarus, Minsk, Belarus

²A.V. Topchiev Institute of Petrochemical Synthesis, Moscow, Russia,

E-mail: plisko.v.tatiana@gmail.com

Introduction

Polyphenylsulfone (PPSU) is a promising membrane forming polymer known for its chemical stability, impact strength and resistance to organic solvents [1-3]. However, scarce studies on PPSU membranes reported up-to-date reveal that a very low pure water flux (PWF) was achieved for ultrafiltration membranes prepared via non-solvent induced phase inversion (NIPS) method [1]. This fact can be attributed to the concentration restrictions of additive and pore former introduction to PPSU solutions in amide solvents (N-methyl-2-pyrrolidinone (NMP), N,N-dimethylformamide etc.) due to the narrow miscibility region on ternary phase diagrams PPSU-solvent-nonsolvent [2,3]. These restrictions require novel approach for PPSU membrane preparation in order to utilize the advantages of this promising membrane-forming polymer. A novel method for PPSU ultrafiltration membrane preparation using the systems PPSU-polyethylene glycol (PEG)-NMP exhibiting lower (LCST) ($T > 100$ °C) and upper (UCST) ($T = 38-40$ °C) critical solution temperatures was developed in this study. This method involves PPSU casting solution processing at the temperature region between LCST and UCST and varying the coagulation bath temperature which allows combining NIPS and thermally induced phase separation (TIPS).

The effect of coagulation bath temperature on the structure, permeation, rejection, hydrophilic/hydrophobic properties of the skin layer, water uptake of PPSU membrane was studied.

Experiments

Polyphenylsulfone (Ultrason P 3010) with average $M_w = 50\,000$ g·mole⁻¹ was purchased from BASF (Germany). Polyethylene glycol of $M_n =$ g·mole⁻¹ (Fluka) was used as additives to the PPSU casting solution. Flat sheet asymmetric PPSU membranes were prepared via the phase inversion method. The casting solution at $T = 40$ °C was cast onto a glass plate using a casting blade at $T = 40$ °C. Immediately after casting, the membrane was immersed in a deionized water bath ($T = 25$ °C, 40 °C, 60 °C, 70 °C) where phase inversion occurred. After 30 min, the membrane was placed in a fresh water bath and left for 24 h to ensure sufficient removal of solvent and stability of the membrane final structure. Lastly, the membranes were stored in deionized water for the further analysis. Prior to SEM studies the membranes were kept in 50 wt% glycerin aqueous solution and then dried at room temperature for 72 hours. Morphology of the flat sheet membranes was studied on a LEO 1420 scanning electron microscope. Cleaved facets of the samples of the membranes were prepared by cryogenic fracture in liquid nitrogen followed by gold coating using cathode sputtering in an EMITECH K 550X vacuum system. Membrane performance was estimated at an average transmembrane pressure of 1.0 bar in ultrafiltration cross-flow mode. Human serum albumin (HSA) ($MW = 66400-66600$ g·mole⁻¹, isoelectric point of pH 4.7) (Sigma-Aldrich) was used as reference solute in permeation and rejection experiments.

Results and Discussion

When the temperature of water coagulation bath is $T = 25$ °C (below UCST) the casting solution undergoes UCST-TIPS which yields in symmetrical bicontinuous structure formation (Fig. 1a). Increase of the coagulation bath temperature up to 40 °C results in the transition structure type (Fig. 1 b), where macrovoids are conceiving due to the change from UCST-TIPS to NIPS process but their formation is suppressed because of high casting solution viscosity resulting in low mass transfer rate. Increasing the coagulation bath temperature up to 70 °C yields in the formation of

asymmetrical structure with macrovoids due to NIPS process to occur and increasing mass transport rate upon phase inversion process (Fig. 1 c). The increase in coagulation bath temperature was found to result in the rise of the pure water flux from 110 to 400 $\text{l}\cdot\text{m}^{-2}\cdot\text{h}^{-1}$ with human albumin rejection maintaining unchanged (86-88%), increase of the pore size of the skin layer (Fig. 1), rise of water uptake and contact angle.

Contact angle was shown to increase from 45° to 53° when the temperature of coagulation bath increases from 25°C to 70°C which can be attributed to faster out-diffusion of high molecular weight PEG from the casting solution during membrane formation at higher coagulation bath temperature. When the temperature of coagulation bath increases the viscosity of the coagulation medium and casting solution decreases which allows PEG to wash out more easily from the nascent membrane matrix leading to the increase of the contact angle.

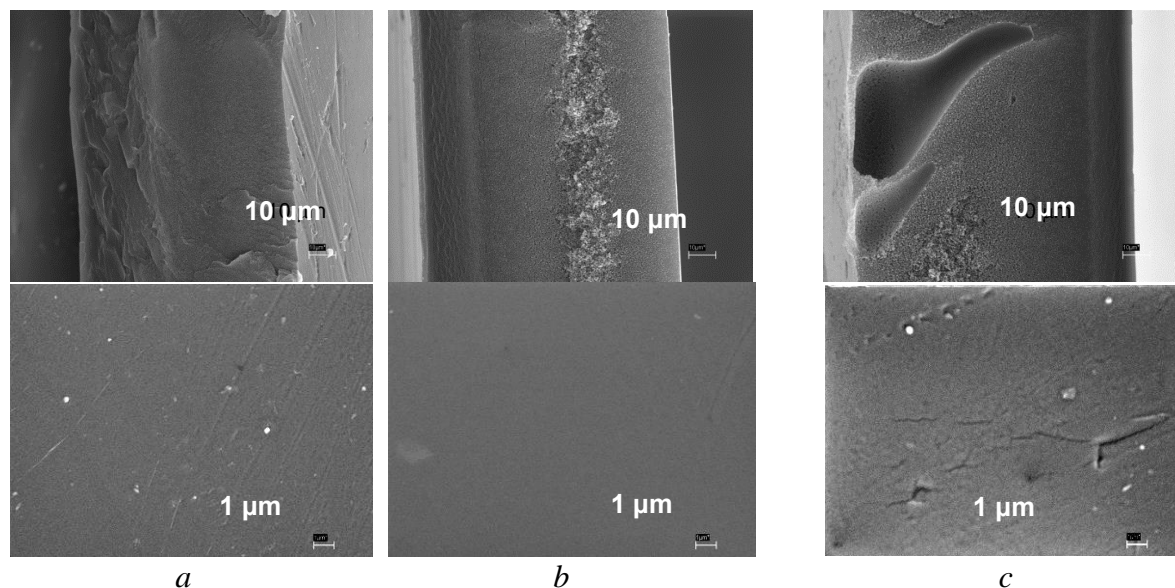


Figure 1. Scanning electron microscope images of the cross section and the inner surface of the skin layer of the flat-sheet PPSU membranes prepared at different coagulation bath temperatures: a - 25°C , b - 40°C , c - 70°C

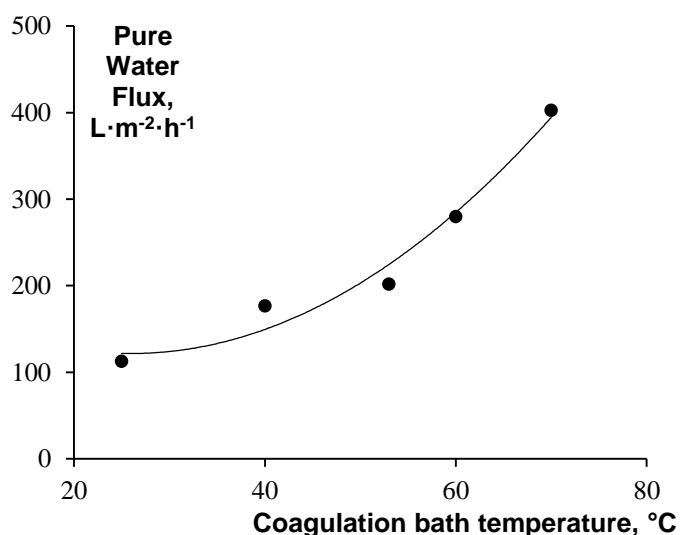


Figure 2. Pure water flux versus coagulation bath temperature for PPSU ultrafiltration membranes

The structure and performance of the PPSU flat sheet membranes prepared from the polymer casting solutions with upper and lower critical solution temperatures was shown to depend on

coagulation bath temperature significantly which is attributed to different phase inversion mechanism to occur (NIPS or UCST-TIPS).

Acknowledgements

This work was performed at the Topchiev Institute of Petrochemical Synthesis and supported by the Russian Science Foundation, project no. 14-49-00101.

References

1. *Praneeth K., Bhargava Suresh K.* Design of novel ultrafiltration systems based on robust polyphenylsulfone hollow fiber membranes for treatment of contaminated surface water // *Chem. Eng. J.* 2014. V. 248. P. 297-306.
2. *Darvishmanesh S., Jansen C. J., Tasselli F.* Preparation of solvent stable polyphenylsulfone hollow fiber nanofiltration membranes // *J. Membr. Sci.* 2013. V. 384. P. 89-96.
3. *Jansen C. J., Darvishmanesh S., Tasselli F.* Influence of the blend composition on the properties and separation performance of novel solvent resistant polyphenylsulfone/polyimide nanofiltration membranes // *J. Membr. Sci.* 2013. V. 447. P. 107-118.

INFLUENCE OF HEAT TREATMENT ON STRUCTURAL CHARACTERISTICS OF ION-EXCHANGE MEMBRANES

¹Kristina Pogosyan, ¹Natalia Kononenko, ²Vera Vasil'eva

¹Kuban State University, Krasnodar, Russia, E-mail: pogosyan.chris@gmail.com

²Voronezh State University, Russia

The operating conditions of ion-exchange membranes are often associated with the elevated temperatures (high-temperature or intensive current regimes electro dialysis). Small increase in temperature can significantly affect the structure of the ion exchange membrane that leads to change of membrane transport characteristics.

The aim of this work is investigation the influence of heat treatment on the structural characteristics of heterogeneous ion-exchange membranes. The objects of the study were commercial MK-40 and MA-41 membranes manufactured by JSC "ShchekinoAzot" (Russia). Each membrane was exposed at certain temperature for 50 hours.

The method of standard contact porosimetry was used to determine the water distribution on the binding energy or the effective pore radii in the membrane [1, 2]. The maximum porosity was obtained from porosimetric curves as water volume per gram of the dry sample (V_0 , cm³/g). The specific internal surface area (S , m²/g) was calculated according [2]. The volume of hydrophilic unselective macropores filled with unbound "free" water (V_{macro}) and the volume of micro and mesopores (V_{micro}) having radius below 25 nm and nearly ideal selectivity was found from the porosimetric curves as well. The volume fraction of macropores in swollen membrane ($\frac{V_{macro}}{V_{sw.m}}$) characterizes the membrane heterogeneity. The fraction of micro and mesopores in the total volume of water in the membrane ($\frac{V_{micro}}{V_0}$) is concerned with the membrane ion selectivity.

The curves of water distribution on the binding energy and the effective pore radii for MK-40 and MA-41 membranes are shown in Fig. The structural parameters found from the porosimetric curves are presented in Table.

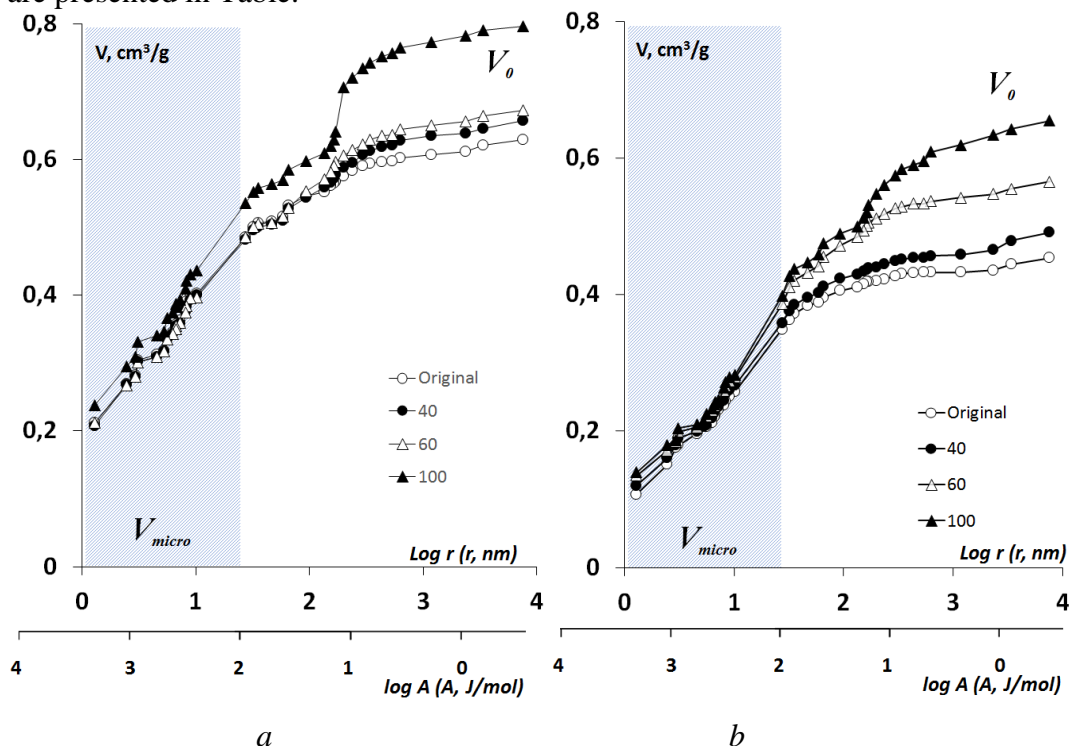


Figure. Integral curves of water distribution on the effective pore radii and the binding energy for MK-40 (a) and MA-41 (b) membranes

Table: Structural characteristics of the membranes

Membrane	Q, mmol/g	V_0 , cm ³ /g	V_{macro} , cm ³ /g	$\frac{V_{macro}}{V_{sw.m}}$	S, m ² /g	$\frac{V_{micro}}{V_0}$
MA-41 original	1.18±0.06	0,45	0,20	0,15	323	0,89
MA-41 after 100°C	0.72±0.06	0,65	0,37	0,22	382	0,75
MK-40 original	1.52±0.08	0,63	0,23	0,15	554	0,87
MK-40 after 100°C	1.19±0.03	0,80	0,36	0,25	611	0,75

Analysis of the obtained data shows that the heat treatment of membranes leads to the change of both physicochemical characteristics and structural parameters. It can be seen from the Figure that increase in the treatment temperature from 40 to 100°C, causes the growth of total pore volume in the membranes (V_0). The most significant changes occur in membranes after 100°C. The growth of macropores volume with a radius greater than 25 nm correlates with scanning electron microscopy data [3]. The volume fraction of macropores $\frac{V_{macro}}{V_{sw.m}}$ increases (Table). As result membrane diffusion permeability and electrical conductivity grow [3]. The temperature treatment of the membranes leads to reduction in membrane selectivity. The fraction of selective micro and mesopores in the membranes $\frac{V_{micro}}{V_0}$ decreases with growth of treatment temperature for both cation- and anion-exchange membranes (Table).

Thus, the results obtained indicate a correlation between structural characteristics and electrottransport properties of membranes after heat treatment.

The present work is supported by the Russian Foundation for Basic Research, grant 15-08-05031.

References

1. *Volfkovich Yu.M., Filippov A.N., Bagotsky V.S.* Structural properties of porous materials and powders used in different fields of science and technology. Springer-Verlag; 2014.
2. *Berezina N.P., Kononenko N.A., Dyomina O.A., Gnusin N.P.* // Adv. Colloid Interf. Sci. 2008. V.139. P. 3.
3. *Vasil'eva V.I., Akberova E.M., Demina O.A., Kononenko N.A., Malykhin M.D.* // Elektrokhimiya, 2015, Vol. 51, No. 7. P. 711.

THE FUNCTIONAL PROPERTIES OF NEW PROTON ELECTROLYTES BASED ON CESIUM DIHYDROGEN PHOSPHATE AND HIGH WATER RETENTION MATRIX

Valentina Ponomareva^{1,2}, Galina Lavrova¹, Elena Shutova¹

¹Institute of Solid State Chemistry and Mechanochemistry SB RAS, Novosibirsk, Russia,
E-mail: ponomareva@solid.nsc.ru

²Novosibirsk State University, Novosibirsk, Russia

Introduction

Cesium dihydrogen phosphate is one of the most conductive proton electrolytes in the intermediate temperatures and is of great scientific and practice interest to be used as a proton membrane in fuel cells. It has one of the highest value of proton conductivity, $6 \cdot 10^{-2} \text{ S} \cdot \text{cm}^{-1}$ in superionic phase; the low temperature phase (LT) (P2₁/m) conductivity is less than 10^{-6} Scm^{-1} . However superionic phase of CsH₂PO₄ is stable at 30 mol% of water vapor. Dispersed SrZrO₃ and SnP₂O₇ compounds are known to have high water retention at relatively high temperatures; it should be important for the improvement of thermal stability of CsH₂PO₄ superionic state at the lower water partial pressure in the composite electrolytes.

This work was directed to the investigation of the new types of composite (1-x)CsH₂PO₄-xA electrolytes, where A=SrZrO₃ and SnP₂O₇, x=0.1-0.8. The microstructure, phase composition, electrotransport and thermal properties of proton composite electrolytes were investigated firstly in a wide range of compositions at different water vapor partial pressures at 40-260°C.

Experiments

(1-x)CsH₂PO₄-xSrZrO₃ and (1-x)CsH₂PO₄-xSnP₂O₇ composites were synthesized by prolong mechanical mixing of the stoichiometric quantities of CsH₂PO₄ and dispersed matrix followed by heating at temperatures ~220°C. The investigation was carried out using IR and a.c. impedance spectroscopy, XRD, DSC, TGA analysis and high resolution electron microscopy.

Results and Discussion

According to X-ray diffraction, the crystalline structure of CsH₂PO₄ was preserved and the chemical interaction of the salt with the matrix was not observed. Thermodynamic and structural properties of CsH₂PO₄ in composites differ significantly from the ones of individual salt due to the structural disordering and partial amorphization. With increase of the mole fraction of high dispersed SrZrO₃ or SnP₂O₇ in the composites, a gradual increase of proton conductivity up to 1-3 orders of magnitude in the low temperature phase was observed, due to the dispersion of salt at small x values and the subsequent partial amorphization with the increase of heterogeneous additive content. The conductivity in superionic phase does not depend on the heterogeneous additive content up to x=0.2 and then decreases with x increase at x>0.3. The optimal compositions were developed and studied more detailed in different conditions with its variable water vapor pressure. The composites were shown to have significant thermal stability and high conductivity $\sim 10^{-2} \text{ S/cm}$ during a long term storage at the significantly lower water partial pressure (7.5-12.5 mol %) in comparison with an individual CsH₂PO₄. The substantial effect of the heterogeneous matrix with high water retention SrZrO₃ or SnP₂O₇ on the stability of CsH₂PO₄ in superionic phase at 230-260°C in nanocomposites (1-x)CsH₂PO₄-xSnP₂O₇ and (1-x)CsH₂PO₄-xSrZrO₃ has been detected firstly. The comparison of two types of electrolytes has been carried out. Such effects are extremely important for creating intermediate-temperature proton membrane for the fuel cells.

The work was carried out with a partial financial support from complex program of SB RAS.

PHASE COMPOSITION, TRANSPORT AND THERMAL PROPERTIES OF BARIUM DOPED CESIUM DIHYDROGEN PHOSPHATE SYSTEM

Valentina Ponomareva^{1,2}, Irina Bagryantseva^{1,2}, Elena Shutova¹

¹Institute of Solid State Chemistry and Mechanochemistry SB RAS, Novosibirsk, Russia,

E-mail: ponomareva@solid.nsc.ru

²Novosibirsk State University, Novosibirsk, Russia

Introduction

CsH₂PO₄ is one of the most promising compounds in the family of solid acids of alkali metals M_nH_m(AO₄)_p, where M = Cs, Rb, K, Na, Li, NH₄; A = S, Se, As, P to be used as a proton membrane in intermediate temperature fuel cells. It has one of the highest value of proton conductivity, 6·10⁻² S·cm⁻¹ in superionic phase. The CsH₂PO₄ low temperature phase (LT) (P2₁/m) conductivity is less than 10⁻⁶ Scm⁻¹. LT proton conductivity of CsH₂PO₄ is strongly sensitive to cation and anion substitution due to possible formation of solid solutions or disordered phases on the interphase and corresponding changes of hydrogen bond network. The electrotransport and structural properties of Cs_{1-x}M_xH₂PO₄ where M=Rb, K, Na, were investigated in details and solid solutions isostructural to CsH₂PO₄ were shown to be formed with decreasing unit cell parameters. The existence of Cs_{1-x}M_xH₂PO₄ solid solutions depends markedly on the substituting cation. A wide range of solid solutions up to x=0-0.9 was observed for Cs_{1-x}Rb_xH₂PO₄ and it significantly was decreased with a diminishing in the size of the substitutive cations. The scientific interest for formation of more disordered systems deals with the isovalent substitution in CsH₂PO₄. Modification of CsH₂PO₄ by double-charged cations results in vacancies in Cs-sublattice, determining changes in hydrogen bond energy and the degree of structure disordering. This work was directed to the investigation of proton conductivity, structural, thermodynamic properties of (1-x)CsH₂PO₄-xBa(H₂PO₄)₂ system in wide range of substitution of Cs⁺ by Ba²⁺ (x=0-0.4) and to the conductivity of additive Ba(H₂PO₄)₂ compound which were studied firstly.

Experiments

Cs_{1-2x}Ba_xH₂PO₄ were synthesized by prolong mechanical mixing of the stoichiometric quantity of CsH₂PO₄ and Ba(H₂PO₄)₂ followed by heating. Ba(H₂PO₄)₂ and CsH₂PO₄ single crystals were synthesized from aqueous solutions. The investigation was carried out using IR and a.c. impedance spectroscopies, XRD, DSC, TGA analysis and high resolution electron microscopy.

Results and Discussion

Careful studies of the thermal and transport properties of Ba(H₂PO₄)₂ initial salt have been carried out at a first time. Ba(H₂PO₄)₂ single crystals were analyzed in detailed by impedance spectroscopy. Measurements of the proton conductivity have been realized in different atmospheres (nitrogen, argon, air) and showed the significant influence of adsorbed water on its values at 30-160°C. The presence of anisotropy of proton conductivity was found in Ba(H₂PO₄)₂. The anisotropy of proton conductivity is caused by peculiar structural features of the salt: the presence of corrugated sheets of phosphate tetrahedra lying in the ac plane alternating with Ba²⁺ cations. The higher values of proton conductivity (4·10⁻⁹ - 1.5·10⁻⁷ S/cm at 60-160°C) were observed along the [100] crystallographic direction in comparison with [010]. The energy of activation of proton conductivity was determined.

The Xray diffraction data of Cs_{1-2x}Ba_xH₂PO₄ shown the formation of solid solution isostructural to CsH₂PO₄ (P2₁/m) at x= 0.03-0.1 with negligible decrease of unit cell parameters. While the proton conductivity of Cs_{1-2x}Ba_xH₂PO₄ increases more than three orders of magnitude in the low temperature phase and the superionic phase transition practically disappears with x increase. In contrast to substitution of monovalent cation, the formation of Cs⁺ vacancies takes place due to heterovalent substitution of CsH₂PO₄. It facilitates the structural disordering and reorientation of phosphate tetrahedra, CsH₂PO₄ amorphization at higher x, improves the proton mobility and conductivity. The conductivity in superionic phase doesn't change. The stability of high conductivity values has been verified at high temperatures for the long term storage. A mechanism

of conductivity improvement includes the formation of Cs vacancies during heterovalent replacement which lead to phosphate tetrahedra reorientation and structural disordering of the salt up to its amorphization with x increase with weakening of hydrogen bond network. Significant changes of $\text{Cs}_{1-2x}\text{Ba}_x\text{H}_2\text{PO}_4$ thermal properties were revealed, which were in accordance with structural and transport characteristics.

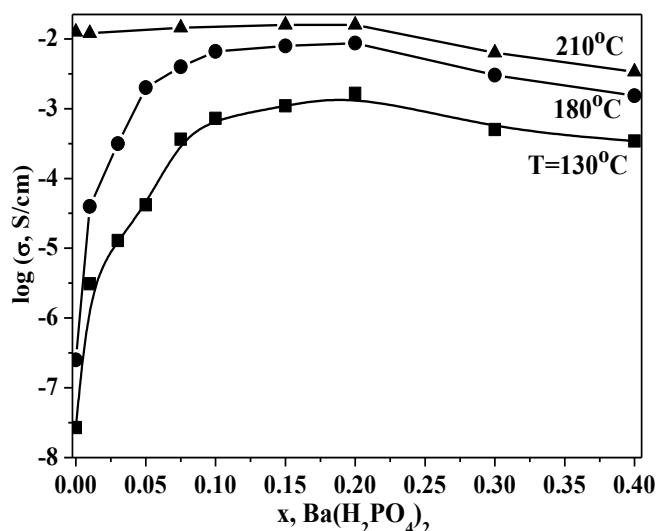


Figure 1. Isotherm of proton conductivity of $(1-x)\text{CsH}_2\text{PO}_4-x\text{Ba}(\text{H}_2\text{PO}_4)_2$ for different x content.

With the growth of Ba^{2+} mole fraction, $x > 0.10$ the solid solutions are not observed; the reflexes of $\text{Ba}(\text{H}_2\text{PO}_4)_2$ are appeared and two phases coexist, forming a composite system. The heterophase high-conductivity systems was revealed in the range $x = 0.15-0.4$. Superionic phase transition disappears with x increase. The further proton conductivity increase takes place up to $x=0.25$ while the initial salts have the extremely low conductivity values (Figure 1). The high conductivity deals with the formation of composite electrolytes based on salts where the protons of water molecules adsorbed on the grain boundaries also participate in the proton transport. The mechanism of proton transport for $(1-x)\text{CsH}_2\text{PO}_4-x\text{Ba}(\text{H}_2\text{PO}_4)_2$ system in wide range of $\text{Ba}(\text{H}_2\text{PO}_4)_2$ is discussed.

Formation of composite systems with the optimal x values at 0.15-0.2 with the highest proton conductivity $\sim 10^{-2}$ S/cm, chemically stable at a temperature of $\sim 200-210$ ° C in an atmosphere with low humidity was determined. It creates perspectives for the development of new functional highly conductive proton membranes for medium-temperature electrochemical devices.

The work was carried out with a financial support from the grant of RFBR n 15-08-08961.

NEW PROTON CONDUCTING ELECTROLYTES IN CESIUM MONO AND DIHYDROGEN PHOSPHATES SYSTEM

Valentina Ponomareva^{1,2}, Galina Lavrova¹, Boris Zakharov^{1,2}, Irina Bagryantseva^{1,2}

¹Institute of Solid State Chemistry and Mechanochemistry SB RAS, Novosibirsk, Russia,

E-mail: ponomareva@solid.nsc.ru

²Novosibirsk State University, Novosibirsk, Russia

Introduction

CsH₂PO₄ in superionic phase has a high proton conductivity and can be used in a variety of electrochemical devices at moderate temperatures (200-250°C). It is determined that minor quantities of the other phases may give a noticeable effect on the thermal and transport properties of CsH₂PO₄. The small additives of Cs₂HPO₄ or CsH₅(PO₄)₂ may results in significant changes in proton conductivity and thermal properties. The CsH₂PO₄-Cs₂HPO₄-H₂O system wasn't investigated earlier.

This work is devoted to detailed study of phase composition, their thermal stability and transport properties in the (1-x)CsH₂PO₄-xCs₂HPO₄*yH₂O system.

Experiments

The single crystals were synthesized from aqueous solutions of the stoichiometric quantities of Cs₂HPO₄*2H₂O and CsH₂PO₄. Their physics-chemical properties were investigated in a wide range of compositions (x=0-1) using IR and a.c. impedance spectroscopy, XRD, DSC, TGA analysis.

Results and Discussion

The crystal structure P2₁/c was determined for synthesized Cs₂HPO₄*2H₂O compound with lattice parameters a=7.4761 Å, b=14.2125 Å, c=7.9603 Å, β=116.914°, Z=4. The thermal transformations of Cs₂HPO₄*2H₂O up to 450° C and electrotransport properties in the different H₂O partial pressure were investigated for the first time.

A new phase was firstly discovered in the (1-x)CsH₂PO₄-xCs₂HPO₄*yH₂O system at x=0.5. Its final composition corresponds to Cs₃(H₂PO₄)(HPO₄)*2H₂O. Its crystalline structure was determined: space group Pbca, unit cell parameters: a=11.4412 Å, b=14.8774 Å, c=7.4692 Å, β=90°. The proton conductivity of Cs₃(H₂PO₄)(HPO₄)*2H₂O in different H₂O partial pressure and dehydrated phase was investigated firstly.

In the range x=0.5-0.9 the solid solutions are not observed and Cs₃(H₂PO₄)(HPO₄)*2H₂O phase coexists with Cs₂HPO₄*2H₂O, giving composite electrolytes. Dehydrated systems have the low conductivity at x = 0.5-0.9 not exceeding 10⁻⁵- 10⁻⁸ S/cm at ~100-230°C.

With the decreasing of Cs₂HPO₄ content the phase composition of the system is changing. Along with Cs₃(H₂PO₄)(HPO₄)*2H₂O the reflexes of CsH₂PO₄ (P2₁/m) appear with increasing their intensities. CsH₂PO₄ (P2₁/m) becomes the main phase for or x = 0.3. The solid solutions weren't formed; it was associated with a significant difference in the crystalline structures of cesium hydrogen phosphates with varying degrees of hydrogen replacement. Very interesting results for electrotransport properties were obtained with the increasing ratio of CsH₂PO₄. The temperature dependence of conductivity changes significantly and superionic conductivity, ~10⁻² S/cm, appears. The conductivity in the low temperature phase of (1-x)CsH₂PO₄-xCs₂HPO₄*yH₂O depends markedly on x and increases almost 5 orders of magnitude for x = 0.1 - 0.3. Significant growth of conductivity deals with the formation of proton composite electrolytes with modified salt properties on the interface and partial participation of the water molecules adsorbed on the interface in the transfer of protons. The values of proton conductivity ~ 10⁻² S/cm were stable at a high temperatures for a long term storage, that is perspective for proton membranes.

The work was carried out with a basic financial support of ISSCM SB RAS.

ORGANIC-INORGANIC ION-EXCHANGER BASED ON WEAKLY AND STRONGLY ACIDIC RESINS

¹Ludmila Ponomarova, ²Yuliya Dzyazko, ³Yurii Volfkovich, ³Valentin Sosenkin

¹Sumi National Agrarian University, Sumy, Ukraine

E-mail: ponomarouva@gmail.com

¹V.I. Vernadskii Institute of General & Inorganic Chemistry of the NAS of Ukraine, Kyiv, Ukraine

E-mail: dzyazko@ionc.kiev.ua

²A.N. Frumkin Institute of Physical Chemistry & Electrochemistry of the RAS, Moscow, Russia,

E-mail: yuvolf40@mail.ru

Introduction

Strongly acidic resins (SARs) are widely used for removal of toxic cationic components from water. Their main disadvantage is difficult regeneration: strong acid as well as a large volume of water for washing are necessary. In opposite to SARs, weakly acidic resins (WARs) containing –COOH groups can be regenerated easier. Additionally, incorporated nanoparticles of zirconium hydrophosphate (ZHP) are expected to facilitate desorption: this effect was observed for organic-inorganic resin based on SAR loaded with uranyl-ions [1, 2]. Moreover, the embedded ZHP particles affect functional properties of the ion-exchange resin particularly swelling, exchange capacity, sorption kinetics [3, 4]. The aim of the investigation is to establish the effect of the inorganic constituent on functional properties of WAR and compare the composites based on this type of the matrix and SAR.

Experiments

Such macroporous WAR as DOWEX MAC-3 has been chosen as a model matrix. Gel-like Dowex HCR-S SAR and amorphous ZHP were also investigated for comparison. The resins were immersed in a $ZrOCl_2$ solution followed by treatment with H_3PO_4 . Porous structure of the samples was investigated with standard contact porosimetry method, which can be applied to polymers [5]. The measurements were carried out by means of a home-made device (A.N. Frumkin Institute of Physical Chemistry & Electrochemistry of the RAS) using water as a working liquid. Morphology of the samples was researched using transmission electron microscopy. Adsorption of Malachite Green was researched under batch conditions. Sorption of Ni^{2+} ions was investigated under dynamic conditions, the solution (1 mmol dm^{-3}) was prepared using tap water containing (mmol dm^{-3}): Ca^{2+} –1.3, Mg^{2+} –0.4.

Results and Discussion

Both non-aggregated ZHP nanoparticles (5-10 nm) and their aggregates (from 0.2 up to several μm) are observed for the modified WAR matrix (Fig. 1). Larger nanoparticles (up to 20 nm) have been found earlier for the SAR resin [3]. The nanoparticles stabilized with polymer are placed inside the clusters and channels of gel phase, the aggregates are outside it.

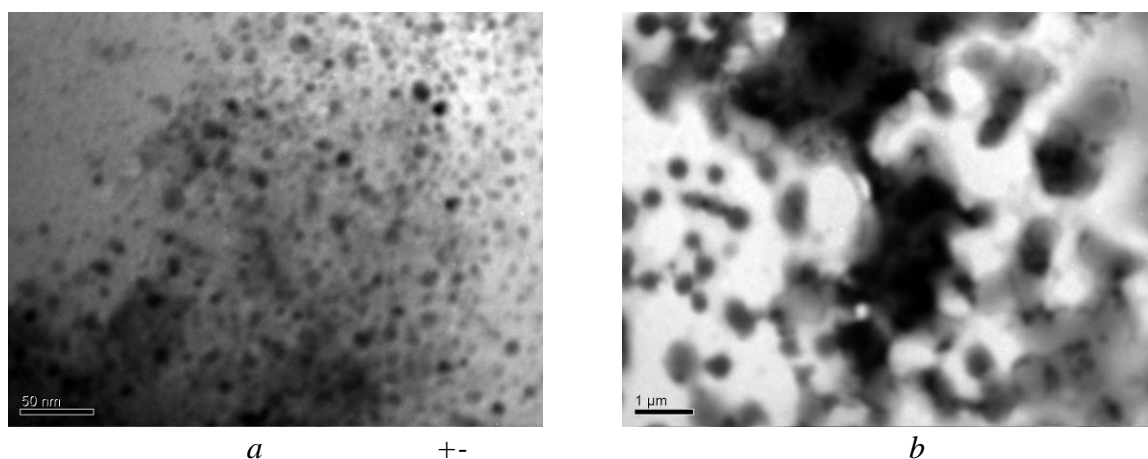


Figure 1. TEM images of the modified WAR resin. Single nanoparticles (a) and aggregates (b) are seen

Before the porometric measurements the samples were previously vacuumized at 353 K. Removal of bonded and free water from ZrPh phase is impossible under these conditions. Thus only polymer structure has been recognized. As seen from the pore size distributions for the WAR, the mesopores (clusters and voids between gel regions) are both ordered and disordered (Fig. 2). The structure defects (peaks at $\log r=3-4$ and 4.2 (nm)) are related to ordered pores. Only disordered meso- and macropores are observed for the SAR. Insertion of ZHP into the WAR matrix decreases a volume of pores probably due to corking of clusters and channels with the nanoparticles. Simultaneously the volume of structure defects also decreases. Regarding the SAR, modification causes reduction of volume of clusters and voids between gel regions, however, structure defects become larger.

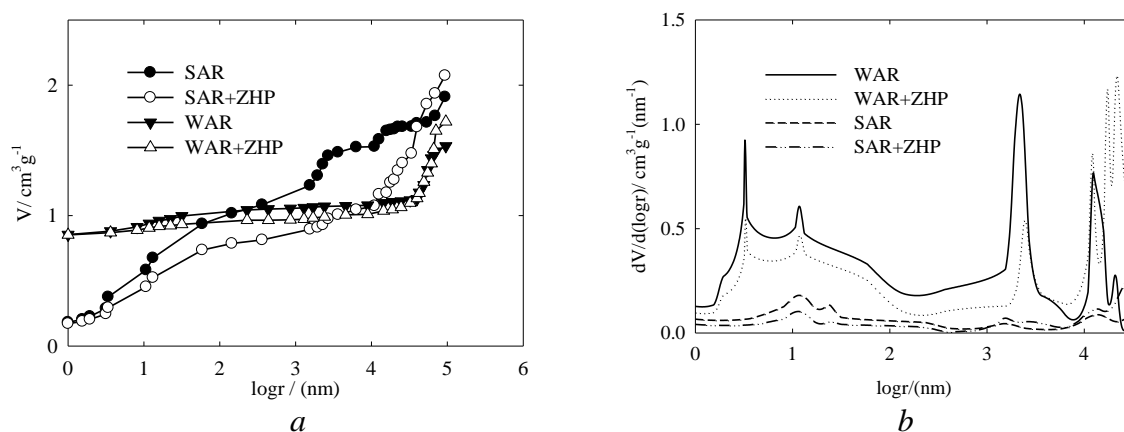


Figure 2. Integral (a) and differential (b) pore volume distributions

Chemical composition of the ion-exchangers as well as porous structure of polymer matrix affect sorption properties. The models of chemical reactions were applied to rate of adsorption of Malachite Green/ The model of pseudo-first order is described by the Lagergren equation [6]:

$$\ln(A_{\infty} - A) = \ln A_{\infty} - K_1 \tau. \quad (1)$$

The model of pseudo-second order is:

$$\frac{\tau}{A} = \frac{1}{K_2 A_{\infty}^2} + \frac{1}{A_{\infty}} \cdot \tau \quad (2)$$

where K_1 and K_2 are the rate constants, τ is the time, A and A_{∞} are the adsorption capacity at predetermined time and $\tau=0$. As follows from Table 1, kinetics is described by the model of pseudo-second order.

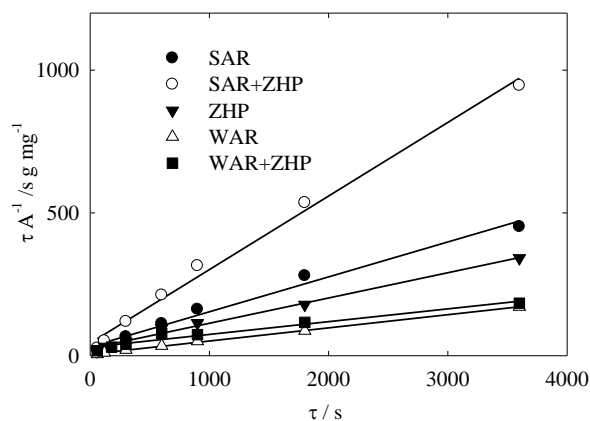


Figure 3. Application of the model of pseudo-second order to adsorption of Malachite Green

Table 1. Kinetics of cationic dye sorption under batch conditions and Ni^{2+} removal from water under dynamic conditions

Sample	$A_{\infty}(\text{exp}),$ mg g^{-1}	Sorption of Malachite Green					Ni^{2+} sorption	
		1-st order		2-nd order			Break-through capacity, mg cm^{-3}	$\text{C}_{\text{Ni}}, \text{mg dm}^{-3}$ In the effluent
		$A_{\infty}(\text{th}),$ mg g^{-1}	R^2	$A_{\infty}(\text{th}),$ mg g^{-1}	R^2	$K_2,$ $\text{g mol}^{-1}\text{s}^{-1}$		
SAR	7.96	4.24	0.90	8.33	0.98	4.59×10^{-4}	4.13	0.52
SAR+ZHP	3.81	1.61	0.98	3.88	0.99	1.52×10^{-3}	2.95	0.41
WAR	21.06	10.84	0.97	21.60	0.99	4.07×10^{-4}	4.17	1.31
WAR+ZHP	19.58	16.11	0.98	20.32	0.99	8.20×10^{-5}	4.05	1.11
ZHP	10.53	8.28	0.96	11.28	0.99	3.15×10^{-4}	0.59	7.88

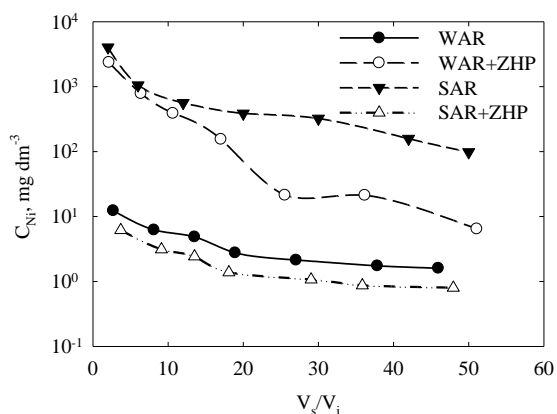


Figure 4. Desorption of Ni^{2+} ions under dynamic conditions using a 1 M H_2SO_4 solution

The K_2 values show that ZHP particles reinforce interaction with SAR and weaken with WAR. It means, each molecule of the dye interacts with two adsorption centers, probably they are located outside clusters and channels. Taking the change of volume of one or another pores into consideration, the adsorption centers can be placed in structure defects. Alternately, no significant change of break-through capacity was found for the WAR due to ZHP.

As follows from Fig. 4, ZHP particles facilitate desorption of Ni^{2+} ions.

Conclusions

Modification of ion-exchange resins with ZHP causes transformation of porous structure of the polymer. Single nanoparticles and their aggregates determine functional properties of the composites. They reinforce interaction of molecules of cationic dye with SAR and weaken with WAR. Adsorption centers are supposed to locate in structure defects. At the same time, the inorganic constituent decreases the break-through capacity of the SAR and increase it for the WAR. In all cases, ZHP facilitates desorption of Ni^{2+} ions.

References

1. Perlova N., Dzyazko Y., Perlova O., Palchik A., Sazonova V. Formation of Zirconium Hydrophosphate Nanoparticles and Their Effect on Sorption of Uranyl Cations // *Nanoscale Research Letters*. 2017. V. 12, P. 209.
2. Dzyazko Yu. S., Perlova O.V., Perlova N.A., Volfkovich Yu.M., Sosenkin V.E., Trachevskii V.V., Sazonova V.F., Palchik A.V. Composite cation-exchange resins containing zirconium hydrophosphate for purification of water from U(VI) cations // *Desalination and Water Treatment*. 2017. *in press*.
3. Dzyazko Yu.S., Ponomaryova L.N., Volfkovich Yu.M., Sosenkin V.E., Belyakov V.N. Polymer Ion-Exchangers Modified with Zirconium Hydrophosphate for Removal of Cd^{2+} Ions from Diluted Solutions // *Separ. Sci. Technol.* 2013. V. 48. P. 2140-2149.
4. Dzyazko Yu. S., Ponomaryova L. N., Volfkovich Yu. M., Trachevskii V.V., Palchik A. V. Ion-exchange resin modified with aggregated nanoparticles of zirconium hydrophosphate. Morphology and functional properties // *Micropor. Mesopor. Mater.* 2014. V. 198. P. 55-62.
5. Volfkovich Yu.M., Sosenkin V.E., Bagotzky V.S. Structural and wetting properties of fuel cell components // *J. Power Sources*. 2010. V. 195. P. 5429--5441.
6. Helfferich F. *Ion Exchange*. New York: Dover, 1995.

INVESTIGATION OF ANISOTROPIC PERFLUORINATED MEMBRANES MODIFIED BY POLYANILINE BY SPECTRAL METHODS

Darya Popova, Irina Falina, Natalia Loza, Marya Salashenko

Physical Chemistry Department, Kuban State University, Krasnodar, Russia

E-mail: irina_falina@mail.ru

Introduction

Nowadays intensive research in the field of developing a new materials for hydrogen energy is being carried out. Membranes modified with polyaniline (PANI) are prospective as carrier of a platinum catalyst in air-hydrogen fuel cell, because of their proton and electronic conductivity. For practical application, such membranes must preserve stable properties. Present work is devoted to investigation the stability of anisotropic composites on the base of MF-4SK and polyaniline by spectral methods.

Experiments

The objects of investigation were perfluorinated sulfocationic membrane MF-4SK and composites with polyaniline on its basis. Asymmetric composite membranes were prepared in a two-chamber cell by the one-sided diffusion of an oxidant solution through a membrane into water. Before synthesis, the samples were saturated with a monomer solution (protonated aniline).

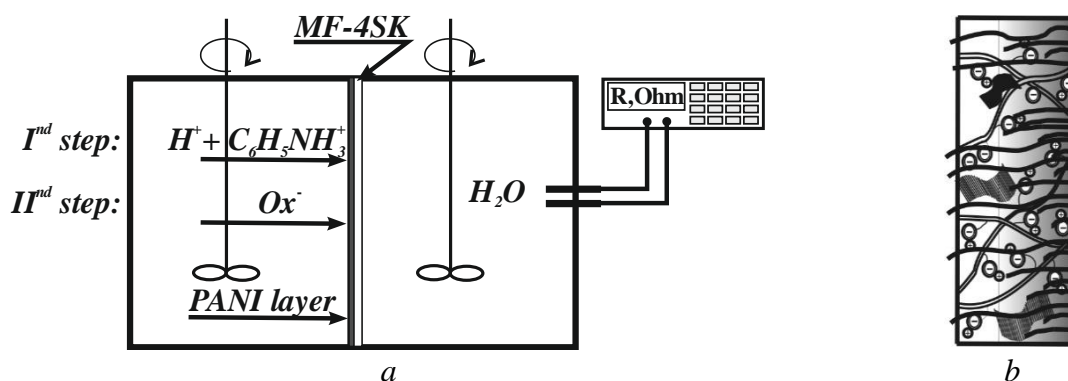


Figure 1. Scheme of the cell for modification MF-4SK membranes with polyaniline (a) and the anisotropic composite membrane MF-4SK/PANI (b)

As the oxidant, we used $S_2O_8^{2-}$ or Fe^{3+} which are co- and counter-ions to the membrane matrix respectively. The synthesis time varied from 0.5 to 2 h. UV-vis electronic spectra were measured by LEKI SS2109UV spectrometer with scan step 1 nm. The FTIR spectra of the surfaces of the initial and composite membranes were measured on a Bruker Vertex 70 FTIR spectrometer with an annex of broken total internal reflection on a diamond crystal.

Results and Discussion

To evaluate the stability of composites after contact with oxidizer, the study of UV-vis absorbance spectra was done. One can see from Fig. 2 that maxima at 400 and 800 nm corresponding to polaron- π^* and π -polaron transitions of polyaniline in the emeraldine-salt form present in electron spectra of composites [2]. Analysis of the peaks intensity allows to estimate the amount of the modifier in the structure of the ion-exchange membrane. According to figure 1a in the case of using Fe^{3+} as an oxidizer, the absorbance of the samples changes with time that is associated with an increase of PANI content inside the membrane. At the same time, using $S_2O_8^{2-}$ permits to obtain reproducible results, and there is no increase of peaks maxima during at least one month (Fig. 2b). This indicates the quantitative progress of the polymerization reaction and the possibility of stopping it upon termination the contact with the oxidant solution. At the same time, in the case of Fe^{3+} (counter-ion), the sorption of oxidant by a polymer matrix takes place, and the polymerization continues in the cluster area of the membrane even after stopping the contact with the oxidant solution.

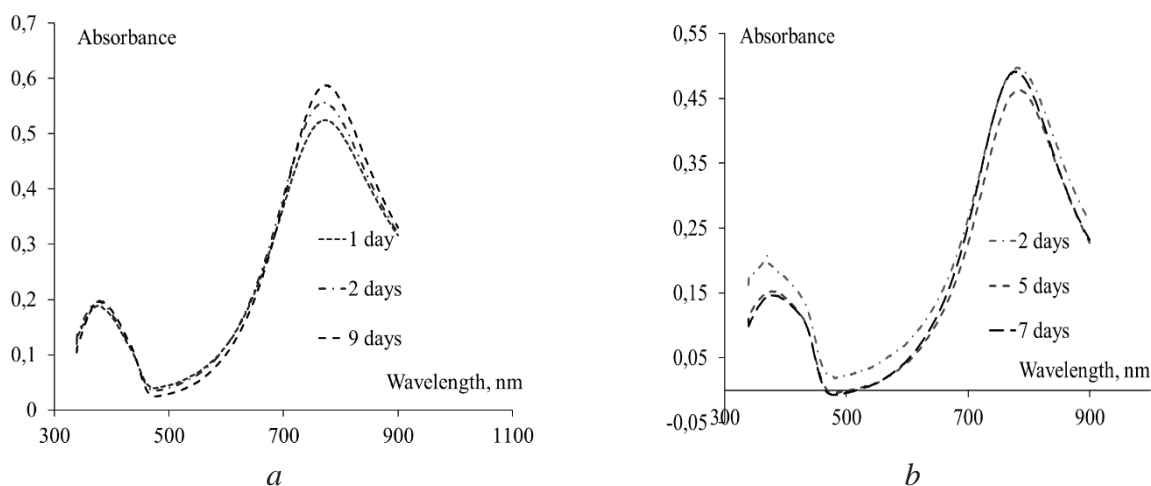


Figure 2. UV-vis spectra of composite membranes obtained with Fe^{3+} (a) and $S_2O_8^{2-}$ (b)

Analysis of the FTIR spectra of the surfaces of the initial and composite membranes (Fig. 3) showed that composite spectra contains peaks at 1500 cm^{-1} and 1581 cm^{-1} , corresponding to polyaniline in the emeraldine-salt form [3]. One can see that when we use $S_2O_8^{2-}$ as oxidizer, one surface contains polyaniline, and the other side is identical to the surface of the initial membrane even after 2 hour of contact with oxidizer (Fig.3b). It points out to the non-growth of the modifier through the membrane. In the case of using Fe^{3+} as an oxidizer, the membrane surfaces have identical spectra after 0.5 hours synthesis.

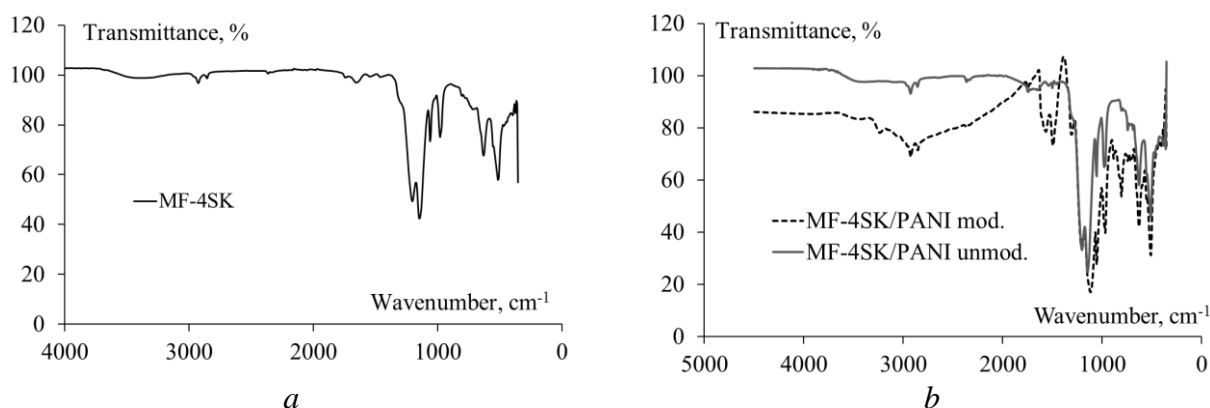


Figure 3. FTIR spectra of surfaces of initial MF-4SK (a) and composite MF-4SK/PANI (b) membranes

The formation of an asymmetric structure was confirmed by membrane voltammetry data in NaCl solution. For a membrane, prepared by using Fe^{3+} , the polarization curves measured for different orientation of the membrane towards the counterion flow are identical. For the membranes, obtained by using $S_2O_8^{2-}$ as an oxidant, a noticeable asymmetry of the current-voltage characteristic was observed. Thus, in order to obtain composites with stable anisotropic structure, it is preferable to use the co-ions as the oxidant of aniline template polymerization in cation exchange membrane.

Acknowledgements

The present work is supported by Russian Foundation for Basic Research and Krasnodar Region Administration (project No 16-48-230545r_a)

References

1. Sapurina I.Yu., Stejskal J. // Russian chemical reviews. – 2010. – V. 79. – P. 1–22.
2. Choi B.G., Park H.S., Im H.S., Kim Y.J., Hong W.H. // Journal of Membrane Science, 2008, V. 324, P. 102–110.
3. Loza N.V., Falina I.V., Popova D.S., Kononenko N.A. // Sorption and chromatographic processes 2016. V. 16, № 5. P. 663–671.

CONCENTRATION DEPENDENCE OF CONDUCTIVITY AND DIFFUSION PERMEABILITY OF ION EXCHANGE MEMBRANES EMBEDDED WITH MINERAL OR ORGANIC NANOPARTICLES. MODELLING AND EXPERIMENT

Mikhail Porozhnyy¹, Stefano Deabate², Patrice Huguet², Victor Nikonenko¹

¹ Membrane Institute, Kuban State University, Krasnodar, Russia, *E-mail: porozhnyj@mail.ru*

² University of Montpellier, Montpellier, France

Introduction

Immobilization of inorganic nanoparticles (like ZrO_2 , TiO_2 and SiO_2) allows essential improvement of proton-exchange membrane properties pertinent for fuel cell applications [1]. It has been shown that such kind of modification can improve water retention and, under certain conditions, leads to an increase of conductivity [2]. When inserted nanoparticles exhibit relatively high acidic properties, the membrane shows a decrease of diffusion permeability [3].

No less important for scientific interest is formation of organic colloid aggregates in membrane structure. Unlike the deliberate modification with inorganic particles, formation of these organic colloids on a surface and in membrane pores (known as fouling) occurs spontaneously when ion exchange membranes (particularly AEM) are used for electro dialysis (ED) treatment in food industry applications. Fouling leads to a number of undesirable effects: an increase in diffusion permeability, a decrease in selectivity and electrical conductivity of membranes, as well as a decrease in ion-exchange capacity [4].

Hence, the better understanding of the structure influence on membrane properties is of a great interest. On this purpose, we have developed a new mathematical model based on the well-established microheterogeneous model [5].

Results and discussion

The microheterogeneous model takes into account the microporous (gel phase) and meso/macroporous (intergel spaces solution) membrane structure. Since the intergel space solution conductivity is proportional to the external solution concentration, the presence of meso/macroporous domains defines the membrane conductivity dependence on the external solution concentration.

In the case of membranes modified with metal oxides and other oxides (ZrO_2 , TiO_2 , SiO_2), we assume nanoparticles to occupy some part of the meso/macropore volume and displace electroneutral solution from this domain. It could lead to several effects.

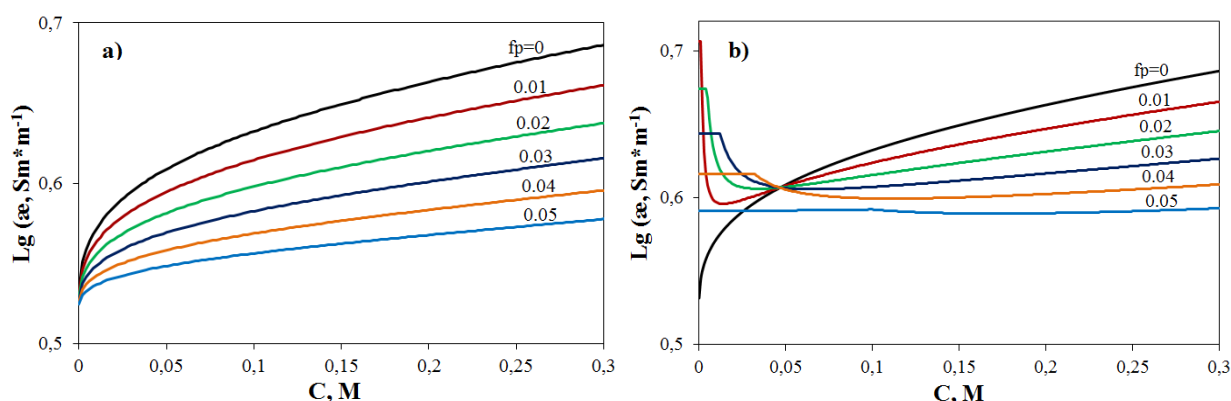


Figure 1. Concentration dependence of the conductivity for the membranes with different volume fractions (fp) of a) uncharged and b) charged nanoparticles.

For a membrane modified with uncharged nanoparticles, we observe a decrease in conductivity and diffusion permeability when the nanoparticle volume fraction increases over the whole range of concentrations (Figs. 1a and 2a). It is explained by the fact that the nonconductive nanoparticles replace the electrolyte in the pores and at the same time reduce the space available for electrolyte diffusion.

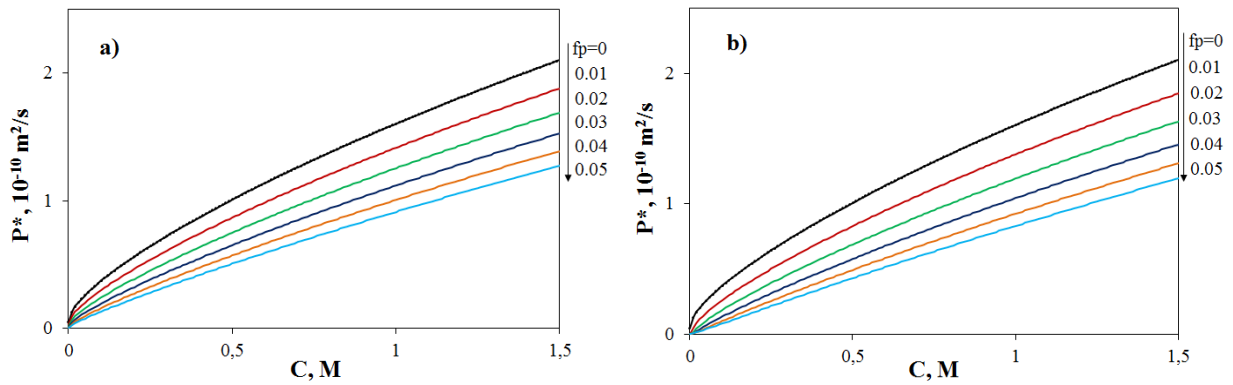


Figure 2. Concentration dependence of the diffusion permeability for the membranes with different volume fractions (f_p) of a) uncharged nanoparticles and b) charged nanoparticles.

For a membrane modified with charged nanoparticles, the behavior is different, especially in the range of low concentrations (Fig. 1b). In this concentration range, the thickness of an electric double layer (EDL) at the particle interface is high. This gives rise to elevated conductivity, as the ionic concentration in the EDL is much higher than in the pore bulk solution. With increasing concentration, the EDL thickness decreases and its impact on conductivity vanishes. On the other hand, the reduced concentration of co-ions in the EDL causes a decrease in the diffusion permeability in the whole range of concentrations (Fig. 2b).

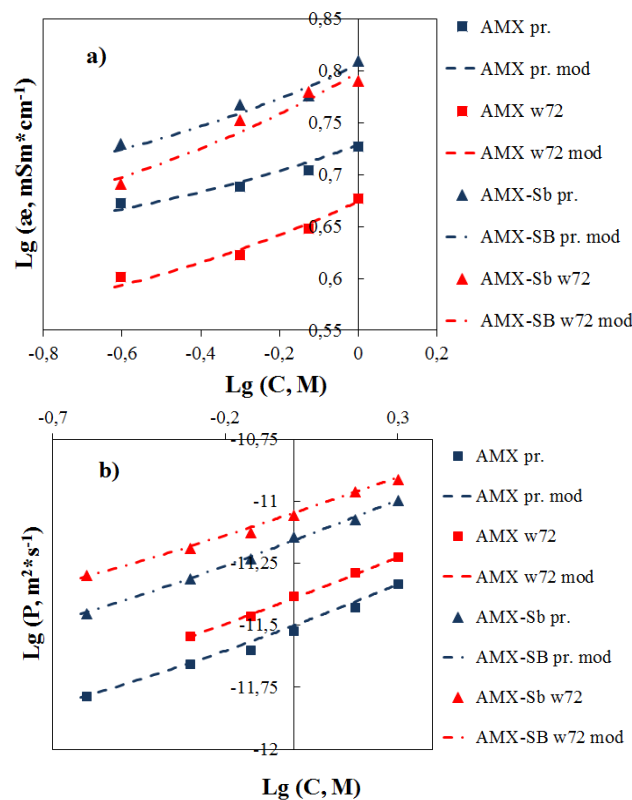


Figure 3. Concentration dependences of (a) electrical conductivity and (b) diffusion permeability of pristine anion exchange membranes (AMX and AMX-SB) and the samples of the same membranes after 72 hours of soaking in red wine. The dashed and dash-dot lines correspond to the results of calculations.

In the case of organic fouling, we assume that the formation of colloidal particles in the intergel solution causes a decrease of the ion mobility. Furthermore, these particles can deprotonate some part of fixed ions, thereby decreasing the membrane ion exchange capacity. High hydration degree of these particles leads to increasing the volume fraction of intergel spaces. Numerical simulation using the relevant parameters shows a good agreement with experimental results (Fig. 3).

Acknowledgements

This investigation was carried out within French-Russian laboratory "Ion-exchange membranes and related processes". The authors are grateful to RFBR, Russia (grants 15-58-16004NCNIL, 16-48-230919 reg_a) for financial support.

References

1. *Jalani N.H., Dunn K., Datta R.* Synthesis and characterization of Nafion®–MO₂ (M= Zr, Si, Ti) nanocomposite membranes for high temperature PEM fuel cells// *Electrochim. Acta.* 2005. V. 51. P. 553–560.
2. *Pereira F., Valle K., Belleville P., Morin A., Lambert S., Sanchez C.* Advanced mesostructured hybrid silica–Nafion® membranes for high-performance PEM fuel cell// *Chem. Mater.* 2008. V. 20. P. 1710–1718.
3. *Safronova E.Yu., Prikhno I.A., Yurkov G.Yu., Yaroslavtsev A.B.* Nanocomposite membrane materials based on nafion and cesium acid salt of phosphotungstic heteropolyacid// *Chem. Eng. Transactions.* 2015. V. 43. P. 679-684.
4. *Ghalloussi R., Garcia-Vasquez W., Bellakhal N., Larchet C., Dammak L., Huguet P., Grande D.* Ageing of ion-exchange membranes used in electro dialysis: investigation of static parameters, electrolyte permeability and tensile strength// *Sep. Purif. Technol.* 2011. V. 80. P. 270–275.
5. *Zabolotsky V., Nikonenko V.* Effect of a structural membrane inhomogeneity on transport properties // *J. Membr. Sci.* 1993. V. 79. P. 181-198.

MEMBRANE-BASED PROCESSES FOR DESALINATION & WATER TREATMENT AND SUSTAINABLE POWER GENERATION

¹Gérald Pourcelly, ²Victor Nikonenko

¹European Membrane Institute¹, University of Montpellier, France

E-mail: Gerald.pourcelly@umontpellier.fr

²Membrane Institute, Kuban State University, Krasnodar, Russia, *E-mail: v_nikonenko@mail.ru*

One of the most pervasive problems afflicting people throughout the world is inadequate access to clean water and sanitation. Problems with water are expected to grow worse in the coming decades, with water scarcity occurring globally, even in regions considered water rich. Addressing these problems calls out for a tremendous amount of research to be conducted to identify robust new methods of purifying water (sea and brackish water) at lower cost and less impact on the environment. Membrane processes appear as one of the most suitable solutions [1, 2]. Together, water and wastewater treatment are the most well-established end uses for membranes so that world demand for membranes is forecast to rise 8.5 percent annually to \$26.3 billion in 2019. Over the 20 last years, more than 17,000 scientific papers and 18,000 patents were generated in the domains covering MF, UF, NF, RO, ED, PV and Liquid Membranes. If UF, RO, NF are hotspots in SCI papers, RO, Liquid Membranes are hotspots in patents [3]. Literature clearly shows the necessity to promote the membrane technologies in water treatment through 3 axes: (i): Materials (membranes, spacers), (ii): Design (fluidics, operating conditions etc...) and (iii): Global approach (waste management, costs etc...).

This presentation aims to resume the last development of research focusing on the three sub-topics such as profiled membranes [4], membranes with integrated spacers [5], carbon nanomaterials (Carbon NanoTubes or Graphen Oxide) for advancing separation membranes [6, 7], the inputs of 3D printing technologies available for modules and stack components [8], the promising opportunities of microfluidic inputs for water desalination or purification of brines [9, 10] and as far as electroconvection is involved as a major mechanism of overlimiting transfer, the inputs of specific knowledge and practice acquired in nano- and microfluidics into desalination [11]. At last, several approaches to capture salinity gradients energy have been developed, among them pressure-retarded osmosis and reverse electrodialysis. The main challenges remain: developing low cost materials and achieving high power densities, which could be addressed by significantly improved membranes [12].

Acknowledgement

This investigation was realized in the frame of a joint French-Russian PHC Kolmogorov 2017 project of the French-Russian International Associated Laboratory "Ion-exchange membranes and related processes" with the financial support of Minobrnauki (Ref. N° RFMEFI58617X0053), Russia, and CNRS, France (project N° 38200SF).

References

1. Shannon M.A., Bohn P.W. *et al*, Science and technology for water purification in the coming decades // *Nature* 2008. V. 452. P. 301-310.
2. Elimelech M., Philip W.A. The future of seawater desalination: energy, technology and the environment // *Science* 2011. V. 333. P. 712-717.
3. Dai Y., Song Y *et al*, Bibliometric analysis of research progress in membrane water treatment technology from 1985 to 2013 // *Scientometrics* 2015. V.105. P. 577-591.
4. Strathmann H. ED, a mature technology with a multitude of new applications // *Desalination* 2010. V. 264. P. 268-288.
5. Balster J., Stamatialis D.F., Wessling M. Membrane, with integrated spacer // *J. Membr. Sci.* 2010. V. 360. P. 185-189.
6. Goh K., Karahan H.E. *et al*, Carbon nanomaterials for advancing separation membranes : a strategic perspective // *Carbon* 2016. V.109. P. 694-710.

7. *Baoxia M.*, Graphene oxide membranes for ionic and molecular sieving // *Science* 2014. V.343. P. 740-742.
8. *Lee J.Y., Tan W.S. et al*, The potential to enhance membrane module design with 3D printing technology // *J. Membr Sci* 2016. V.499. P. 4801-490.
9. *Kwak R., Han J. et al*, Enhanced salt removal by unipolar ion conduction in ion concentration polarization desalination // *Scientific Reports, Nature* 2016. V. 6. P. 25349.
10. *Kim B., Kwak R. et al*, Purification of high salinity brine by multi-stage ion concentration polarization desalination, // *Scientific Reports, Nature* 2016. V. 6. P. 31850.
11. *Nikonenko V.V., Kovalenko A.V., Urtenov M., Pismenskaya N.D., Han J., Sizat P., Pourcelly G.* Desalination at overlimiting currents: state-of-the-art and perspectives // *Desalination* 2014. V. 342. P. 85-106.
12. *Logan E.B., Elimelech M.*, Membrane-based processes for sustainable power generation using water // *Nature* 2012. V. 488. P. 313-319.

HYBRID MEMBRANES BASED ON NAFION POWDER AND DIFFERENT DOPANTS OBTAINED BY HOT PRESSING

¹Ivan Prikhno, ¹Ekaterina Safronova, ¹Andrey Yaroslavtsev

¹Kurnakov Institute of General and Inorganic Chemistry, Moscow, Russia

E-mail: *ivan_prikhno@mail.ru*

Introduction

It was proposed to solve such urgent problem as pollution of the environment with help of alternative energy sources, for example, fuel cells. A proton-conducting membrane is one of the key elements of this device, and Nafion type membranes are now most often used as such. To overcome their drawbacks, for example, unsatisfactory conductivity at low relative humidity, such approaches, as modification with different dopants, are used. As a rule, modification is accomplished either by synthesis of dopant in the pores of already prepared membrane or by casting of membrane from solution containing dopant particles. At the same time it seems interesting to use a method of obtaining of a hybrid membrane by hot pressing of polymer powder and dopant powder. Though this approach practically isn't described in literature. So the goal of this research was to obtain hybrid membranes based on Nafion powder and different dopants.

Experiments

Commercial Nafion membrane was treated by tetrabutylammonium (TBA) hydroxide solution in methanol, then dissolved in solvothermal conditions in methanol. The solution was evaporated, and the residue was ball-milled. The obtained powder was studied by XRD, according to which it is amorphous. IR spectrum proves the composition of the powder.

SiO₂, Cs_xH_{3-x}PW₁₂O₄₀ (CsHPWA) and carbon nanotubes (CNT) were used as dopants. Silica was obtained by standard sol-gel method from tetraethoxysilane by hydrolysis. CsHPWA was obtained by precipitation of a neutral salt from cesium carbonate solution by phosphotungstic acid with following treatment of the neutral salt with diluted nitric acid. Carbon nanotubes Taunit S12, purified by treatment with diluted nitric acid, were used. XRD and IR spectroscopy were used to prove composition of the dopants.

Membranes were obtained by hot pressing of Nafion powder in TBA-form with appropriate quantity of dopant at 145°C during 20 minutes. The obtained membranes were treated by 4M solution of sulfuric acid in isopropanol at 70°C for an hour and twice with deionized water at 80°C for an 1.5 hours for conditioning. The obtained samples were named as Nafion (unmodified sample), Nafion-SiO₂, Nafion-CsHPWA и Nafion-CNT (samples, modified by 1 wt. % of the corresponding dopant).

Results and Discussion

TEM microphotographs prove existence of dopants nanoparticles in the obtained samples. Water uptake of all samples is greater than 30%, which is significantly higher than for cast/extruded membranes, it is the highest for Nafion-CNT sample (36.9%). Figure 1 shows results of conductivity measurement of obtained samples. The conductivity of hot-pressed Nafion membrane is higher, than for commercial membranes, in contact with water, but lower at low relative humidity (RH). Nafion-CNT has the highest conductivity at both RH and in contact with water (0.070 S/cm at 30°C in contact with water and $1.5 \cdot 10^{-4}$ S/cm at RH=32% and 30°C).

Measurement of diffusion permeability of 0.1M HCl solution was made to study anion transport across the membranes. Results are shown in table 1. Diffusion permeability of Nafion hot-pressed membrane is quite comparable to commercial Nafion membrane. Nafion-CNT sample has the lowest rate of anion transport ($2.43 \cdot 10^{-7}$ cm²/s against $3.80 \cdot 10^{-7}$ cm²/s for the unmodified sample).

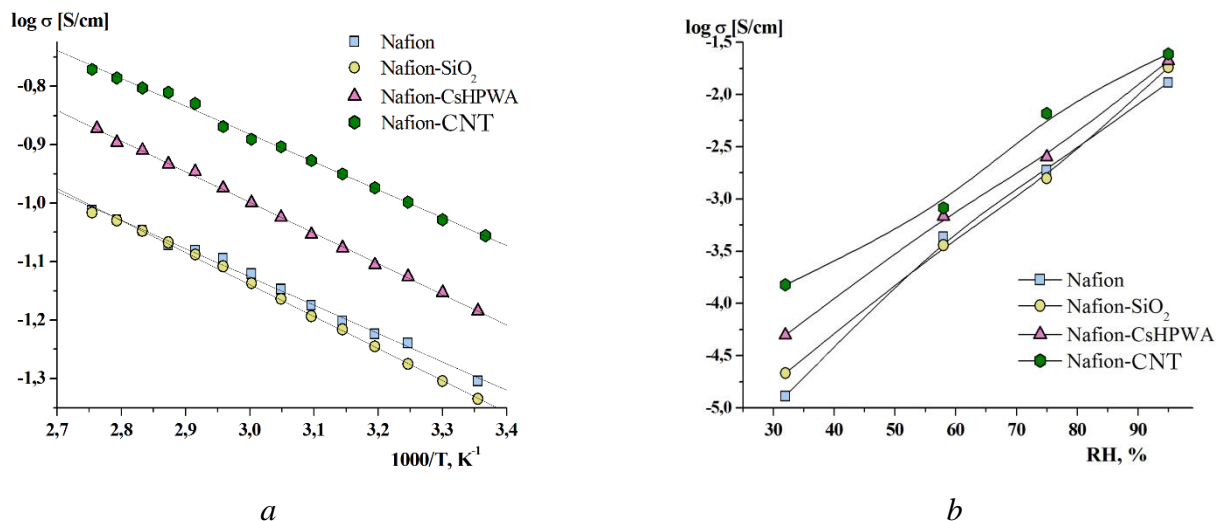


Figure 1. Proton conductivity of the membranes as function of temperature (a) and relative humidity at 30°C (b).

Table 1: Diffusion permeability of 0.1 M hydrochloric acid solution across the membranes

Sample	P·10 ⁷ , cm ² /s
Nafion	3.80
Nafion-SiO ₂	2.95
Nafion-CsHPWA	3.88
Nafion-CNT	2.43

So hybrid membranes, useful for fuel cells, were obtained by hot pressing. The sample, containing carbon nanotubes, is the most effective and the most promising.

Acknowledgements

This work was financially supported by Russian foundation for basic research (project 15-38-70005).

ON THE SCHROEDER PARADOX FOR ION-EXCHANGE AND NONIONIC POLYMERS

¹Vjacheslav Roldugin, ²Larisa Karpenko-Jereb, ¹Tat'yana Kharitonova

¹Frumkin Institute of Physical Chemistry and Electrochemistry of RAS, Moscow, Russia

E-mail: vroldugin@yandex.ru

²Institute of Electronic Sensor Systems, Graz University of Technology, Graz, Austria

E-mail: larisa.karpenko-jereb@tugraz.at

Introduction

An effect that was discovered about 100 years ago and is referred to as the “Schroeder paradox” remains to be discussed in the scientific literature [1]. Its essence consists in the following. A polymer swells in different manners in vapor and liquid phases, which are at equilibrium with one another. It is the difference in the swelling that is the Schroeder paradox, because the polymer swells due to solvent molecule sorption, while the chemical potentials of molecules in liquid and vapor phases are obviously equal. That is, solvent molecules having the same chemical potential cause different degrees of swelling depending on the polymer environment, which, seemingly, should not be. This effect plays a key role in membrane processes, because polymer membranes may simultaneously be in contact with vapor and liquid phases. Therefore, repeated attempts were made to explain the paradox theoretically. For this purpose, diverse (sometimes, exotic) models have been proposed (a long list of works devoted to the Schroeder paradox may be found in [2, 3]). It should only be noted that the Schroeder effect is of a general character; i.e., it is observed in diverse systems. Therefore, its explanation must, in our opinion, be based on fundamental laws. Below, we propose a simple explanation of the Schroeder paradox for ion-exchange and nonionic polymers, with this explanation being based on fundamental principles. In fact, our explanation does not involve any model considerations. We shall just draw attention to the obvious difference between the states of an ion-exchange and nonionic polymer occurring in contact with vapor and liquid phases and show that, in the case of the liquid phase, additional forces arise to stretch the polymer. The estimated value of these additional forces shows that they are sufficient to explain the “Schroeder paradox.”

Formal Explanation

Now, we shall show that the states of an ion-exchange polymer in vaporous and liquid water are different. Indeed, the vapor phase consists of just water molecules (if we ignore an inert gas medium). The liquid phase does not represent just water molecules; it contains H⁺ and OH⁻ ions (if we consider a primitive model). If an ion-exchange polymer occurs in (to be more specific) a sodium form, Na⁺ ions cannot pass to the vapor phase, while they freely pass to liquid water. This leads to the appearance of the Donnan potential, which cannot exist for a polymer in a vapor phase. Quantum-chemical calculations have shown that ionogenic groups of a membrane dissociate after water molecules are sorbed [4]. That is, “free” ions are also present in a polymer swollen in water vapor. However, the ions are not evaporated into the vapor at normal temperature (image forces prevent the ions from leaving the polymer or electrolyte). Therefore, the Donnan potential cannot be introduced for a polymer in water vapor. Thus, even with a cursory glance at polymer/vapor and polymer/water systems, we can see that the states of the polymer in them must be different. It is quite obvious that the aforementioned equilibrium conditions are not identical. Thus, there is no reason to require the same degree of swelling for polymers occurring in different states, in particular, with respect to the concentrations of H⁺, OH⁻, and Na⁺ ions and, hence, the concentration of water molecules. That is, the difference in polymer swelling is due to the non identity in the conditions of the thermodynamic equilibrium in the two cases under consideration. Moreover, in the case of ion-exchange polymers occurring in liquid water, there is one more mechanism for their increased swelling, this mechanism being incapable of manifesting itself in water vapor.

Excess Ion-Exchange Polymer Swelling in Liquid Water

We consider the standard mechanism for the appearance of Donnan potential φ_D . The Donnan potential results from the passage (or exchange) of ions from a polymer to a liquid water phase (aqueous electrolyte solution). It is generated by immobile charges that are located in a thin surface layer and screened by mobile ions present in an electrolyte. It is known that the charges distributed over the surface of a conductor (an ion-exchange polymer may be considered to be a conductor) do not create a field in its internal part. In this case, the distribution of a field at the polymer surface may be represented as follows. In a polymer, the field exists only in the region of a thin charged layer, while it does not exist in the internal region. In an electrolyte solution, the field is generated by all charges of the surface layer and reaches the thickness of the Debye layer, beyond which it is screened by counterions. An important difference between vapor and liquid phases surrounding the polymer consists in the following: in the case of liquid water, the charge on a polymer surface is screened by ions of an external electrolyte, while, in a vapor phase, all charges are screened by ions located in the polymer. In other words, in the case of a liquid phase, the polymer is charged (in a thin surface layer), while, in the case of water vapor, it is not. It should be emphasized that, in liquid water, a polymer must be charged to provide the equality of the electrochemical potentials of ions located in water and the polymer. This equality is provided by the charges rigidly bonded to the polymer (the mobile ions are involved in the formation of an electrical double layer).

Now, let us discuss what transpires with charged surface groups of a polymer. These groups are repulsed from each other by electrostatic (Coulomb) forces. This repulsion stretches the polymer. These tensile stresses are equal to

$$\Pi_{Mmn} = \frac{1}{2} q_s E, \quad (1)$$

where Π_{Mmn} is the stress tensor component normal to the polymer surface (the Maxwell stresses), q_s is the surface charge density, and E is the electric field strength at the polymer surface.

Then, the physical meaning of these stresses becomes quite obvious. Parameter $q_s E$ is the force applied from the side of an electric field to the surface charges. Since the field is generated by the same charges, a factor of 1/2 arises, which excludes the action of each charge on itself. Note that these stresses lead to other well-known effects: a reduction in the surface tension of charged droplets and breakage of strongly charged solids.

The Π_{Mmn} value of a typical ion-exchange polymer is determined as follows. For a polymer charged to potential φ_D , the electric field strength at its surface on the side of a 1:1 electrolyte is equal to

$$E = \left| \frac{d\varphi}{dx} \right| = \frac{1}{r_D} \frac{2kT}{e} \sinh\left(\frac{e\varphi_D}{2kT}\right) \quad (2)$$

where k is the Boltzmann constant, T is the temperature, and e is the proton charge. For the Donnan potential, we take a moderate value $\varphi_D = 100$ mV; then, $E \approx 330$ mV/ r_D . Assuming that $r_D = 3$ nm (a centimolar electrolyte solution), we obtain $\Pi_{Mmn} \approx 4 \times 10^6$ Pa. Note that the normal component of the pressure tensor (this component governing the action from the side of the electrolyte on the charged surface) coincides with the hydrostatic pressure in the electrolyte far from the surface. Therefore, the total “excess” effect is determined by the aforementioned value of Π_{Mmn} . It should be noted once more that this is the additional tensile stress applied to the polymer in the liquid water phase.

Using the elasticity modulus of Nafion membranes equal to nearly 50 MPa [5] at 95% humidity (i.e., a strongly overestimated value), we obtain that the linear degree of swelling (a change in the radius) related to the action of the electrostatic forces is 4–8% and, accordingly, the change in the

polymer sample volume is 12–30%. As the humidity increases, the elasticity modulus of the polymer decreases, and its swelling, accordingly, increases.

Excess Nonionic Polymer Swelling in Liquid Solvent

In the case of nonionic polymers, we take into account the force acting at the interface of two dielectric media and associated with the fluctuating electromagnetic field

$$f = \frac{kT}{4\pi\hbar c^2} \sum_l' (\nabla \varepsilon(\mathbf{r}, i\zeta_l)) D_{mm}^E(\mathbf{r}, \mathbf{r}, i\zeta_n), \quad (3)$$

where \hbar is the Plank constant, c is the speed of light, “frequencies” $\zeta_l = 2\pi lkT/\hbar$, the prime for the sum means that the term with $l = 0$ is taken with a weight of 1/2, the repeated index m denotes summation over indices, $D_{mm}^E(\mathbf{r}, \mathbf{r}, i\zeta_n)$ is the Green function of fluctuating electromagnetic field, \mathbf{r} is the space coordinate vector.

The force f provide the following excess stress for polymer in liquid solvent

$$\Pi_{mm} \approx c_{ss} \frac{\hbar}{\pi} \int_0^\infty (\varepsilon_s(i\zeta) - 1) \frac{\zeta^2}{c^2 a} \exp\left(-\frac{\zeta}{c} \sqrt{\varepsilon_s(i\zeta)} a\right) d\zeta, \quad (18)$$

where $\varepsilon_s(i\zeta)$ is dielectric permittivity of solvent, a is a cutoff parameter, c_{ss} is the constant of the order of unity.

Using the known frequency dependencies of $\varepsilon_s(i\zeta)$ we obtain for $a = 1$ nm that $\Pi_{mm} \approx 10^6$ Pa. The stresses of this magnitude are sufficient to ensure the excess polymer swelling observed in the experiments.

Conclusion

It has been shown that ion-exchange and nonionic polymers must have different swell abilities in liquid solvent and its vapor. The specific physicochemical analysis has shown the unavoidability of such behavior of a polymer in these two phases; i.e., the Schroeder paradox comprises no paradoxicality. The increased swelling of ion-exchange polymers in liquid water is due to the Maxwell stresses acting on their charged surfaces, with these stresses being absent in the case of water vapor. The estimation of the stresses for the polymer Nafion in water yields values of “excess” swelling comparable with those observed in real experiments. The increased swelling of nonionic polymers is due to molecular forces, which stretch a polymer in liquid solvent and compress it in a vapor phase.

The work supported by Russian Foundation for Basic Researches, grant № 17-08-00315_a.

References

1. *Shroeder P.* Über Erstarrungs- und Quellungserscheinungen von Gelatine // *Z. Phys. Chem.* 1903. V. 45. P. 75-117.
2. *Eikerling M.H., Berg P.* Poro-electroelastic theory of water sorption and swelling in polymer electrolyte membranes // *Soft Matter.* 2011. V. 7. P. 5976-5990.
3. *Davankov V.A., Pastukhov A.V.* Swelling of crosslinked polymers in liquids and vapors. Rational explanation of thermodynamic paradoxes // *Z. Phys. Chem.* 2014. V. 228. P. 691-710.
4. *Karpenko-Jereb L.V., Kelterer A.-M., Berezina N.P., Pimenov, A.V.* Conductometric and computational study of cationic polymer membranes in H^+ and Na^+ -forms at various hydration levels // *J. Membr. Sci.* 2013. V. 444. P. 127-138.
5. *Safronova E., Golubenko D., Pourcelly G., Yaroslavl'tsev A.* Mechanical properties and influence of straining on ion conductivity of perfluorosulfonic acid Nafion®-type membranes depending on water uptake // *J. Membr. Sci.* 2015. V. 473. P. 218-225.

GENERALIZED DUSTY-GAS MODEL FOR GAS MIXTURE FLOW THROUGH NANOPOROUS BODIES

¹Vjacheslav Roldugin, ²Vladimir Zhdanov, ¹Andrey Shabatin

¹Frumkin Institute of Physical Chemistry and Electrochemistry of RAS, Moscow, Russia

E-mail: roldugin@phyche.ac.ru

²National Research Nuclear University "MEPhI", Moscow, Russia, *E-mail:* VMZhdanov@mail.ru

Introduction

In [1], the generalization of the dusty-gas model [2] has made it possible to take into account the effect of surface forces on a simple gas flow in porous media. As has been shown in [3, 4], the surface forces must be taken into account when considering transport in nanosized channels. The dusty-gas model [2] is known to be used when considering the transport of both one- and multicomponent gases and liquids in porous bodies. Initially, this model was proposed for describing the flow and diffusion of a gas mixture in a porous body within the framework of a unified approach in the entire range of Knudsen numbers from the free-molecular to the viscous (hydrodynamic) flow regimes. The success of the model in describing gas fluxes seems to be due to the fact that it is based on the rigorous relations of the kinetic theory and rather simple physical assumptions. Later [2], it turned out that the same equations may be employed to describe liquid fluxes. The wide field of application of the equations of the dusty-gas model has been predetermined by their simplicity and the absence of a necessity to use cumbersome calculations for solving specific problems.

The creators of the model [2] noted that it needed to be improved, especially when the transfer of molecules in adsorbed layers must be taken into account. Such a situation arises when a gas flow in nanoporous systems is considered. However, the model was not previously generalized for this case. Some progress in the direction of allowance for the contribution of surface forces within the framework of the dusty-gas model was made in our previous work [1]. It was shown that the effect of the surface forces on a gas flow in a porous medium becomes especially pronounced for a gas that is nonuniform with respect to temperature. A simple gas flow was studied in [1]. In this work, we shall consider a gas mixture flow. We shall derive an analog of the Stefan–Maxwell equation, this analog taking into account the contribution of the surface forces and, then, obtain generalized equations of the dusty-gas model for a gas mixture using the traditional scheme [2].

Basic equations

We shall try to derive modified transport equations by a partial modification of the Boltzmann kinetic equation. Instead of the classical Boltzmann equation in which the intermolecular interaction is taken into account only in the collision integral, we shall consider the generalized kinetic relation [1], in which the long-range component of the interaction potential between gas molecules and dust particles (an analog of surface forces) is isolated as a separate term. Therewith, collisions with dust particles are considered to be collisions with solid spheres. Thus, the equation for the $f_\alpha(\mathbf{v}_\alpha)$ function of component α distribution over velocities \mathbf{v}_α has the following form [1]:

$$\frac{\partial f_\alpha}{\partial t} + \mathbf{v}_\alpha \cdot \frac{\partial f_\alpha}{\partial \mathbf{r}} + \frac{(\mathbf{F}_{\alpha e} + \mathbf{F}_{\alpha s})}{m_\alpha} \cdot \frac{\partial f_\alpha}{\partial \mathbf{v}_\alpha} = \sum_\beta I_{\alpha\beta}(f_\alpha, f_\beta), \quad (1)$$

where \mathbf{r} is the vector of spatial coordinates, m_α is the mass of α -type molecules, $\mathbf{F}_{\alpha e}$ is the external force applied to them, $\mathbf{F}_{\alpha s}$ is the surface force applied to the α -type molecules from the side of the dust particles, and $I_{\alpha\beta}(f_\alpha, f_\beta)$ is the Boltzmann collision integral.

Let us introduce long-range dust particle–gas molecule interaction potential $U_\alpha(\mathbf{r} - \mathbf{r}_{dk})$ where \mathbf{r}_{dk} characterizes the position of a k th particle of a dusty gas. Then,

$$\mathbf{F}_{\alpha s} = -\frac{\partial}{\partial \mathbf{r}} \sum_k U_\alpha(\mathbf{r} - \mathbf{r}_{dk}), \quad (2)$$

where summation is carried out over all dust particles.

Due to the mesoscopic size of dust particles, the long-range interactions and gas–particle collisions may be physically separated in a distinct manner. After the introduction of the self-consistent long-range interaction into the kinetic equation, the equations actually retain the form of those obtained by the Grad method; an additional term is just added to the external forces. Therefore, we may, at once, write the final variant of diffusion equations used in the dusty gas model [1] assuming that all gas parameters vary along one coordinate z , as commonly takes place in membrane transport,

$$\begin{aligned} \sum_{\alpha=1}^N \frac{n_{\alpha}}{n D_{\alpha\beta}} \left(\frac{J_{\alpha z}}{n_{\alpha}} - \frac{J_{\beta z}}{n_{\beta}} \right) + \frac{1}{D_{\alpha K}} \left[\frac{J_{\alpha z}}{n_{\alpha}} + \frac{B_0}{\eta} (\nabla p - \sum_{\beta=1}^N n_{\beta} F_{\beta z}) \right] = \\ = -\nabla \ln c_{\alpha} - \nabla \ln p + \frac{F_{\alpha z}}{kT} - \frac{1}{n'} \left[\sum_{\beta=1}^N n_{\beta} \alpha'_{T\alpha\beta} + n_d \alpha'_{T\alpha d} \right] \nabla \ln T, \end{aligned} \quad (3)$$

where \mathbf{J}_{α} is the flux density of component α , c_{α} is its molar fraction, $\mathbf{F}_{\alpha} = \mathbf{F}_{\alpha e} + \mathbf{F}_{\alpha s}$ is the total force applied to the molecules of component α , $p_{\alpha} = n_{\alpha} kT$ is the partial pressure, $n = \sum_{\alpha} n_{\alpha}$, $p = \sum_{\alpha} p_{\alpha}$, $n' = n + n_d$, n_d is the concentration of dust particles, ∇ is the gradient in the direction of the z axis, N is the number of mixture components, and $D_{\alpha\beta}$ is the effective interdiffusion coefficient of the components in a porous medium. Parameter $D_{\alpha\beta} = (\varepsilon/q)[D_{\alpha\beta}]_1/(1-\Delta_{\alpha\beta})$, $[D_{\alpha\beta}]_1$ is the coefficient of the binary diffusion of components α and β , this coefficient being calculated in the first approximation of the Chapman–Enskog theory; $\Delta_{\alpha\beta}$ is the correction to this coefficient; ε is the medium porosity; q is the tortuosity; and $D_{\alpha K}$ is the Knudsen diffusion coefficient. Value $\alpha_{T\alpha\beta} = -\alpha_{T\beta\alpha}$ is the generalized thermodiffusion relation, which determines the relative motion of components α and β in the field of a temperature gradient; subscript d relates all values to the dust component; η is the gas viscosity; and B_0 is the hydrodynamic permeability of the porous medium (Darcy constant). The prime symbol at some values indicates that they must be calculated for a multicomponent mixture, in which a dusty-gas represents one of the components. Parameters $\Delta'_{\alpha d}$, $\alpha'_{T\alpha\beta}$, and $\alpha'_{T\alpha d}$ have been considered in detail in [2]; therefore, we shall not discuss them here, but rather consider allowance for the gas–dust particles interaction forces alone.

Some examples

We assume that the molecules interact with the pore surface through a potential

$$U_{\alpha s}(r_s)/kT = -\frac{a_{\alpha s}}{4[(R_c - r_s)^2 + \Delta_s]^{3/2}} \frac{T_0}{T}, \quad (4)$$

where T_0 is room temperature, the distance is measured in nanometers, the coefficients have been selected in a manner such that parameter $a_{\alpha s}$ is equal to unity for an argon/glass system, and Δ_s is a parameter that ensures the finiteness of the potential at $r_s = R_c$.

Figure 1 presents the dependence of ratio between the viscous fluxes on the capillary radius for an equimolar mixture, the potentials of the interaction of molecules of which with the walls differ by a factor of 2 ($a_{1s} = 1$ and $a_{2s} = 0.5$). The figure shows that, for 10-nm capillaries, the reverse-osmotic separation of a gas mixture becomes efficient even due to the purely hydrodynamic factor. For capillaries with a radius of 5 nm, the flow of a component that more weakly interacts with a wall is already reduced by 20%.

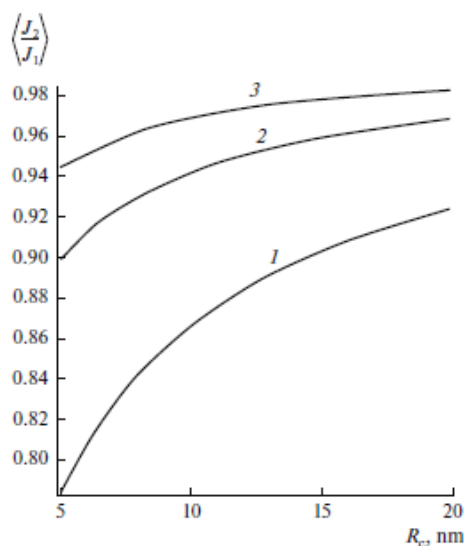


Figure 1. Flux ratios as functions of capillary radius at $\Delta_s = (1) 0.3$, (2) 0.5, and (3) 0.8.

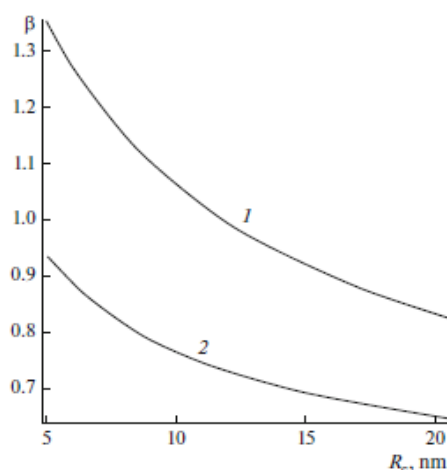


Figure 2. Thermomolecular pressure differences as functions of capillary radius for helium/argon mixture at (1) $\Delta_{sAr} = 0.3$, $\Delta_{sHe} = 0.159$ and (2) $\Delta_{sAr} = \Delta_{sHe} = 0.3$.

Figure 2 illustrates the dependence on pore size of the coefficient β , which characterizes the value of the thermomolecular pressure difference, via the following relation:

$$\frac{d \ln p}{d \ln T} = \beta \Rightarrow \frac{p_2}{p_1} = \left(\frac{T_2}{T_1} \right)^\beta \quad (5)$$

It can be seen that, as the capillary radius decreases, the role of the surface forces increases, with the character of the interaction between the components and the wall playing a substantial role. As we have already mentioned in [1], deviations of coefficient β from 0.5 were also observed in a numerical experiment for a simple gas.

Conclusion

The dusty gas model has been generalized to the flow of a gas mixture in a porous body under the conditions of the influence of the surface forces on the transfer of mixture components. It has been shown that the action of the surface forces accompanying the interaction of molecules with walls substantially changes the regularities of transport processes. The surface forces may either enhance or weaken (noticeably) the efficiency of the separation of mixture components depending on the character of the interaction between their molecules and the walls. They affect the value of the coefficient that determines the thermomolecular pressure difference, because its value noticeably deviates from the classical one in the range of the free-molecular flow.

The work supported by Russian Foundation for Basic Researches.

References

1. Roldughin V.I., Zhdanov V.M. Dusty-gas model. Allowance for surface forces // Colloid J. 2016. V. 78. P. 363-370.
2. Mason E.A., Malinauskas A.P. Gas transport in porous media: the dusty-gas model. Elsevier, Amsterdam – New York, 1983.
3. Roldughin V.I., Zhdanov V.M. Effect of surface forces on the gas flow in nanosized capillaries // Colloid J. 2003. V. 65. P. 598-601.
4. Roldughin V.I., Zhdanov V.M. Kinetic phenomena in the gas mixture flow through nanodimensional capillaries: the effect of surface forces // Technical Physics. 2006. V. 51. P. 436-443.

NON-EQUILIBRIUM THERMODYNAMICS OF HEAT AND MASS TRANSFER THROUGH THE MEMBRANE SURFACE FOR TWO-COMPONENT MIXTURE

¹Vjacheslav Roldugin, ²Vladimir Zhdanov, ¹Andrey Shabatin

¹Frumkin Institute of Physical Chemistry and Electrochemistry of RAS, Moscow, Russia

E-mail: roldugin@phycbe.ac.ru

²National Research Nuclear University "MEPhI", Moscow, Russia, *E-mail:* VMZhdanov@mail.ru

Introduction

In this work, we consider the non-equilibrium thermodynamics of transport processes for gas/fluid mixture at gas/fluid/membrane interface, using the kinetic theory to formulate phenomenological equations. As it shown earlier in [1], the Fokker–Planck kinetic equation well applied for such calculations. This equation has a broad spectrum of possible applications, which, however, makes the values of the kinetic coefficients less specific. The fact, that the calculation of the kinetic coefficients for liquids is still unsolved problem can be pointed out to explain this simplification.

Combination of non-equilibrium thermodynamics and kinetic Fokker–Planck equation have a certain advantage. It gives good results and allows in some cases to include in the consideration some non-linear effects staying within the framework of the linear approximation of non-equilibrium thermodynamics [2]. This is implemented when a chemical reaction can be considered as the diffusion along the reaction coordinate over the energy potential barrier. The transfer through the surface layer of the membrane may also be treated as a chemical reaction of a mass or energy transfer from fluid bulk into the subsurface layer of the membrane, wherein the reaction coordinate is normal to the surface spatial coordinate. The presence of the energy of the potential barrier at the surface of the membrane is a rather common situation.

Basic relations

Thus, we consider the classical Fokker–Planck equation for two-component mixture

$$\begin{aligned} \frac{\partial f_i(\mathbf{v}_i, \mathbf{r}_i, t)}{\partial t} + \mathbf{v}_i \cdot \frac{\partial f_i(\mathbf{v}_i, \mathbf{r}_i, t)}{\partial \mathbf{r}_i} + \frac{\mathbf{F}_i}{m_i} \cdot \frac{\partial f_i(\mathbf{v}_i, \mathbf{r}_i, t)}{\partial \mathbf{v}_i} = \\ \frac{\xi_{fi}}{m_i} \frac{\partial}{\partial \mathbf{v}_i} \cdot \left(\mathbf{v}_i + \frac{kT}{m_i} \frac{\partial}{\partial \mathbf{v}_i} \right) f_i(\mathbf{v}_i, \mathbf{r}_i, t) + \left(\frac{\partial f_i(\mathbf{v}_i, \mathbf{r}_i, t)}{\partial t} \right)_{\text{coll}}, \\ \left(\frac{\partial f_i(\mathbf{v}_i, \mathbf{r}_i, t)}{\partial t} \right)_{\text{coll}} = J_1(f) + J_2(f), \\ J_1(f) = \mathbf{v}_1 \frac{\partial}{\partial \xi_r} \left\{ RT \frac{\partial f}{\partial \xi_r} + (\xi_r - u_r) f \right\}, \\ J_2(f) = \mathbf{v}_2 \frac{\partial}{\partial \xi_r} \left\{ RT \frac{\partial f}{\partial \xi_r} + (\xi_r - \bar{u}_r) f \right\}, \end{aligned} \quad (1)$$

where $f_i(\mathbf{v}_i, \mathbf{r}_i, t)$ is the distribution function of fluid molecules over velocity \mathbf{v}_i , \mathbf{r}_i is spatial coordinate vector, t is time, \mathbf{F}_i is the force acting on the molecules, T is the absolute temperature, k is the Boltzmann constant, m_i is the molecule mass, ξ_{fi} is the generalized friction coefficients related to self-diffusion coefficients D_i :

$$D_i = \frac{kT}{\xi_{fi}}. \quad (2)$$

We can obtain the following expression for local entropy production for stationary state

$$\Delta S_{\text{st}} = k \sum_i \int \varphi_i(\mathbf{v}_i, \mathbf{r}_i, t) \left[\mathbf{v}_i \cdot \frac{\partial f_i(\mathbf{v}_i, \mathbf{r}_i, t)}{\partial \mathbf{r}_i} + \frac{\mathbf{F}_i}{m_i} \cdot \frac{\partial f_i(\mathbf{v}_i, \mathbf{r}_i, t)}{\partial \mathbf{v}_i} \right] d\mathbf{v}_i. \quad (3)$$

Then we write the non-equilibrium distribution function $f_i(\mathbf{v}_i, \mathbf{r}_i, t)$ in the form

$$f_i(\mathbf{v}_i, \mathbf{r}_i) = \exp\left(-\frac{m_i \mathbf{v}_i^2}{2kT} + \frac{\mu_{iT}}{kT}\right), \quad (4)$$

where μ_{iT} is the thermodynamic part of the chemical potential for each component of mixture, and here we assume that this is the non-equilibrium chemical potential and it does not depend on the velocity of the molecules. So the entropy production (3) is converted to the expected [2] form

$$\Delta S_{st} = -\mathbf{J}_q \cdot \frac{\nabla T}{T^2} + \sum_i \mathbf{J}_{ni} \cdot \frac{(\nabla \mu_{iT})_T}{T} - \sum_i \frac{\mathbf{F}_i \cdot \mathbf{J}_{ni}}{T}, \quad (5)$$

where $\mathbf{J}_{ni} = \int \mathbf{v}_i \varphi_i(\mathbf{v}_i, \mathbf{r}_i, t) f(\mathbf{v}_i, \mathbf{r}_i) d\mathbf{v}_i$ is the number flux density of particles,

$\mathbf{J}_q = \sum_i \int \mathbf{v}_i \left(\frac{m_i \mathbf{v}_i^2}{2} - h_i\right) \varphi_i(\mathbf{v}_i, \mathbf{r}_i, t) f_i(\mathbf{v}_i, \mathbf{r}_i) d\mathbf{v}_i = \mathbf{J}_e - \sum_i h_i \mathbf{J}_{ni}$, where \mathbf{J}_e is the energy flux

density, \mathbf{J}_q is the heat flux density h_i is the partial enthalpy, symbol $()_T$ means that the derivative of chemical potential is taken at constant temperature.

Separating the motion of the mixture as a whole and introducing the renormalized chemical potentials $\mu_i = \mu_{iT} + U_i$, where U_i are the potentials of the external forces, we can obtain

$$\Delta S_{st} = \frac{\mathbf{u}_v \nabla p}{T} + \mathbf{J}_q \cdot \frac{\nabla T}{T^2} + \frac{n_1 n_2}{n} (\mathbf{u}_1 - \mathbf{u}_2) \cdot \frac{\nabla(\mu_1 - \mu_2)_T}{T}. \quad (6)$$

Here $\mathbf{u}_v = \frac{1}{n} \sum_i \mathbf{J}_{ni}$ is the molar-averaged velocity of the mixture, $\mathbf{u}_i = \mathbf{J}_i / n_i$, n_i is the number concentration of particles of kind i , $n = n_1 + n_2$.

Phenomenological equations

Basing on entropy production (6), we can write down the phenomenological equations of non-equilibrium thermodynamics

$$\begin{aligned} \mathbf{u}_v &= \Lambda_{00} \nabla p + \Lambda_{01} \frac{\nabla T}{T} + \Lambda_{02} \nabla(\mu_1 - \mu_2)_T, \\ \mathbf{J}_q &= \Lambda_{10} \nabla p + \Lambda_{11} \frac{\nabla T}{T} + \Lambda_{12} \nabla(\mu_1 - \mu_2)_T, \\ \frac{n_1 n_2}{n} (\mathbf{u}_1 - \mathbf{u}_2) &= \Lambda_{20} \nabla p + \Lambda_{21} \frac{\nabla T}{T} + \Lambda_{22} \nabla(\mu_1 - \mu_2)_T. \end{aligned} \quad (7)$$

We can draw certain conclusions about the kinetic coefficients, which satisfy the Onsager symmetry relations $\Lambda_{lm} = \Lambda_{ml}$. Λ_{00} coefficient characterizes the hydrodynamic permeability of the surfaces layer, Λ_{01} is related to thermo-osmosis and Λ_{02} to the diffusion osmosis in the surface layer. Λ_{10} and Λ_{20} coefficients are related to mechanocaloric effect and pressure diffusion, respectively. We can estimate some coefficients as follows: $\Lambda_{11} = \kappa T$, where κ is thermal conductivity; $\Lambda_{22} = kTD$ where D is mutual diffusion coefficient of molecules in the membrane surface layer, $\Lambda_{21} = nD_T$, D_T is the thermal diffusion coefficient, $\Lambda_{12} = \Lambda_{21}$ characterizes the Dufour effect. It was shown (see [1]) that $\Lambda_{10} = \Lambda_{01} \approx D$.

Let us consider the isothermal flow of a mixture as an example. Then we can rewrite the system (7) in the form

$$\begin{aligned} \nabla p &= \Lambda_{00}^* \mathbf{u}_v + \Lambda_{20}^* (\mathbf{u}_1 - \mathbf{u}_2), \\ \nabla(\mu_1 - \mu_2)_T &= \Lambda_{00}^* \mathbf{u}_v + \Lambda_{20}^* (\mathbf{u}_1 - \mathbf{u}_2). \end{aligned} \quad (8)$$

Using the procedure proposed in [1] we express now the fluxes through the values characterizing the deviation of the surface layer from the equilibrium:

$$\begin{aligned}
 u_v &= \langle \Lambda_{00} \rangle \frac{p_{\text{ex}} - p_{\text{in}}}{T} + \langle \Lambda_{02} \rangle e^{\frac{(\mu_1 - \mu_2)_{\text{ex}}}{kT}} \left(1 - e^{-\frac{\Delta(\mu_1 - \mu_2)}{kT}} \right), \\
 u_1 - u_2 &= \langle \Lambda_{20} \rangle \frac{p_{\text{ex}} - p_{\text{in}}}{T} + \langle \Lambda_{22} \rangle e^{\frac{(\mu_1 - \mu_2)_{\text{ex}}}{kT}} \left(1 - e^{-\frac{\Delta(\mu_1 - \mu_2)}{kT}} \right),
 \end{aligned} \tag{9}$$

where $\Delta(\mu_1 - \mu_2) = (\mu_1 - \mu_2)_{\text{in}} - (\mu_1 - \mu_2)_{\text{ex}}$ is the effective affinity of the reaction of fluid molecules transfer from the bulk phase into the subsurface layer of the membrane, $\langle \Lambda_{lm} \rangle$ are transport coefficients averaged in a special manner. The relations (9) generalize the approach proposed in [1] for flow of a mixture.

The advantage of this approach is as follows. It allows for the linear non-equilibrium thermodynamics actually get a nonlinear transport equation, when instead of chemical potential difference as a thermodynamic forces appears another thermodynamic force i.e. the combination $e^{\frac{(\mu_1 - \mu_2)_{\text{ex}}}{kT}} \left(1 - e^{-\frac{\Delta(\mu_1 - \mu_2)}{kT}} \right)$. The resulting equations of non-equilibrium thermodynamics remaining linear in thermodynamic force are nonlinear in the chemical potential difference. Furthermore, transport coefficients include an explicit dependence on the height of potential energy barrier which molecule must to overcome to 'react'.

Conclusion

Using the Fokker Plank kinetic equation we found the transport equations, which describes the transport processes at the surface of the membrane for two-component mixture. We confirmed the presence of jumps of the thermodynamic parameters predicted earlier within the phenomenological approach and determined the kinetic coefficients.

The work was supported by Russian Foundation for Basic Research, project No 17-08-00315_a.

References

1. *Roldughin V.I., Zhdanov V.M., Kharitonova T.V.* Nonequilibrium Thermodynamics of Transport Processes on Membrane Surfaces // *Colloid Journal*, 2016, Vol. 78, No. 5, P. 652–657.
2. *de Groot S.R., Mazur P.* Non-Equilibrium Thermodynamics. North-Holland, Amsterdam, 1962.

INFLUENCE OF HYBRID FULLERENE-CONTAINING MODIFIERS ON PHYSICO-CHEMICAL AND TRANSPORT PROPERTIES OF POLYPHENYLENE OXIDE MEMBRANES

¹Valeriia Rostovtseva, ¹Alexandra Pulyalina, ²Ludmila Vinogradova, ^{1,2}Galina Polotskaya

¹Saint Petersburg State University, Saint Petersburg, Russia, *E-mail: Valfrank56@gmail.com*

²Institute of macromolecule compounds, Russian academy of sciences Saint Petersburg, Russia

Introduction

Mixed matrix membranes (MMMs) are a current trend in novelty membrane materials for gas and liquid separation that are primarily configured through a combination of organic and inorganic phases. Due to their combined effects, MMMs exhibit higher thermal stability and mechanical properties compared to those of pure polymer membranes and enhance permeability and separation performance by the incorporation of an inorganic phase.

The aim of the present work was the development and investigation of effective MMMs. Glassy poly(2,6-dimethyl-1,4-phenylene oxide) (PPO) was selected as the polymer matrix due to its low cost and high mechanical strength. Two types of hybrid star-shaped macromolecules were used as fillers to PPO matrix. First consist of a small core C₆₀ and 6 arms of nonpolar polystyrene (PS), second one has 2 types of arms of different nature: 6 PS and 6 polar copolymer of poly(2-vinylpyridine-block-poly-tret-butylmetacrylate) (PVP - PTBMA).

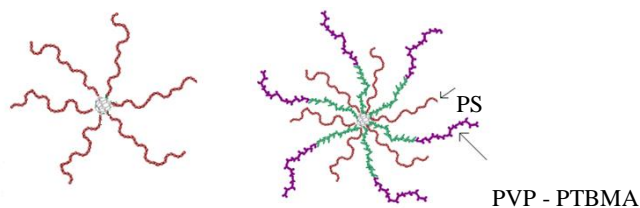


Figure 1. Two types of hybrid star-shaped macromolecule.

Experiments

PPO, PPO/FPS and PPO/HSM thin film membranes of ~40 μm thick were obtained by casting 3 wt% polymer solution in chloroform on a cellophane surface. The solvent was removed by evaporation at 40 $^{\circ}\text{C}$; the membrane was separated from the substrate and dried in a vacuum oven at 60 $^{\circ}\text{C}$ up to the constant weight. The structure and properties of the MMMs were examined using scanning electron microscope (SEM), determination of the density by flotation method and differential scanning calorimetry (DSC). Gas transport permeability measurements were carried out by using a laboratory high vacuum apparatus with a static permeation cell for a number of pure gases: H₂, O₂, N₂, CH₄. Swelling experiments were performed by immersion of membrane samples in individual liquid (methanol or ethylene glycol) at atmospheric pressure and temperature 20 $^{\circ}\text{C}$. These two components have different molecular masses, sizes, and solubility parameters. In fact, the separation of methanol from ethylene glycol is industrially important in the production of poly(ethylene terephthalate) for polyester industry. The transport properties in pervaporation of the methanol and ethylene glycol (EG) mixture were measured using a laboratory cell having an effective membrane area of 14.8 cm² at 50 $^{\circ}\text{C}$ with stirring. The composition of permeate was determined using both chromatograph «Chromatec–Crystal 5000.2» (Chromatec, Russia) with thermal conductivity detector.

Results and Discussion

PPO/HSM and PPO/FSP membranes containing up to 5 wt.% modifier are transparent films, pointing to good compatibility of the composite's components. The inclusion of different types of additive in the polymer matrix leads to the change of membrane structure that was studied by scanning electron microscopy. Fig. 2 shows micrographs of membrane cross section of PPO and its composites containing 5 wt.% FSP and HSM. The morphology of the membranes changes with the introduction of fullerene-containing modifier in the matrix polymer. The PPO film cross-section exhibits comparatively smooth structure.

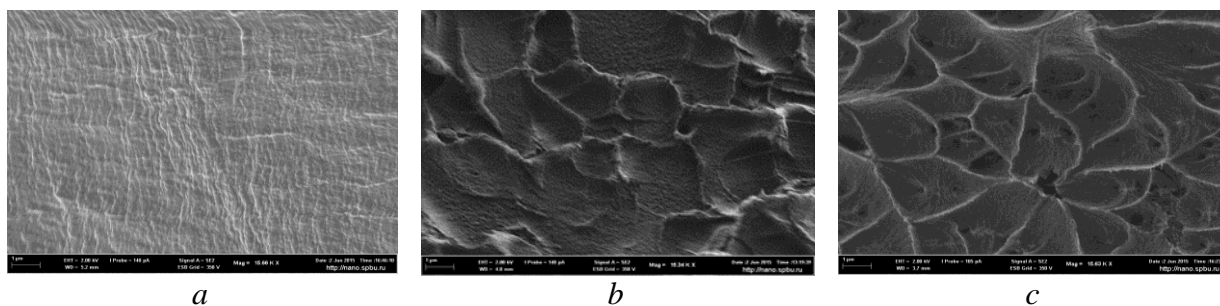


Figure 2. SEM micrographs of the membrane cross section: (a) PPO, (b) PPO/FPS (5%), (c) PPO/HSM (5%), magnification 15000.

To determine sorption and diffusion parameters of PPO/FPS samples, sorption (swelling) and desorption experiments were carried out toward individual liquids (methanol and ethylene glycol). Table 1 shows data on the equilibrium sorption degree and diffusion coefficients determined for membranes containing 0-5 wt% modifier. The inclusion of FPS into PPO matrix resulted in the decreasing magnitudes of the sorption degree and the diffusion coefficient for both liquids. The sorption degree of methanol is more than twice higher than that of ethylene glycol. Kinetics of sorption/desorption is controlled by the diffusion of penetrant molecules between the polymer chains. As it follows from the data of Table 1, the diffusion coefficients of methanol are higher than that of ethylene glycol; their difference is about two orders of magnitude. The methanol molecules can diffuse through the polymer matrix faster than the ethylene glycol molecules due to the smaller size. Thus, the methanol could sorb and penetrate through PPO/FPS membrane better in comparison with the other alcohol. This can play an important role in separation of methanol – ethylene glycol mixture by the pervaporation.

Table 1: Membrane sorption and diffusion characteristics for methanol and ethylene glycol

Modifier, wt%	Sorption degree MeOH, %		Sorption degree EG, %		Diffusion coefficient MeOH, $D \cdot 10^{12} \text{ m}^2/\text{s}$		Diffusion coefficient EG, $D \cdot 10^{14} \text{ m}^2/\text{s}$	
	FPS	HSM	FPS	HSM	FPS	HSM	FPS	HSM
0	14.0	14.0	5.2	5.2	2.27	2.27	3.70	3.70
1	13.7	14.6	5.1	5.7	2.10	2.83	0.16	4.18
3	12.5	15.3	5.0	6.6	2.00	3.14	0.12	5.70
5	12.4	16.1	4.9	7.0	1.90	4.52	0.05	6.91

Separation of methanol – ethylene glycol mixture through PPO, PPO/FPS and PPO/HSM membranes was studied by pervaporation experiments in the concentration range of 10 ÷ 30 wt% methanol in the feed at 50°C. In pervaporation, the transport of small molecules through a membrane proceeds according to the “solution-diffusion” model i.e. permeability is directly proportional to solubility (sorption) and diffusivity. The separation factor decreases with growing methanol concentration in the feed (Fig. 3a). It is important that membranes containing FPS or HSM are more efficient in separation of methanol –ethylene glycol mixture than unmodified membranes. But PPO/HSM is occurred to be the most selective one due to the greater difference in values of sorption of methanol and EG than for PPO and PPO/FPS. Fig. 3b shows that the total flux increases with methanol concentration in the feed for all membranes, but its magnitude decreases with a growth of FPS content in the membrane. In case of PPO/HSM membranes flux is also greater than others on account of higher diffusion coefficients.

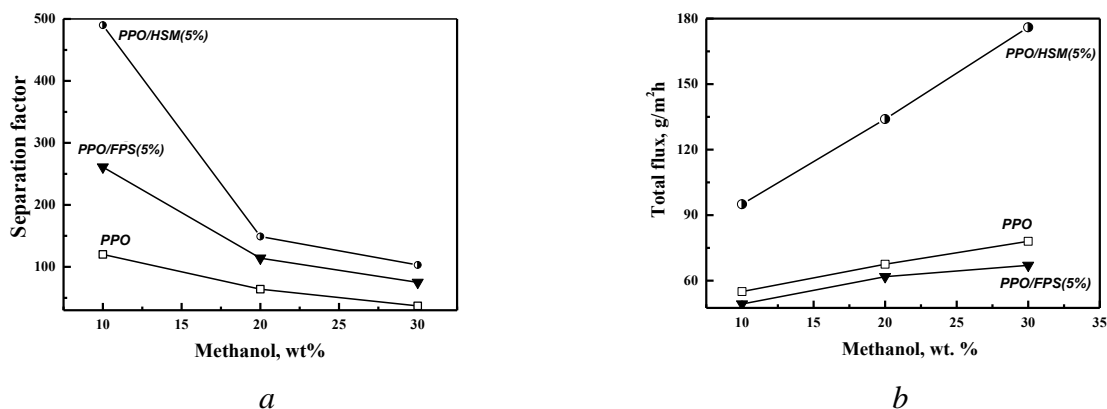


Figure 3. Dependence of (a) separation factor and (b) total flux on methanol concentration in the feed for pervaporation of methanol - ethylene glycol mixture using PPO, PPO/FPS and PPO/HSM membranes, 50 °C.

It was established that the fullerene-containing modifier exerts positive effect on gas separation properties of PPO membrane. As it is shown in Table 2, selectivity separation of H₂/N₂, H₂/CH₄ and O₂/N₂ mixtures increases with adding of FPS content in the membrane. The selectivity for PPO/HSM membrane also exhibited similar trend but the difference between pure PPO membrane and PPO/HSM (5%) is higher. In all cases, gas permeability decreases with an increasing gas molecule sizes.

Table 2: Gas permeability of membranes, 30 °C

Membrane	Permeability coefficient, Barrer				Selectivity		
	H ₂	N ₂	O ₂	CH ₄	O ₂ /N ₂	H ₂ /N ₂	H ₂ /CH ₄
PPO	188.0	10.2	33.2	14.0	3.3	18.4	13.4
PPO/FPS (5%)	135.7	5.9	25.9	9.3	4.4	22.8	14.8
PPO/HSM (5%)	116.9	4.7	20.2	6.2	4.3	24.7	18.9

Conclusions

Novel mixed matrix membranes with star-shaped fullerene-containing nanomodifiers characterized by high thermal stability, mechanical strength and chemical stability have been developed. The mass transfer through membranes is accurately described on the basis of thermodynamic and kinetic parameters (sorption and diffusion). It is shown that the mixed matrix membranes have improved transport properties, demonstrated good selectivity in gas separation and are highly efficient in the process of separation of a mixture of monohydric and polyhydric alcohols, including an azeotropic composition, allowing the extraction of ethylene glycol much more energy and resource-saving compared to standard industrial methods.

Acknowledgments

A.M.T. and G.A.P. acknowledge the Russian Foundation for Basic Research (project 15-03-02131). A.Yu.P. is also grateful for the support by Fellowship of the President of Russian Federation (project № 184, SP-1469.2015.1). Equipment of Resource Centers of St. Petersburg State University, namely "Thermogravimetric and calorimetric methods of investigation", "Chemical Analysis and Materials Research Centre", Interdisciplinary Resource Center "Nanotechnologies", "X-ray diffraction studies" and Education Resource Centre in the direction of chemistry were used for membrane investigation.

ION TRANSPORT IN CARBON COATED ALUMINA NANOFIBER MEMBRANES: MATHEMATICAL MODELLING AND EXPERIMENT

¹Ilya Ryzhkov, ¹Denis Lebedev, ¹Victoria Bykanova, ¹Vera Solodovnichenko, ¹Alexey Shiverskiy, ^{1,3}Mikhail Simunin

¹Institute of Computational Modeling SB RAS, Krasnoyarsk, Russia

²Molecular Electronics Department KSC SB RAS, Krasnoyarsk, Russia

³National Research University of Electronic Technology – MIET, Zelenograd, Moscow, Russia

E-mail: rii@icm.krasn.ru

Introduction

Separation of species with the help of selectively permeable membranes is widely used in various fields of industry including chemical, pharmaceutical, energy, and biotechnology sectors. The removal of ionic species and organic solutes from aqueous solutions can be accomplished with the help of nanofiltration and ultrafiltration. These pressure-driven membrane processes received much attention in the last decades due to their applications in textile, paper, and food industries including water desalination and purification.

Most of nanofiltration membranes acquire an electric charge when brought in contact with a polar medium due to dissociation of functional groups or adsorption of charged species from the solution onto the pore walls. The fixed charge significantly affects the electrolyte transport through membrane pores. If pore walls are made of conductive material, this charge can be altered by applying a prescribed potential to the membrane. In this way, the membrane selectivity characteristics can be externally varied and controlled [1].

This work deals with studying the ion transport in carbon coated alumina nanofiber membranes and interpretation of results on the basis of mathematical modelling.

Experimental

The membranes are produced from highly aligned alumina nanofibers – Nafen™ (ANF Technologies). The nanofibers have the diameter of 10 – 15 nm and length in the cm range. The membranes are prepared by filtration of aqueous nanofiber suspension through a porous support followed by drying and sintering. Electrical conductivity and ionic selectivity are achieved by depositing a thin carbon layer by catalytic-free chemical vapor deposition (CVD) [2]. Membranes without and with carbon layer are further referred to as Nafen and C-Nafen membranes.

The ionic selectivity of prepared membranes is studied by measuring the potential difference between two electrolyte solutions with different concentrations separated by a membrane. Measurements were carried out in the laboratory made electrochemical cell consisting of two compartments (half-cells) with Ag/AgCl electrodes connected to a potentiostat PI-50Pro (ELINS Ltd., Russia). KCl aqueous solution was used as electrolyte. The concentration in the right half-cell was fixed at $C_R=1$ mM or $C_R=10$ mM, while the concentration in the left half-cell was varied from C_R up to 4.2 M.

Theoretical

According to the theory of Teorell, Meyer and Sievers (TMS theory), the total potential difference $\Phi = \Phi_R - \Phi_L$ across the membrane for binary monovalent electrolyte is given by [3]

$$\Phi = \ln \frac{C_L}{C_R} \left(\frac{-X + \sqrt{X^2 + 4C_R^2}}{-X + \sqrt{X^2 + 4C_L^2}} \right) - \frac{D_+ - D_-}{D_+ + D_-} \ln \left(\frac{-DX + \sqrt{X^2 + 4C_R^2}}{-DX + \sqrt{X^2 + 4C_L^2}} \right), \quad (1)$$

where the first and second terms represent the contributions from Donnan potential and diffusion potential, respectively. In formula (2), C_L and C_R are the electrolyte concentrations in the left and right half-cells ($C_L > C_R$), respectively, D_{\pm} are the diffusion coefficients of positive and negative ions, and X is the volume density of membrane fixed charge, which is related to the surface charge density σ by the formula

$$X = \frac{2\sigma}{Fr}. \quad (2)$$

Here r is the pore radius. Anion- and cation-selective membranes correspond to the cases $X > 0$ and $X < 0$, respectively. The volume density of fixed charge X can be determined by fitting the experimentally measured values of Φ at constant C_R and varying C_L to formula (2). It will be referred to as one-parameter fit of TMS model. The two-parameter fit corresponds to the simultaneous determination of volume charge density X and counter-ion diffusion coefficient by fitting the TMS model to the experimental data. It is based on the assumption that the counter-ion diffusion coefficient is lowered in comparison with the external solution due to attractive interaction between counter-ions and membrane fixed charge [4]. The prediction of membrane potential by the TMS model (1) can be greatly improved by replacing the concentrations C_R and C_L with the corresponding activities a_R and a_L [4].

More precise description of membrane potential can be obtained with the help of Space-Charge model, which takes into cross-sectional variation of potential and electrolyte concentration [5, 6]. In this work, we have used this model as well for determining the membrane surface charge and compared the results with those obtained from TMS model.

A simplified approach to interpreting the potential difference between two half-cells separated by a membrane is provided by the equation [7]

$$\Phi = 2.303 (t_+ - t_-) \frac{RT}{F} \log \frac{a_L}{a_R}, \quad (3)$$

where t_+ and t_- are transference numbers of anions and cations in membrane, respectively, which obey the relation $t_+ + t_- = 1$.

Results and discussion

The results for Nafen membrane presented in Fig. 1a show that the potential difference between half-cells with larger and smaller electrolyte concentration is negative. It means that the membrane is anion-selective ($t_- > t_+$), see Eq. (3). The absolute value of membrane potential first increases with the increase of activities ratio, then reaches maximum, and finally decreases. The weak anion selectivity is related to positive charge due to adsorption of cations on the alumina surface [2]. The values of volume and surface charge density determined from one-parameter fit of TMS model (1) are given in Table 1. Note that the pore radii $r = 14$ nm and $r = 8$ nm were taken for the Nafen and C-Nafen membranes, respectively. These values correspond to the maxima in pore size distributions.

The experimentally determined membrane potential for the C-Nafen membrane shown in Fig. 1b gives evidence of high anion selectivity. In this case, the experimental results are very well fitted by equation (3) with anion transference numbers $t_- = 0.91$ for $C_R = 1$ mM and $t_- = 0.94$ for $C_R = 10$ mM, see Table 1. The one-parameter fit by the TMS model (1) is not so good, but still can be used to estimate the membrane fixed charge. The increase of concentration from $C_R = 1$ mM to $C_R = 10$ mM decreases the Debye length, which should reduce the ionic selectivity. At the same time, it leads to the increase of fixed charge by ~ 10 times, which enhances the ionic selectivity. For the C-Nafen membrane, the former effect slightly overcomes the latter one, which results in higher anion transference number for the increased concentration. The increase of membrane selectivity after deposition of carbon can be explained by a strong adsorption of cations on the structural defects of carbon layer.

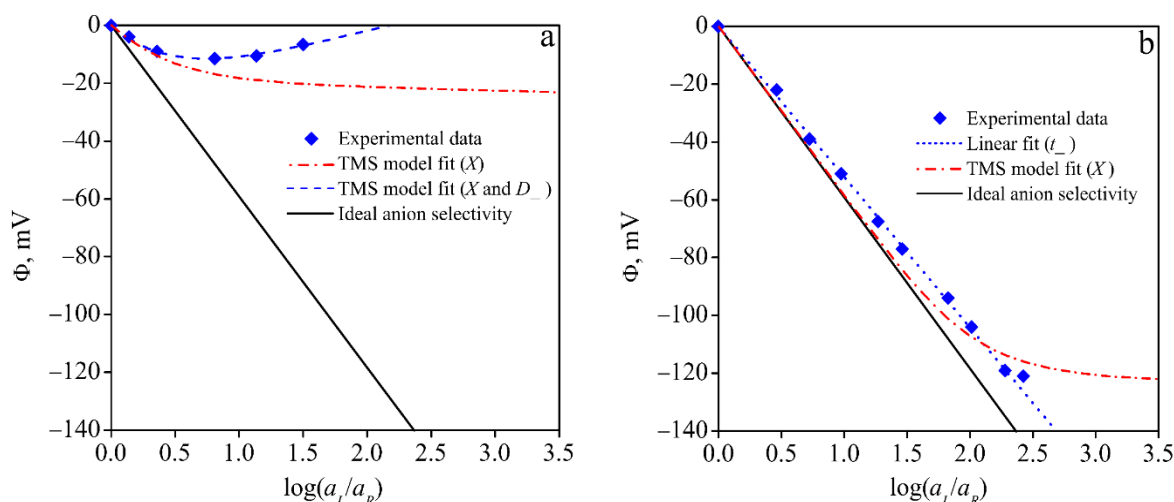


Fig. 1. The dependence of membrane potential Φ on the logarithm of activities ratio for the Nafen membrane (a) and C-Nafen membrane (b), $C_R = 10$ mM.

Table 1: Transference numbers, volume density X and surface density σ of fixed membrane charge for different concentrations C_R in the right half-cell

Membrane	C_R , mM	t_+	t_-	X , mM	σ , 10^{-3} C m $^{-2}$
Nafen	1	–	–	1.5	1.0
Nafen	10	–	–	14.8	10.0
C-Nafen	1	0.09	0.91	116.1	44.8
C-Nafen	10	0.06	0.94	1021.1	394.0

The potential applications of produced membranes include nano- and ultrafiltration as well as separation of charged species. The deposition of conductive carbon layer on nanofibrous structure is a promising technique for preparing membranes with switchable ion-transport selectivity.

This work is supported the Russian Science Foundation, Project 15–19–10017.

References

1. Martin C.R., Nishizawa M., Jirage K., Kang M. Investigations of the transport properties of gold nanotubule membrane. *J. Phys. Chem. B*, 2001. V. 105, P. 1925–1934.
2. Lebedev D.V., Shiverskiy A.V., Simunin M.M., Solodovnichenko V.S., Parfenov V.A., Bykanova V.V., Khartov S.V., Ryzhkov I.I. Preparation and Ionic Selectivity of Carbon-Coated Alumina Nanofiber Membranes *Petroleum Chemistry*, 2017, Vol. 57, P. 306–317.
3. Tanaka Y. Ion exchange membranes: fundamentals and applications. Elsevier, Amsterdam, 2015.
4. Galama A.H., Post J.W., Hamelers H.V.M., Nikonenko V.V., Biesheuvel P.M. On the origin of the membrane potential arising across densely charged ion exchange membranes: how well does the Teorell–Meyer–Sievers theory work? *J. Membr. Sci. & Res*, 2016. V. 2, P. 128–140.
5. Peters B.B., Van Roij R., Bazant M.Z., Biesheuvel P.M. Analysis of electrolyte transport through charged nanopores, *Phys. Rev. E*, 2016. V. 93, 053108.
6. Ryzhkov I.I., Minakov A.V. Theoretical study of electrolyte transport in nanofiltration membranes with constant surface potential / charge density. *J. Membrane Science*, 2016. V. 520, P. 515–528.
7. Strathmann H. Introduction to membrane science. Wiley–VCH, Weinheim, Germany, 2011.

THE EFFECT OF THE CONCENTRATION OF NICKEL CHLORIDE ON THE SURFACE CHARGE AND THE SELECTIVITY OF THE NANOFILTRATION MEMBRANE

¹Konstantin Sabbatovskiy, ²Polina Epifanova, ²Nadezhda Golovaneva, ¹Vladimir Sobolev, ²Elena Farnosova, ²Georgy Kagramanov

¹Russian academy of sciences A.N. Frumkin Institute of Physical chemistry and Electrochemistry RAS, 119071, Moscow, Leninsky prospect 31, b.4. E-mail: vsobolev@phych.e.ac.ru

²Dmitry Mendeleev University of Chemical Technology of Russia, Moscow 125047, Miusskaya square, 9. E-mail: farelena@rambler.ru

Introduction

The method of nanofiltration is widely used in industrial technological schemes to reduce the concentration of solutions of electrolytes and organic substances. At the same time, the factors and causes that affect the selectivity of nanofiltration membranes have not been adequately studied. Often, the technology uses acidification of the electrolyte solution, it is also possible to change the pH of the electrolyte solution during the process itself. The change in pH and concentration of ions of electrolytes (especially multiply charged) affects the surface properties of the membrane and, ultimately, its selectivity, as well as the competition factor for transport through the membrane between the metal and hydrogen cations.

Under these conditions, it is important to predict the change in membrane selectivity.

Materials and Methods

The purpose of our work was to study the effect of pH and the concentration of nickel chloride on the selectivity of the nanofiltration membrane synthesized at the ZAO Vladipor Science and Technology Center. The selective layer of the membrane is formed by the interphase polycondensation of piperazine and trimesoyl chloride.

A special apparatus [1] was used for the studies, which makes it possible to measure the flow potential, which is a characteristic of the change in the electro-surface properties of the membrane, as well as the electrical resistivity and permeability of the membrane directly during membrane separation. NiCl₂ solutions with a concentration of 3×10^{-4} , 10^{-3} , 3×10^{-3} , and 10^{-2} g-equiv/l in the pH range of 3-6.5 were used for the studies. To analyze the concentration of nickel and hydrogen cations in the filtrate of the solution that passed through the membrane, conductometry, ionometry and atomic absorption spectrometry methods were used.

The experiment and discussion of results

In the concentration range of nickel chloride 0.0001-0.03 g-eq/l, the selectivity of the membrane increased from 0.7 to 0.94. The streaming potential changed the sign from negative to positive in the concentration region 0.0025 g-equiv/l (Fig.1).

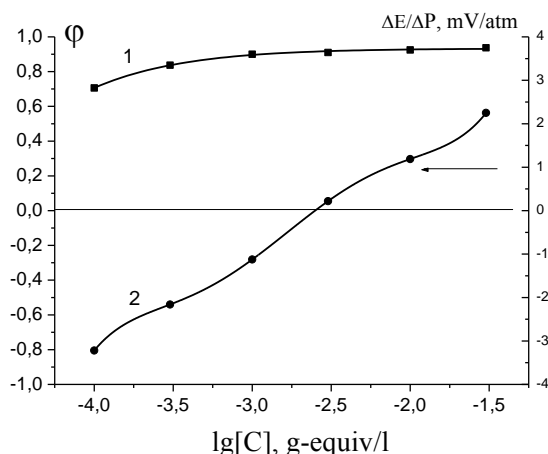


Figure 1. Dependences of the selectivity coefficient ϕ of nickel cations (1), and the streaming potential $\Delta E/\Delta P$ (2) of nanofiltration membrane from nickel chloride concentration C

Upon acidification of the salt solution, the dissociation of the carboxyl groups is suppressed and the simultaneous protonation of the NH groups of the membrane occur, which leads to a change in the sign of the membrane flow potential. The isoelectric point of the membrane (IET), for the 0.01N KCl solution, was in the pH 4.2 range.

The membrane IET is in the pH range 4.1 (Fig.2, curve 3). We note that with an increase in the salt concentration, the isoelectric point of the membrane is shifted to the neutral region. Thus, for 0.001 N solution of the IET membrane is already in the pH range 5.0, and at higher nickel concentrations, in the neutral region, due to the specific adsorption of nickel ions on the charged groups of the copolymer of the membrane. The centers of adsorption for nickel cations can be carboxyl groups, as well as carbonyl oxygen.

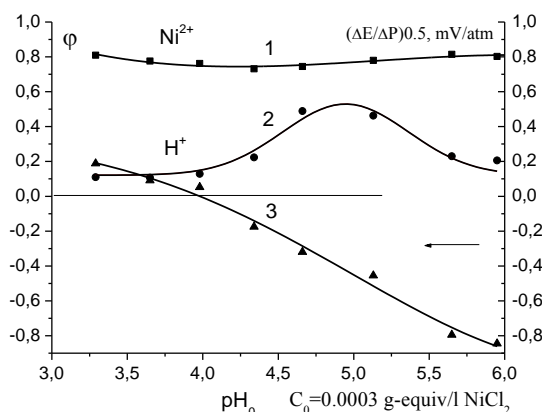


Figure 2. Dependences of the selectivity coefficient ϕ of nickel cations (1), hydrogen (2) and the streaming potential $\Delta E/\Delta P$ (3) of nanofiltration membrane at different pH 0.0003 N of nickel chloride solution

It is seen from Fig. 2, that for 0.0003 N nickel chloride solution in a weakly acid medium, a minimum of selectivity is observed for nickel cations and a maximum for hydrogen cations. Further, when the pH is lowered, the membrane selectivity increases with respect to nickel cations and its decrease in hydrogen cations. The observed changes in the selectivity of the membrane cannot be fully described using only the classical mechanism of Donnan exclusion of co-ions from the pore space of the membrane, which leads to a decrease in the concentration of ions in the filtrate. Thus, for all initial concentrations of nickel chloride, minima of selectivity for nickel cations and maxima for hydrogen cations, were observed in approximately the same weakly acidic pH region, regardless of the position of the IET membrane. At higher starting concentrations of nickel chloride, similar trends in the selectivity of nickel cations were recorded, while negative membrane selectivity was observed for hydrogen cations. In the filtrate, the concentration of hydrogen cations was higher than in the initial solution.

To interpret the results, we consider three main factors: the Donnan exclusion of ions from the pore space of the membrane, the competition for transport through the membrane between the cations of nickel and hydrogen, and the change in the energy of the adsorption centers.

Conclusion

It is shown that the selectivity and charge of the nanofiltration membrane depends on the concentration of nickel chloride. The high adsorption potential of nickel cations affects the electro-surface properties of the membrane, which causes an increase in its selectivity. The presence of hydrogen cations in a solution of nickel chloride has an additional effect on both the charge and the selectivity of the membrane over nickel cations.

References

1. Sabbatovskii K.G., Sobolev V.D., Churaev N.V. Effect of pH of the solution on membrane selectivity//Colloid. Jour. 1991. V. 53(1). P.74-78.

CHOLINE CHLORIDE BASED DEEP EUTECTIC SOLVENTS AND THEIR INFLUENCE ON THE TRANSPORT PROPERTIES OF CHITOSAN MEMBRANES

¹Artemiy Samarov, ¹Maria Sokolova, ²Michael Smirnov, ¹Oleg Medvedev, ¹Alexander Toikka

¹Saint Petersburg State University, St. Petersburg, Russia, *E-mail: samarov@yandex.ru*

²Institute of Macromolecular Compounds, Russian Academy of Sciences, St. Petersburg, Russia

Introduction

Deep eutectic solvents (DES) attract much attention during last years as green and cheap alternative for ILs. DES demonstrate all benefits of ILs and, at the same time, they can be prepared from biocompatible and cheap components.

DES based on choline chloride is highly effective for selective sorption of ethanol. It seems to be interesting task to use this property of DES for separation of liquid mixture via pervaporation through polymeric membrane.

In the present work the possibility of preparation of composite membranes based on DES and chitosan as natural and promising green polymer was investigated. The membrane was tested for separation of n-hexane - ethanol azeotropic mixture and it was demonstrated that chitosan-DES membranes are promising candidate for separation of organic/organic mixtures.

Experiments

The DES was prepared by mixing choline chloride as a hydrogen bond acceptor (HBA) with malonic acid as a hydrogen bond donor (HBD) in screw-capped bottles. The mixture was kept in an ultrasonic bath at 60 ± 0.1 °C until a clear liquid was formed (3-4 hours).

For preparation of composite membranes, the solution containing of 0.33 mass % of chitosan and 67 mass % of DES components were prepared. Membranes were formed by a solution casting of in the Petri dishes with subsequent solvent evaporation. For comparison the membrane containing only chitosan was prepared by the same procedure using of 1 mass % solution of chitosan in the acetic acid (1 mass %).

Scanning electron microscopy (SEM) micrographs were obtained with a Zeiss Merlin SEM (Carl Zeiss, Oberkochen, Germany) at 1.5 kV voltage. For investigation of cross-sections, the membranes were submerged in liquid nitrogen and fractured perpendicularly to their surface.

Pervaporation experiments were conducted with home-made apparatus at 60°C. The membrane surface area was 2,54 cm². The permeate was blown from the membrane surface with nitrogen at flow rate 60 ml min⁻¹ and collected in glass trap cooled down to -20°C with cryostat. Performance of membranes was characterized with flux (amount of penetrant passed through membrane per units of surface and time) and selectivity coefficient (α). The composition of feed and permeate mixtures were obtained via GC by the same method as was used for investigation of LLE.

Results and Discussion

It is known that chitosan is not compatible with hydrocarbons and also used for dehydration of alcohols. So for membrane prepared from pure polymer expectable results was obtained: the flux of both components was not observed. Anyhow, for composite membrane the significant flux of ethanol was fixed. Selectivity respectively to ethanol and its flux through the composite membrane is presented in Figure 1. It is seen that increasing of ethanol concentration in feed mixture from 4 to 10% leads to the increasing of flux from 0.001 to 0.350 kg m⁻² h⁻¹. Taking into account that initial chitosan is not permeable for ethanol at all and comparing these results with literature data, obtained values are good. Selectivity of composite membrane is excellent its lies in the range 1874-23668 respectively to ethanol. For the best of our knowledge this is maximum values reported in literature for pervaporation of n-hexane - ethanol with organic membranes. This achievement can be connected with two reasons: high sorption capacity of DES respectively to ethanol and specific nanostructure of the prepared membrane.

Membrane fouling increased significantly as operating flux increased. Figure 1 suggests that enhanced hydraulic resistance of the fouling layer induced by filtrate flow also contributed to increased fouling observed at high operating flux.

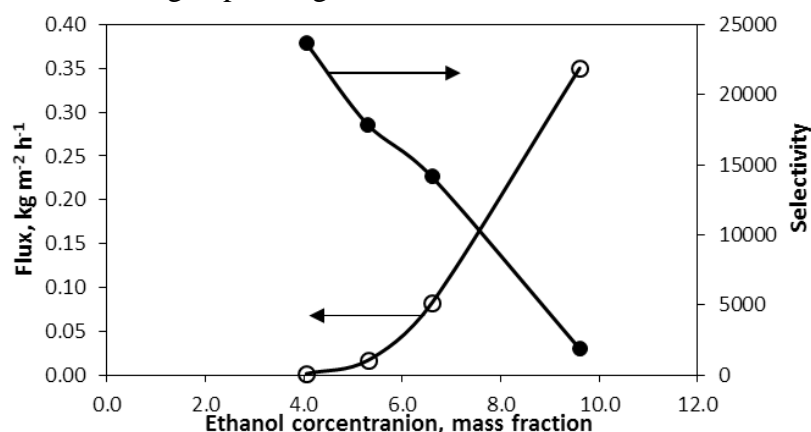


Figure. 1. Selectivity (●) of composite membrane chitosan-DES to ethanol and flux (○) of ethanol through the membrane

SEM was used for the visualization of the morphology of the membranes. SEM images of the surface and the cross-sections of initial chitosan membrane and composite membrane are shown in Figure 2 a and c, respectively. It can be seen that the surface of the chitosan membrane is smooth. Dense packing structure with multiple fracture lines was observed in cross-section SEM images of initial chitosan membranes (Figure 2 b). The introduction of 65% of DES led to a significant change of the morphology of chitosan (Figure 2 c and d). With wrinkled surfaces with large number of pores with sizes of 100-400 nm are observed. The wrinkled morphology can also be seen in the image of cross-section of chitosan-DES membrane presented in Figure 2 d. This It can be supposed that during the formation of membrane the strong interaction between components of DES force chitosan macromolecules to form separate phase. Such phase separation leads to the formation of chitosan skeleton of the membrane, which is filled with DES. At the same time, interaction of DES with chitosan is also possible due to hydrogen bonding between -OH and -NH₂ groups of polymer and -COOH groups of malonic acid. These lead to mechanical stability of the whole system making it suitable for using in pervaporation.

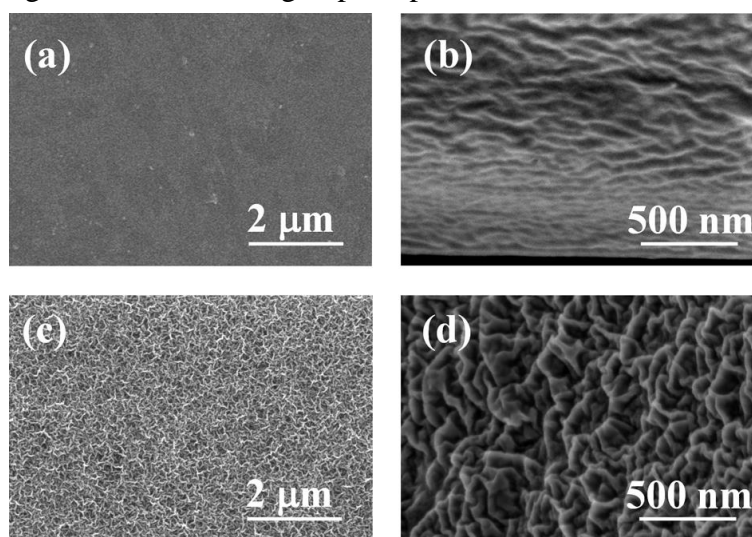


Figure. 2. SEM images of surfaces (a,c) and cross-sections (b,d) of initial chitosan membrane (a, b) and composite chitosan membrane (c,d).

Acknowledgment

The reported study was funded by RFBR, according to the research project No. 16-33-60128 mol_a_dk.

EFFECT OF AMPHOLYTE NATURE ON TRANSPORT CHARACTERISTICS OF ANION-EXCHANGE MEMBRANES

Veronika Sarapulova, Mariya Fomenko, Liudmila Arzaniaeva, Natalia Pismenskaya
Membrane Institute, Kuban State University, Krasnodar, Russia, E-mail: vsarapulova@gmail.com

Introduction

Ion exchange membranes (IEM) are increasingly used in the processes of concentration, purification, separation of biochemical biomass processing products, as well as stabilization and conditioning of liquid media in the food industry. As a rule, these media are multicomponent. For example, wine materials can contain up to 600 substances, including highly hydrated polysaccharides and tannins, as well as ampholytes (polybasic carboxylic acids, amino acids, anthocyanins, etc.). Polar groups of ampholytes enter protonation / deprotonation reactions in aqueous solutions. Therefore, the charge of ampholyte directly depends on the pH of the medium. Coupling of chemical reactions with the transfer of ampholytes in membrane systems greatly complicates the study of these processes. In the works [1-3] it was established that the transport of ampholytes is accompanied by barrier, circulation effects, as well as the effects of facilitated diffusion and electrodiffusion. In the experimental work [4], it was shown that dilution of ampholyte containing solutions leads to an increase in the electrical conductivity of anion-exchange membranes. This phenomenon is explained by the Donnan exclusion of protons which are products of ampholyte protonation / deprotonation reaction. It is established that anion-exchange membranes degrade in greater extent in comparison to cation-exchange membranes when processing ampholyte containing solutions from the food industry. It is suggested that polyphenols and their polymerization and polycondensation products are responsible for the poisoning of anion-exchange membranes in electro dialysis wine stabilization [5]. However, this assumption was not tested. The actual task for today is to obtain new knowledge about the mechanisms of the influence of ampholytes, which are part of model wine solutions, on the structure and transport characteristics of anion exchange membranes (AEM).

Experiment

As the objects of investigation, the commercially available (AMX-Sb) and experimental (MA-41P) anion exchange membranes were selected. Using the atomic force and optical microscopy, the reference contact porosimetry, the structure of the surface and volume of the membranes under study was investigated. Their transport characteristics in ampholyte containing model wine solutions, such as diffusion permeability and specific conductivity, were also studied.

Results and Discussion

Theoretical and experimental evidence of increase in pH of the internal AEM solution due to the Donnan effect of protons exclusion (which are the products of ampholytes protonation / deprotonation reaction) was obtained. It is shown that this change in pH resulted in an increase in the contribution to charge transfer of doubly charged anions in the gel phase of the membrane, which are formed due to deprotonation of singly charged ampholyte forms. This contribution increases with dilution of the external solution and with decrease in the difference in the values of the first and the second protonation / deprotonation constants of the ampholyte. An increase in the pH of the internal solution may lead to a change in the sign of the charge of anthocyanins in comparison to the external solution. Prolonged contact of AEM with strongly hydrated ampholytes leads to an increase in the effective pore radius (fig.1), which results in an increase in the volume fraction of the gel phase (table 1) and the linear dimensions of the membranes (fig.2) as compared to NaCl solutions. The reason is follow. The high ability of ampholytes to water structuring leads to an increase in osmotic pressure in the pores of AEM resulted in stretching of the elastic ion exchange matrix. The influence of this effect increases with increasing counterion hydration number, a decrease in the cross-linking degree of the ion exchange matrix, and an increase in the duration of contact of the ion-exchange material with the ampholyte containing solution. An increase in the effective pore radius of samples situated in multicomponent ampholyte containing

model solutions or in wine promotes the penetration of large molecules of tannins and, apparently, proteins. The association of these molecules with anthocyanin derivatives and the partial deprotonation of carboxyl and hydroxyl groups due to the shift in the pH of the internal solution towards the alkaline values leads to the formation of network structures, which are able to form hydrogen bonds with secondary and tertiary fixed groups on the pore walls. These structures are the reason for a marked decrease in the diffusion permeability and electrical conductivity (fig. 3) of AEM.

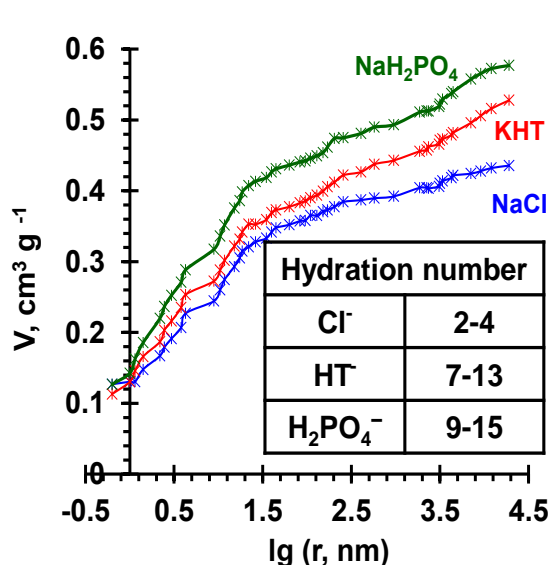


Figure 1. Water distribution by effective pore radius of MA-41 after its contact with NaCl and ampholyte solutions during 150 hours

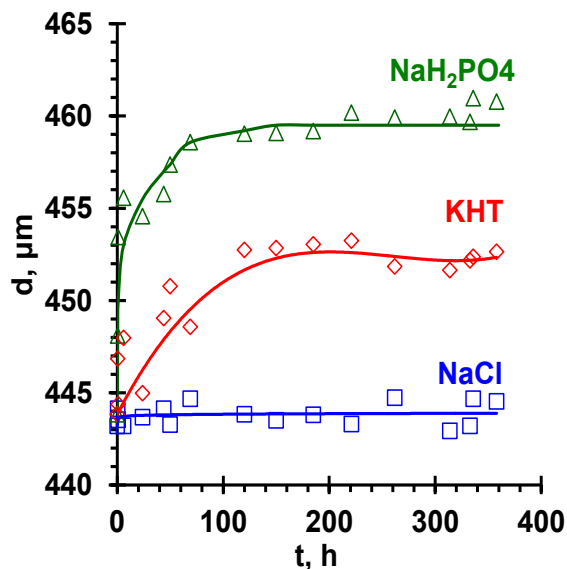


Figure 2. Kinetic dependences of the MA-41 membrane thickness in contact with NaCl and ampholyte solutions

Table 1. The area of specific integral internal surface (per 1 g of dry membrane) of pores (S_t) and the value of the volume fraction of the intergel phase of AEM after treatment in 0.02 M of NaCl and KHT solutions during 150 hours

AOM	$S_t, m^2 g^{-1}_{dry}$		f_2	
	NaCl	KHT*	NaCl	KHT*
AMX	290	340	0.10±0.1	-
AMX-Sb	290	340	0.12±0.1	0.16±0.2
AX	380	450	0.12±0.1	
MA-41	370	410	0.21±0.1	0.27 ±0.2

*measured in NaCl solution after AEM contact with KHT during 150 hours

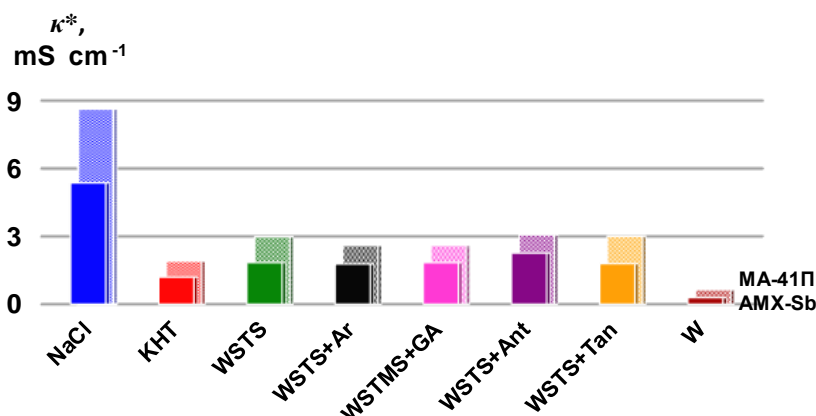


Figure 3. Electrical conductivity of anion-exchange membranes under study after contact with model wine solutions during 72 hours. Where **Ant** is the anthocyanin, **Tan** is the tannin, **Ar** is the arabinose, **Ga** is the galacturonic acid, **W** is the dry red wine.

Acknowledgements

We are grateful for financial support to the Russian Scientific Foundation (grant No 17-19-01486).

References

1. *Shaposhnik V.A., Eliseeva T.V.* Barrier effect during the electro dialysis of ampholytes // *J. Membr. Sci.* 1999. Vol. 161. P. 223-229.
2. *Vasileva V.I., Shaposhnik V.A., Zemlyanukhina I.A., Grigorchuk O.V.* Facilitated diffusion of amino acids in ion-exchange membranes (in Russian) // *Rus. J. Phys. Chem. A.* 2003. V. 77, № 6. P. 1017-1019.
3. *Eliseeva T.V., Shaposhnik V.A.* Effects of circulation and facilitated electromigration of amino acids in electro dialysis with ion-exchange membranes (in Russian) // *Rus. J. Electrochemistry.* 2000. V. 36, № 1. P. 64-67.
4. *Pismenskaya N., Laktionov E., Nikonenko V., El Attar A., Auclair B., Pourcelly G.* Dependence of composition of anion-exchange membranes and their electrical conductivity on concentration of sodium salts of carbonic and phosphoric acids // *J. Membr. Sci.* 2001. V. 181. P.185-197.
5. *Moreno-Arribas M. V., Polo M. C.* Wine chemistry and biochemistry, Springer, NY, 2009.

USE OF IMPEDANCE SPECTROSCOPY FOR STUDYING THE ELECTROCHEMICAL BEHAVIOR OF ION-EXCHANGE MEMBRANES AFTER THEIR CONTACT WITH WINE

Veronika Sarapulova^a, Ekaterina Nevakshenova^a, Natalia Pismenskaya^a, Anton Kozmai^a, Philippe Sizat^b

^a Membrane Institute, Kuban State University, Krasnodar, Russia, *E-mail: n_pismen@mail.ru*

^b Institut Européen des Membranes, CNRS - Université Montpellier, France
E-mail: philippe.sizat@iemm.univ-montp2.fr

Introduction

Membrane-based processes are playing a critical role in the field of separation/purification, clarification, stabilization, concentration, and de-alcoholization of wine products [1, 2]. Wine contains more than 600 components, including polyphenols (anthocyanins, tannins, etc.), polysaccharides, amino acids and proteins. Their interactions with each other and membrane material inevitably lead to fouling [2,3]. The control of fouling, as well as the development of methods for its prevention, are of the primary importance for the successful operation of membrane modules in the food and beverage industry.

Experiment

A homogeneous anion-exchange membrane AMX-Sb (Astom, Japan) was selected as the object of investigation. In experiments we used: distilled water (electrical conductivity $0.5 \mu\text{S cm}^{-1}$, pH = 5.5; $t = 25^\circ \text{C}$), solid NaCl (OJSC Vekton), as well as red dry wine, made from the varieties of the grape of Murvedr, Syrah, Grenache. Before experiments, all membrane samples underwent standard salt pretreatment [4], and were equilibrated with 0.02 M NaCl. One of these samples was used for comparison. Other samples were placed in a two-chamber flow cell. The distilled water circulated through one of the chambers, and the red wine (these samples are denoted by the index w) through the other. Electrochemical impedance spectroscopy of the system with the membrane under investigation was carried out by the method described in [5].

Results and Discussion

Optical images of surface and cross-sections of wet membranes AMX-Sb, AMX-Sbw10, AMX-Sbw72, are shown in Figure 1. The reddish-brown components of the wine are recorded on the surface of the AMX-Sbw10. Their localization is of an island-type. A continuous red-brown layer covers the membrane surface after 72 hours of contact with the wine. This layer consists of highly hydrated colloidal structures. The shape of the electrochemical impedance spectra (EIS) of the pristine membrane and the sample contacted with the wine are significantly different (fig. 2). These differences are traced in all three (high-frequency, mid-frequency, low-frequency) domains. Let us consider the high-frequency region. In the case of the AMX-Sb membrane, the EIS in the frequency range from 10Hz to 130kHz have the form of a semicircle (fig. 3). They can be interpreted using the RC element (fig. 3), where the resistance R is equivalent to the ohmic resistance of the membrane, its interphase boundaries and adjacent diffusion boundary layers (DBL). The effective electrical capacitance C is mainly controlled by the capacity of electric double layers on the interphase boundaries. The spectrum of the system with AMX-Sbw10 in a similar frequency range has a specific shape (fig. 3). Such a form of EIS, as a rule, becomes apparent in the presence of two layers; each of these layers is characterized by a noticeably different effective capacitance [6]. A schematic representation of such a membrane system and its equivalent circuit is shown in figure 3. This scheme consists of two series-connected RC elements, the first of which describes the characteristics of the membrane, its interphase boundaries and diffusion layers (denoted by index 1) that have changed as a result of the penetration of wine components, and the second (denoted by index 2) characterizes the layer of wine components on its surface. In the under-limiting current regimes ($0 < i/i_{lim}^{theor} < 1$), R slowly increases with increasing current (fig. 4). At a current close to the limiting value, R increases sharply. An increase in i in the over-limiting current regimes leads to a decrease in R .

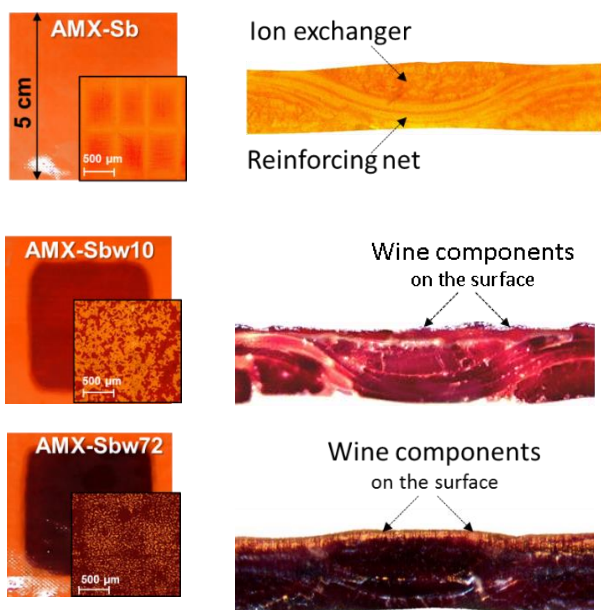


Figure 1. Optical images of surface and cross-sections of swollen samples. The numbers (10 and 72) indicate the time of contact of the membrane with the wine in hours.

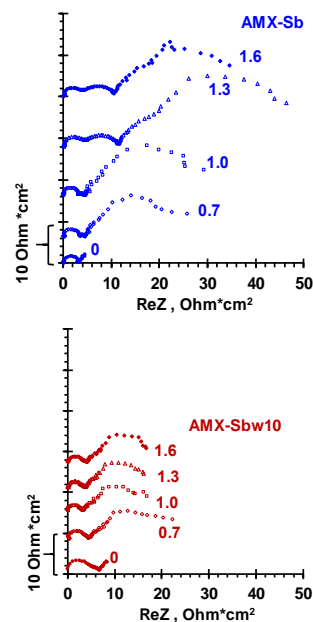


Figure 2. Impedance spectra of AMX-Sb and AMX-Sbw10 membranes. The numbers near the curves denote the values of i/i_{lim}^{theor} .

Such dependence for the under-limiting and close to the limiting currents is mainly determined by changes in the resistance of the DBLs, primarily the depleted DBL. The total ($R_1 + R_2$) resistance of the AMX-Sbw10 contacted with wine is 2 times higher than that of the pristine membrane (fig. 4). The contribution of the resistance of wine components layer on the membrane surface to this total resistance is no more than 15%. In the range $0 < i/i_{lim}^{theor} \leq 1$, the value of R_1 decreases rapidly. At currents close to the limiting one $i = i_{lim}^{theor}$, the values of R_1 become lower than the values of R obtained for the pristine membrane.

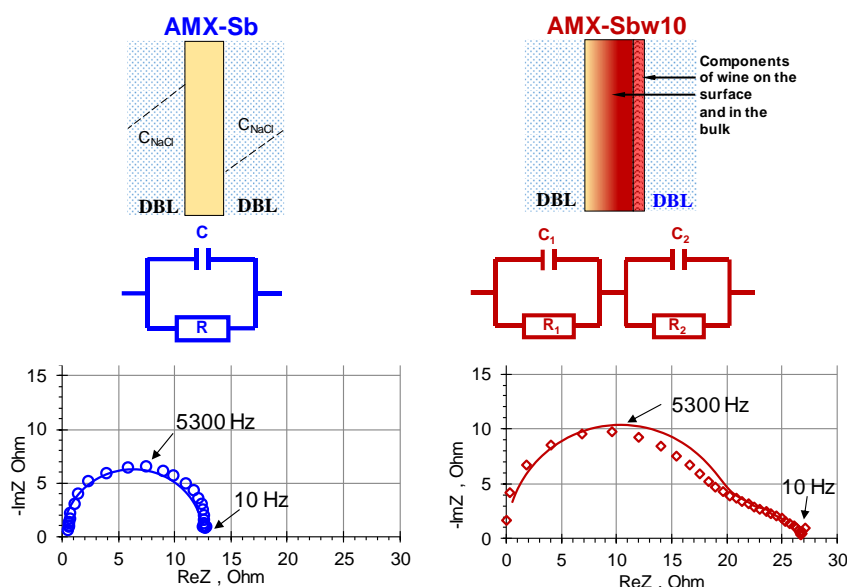


Figure 3. Equivalent electric circuits for membranes AMX-Sb and AMX-Sbw10 and adjacent diffusion layers, as well as high-frequency (10 Hz - 130 kHz) impedance spectra obtained at $i/i_{lim}^{theor} = 0$. Experiment (points); approximation using equivalent circuits (solid line).

At over-limiting current regimes, R_1 gradually increases with increasing current density. The decrease in ohmic resistance R_2 , most likely, is due to a decrease in the thickness of this layer with an increase in the duration of the membrane operation under current. Apparently, under the electric field imposed, anthocyanins, which contain positively charged chromophore groups (flavylium cations) and are retained in the formed layer only due to hydrogen bonds and Van der Waals forces,

move to a negatively charged cathode. The determining factor for reducing the thickness of the layer is the duration of the membrane functioning in the electric field. This factor is more important than the current strength.

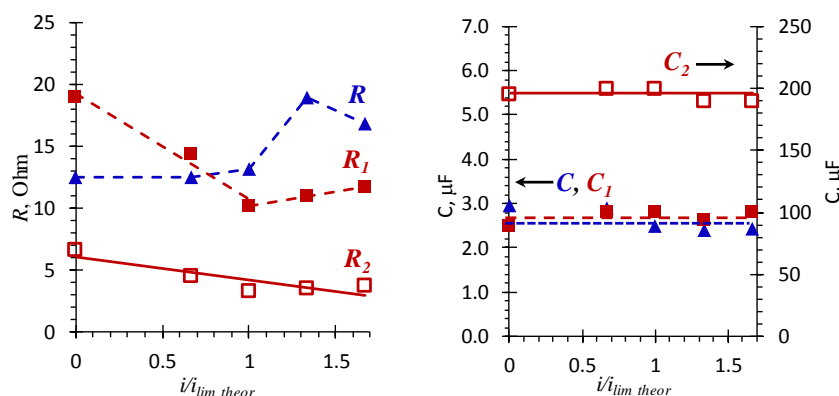


Figure 4. Dependence of the resistances and effective capacitances of the AMX-Sb (R , C) and AMX-Sbw10 (R_1 , C_1 and R_2 , C_2) membranes on the DC current density normalized to the limiting current calculated by the Leveque equation.

The decrease in the resistance R_1 in the under-limiting current modes and its smoother growth in the over-limit current modes in comparison to R are most likely due to the partial destruction of the complex colloidal structures that are formed by the wine components in the pores of AMX-Sbw10. With regard to effective capacities (C_1 , C_2) (fig. 4), their values do not depend on the current density, just as in the case of the initial membrane (C). Moreover, the value of C_1 for AMX-Sbw10 is only slightly higher than C , while C_2 is two orders of magnitude higher. The growth of C_2 , most likely, is due to a significant increase in the roughness factor and the real area of the AMX-Sbw10/solution interface caused by formation of branched colloidal structures with distributed positive and negative charges.

Acknowledgements

We are grateful for financial support to the Russian Foundation for Basic Research (grant No 15-58-16019NCNIL_a).

References

1. El Rayess Y., Mietton-Peuchot M. Membrane Technologies in Wine Industry: An Overview // Crit. Rev. Food Sci. Nutr. 2016. V. 56. P. 2005.
2. Ghalloussi R., Garcia-Vasquez W., Chaabane L., Dammak L., Larchet C., Deabate S.V., Nevakshenova E., Nikonenko V., Grande D. Ageing of ion-exchange membranes in electro dialysis: A structural and physicochemical investigation // J. Membrane Sci. 2013. V. 436. P. 68.
3. Madaeni S. S., Mohamamdi T., Moghadam M. K. Chemical cleaning of reverse osmosis membranes // Desalination 2001. V. 134. P. 77.
4. Berezina N.P., Kononenko N.A., Dyomina O.A., Gnusin N.P. Characterization of ion-exchange membrane materials: Properties vs structure // Adv. Colloid and Interface Sci. 2008. V. 139. P. 3.
5. Sistat P., Kozmai A., Pismenskaya N., Larchet C., Pourcelly G., Nikonenko V. Low-frequency impedance of an ion-exchange membrane system // Electrochim. Acta 2008. V. 53. P. 6380.
6. Nikonenko V., Kozmai A. Electrical equivalent circuit of an ion-exchange membrane system // Electrochim. Acta 2011. V. 56. P. 1262.

THE CORRELATION OF GAS SEPARATION PROPERTIES OF NONPOROUS POLYMERIC MEMBRANES WITH ITS TOPOGRAPHY

Tatyana Sazanova, Alsu Akhmetshina, Artem Atlaskin, Ksenia Otvagina, Ilya Vorotyntsev

Nizhny Novgorod State Technical University n.a. R.E. Alekseev, Nizhny Novgorod, Russia
E-mail: yarymova.tatyana@yandex.ru

Introduction

The creation of high-performance membranes for gas separation is closely associated with different physical, chemical and material science problems [1]. Fundamental research of a structure and membrane functional properties is needed for the solution of those problems.

Now there are a variety of methods for studying polymeric membranes including both physical research and techniques based on a membrane behavior in different conditions and environments [2, 3]. Each of the methods with a variety of advantages and drawbacks has the specific application.

An important task is research the effect of surface topography of polymeric membranes on their gas transport properties, since one of the first stages in gas separation is a contact of gas mixture with a membrane surface.

A membrane surface morphology can be assessed by an atomic force microscopy (AFM) [4-6]. This method is suitable for an investigation of polymeric membranes, not only because of high lateral and vertical resolutions, but also its ability of gaining quantitative three-dimensional information about surface topography, a roughness, a height and a tilt angle of topographic structures without destruction of a soft polymer surface. It is worth noting is that it is necessary to emphasize characteristic parameters of different polymer surfaces during the AFM analysis. For example, for porous membranes, such parameters are porosity and a pore size distribution, and for non-porous membranes, such parameters are a surface structure and its roughness.

However, AFM imaging results alone are not enough to assess the impact of morphological features of polymeric membranes on their transport properties. For studying non-porous polymeric membranes, AFM imaging is useful to combine with a Daynes-Barrer method [7, 8].

In this paper, the AFM combined with the Daynes-Barrer method has been applied to investigate the non-porous polymeric membranes based on polysulfone (PS), which have been casted on substrates with a different roughness.

Experiments

The samples of the polymeric membranes based on polyamide were prepared as follows. The 25 wt. % solution of polyamide in dimethylformamide (DMF) was prepared and applied by curtain coating on glass substrates with a different roughness. One substrate was a standard glass plate, and the other was a glass plate treated with a finely dispersed abrasive. The formation of the polymeric membranes on the substrates was due to evaporation of the solvent under equilibrium conditions at 60 °C for 24 hours. The obtained samples were detached from the substrates in distilled water.

The investigation of the membrane surface morphologies was carried out using the AFM method by a scanning probe microscope SPM-9700 (Shimadzu, Japan). The maximum scanning field was 30 μm. The scans were data arrays with a dimension of 256 × 256 pixels. For checking purposes reproducibility, AFM scanning was carried out on different sites of the studied surfaces.

Before AFM scanning, fragments of the polymer samples were fixed to metal sample discs using adhesive carbon tabs (SPI Supplies Division of Structure Probe Inc., USA) and were cleaned of dust with ethanol.

Since polymeric membranes have a loosely-coupled surface structure, AFM scanning was performed using a tapping mode by silicon vibrating cantilevers POINTPROBE FMR-20 (Nano World Innovative Technologies, USA) with a stiffness coefficient of 1.3 N/m and a typical tip radius of no more than 8 nm (guaranteed - no more than 12 nm), a tip height was from 10 to

15 microns. The experiments were carried out under ambient conditions. Automatic correction of linear noise was applied during scanning.

Digital imaging of the measurement results consisted in representation of topographic maps (heights are reflected by colors) and three-dimensional images. Processing of the obtained AFM images and their analysis were performed by a software SPM Manager ver. 4.02 (Shimadzu, Japan).

Gas transport properties of the polyamide membranes were determined by the Daynes-Barrer method in a constant-volume variable-pressure apparatus for gas permeability measurements at an operating pressure of 0.11 MPa. The permeate pressure variation was recorded with a sampling rate of 10 ms. Analyzed gases were helium (He) and methane (CH₄). Each single-gas test was repeated at least three times.

Physicomechanical properties of the membranes (namely, values of a breaking stress (σ) and elasticity (ϵ)) were determined on a universal test machine Zwick Z005 (Zwick Roell, Germany) at a pulling speed of 50 mm/min.

Results and discussion

According to the scanning results, an arithmetic average roughness height (R_a) and a mean roughness depth (R_z) were obtained. A base length (a length of a line used for unevennesses selection) was 10 μm (Table 1). These data indicate that the surface topography of the obtained membranes is directly proportional to the surface roughness of the substrates. At that, the surface character remains constant (Figure 1).

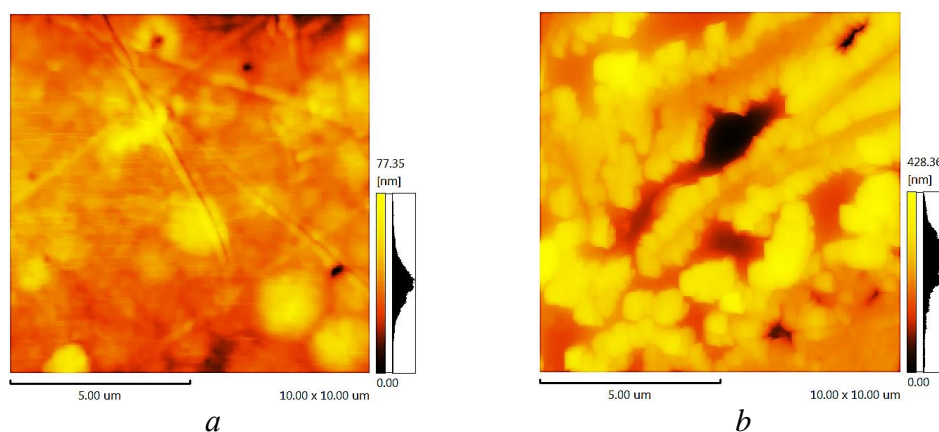


Figure 1. The AFM images of the polyamide membranes casted on: a) the standard glass plate; b) the glass plate treated with an abrasive

The comparative analysis of the AFM results and the gas transport properties (Table 1) shows that the permeability coefficient (P) of the «rough» sample is almost 7 times more than one of the «smooth» sample, and the selectivity (α) of both sample remains constant. The growth of the permeability coefficient can be explained by the fact that a real working area (and, as a consequence, a contact area of a membrane with gas mixture) increases with increasing roughness of a membrane surface. The consistency of the membranes selectivity is confirmed by the fact that selective properties of non-porous polymeric membranes depend only on physicochemical properties of a polymer.

Table 1: Parameters of the polyamide membranes

Substrate	R_a , nm	R_z , nm	P, Barrer		α	σ , MPa	ϵ , %
			He	CH ₄			
«Smooth»	7.07 ± 0.01	34.4 ± 0.01	4 ± 0.009	1 ± 0.007	4 ± 0.007	32.28	1.91
«Rough»	52.81 ± 0.02	207.1 ± 0.02	26.5 ± 0.14	6.8 ± 0.07	3.9 ± 0.005	30.03	1.74

In addition, it is worth noting is that the comparative analysis of the AFM results with the physicochemical parameters shows that the breaking stress and the elasticity slightly decrease with increasing the roughness (Table 1).

Thus, it is possible to control a permeability coefficient of non-porous polymeric membranes without change of selectivity and physicochemical properties by varying their surface roughness.

This work was financially supported by Russian Science Foundation, project 15-19-10057.

References

1. Wang Sh., Li X., Wu H., Tian Zh., Xin Q., He G., Peng D., Chen S., Yin Y., Jiang Zh., Guiver M.D. Advances in high permeability polymer-based membrane materials for CO₂ separations // *Energy & Environmental Science*. 2016. V. 9. P. 1863-1890.
2. Agarwal C., Pandey A.K., Pattyn D., Ares P., Goswami A., Cano–Odena A. Neck-size distributions of through-pores in polymer membranes // *Journal of Membrane Science*. 2012. V. 415-416 (1). P. 608-615.
3. Mulder, J. Basic principles of membrane technology, Kluwer Academic Publishers, Dordrecht, The Netherlands, 1996.
4. Sazanova T.S., Vorotyntsev I.V., Kulikov V.B., Davletbaeva I.M., Zaripov I.I. An atomic force microscopy study of hybrid polymeric membranes: surface topographical analysis and estimation of pore size distribution // *Petroleum Chemistry*. 2016. V. 56 (5). P. 427-435.
5. Akhmetshina A.I., Davletbaeva I.M., Grebenshikova E.S., Sazanova T.S., Petukhov A.N., Atlaskin A.A., Zaripov I.I., Vorotyntsev I.V. Supported ionic liquid membranes based on microporous polymers for hazardous gasses removal // *Membranes*. 2016. V. 6 (1). № 4.
6. Otvagina K.V., Mochalova A.E., Sazanova T.S., Petukhov A.N., Moskvichev A.A., Vorotyntsev A.V., Afonso C.A.M., Vorotyntsev I.V. Preparation and characterization of facilitated transport membranes composed of chitosan-styrene and chitosan-acrylonitrile copolymers modified by methylimidazolium based ionic liquids for CO₂ separation from CH₄ and N₂ // *Membranes*. 2016. V. 6 (2). № 31.
7. Daynes H.A. The process of diffusion through a rubber membrane // *Proceedings of The Royal Society a Mathematical, Physical and Engineering Sciences*. 1920. V. 97 (685). P. 286-307.
8. Barrer R.M., Rideal E.K. Permeation, diffusion and solution of gases in organic polymers // *Transactions of the Faraday Society*. 1939. V. 35. P. 628-643.

INVESTIGATION OF ION BIOCIDAL ACTIVITY OF CHITOSAN MEMBRANES

Valentin Sedelkin, Dmitry Cherkasov, Olga Lebedeva

Engels Technological Institute of Yuri Gagarin State Technical University of Saratov, Engels, Russia

E-mail: sedelkinvm@mail.ru

Introductions

Chitosan is derived from chitin, a polysaccharide complex by partial or total deacetylation it is a promising raw material for the manufacture of semi-permeable barofiltration membranes. Attractiveness of chitosan is the fact that due to the presence of a large number of functional groups with the polar activity it is relatively easy to modify the physico-chemical, has a good balance of hydrophilic and hydrophobic properties, molding enables to produce solutions at a sufficiently large number of inexpensive solvent, has a high film-forming properties. Furthermore, chitosan under certain conditions can have an inhibitory antibacterial, antifungal and antimycotic action, which further increases its attractiveness as a raw material for producing the membrane products.

The biocidal activity of chitosan-based products is dependent on a number of factors: the molecular weight, degree of deacetylation, the polymer concentration in the spinning solution, and species of microorganism and other. It is currently believed that the biocidal activity of chitosan is mainly caused by the action of positively charged free amino groups NH_3^+ , appearing in media with acidic pH values, on the negatively charged surface structure of microbial cells, which leads to disruption of normal metabolism with the surrounding cell environment and inhibiting their development. With the penetration of macromolecules and supramolecular structures of chitosan into the microorganisms is also possible interaction of these structures with the various components of the cytoplasmic contents of the cells of microorganisms, leading to their death. Thus, chitosan, unlike classical biocidal substances has not only a target for their action, and its antibacterial, antifungal and antimicrobial effects are a set of several possible mechanisms of developing in a complex process that leads ultimately to the death of the pathogenic microbial cells. An important prerequisite for the determination of biocidal activity of chitosan-based products is the availability of reliable physical and chemical characteristics of the polymer and the detailed methodology for biological experiments.

Experiments. Results and Discussion

This paper presents the results of a study of chitosan membrane biocidal activity against Gram-negative bacteria *E.coli*. Membranes were formed from solutions of chitosan in acetic acid and water of varying concentrations. In the experiments it was used chitosan derived from crab chitin chemical (alkaline) method. The molecular weight of chitosan $\text{MW} = 420$ kDa, and the degree of deacetylation $\text{SD} = 80\%$.

Disco-diffusion method (DDM) was used to study membranes biocidal activity. Due to technical availability, flexibility and low cost of testing the DDM is the most common method for determining the sensitivity of microorganisms to biocidal agents. In determining the sensitivity of the DDM method to the surface of agar Petri dishes coated, which is a breeding ground for microorganisms. Then, on the agar surface by seeding the grass (with a spatula) was applied to the suspension of the test microorganism. After that, the disk samples was placed lawn chitosan membranes. Diffusion of chitosan in layer agar seeded with microorganisms in the formation zone resulting in the suppression of growth around the test microorganism membrane disk samples. The result is taken into account largest diameter of microbial growth inhibition zone around the disc, measured in millimeters, as shown in Fig. 1. The sensitivity of the bacterial culture to the chitosan assessed after measuring the diameters of the sterile zones according to Table 1.

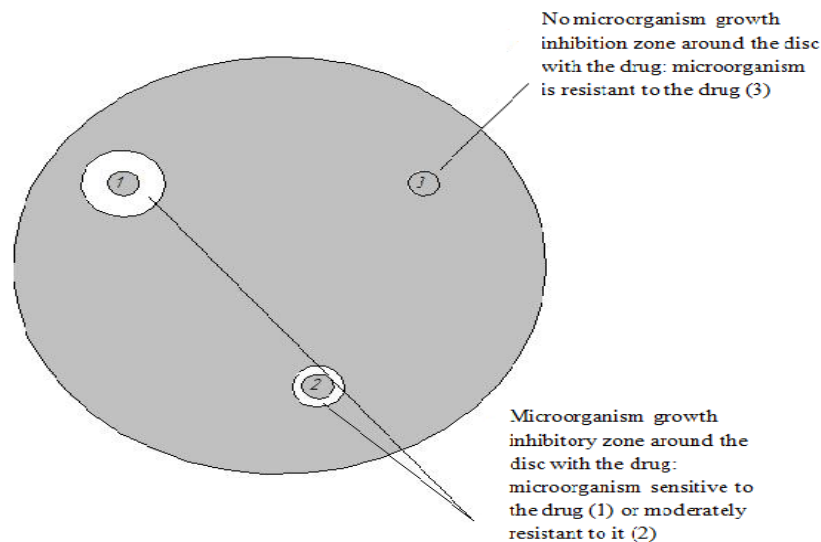


Figure 1. Disco-diffusion method for applying the product to the environment

Table 1: The degree of sensitivity to the drugs by zones of growth retardation

The diameter of the growth inhibition zone, mm	The degree of sensitivity
0	Stable
1 – 15	are unstable
16 - 25	Sensitive
More than 25	highly sensitive

Fig. 2 shows the results of the sensitivity study E.coli bacteria to membranes made from solutions of acetic uisloty and water with a concentration chitosan 2 and 4 wt. %.

The results showed that the studied microorganisms exhibit a high sensitivity to be used for the manufacture of high molecular chitosan membranes.

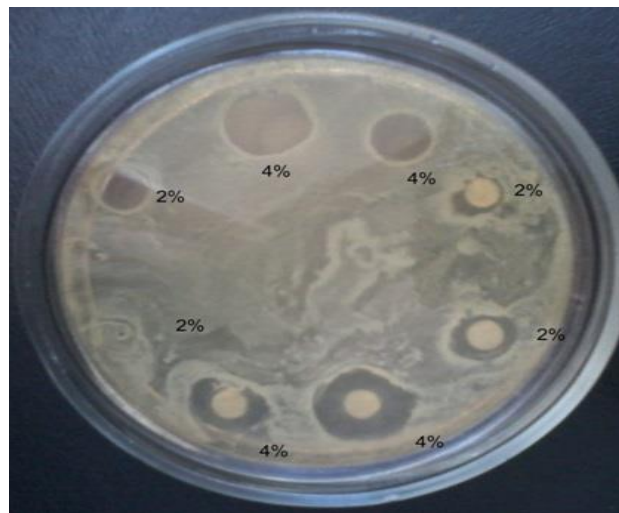


Figure 2. Zone of growth inhibition at concentrations of 2% chitosan solution and 4%

To determine the biocidal activity of chitosan membrane was used as the serial dilution method for assessing the minimum bactericidal concentration of chitosan in the test sample. When conducting experiments using the method of serial dilutions in agar chitosan should be carried out on the culture growth control Petri dish with nutrient medium containing no antibacterial drugs. The most important requirement is that quality control seeding was used to inoculate the suspension on solid non-selective medium to confirm culture purity. In our experiments, each batch of tested strains was accompanied by an internal quality control studies using appropriate control (reference) strains.

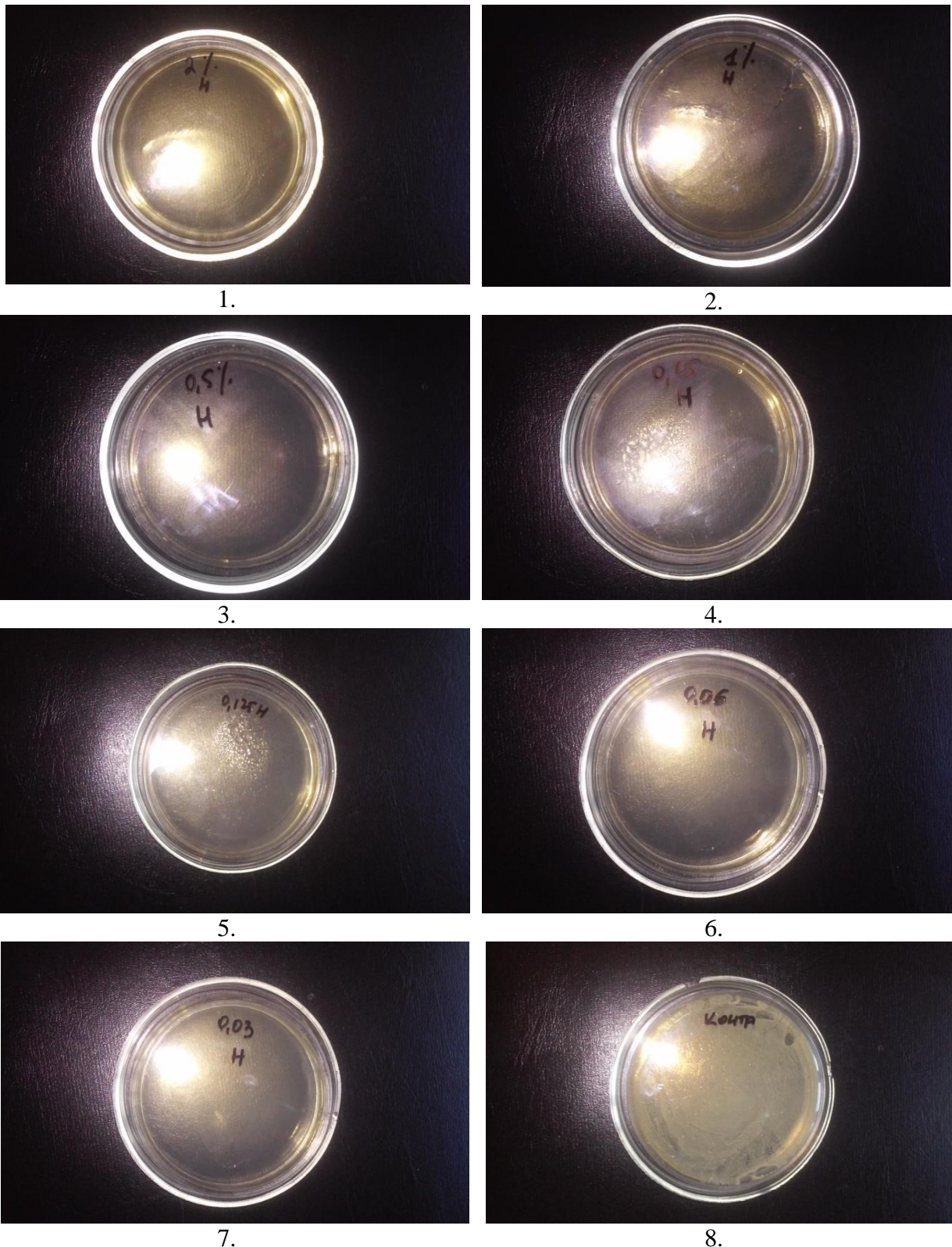


Figure 3. Study of bactericidal activity of chitosan solution at a concentration of: 1) 2.0%; 2) 1.0%; 3) 0.5%; 4) 0.25%; 5) 0.125%; 6) 0.06%; 7) 0.03%; 8) control.

Conclusion

Results from studies using the serial dilution method shown in Fig. 3. An analysis of the experimental data showed that the minimum concentration of chitosan in the spinning solution, the overwhelming visual E.coli growth is 0.03%.

AMORPHOUS-CRYSTALLINE STRUCTURE OF THE FILTRATION MEMBRANE MADE OF A CHITOSAN IN SALT AND THE BASIC FORM

Valentin Sedelkin, Olga Lebedeva, Dmitry Cherkasov

Engels Technological Institute of Yuri Gagarin State Technical University of Saratov, Engels, Russia
E-mail: sedelkinvm@mail.ru

Introduction

Chitosan membrane made by casting a chitosan solution on various solid substrates (glass, plastic, fabric, Teflon). Thus in the initial chitosan powder feed is in the base form, then proceeds by dissolving chitosan in the salt form (salt form depends on the type of solvent used), and which is retained in fresh-formed membrane. After treatment with alkali chitosan salt membrane passes into the main form and the membranes are insoluble in water.

Obviously, the amorphous-crystalline structure of the chitosan membrane as well as their operating characteristics (permeability and selectivity), will depend on the structure of the source of chitosan, the nature of the solvent and conditions of the membrane (basic or salt form of chitosan). It is therefore of considerable scientific interest in the identification of changes in amorphous-crystalline structure in the chain: raw chitosan - spinning solution - gel casting chitosan acetate (chitosan in salt form) - redeposition in alkali salt membrane (chitosan in basic form).

Experiments. Results and Discussion

The report presents the results of the study of amorphous-crystalline characteristics of chitosan and its solutions made of water and acetic acid for saline and alkaline membranes.

For barofiltration chitosan membranes in this study it was used crab air-dried chitosan with a molecular weight $MW = 420$ kDa and a deacetylation degree of 0.8, which is obtained from chitin, released from the shell of walking limbs Kamchatka king crab.

A study of amorphous-crystalline structure of chitosan membranes derived therefrom was carried out by diffractometer method on diffractometer "DRON-3" at the angles 2θ of 2 to 40° with automatic recording on a personal computer in the geometry of reflection. Of the radiation $CuK\alpha$ ($\lambda = 1,54\text{\AA}$). Providing monochromatic carried Ni-filter.

Figure 1 shows the diffraction pattern captured with the pelletized sample of powdered crab chitosan with $MW = 420$ kDa and $SD = 0.8$.

It can be seen that the diffraction pattern is an amorphous halo, where you can select a strong reflection peak at angle $2\theta = 19,35\text{\AA}$ and three weak diffuse reflections with maxima at angles 2θ equal to 21.77; 28.5 and 33.4 degrees.

Figures 2 and 3 show diffractograms of the two air-dried chitosan membranes prepared from 2% solutions of chitosan in the 2% aqueous acetic acid irrigation method on a glass substrate.

As seen in Figure 2, which shows the diffraction pattern for a membrane with chitosan in salt form curve of intensity X-ray scattering includes four crystalline sufficiently strong reflections with peaks at angles 2θ 8,58; 11,56; 18,25 and 22,89 $^\circ$ and four weaker blurry reflections with peaks at angles 2θ 16,19; 20,31; 25,68 and 29,9 $^\circ$. In the diffractogram for the membrane, which was transferred from a salt form by treating the basic with 10% aqueous NaOH solution for 8 hours and subsequent washing with water until neutral, and found four crystalline sufficiently strong

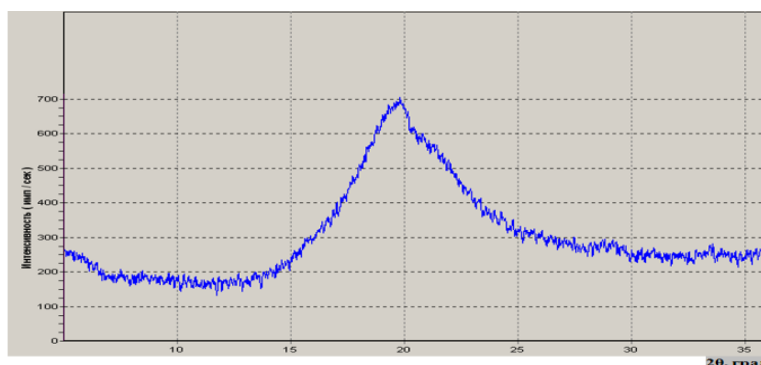


Figure 1. Diffraktogramma chitosan crab. $MW = 420$ kDa; $SD = 0.8$. Chitosan air-dry



Figure 2. The XRD pattern of chitosan film in salt form. $MMhtz = 420$ kDa, $SD = 0.8$. Composition spinning solution: $Shtz = 2$ wt%, $Suk = 2$ wt%, $CH_2O = 96$ wt%. Film air-dry

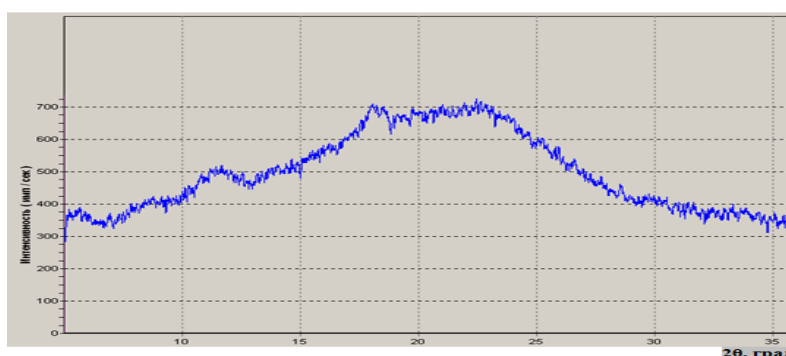


Figure 3 - The XRD pattern of chitosan film in basic form (reprecipitation NaOH solution). $MMhtz = 420$ kDa, $SD = 0.8$. Composition spinning solution: $Shtz = 2$ wt%, $Suk = 2$ wt%, $CH_2O = 96$ wt%. Film air-dry

reflections with peaks at angles 2θ 8, 7; 11.43; 18.08 and 22.9 °, and four low-intensity diffuse reflections with peaks at angles 2θ 15,44; 20.34; 25,69 and 29,97 ° (see. Figure 3).

Comparative analysis of the three diffraction patterns in Fig. 1-3, they showed significant differences in the intensity of X-ray scattering, and the number of the angular position of the crystal reflections half-width of the peak.

Common to all of the samples studied is that in their matrix contains two phases - crystalline and amorphous. To determine the quantitative ratio of these phases (degree of crystallinity K), as well as the main parameters of the chitosan is in calculations values of K samples were conducted, as well as full-profile analysis (PPA) curves intensity X-ray scattering.

The values of the degree of crystallinity were equal to 0.5; 0.14 and 0.175 respectively for the original chitosan salt and alkaline membranes. Thus, in the processes of dissolving chitosan in solvent of water and acetic acid and subsequent molding of saline solution, and then the membrane is rearranged alkaline amorphous-crystalline structure of the chitosan samples.

The report examines the mechanism and stages of restructuring amorphous-crystalline structure of the polymer matrix in the chain: the initial chitosan - its swelling and dissolution - forming a membrane from the solution with a fresh matrix of chitosan acetate membrane -reprecipitation salt with alkali chitosan in the transfer base form.

On the basis of full profile analysis of the scattering of the radiation intensity curves calculated changes in the values of these parameters of the structure of the original chitosan and chitosan membrane as the half-width of the peak of the crystalline reflex β (deg), the crystallographic lattice spacings d (Å), the dimensions of the crystallites Lcr . (Å).

Conclusion

Thus, it is found that the diffraction patterns of all the samples for a large half-width of the peaks are different, indicating that the small size of the samples contained in these crystallites. The calculated values Lcr all samples are located within the range of 14 to 38 Å, indicating that the structure of microcrystalline chitosan and studied membranes made of it.

STABILITY OF BROMATE ANION IN STRONGLY ACIDIC SOLUTIONS

^{1,2}Olga Sereda, ¹Natalia Sherstneva, ^{1,3}Dmitry Konev, ^{1,2}Anatoly Antipov,
^{1,2,3,4}Mikhail Vorotyntsev

¹D. I. Mendeleev University of Chemical Technology of Russia, Moscow, Russia

²M. V. Lomonosov Moscow State University, Moscow, Russia

³Institute of Problems of Chemical Physics, Russian Academy of Sciences, Chernogolovka, Russia

⁴ICMUB, UMR 6302 CNRS-Université de Bourgogne, Dijon, France

E-mail: mivo2010@yandex.com

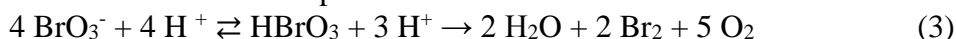
The electroreduction process of the non-electroactive bromate anion via autocatalytic cycle composed of the electrochemical Br₂-to-Br⁻ transformation:



and the comproportionation reaction between BrO₃⁻ and Br⁻ anions:



is prospective for applications in a broad variety of electrochemical energy sources. Necessary conditions for performing such a process are the reversibility of the electrode process in combination with irreversibility of the comproportionation reaction. The latter requires for the bromate solution to be strongly acidic. At the same time the bromic acid has got a tendency to a chemical decomposition. It is why it is of importance for the practical applicability of the bromate electroreduction process inside electric energy sources to establish the relation between the acidity of the bromate solution and its rate of its decomposition:



depending on the composition of the solution, primarily on its pH.

The concentration of bromine in solution is often determined electrochemically, via its diffusion-limited reduction current. However, this method cannot be used in the presence of a high concentration of bromate, since the reduction of bromine is accompanied by the reduction of bromate owing to the comproportionation reaction, Eq (2) [1].

Therefore, spectroscopy in the UV-visible range was used as the main method for controlling the bromine concentration in solution, since this substance in the aqueous solution possesses an intensive characteristic absorption band with a maximum near 400 nm.

In a series of calibration experiments, aqueous solutions were prepared by mixing of three components inside their aqueous solutions: 1 M NaBrO₃ + 1M H₂SO₄ + x mM NaBr, where the amount of bromide added varied from x = 5 to x = 20. Due to the rapid comproportionation reaction, Eq (2), and excess of bromate acidic bromate solutions containing bromine of concentrations from 3 to 12 mM is produced.

Fig. 1a shows the spectrum of the mixed solution after such addition of 10 mM NaBr, which corresponds to 6 mM Br₂ after termination of reaction (2), in comparison with spectra of individual components at the same concentrations. Sulfuric acid and bromide do not absorb markedly in the wavelength range above 250 nm, whereas one can see a rapidly growing branch in the region below 320 nm in the bromate spectrum, which makes impossible to perform measurements in the bromate-containing solution below 260 nm.

In the wavelength region above 320 nm none of these substances absorbs the light so that the observed band with maximum at 392 nm refers to bromine< in conformity with the literature data.

This assignment of the band agrees with its dependence on the bromine concentration in the mixed solution (Fig. 1b), the maximum absorption (at 394 nm) being proportional to Br₂ concentration.

The extinction coefficient at 394 nm (about 170 M⁻¹ cm⁻¹) determined from these data agrees with literature data. The intensity of absorption in 0.01 corresponds to the bromine concentration of about 0.06 mM, i.e. this method of monitoring of Br₂ is convenient and sufficiently sensitive for our needs.

To study the stability of bromate anion in sulfuric acid where a certain amount of undissociated bromic acid, HBrO₃, is inevitably formed at a high concentration of added acid,

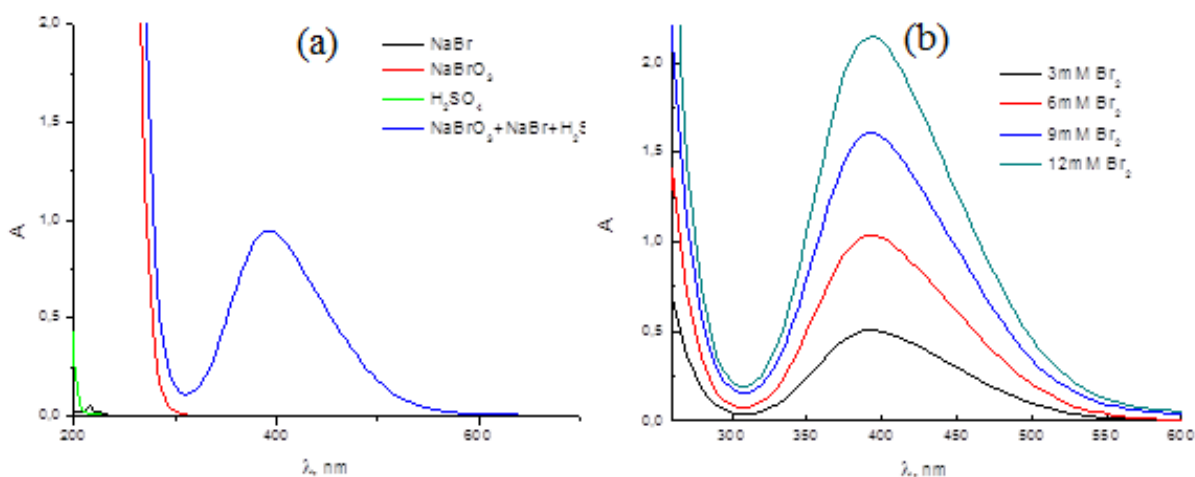


Figure 1. (a) Absorption spectrum of the aqueous solution (blue line) formed by mixing solutions of bromate, sulfuric acid and bromide (final concentrations: 1M, 1M and 10 mM, respectively). Spectra of these individual substances for the same concentrations are also shown. (b) Spectra of mixed solutions in the 260 - 600 nm range for a series of mixed solutions with bromine concentrations from 3 to 12 mM. Optical path length: 1 cm

evolution of the spectra of mixed solutions of 0.5 M sodium bromate and of sulfuric acid (for its various concentrations) in time was studied, by the spectrum recording every 10 minutes.

First series of such measurements was performed for 1 M H₂SO₄. No formation of noticeable amounts of Br₂ was registered. Therefore, we can conclude that decomposition of bromate in 0.5 M NaBrO₃ + 1M H₂SO₄ solution practically does not occur for at least one hour.

Fig. 2a demonstrates results for the 2 M H₂SO₄. One can note that the branch of intensive absorption within the wavelength region below 300 nm has shifted noticeably to the right. This effect can be attributed to a significant increase in the concentration of non-dissociated acid, HBrO₃, due to the pH shift in the negative direction. At the same time there is no increase of absorption in the range near 400 nm (Fig. 2a) where absorption of dissolved bromine is expected (Fig. 1), no change of the initial spectrum in time is observed. Thus, one can conclude again of no decomposition of bromate in 0.5 M NaBrO₃ + 2M H₂SO₄ solution at the time scale of about one hour.

The change in the spectrum of the mixed solution with increase of sulfuric acid concentration, compared to those for lower acidities (Figs. 1 and 2a), i.e. a shift of the short-range absorption branch immediately after mixing, becomes even more pronounced for the 3M solution (Fig. 2b). Besides, absorption band of low intensity near 400 nm appears at the time scale of about one hour after mixing the solutions. After exposure for about one day, the bromine concentration has increased to about 10 mM concentration (Fig. 2b).

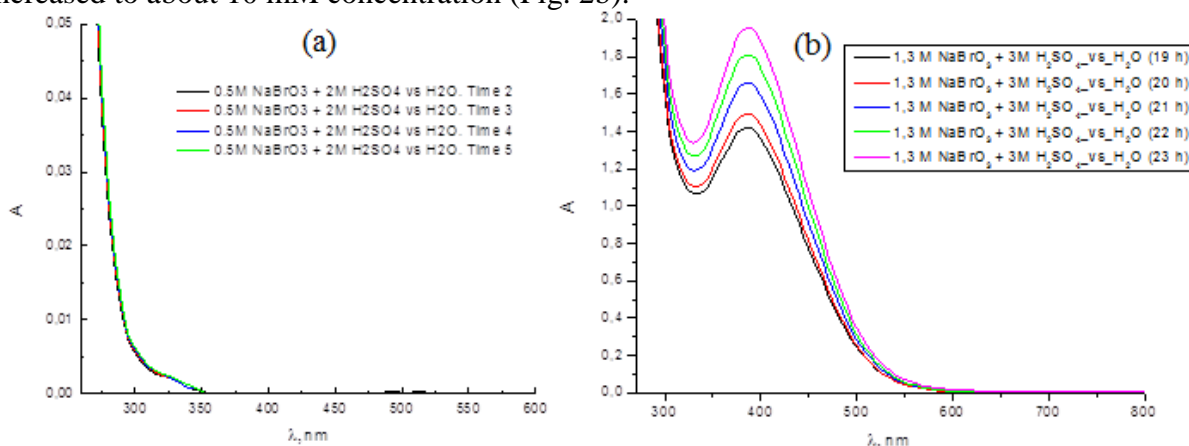


Figure 2. (a) Evolution of the spectrum of a mixed aqueous solution of 0.5 M NaBrO₃ + 2 M H₂SO₄ in time (recorded every 10 minutes). (b) Spectra of a mixed aqueous solution of 1.3 M NaBrO₃ + 3 M H₂SO₄ after exposure for 19 to 23 hours after mixing.

As a whole one can conclude that bromate anion remains chemically stable in strongly acidic solutions, i.e. up to 3 M sulfuric acid for the time interval of one hour, and up 2M sulfuric acid for the time interval of 24 hours.

Acknowledgements

Supported by the Russian Science Foundation (grant 15-13-20038).

References

1. *Vorotyntsev M. A., Konev D. V., Tolmachev Y. V.* *Electrochim. Acta.* 2015. Vol. 173. P. 779–795.

SUPRAMOLECULAR CHEMISTRY OF ION EXCHANGE MEMBRANES

Vladimir Shaposhnik

Voronezh State University, Russia, E-mail: v.a.shaposhnik@gmail.com

Henri Poincare wrote that it is difficult to imagine what a huge economy of thought can be effected by a *well-chosen* word, and this word may become a creator. Among these well-chosen words is supramolecular chemistry, the term introduced by Nobel Prize Laureate in Chemistry Jean-Marie Lehn [1]. The essence of supramolecular chemistry is the synthesis of the traditional molecular chemistry based on the combination of atoms into molecules by a covalent bond with the chemistry in which intermolecular bonds play an essential role.

Ion exchangers in the form of membranes, as well as in the form of granules are supermolecules, since they comprise a stable polymer matrix with covalent bonds and a labile part of hydrated counter-ions. Both the ion exchange and the membrane transport are possible only if there is a labile component of the supermolecule. The most wide-spread type of ion exchangers is a strongly acidic sulfo cation exchanger, and among the ion-exchange membranes the cation exchange membrane made on its basis. Fig. 1 shows a portion of the cation exchanger KU-2, which we calculated using ab initio quantum chemistry LCAO MO method [2]. The left side of the figure shows a portion of polystyrol which represents a stable part of the supermolecule in which carbon, hydrogen and sulfur atoms are joined by strong covalent bonds. The quantum chemistry methods allow one to calculate most accurately the internuclear distances, and the shorter the distance, the stronger the covalent bond. In the benzene molecule the bonds C-H 1.09 Å calculated by us are in good agreement with the experimental bond lengths measured by the X - ray diffraction method [3]. There is an accurate agreement between the calculated and experimental aromatic C-C bonds (1.39 Å) and C-S sulphur bonds (1.82 Å). Ion - dipole distances between the sodium counter-ion and oxygen atoms of the first hydration layer have the calculated values of 2.10 Å and indicate the presence of a strong bond.

In the labile part of supermolecules of ion exchangers the atoms are joined by ionic, coordination and hydrogen bonds. While investigating the structures of cation exchange membranes in the form of alkali metals we have obtained a paradoxical result: the chemical ionic bonds had much larger internuclear distances than the hydrogen ones formed by hydrogen and oxygen atoms of hydrated water molecules. In particular, for the sodium form of sulfo cation exchange membrane the length of the hydrogen bond 2.57 Å was close to the hydrogen bond in free water, while the ionic bond had an average internuclear distance of 4.84 Å, which indicates a greater strength of intermolecular hydrogen bond in comparison with the ionic bond. This is caused by the fact that upon hydration of contact ion pairs between the counter ions and fixed ions the water molecules intrude increasing the distance between the ions and the dielectric permittivities. According to Coulomb's law, this results in the weakening of the electrostatic interaction between counter-ions and fixed ions. One can draw an analogy with the role of the hydrogen bond in the most important natural compounds (water, proteins, RNA, DNA, etc.). With increasing charge of the counter-ions the electrostatic interaction between the fixed ions and counter-ions increases. For three-charge cations the energies of ionic and hydrogen bonds become nearly equal. The increase in electrostatic interaction results in the increase in the activation energies and the reduction of the ion fluxes, as we have shown theoretically and experimentally [4,5]. The four-charge ions are irreversibly sorbed by fixed ions and the membrane alters the charge sign of the fixed ion.

Man did not invent a membrane, but borrowed the ready-made idea from nature. Biological membranes, due to protein ion channels, have an ideal selectivity with respect to ions. The ion channels researchers have been awarded the Nobel Prizes in chemistry, even though the primary structure of protein has not been deciphered. There is a possibility of grafting into channels of macroporous ion-exchange membranes of amino acids and thus to carry out protein synthesis using R. Merrifield method. This will make it possible to solve the problem of synthesis of ideally

selective membranes in potentiometry as well as selectively extract ions during electro dialysis. A selective extraction of sodium from sea and brackish waters can serve as an example.

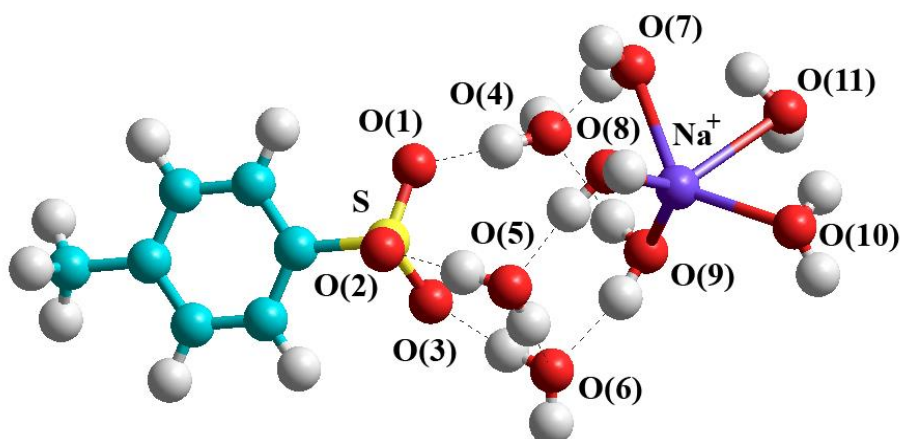


Fig. 1. The structure of the fragment of sulfo cation exchange membrane in the form of sodium ions calculated by LCAO MO method.

Man did not invent a membrane, but borrowed the ready-made idea from nature. Biological membranes, due to protein ion channels, have an ideal selectivity with respect to ions. The ion channels researchers have been awarded the Nobel Prizes in chemistry, even though the primary structure of protein has not been deciphered. There is a possibility of grafting into channels of macroporous ion-exchange membranes of amino acids and thus to carry out protein synthesis using R. Merrifield method. This will make it possible to solve the problem of synthesis of ideally selective membranes in potentiometry as well as selectively extract ions during electro dialysis. A selective extraction of sodium from sea and brackish waters can serve as an example.

One of the major problems that today seem unrealistic is the synthesis of living organisms. However, this task cannot be called fundamentally unsolvable. D. Haldane argued [4] that the critical moment, which can be called the origin of life, was when several different self-replicating polymers inside a semi-permeable membrane became isolated. The gene and catalytic mechanisms will not function if the substances with a small molecular weight that serve as substrates and precursors will not be held by a membrane and this membrane cannot be inert.

References

1. *Lehn J.-M.* Supramolecular Chemistry, Weinheim, N.Y., Basel, Cambridge, Tokyo, VCH Verlagsgesellschaft mbH, 1995.
2. *Shaposhnik V.A., Buturskaya E.V.* Computer Simulation of Cation-Exchange Membrane Structure // Rus.J. Electrochem. Soc., 2004, V.40. P. 880-883.
3. *Gordon A., Ford R.* A Handbook of practical Data, Techniques and References, John Wiley & Sons, N.Y., 1972.
4. *Badessa T.S., Shaposhnik V.A.* The electro dialysis of electrolyte solutions of multi-charged cations // J. Membr.Sci. 2016. V.498. P. 86-93.
5. *Badessa T.S., Shaposhnik V.A.* Electrical conductance studies on ion exchange membrane using contact-difference method // Electrochimica Acta. 2017. V.211. P. 453-459.
6. *Haldane J.* The origin of life, New Biology, 16 (1954) 12

IONS' TRANSPORT THROUGH ION EXCHANGE MEMBRANES IN THE SYSTEMS USED TO OBTAINING ORGANIC ACIDS AND BASES BY BIPOLAR ELECTRODIALYSIS

Nikolay Sheldeshov, Konstantin Lebedev, Victor Zabolotsky
 Kuban State University, Krasnodar, Russia, E-mail: sheld_nv@mail.ru

Bipolar ion-exchange membranes produced in industrial scale, helped to create the electro dialysis processes are capable of competing with membrane electrolysis [1-4]. Electro-membrane methods of obtaining acids, alkalis and bases with the use of bipolar membranes from the respective salts and water by the reaction $CatAn + H_2O = CatOH + HAn$ have a lot of advantages in comparison with classical electrochemical methods. During the flow of electric current through a bipolar membrane it produces hydrogen and hydroxyl ions $H_2O = H^+ + OH^-$ transporting into the solutions surrounding the bipolar membrane (Figure 1).

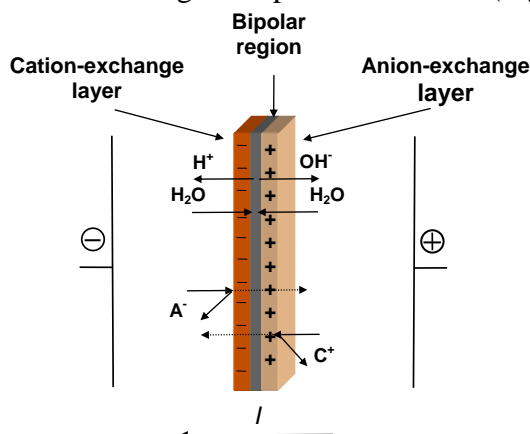


Figure 1. The main processes occurring in the bipolar membrane when electric current is passing

To obtain a weak organic acids, two-compartment unit cell formed by the bipolar membrane and cation-exchange membrane are used (Figure 2). In such a cells solution of the weak acid salt is enter in the acid chamber so its electrical resistance is small as it contains a mixture of salt and weak acid. The process is carried out so that at the end of the process the acid solution contains the small amount of salt, providing sufficient conductivity of the solution. Concentration of organic acids is limited only by its solubility. In the same way, weak bases may be produced, but in this case instead of cation-exchange an anion-exchange membrane is used. Current efficiency of weak organic acids and weak organic bases during electro dialysis synthesis from the corresponding salts is always less than 100%. It is due to the imperfect selectivity of the bipolar and cation-exchange (anion-exchange) membranes, which leads to "leaks", losses of ions and molecules in the adjacent chambers.

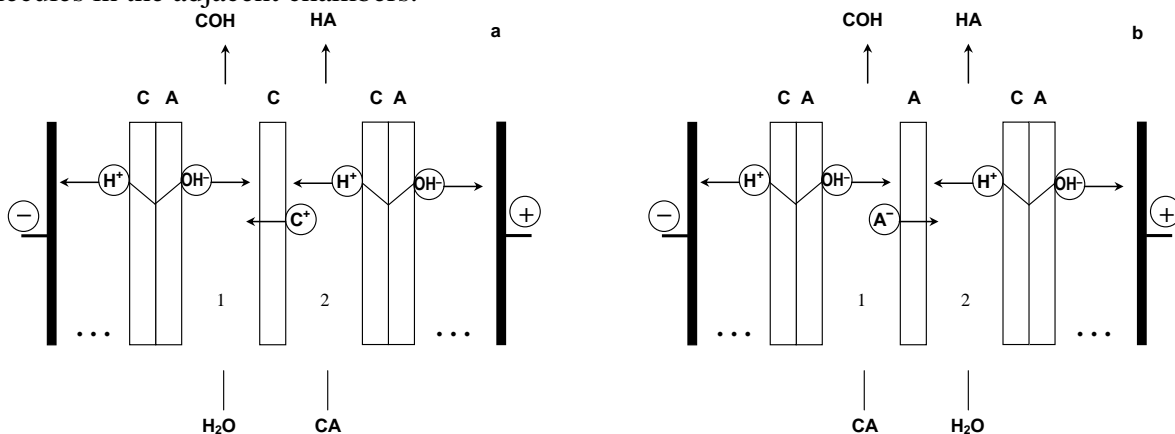


Figure 2. Schematic drawing of two-compartment unit cells for producing weak acids (a) and weak organic bases (b)

Currently there are only a few studies in which the flow of ions and molecules through the membrane (bipolar, cation and anion exchange) in the solutions used for the synthesis of organic acids and bases during the flow through the membrane electric current are measured. This is probably due to, on the one hand, the experimental difficulties of studying the transport of ions and molecules across membranes in a multicomponent, asymmetric chemical composition systems containing on opposite sides of the membrane solutions of salts and alkalis, or salt solutions and mineral acid. On the other hand, some difficulties arise in the mathematical description because of the spontaneous occurrence in such systems of reaction layers, in which chemical reactions run, regions of space charge which further complicate the mathematical description of the membrane system.

To calculate the local values of the flow of ions and molecules in membranes and the diffusion layers the mathematical model, which is based on the equations of Nernst – Planck is formulated. Chemical reactions occurring in the membrane and diffusion layers are described by equations of chemical kinetics. At interfaces of the membrane system the local equilibrium is taken into account and Donnan and Nikolsky equations are used.

The results of calculations on mathematical model are discussed. It is shown that the current efficiency of produced acid (base) is dependent on the initial concentration of salt in solution, the concentration of produced alkali (mineral acid) in this process and the concentration of weak organic acid (weak organic base). An important characteristic of such membrane systems is the voltage drop across each membrane and the system as a whole. This value also depends on many factors, including the dissociation constant of weak organic acids or bases, the charge of the anion (cation), the size of the ion and the molecules, which increases with increasing molar mass of the particles, the specific interaction between ions and molecules of acids and bases with the polymer contained in the membrane. Relationship between the thermodynamic and kinetic characteristics of organic acids and bases molecules, and electrochemical characteristics of membrane systems, in particular, the effective transport numbers of ions and molecules through the membrane and voltammetric characteristics of membranes is an extremely important task. This relationship influences on the main parameters of synthesis of organic acids and bases from their salts. The structure of the reaction layers formed in the diffusion layers and local fluxes of ions and molecules in membrane systems are discussed.

Study was supported by Russian Foundation for Basic Research, research project № 17-08-01689.

References

1. Handbook in Bipolar Membrane Technology, Kemperman, A.J.B. (Ed), Enschede : Twente University Press, 2000.
2. *Pourcelly G.* Electrodialysis with bipolar membranes: principles, optimization, and applications // *Russ. J. Electrochem.* 2002. V. 38. P. 919–926.
3. *Xu T.* Electrodialysis processes with bipolar membranes (EDBM) in environmental protection – a review // *Resources, Conservation and Recycling.* 2002. V. 37. P. 1-22.
4. *Shel'deshov N. V., Zabolotsky V. I.* Bipolar ion-exchange membranes. Synthesis. Properties. Application // *Membranes and membrane technologies.* Collective of authors. Responsible Editor Yaroslavtsev A. B. The Scientific World, 2013. 612 p. (in Russian)

THE EFFECT OF SURFACE CHARGE ON THE CATIONIC POLYELECTROLYTE ADSORPTION

Vladimir Sobolev, Inessa Sergeeva

A.N. Frumkin Institute of Physical Chemistry and Electrochemistry RAS, Leninsky prospect 31, Moscow, 119991, Russia. E-mail: vsobolev@phych.ea.ru

Introduction

Adsorption of the oppositely charged polyelectrolyte on the inner pore surface yields membranes with new properties. As a membrane pore model can serve a thin capillary of fused quartz. Properties of the modified membranes depend on the original surface of the pores and on the adsorption conditions. The adsorption of polyelectrolyte onto oppositely charged surfaces has been under extensive theoretical and experimental study for many years due to a number of potential applications in many industrial processes. However, there few experimental results concerning polyelectrolyte adsorption under wet condition obtained by *in situ* experimental techniques. The capillary electrokinetics method allows us to obtain such information.

Quartz surface charge depends on the pH of the solution. The aim of this work is to study the effect of the surface charge on the kinetics and adsorption value.

Experiments

The electrokinetic studies were performed using homemade capillary setup, described in [1]. The streaming potential was measured in quartz capillaries with radii $r = 5-6 \mu\text{m}$ and length $l = 8-9 \text{ cm}$. We performed the experiments with capillaries, for which $\kappa r > 100$ (where κ is the inverse Debye length, r is radius of the capillary). Thus, the ζ -potential can be calculated on the basis of the Helmholtz-Smoluchowski equation (1):

$$\zeta = -\frac{\Delta E \eta \kappa^*}{\Delta p \varepsilon \varepsilon_0} \quad (1)$$

where ε and ε_0 are the relative dielectric permittivity of the solution and the vacuum permittivity, respectively, η is the solution viscosity, κ^* is the electrical conductivity, which is determined from the slope of the current-voltage diagram of the capillary, ΔE is the streaming potential and ΔP is the pressure drop over the capillary.

We have also used the measurements of streaming current I_s to calculate the ζ -potential according to equation 2, which is valid for zero value of the slip coefficient:

$$\zeta = \frac{I_s \eta l}{\pi \varepsilon \varepsilon_0 r^2 \Delta p} \quad (2)$$

where l and r are the length and the radius of the capillary, respectively.

For the experiments the capillaries with potential value about 90 – 100 mV in KCL 10^{-4} M solution at pH 6.5 were chosen.

As a cationic polyelectrolyte (poly (dialildimethylamine) ammonium chloride, (PDDA), $M = 400000-500000$, Aldrich) was used. Polyelectrolyte concentration was the same in all solutions, 10^{-3} g/l. Measurements were carried out in the background solutions KCL 10^{-2} M at different pH. pH values were varied by adding appropriate amounts of KCl or KOH solutions.

First we measured potential in a neutral KCL 10^{-2} M solution, then in a solution at appropriate pH value. After that the kinetics of PE adsorption was studied in a streaming current measurement mode. After the establishment of the ζ - potential constant values measurements in the neutral solutions KCL 10^{-4} M were carried out to compare the absorption under identical conditions.

Results and Discussion

Cationic polyelectrolyte (CPE) adsorption to the negative silica surface leads to a reduction of the charge and hence the surface potential. Thus, estimation of adsorption can be carried out by the changing ζ - potential. We studied the adsorption in the neutral (pH 6.25), acidic (pH 3.8) and alkaline (pH 9) solutions. Quartz surface charge increases with pH. The point of zero charge corresponds to pH 2-3.

Our measurements have shown that the adsorption value increases with surface charge increasing. Potential values measured in a KCl 10^{-4} M solutions are, respectively, -90 mV (pH 3.8), -140-150 mV (pH 6.25) and -160-200 mV (pH 9). The charge reversal time also increases with surface charge, 5-7 sec (pH 3.8), 60-70 sec (pH 6.25) and 140 sec (pH 9). Times of establishment of constant adsorption values in acidic and neutral media differ slightly, in an alkaline environment increases significantly. For pH 9 course of adsorption depends on the conditions of the experiment. If PE alkaline solution is passed through the capillary after the measurement in a neutral environment, there is a curve with a minimum and time of equilibrium is significantly increased. In this case, there are two processes at the same time, the negative surface charge increase with pH and its neutralization by CPE adsorption. If we start measuring in an alkaline solution and then carry out the adsorption at pH 9, a normal curve is obtained (fig.1). Adsorption of CPE molecules on the quartz surface in neutral and alkaline media occurs mostly due to electrostatic forces. Recharging indicates that thereafter (or simultaneously) the adsorption occurs due to hydrophobic interactions or entropy contribution. At pH 3.8 the surface charge of the silica is small (recharging time is 5-7 seconds) and the adsorption can occur due to hydrophobic interactions and entropy change. The polyelectrolyte molecules attraction to the surface in this case is considerably weaker and, as a result, desorption is observed. In an alkaline and neutral solutions adsorption is irreversible.

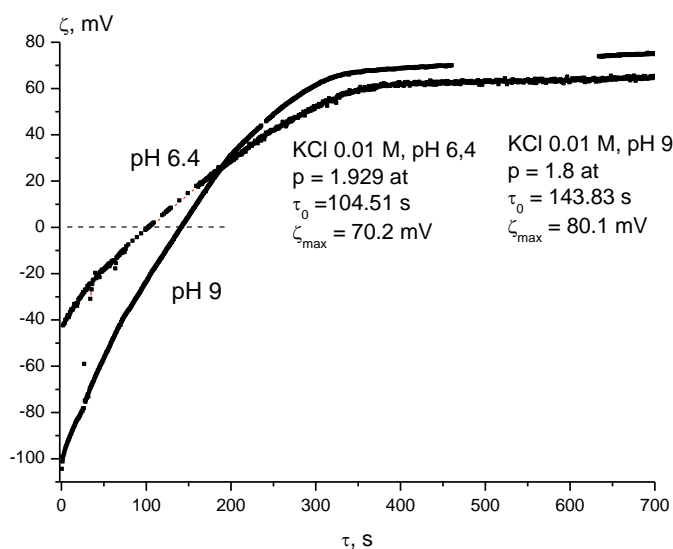


Fig. 1. The dependence of zeta-potential as a function of time in the course of PDDA adsorption on quartz surface at pH 6.4 and 9.

References

1. Churaev, N. V.; Sergeeva, I. P.; Sobolev, V. D.; Derjaguin, B. V. Examination of the Surface of Quartz Capillaries by Electrokinetic Methods. *J. Colloid Interface Sci.* **1981**, *84*, 451–460.

SYNTHESIS AND CHARACTERIZATION OF COMPOSITE ALUMINA–MULLITE AND ALUMINA–CORDIERITE MEMBRANES

¹Vera Solodovnichenko, ¹Denis Lebedev, ¹Victoria Bykanova, ^{1,2}Alexey Shiverskiy, ¹Ilya Ryzhkov, ³Tatiana Azarova, ³Sergei Azarov, ³Vladimir Prozorovich, ⁴Elena Krivoshapkina, Andrei Ivanets³

¹Institute of Computational Modeling SB RAS, Krasnoyarsk, Russia,

²Molecular Electronics Department, Krasnoyarsk Scientific Center, Russia

³Institute of General and Inorganic Chemistry, NAS Belarus, Belarus

⁴Institute of Chemistry, Komi Science Center, Syktyvkar, Russia

E-mail: vsolodovnichenko@gmail.com

Introduction

The modern stage of nanotechnology development allows synthesizing materials with unique physicochemical and functional properties. NafenTM (ANF Technologies) provides an example of such unique materials. It is represented by an array of γ -phase alumina nanofibers with the diameter of 10–15 nm and length up to several centimeters. Its specific surface area reaches $155 \text{ m}^2\text{g}^{-1}$ [1]. The range of Nafen applications includes additives to paints and coatings [1], catalyst supports [2], and synthesis of ultrafiltration [3] as well as ion-selective [4] membranes.

The Nafen material can be used for the preparation of composite membranes, where the Nafen nanofibers form a mesoporous selective layer on a macroporous support. The aim of this work is the formation of composite membranes Nafen–mullite and Nafen–cordierite membranes with further testing of their permeability properties.

Experimental

1. Mullite macroporous substrates

Macroporous ceramic in tablet form (19 mm in diameter and 3–4 mm in height) was obtained from fine dispersed mullite ($2\text{Al}_2\text{O}_3 \cdot \text{SiO}_2$) powder with particle size of 10–30 μm by compression in a laboratory hydraulic press. After drying at room temperature, the samples were sintered in an air atmosphere at 1150°C in a SNOL 7.2/1100 laboratory furnace according to [5].

2. Cordierite macroporous substrates

Macroporous cordierite supports were prepared from natural raw materials. Components required to obtain the cordierite with formula $\text{Mg}_2\text{Al}_4\text{Si}_5\text{O}_{18}$ were mixed in the stoichiometric ratio as follows: 42 wt% bauxite, 21 wt% silica sand, 37 wt% talc or 52 wt% kaolinite, 36 wt% talc, and 12 wt% alumina. The mixture was ground in a porcelain mortar and subsequently in the colloid mill for 3 h. The particle size of obtained powder was 20–30 μm . Forming of samples of the ceramic discs were performed by compression in a laboratory hydraulic press. After drying at room temperature, the samples were sintered in an air atmosphere at 1350°C .

3. Synthesis of composite membranes

The formation of $\gamma\text{-Al}_2\text{O}_3$ layers on the mullite and cordierite substrates was performed by the vacuum filtration technique, in this case the pore size of a selective layer will be defined by a difference of the applied pressure. Nafen nanofibers (0.5% wt) were dispersed in deionized water and agitated with a magnetic stirrer for 30 minutes followed by 15 minutes of ultrasonic treatment. The resulting colloidal solution was filtered through the prepared substrates using a Sartorius AG system and a fore-vacuum pump. The obtained samples were dried at 120°C for 2 hours with further thermal treatment at 800°C for 4 hours.

At the next step, the carbon is deposited on the membrane by chemical vapor deposition (CVD). The surface of $\gamma\text{-Al}_2\text{O}_3$ is catalytically active in reactions of carbon structure formation, so the process can be performed without additional catalysts. The synthesis of carbon layer was carried out in ethanol / argon mixture (1:1) at 900°C during 20 min.

Result and discussion

The porosity of the mullite substrates determined by hydrostatic weighing was in the range of 25–27 %. The average pore size of the mullite substrates was $1.0 \pm 0.2 \mu\text{m}$ (“bubble point” method).

For cordierite supports according to mercury porosimetry average pore size is equal to 9.5 μm with a narrow pore size distribution. Open porosity of ceramic was estimated to be 30%.

Membranes produced solely from Nafen alumina nanofibers have the porosity of around 75 %, and the average pore size of 20 nm according to the low-temperature nitrogen adsorption/desorption [4].

The morphology of resulting composite membranes was studied by scanning electron and transmission electron microscopy. Analysis of composite membranes morphology showed that Nafen nanofibers form a grid in larger pores of the support membrane, with average thickness of 10–20 μm .

Permeability of membranes for water was measured by the "dead-end" method. Results of measurements have shown that formation of a selective layer leads to permeability reduction approximately 4 times. Permeability of composite alumina–cordierite membranes for water was around 4000 $\text{l m}^{-2}\text{h}^{-1}\text{bar}^{-1}$.

The selective properties is investigated by measuring the potential difference between two KCl aqueous solutions with different concentrations separated by a membrane. The composite membranes with carbon layers demonstrate cation selectivity.

The prepared membranes can be used for ultrafiltration. The main advantage of the obtained ceramics using is low cost and availability of raw materials. Membranes with conductive carbon layer on nanofibrous structure is a promising material for separation of charged species as well as switchable ion- transport selectivity.

This work is supported by the Russian Science Foundation, Project 15–19–10017.

References

1. Features of Nafen alumina nanofibers, <http://www.anftechnology.com/nafen/>
2. *Hussainova I., Ivanov R., Stamatina S.M., Anoshkin I.V., Skou E.M., Nasibulin A.G.* A few-layered graphene on alumina nanofibers for electrochemical energy conversion // *Carbon* 2015. V. 88. P. 157–164.
3. *Su V.M.T., Clyne T.W.* Hybrid filtration membranes incorporating nanoporous silica within a nanoscale alumina fiber scaffold // *Adv. Engineer. Materials*. 2016. V. 18. P. 96–104.
4. *Lebedev D.V., Shiverskiy A.V., Simunin M.M., Solodovnichenko V.S., Parfenov V.A., Bykanova V.V., Khartov S.V., Ryzhkov I.I.* Preparation and ionic selectivity of carbon-coated alumina nanofiber membranes // *Petrol. Chem.* 2017. V. 54 (4). P. 306–317.
5. *Ivanets A.I., Agabekov V.E.* Ceramic microfiltration membrane based on natural silica // *Petrol. Chem.* 2017. V. 57, № 2. P. 117–126.

SYNTHESIS OF ION-SELECTIVE CERAMIC MEMBRANES BASED ON ALUMINA NANOFIBERS

¹Vera Solodovnichenko, ^{1,2}Alexey Shiverskiy, ^{1,3}Mikhail Simunin, ¹Denis Lebedev, ¹Victoria Bykanova, ¹Ilya Ryzhkov

¹Institute of Computational Modeling SB RAS, Krasnoyarsk, Russia

²Molecular Electronics Department, Krasnoyarsk Scientific Center, Russia

³National Research University of Electronic Technology – MIET, Zelenograd, Moscow, Russia

E-mail: vsolodovnichenko@gmail.com

Introduction

In recent decades, the interest in membranes produced from inorganic materials has been greatly increased. Ceramic membranes offer a number of advantages over polymeric membranes, such as higher thermal and mechanical stability and enhanced chemical resistance. We believe that the combination of ceramic nanofibers and carbon materials is promising for the preparation of membranes with selective ion transport. The carbon surface layer can form a wide range of functional groups, which could be utilized to control the membrane selectivity.

This work is devoted to a novel type of ion-selective membranes based on alumina nanofibers, which combine the advantages of ceramic nanofibrous media and good electrical conductivity [1].

Experimental

The membranes are produced from highly aligned alumina nanofibers – Nafen™, ANF Technologies [2]. The membranes are prepared by filtration of nanofiber suspension through a porous support followed by drying and sintering (Fig. 1). Electrical conductivity and ionic selectivity are achieved by depositing a thin carbon layer by catalytic-free chemical vapor deposition (CVD) due to catalytic activity of alumina in carbon structure formation [3].

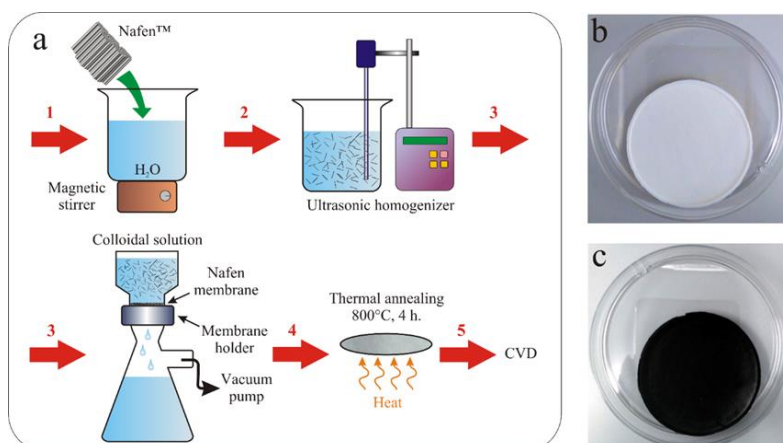


Figure 1. Membrane preparation technique (a), top view of Nafen membrane before (b) and after (c) deposition of carbon by CVD method.

Result and discussion

According to SEM and TEM images, resulting membranes consist of randomly oriented alumina nanofibers with high aspect ratio (~100) and small diameter (~ 8 nm) covered by 2–3 carbon layers with the total thickness around 1–2 nm (Fig. 2).

The pore size characteristics and ionic permselectivity properties of produced membranes can be regulated widely by changing the synthesis conditions. So, variation of pH and ultrasonic treatment of nanofibers dispersions allows formation of membranes with average pore size from 25 to 50 nm and total pore volume from 0.5 to 1.0 cm³/g.

According to FTIR, Raman and X-ray fluorescence spectroscopy, changing the CVD process conditions (T, P and carbon precursor) enables controlling the properties of carbon coating, such as number of layers, disordering degree, quality and quantity of functional groups. In all cases, the pore size distribution (N₂ adsorption, 77 K) shows that deposition of carbon reduces the average pore diameter by half and decreases the total porosity of membranes.

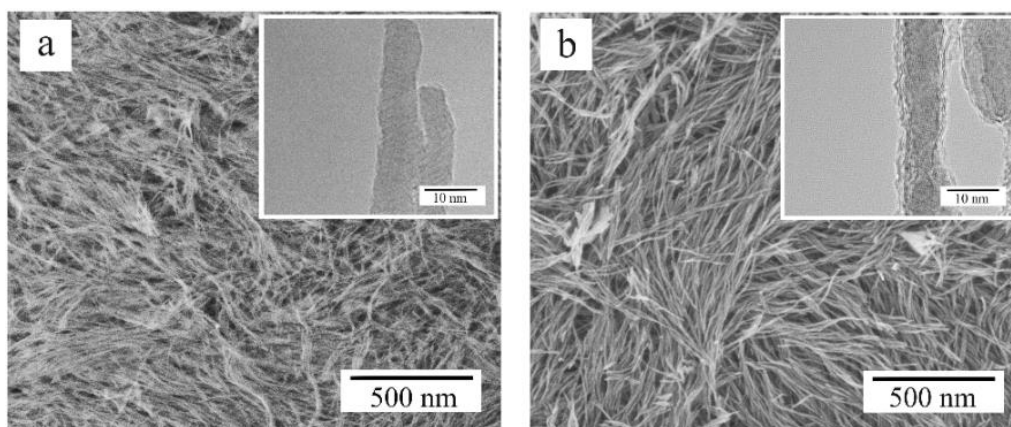


Figure 2. SEM and TEM (in the inserts) images of the Nafen membrane before (a) and after (b) deposition of carbon.

The formation of conductive material after deposition of carbon is confirmed by measuring the electrical resistance. It reduces by 10^9 times to $0.002 \Omega\text{m}$, which is typical for conductive carbon layers.

Variation of synthesis conditions is used to control the membrane ionic selectivity. Carbon deposition on Nafen membranes allowed us to obtain anion-selective membranes with transfer numbers 0.94 for anion and 0.06 for cation in KCl aqueous solution.

The potential applications of proposed membranes include nano- and ultrafiltration as well as separation of charged species. The deposition of conductive carbon layer on nanofibrous structure is a promising technique for preparing membranes with switchable ion- transport selectivity.

This work is supported by the Russian Science Foundation, Project 15–19–10017. The physicochemical analysis of materials was carried out on equipment of Krasnoyarsk Scientific Center of Shared Facilities SB RAS.

References

1. Lebedev D.V., Shiverskiy A.V., Simunin M.M., Solodovnichenko V.S., Parfenov V.A., Bykanova V.V., Khartov S.V., Ryzhkov I.I. Preparation and Ionic Selectivity of Carbon-Coated Alumina Nanofiber Membranes *Petroleum Chemistry*, 2017, Vol. 57, P. 306–317.
2. Features of Nafen alumina nanofibers, <http://www.anftechnology.com/nafen/>
3. J. Pang, A. Bachmatiuk, I. Ibrahim et al. CVD growth of 1D and 2D sp^2 carbon nanomaterials, *J Mater Sci*, 2016, Vol. 51, PP. 640–667.

ELECTROCHEMICAL PROPERTIES OF PRUSSIAN BLUE-POLYPYRROLE COMPOSITE

^{1,2}Natalia Talagaeva, ^{1,2,3}Ekaterina Zolotukhina, ^{1,2,3}Mikhail Vorotyntsev

¹The Institute of Problems of Chemical Physics RAS, Chernogolovka, Russia

E-mail: talagaevanv@gmail.com

²D. Mendeleev Russian University of Chemical Technology, Moscow, Russia

³Lomonosov Moscow State University, Moscow, Russia

Introduction

Prussian Blue (PB) is a promising material for electrocatalytic application (H₂O₂, glucose, SO₃²⁻ sensors) nevertheless attracts little attention as an electrocatalyst because of fast degradation of its electrocatalytic properties, mostly due to peeling off fragments of the electroactive film from the substrate. One of the ways to solve this problem is to create any composite material based on matrix for PB particles (conductive polymers affect stabilizing are often used). It is important to select the synthesis conditions permit to obtain the most stable composite films PB-polypyrrole (PPy) on the surface of inert electrode for electrocatalytic application.

Experiments

PB-PPy composites were generated via a one-pot one-step redox reaction between the oxidizer (equimolar mixture of iron(III) and ferricyanide salts) and the reducing agent (pyrrole, Py, taken in excess) in their mixed aqueous solution, with addition of a background electrolyte. It was found that the anion type in the synthetic mixture strongly affects the characteristics of deposited composite films [1,2]. For the further experiments the nitrate background solution was selected as the use of this one results in high quality films without cracks [2].

The concentrations of PB and PPy precursors in the synthetic mixture were varied. PB-PPy films were deposited from reaction mixtures with 0.1 mM Fe³⁺, 0.1 mM [Fe(CN)₆]³⁻, and 0.5 mM Py (system 1:1:5); 0.1 mM Fe³⁺, 0.1 mM [Fe(CN)₆]³⁻, and 1.0 mM Py (system 1:1:10); 0.5 mM Fe³⁺, 0.5 mM [Fe(CN)₆]³⁻, and 0.5 mM Py (system 1:1:1); and 0.5 mM Fe³⁺, 0.5 mM [Fe(CN)₆]³⁻, and 1.0 mM Py (system 1:1:2). PB-PPy composite was deposited at the surface of Pt and ITO-coated glass working electrodes. To modify the electrode surface with PB-PPy film, the electrode was placed in reaction mixture for 48 h and then rinsed thoroughly with distilled water.

Electrochemical measurements were performed in single-compartment three-electrode cell with coiled Pt wire as counter electrode and Ag/AgCl as reference electrode. Redox activity of PB modified electrodes related to reversible transformation of PB to PW due to reduction of Fe(III) ions inside the PB lattice was characterized by cyclic voltammetry (CV). Stability tests of composite films were carried out either under conditions of the hydrogen peroxide electroreduction and sulfite electrooxidation or in the course of multi-cycle experiments. The film-coated electrode was subjected to such repeating CV treatment until the cathodic (or anodic) charge of the cycle has become lower than 25–30 % of the charge of the second cycle. Electrochemical measurements were carried out at room temperature. Redox activity of synthesized PB-PPy composites immobilized on electrode surface was tested in the same nitrate background electrolyte which was used for their synthesis. Tests of the electrocatalytic activity of PB-PPy films in H₂O₂ and Na₂SO₃ solutions were performed with the use of potassium phosphate buffer (pH 6.0). Electroreduction of hydrogen peroxide and electrooxidation of sulfite anions at these modified electrodes were performed in potentiostatic conditions.

Results and Discussion

The one-step method of the chemical deposition of PB-polypyrrole films on a conducting or insulating solid substrate (including an electrode surface) from the mixed solution of pyrrole, iron (III) and ferricyanide salts have been elaborated. It has been found that such films consist of composite particles where small PB single crystals are incorporated into PPy surrounding. It is important to mention that PB inside the composite film retains its crystalline structure even after its long-time functioning as electrocatalyst in 1 mM hydrogen peroxide solution, the size of PB

crystals remaining unaffected (according to XRD spectra). It means that the progressive loss of its catalytic properties is not due to a progressive dissolution of the reduced form, PW. The stability period of the H₂O₂ electroreduction for nitrate-synthesized films on Pt substrate was about eighty times longer than that of pure Prussian Blue films without polymeric support.

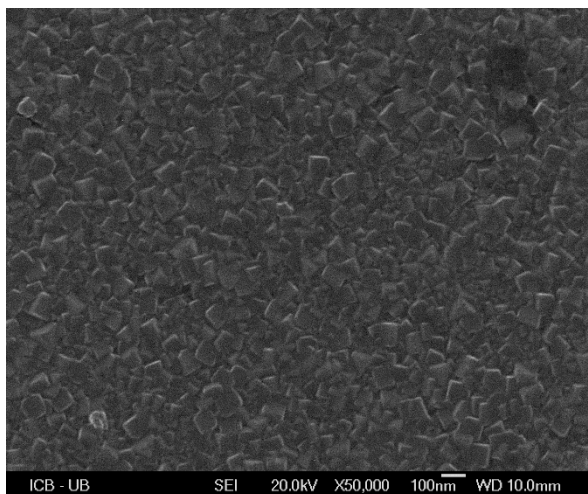


Figure 1. SEM image of PB-PPy composite films on ITO support obtained in nitrate electrolyte

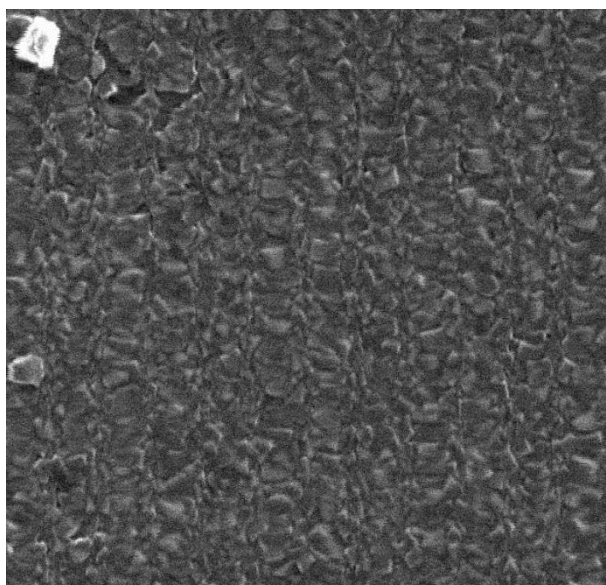


Figure 2. SEM images of PB-PPy films on ITO surface after electroreduction in 1 mM solution of H₂O₂

Table 1: Principal characteristics of Prussian blue–polypyrrole composite films

Composition of mixed solution	"System"	Number of cycles performed, <i>i</i>	Degradation degree, χ_i (%)
0.1 mM [Fe ³⁺ + Fe(CN) ₆ ³⁻] + 0.5 mM Py	1:1:5	3000	25
0.1 mM [Fe ³⁺ + Fe(CN) ₆ ³⁻] + 1.0 mM Py	1:1:10	1600	9.5
0.5 mM [Fe ³⁺ + Fe(CN) ₆ ³⁻] + 0.5 mM Py	1:1:1	1700	30
0.5 mM [Fe ³⁺ + Fe(CN) ₆ ³⁻] + 1.0 mM Py	1:1:2	2000	30

So, composites based on PPy matrix demonstrate more stable electrochemical properties compared to pure PB (stability period of PB-PPy films is 10 times greater than that for pure PB films). Electrochemical stability of composite films depends on the amount of Py in synthetic solution. It was found that characteristics of PB-PPy films essentially depend on synthesis solution. Composite films formed via redox synthesis procedure from solution where molar ratio

$\text{Fe}^{3+}:[\text{Fe}(\text{CN})_6^{3-}]:\text{Py}$ was 1:1:10 and 1:1:5 with nitrate supporting electrolyte demonstrate the lowest degradation degree [3].

In the reaction of SO_3^{2-} electrooxidation electrochemical properties of composite films formed via redox synthesis procedure from solution with molar ratio $\text{Fe}^{3+}:[\text{Fe}(\text{CN})_6^{3-}]:\text{Py}$ 1:1:5 were the most stable. Such films demonstrate electrocatalytic activity both in sulfite model solutions and in wine. It was shown that PB-PPy films synthesized on ITO electrodes demonstrate the similar to obtained by the use of titrimetric method results.

It was estimated that sensitivity coefficient and amperometric response stability of PB-PPy films in various electrochemical tests depend on not only component ratio in film but also on adhesion of composite film to electrode surface.

Acknowledgments

This work was supported by the RFBR (project no. 15-03-06351 A).

References

1. *Itaya K., Uchida I.* Nature of Intervalence Charge-Transfer Bands in Prussian Blues // *Inorg. Chem.* 1986. V. 25. P. 389-392.
2. *Talagaeva N.V., Zolotukhina E.V., Bezverkhyy I., Konev D.V., Lacroute Y., Maksimova E.Y., Koryakin S.L., Vorotyntsev M.A.* Stability of Prussian blue–polypyrrole (PB/PPy) composite films synthesized via one-step redox-reaction procedure // *J. Solid State Electrochem.* 2015. V. 19. P. 2701–2709.
3. *Talagaeva N.V., Zolotukhina E.V., Pisareva P.A., Vorotyntsev M.A.* Electrochromic properties of Prussian blue–polypyrrole composite films in dependence on parameters of synthetic procedure // *J. Solid State Electrochem.* 2016. V. 20. P. 1235–1240.

SYNERGETIC APPROACH IN ANALYSIS OF COMPOSITE MATERIALS FRACTAL MORPHOLOGY

Denis Terin, Sergey Korchagin

Yuri Gagarin State Technical University of Saratov, Saratov, Russia

E-mail: terinden@mail.ru, korchaginser@gmail.com

Introduction

Many materials have a self-similar structure, similar to the formation of fractal and have unique properties compared to conventional materials morphologies [1]. The possibility of their use in applied research requires a detailed understanding of the fundamental principles of the interaction of radiation with matter. In the process of designing composite media must not lose sight of the presence of thermodynamic, kinetic, electromagnetic effects and functional links between them. In the simulation of such systems, for a more detailed description and analysis of efficient to synergetic approach, this includes the apparatus of quantum mechanics, classical electrodynamics (with certain restrictions), nonlinear dynamics in chemical processes, programming methods, as well as elements of fractal analysis.

Computer experiment

A software package [2], for realization of computing experiment to study the properties of the composite, fractal morphology, considered in [3].

The anisotropic electrical properties are taken into account, so the complex dielectric permittivity of the composite is represented, in the form of a tensor. For the calculation of the dielectric tensor elements of up to 10 nm in size structure of the material, where the experimental determination is difficult, and the dimensional effects can be significant, we used quantum mechanical approach. The mathematical model is based on the Agranovich-Ginzburg relation, in which the matrix elements of dipole transitions are calculated in the interaction of a quantum system with electromagnetic radiation. The relaxation of quasiparticles interacting with the electromagnetic field is neglected and is not taken into account in the mathematical model. The Hartree-Fock method was used to determine the matrix elements.

In the case where the structure element has dimensions of 10 nm to 50 nm, for describing the electrical characteristic of the effective medium model was used. The aggregate of particles of which the composite is composed is regarded as a kind of new medium having the same level of polarization. With respect to the field averaged over the volume, the system is homogeneous, and therefore can be characterized by a certain effective value of the permittivity. This approach is realized using a model consisting of the Poisson equation for the distribution of the electrostatic field in a nonconducting medium in the presence of electric charges, which includes a complex effective dielectric constant.

An analysis of the electrodynamic properties of a material with structural elements larger than 50 nm was carried out using the transmission matrix method. For a description of the qualitative properties of the test composite used methods of fractal analysis. The dimensions of Hausdorff, Minkowski, and the Hurst exponent are calculated.

Results and discussion

Fig. 1 shows the frequency dependence of the complex permittivity of the test composite, where a - level fractal. Fig. 2 shows the dependence of the complex dielectric constant of the volume fractions of the components of the composite.

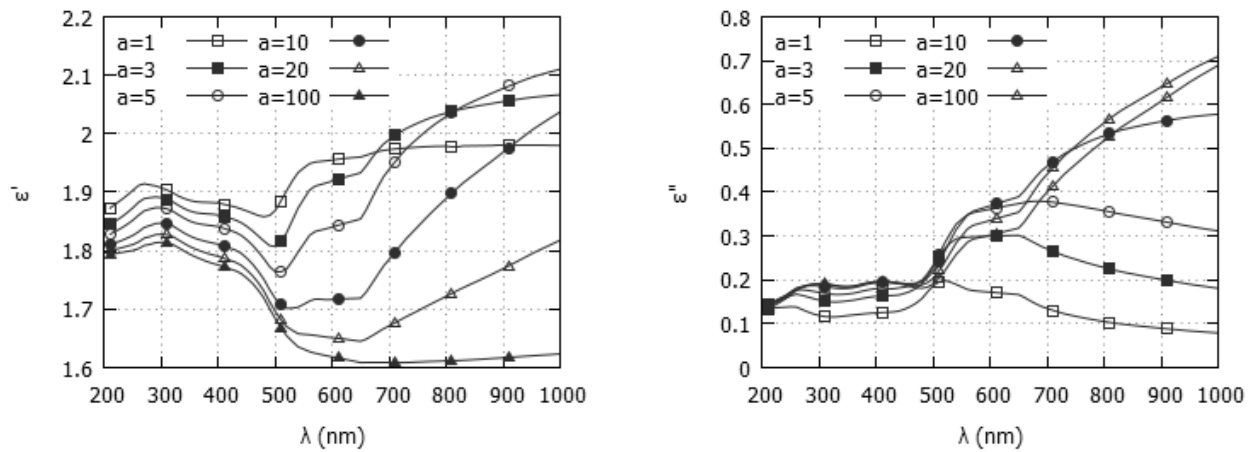


Figure 1. The frequency dependence of the complex permittivity of the composite

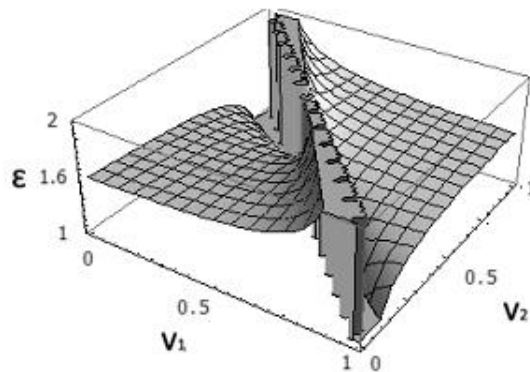


Figure 2. Dependence of the complex dielectric constant on the volume fractions of the components of the composite

It is clear from the graphs that the level of the composite fractal has a significant influence on its properties. The frequency dependence of the dielectric constant was exhibit nonlinear. By varying the geometric parameters of the object, you can control a maximum of difference loss and resonant absorption maxima. Fractal analysis shows that the investigated composite fractal level 3-10 has the property of persistence (the ongoing trend is supported). The fourth level fractal shows the closest value to the Hurst exponent of natural processes. Thus, the probability of occurrence of such a fractal in nature is higher than with composites studied the morphology of the other levels of factuality.

References

1. *Cristina Ramirez, Filipe M. Figueiredo, Pilar Miranzo, P. Poza, M. Isabel Osendi.* Graphene nanoplatelet/silicon nitride composites with high electrical conductivity //CARBON, 50, 2012, p. 3607 - 3615.
2. *Korchagin S.A.* Research electrodynamics properties of layered composite the fractal structure / *Korchagin S.A., Terin D.V.* // Conference Proceedings - 2016 International Conference on Actual Problems of Electron Devices Engineering, APEDE 2016
3. *Onosov I.A.* The complex programs for research of composite media of various structures. *Onosov I.A., Pishkinas S.A., Korchagin S.A., Romanchuk S.P., Terin D.V.:* Mathematical modeling and information technology in research and education. Collection of scientific articles. Saratov, 2015. S. 86-89.

EXPERIENCE OF SOLID-POLYMER WATER ELECTROLYSERS USING WITH MF-4SK MEMBRANES

Sergej Timofeev, Gennadiy Belyakov, Vladimir Gursky

OAo Plastpolymer, St. Petersburg, Russia

OOO Eldis Firm, Moscow, Russia

Aleksandrov Research Institute of Technology, Sosnovyi Bor, Russia

Electrochemical hydrogen generators with solid polymer electrolyte (ECHG) are increasingly used in various fields of science and technology. In Russia there are generally a number of small-scale plants with a capacity of several tens to several hundred liters of hydrogen per hour presented. The developer of the first commercial units, introduced in the market in the late 80s of last century, was OOO Eldis Firm, which is still producing a range of ECHG of various capacities.

Perfluorinated sulphocathionite membranes MF-4SK are used as a solid polymer electrolyte of Russian-manufactured ECHG. Together with ECHG developers the requirements to membranes (thickness, equivalent weight, volume resistivity) are determined, which high operational characteristics of the plants ensure. The nature of the electrocatalyst (Pt-black, Ir-black, Pt on charcoal, chemically reduced Pt), porous electrodes types (porous titanium, platinized porous titanium, porous carbon paper) as well as membrane-electrode assembly forming method (application of a finely dispersed catalyst to an electrode, deposition of a finely dispersed catalyst on the membrane surface, chemical reduction of Pt on the membrane surface) were estimated. In this work, a conclusion is made about the most preferred method of manufacturing a membrane-electrode assembly.

In the electrolysis process produced hydrogen usually contains 1-2% oxygen. For a number of applications (for example, in gas chromatography) it is important to obtain pure hydrogen without further purification. We have established that the introduction of Pt into the membrane to a depth of 3-5 μm from the surface makes it possible to obtain hydrogen of high purity (at least 99.99%) as a result of diffusing ballast oxygen reduction. A method has been developed for introducing Pt into the membrane using an ammonia complex Pt, which provides a Pt concentration of 0.15-0.25 mg / cm^2 .

Examples are given of the use of ECHG in the manufacture of hydrogen-oxygen welding sets, water deoxygenation units, hydrogen supply devices in fuel cells, and configuration of gas chromatographs (including those with the removal of moisture from the gas using TF-4SK tubes).

TRANSPORT PROPERTIES OF PERFLUORINATED MEMBRANES MODIFIED BY HALLOYSITE NANOTUBES

¹Ekaterina Titskaya, ¹Irina Falina, ²Anatoly Fillipov

¹Kuban State University, Krasnodar, Russia, E-mail: irina_falina@mail.ru

²Gubkin University, Moscow, Russia, E-mail: filippov.a@gubkin.ru

Introduction

Nowadays functional materials for hydrogen energy are under the great interest of investigators. The main part of a hydrogen-air fuel cell is the membrane-electrode assemble (MEA), which consists of proton exchange membrane, catalyst and gas diffusion layers. Sulfocationite perfluorinated membrane traditionally serve as polymer electrolyte in a low temperature fuel cell. Its modification by various additives permits to attach special properties to the membrane. The halloysite nanotubes can serve as a carrier of platinum nanoparticles, and modification of the membrane by Pt-containing halloysite nanotubes could improve the efficiency of the hydrogen-air fuel cell. The purpose of present work was to explore the electrotransport characteristics of bilayer perfluorinated membranes MF-4SK modified by halloysite nanotubes and platinum dispersion.

Experimental

The Table presents the set of investigated membranes, which included industrial MF-4SK membrane (No 1, JSC Plastpolymer, St. Petersburg) and bi-layer laboratory samples, prepared from MF-4SK dispersion of halloysite nanotubes and platinum nanoparticles immobilized on the outer nanotube surface (Gubkin University, Moscow) [1]. Samples 2 and 3 consisted of two layers: modified by Pt-containing halloysite layer and non-modified one. Non-modified layer was cast from LF-4SK solution in dimethylformamide (DMF), and modified layer was prepared from LF-4SK solution in DMF (sample 2) or isopropyl alcohol (IPA) (sample 3) containing modifier.

Table: Objects of research

No	Membrane	Thickness $\times 10^5$, m	Layers	Solvent	Modifier
1.	MF-4SK	5	Single-layer	DMF	-
2.	MF-4SK/2-DMF	17.7	Bilayer $h_{(mod.)}=20\%$ $h_{(unmod.)}=80\%$	DMF	I layer: 2% Hall +Pt II layer: MF-4SK
3.	MF-4SK/2-DMF+IPA	14.8	Bilayer $h_{(mod.)}=20\%$ $h_{(unmod.)}=80\%$	I layer: isopropyl alcohol II layer: DMF	I layer: 2% Hall +Pt II layer: MF-4SK

Electric conductivity of the membranes in solutions of hydrochloric acid was measured by the mercury-contact method as the active part of the cell impedance. Diffusion permeability of membranes was determined in two-compartment cell filled with electrolyte solution and water at opposite sides of the membrane. The diffusion flux through the membrane was determined on the basis of kinetic dependencies of electrolyte concentration in chamber with water, measured by conductometric method [2].

Testing of membranes in hydrogen-air fuel cell of MEA was carried out at temperature 25°C; hydrogen flow rate was 20 L/h, the air flux – 300 L/h, the platinum loading of the electrodes was 0.4 mg/cm².

Results and Discussion

There were obtained concentration dependences of the electric conductivity of membranes MF-4SK modified with halloysite nanotubes and platinum nanoparticles. It was established that the investigated samples possess proton conductivity sufficient for use in a fuel cell.

Concentration dependencies of diffusion permeability of the membranes in HCl solutions are presented in Fig. 1b. Preparation of the multilayered membranes allows to assign asymmetric properties to them, so investigation of the diffusion characteristics of the bilayer membranes was performed for different orientation of the samples towards the electrolyte flux. As can be seen

from the Fig. 1b, the considerable asymmetry of the diffusion permeability presents for anisotropic samples and its value is 15-20% and greater in the case when modified surface faces the electrolyte flux.

The results of measurement of the current-voltage and power characteristics of MEA of a hydrogen-air fuel cell with the studied membranes are presented in Fig. 2.

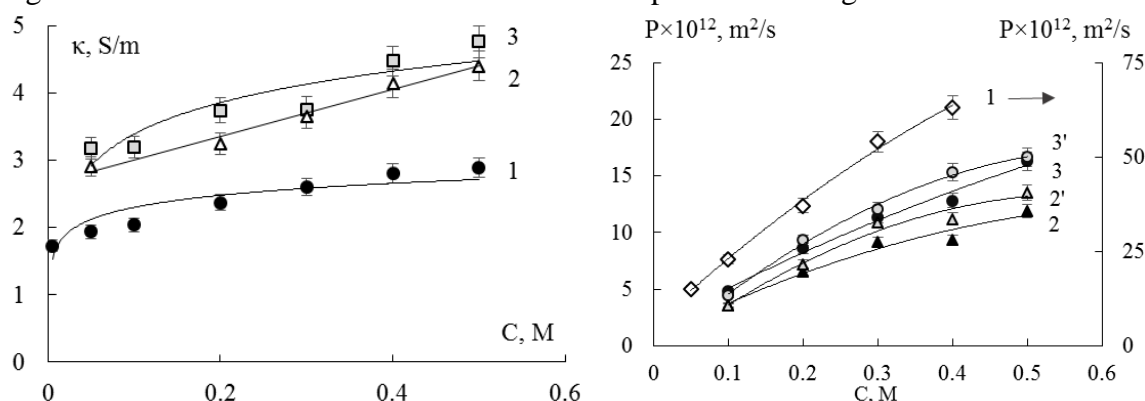


Figure 1. The concentration dependence of the electric conductivity (a) and diffusion permeability (b, nonmodified (2, 3) and modified (2', 3') surface meets the electrolyte flux) of the membranes in HCl solutions. The curve numbers correspond to the sample numbers in the Table.

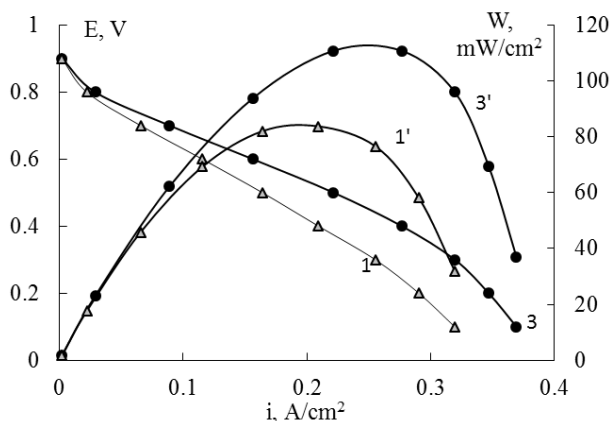


Figure 2. The current-voltage (1, 3) and power (1', 3') characteristics of the membrane-electrode assembly of a hydrogen-air fuel cell with investigated samples (the curve numbers correspond to sample numbers in the Table)

One can see that the membrane modification with Pt-containing halloysite nanotubes significantly improves the maximum of power density. This could be caused by the catalytic activity of the platinum dispersion immobilized on the nanotube surface.

Acknowledgements

This study was supported by the Ministry of Education and Science of the Russian Federation (Grant No 14.Z50.31.0035).

References

1. Filippov A., Afonin D., Kononenko N., Lvov Yu., Vinokurov V. New approach to characterization of hybrid nanocomposites // Colloids Surf. A. 2017. V.521. P.251-259.
2. Berezina, N.P., Kononenko N.A., Dyomina O.A., Gnusin N.P. Characterization of ion-exchange membrane materials: Properties vs structure // Advances in Colloid and Interface Science. 2008. V. 139. P. 3-28.

FLOW BATTERY OF A NOVEL TYPE PROSPECTIVE FOR STATIONARY ENERGY STORAGE, FULLY ELECTRIC VEHICLES AND DIRECT SOLAR-TO-CHEMICAL ENERGY CONVERSION

¹ Yuriy Tolmachev, ¹ Oleg Tripachev, ¹ Olga Istakova, ^{1,3} Dmitry Konev, ^{1,2} Anatoly Antipov, ^{1,2,3,4} Mikhail Vorotyntsev

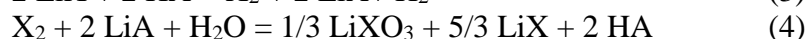
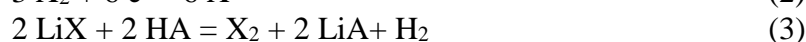
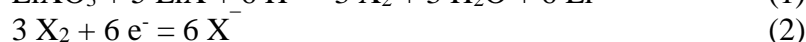
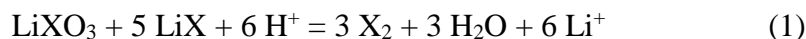
¹D. I. Mendeleev University of Chemical Technology of Russia, Moscow, Russia

²M. V. Lomonosov Moscow State University, Moscow, Russia

³Institute for Problems of Chemical Physics, Russian Academy of Sciences, Chernogolovka, Russia

⁴ICMUB, UMR 6302 CNRS-Université de Bourgogne, Dijon, France, *E-mail: mivo2010@yandex.com*

We propose a flow battery employing H₂ as the fuel and one or more of highly soluble halate salts (such as 50% w/w aqueous solution of LiBrO₃) as the oxidant achieving the energy density > 400 Wh/kg at the system level, which is sufficient for fully electric vehicles with a driving range of 500 km on a single refill [1]. Moreover, such a battery can reach very high areal power density (> 1 W/cm²) when the rate limiting steps (halate-halide comproportionation (1) on discharge and halogen disproportionation (4) on charge) are performed in a 3D solution phase within a porous carbon electrode rather than on a 2D electrode surface [1-4]:



The pH manipulation required for switching between the charge and discharge modes is conveniently accomplished using reagent-free small-size and low-cost Orthogonal Ion Migration Across Laminar Flow Reactor (OIMALF™) akin to the ion suppression reactor of ion chromatography. Photoelectrochemical splitting process (3) of LiBr, which can be done using low cost silicon photopanel or microparticles, when coupled to the disclosed disproportionation process (4), may finally enable the human civilization to use sunlight (with its average power striking the planet exceeding the 13 TW need of our civilization by a factor of over 10,000) as the primary energy source at a cost competitive with the more traditional methods such as coal combustion and uranium fission.

Acknowledgements

Financially supported by the Russian Science Foundation (grant 15-13-20038).

References

1. Tolmachev Y. V., Pyatkivskiy A., Ryzhov V. V., Konev D. V., Vorotyntsev M. A. J. Solid State Electrochem., 19 (2015) 2711-2722.
2. Vorotyntsev M. A., Konev D. V., Tolmachev Y. V. Electrochim. Acta 173 (2015) 779–795
3. Vorotyntsev M.A., Antipov A.E., Tolmachev Yu.V., Antipov E.M., Aldoshin S.M., Doklady Phys. Chem., 468 (2016) 141-147.

DESIGN AND FABRICATION OF MULTIFUNCTIONAL NANOCOMPOSITE MATERIALS «POLIKON A»

Sergey Tsyplyayev, Marina Kardash, Ilya Strilets

¹Engels Technological Institute of Yuri Gagarin State Technical University of Saratov, Russia

E-mail: tsiplyayev@mail.ru; E-mail: m_kardash@mail.ru

Introduction

The ion-exchange membranes are nanoporous polymeric materials. They are widely used in modern technology. They are some of the most modern and technological types of materials [1]. At the department «Chemical technology» (Engels Technological Institute of the Gagarin State Technical University of Saratov) the materials «Polikon A» were fabricated and developed its modifications. «Polikon A» is produced by polycondensation filling [2, 3]. These materials make it possible to increase the efficiency of electro dialysis by modifying the characteristics of «Polikon A» and reduce environmental stress.

Experiments

The anion-exchange fibrous material «Polikon A» polycondensation filling method with introduction of modifying additives into the matrix (at the synthesis stage) was obtained. Material «Polikon A» with different fibers for reaching the most optimal properties was investigated. Modifying additives - ultrafine powders: Fe, Ni, B were used. Method of differential scanning calorimetry was used, for studying kinetics and thermodynamics of occurring processes. Experimentally, the exchange capacity and the efficiency of sorption materials «Polikon A» were determined.

Results and Discussion

Ultrafine powders: Fe, Ni, B were implemented into material «Polikon A» for giving in membrane more evenly-crosslinked structure. Selection of optimal basis for filling fiber material «Polikon A» was made. Heterophase medium was introduced in monomerization composition and this has resulted to changes in the kinetics and thermodynamics of chemical reactions. We observed a higher speed of synthesis reaction and curing. The thermal effect of the curing reaction is increases. More extensive cross-linked structure «Polikon A» is formed. The effectiveness of the materials «Polikon A» in the purification of water from sulfates was proved.

References

1. *Prikhno I.A., Safronova E.Yu, Yaroslavtsev A.B.* Hybrid materials based on perfluorosulfonic acid membrane and functionalized carbon nanotubes: Synthesis, investigation and transport properties // *International Journal of Hydrogen Energy*. 2016. T. 41. C. 15585-15592.
2. *Kardash M.M.* Sposob poluchenija polimernogo press-materiala [The method of polymer press-material producing]. Patent RU, no. 2013101387/04, 2013.
3. *Jaroslavcev A. B., Nikonenko V. V., Zabolockij V. I.* Ion transport in membrane and ion exchange materials. *Uspehi himii*, 2003. vol. 72, no. 5, pp. 438-470. (in Russian).
4. *Tsyplyayev S.V., Kardash M.M., Strilets I. D.* Structure and properties of the "Polikon A" modernized by ultrafine additives // *New polymer composite materials: Materials of XI International scientific-practical conference.- Nalchik.- 2016. C. 258-261.*

ELECTROCHEMICAL SYNTHESIS OF COPPER OXIDES AND THEIR ELECTROCATALYTIC PROPERTIES IN DIRECT ALCOHOL FUEL CELLS

Anna Ulyankina, Nina Smirnova

Platov South-Russian State Polytechnic University (Novocherkassk Polytechnic Institute), Russia

E-mail: anya-barbashova@yandex.ru

Introduction

The synthesis of micro/nanoparticles of transition metal oxides with different morphology has attracted a considerable amount of interest because of structure-dependent material properties with potential application in direct methanol fuel cells (DMFCs). Of the different transition metal oxides that are available, copper oxides are a promising material due to their low cost, larger abundance, chemical stability and environmentally friendly nature. The various nanostructured copper oxides have been synthesized using a variety of methods. Electrochemical synthesis under pulse alternating current offers a simple, one-step, room-temperature and relatively cost-effective technique that can be used for large-scale applications.

Experiments

In this paper we investigated the copper oxides which were firstly prepared by means of electrochemical oxidation/dispergation under pulse alternating current of different current densities (0.5; 1.0 and 1.5 A/cm² for CuO_x-0.5, CuO_x-1.0 and CuO_x-1.5 samples, respectively). This technique was also used for synthesis of different metal oxides such as NiO[1] and SnO₂[2].

The electrocatalytic activity of the copper oxides for methanol oxidation was investigated by cyclic voltammetry (CV). Solutions containing 0.1M NaOH with and without 0.25M CH₃OH were used as the electrolyte.

Results and Discussion

It was shown that the current density has a significant effect on shape, size and composition of the prepared powders. The CuO_x-0.5 powder is pure Cu₂O with octahedral particles of 1 μm. When the current density increases the CuO phase appears. The CuO_x-1.0 consists of polyhedral particles of Cu₂O (50-400 nm) with small amount of CuO. The CuO_x-1.5 particles can probably reveal Cu₂O/CuO core-shell structure[3].

Figure 1 (a-c) shows the CV curves measured at a scan rate of 50 mV/s for the CuO_x-0.5, CuO_x-1.0 and CuO_x-1.5 samples in 0.1M NaOH and (0.1M NaOH+0.25M CH₃OH) electrolytes. It can be seen that after the addition of 0.25 methanol in 0.1M NaOH electrolyte, during the forward scan, the anodic current density remains nearly the same up to 0.4 – 0.47 V and, above this potential, the copper oxide surface is converted into CuOOH in NaOH electrolyte. Also, methanol is oxidized at a certain potential, which forms Cu(OH)₂ and CO₂ with a sharp increase in the anodic current density. This indicates that the electrooxidation of methanol takes place on the surface of the electrodes[4].

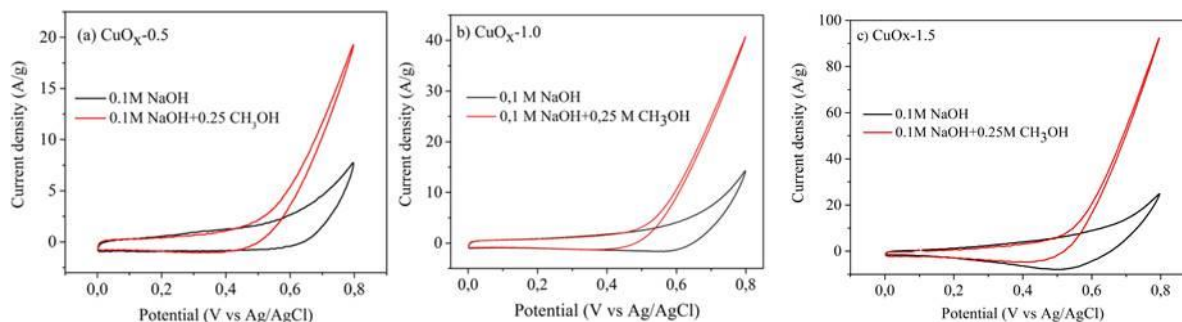


Figure 1. Cyclic voltammograms (CVs) at a scan rate of 50 mV/s for (a) CuO_x-0.5, (b) CuO_x-1.0 and (c) CuO_x-1.5 measured in 0.1M NaOH and (0.1M NaOH+0.25M CH₃OH) electrolytes

It is well known that two important parameters for methanol electrooxidation are the onset potential and the anodic current density. The results in Figure 1 show that the onset potentials for all samples are almost similar (0.44, 0.46 and 0.5 V for CuO_x-0.5, CuO_x-1.0 and CuO_x-1.5, respectively). However, the anodic current density of the CuO_x-1.5 (92 A/g) is much higher than that of the CuO_x-0.5 (19 A/g) and CuO_x-1.0 (41 A/g). It may be related to a higher electrocatalytic activity of CuO phase compared to Cu₂O[4]. Moreover, the anodic current density at the methanol oxidation potential for copper oxides may vary depending on the exposed crystal plane. In paper[5] it was shown that plate-like copper exhibits enhanced catalytic activity toward methanol oxidation compared to octahedron-like copper crystals depending on the exposed crystal plane. The results of the electrocatalytic performance clearly indicate that the copper oxides prepared by electrochemical oxidation/dispersion under pulse alternating current are suitable for use in methanol oxidation.

References

1. *Leontyeva D.V., Leontyev I.N., Avramenko M.V., Yuzyuk Y.I., Kukushkina Y.A., and Smirnova N.V.* Electrochemical dispersion as a simple and effective technique toward preparation of NiO based nanocomposite for supercapacitor application // *Electrochimica Acta*. 2013. V. 114. P. 356-362.
2. *Kuriganova A.B., Vlaic C.A., Ivanov S., Leontyeva D.V., Bund A., and Smirnova N.V.* Electrochemical dispersion method for the synthesis of SnO₂ as anode material for lithium ion batteries // *Journal of Applied Electrochemistry*. 2016. V. 46(5). P. 527-538.
3. *Ulyankina A., Leontyev I., and Smirnova N.* Electrochemical Synthesis and Photocatalytic Activity of Differently Shaped CuO_x Particles // *Nano Hybrids and Composites*. 2017. V. 13. P. 330- 333.
4. *Pawar S.M., Kim J., Inamdar A.I., Woo H., Jo Y., Pawar B.S., Cho S., Kim H., and Im H.* Multi-functional reactively-sputtered copper oxide electrodes for supercapacitor and electro-catalyst in direct methanol fuel cell applications // *Scientific Reports*. 2016. V. 6. P. 21310.
5. *Venkatasubramanian R., He J., Johnson M.W., Stern I., Kim D.H., and Pesika N.S.* Additive-Mediated Electrochemical Synthesis of Platelike Copper Crystals for Methanol Electrooxidation // *Langmuir*. 2013. V. 29(43). P. 13135-13139.

2D MODELLING OF THE MAIN COUPLED EFFECTS OF CONCENTRATION POLARIZATION IN ELECTROMEMBRANE SYSTEMS AND THEIR IMPACT ON ION TRANSPORT IN BINARY ELECTROLYTES

¹Makhamet Urtenov, ¹Anna Kovalenko, ¹Alexander Pismenskiy

¹ Kuban State University, Krasnodar, Russia, *E-mail: urtenovmax@mail.ru*

Introduction

Ion transport in membrane systems at overlimiting currents is accompanied by a number of coupled effects. The main ones are electroconvection and gravitational convection, the dissociation / recombination reaction of water molecules, and the Joule heating. At present, electroconvection is considered as the main cause of overlimiting ion transport in narrow cells of membrane systems [1].

At the same time, in the relatively wide cells, according to the results of theoretical [2] and experimental studies [3], the role of gravitational convection is also important.

Water splitting affects both gravitational convection and electroconvection. The dissociation of water molecules is accompanied by absorption of heat, and the recombination by release of heat. The appearance of new charge carriers can reduce the space charge and prevent electroconvection.

Experiments

In [4], a 2D model of salt ion transport in membrane systems was first constructed, taking into account the forced solution flow, the dissociation of water molecules and electroconvection, but without gravitational convection. With the use of this model, it is shown that with a low dissociation intensity of water molecules, the electroconvection actually weakens, and, as a consequence, there is a decrease in the overlimiting transport of salt ions.

However, with a further increase in the jump in the potential (or time), the electroconvection arises and starts to effectively mix the solution, which contributes to the enhancement of the overlimiting transport of salt ions. On the other hand, an increase in the potential jump leads to an increase in the dissociation reaction of water molecules in the membrane, and, accordingly, to an increase in the absorption of heat in the membrane and the release of heat in the solution due to the recombination of hydrogen ions and hydroxyl in solution. And this, in turn, can strengthen gravitational convection and hinder electroconvection.

Thus, when taking into account forced convection, the presence of opposing trends makes an actual problem theoretical and experimental study of the transfer of salt ions gravitational and electroconvection, the dissociation-recombination reaction of water molecules, and also the joule heating of the solution.

Results and Discussion

In this study, a mathematical model is constructed using the Nernst-Planck-Poisson equations, thermal conduction and Navier-Stokes equations, and natural boundary conditions.

For a numerical solution, the finite element method is used, with the splitting of the solved problem into three sub-tasks on each new time layer:

1) the electrochemical problem (the 2D Nernst-Planck and Poisson equations and the equation of dissociation / recombination reaction of water molecules), the solution of which gives the distribution of salt ion concentration, electric field strength, power of heat sources and sinks.

2) the thermal conductivity problem (the 2D thermal conductivity equation with the source and heat sink caused by the Joule heating of the solution (heat source) and the recombination of water molecules (heat flow)).

3) the hydrodynamic problem (the 2D Navier-Stokes equations with lifting Archimedean forces responsible for thermal convection and concentration convection, as well as electroconvection).

This approach to the development of numerical methods is original and allows us to solve the boundary value problems arising for modeling for a nonlinear system of partial differential equations.

Acknowledgments

This work was supported by Russian Science Foundation, grant № 16-08-00128 A.

References

1. *Nikonenko V., Kovalenko A., et al*, Desalination at overlimiting currents: State-of-the-art and perspectives // *Desalination* 2014. V. 342. P. 85-106.
2. *Pismenskiy A.V., Urtenov M.Kh., et al*, Model and experimental studies of gravitational convection in an electromembrane cell // *Russian Journal of Electrochemistry* 2012. V.48 (7), P. 756-766.
3. *Pevnitskaya M.V.* Intensification of mass transfer during electro dialysis of dilute solutions // *Electrochemistry* 1992. V.28. No. 11. P. 1708-1715.
4. *Kovalenko A.V.* Influence of Water Dissociation on the Development of Electroconvection in Membrane Systems // *Condensed Media and Interphase Boundaries* 2014., V. 16. No. 3. P. 288-293.

INFLUENCE OF THE DEGREE OF FUNCTIONALIZATION OF CARBOXYLATED HYPERBRANCHED POLYMERS ON ELECTROCHEMICAL CHARACTERISTICS OF ASYMMETRICAL BIPOLAR MEMBRANES

Stanislav Utin, Sergey Loza, Victor Zabolotsky, Alexander Besspalov, Victor Dotsenko
Kuban State University, Krasnodar, Russia, E-mail: utinstanislav@mail.ru

Introduction

Hyperbranched polymers are promising precursors for synthesis the modifiers that improve electrochemical properties of the bipolar membranes. The significant potential of hyperbranched polymers is the availability of a much higher number of reactive terminal groups than in a linear polymers (Fig. 1). The imparting to these polymers properties of catalysts for the dissociation of water is carried out through their chemical functionalization. In the present work asymmetric bipolar membranes modified by carboxylated hyperbranched polymers with different degrees of functionalization were obtained. The process of the pH correction of a dilute sodium chloride solution using modified membranes was investigated.

Objects and methods of research

The objects of research were the initial and modified asymmetric bipolar membranes, as well as the electro dialysis chambers formed by these membranes [2].

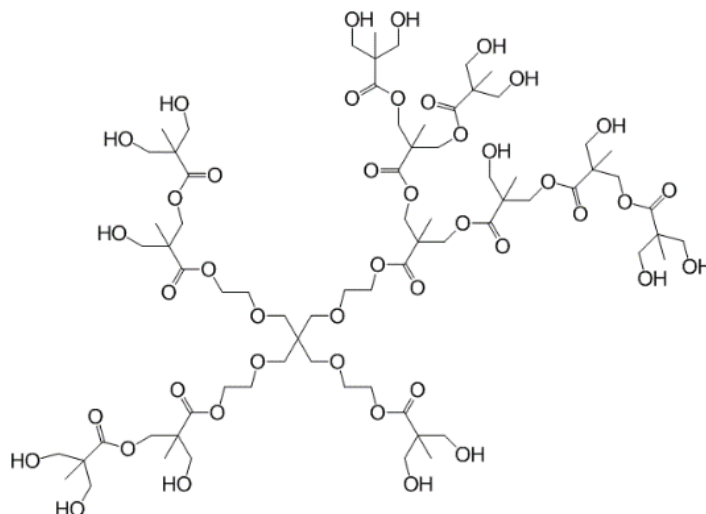


Figure 1. Structure of hyperbranched polymer Boltorn H20 [3]

The component composition of the ion exchange layers of the asymmetric and modified asymmetric bipolar membranes under investigation are presented in Table 1.

Table 1. Composition of ion exchange layers of asymmetric bipolar membranes

Asymmetric bipolar membrane	Anion exchange layer (Anion exchange resin)	Cation exchange layer
ABM	MA-41 (AV-17)	film of MF-4SK
ABM-M1	MA-41 (AV-17)	film of MF-4SK + Boltorn H20-COOH ⁶
ABM-M2	MA-41 (AV-17)	film of MF-4SK + Boltorn H20-COOH ¹⁰

The thickness of the cation-exchange homogeneous MF-4SK film for all investigated asymmetric bipolar membranes was 20 μm . As a modifying component of the cation exchange layer of the ABM-M1 membrane, a carboxylated Boltorn H20 polymer containing 6 terminal carboxyl groups was used. The modifier of the membrane ABM-M2 contained 10 carboxyl groups. As anion-exchange membranes, forming together with asymmetric bipolar membranes of the electro dialysis cell chamber, the commercially available strongly basic anion-exchange membrane MA-41 was used. In detail, the scheme of the electro dialysis cell and the procedure for obtaining asymmetric and modified asymmetric bipolar membranes are presented in [1].

Results and discussion

The modifiers based on hyperbranched polymers with a different number of carboxyl groups were obtained depending on the ratio of the initial reagents (Table 2). With the stoichiometric ratio of the reacting groups, a product with a degree of functionalization of 37.4% is formed, which leads to the conclusion that six hydroxyl groups from sixteen possible are acylated. It should be noted that with a double excess of phthalic anhydride, the degree of functionalization of the resulting carboxylated polymer increases to 62% as compared to the product obtained with the stoichiometric ratio of the reacting groups. At the same time, the sample obtained with a fourfold excess of phthalic anhydride, practically does not differ from the previous sample by the degree of functionalization, which indicates the attainment of the maximum possible degree of functionalization of the superbranched polymer used with phthalic anhydride, which is 62%.

Table 2. Effect of the initial reagent ratio on the degree of functionalization of Boltorn H20 with phthalic anhydride

[OH ⁻ groups] : [phthalic anhydride] ratio	Carboxyl groups content *, mmol/g	Functionalization degree, % *	Functionalization degree, % **	The average number of acylated hydroxyl groups
1:1	2.00	37.4	38.2	6
1:2	3.08	61.8	62.4	10
1:4	3.09	62.3	62.2	10

* - obtained by potentiometric titration

** - obtained by NMR ¹H

Modification of asymmetric bipolar membranes leads to a decrease in voltage drop on the membranes. Figure 2 shows the current-voltage characteristics of various asymmetric bipolar membranes in the process of the pH correction of the sodium chloride.

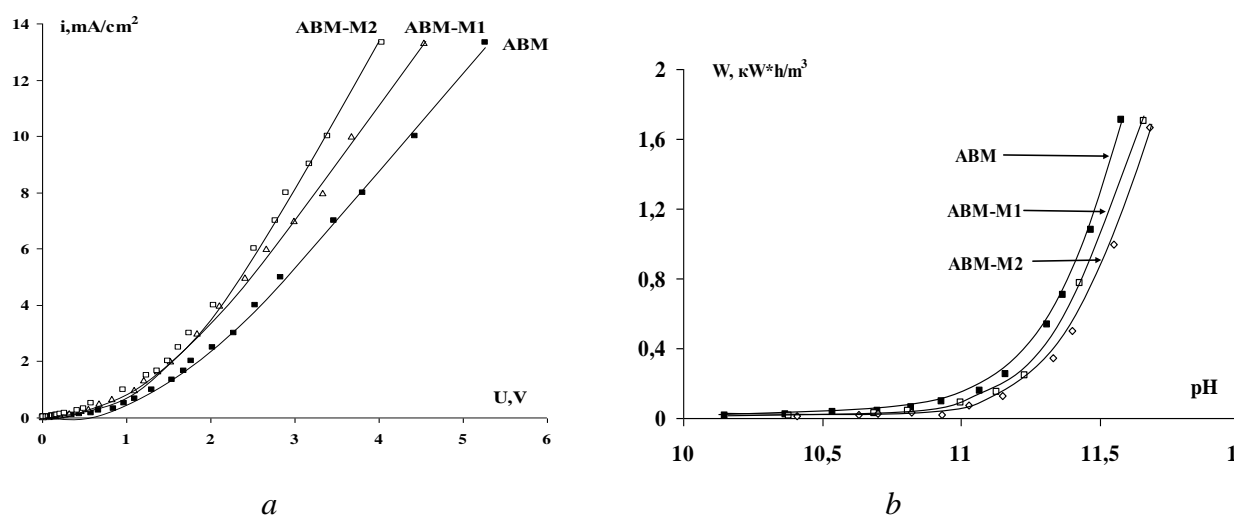


Figure 2. a - current-voltage characteristics of various asymmetric bipolar membranes in the process of correcting pH 0.01 M NaCl solution; b - dependence of energy consumption of the pH of the solution in alkaline electrodialysis chambers formed by the MA-41 membrane and various asymmetric bipolar membranes

The current efficiency for hydrogen and hydroxyl ions for membranes modified with carboxylated hyperbranched polymers have similar values (88% for the ABM-M1 membrane, 92% for the ABM-M2 membrane) and exceed the corresponding values for the initial unmodified asymmetric bipolar membrane (77%). The dependence of energy consumption of the pH values of the solution achieved in alkaline chambers (Fig. 2a) for chambers formed by various asymmetric bipolar membranes also confirms the high efficiency of modified asymmetric bipolar membranes.

The highest pH shift at the same energy expenditure is observed for an asymmetric bipolar membrane modified with a polymer with a degree of functionalization of 62%.

It was found that the maximum value of the degree of functionalization of the Boltorn H20 polymer is 62%. Asymmetric bipolar membranes modified with a carboxylated hyperbranched polymer with a higher degree of functionalization make possible to reduce the membrane voltage drop and energy consumption for the electro dialysis correction of the pH of a dilute sodium chloride solution.

The present work was supported by the Ministry of Education and Science of Russia within the framework of the base part project №10.9572.2017/BP.

References

1. *Zabolotsky V. S. Utin, A. Bespalov, V. Strelkov // Journal of Membrane Science – 2015. – Vol. 494. – P. 188-195.*
2. *S. Utin, V., Zabolotskii, K. Lebedev // Sorbtzionnye i khromatograficheskie protsessy 2015. V. 15. №6. P. 811.*
3. *E. Žagar, M. Žigon // Prog. Polym. Sci. 36 (2011) 53–88.*

TWO-DIMENSIONAL MATHEMATICAL MODEL OF OVERLIMITING TRANSFER IN MEMBRANE SYSTEMS TAKING INTO ACCOUNT ELECTROCONVECTION AND FORCED FLOW FOR THE GALVANOSTATIC MODE

¹Aminat Uzdenova, ²Makhamet Urtenov, ²Anna Kovalenko, ²Victor Nikonenko

¹Karachaevo-Cherkessky State University named after U.D. Aliev, Lenina Str., 29, 369200 Karachaevsk, Russia, E-mail: uzd_am@mail.ru

²Kuban State University, Stavropolskya Str. 149, 350040 Krasnodar, Russia

In this study we are developing a two-dimensional mathematical model of overlimiting transfer in membrane systems taking into account electroconvection and forced flow, which can be applied in the galvanostatic mode. The model is based on the decomposition of the Nernst-Planck-Poisson-Navier-Stokes equations system. If in the case of potentiostatic mode, the model is well established [1, 2], for the galvanostatic mode some mathematical difficulties are not overcome yet. We propose a new boundary condition and a new algorithm of calculations, which allows for effective computations and assures a good agreement between the results obtained for both electric modes in comparable conditions.

The chronopotentiograms calculated by the proposed model for different values of current density are shown in Fig. 1. Fig. 1 also shows the calculations for the potentiostatic model [2] for the potential drop values corresponding to the indicated current densities.

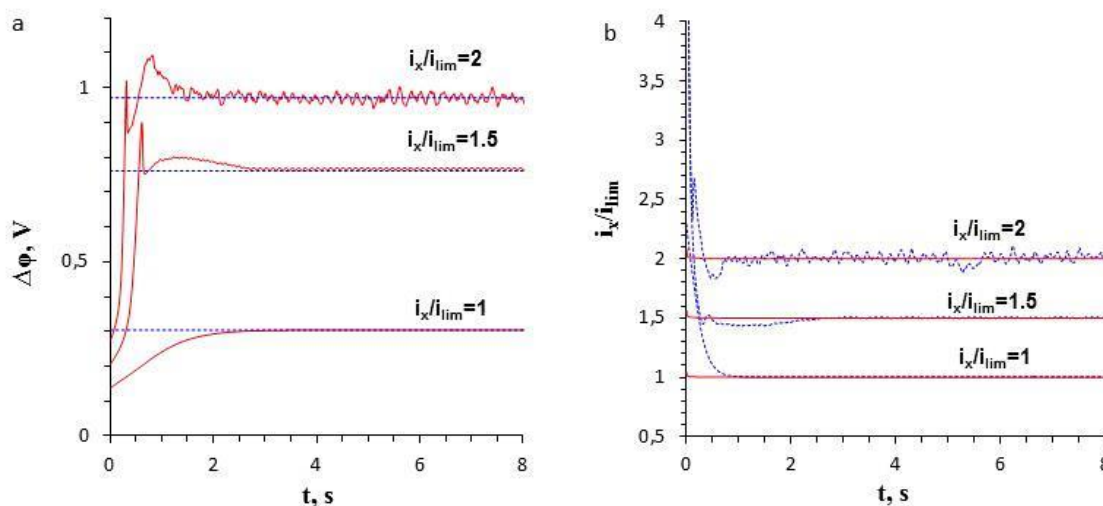


Figure 1. The dependence of the potential drop on time (a); the dependence of the average current density on time (b). The results of computation for galvanostatic model (solid lines) and potentiostatic model (dashed lines) for the current density $i_x/i_{lim}=1$; 1.5; 2.

As Fig. 1 shows, the results of calculation of potential drop / current density in quasi-steady state using galvanostatic / potentiostatic models are in good agreement.

Acknowledgements

We are grateful for financial support to the Russian Foundation for Basic Research (grant No 15-58-16005NCNIL_a).

References

1. Kwak R., Pham V.S., Lim K.M., Han J. Shear flow of an electrically charged fluid by ion concentration polarization: scaling laws for convection vortices // Phys. Rev. Lett. 2013. V. 110. P. 114501.
2. Urtenov M.K., Uzdenova A.M., Kovalenko A.V., Nikonenko V.V., Pismenskaya N.D., Vasil'eva V.I., Sistat P., Pourcelly G. Basic mathematical model of overlimiting transfer enhanced by electroconvection in flow-through electro dialysis membrane cells // J. Membr. Sci. 2013. V. 447. P. 190-202.

NEW REDOX-SORPTION MODEL AS WATER DEOXYGENATION DESCRIPTION METHOD

Dmitrii Vakhnin, Valeriya Pridorogina, Lev Polyanskii, Tamara Kravchenko
Voronezh State University, Voronezh, Russia, E-mail: krav280937@yandex.ru

Introduction

The mathematical model is developed. Numerical solution Cauchy problem for two migrating fronts of sustained chemical reaction's distinct stages is performed. The analysis of a polarizing current density effect to a velocity of reaction fronts migration, active substance concentration, the degree of redox sorption and the contribution from electrochemical and chemical components to the total rate is complete. The process of water-dissolved oxygen redox sorption by a copper-containing nanocomposite under the influence of electrochemical polarization was studied.

Results and Discussion

We obtained the Cauchy problem for ordinary differential equations (1) and (2) in relation to unknown functions of time $R_i(t)$, ($i = 1, 2$):

$$\frac{dR_1}{dt} = -\frac{2}{\varepsilon} D_1 \left. \frac{\partial c_1}{\partial R} \right|_{R=R_1}, \quad (1)$$

$$\frac{dR_2}{dt} = -\frac{2}{\varepsilon} \left(D_2 \left. \frac{\partial c_2}{\partial R} \right|_{R=R_2} - D_1 \left. \frac{\partial c_1}{\partial R} \right|_{R=R_2} \right), \quad (2)$$

where ε is the nanocomposite's content of the metal component, D_i и c_i are the coefficient of diffusion and the concentration of active substance (oxygen A), respectively. Than new dimensionless time τ was introduced. So equations (1), (2) are expressed in dimensionless variables as

$$\frac{d\xi_1}{d\tau} = -\frac{D_1}{D_2} \left. \frac{\partial C_1}{\partial R} \right|_{R=\xi_1}, \quad (4)$$

$$\frac{d\xi_2}{d\tau} = -\left. \frac{\partial C_2}{\partial R} \right|_{R=\xi_2} + \frac{D_1}{D_2} \left. \frac{\partial C_1}{\partial R} \right|_{R=\xi_2}, \quad (5)$$

$$\tau = 0: \quad \xi_1(0) = 1, \quad \xi_2(0) = 1. \quad (6)$$

Here, $\xi_1 = R_1 / R_0$ and $\xi_2 = R_2 / R_0$ are the dimensionless coordinates of the fronts of the metal oxidation products at the intermediate and final stages of the chemical reaction between metal nanoparticles and oxygen; $C_i = c_i / c_0$ is dimensionless oxygen concentration in nanocomposite; and $R = R / R_0$ is a dimensionless coordinate. Note that equations (4)–(6) include only one dimensionless parameter – the ratio of diffusion coefficients in subregions δ_i ($i=1,2$).

After substituting the expressions for concentrations C_i ($i=1,2$) from [1] into eqs. (4), (5) we finally obtained the following ordinary differential system described the distribution of distinct stages fronts of a sustained chemical reaction:

$$\frac{d\xi_1}{d\tau} = -\left(1 - \frac{i}{i_{\text{lim}}}\right) \frac{d_{12}\xi_2}{Z_s}, \quad (7)$$

$$\frac{d\xi_2}{d\tau} = -\left(1 - \frac{i}{i_{\text{lim}}}\right) \frac{\xi_1(\xi_2 - \xi_1) + d_{11}\xi_2}{Z_s}, \quad (8)$$

where $Z_s = [1 - (1 - Bi^{-1})\xi_2][\xi_1\xi_2(\xi_2 - \xi_1) + d_{11}\xi_2^2 + d_{12}\xi_1^2] - d_{22}(\xi_1^2 - \xi_1\xi_2 - d_{11}\xi_2)$, $d_{ij} = D_i / (k_j\delta'_jR_0)$ is a dimensionless set of kinetic constants; $Bi = D_3R_0 / (\delta D_2\gamma)$ is Biot's dimensionless diffusion criterion; D_3 is the coefficient of the external diffusion of the active component; δ and δ'_j are the widths of the external diffusion and reaction layers; k_j is the reaction rate constant; i is the density of the polarizing current; and i_{lim} is the density of the limiting diffusion current for component A. Analysis of the system of two ordinary differential equations shows that when condition $i = 0$ is met, the system of eqs. (1) and (2) is transformed into the familiar problem for a grain with no external polarizing electric current. The obtained values ξ_i are used for calculation of oxygen relative concentration on a solution/nanocomposite grain boundary surface, degree of redox sorption α , and the contribution of external diffusion stage. Value α can be presented as the sum of two terms:

$$\alpha = \alpha_{ch} + \alpha_{elch}, \quad (9)$$

where α_{ch} and α_{elch} are the degrees of redox sorption due to the reduction of oxygen in chemical (without electric current) and electrochemical reactions, respectively. Value α_{ch} is associated with the coordinates of distinct stages of the chemical reaction

$$\alpha_{ch} = 1 - \frac{\xi_1^3 + \xi_2^3}{2}, \quad (10)$$

while value α_{elch} is associated with the flowing charge,

$$\alpha_{elch} = \frac{Q(I)}{Q(I_{lim})} = \frac{I}{I_{lim}}. \quad (11)$$

Here, $Q(I)$ and $Q(I_{lim})$ represent the charge spent on the electroreduction of oxygen using electric currents I and I_{lim} , respectively. Also the relative surface oxygen concentration on a solution/nanocomposite grain boundary and contribution of external diffusion can be described.

Experiments

Kinetic dependences $\xi_i(\tau)$, $\alpha(\tau)$ were calculated for different densities of the cathode polarizing current. Figures 1 and 2 show that the velocity of front migration slows and the degree of redox sorption increases as the density of current grows.

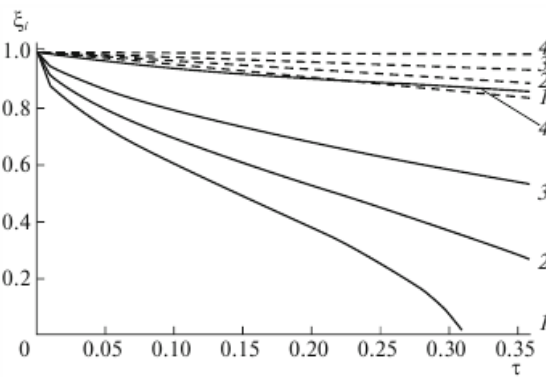


Figure 1. Kinetic curves for the coordinates of chemical reactions $\xi_1(\tau)$ and $\xi_2(\tau)$ in for different densities i/i_{lim} of the electric current: (1) 0; (2) 0.25; (3) 0.5; (4) 0.75. Solid curves are for $\xi_1(\tau)$; dashed curves, $\xi_2(\tau)$

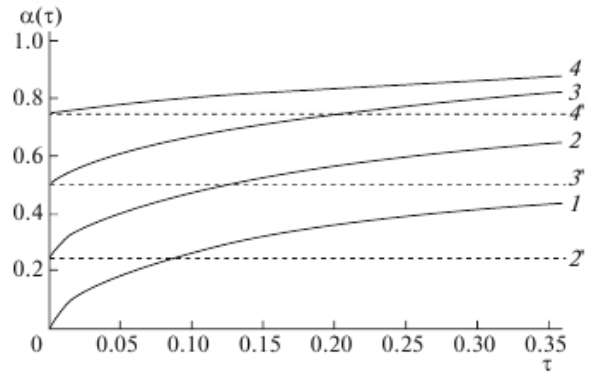


Figure 2. Degree of completion of the redox sorption of oxygen for different densities i/i_{lim} of the electric current: (1) 0, (2) 0.25, (3) 0.5, (4) 0.75. Solid curves $\alpha(\tau)$; dashed lines $\alpha_{elch}(\tau)$

The oxidation by oxygen of the copper-containing nanocomposite with electrochemical polarization lasted 150 hours. The grain sections were periodically examined, tracking the migration of fronts at the intermediate $\xi_1(t)$ ($Cu \rightarrow Cu_2O$) and final $\xi_2(t)$ ($Cu_2O \rightarrow CuO$) stages of metal particle oxidation sustained chemical reaction. It should be noted that variations in the positions of boundaries of separate reaction stages occur randomly (fig. 3) with the preferential

formation of copper (I) oxide. The expansion of the Cu_2O oxide layer and its propagation inside the grain were found to grow in proportion to the length of the experiment.

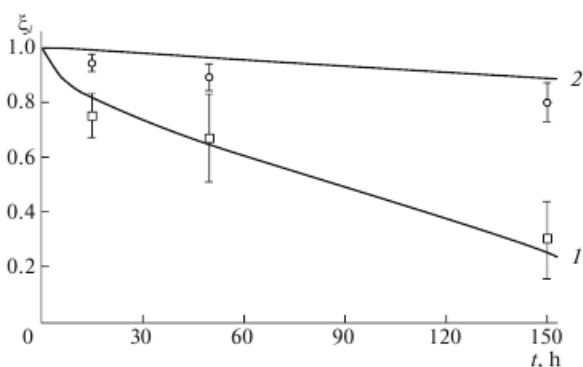


Figure 3. Kinetic curves for the coordinates of chemical reactions ξ_1 (1) and ξ_2 (2) upon electrochemical polarization of a thin granular layer of Cu-KU-23 (Na^+). The curves are for a granular layer with height $l = 1.0 \times 10^{-2}$ m; the water flow rate was 0.23 cm/s; the concentration of dissolved oxygen was 2.4×10^{-7} mol/L. The relative density i/i_{lim} of the current was 0.7. Experimental data are represented by points; data is calculated [2].

Conclusion

Solving the problem of two moving fronts from the chemical reactions of sustained metal oxidation during sorption in metal – ion exchange nanocomposites upon electrochemical polarization showed that polarization slows the rate of the radial outspread of the fronts from the formation of intermediate and end products of metal component oxidation. The degree of oxygen redox sorption from water increased due to the reduction of oxygen by electric current. The process was shifted to the region of external diffusion.

Acknowledgments

This work was supported by the Russian Foundation for Basic Research (grant № 17-08-00426_a) and by the Russian Ministry of Education and Science (grant № 675, 2014-2016, Voronezh State University).

References

1. Polyanskii L.N., Korzhov E.N., Vakhnin D.D., Kravchenko T. A. Macrokinetic model of redox sorption on metal-ion exchange nanocomposites at electrochemical polarization // Russ. J. Phys. Chem. 2016. V. 90. № 8. P. 1675-1681.
2. Polyanskii L.N., Korzhov E.N., Vakhnin D.D., Kravchenko T. A. Redox-sorption in metal-ion-exchanger nanocomposites upon electrochemical polarization // Russ. J. Phys. Chem. 2016. V. 90. № 9. P. 1889-1895.

THE CONFIGURATION OF THE LABORATORY UNIT FOR REVERSE ELECTRODIALYSIS PROCESS

Vladimir Vasilevsky, Eduard Novitsky, Evgeniy Trofimenko, Evgenia Grushevenko, Kirill Kutuzov, Alexey Volkov

A.V. Topchiev Institute of Petrochemical Synthesis, Moscow, Russia, E-mail: ednov@ips.ac.ru

Introduction

Nowadays, the use of various ethanolamines (mostly monoethanolamine (MEA)) as carbon dioxide absorbent in industry is widespread. MEA is the most common compound for the carbon dioxide absorption from fuel gases from oil, coal and energy industries [1]. However, its thermal regeneration to remove carbon dioxide is an energy-intensive process [2-4]. To compensate for at least part of the energy costs it is proposed to use reverse electro dialysis process. The basic principle of this process is the following: creation two streams with different concentration of electrolytes, what is lead to directional movement of charged particles through anion- and cation exchange membranes, thus creating an additional source of electricity. In this work configuration of the laboratory unit for reverse electro dialysis process for carrying out search study on the possibility of use reverse electro dialysis process of carbonized MEA solution for energy generation.

Experimental

Laboratory unit (fig. 1) for reverse electro dialysis is flat frame construction including two platinum electrodes 2 and 7 with active area 1 dm², gasket kit 3 made of polyvinylidenechloride, cation exchange 4 and anion exchange 6 membranes, MK-40 and MA-41 respectively, made by chemical industrial complex Shekinoazot, and turbulent mesh 5. Therefore, laboratory unit has three compartment: anode compartment, cathode compartment and buffer compartment.

The principle of the unit works is as follows:

1) Buffer compartment is filled carbonized MEA solution (concentration of MEA in this work was 7.5, 12 and 30%wt., carbonization degree – 0.7 mol CO₂/mol MEA) and electrode compartment is filled distillation water.

2) Under the influence of the concentration difference, directed diffusion of charged particles through ion-selective membranes occurs, as a result of which their discharge on the electrodes occurs with the formation of an electric current.

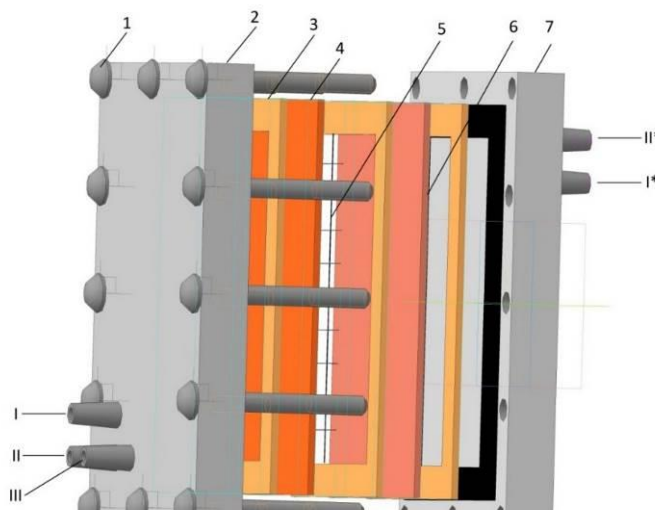


Figure 1. Laboratory installation of reverse electro dialysis.

1- Bolts M6x55 (12 pcs.); 2- Cathode; 3- Gasket (3 pieces); 4-Anion exchange membrane MA-41; 5- Turbulent mesh; 6- Cation-exchange membrane MK-40; 7- Anode. I-I * - Motion of the MEA flow inside the apparatus; II-II * - Movement of the near-cathode stream; III-III * - Movement of the pre-anode flow.

To determine the concentration of carbon dioxide in the reverse electro dialysis process, calibration curves were constructed for the dependence of the specific electrical conductivity on the carbonization degree of aqueous monoethanolamine solutions (Fig. 2).

Results and Discussion

The experimental start-up of the apparatus was carried out on model MEA solutions, while the solution was continuously circulated inside the chamber. In the case of a 12% MEA solution, with a parallel connection of a voltmeter and an ammeter to the system, the indicators on the instruments recorded a value of 0.07 V and 0.22 mA, which corresponds to a power of 0.154 W / (m² electrode). In the experiment in the absence of solution circulation in the buffer chamber, the readings of the ammeter and voltmeter coincide with the values in the case of circulation of the solution. The report will present data on process optimization: selection of the optimal concentration of MEA solution, saturated with carbon dioxide, fed into the buffer chamber and selection of the optimal composition of the solution feeding the pre-cathode and pre-anode chamber to increase the electromotive force (EMF) of the system, which leads to the maximum value of the energy received.

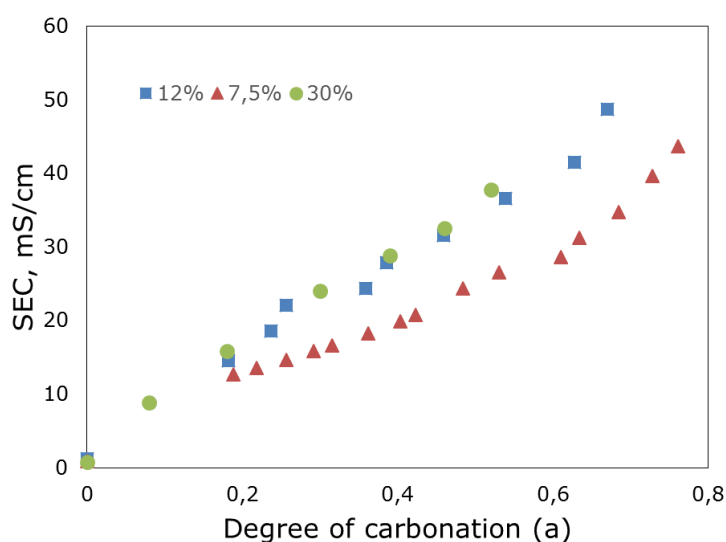


Figure 2. Calibration curves of the degree of saturation of the solution of MEA with carbon dioxide from the specific electrical conductivity.

Acknowledgements

This work was supported by the Russian Foundation for Basic Research, project no. 17-08-00312.

Reference

1. Lapidus A.L., Golubeva I.A., Zhagfarov F.G. Gas chemistry: a study guide. - M.: CentrLit-Neftegaz, 2008. - 450 p.
2. Vakk E.G., Shuklin G.V., Leites I.L. Production of process gas for the production of ammonia, methanol, hydrogen and higher hydrocarbons. Theoretical bases, technology, catalysts, equipment, control systems - 2011, Moscow. 480 p.
3. Dow. Gas Conditioning Fact Book. — Midland, MI, USA : Dow Chemical Company, 1962.
4. IAGHG, Evaluation of reclaimer sludge disposal from post-combustion CO₂ capture, 2014/02, March 2014.

THE SURFACE ANALYSIS OF THE CM PES ION EXCHANGE MEMBRANES WITH THE DIFFERENT DEGREE OF ION EXCHANGER DISPERSION BY SEM AND AFM METHODS

¹Vera Vasil'eva, ¹Elmara Akberova, ¹Evgeniya Kozhuhova, ²Lubos Novak, ³Victor Zabolotsky, ³Konstantin Lebedev

¹Voronezh State University, Voronezh, Russia, *E-mail: viv155@mail.ru*

²Mega a.s., Strazh pod Ralskem, Czech Republic

³Kuban State University, Krasnodar, Russia

Introduction

At present, one of the directions in improvement of electromembrane methods of substances separation and isolation is the development of new membranes with optimized surface morphology. The use of such membranes in electrodialysis processes creates the prerequisites for a significant increase in the efficiency of processes in overlimiting current regimes due to the development of electroconvection. The purpose of this work is a comparative analysis of the surface microstructure of the experimental samples of membranes with different ion exchanger dispersion degrees.

Experiments

In the study there was evaluated the electrical homogeneity degree of experimental samples of heterogeneous cation-exchange CM Pes membranes (Mega a.s., Czech Republic). The membranes were obtained by rolling the homogenised mixture of milled ion-exchanger with varying dispersion degrees with polyethylene. The dispersion degree of sulfocation-exchanger was varied by using of different time of its milling. The used membranes were chemically conditioned by sequential treatment with solutions of acids and alkalis.

The experimental studies of surface morphology of hydrated and dry membranes were conducted using the method of scanning electron microscopy at JSM-6380 LV microscope (Japan) equipped with regulated pressure, what allows the ion exchange material to be studied under real conditions of its operation (water swollen state). Microphase fractions and sizes were estimated by means of an original software system [1]. The ion-exchange particles dispersion degree D was assumed to be the reciprocal of their diameter. The AFM images of dry membrane samples were processed by means of the Nova RC1 software of a Solver P47 Pro microscope. The typical amplitude parameters of the surface roughness were analyzed according to the international standards ISO 4281 and ANSI B.46.1.

Results and Discussion

The electrical heterogeneity of the membrane surface is characterized by the proportion and sizes of the conducting regions (ion exchanger particles and pores near them). From the analysis of SEM-images (Fig. 1) of membrane samples, it was found that the proportion of ion exchanger for heterogeneous membranes CM Pes is 15-17% (Table 1).

Table 1: Surface characteristics of heterogeneous CM Pes samples after conditioning

Milling time, min	$S, \%$	$\bar{R}, \mu\text{m}$	$R_{\min} - R_{\max}, \mu\text{m}$	$P, \%$	$\bar{r}, \mu\text{m}$	$r_{\min} - r_{\max}, \mu\text{m}$	$D_{\min} - D_{\max}, 10^4 \text{ m}^{-1}$
5	16.6±0.7	1.85±0.07	0.6 – 15.0	2.7±0.2	1.55±0.03	0.4 – 7.0	3 – 83
40	16.8±0.5	1.76±0.06	0.5 – 8.0	2.6±0.3	1.43±0.05	0.5 – 4.0	6 – 120
80	15±1	1.52±0.03	0.4 – 9.0	1.81±0.05	1.27±0.04	0.3 – 5.0	6 – 125

where S is the proportion of the ion exchanger; P is the porosity; \bar{R} and \bar{r} are the radii of the ion exchangers and macropores, respectively; D is the ion exchanger dispersion degree.

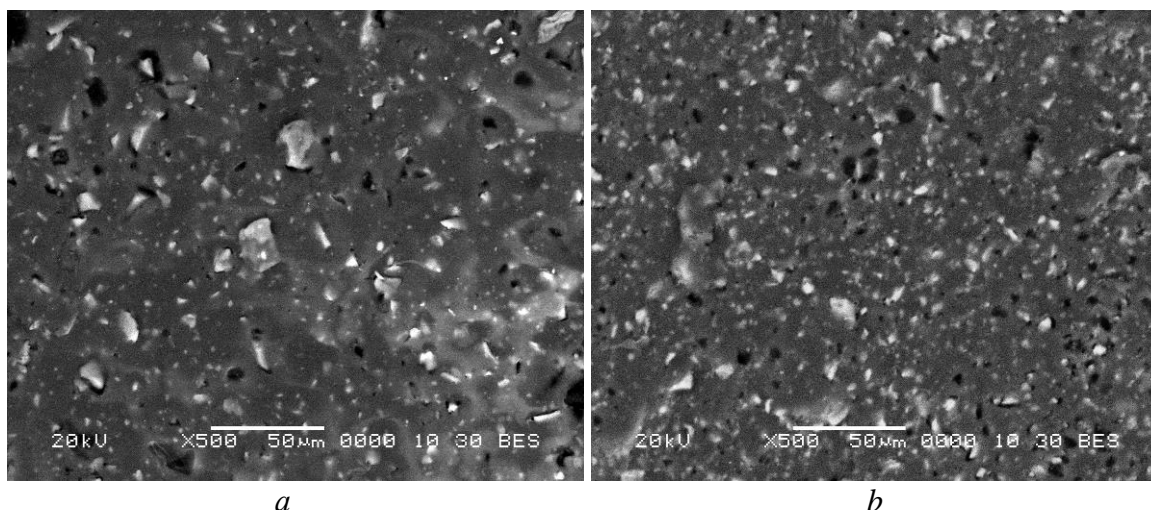


Figure 1. Micrographs of the surface of sulfonation-exchange membranes in swollen state. Time of ion-exchanger milling: 5 min (a) and 80 min (b).

A comparative analysis of the distribution of ion-exchange areas over the radii shows that the maximum on the distribution curve for all membrane samples was in the 1-2 μm region (Fig. 2). With the increase in the time of ion-exchange particles milling, an increase in their total quantity and a significant increase in the fraction of the ion exchanger with a radius of less than 0.7 μm is established. For membrane samples with the milled ion exchanger for 5 and 80 min, the range of the dispersion degree is $(3 - 80) \cdot 10^4 \text{ m}^{-1}$ and $(6 - 120) \cdot 10^4 \text{ m}^{-1}$ respectively. With an increase in the degree of dispersion of ion-exchange particles on the surface of swollen samples of CM Pes membranes, the value of their average radius decreases by 20% and amounts to $1.52 \pm 0.03 \mu\text{m}$ for membranes with the maximum ion exchangers grinding time. According to estimates made in [2], the value of the average radius \bar{R} for the Ralex CM Pes sulfonation exchange membrane that is serially produced by the «MEGA a.s.» company is 1.88 μm .

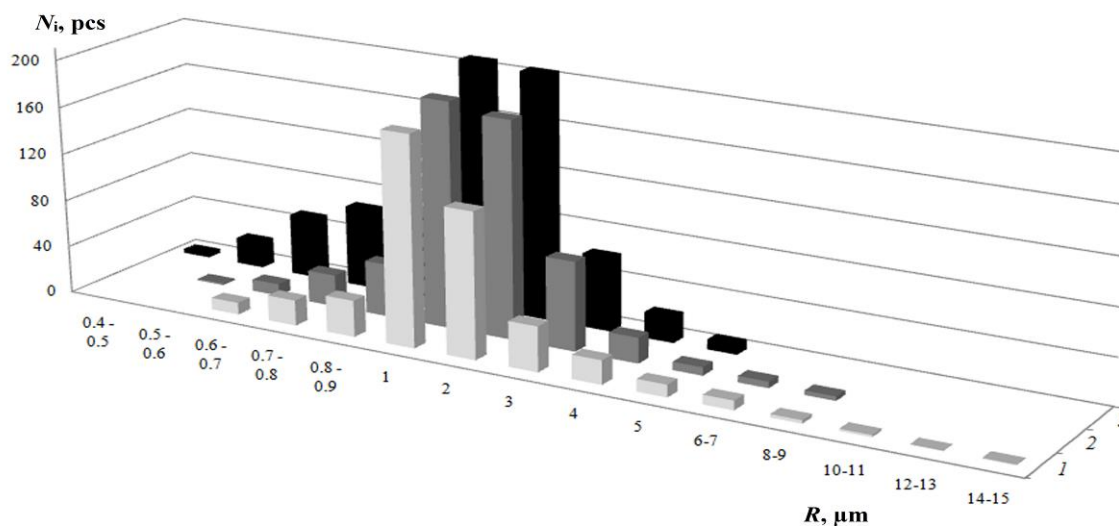


Figure 2. Distribution of ion-exchanger over radii for swollen conditioned samples of CM Pes membranes with time of ion-exchanger milling: 5 (1), 40 (2) and 80 min (3).

The reduction in the sizes of the ion exchanger regions on the surface of the experimental CM Pes membranes is accompanied by the convergence of the conducting surface zones: the effective distance between the ion exchangers is more than twice and amounts to 11.45 and 5.49 μm for a milling time of 5 and 80 min, respectively.

A significant difference is found between the total surface porosity of CM Pes membranes with the different degree of the ion exchanger dispersion. With increase in time of ion-exchange particles milling from 5 to 80 min, the macroporosity on the surface of the conditioned membranes

in the swollen state decreases from 2.7 to 1.8%, wherein the average pore radius values are 1.55 ± 0.03 and 1.27 ± 0.04 μm , respectively. An increase in the degree of ion exchanger dispersion is one of the main reasons for the reduction in the radius and area of macropores on the surface.

A comparison of the surface microrelief of the experimental CM Pes heterogeneous cation exchange membranes in the dry state is shown in Fig. 3a. The membrane with a higher degree of ion exchanger dispersion was characterized by a smoother surface on a micrometric scale: the maximum height R_y and the average arithmetic roughness R_a were 286 nm and 12 nm, respectively. Wherein, the maximum density distribution of the heights on the entire surface of the membrane sample was 1 μm (Fig. 3b). The microprofile of the membrane containing the ion exchange particles after 5 minutes of grinding had the appearance of a more developed chaotic structure with an average roughness scale R_a twice as large (Fig. 4). The maximum of density of the height distribution corresponded to a region of 4-6 μm .

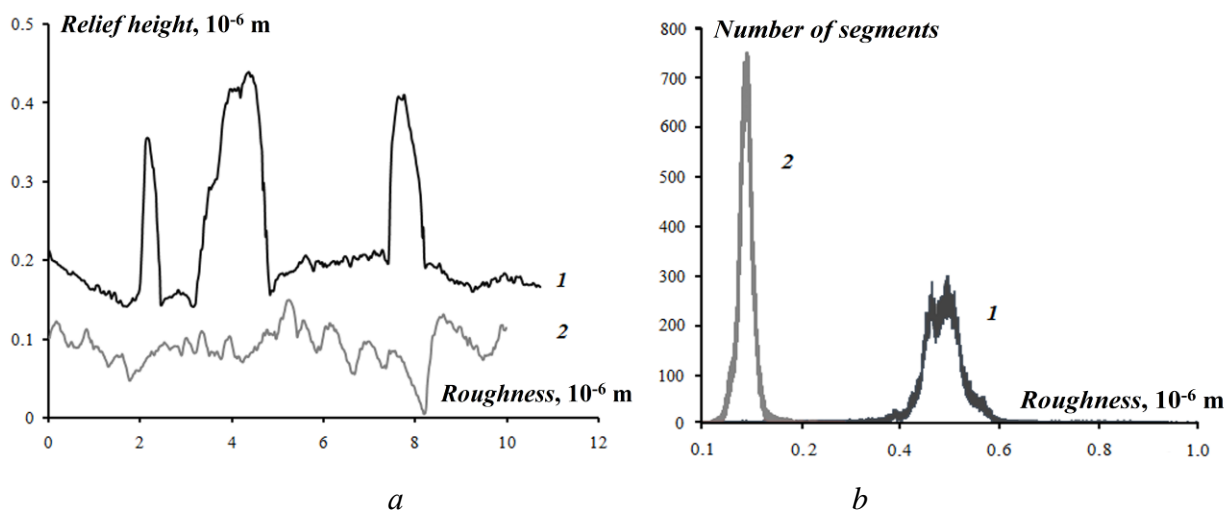


Figure 3. The microprofiles (a) and histogram of the density distribution of the heights for the entire image (b) of the samples of the CM Pes membranes with the ion exchanger milling time of 5 (1) and 80 (2) min. Scanning area of 10×10 μm .

Thus, the differences in the surface microstructure of the swollen samples of the experimental Ralex CM Pes heterogeneous sulfocation exchange membranes (Czech Republic) with different time of the ion exchanger milling are visualized by microscopic analysis methods. The reduction in the size and the convergence of the conducting phase zones, the decrease in the porosity and roughness of the surface of the membranes containing the ion exchanger subjected to a longer grinding time are revealed.

Acknowledgements

The present work is financially supported by the RFBR (project No 16-48-230433). Microphotographs of the membranes surface were obtained at the CCUSE of VSU.

References

1. Sirota E.A., Kranina N.A., Vasil'eva V.I., Malykhin M.D., Selemenev V.F. Development and experimental approbation of software for determining the fraction of the ion-conducting surface of membranes from scanning electron microscopy data // Vestnik VGU, Seriya: Himiya, Biologiya, Farmaciya. 2011. № 2. P. 53-59. (in Russian)
2. Vasil'eva V. I., Zhil'tsova A. V., Akberova E. M., Fataeva A. I. Influence of surface heterogeneity on current-voltage characteristic of heterogeneous ion-exchange membranes // Kondensirovannye sredy i mezhfaznye granitsy. 2014. Vol. 16. No. 3. P. 257-261. (in Russian)

THE STUDY OF RADIOLYSIS PRODUCTS IN THE TRACKS OF POLYETHYLENE TEREPHTHALATE AND POLYCARBONATE AS THE DISTANCE FROM THE ION TRAJECTORY

Alexander Vilensky

Institution crystallography and fotoniki A.V. Shubnikov RAS, 119333, Moscow, Leninsky prosp. 59.

E-mail: track@eimb.ru

Introduction

Latent tracks and track-etched membranes, the formation of micro - and nanometer range, are promising objects for research. The peculiarity of these structures lies in the fact that they have a discrete character. As the distance from the axis of the track of physical and chemical characteristics of such entities are changed to their initial values. The size of the tracks also depends on the mass and energy of energetic ions. So, for example, Kg for ions with energies of 1-2 MeV/a.e.m. the maximum size, according to preliminary data, 50 nm. The aim of this work is the study of changes in the area of the track as the distance from the ion trajectory.

Experiments

We used a standard film of polyethylene terephthalate (PET) and polycarbonate (PC) with a thickness of 10 μm is irradiated at JINR (Dubna) with accelerated ions of Xe, Kr, Ar, or the uranium fission fragments with the density of ion 10^9 ion/cm² and energy of 2 MeV/a.e.m. The density of tracks and their size was controlled by electron and atomic force microscopy. Track-etched membranes were obtained by etching in 1M aqueous KOH solution.

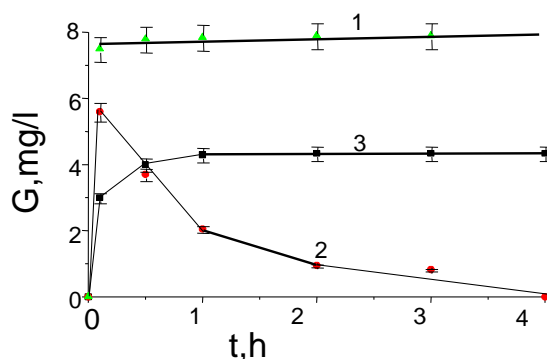


Figure 1. The accumulation of radiolysis products (2) and terephthalic acid (3) in water from PET irradiated Xe. 1 - Accumulation of TPA in the control sample.

To study changes in polymers, as the distance from the ion trajectory, a method is developed layer-by-layer etching. It is a sequential (layer by layer) the etching of the polymer up to a certain diameter and investigation (at each stage of etching) as products, passed into solution, and changes in the polymer. Each layer includes the following operations: determination of areas of etching (pore size before and after etching); the analysis of products, both in solution and in the remaining region tracks.

To research products etched in a solution using high-performance liquid chromatography (HPLC), UV - and IR-spectroscopy.

To study the polymer after each stage of etching used IR and UV spectroscopy, the spectroscopy of Raman scattering (RS) and atomic force microscopy (AFM).

The kinetics of accumulation of radiolysis products in solution are presented in Fig. 1. Products from RT for 15 min diffuse into the water, and then gradually dissolved with the formation of terephthalic acid Fig1, кривые 2,3). In addition, from Fig.1 also, of the irradiated polymer products extracted less than from non-irradiated, probably due to the formation of crosslinks.

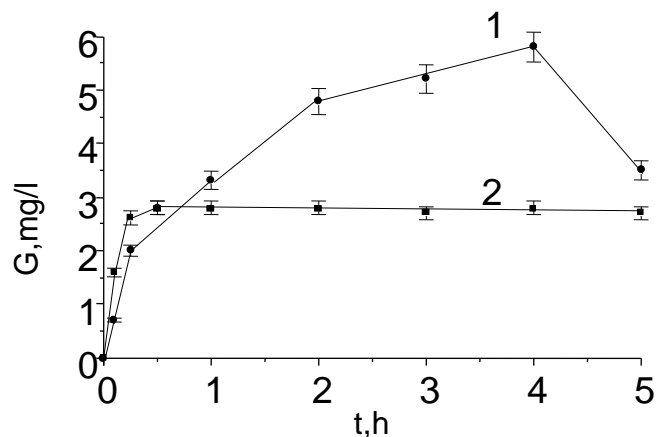


Figure 2. The accumulation of radiolysis products (1) and TPA (2) in water from PET irradiated Ar ions (1 MeV/a.e.m.) a fluence of 10^9 cm^{-2}

Chromatogram analysis of radiolysis products from tracks Ar (Fig. 2) shows that their accumulation in water occurs within 4 h, much more slowly than the tracks Xe. This difference is due to the fact that the area of damage of polymer Ar ions is much less than Xe ions. In addition, it is clear that the major share of radiolysis products is terephthalic acid. Slightly different look chromatogramme of radiolysis products allocated to water from tracks in PETP irradiated with fission fragments of uranium (Fig. 3). In this case, the retention time of the products of radiolysis on the hydrophobic stationary phase is greater than that of terephthalic acid (TPA retention time of 3.8 min), i.e. these products are more hydrophobic.

The kinetics of accumulation of radiolysis products in water tracks from PET irradiated with fission fragments of uranium, represented Fig 3. From comparison of the kinetic curves presented, it follows that LT Xe in the initial moment of time in the water radiolysis products of the forms times more TFA and approximately as many times less than that of LT of uranium fission fragments. This difference is probably due to the fact that in a nuclear reactor irradiation of the polymer by fission fragments is at an elevated temperature ($\sim 100^\circ\text{C}$) and, in addition, is accompanied by γ -irradiation.

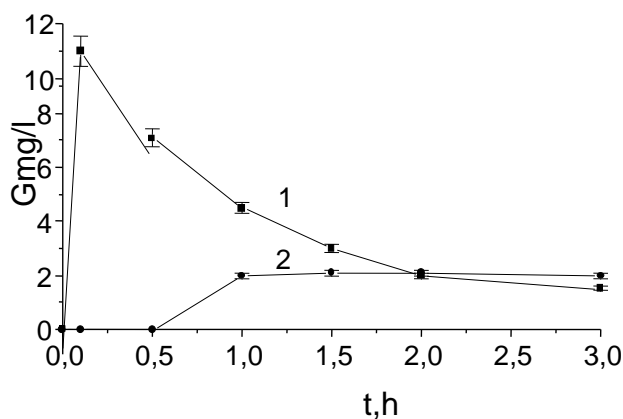


Figure 3. The accumulation of radiolysis products (1) and TPA (2) in water after irradiation of PET to the uranium fission fragments. Fluence $2 \cdot 10^9 / \text{cm}^2$

The kinetics of accumulation of radiolysis products in water tracks from PET irradiated with fission fragments of uranium, represented Fig 3. From comparison of the kinetic curves presented, it follows that LT Xe in the initial moment of time in the water radiolysis products of the forms times more TFA and approximately as many times less than that of LT of uranium fission fragments. This difference is probably due to the fact that in a nuclear reactor irradiation of the polymer by fission fragments is at an elevated temperature ($\sim 100^\circ\text{C}$) and, in addition, is accompanied by γ -irradiation.

Thus, on the basis of the results presented in this section, we can conclude that the composition of radiolysis products depends on the mass and energy of high energy particles. These products are hydrolytically unstable. They decompose with the formation of mainly terephthalic acid. By the nature of the chromatograms, retention time, we can assume that some of the products isolated from the tracks Xe, are esters of terephthalic acid. Similar products found at deep pyrolysis of PET. The other part of products, extractable with chloroform, are aromatic peroxides structure.

CAPACITIVE DEIONIZATION OF WATER USING MEMBRANE OF MOSAIC STRUCTURE

¹Yurii Volfkovich, ¹Alexey Rychagov, ¹Alexey Mikhailin, ²Marina Kardash, ³Natalia Kononenko, ²Denis Ainetdinov, ³Svetlana Shkirskaia, ¹Valentin Sosenkin

¹A.N. Frumkin institute of Physical Chemistry & Electrochemistry of the RAS, Moscow, Russia

E-mail: yuvolf40@mail.ru

²Engels State Tehnology University, Russia

E-mail: m_kardash@mail.ru

³KubanStateUniversity, Krasnodar, Russia

E-mail: kononenk@chem.kubsu.ru

Introduction

Production of pure drinking water using capacitive deionization (CDI) is complicated by high energy consumptions due to high ohmic losses caused by a huge resistance of deionized water. However, electrical conductivity of electrodes made of activated carbon (AC) is rather high even in pure water, since AC contains surface functional groups, which provide surface conductivity [1]. During the final stage of the CDI process, energy consumptions are limited by low conductivity of water inside pores of the separator, which is placed between the electrodes. The aim of the work was to develop membrane-electrode assembly (MEA) for CDI and investigate its operation. In opposite to known assemblies, the original mosaic membrane (MM) containing both cation- and anion exchange groups has been proposed as a porous separator.

Experiments

The film and fibrous heterogeneous MM (Fig. 1) were prepared by mixing of powders of KU-2 cation-exchange and AV-17 anion-exchange resins, their mass ratio was 7:3. The technique has been developed based on the method of Polycan membrane preparation.

Two types of AC electrodes were used, namely AC textile (*Kuraray, Japan*) and materials prepared from disperse AC (*Norit, the Netherlands*). The electrodes were characterized by both cation- and anion exchange capacity that is necessary for CDI. Porous structure of the MM and AC electrodes was researched by means of a standard contact porosimetry method using octane and water as working liquids [2]. This gave a possibility to determine both hydrophilic and hydrophobic pores.

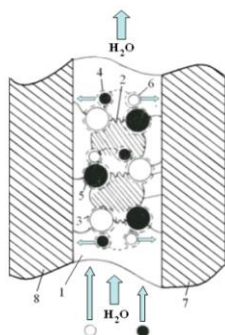


Figure 1. Scheme of MEA involving MM structure: 1 - inert polymer, 2 - micropores, 3 - anion exchange groups in anion-exchanger, 4 - anions; 5 - cation-exchange groups in cation-exchanger, 6 - cations; 7 - cathode; 8 - anode.

Results and Discussion

Fig. 2 illustrates electrical conductivity of film and fibrous MM immersed with NaCl solutions of different concentration. Extrapolation of the curves to zero concentration gives significant values of specific conductivity caused by functional groups.

MM and two similar AC electrodes were immersed with twice deionized water in a symmetric static cell (without water flow). Cyclic curves, which reflect a dependence of capacitance on voltage show extremes. The extremes are caused by charging of electric double layer and by rather high resistance. High values of maximal specific capacitance of the AC electrodes ($55\text{--}66\text{ F g}^{-1}$) confirm the possibility to obtain pure water using MM and AC electrodes.

Electrical conductivity of very low concentrated KCl solution (0.005 M) was measured for stages of deionization and concentration. The measurements were performed in a dynamic cell, where a flow of water was provided. The fibrous MM was used as a separator. Deionization occurred, when voltage was applied. The concentration stage began under closed circuit

conditions. Fig. 4 illustrates a change of the solution concentration over time during charging-discharging of the electrodes.

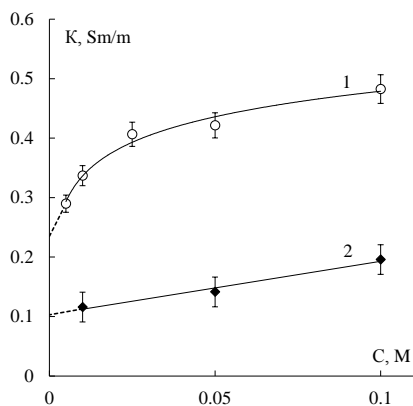


Figure 2. Conductivity of film (1) and fibrous (2) MM as a function of concentration of equilibrium NaCl solution:

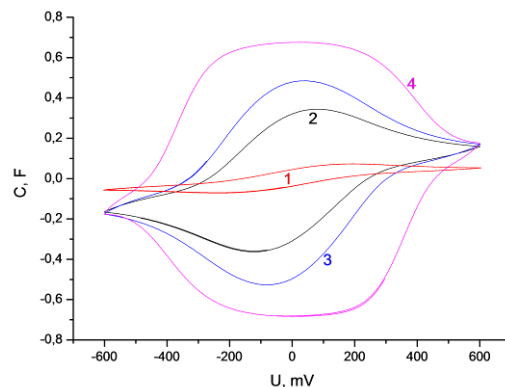
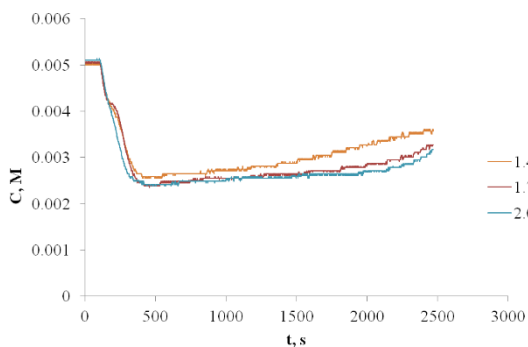
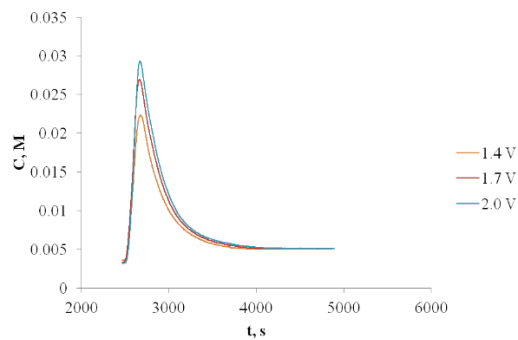


Figure 3. Capacitance of the static cell as a function of applied voltage. Scan rate was 20 (1), 2 (2), 1 (3), 0.1 (4) mV s^{-1}



a



b

Figure 4. KCl content in the solution during deionization (a) and concentration (b). The flow rate was $5 \text{ cm}^3 \text{ min}^{-1}$

Increasing in voltage slightly improves both deionization (Fig. 4a) and concentration (Fig. 4b). During the concentration stage (energy regeneration), the CDI cell is supplied by energy. This compensates the energy consumptions for deionization. The resulting energy (W_{CDI}) is equal to $W_{deion} - W_{conc}$, where W_{deion} is the energy spent to deionization, W_{conc} is the energy released during concentration. It is the W_{CDI} energy that must be taken into consideration during the CDI stack operation, since there is a gain due to the energy released during the concentration stage.

The energy consumptions of the cells with fibrous MM and porous glass separator were compared for deionization-concentration stages and resulting energy (Fig. 5). As follows: the energy decreases sufficiently for the cells with two types of separators due to concentration stage. This causes much lower energy consumption of the CDI process in comparison with reverse osmosis. It should be also noted that all types of energies increase with a growth of voltage. Moreover, the values of resulting energy are lower for the cell with MM than those for the cell containing porous glass separator.

The dependencies of specific resulting CDI energy (per 1 mol of salt desorbed from the electrodes) on voltage are plotted in Fig. 6 for the cells with fibrous MM and porous glass separator. As seen, the energy consumption reduces with decreasing in voltage. The curves demonstrate plateau at $U \leq 1.4 \text{ V}$ in the case of MM. The values of energy consumption are lower than those for the cell with glass separator. This is caused by features of ion transport in solids of different types. When the solution concentration is minimal, the transport in the cell containing MM is due to counter-ions of functional groups located not only in the AC electrodes, but also in

the membrane. At the same time, the glass separator is practically free from mobile ions.

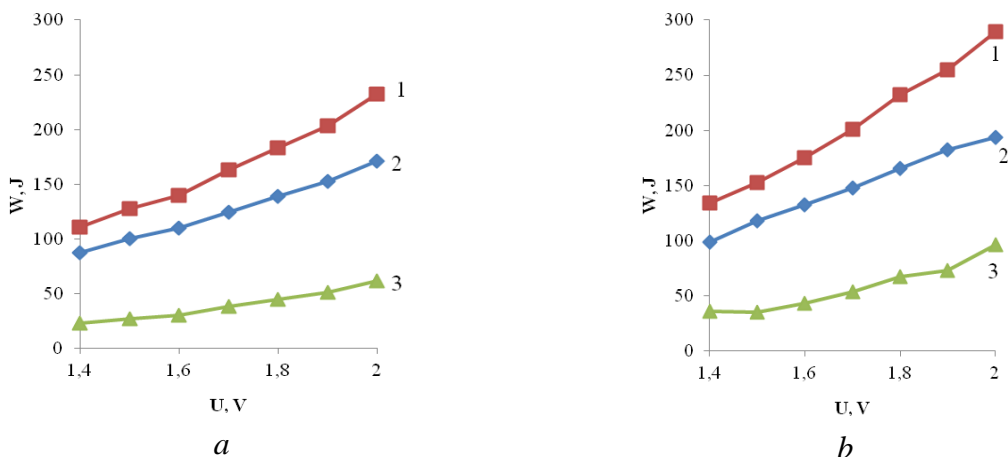


Figure 5. Energy, which is necessary for deionization (1), released during concentration (2) and resulting value as a function of applied cell voltage. The CDI cell contained MM (a) and porous glass separator (b). The flow rate was $5 \text{ cm}^3 \text{ min}^{-1}$.

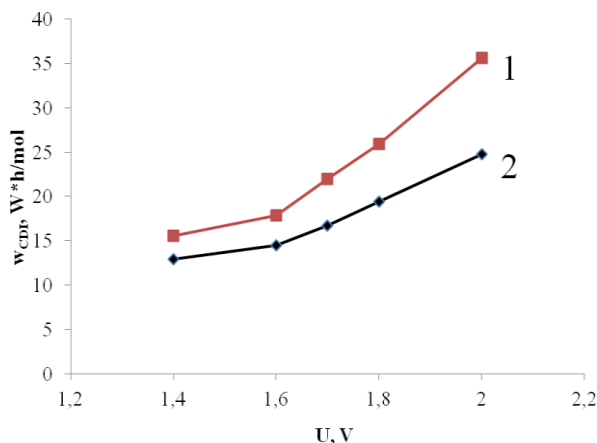


Figure 6. Specific resulting deionization energy as a function of applied voltage for the cell containing porous glass separator (1) and MM (2). The flow rate was $5 \text{ cm}^3 \text{ min}^{-1}$.

Conclusions

In order to compare two types of separators (MM and glass), it is necessary to take their different thickness and porosity into consideration. The thickness of fibrous MM is $450 \mu\text{m}$, its porosity is 53%. Regarding the glass separator, these characteristics are $300 \mu\text{m}$ and 93%. Based on data of Figs. 4a and 6, it is possible to conclude that optimal voltage is 1.4 V for the cell with MM: minimal energy consumptions and maximal deionization degree are reached under these conditions. In general, CDI process involving MM is more attractive from the economical point of view than the process, when inert porous separator is used.

References

1. Volkovich Yu.M., Mikhailin A.A., Rychagov A.Yu. Surface conductivity measurements for porous carbon electrodes // Russ. J. Electrochem. 2013. 49. P. 594–598.
2. Volkovich Yu.M., Sosenkin V.E., Bagotzky V.S. Structural and wetting properties of fuel cell components // J. Power Sources. 2010. V. 195. P. 5429–5441.

BROMATE ANION REDUCTION VIA AUTOCATALYTIC CYCLE AND ITS IMPLICATIONS FOR ELECTRICAL ENERGY SOURCES

¹⁻⁴ Mikhail Vorotyntsev, ¹ Yuriy Tolmachev, ^{1,3} Dmitry Konev, ^{1,2} Anatoly Antipov

¹D. I. Mendeleev University of Chemical Technology of Russia, Moscow, Russia

²M. V. Lomonosov Moscow State University, Moscow, Russia

³Institute of Problems of Chemical Physics, Russian Academy of Sciences, Chernogolovka, Russia

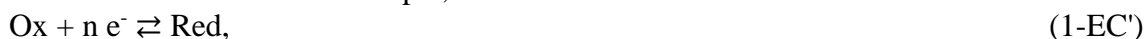
⁴ICMUB, UMR 6302 CNRS-Université de Bourgogne, Dijon, France

E-mail: mivo2010@yandex.com

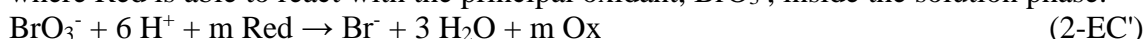
Redox flow batteries (RFB) represent a prospective direction in electrochemical energetics owing to their functioning without precious, deficient or hazardous elements [1]. Being mostly based on dilute reversible redox systems, they provide relatively low power densities [1,2]. Significantly higher power densities (about 1 W/cm²) have recently been achieved [3,4] for H₂-Br₂ RFBs. But their energy density still remains insufficient for mobile applications.

Much higher redox-charge and energy densities (790 A h and 1100 W h per kg, 1400 A h and 2000 W h per dm³ of solution) have been predicted [5,6] for the cathodic process of RFBs based on H₂-BrO₃⁻ chemistry, owing to a very high solubility of LiBrO₃ (almost 9 M at room temperature), the 6-electron character of its reduction to Br⁻ and a relatively high (for aqueous solutions) standard potential of this process (1.41 V SHE). However, the bromate anion is non-electroactive within the proper potential range.

Conventional approach to overcome this difficulty is based on the EC' mechanism, i.e. via addition of a reversible redox couple, Ox/Red:



where Red is able to react with the principal oxidant, BrO₃⁻, inside the solution phase:



Set of reactions (1-EC') and (2-EC') forms a cycle transforming bromate anions to bromide ones.

However, it has been demonstrated [6] that current densities acceptable for applications of this system for electric energy sources can only be achieved for *high* concentrations of the added redox couple which diminishes automatically the redox-charge and energy densities of the process. Besides, it is difficult to find a redox couple compatible with the requirement of a low crossover of its components across the proton-exchange membrane.

Quite unexpectedly our theoretical analysis [1] has revealed that a *miracle* solution of this problem is provided by the Br₂/Br⁻ redox couple:



which is reversible even at low-cost carbon electrodes, in combination with the comproportionation reaction



which is irreversible in strongly acidic solutions. One should keep in mind that at least a tracer amount of Br₂ is always present in such solutions, owing to BrO₃⁻ chemical decomposition.

One should note that the sets of electrochemical and chemical steps, Eqs (1-EC'), (2-EC') or (1), (2), *look* very similar. However, their predictions are *radically different*. An astonishing example is shown in Fig. 1 for the dependence of the "maximal current density", j^{max} , on the revolution frequency of the rotating disc electrode (RDE), f [6].

Lines EC' and 1 for two reaction mechanisms are close to one another in the ranges of extremely high and extremely low frequencies, f . However, there is a tremendous difference between these lines within the medium range of f values, which occupies many orders of magnitude for a great difference in the bromate anion and bromine concentrations in the bulk solution, BrO₃⁻⁰ and Br₂⁰ (Fig. 1). Within this interval of RDE frequencies the EC' mechanism predicts an almost *constant* value of the maximal current that is *proportional to the bromine concentration*, Br₂⁰, and it is *much smaller than the bromate diffusion-limited current density*, $j_{\text{BrO}_3^-}^{\text{lim}}$. On the contrary, line 1 based on the bromate-bromine reaction scheme, Eqs (1), (2),

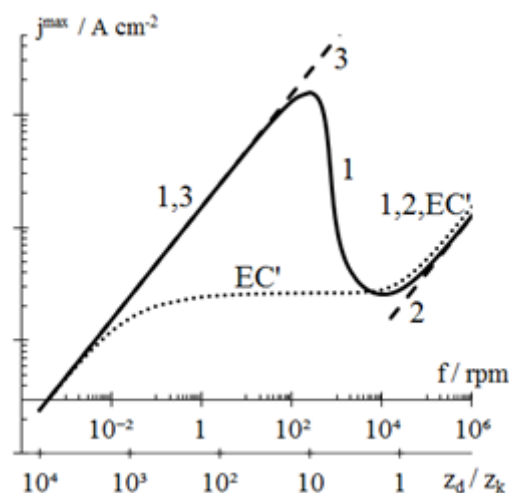


Figure 1. Dependence of j^{\max} , on the RDE rotation rate, f , or on the ratio of the diffusion and kinetic layer thicknesses, z_d/z_k . Maximal current density, j^{\max} , is defined as the upper limit of the current density, j , for sufficiently high cathodic overpotentials, for a fixed value of f . Line (EC') corresponds to the EC' mechanism [6], line 1 is calculated for the reaction scheme given by Eqs (1) and (2) [7], straight lines 2 and 3 show the Levich plots: $j^{\max} = j_{\text{Br}_2}^{\text{lim}}$ and $j^{\max} = 1.2 j_{\text{BrO}_3^-}^{\text{lim}} + j_{\text{Br}_2}^{\text{lim}}$

predicts an **anomalous** behavior within this frequency range. First of all, there is a range of frequencies where the maximal current **increases by several orders of magnitude** in parallel to **diminution of the frequency**, i.e. for weaker agitation of the solution. As a result of this maximal current growth its value becomes comparable (near the **maximum** of line 1) and even **greater than the diffusion-limited current density of bromate**, $j_{\text{BrO}_3^-}^{\text{lim}}$ (line 3).

This crucial difference between the predictions of the EC' mechanism and Eqs (1), (2) is a direct consequence of **transformation of BrO_3^-** in Eq (2) to Br_2 (rather than into an inert species), i.e. **into a component of the redox couple**, Eq (1). Therefore, passage of the cycle, Eqs (1) and (2), leads to progressive accumulation of the total amount of the redox couple components, with resulting acceleration of the bromate reduction via Eq (2), up to its diffusion-limited regime (line 3). Thus, the bromate reduction process described by Eqs (1) and (2) corresponds to a **novel mechanism** (which we called **EC'' mechanism** [7]) based on **redox-mediator autocatalysis** since the **reaction product**, Br_2 , represents a **catalyst**.

The origin of the anomalous branch of line 1 where the direction of variation of j^{\max} inverses the sign (compared to the "normal one", see line EC') may be understood from the values of the ratio of the diffusion and kinetic layer thicknesses, z_d/z_k .

If its value is smaller than 1 Br^- ions generated at the electrode surface passes across the thin diffusion layer practically without reaction with BrO_3^- ions, Eq (2), so that the comproportionation reaction takes place outside this layer and its product, Br_2 , does not return to the electrode surface. Then, no catalysis occurs, and the current is determined by reaction of Br_2 species at the surface after their diffusion across the diffusion layer (line 3).

If the ratio, z_d/z_k , becomes greater than 1, a significant fraction of Br^- is subject to comproportionation reaction (2) inside the kinetic layer, i.e. inside the diffusion layer, and its product, Br_2 , returns partially to the electrode surface, to participate again in electrode reaction (1). It implies consumption of BrO_3^- anions inside the kinetic layer because of its catalysis transformation.

The larger is the ratio of the thicknesses, z_d/z_k , the greater is the fraction of Br_2 species participating in the redox cycle. Near a critical value of this ratio equal to 6, the losses of Br_2 species due to their diffusion towards the bulk solution across the outer part of the diffusion layer become so low that passage of the redox cycle leads to accumulation of very high concentrations of the redox couple components, Br_2 and Br^- , inside the kinetic layer. Then, it is the diffusion of the

principal oxidant, BrO_3^- , across the outer part of the diffusion layer which becomes a current-determining step of the whole process.

The thickness of this spatial zone, $z_d - z_k$, is smaller than z_d , because of a finite thickness of the kinetic layer, z_k . Under steady-state conditions the loss of Br_2 via diffusion to the bulk solution should be equal to 1/6 of its overall amount generated by reaction (2) inside the kinetic layer. Therefore, this layer thickness, z_k , should be about 1/6 of the diffusion layer one, z_d , while the outer layer thickness is $5 z_d/6$. Since the final product of reactions (1) and (2) is Br_2 it means the transfer of 5 electrons per consumed BrO_3^- anion. It explains why the limiting behavior of j^{\max} in Fig. 1 for large values of the ratio, z_d/z_k , is $(6/5) j_{\text{BrO}_3^-}^{\text{lim}}$ (besides a minor contribution, $j_{\text{Br}_2}^{\text{lim}}$, due to Br_2 diffusion from the bulk solution, line 3), i.e. j^{\max} may even exceed noticeably $j_{\text{BrO}_3^-}^{\text{lim}}$.

Acknowledgements

Supported by the Russian Science Foundation (grant 15-13-20038).

References

1. A. Z. Weber, M. M. Mench, J. P. Meyers, P. N. Ross, J. T. Gostick, Q. Liu, *J. Appl. Electrochem.*, 41 (2011) 1137–1164.
2. Y. V. Tolmachev, M. A. Vorotyntsev, *Russ. J. Electrochem.* 50 (2014) 403-411.
3. W. A. Braff, M. Z. Bazant, C. R. Buie, *Membrane-less hydrogen bromine flow battery*, *Nature Comm.* 4 (2013), Article number: 2346, doi:10.1038/ncomms3346
4. K. T. Cho, P. Albertus, V. Battaglia, A. Kojic, V. Srinivasan, A. Z. Weber, *Energy Technology* 1 (2013) 596–608.
5. Y. V. Tolmachev, A. Pyatkivskiy, V. V. Ryzhov, D. V. Konev, M. A. Vorotyntsev, *J. Solid State Electrochem.*, 2015, vol. 19, 2711-2722.
6. M. A. Vorotyntsev, A. E. Antipov, D. V. Konev, *Pure Applied Chem.*, submitted.
7. M. A. Vorotyntsev, D. V. Konev, Y. V. Tolmachev, *Electrochim. Acta* 173 (2015) 779-795.

INFLUENCE OF THE PHASE COMPOSITION ON THE PARAMETERS OF HYDROGEN PERMEABILITY OF Pd53Cu FILM ELECTRODES

Alexander Vvedenskii, Anastasiya Fedoseeva, Natalya Morozova, Elvira Leschenko, Alexey Dontsov

Voronesh State University, Voronezh, Russia, E-mail: *alvved@chem.vsu.ru*

Introduction

The development of hydrogen energy increases the need for high-purity gaseous hydrogen. Its extraction from gas mixtures in the course of the diffusion through palladium membranes is most effective production. Alloys based on palladium have a wide range of applications. They are used as electrode materials in the electrocatalysis of organic compounds, in the electroreduction of hydrogen and for super deep purification of hydrogen from impurities. In this regard thin-layer membranes manufactured in various ways from alloys of the Cu-Pd system and highly selective with respect to H are especially promising. The Cu-Pd alloy with a palladium content of $X_{Pd} = 30-55$ at.% has a high hydrogen permeability [1]. Such a Cu-Pd alloy can crystallize both in the fcc (α -phase) and in the bcc (β -phase) crystal lattice. The purpose of this study is to establish the role of the β -phase in the hydrogen permeability of film samples of copper-palladium alloy.

Experiments

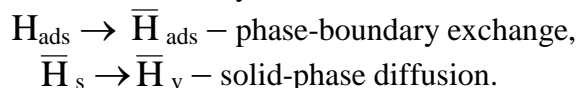
The investigations were carried out on copper-palladium film electrodes of composition 53 at.% Cu and 47 at.% Pd, obtained by magnetron sputtering in vacuum on SiO₂ substrates. The substrate temperature of the investigated films is $T_{sub} = 700$ K. The influence of the β -phase content was carried out on two film samples. The sample (1) contains 100% of the β -phase (bcc lattice), and the sample (2) is a mixture of the α - and β -phases. The phase composition of the sample sides slightly differs, namely, the outer side of the sample contains 52% of the β -phase and internal side contains 41%. The thickness of the investigated electrodes is $L_1 \approx 11$ μ m, and $L_2 \approx 2.6$ μ m. The influence of the thickness of film samples is manifested only on samples with L up to 1 μ m, where the main change in the size of the crystallites occurs. With a subsequent increase in the thickness of the samples, the dimension of the crystallites remains practically unchanged [2].

The inner surface of film electrodes facing the substrate and the outer surface differ by roughness, substructure and phase composition [3], therefore electrochemical studies were carried out on both surfaces. In electrochemical measurements a sample of a metallic film was applied on electrode from spectrally pure graphite which using a conductive graphite glue. The area of film samples did not exceed 1 cm². Each sample was used only once.

The investigations were carried out using cyclic voltammetry and a two-step cathodic-anodic chronoamperometry in a solution of 0.1 M H₂SO₄ (especially pure). The solution was deoxygenated by chemically pure argon. Electrochemical measurements were carried out using an IPC-Compact potentiostat connected to a computer. The potentials are calculated relative to the s.h.e. The hydrogen saturation potential (E_c) was -0.08 V. The ionization potential E_a corresponded to the ionization potential of atomic hydrogen, which was found from the previously obtained voltammograms. The values of E_a for different samples were slightly different. The hydrogenation time t_c did not exceed 10 s, which practically eliminated the possibility of the formation of palladium hydride.

Results and Discussion

It is established [4] that the cathode injection of H into the film of the Pd53Cu alloy is carried out in the regime of mixed diffusion-phase-bound kinetics, taking into account the difficulties in the entry of an atom into the crystal lattice of the alloy:



Here \bar{H} is atomic hydrogen in a metal film.

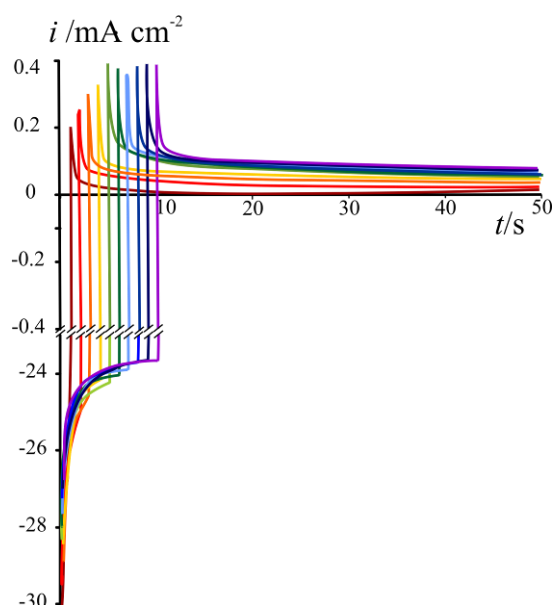


Figure 1. Chronoamperograms obtained on a film electrode for different hydrogenation times $t_c = 1 \div 10$ s

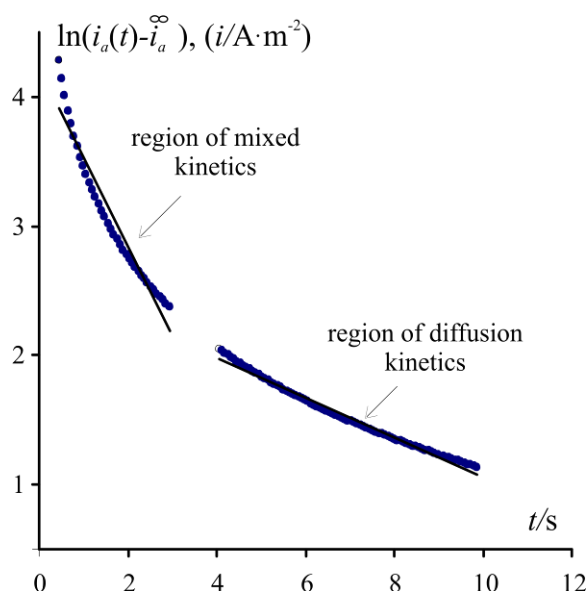


Figure 2. An example of a linearized cathode chronoamperogram

Typical chronoamperograms obtained on film electrodes are shown in Fig. 1. As the hydrogenation time t_c increases from 1 to 10 s, the rate of ionization of atomic hydrogen from the film electrode increases.

The obtained cathodic and anodic chronoamperograms were used to calculate the hydrogenation parameters. The mathematical processing of the i, t -curves was carried out according to the procedure described in [5]. An example of the linearization of cathode current decays is shown in Fig. 2. The presence of two linear sections, at small times ($t \leq 3$ s) and at large times ($t \geq 4$ s) correspond to different kinetic regimes of hydrogen injection.

The calculated parameters of hydrogen permeability are presented in Table 1. They are the diffusion coefficient $D_{\bar{H}}$, the concentration of atomic hydrogen in the film $\Delta c_{\bar{H}}$, the coefficient of hydrogen permeability $K_D = D_{\bar{H}}^{1/2} \Delta c_{\bar{H}}$ and the effective equilibrium constant of the phase-boundary exchange stage $K = \bar{k} / \bar{k}$. Here \bar{k} and \bar{k} are the rate constants of injection and extraction of atomic hydrogen respectively.

Table 1: Parameters of the cathode injection process in the films of the Pd53Cu alloy of different phase composition (inner side – num., outer side – den.)

N sample	X_{β} , %	$D_{\bar{H}} \cdot 10^9$, $\text{cm}^2 \cdot \text{s}^{-1}$	$\Delta c_{\bar{H}} \cdot 10^5$, $\text{mol} \cdot \text{cm}^{-3}$	$K_D \cdot 10^9$, $\text{mol} \cdot \text{cm}^{-2} \cdot \text{s}^{-1/2}$	$\bar{k} \cdot 10^4$, $\text{cm} \cdot \text{s}$	$\bar{k} \cdot 10^8$, $\text{mol} \cdot \text{cm}^{-2} \cdot \text{s}^{-1}$	$K \cdot 10^5$, $\text{mol} \cdot \text{cm}^{-3}$
1	100	59.3 ± 0.3	4.83 ± 0.06	12.6 ± 0.2	5.38 ± 0.02	4.61 ± 0.06	8.50 ± 0.11
	100	45.8 ± 0.7	4.31 ± 0.05	6.2 ± 0.1	5.65 ± 0.04	3.90 ± 0.07	6.53 ± 0.08
2	41	2.84 ± 0.09	8.79 ± 0.21	4.68 ± 1.34	1.38 ± 1.69	3.73 ± 1.22	13.31 ± 3.62
	52	2.85 ± 0.01	9.83 ± 1.36	5.24 ± 0.81	1.38 ± 0.04	4.17 ± 0.64	14.87 ± 2.30

Most of the parameters of hydrogen permeability were sensitive to the choice of the side of the film. For both samples, the diffusion parameters on the inner side of the film, characterized by a smaller crystallite size, are greater than for the external one. At the same time, the kinetic parameters (\bar{k} , \bar{k} and K) practically do not change during the transition from the outer to the inner sides of the film samples, i.e. they are dimension-independent parameters. With an increase in the fraction of the β -phase in the sample, the diffusion coefficient increases by a factor of 15-20, but the concentration of atomic hydrogen in the alloy decreases approximately by a factor of two. As

a consequence, some growth of the hydrogen permeability of the films occurs. The rate constant of injection of \bar{H} (\bar{k}) remains approximately constant, while the extraction rate constant (\bar{k}) increases almost 5 times. Since the injection of hydrogen is facilitated with an increase on β -phase fraction, it can be assumed that hydrogen moves along the body of the grain, and not along the grain boundaries.

Anodic chronoamperograms characterize the process of extraction of atomic hydrogen. The main current drop practically terminates in 100 s and reaches its steady-state value. The obtained anode i, t -dependencies are also linearized in the corresponding criterial coordinates [5]. But the method used does not allow to split experimentally the parameters of the phase-boundary and diffusion stages. Therefore, the parameters were calculated within the framework of the mixed kinetics model. The results are shown in Table 2.

Table 2: Characteristics of diffusion transfer for the Pd53Cu alloy obtained under the conditions of anodic polarization of hydrogenated samples

N sample	X_{β} , %	$D_{\bar{H}} \cdot 10^9, \text{cm}^2 \cdot \text{s}^{-1}$		$\Delta c_{\bar{H}} \cdot 10^5, \text{mol} \cdot \text{cm}^{-3}$		$K_D \cdot 10^9, \text{mol} \cdot \text{cm}^{-2} \cdot \text{s}^{-1/2}$	
		inner	outer	inner	outer	inner	outer
1	$\frac{100}{100}$	29.1 ± 0.3	29.0 ± 0.5	6.78 ± 0.09	5.57 ± 0.06	10.0 ± 0.1	7.87 ± 0.07
2	$\frac{41}{52}$	1.11 ± 0.15	0.89 ± 0.08	11.52 ± 7.74	10.80 ± 2.47	3.84 ± 1.77	3.22 ± 0.37

The values of the parameters of hydrogen permeability calculated from anodic current decays also increase with increasing fraction of the β -phase in the alloy, but are insensitive to the crystallite size. However, the $D_{\bar{H}}$ values found from the anodic current decays are almost half that of the cathodic ones, while the other hydrogenation parameters are within the error limits. The latter may be due to the fact that part of the atomic hydrogen is trapped in the defects of the alloy, and therefore it is not possible to extract completely all of the embedded hydrogen.

Thus, an increase in the fraction of the β -phase in the solid solution of the Pd53Cu film electrode leads to an increase in the diffusion coefficient, the concentration of atomic hydrogen in the alloy and consequently an increase in the hydrogen permeability. The fraction of the bcc lattice in the alloy (β -phase) practically does not affect the kinetic parameters of the process, primarily the rate constants of the phase-boundary exchange stage.

References

1. Hydrogen in metals /Ed. by G. Alefeld and J. Völkl. V.2. 1981. 275 p.
2. Ievlev V.M., Roshan N.R., Belonogov E.K., Kushchev S.B., Kannykin S.V., Maksimenko A.A., Dontsov A.I., Glazunova Y.I. Vodorodopronitsaemost folgi splavov Pd–Cu, Pd–Ru i Pd–In–Ru poluchennoi magnetronnym raspyleniem // Kondensirovannye sredy i mezhfaznye granitsy. 2012. V. 14, №4. P. 422-427.
3. Ievlev V.M. Sintez i substruktura plenok uporiadochennogo tverdogo rastvora palladii-med // Vestn. VGTU Ser. Materialovedenie. 2005. № 117. P. 9-18.
4. Morozova N.B., Vvedenskii A.V., Beredina I.P. The phase-boundary exchange and the non-steady-state diffusion of atomic hydrogen in Cu-Pd and Ag-Pd alloys. Part I. Analysis of the model // Protection of Metals and Physical Chemistry of Surfaces. 2014. V.50, №6. P.699-704.
5. Morozova N.B., Vvedenskii A.V. Fazogranichnyi obmen i nestatsionarnaia diffuziia atomarnogo vodoroda v metallicheskoj plenke I. Analiz tokovogo tranzienta // Kondensirovannye sredy i mezhfaznye granitsy. 2015. V.17, №4. P. 451-458.

THE RELATIONSHIP BETWEEN PROTONCONTAINING GROUPS STRUCTURE, MOBILITY AND TRANSPORT PROPERTIES OF ION-EXCHANGE MEMBRANES

Andrey Yaroslavtsev^{a,b}, Daniil Golubenko^a, Andrey Ilyin^b, Irina Stenina^a, Vladimir Tverskoy^c.

^aKurnakov Institute of General and Inorganic Chemistry RAS, Moscow, Russia

E-mail: yaroslav@igic.ras.ru

^bTopchiev Institute of Petrochemical Synthesis. RAS, Moscow, Russia

^cMoscow Technological University, Moscow, Russia

Transport properties of ion-exchange membranes are determined by its pore and channel structure. In accordance with the well-known Gierke model, pores are formed in the membrane matrix, which walls contain functional groups. These pores are filled by the sorbed water molecules together with the counterions produced during dissociation of functional groups. In the case of cation exchange membranes in the hydrogen form there is an aqueous solution inside the pores containing protons, most of which are localized in a thin Debye layer near the pore walls. At the center of the pores there is an electrically neutral solution having a composition corresponding to the composition of the solution contacted with the membrane. If the membrane is in equilibrium with pure water, the last one should be present in the pore center. But a question arises if this water is really pure and how much of such water can be located in the pore. There is no information about this in the literature. In this report, the composition of this solution and the transport processes of such membranes will be considered for the case of not quite traditional membranes based on polyethylene with grafted sulphonated polystyrene.

The choice of such an exotic membrane is due to the fact that their ion exchange capacity and water uptake can be varied in the wide range. In our opinion, this should ensure more correct observation of changes in the structure of the solution in the pores.

The grafting copolymerization of styrene was carried out in a methanol solution containing 70 vol. % styrene at the solution boiling point (68 °C). The grafting solution contained iron(II) sulfate as the homopolymerization inhibitor and co-initiator. Sulfonation of films was carried out in concentrated (96 %) sulfuric acid at 98 °C for 120 min, thus allowing for sulfonation throughout the membrane thickness [1]. According to the microprobe analysis, the sulfur distribution in the sample was uniform.

The thickness and volume of the membranes in swollen state increased with increasing g-PS contents. IEC steadily increased from 0.54 to 2.66 mmol/g with increasing PS grafting degrees from 7 to 71%. For the samples containing a g-PS higher than 26 wt. %, the IEC values were higher than that of Nafion[®] 212 membrane.

At the same time, water uptake for membranes contacting with water varies from 17 to 73%. The ion exchange capacity was found to increase with the increase in polystyrene sulfate content in the and water uptake can be observed. Moreover, the number of water molecules per sulfone group increases also. This index varies from 22 to 57. Thus, as the content of polystyrene increases, the solution becomes more diluted. This is determined by the fact that water is sorbed only by polystyrene sulfate, and the possibility of its swelling is limited by a polyethylene grid. With increase in polystyrene sulfate content, the thickness of this grid falls and the grid can be deformed more easily.

The concentration of this solution can be characterized by the freezing temperature with the use of calorimetry. However, undesirable processes of water freezing and evaporation from pores are possible. Therefore, calorimetric studies were carried out during the heating.

From the low-temperature calorimetric measurements (from -100 to 50 °C), it could be observed that for the highly hydrated membranes an endothermic transition occurred with a peak at ~ 0 °C (Fig. 1a). This transition could be related to the “melting” of water molecules located in the membrane pores at a distance from pore walls, along which the overwhelming majority of protons are localized. As a matter of fact, the so-called electroneutral solution consisted of weakly bound water that was localized around the pore center and almost free of protons for membranes

equilibrated with distilled water. The enthalpy of endothermic process is equal to 99 J/g. From this value, the amount of weakly bound water can be estimated as ~20 molecules per sulfonic group. It is also noteworthy that the heat transferred to membranes, equilibrated at RH = 30 % increases steadily in the low-temperature region below -35 °C (Fig. 1b), before reaching a maximum value at this temperature and coming to a fixed value above 0 °C.

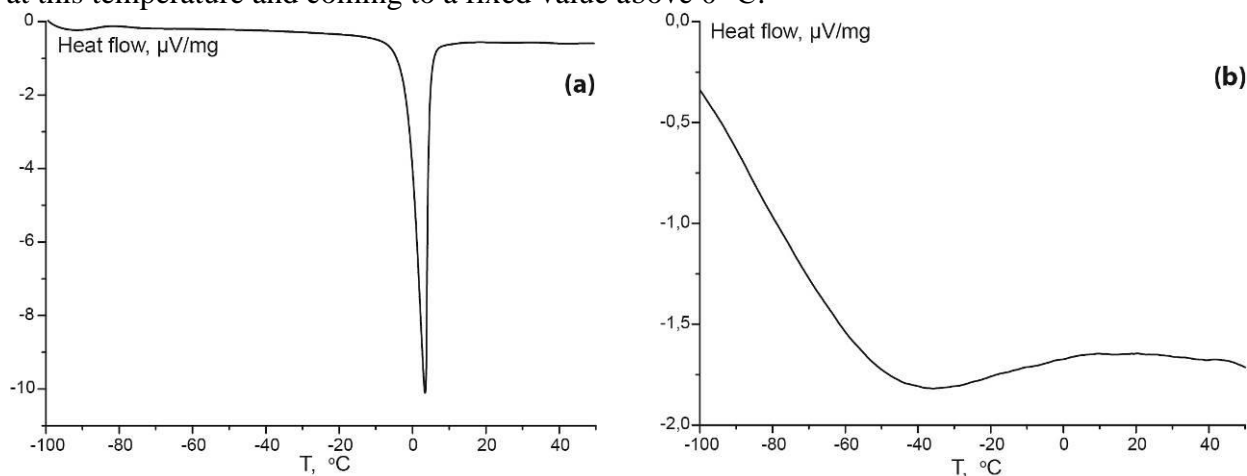


Figure 1. DSC curves for membrane with PS content equal to 65, equilibrated at RH = 100% (a), and RH = 30% (b).

The endothermic effect was determined by a gradual “melting” of water mobility, starting from molecules in the first coordination sphere of the protons (H_5O_2^+ or H_9O_4^+ ions). It is worth mentioning that ^1H NMR measurements at temperatures around -90 $^{\circ}\text{C}$ demonstrated the appearance of mobility of the proton-containing groups in a large number of acid hydrates and acid salt hydrates, with the fraction of mobile protons increasing at higher temperatures due to cooperative effects [2]. At temperatures around 0 $^{\circ}\text{C}$, the process finished, and all the water was transferred to a highly mobile state, corresponding to the plateau on the DSC curve.

According to the calorimetric data, when the relative humidity decreased to 95 %, the phase transition disappeared. Nevertheless, the same trend of gradual transition of water and protons, located within the Debye layer, to the mobile state was observed (Fig. 2).

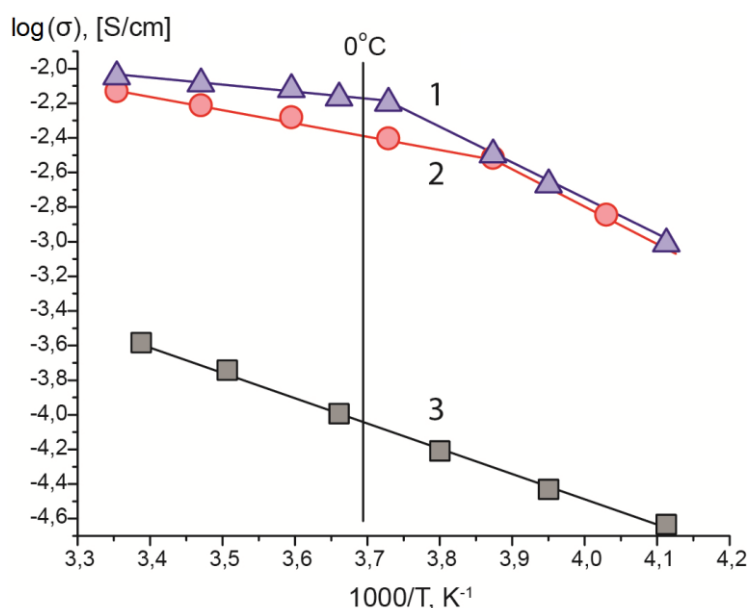


Figure 2. Temperature dependence of conductivity for MSC-65 at different relative humidity values: (1) RH = 100 % (in contact with water), (2) RH = 95 %, (3) RH = 60 %

After the transition occurred, the activation energy of conductivity also decreased, while the resulting conductivity became slightly lower, as compared to the membrane equilibrated with water. This was due to the fact that the reduction of pore volume was inevitably coupled with that of interconnecting channel sizes [3], which limited the conductivity. Further relative humidity decrease to 30% was accompanied by a higher decrease in water uptake, due to a decrease in water content in the Debye layer and an increase in its concentration. As a result, the final temperature of the transition to the mobile state decreased, and no change in activation energy was observed up to $-30\text{ }^{\circ}\text{C}$ (Fig. 2). Comparison of these facts shows that some of the water molecules localized in the pores of such ion-exchange membranes do not participate in the hydration of protons, but the number of such water molecules is not high. About 20-25 molecules per functional group take part in hydration process and ionic transfer, on the contrary.

The high proton conductivity of such membranes should be noted and the possibility of their application in some gas separation processes. Thus, such systems enable selective transfer of ethylene in the complexes with silver ions or protons. The transfer of such complexes also proceeds through an aqueous solution in the membrane pores.

This work was supported by the Russian Science Foundation (Agreement number 16-13-00127).

References

1. Safronova E.Yu., Golubenko D.V., Shevlyakova N.V., D'yakova M.G., Tverskoi V.A., Dammak L., Grande D., Yaroslavtsev A.B. New cation exchange membranes based on cross-linked sulfonated polystyrene and polyethylene for power generation systems // *J. Membrane Sci.* 2016, **515**, 196–203.
2. Yaroslavtsev A.B. Solid electrolytes: main prospects of research and development // *Russ. Chem. Rev.* 2016, **85**, 1255-1276.
3. Yaroslavtsev A.B., Karavanova Y.A., Safronova E.Y. Ionic conductivity of hybrid membranes // *Petroleum Chem.* 2011, **51**, 473-479.

VARIATION OF THE ULTRAFILTRATION POLYACRYLONITILE MEMBRANES PROPERTIES BY THE DIAMINE MODIFICATION

Ala Yaskevich, Victor Kasperchik, Aleksandr Bildyukevich

Institute of Physical Organic Chemistry NASB, Minsk, Belarus, E-mail: ufm@ifoch.bas-net.by

Introduction

Porous membranes made of acrylonitrile copolymers are used for pressure driven processes such as micro- and ultrafiltration (UF). Otherwise polyacrylonitrile (PAN) membrane is convenient material for chemical modification. The nitrile groups in the structure of PAN polymers are able to participate in many variable chemical reactions with the formation of different ionizable (both cationic and anionic) groups, as well as complexing groups [1]. Thus after chemical modification ultrafiltration PAN membrane can exhibit an additional behaviors e.g. improving of chemical stability, appearance of ion exchange properties etc.

Experiments

UF hollow fiber PAN membranes were used as initial matrixes for the chemical modification. Diamine water solutions were used for formation of amino groups as well as intra- and intermolecular cross-linking of initial membrane structure. Formation of carboxylic groups was carried out by hydrolysis in 10% NaOH solutions. In Table are presented the main characteristics of the initial and obtained modified membranes: *c* – concentration of modification agent, *T* – treating temperature, *t* – exposition time, *J* – transmembrane flux, *E_a* and *E_b* – cationic and anionic exchange capacities respectively.

Table: Characteristics of initial and modified membranes

Modification agent	<i>c</i> , %	<i>T</i> , °C	<i>t</i> , h	<i>J</i> , l/m ² h	<i>E_a</i> , meq/g	<i>E_b</i> , meq/g
Before modification	-	-	-	17-22	0.11	0.07
Hydrazine (H)	10	70	1	10	1.01	0.47
	20	80	1	4	0.95	0.64
	30	80	1	2	1.09	0.74
	30	80	1.5	2	1.97	0.62
Ethylenediamine (EDA)	10	60	6	13	3.83	1.68
	20	60	6	15	5.2	1.24
	20	70	6	9	2.38	0.71
	10	80	6	5	1.71	0.83
	30	80	6	8	1.37	1.26

Results and Discussion

Earlier [2] we have shown that the chemical stability of the ultrafiltration PAN membranes can be improved after its short time exposition in 30-40 % hydrazine water solutions at 80-90 °C. The aim of this paper was the investigation of the ultrafiltration PAN membranes variation properties after its treating by the following diamines: hydrazine and ethylenediamine.

As can be seen from the table, the initial PAN membranes practically have no ion-exchange groups. Interaction of membranes with hydrazine solutions at elevated temperatures leads to the appearance of anion-exchange groups and the value of *E_b* increases with increasing of hydrazine concentration and temperature. The amount of carboxyl groups (*E_a*) is practically independent from the degree of hydrazidation at the same process conditions. The increase of the hydrazination time up to 1.5 h did not affect *E_b*, but *E_a* increased by a factor of 2, which may indicate a joint effect of hydrazidation and alkaline hydrolysis on the properties of the modified membrane.

Ethylenediamine as studies have shown is the softer modifying agent compared to hydrazine. With the duration of the amination process of 6 h the ultrafiltration properties of membranes remain almost the same. The constant selectivity to polyvinylpyrrolidone (PVP K15) with a permeability decrease of 1.5-2 times was observed. The sharp change in the properties of membranes occurs after alkaline hydrolysis. These ones become impermeable to water at 0.1 MPa

and have substantial quantity of ion-exchange groups that is larger than after the modification with hydrazine. In the case of EDA there is no good correlation between the number of ion-exchange groups and the modification conditions. With a decrease in exposition time to 2 h and the carrying out of the alkaline hydrolysis the amount of ion-exchange groups practically does not differ from that for the initial membranes.

All the modified membranes had increased the chemical resistance to strong acids. When boiling in 5 N H₂SO₄ for 0.5 h the modified membranes did not change the external form. Under the same conditions in 5 N NaOH the modified membranes swell but do not collapse unlike the initial PAN membranes. It was established also that the modified membranes are insoluble in dimethylformamide for a long time.

References

1. New materials and technologies for environmental engineering. Part I. Syntheses and structure of ion exchange fibers / V. Soldatov, L. Pawlowski, A. Shunkevich, H. Wasag // Polska Akademia nauk. Komitet inżynierii środowiska. Monografie Nr 21. – Lublin 2004.
2. Kasperchik V.P., Yaskevich A.L., Bilyukevich A.V. // Kritich. Tekhnol. Membrany. 2005. № 28. P. 35–40.

DEOXYGENATION OF HIGH-PURITY WATER USING MEMBRANE ELECTRODE UNITS

Ivan Yasnev, Vladimir Gursky

Aleksandrov Research Institute of Technology, Sosnovyi Bor, Russia, E-mail: ivan_yasnev@mail.ru

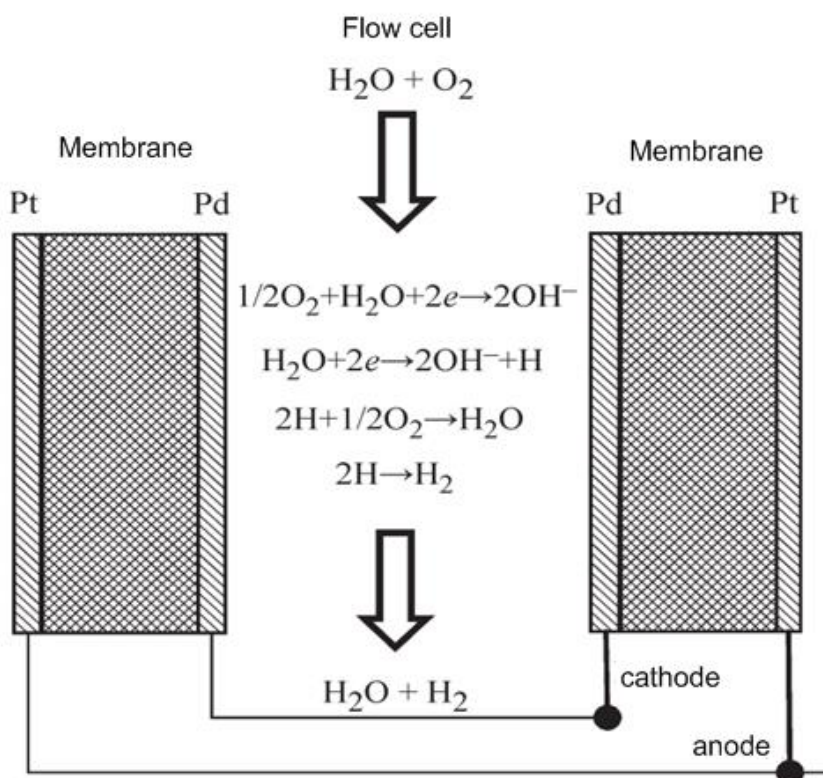
Introduction

Dissolved oxygen is a crucial factor of corrosion in the thermal and nuclear power energetics. Significant corrosion rate reduction can be achieved if dissolved oxygen level in the water is at 20 ppb or less. The raise of dissolved oxygen level from 20 to 100 ppb increases corrosion rate by 10 times.

Experiments

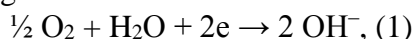
The research of transport processes of substances through the ion exchange membranes coated with electronically conducting layers was made, resulting in using this kind of systems for electrochemical oxidation and reduction of substances on the surface of catalytic electronically conducting layers. A membrane electrode unit (MEU) were constructed. It is a cation exchange membrane whose surfaces are coated with a porous electronically conducting metal layer. This structure allows user to carry out a current drainage (electron conduction of surface) and doesn't prevent electrode reaction on the interphase boundary membrane/porous metal and ion transport through this boundary.

The proposed scheme of water deoxygenation is shown in Fig. 1.

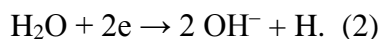


The flow cell is a space restricted from both sides with a cation exchange membrane with surfaces coated with porous layer of catalytically active metal (platinum, palladium). Metal layers facing into the cell are cathode, the outer layers are anode. When water flows through the cell and electric field is applied, the next electrochemical reaction is occurring on the cathode:

ionization of the dissolved oxygen



generation of the atomic hydrogen



Atomic hydrogen reacts with dissolved oxygen on the catalytic surface, with water as the resultant. Due to these processes, concentration of dissolved oxygen is decreasing.

On the anode of MEU the discharge reaction of water from the membrane occurs with generation of the gaseous oxygen. The high permeability of the ion exchange membrane to water allows conducting the electrolysis process with the "dry" anode cell.

An important fact is that the water electrical resistivity at the unit doesn't affect the voltage-current characteristic of the electrode processes, because it is determined primarily by the electrical resistivity of the ion exchange membrane. Therefore, this method can be applied to deoxygenation of high purity water with high electrical resistivity.

Due to diffusion limits of dissolved oxygen transport to the surface of membrane, part of the atomic hydrogen formed on the cathode does not react with oxygen, recombines to molecules and washes out with water flow. Complete removal of dissolved oxygen occurs in the catalytic column, whose surface is covered with a catalytic layer of palladium, and which is filled with the anion exchange resin.

Results and Discussion

The obtained results allowed constructing a pilot sample system for high-purity water deoxygenation. This system contains devices monitoring the quality of feeding and finish water (conductivity, dissolved oxygen). System of electromagnetic valves switches the water flow with indication of analyzers. It provides automatic shutdown of the output water flow from the consumer then quality of water become worse. The system can be operated in automatic or manual mode.

Specifications of a setup shown in Table 1

Table 1: Specifications of a setup

Productivity, L·h⁻¹	500
Readiness time, min	less 30
Concentration of the dissolved oxygen, mg·L⁻¹	
Input water flow	10
Output water flow	less 0.010
Conductivity, μSm·cm⁻¹:	
Input water flow	less 2,0
Output water flow	less 0,2
Concentration of chlorides in output water flow, mg·L⁻¹	less 0,01
Power supply	220 V / 50 Hz
Size, width x depth x height, mm	800x600x2000
Weight, kilograms	120

Selected constructive solutions allow, if required, to increase productivity of the system up to 1000 L·h⁻¹ without significant changes of construction.

The advantages of system are:

- low power consumption (especially compared to thermal deaeration),
- mobility and easy maintenance operations;
- the use of reagents and inert gases is not necessary.

THE CHANGES IN SURFACE AND TRANSPORT PROPERTIES OF ION-EXCHANGE MEMBRANES USED AT ELECTRODIALYSIS TREATMENT OF NATURAL WATERS

Andrey Yatsev, Vera Vasil'eva, Elmara Akberova

Voronezh State University, Voronezh, Russia, *E-mail: yatsev-andrey@mail.ru*

Introduction

An important limitation worsening the efficiency of electrodialysis at demineralization of natural waters is a reduction of the membrane electrochemical activity under the influence of temperature and polarization effects as well as scaling. The purpose of this work is the revealing of the relationship between the structural and transport properties of sulfocation-exchange MK-40 membrane after prolonged operation in the electrodialyzers at desalination and concentration of natural waters.

Experiments

We investigated the MK-40 membrane sample extracted from the near-electrode section of a reverse electrodialysis unit after its 1000-h operation, namely, in the desalination of very hard natural waters in the Aral region. In its composition there was a large amount of chlorides and sulfates. The other MK-40 membrane sample operated for more than 2 months in the near-electrode section of the electrodialyzer-desalinator. The total mineralization of this water was more than 15 g/dm³; the total hardness exceeded 50 mmol/dm³. The operating life of the MK-40 membrane sample extracted from the work packet of a concentrator was about 500 h at a current density of 2.5 A/dm². An electrodialyzer-concentrator with static brine sections was used without current reverse to obtain brine with concentration of 180-200 g/dm³ from chloride class groundwater. Membrane samples after electrodialysis of natural waters were provided by LLP «Membrane Technologies, S.A.», Almaty, Kazakhstan Republic.

Results and Discussion

Comparison of main physical and chemical characteristics of the ion-exchange membrane samples after chemical conditioning and use in various types' electrodialyzers showed a decrease of the total exchange capacity and the density, accompanied by an increase in the water content and the thickness. The MK-40 membrane from the electrode section of the reverse desalter characterized by the maximum change in physicochemical properties, and minimal change were found for the membrane from concentrator without current reverse. For the membrane from the electrodialyzer-desalter electrode section the change of the total capacity was 20%, the thickness and water content increased by 9% and 21%, respectively.

The study of the transport characteristics of MK-40 membranes demonstrated that, as compared to the conditioned samples, long-term operation caused a 1.6-fold increase in the specific conductivity of the membrane from the electrodialyzer-desalinator and a 1.4-fold increase in that of samples from the electrodialyzer-concentrator. For the given membrane samples, significant (up to 50%) growth in diffusion permeability was established.

It is revealed that the operating conditions oppositely affect the properties of membranes from the near-electrode sections of the reverse electrodialysis unit upon the desalination of ground water in the Aral region. In this case, the specific conductivity decreases 1.4 fold and the diffusion permeability reduces by 20–50%. This is caused by not only the destruction of ionogenic groups and an increase in macroporosity due to the action of electrolysis products and overheating, but also substantial changes in the microstructure of their surface and bulk, which arise from the formation of mineral sediments, that occurred during long-term operation of these membranes.

A comparison of X-ray spectrum analysis (XRSA) data on the membrane surface indicate that the compositions of all samples are qualitatively identical, the Ca content being predominant (Table 1). The sediment, grains of which are observed on the surface of the MK-40 membrane from the desalinator, is localized mainly on ion-exchanger particles and, in accordance with the

performed XRSA, contains Ca, Mg, and Fe. In general, its structure is spongy to such an extent that it is removed from the surface by solution flows.

Table 1: Elemental composition of the surface and cut of the MK-40 membrane extracted from electro dialysis apparatuses of various types

Element	Concentration, wt %					
	Membrane samples					
	desalinators		concentrator		reverse electro dialysis unit	
	surface	cut	surface	cut	surface	cut
C	74.73	45.99	88.70	78.73	38.15	52.41
O	16.75	33.58	5.45	12.73	40.10	31.01
S	2.33	2.00	3.82	5.09	0.70	2.89
Ca	4.93	5.45	0.10	0.26	16.17	1.33
Mg	0.24	11.85	0.03	0	1.25	10.88
Fe	0.51	0.32	0	0	1.28	0.58

The contents of depositgenerating elements Ca and Mg (0.10 and 0.03 wt %, respectively) on the surface of MK-40 membrane from the concentrator is small and such a deposit can be detected only in microphotographs. Electron-microscopy images, XRSA data, and maps of the distribution of elements Ca, Mg, and Fe made it impossible to detect sediment in the cross section of the sulfocation-exchange membrane from the concentrator.

In the case of membranes from the reverse electro dialysis unit, sediment firmly attached to the membrane surface, which is localized in well-conducting regions, where ion exchanger particles are placed, but its continuous film covers almost the entire membrane surface, can be observed at the stage of formation thereof. The XRSA data on the elemental composition of the sediment film demonstrated the dominant content of Ca and the existence of Mg and Fe.

Acknowledgements

The present work is financially supported by the RFBR (project No 15-08-05031). Microphotographs of the membranes surface were obtained at the CCUSE of VSU

SYNTHESIS AND DIFFUSION PROPERTIES OF CATION-EXCHANGE MEMBRANES MODIFIED WITH PROTONACTERT AND PROTONDONOR DOPANTS

Polina Yurova, Yulia Karavanova, Andrey Yaroslavtsev

IGIC RAS, Moscow, Russia, E-mail: polina31415@mail.ru, yuka86@mail.ru

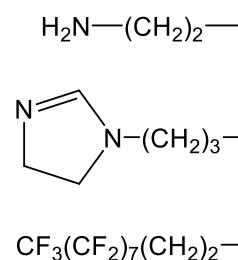
Introduction

For a long time, membranes have been used for water treatment [1] and hydrogen energy [2]. The effectiveness of their use grows every year, due to new researches. Except to finding ways to synthesize fundamentally new membrane materials, a very interesting task is the modification of existing industrial membranes. Using modification, it is possible to obtain materials with previously predicted properties which in the case of the new materials synthesis is difficult. Also, the modification of one industrial membrane by various methods makes it possible to obtain a number of materials with different properties.

Experiments

In the course of this study, the following groups of samples were obtained based on the cation-exchange membrane MC-40:

- 1) with a surface layer of MF-4SC, bulk modified with polyaniline, silica, zirconia with a functionalized surface (Fig. 1),
- 2) bulk modified with ceria by *in situ* method,
- 3) with thickness gradient distribution of zirconia by in situ method due to one-sided, two-sided and synchronous diffusion the precursor and ammonia through membrane.



Conductivity (Table 1) and diffusion parameters were measured for the samples obtained.

Table 1: Conductivity of the obtained samples at 30°C, Ohm⁻¹cm⁻¹

Membrane	No modification					
MC-40	0.029					
Surface modification						
Membrane	Mass fraction PANI					
	0%	1%	2%	3%	5%	15%
MC-40 + MF-4SC+PANI	0.044	0.046	0.054	0.041	0.039	0.026
Groups on the oxide surface						
	-	R ₁	R ₂	R ₃		
MC-40 + MF-4SC + SiO ₂	0.045	0.049	0.041	0.044		
MC-40 + MF-4SC + ZrO ₂	0.048	0.052	0.046	0.049		
MC-40 + MF-4SC + ZrO ₂ (sulf.)	0.050	0.054	0.047	0.050		
Bulk modification						
Mass fraction CeO ₂						
	8%			5%		
MC-40 + CeO ₂	0.003			0.005		
Gradient distribution						
Obtaining from						
	1M solution ZrCl ₄			0.1M solution ZrCl ₄		
MC-40 + ZrO ₂ one-sided	0.021			0.022		
MC-40 + ZrO ₂ two-sided	0.015			0.014		
MC-40 + ZrO ₂ synchr.	0.018			0.021		

Results and Discussion

Modification of membranes with the surface layer with adding of polyaniline leading to increased the rate of proton transfer in an acidic medium due to additional sorption of protons from the solution, which increases the ionic conductivity. Separately, we should note the asymmetry of transport characteristics and its handling of the increase in the concentration of polyaniline in the modifying layer due to the formation of an artificial ion concentration gradient in the membrane.

Modification with the application of MF-4SC containing oxides with a functionalized surface leads to an asymmetry in diffusion parameters and an increase in conductivity, expressed in varying degrees depending on the composition.

Modification with ceria leads to a decrease in conductivity and an increase in the cation selectivity of the membrane.

Samples with a thickness gradient distribution of zirconia show a decrease in conductivity, an increase in diffusion coefficients, and a significant increase in the selectivity to cations.

An increase in the conductivity of most of the samples proves the prospects of the membrane modification methods presented. Samples with a thickness gradient distribution of zirconia show a decrease in conductivity, an increase in diffusion coefficients, and a significant increase in the cation selectivity.

The work was performed by a grant from the Russian Science Foundation (project № 16-13-00127)

References

1. Perfluorinated Ionomer Membranes. Ed by Eisenberg A., Yager H.L. Washington // Am. Chem. Soc. 1982, 500 p
2. Yaroslavtsev A.B., Zabolotskii V.I., Nikonenko V.V. // Uspehi Chimii, 2003, T. 72. C. 438 [in Russian]

INFLUENCE OF IR RADIATION ON MEMBRANES BASED ON POLYACRYLONITRILE

¹Alexey Yushkin, ¹Danila Bakhtin, ¹Mikhail Efimov, ¹Lev Zemtsov, ¹Alexey Volkov

¹A.V.Topchiev Institute of Petrochemical Synthesis, RAS, Moscow, Russia, *E-mail: Halex@ips.ac.ru*

Introduction

Polyacrylonitrile (PAN) is a widely used membrane material for the preparation of solvent-resistant membranes and membrane supports due to its stability over a wide range of organic solvents [1-3]. PAN is also material for the production of carbon fiber [4-5].

This polymer is insoluble in nonpolar and low-polar solvents, such as hydrocarbons and alcohols. But this material is soluble in aprotic solvents, such as DMSO or DMF. Also PAN as a membrane material has some temperature limitations, since its glass transition temperature is about 90°C. In addition, PAN is soluble in aqueous solutions of electrolytes with high ionic strength, which limits the use of filtration membranes.

PAN has a partially crystalline structure with an aspect ratio of crystalline and amorphous phases of 1:1. Increasing the temperature to 200-220°C leads to significant changes in the chemical structure of the polymer, which begin with the cyclization of the nitrile groups of the polymer chain. At temperatures above 220°C decomposition processes occur with loss of weight and evolution of gaseous products of decomposition of main polymer chain and nitrile groups not included in conjugated system. Pyrolysis in an inert atmosphere at higher temperatures leads to carbonization processes followed by ordered carbon structures formation.

PAN has a partially crystalline structure with a crystalline and amorphous phase ratio of 1:1. An increase in temperature to 200-220°C leads to significant changes in the chemical structure of the polymer that begin with the cyclization of the nitrile groups of the polymer chain. At temperatures above 220°C, decomposition processes take place with loss of weight and evolution of the gaseous decomposition products of the main polymer chain and nitrile groups that are not part of the conjugate system. Pyrolysis in an inert atmosphere at higher temperatures leads to carbonization processes followed by the formation of ordered carbon structures. Carbon membranes based on pyrolyzed PAN possess high chemical resistance, but have reduced mechanical properties compared to the initial material.

Process of thermal pyrolysis requires 14-16 hours of heat treatment [1,6]. However, PAN structural changes in the conditions of infrared (IR) pyrolysis occur much faster compared to a common thermal process since cyclization step takes 10-15 min. IR annealing allows to selectively affect on vibrational energy of individual groups of macromolecules, which admits to control the mechanism of structural transformations.

The use of IR radiation allows not only reduce the processing time to several minutes, but also reduces the processing temperature. Rapid increase of chemical reactions rate is observed due to lowering of the activation energy of the vibrationally excited macromolecules. It should be noted that positive effect on the filtration characteristics of the membrane can be achieved due to change in the pore space of the membrane structure during heat treatment.

The purpose of this work is to investigate the effect of treatment of membranes based on PAN IR radiation at temperatures of 100-150°C. It is expected that such a modification of the PAN will yield membranes resistant to aprotic solvents.

Experiments

PAN was synthesized in the presence of a catalytic oxidation–reduction system according to the method in [7]. Polymerization was performed under the following conditions: $[(\text{NH}_2)\text{S}_2\text{O}_8] = 1.6 \times 10^{-3} \text{ mol/l}$, $[\text{Na}_2\text{S}_2\text{O}_4] = 6.2 \times 10^{-4} \text{ mol/l}$, $[\text{H}_2\text{SO}_4] = 1.8 \times 10^{-2} \text{ mol/l}$, and $[\text{acrylonitrile}] = 1.525 \text{ mol/l}$. The monomer and H_2SO_4 were loaded into the reaction vessel in two stages.

The catalytic system was introduced into the vessel containing 2/3 of the necessary volumes of the monomer solution and the acid, and then the reaction was carried out at 60°C for 40 min. Next, the remaining 1/3 of the solution was loaded and the reaction was continued for 4 h. The polymer was filtered; washed with potassium carbonate solution to remove sulfuric acid, with distilled

water up to a neutral reaction, and with methanol; and dried in vacuum up to a constant weight. Characteristics of obtained PAN was $M_n=85900$, $M_w=224700$, $M_w/M_n=2.62$.

For preparation of dense films and porous membranes PAN was dissolved in DMSO at varied concentrations 4-9%. Solution was stirred with magnetic stirrer for 24 hour and with further treatment in ultrasonic bath until complete dissolution of PAN.

Dense films were prepared in Petri dish from 4% PAN solution in DMSO by evaporation of solvent at 50°C. Thickness of obtained films was 40±4 mkm.

To prepare porous membranes, a polymer solution with a thin layer (200 µm) was applied on glass plate and precipitated in distilled water. The time between application of the solution on the glass and immersion in water did not exceed 10 seconds. The resulting membrane was successively washed in distilled water (1 hour), ethanol (1 hour) and hexane (1 hour) and dried at room temperature in air. Thickness of obtained films was varied from 80 to 130 mkm depending on the concentration of the polymer in the solution.

Thermal treatment of films and membranes was carried out in a laboratory setup of pulsed IR radiation at a given temperature from 100 to 150°C under a nitrogen atmosphere for 5 minutes. Halogen lamps KG-220 were used as a source of incoherent IR radiation. The radiation maximum of which falls within the range 0.9-1.2 µm. The lamps were arranged in such a way as to ensure a uniform heating of the entire sample. The PAN film was fixed in a graphite cassette, which was placed in a cylindrical quartz reactor. The intensity of the IR radiation was controlled by the sample heating temperature, measured with a chromel-alumel thermocouple placed directly below the sample. The temperature regulation was accurate to within 0.25°C.

A study of filtration characteristics of membranes was carried out in dead-end cell at a transmembrane pressure of 5 atm. The active area of the membranes in the cells was 8-33 cm². The pressure in the cell was created with helium. The flux of permeate was determined gravimetrically. The membrane performance was characterized by a liquid flow (J), permeability (P) and rejection (R).

Bovine serum albumin (BSA, MM = 69 kDa) was used as the model solute which was dissolved in phosphate buffer (Ph = 7.0) 0.05 M. The concentration of BSA in the solution was determined photometrically on the optical density spectrophotometer PE-5400UF on the wavelength 280 nm. A phosphate buffer containing BSA was used as the reference solution.

Results

Main parameter for membrane material it is stability in organic solvent. For stability tests dense films (2x2cm, thickness 40µm) were immersed in selected solvents for 7 days. Initial samples were soluble in DMSO, NMP, DMAA and DMFA (Table 1). In other solvents absence of significant swelling was observed.

Table 1: Solubility of PAN after IR-treatment

Solvent	Temperature of treatment, °C			
	Initial	100	120	150
Acetone	+	+	+	+
Tetrahydrofuran	+	+	+	+
DMSO	Soluble	Soluble	+	+
NMP	Soluble	+	+	+
DMAA	Soluble	+	+	+
DMFA	Soluble	+	+	+

After IR-treatment films was insoluble in NMP, DMAA and DMFA even if temperature of treatment was 100°C which is much lower than temperature of common thermal treatment. In case of DMSO PAN-films became insoluble only after treatment at 120°C.

It should be noted that strength of films did not change after 100°C but treatment at 150°C makes polymer 3 times less rigid than initial polymer. IR-treated dense films don't swell in any

solvents and are impermeable for all solvents since initial PAN is barrier material and only porous membranes can be used for solvent filtration.

Porous membranes obtained in this work were examined by scanning electron microscopy. Examples of SEM micrographs are shown in Figure 1. As can be seen membrane structure did not change after treatment.

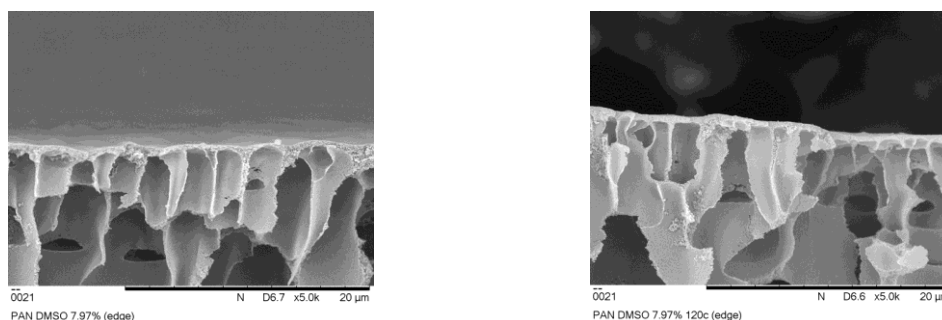


Figure 1. SEM micrographs of PAN membranes before (left) and after (right) treatment

Permeability and membrane rejection were investigated using distilled water and aqueous solutions of bovine serum albumin (BSA) (Figure 2). Permeability of membranes on water after treatment with IR radiation was practically unchanged. The membranes obtained from a 5% solution of PAN in DMSO possessed the greatest permeability. At the same time, these membranes retained about 83% BSA. As the concentration of the polymer in the molding solution increases, the permeability of the membranes decreases, but the retention factor of the BSA increases.

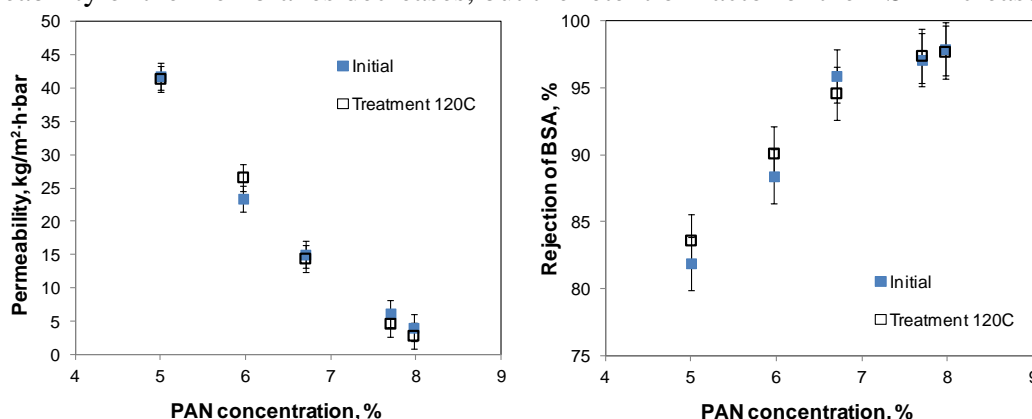


Figure 2. Membrane performance before and after treatment with IR radiation

After treatment membranes had stable permeabilities in DMSO (up to 16 kg/m²·h·bar), DMFA (up to 42 kg/m²·h·bar), DMAA (up to 37 kg/m²·h·bar), NMP (up to 15 kg/m²·h·bar). It should be noted that the proposed modification of the membranes by IR radiation can be applied to commercially produced membranes from PAN without introducing significant changes in the technological process of production.

Acknowledgments

Alexey Yushkin acknowledges Russian Foundation of Basic Research (RFBR project no. 16-38-60152) for financial support.

References

1. Hui-An Tsai et al. *Sep. Purif. Tech.* 100 (2012) 97.
2. In-Chul Kim et al *J. Membr. Sci.* 199 (2002) 75.
3. L.Germic et al. *J. Membr. Sci.* 132 (1998) 131.
4. Ze-Jing Li et al. *Integrated Ferroelectrics*, 152 (2014) 67.
5. S.M.Saufi, A.F.Ismail. *Membrane Sci. & Tech.* 24 (2002) 843.
6. S.M.Saufi, A.F.Ismail. *Carbon* 42 (2004) 241.
7. L.M.Zemtsov et al. *Polym. Sci. A.* 48. (2006) 633.

ELECTROCONVECTION IN SYSTEMS WITH HETEROGENEOUS AND HOMOGENEOUS ION-EXCHANGE MEMBRANES

Victor Zabolotsky¹, Anastasia But¹, Lubos Novak², Vera Vasil'eva³

¹Kuban State University, Krasnodar, Russia, E-mail: nasty310392@mail.ru

²Mega a.s., Strazh pod Ralskem, Czech Republic

³Voronezh State University, Voronezh, Russia

Introduction

It is believed that the mass transfer and the magnitude of the limiting current directly depends on the proportion of the ion exchange material in the membrane. Also, the modification of the membrane contributes to the growth of the limiting current. Given these two facts, it is possible to create a heterogeneous membrane with characteristics exceeding the homogeneous membrane.

The purpose of this paper is to investigate the effect of the morphology of the surface of heterogeneous ion-exchange membranes on vortex structures and on the mass transfer of salt ions. Using a rotating membrane disk method, investigate homogeneous and modified heterogeneous membranes.

Experiments

Strongly basic anion-exchange membranes homogeneous AMX ("Tokuyama Soda", Japan) and modified heterogeneous membrane Ralex AMH-M ("Mega a.s.", Czech Republic) were studied by the rotating membrane disk method. Current-voltage characteristics (CVC), limiting current densities at different rotational speeds of the RMD were studied and the contribution of the electroconvective component was estimated.

Results and Discussion

Scanning electron microscopy images of strongly basic homogeneous AMX and heterogeneous Ralex AMH membranes in the swollen state are shown in Fig. 1 (a, b).

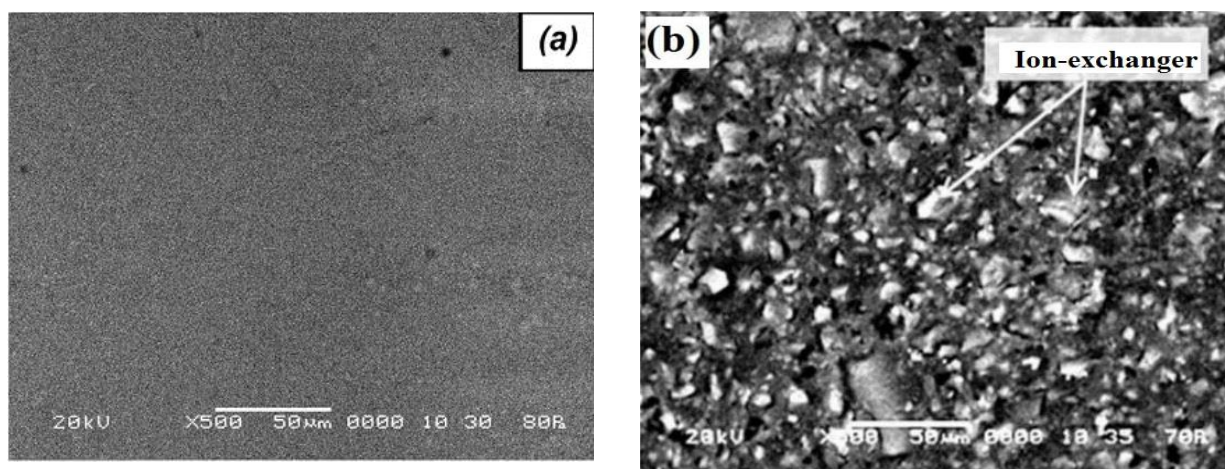


Figure 1. Microphotographs of the surface of homogeneous AMX (a) and heterogeneous modified Ralex AMH (b) membranes.

The surface of the homogeneous membrane AMX is uniform in all directions, with only slight distortions in the places where the reinforcing mesh is presented. The heterogeneous Ralex AMH membrane has a finely dispersed structure.

Table 1 presents the morphology characteristics of the surface of the heterogeneous ion exchange membrane Ralex AMH.

Table 1: Morphology characteristics of membrane surface

Membrane	Share of ion exchanger S,%	Effective radius of ion-exchange areas, μm	Macropores proportion P,%	Effective radius of macropores and structural defects, μm	Effective length between ion exchangers, μm
Ralex AMH	28.94	2.25	1.91	1.13	4.48

As is known [1], the electroconvection is strongly influenced by the dissociation of water, which flows in the electromembrane system under overlimiting current conditions at the same time with electroconvection. The experimental strongly basic membranes AMH were surface-modified with a copolymer of dimethyldialylammonium chloride with acrylonitrile according to the method described in [2]. Surface-modified AMH-M membranes do not contain in the surface layer the functional groups that are catalytically active in the water dissociation reaction. As a result, water dissociation on these membranes is not observed until the electric potential drop on the membrane reaches $\Delta\phi = 3V$. The results of the investigation of AMH-M membranes by the RMD method, presented in Levich coordinates, are shown in Fig. 2.

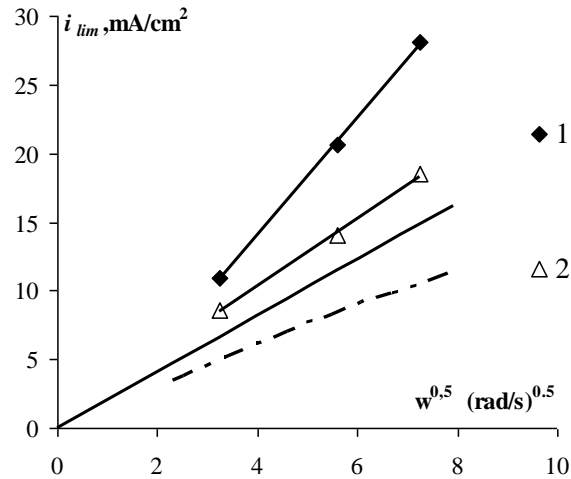


Figure 2. The dependence of the limiting current density on the square root of the angular speed of RMD. The solid line shows the values of limiting current for the AMX membrane, calculated using the Eq. (1). The dashed line - respectively for heterogeneous membranes AMH, calculated according to the Eq. (2) and (3) taking into account the screening of membrane surface by an inert binder. The points are the experimental values of the limiting current for membranes: 1 – AMH-M, 2 – AMX.

The same figure shows the results of the RMD method of homogeneous AMX membranes of Japanese production. For comparison, the dependence of the limiting electrodiffusion current for a homogeneous membrane AMX and a heterogeneous membrane AMH-M calculated with Levich equation (1):

$$i_{lim} = 0,62FzD^{2/3}v^{-1/6}C \frac{1}{(T_i - t_i)} \omega^{1/2} \quad (1),$$

And by the Baltrunas-Bugakov equation of and his colleagues, taking into account the heterogeneity of the membrane [3].

$$\frac{1}{i_{lim}} = \frac{\delta(T_i - t_i)}{zFDC} + \frac{\Theta R}{zFDC} \sqrt{\frac{\ln(1+0,27/\sqrt{1-\Theta})}{2(1-\Theta)}} \quad (2),$$

The thickness of the diffusion layer was calculated by the equation 3:

$$\delta = 1,61\omega^{-1/2}v^{1/6}D^{1/3} \quad (3)$$

The contribution of the electroconvective component of the limiting current measured for the homogeneous membrane AMX and the modified heterogeneous membrane AMH-M can be compared by comparing the experimental limiting currents with the calculated electrodiffusion limit currents for the homogeneous (solid line) and the modified heterogeneous (dashed line) membranes, respectively (fig. 2). The contributions of the electroconvective component for the membranes under study are given in Table 2.

Table 2: The relative contributions of the electroconvective component of the limiting current in the total mass transfer in percent for the investigated membranes at different rotation speed of the membrane disk (ω)

Membrane	$\omega = 100$ rpm	$\omega = 300$ rpm	$\omega = 500$ rpm
AMX	23.1	18.7	19.9
AMH-M	53.1	57.6	60.9

It can be seen that heteroelectroconvection on heterogeneous membranes AMN-M, developed as an electroosmosis of the second kind, is substantially higher than electroconvection on a homogeneous membrane of AMX (first-kind electroosmosis). At high current densities ($i > i_{lim}$), heteroelectroconvection becomes the dominant mechanism of ion transport.

Acknowledgements

The present work is supported by the State Task of the Ministry of Education and Science of the Russian Federation, project No. 10.3091.2017 / PP.

References

1. V.I. Zabolotskiy, A.Yu. But, V. I. Vasil'eva, E. M. Akberova Mel'nikov S.S. // *J. Membr. Sci.* 2017. V.526. P.60.
2. V.I. Zabolotsky, M.V. Sharafan, R. Kh. Chermit, RF Patent No 2013133028 dated 2015.
3. V.I. Zabolotsky, V.V. Nikonenko, M. H. Urtenov, K.A. Lebedev, V.V. Bugakov // *Rus. J. Electrochem.* 2012. V.48. P.766

INFLUENCE OF NATURE OF CATION EXCHANGE LAYER ON ELECTROCHEMICAL CHARACTERISTICS OF ASYMMETRIC BIPOLAR MEMBRANES

Victor Zabolotsky, Stanislav Melnikov, Stanislav Utin

Kuban State University, Krasnodar, Russia

Introduction

Bipolar membranes (BPM) are bilayer composites, in which cation- (CEL) and anion-exchange (AEL) layers possess ion-selective properties. They occupy a unique place among ion-exchange membranes due to their ability to generate hydrogen and hydroxyl ions from the water molecules under direct current polarization. Water splitting reaction occurs in the bipolar region (a place where CEL and AEL are conjoined) of a BPM.

The primary distinction of asymmetric bipolar membranes from the classical ones lies in the fact that salt transport numbers across such membrane can be equal to the transport numbers of water splitting products. Previously we have shown how cation-exchange layer thickness affects asymmetric bipolar membrane electrochemical characteristics [1].

To improve water splitting capabilities, a catalyst is usually introduced into the reaction zone of the bipolar membrane, which is situated on a bipolar border between a cation- and anion-exchange layers of a BPM. However, given the procedure of asymmetric bipolar membrane creation, a catalyst may be easily introduced into a cation-exchange layer. Following a series of ionogenic groups catalytic activity towards water splitting reaction [2], carboxylic and phosphoric acid groups have the highest activity. To date, various methods have been known for introducing the catalyst into the bipolar region [3]. One of the promising directions is the use of functionalized dendrimers [4] since such modifiers have a significant number of reaction centers per one molecule. Also, they are readily responsive to the introduction of various functional groups.

In this work, we present the results of studying the effect of the chemical nature of the cation exchange layer on the electrochemical characteristics of asymmetric bipolar membranes.

Experiments

To investigate the effect of a cation-exchange layer on the electrochemical and transport characteristics of asymmetric bipolar membranes three asymmetric bipolar membranes obtained in a way similar to the one described in [1] with different catalytic additives were studied. Anion-exchange layer thickness remained equal to 450 μm . Ralex AMH-Pes was used as an anion-exchange layer and NafionTM type membrane as a cation-exchange coating.

The current-voltage characteristics measurements were carried out in an electrochemical cell (Fig. 1) with working membrane surface of 2.27 cm^2 in the NaCl | aBPM | NaCl system. The salt solution was chosen to allow simultaneous study of electrochemical and transport characteristics of the membranes. The cation-exchange layer was facing towards the cathode, and the anion-exchange layer was facing towards the anode. The concentration of all solutions was 0,01 M. For the measurement of current-voltage curves (CVC) Luggin-Haber capillaries connected to Ag/AgCl electrodes were used. In the present study dynamic method was used for measuring the current-voltage characteristic of asymmetric bipolar membranes. Linearly increasing and decreasing current was applied to the cell, and CVC recorded. Current sweep rate was set at 2×10^{-5} A/s that gives a minimal hysteresis sweep between forward and backward CVCs.

The results were normalized on the value of the ohmic potential drop:

$$\Delta\varphi' = \Delta\varphi - iR_{ef}, \quad (1)$$

where R_{ef} is the effective resistance of the membrane system at low current densities, which includes the ohmic resistance between the measuring electrodes and the diffusion resistance of both diffusion layers. R_{ef} is determined experimentally by the initial slope of the CVC.

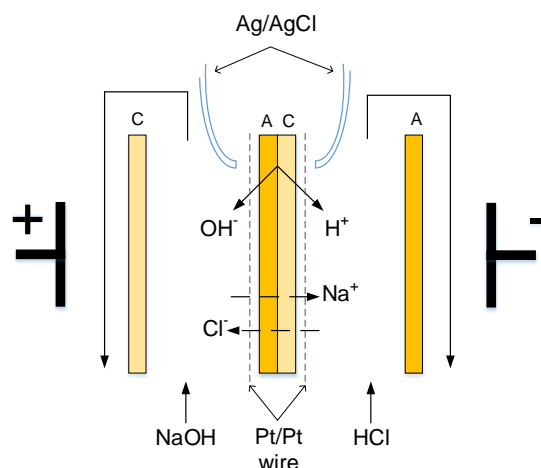


Figure 1. Experimental cell and ions fluxes through the membrane under investigation. A – anion-exchange membrane/layer; C – cation-exchange membrane/layer; Pt/Pt wire –platinized platinum wire used for impedance measurement.

Results and Discussion

The shape of the current-voltage curves obtained after the correction of the potential is substantially distorted (Fig. 2). This behavior is most likely due to the fact that the rate of decrease in resistance when the membrane is in the generation mode is greater than the ohmic component of the resistance. As a result, using the equation (1), the second term becomes larger than the first. This effect is directly related to the ability of the membrane to generate alkali and acid. During this process, the salt ions are slowly removed from the solution near the membrane, and the mobile ions of hydrogen and hydroxyl from the membrane come in for replacement in large numbers. Due to the high mobility of the latter ions, the resistance of the solution near the surface of the membrane decreases in comparison with the initial one. At the same time, as the density of the polarizing current increases, the rate of this process increases, which further reduces the resistance of the impurity membrane. As a result, when the initial ohmic resistance is subtracted, the shape of the volt-ampere characteristic of the membrane is distorted.

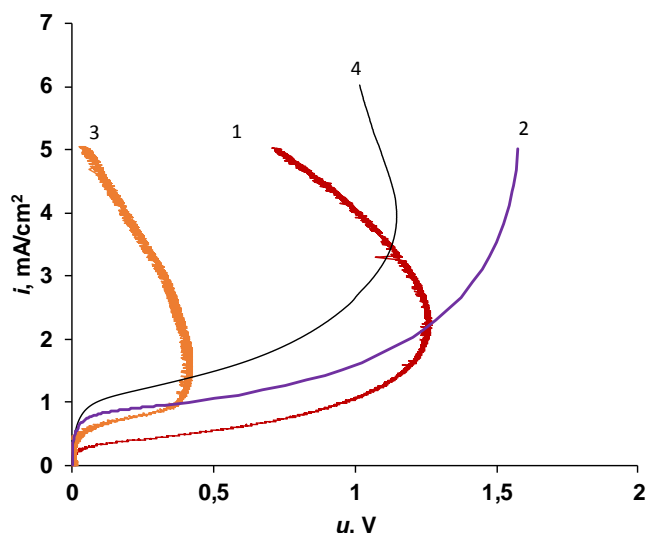
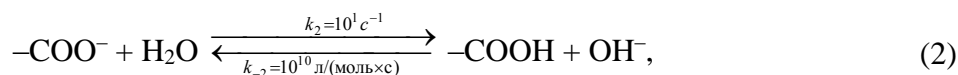


Figure 2. Current-voltage characteristics of the studied asymmetric bipolar membranes: 1 – initial membrane without catalyst, 2 – membrane with carboxylic catalyst, 3 – membrane with phosphoric acid catalyst, 4 – membrane with microsized phosphoric acid particles.

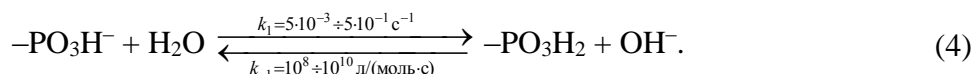
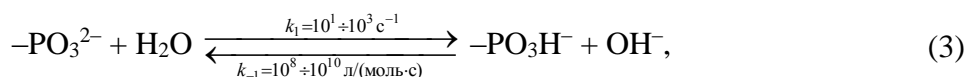
As can be seen from the data given in Fig. 2, the introduction of catalytically active substances into the cation-exchange membrane layer leads to a significant decrease in the potential at which the dissociation of water begins.

The introduction of ionopolymers (functionalized dendrimers) into the cation exchange layer should substantially reduce the potential of water splitting reaction, due to the high degree of functionalization and localization of ionosphere molecules in the reaction region. However, as can be seen from the data obtained, the dissociation of water on membranes 2 and 3 occurs only slightly earlier than in the unmodified membrane 1. This can be explained by blocking part of the dendrimer by the chains of the sulfonated perfluorocarbon from which the cation exchange layer consists and, moreover, by its uniform distribution over Thickness of the cation exchange layer, as a result of which only a part of the molecules are in the reaction zone. It is also worth noting that the limiting electrodiffusion currents for these membranes are somewhat higher, compared with the original membrane, which indicates a decrease in the selectivity of these membranes with respect to salt ions.

With an increase in the polarizing current, the fluxes of hydrogen and hydroxyl ions increase, which leads to a decrease in the pH of the cation exchange layer and its gradual transition into the hydrogen form. Since carboxyl and phosphoric acid ionogenic groups are weakly acidic, with large pKa values (3.5-7 for phosphoric acid and 4-6 for carboxylic acid), their form is directly linked to pH. When the pH is lowered inside the cation exchange layer, the ionic groups of the modifier are protonated by reactions:



and



Protonated ionogenic groups no longer possess a charge and are no longer able to participate in ion exchange. Thus, a part of the volume of the cation exchange layer is removed from the ion exchange, which causes a decrease in the selectivity of the cation exchange layer over the anions present in the solution.

Thus, it has been shown that the introduction of catalytic additives into the cation exchange layer can improve the electrochemical properties of asymmetric bipolar membranes, in particular, to decrease the potential difference at which the water dissociation reaction begins. At the same time, to increase their effectiveness, it is worthwhile to introduce modifiers only in the reaction zone, since the introduction of the modifier into the cation exchange layer causes only blocking of the modifier part and a decrease in membrane selectivity. Perhaps to increase the efficiency of these catalysts, it is necessary to use the multilayer irrigation method, when a second cation exchange layer is applied over the thin layer of the containing modifier, giving the membrane the required selectivity.

Acknowledgments

This work was supported by Russian Federation presidents scholarship, № SP 1545.2016.1.

References

1. V. Zabolotskii, N. Sheldeshov, S. Melnikov // J. Appl. Electrochem., 2013, vol. 43, p. 1117.
2. V.I. Zabolotskii, N.V. Shel'deshov, N.P. Gnusin // Russ. Chem. Rev., 1988, vol. 57, p. 801.
3. V. Zabolotskii, N. Sheldeshov, S. Melnikov // Desalination, 2014, vol. 342, p. 183.
4. V. Zabolotsky, S. Utin, A. Besspalov, V. Strelkov // J. Membr. Sci., 2015, vol. 454, p. 188.

STABILIZATION OF COPPER NANOPARTICLES IN ION EXCHANGE MEMBRANE MATRIX TO CREATE COMPOSITE MATERIALS WITH DUAL FUNCTION - ION TRANSPORT AND ELECTROCATALYSIS OF NITRATE ION REDUCTION REACTION

Victor Zabolotsky, Oleg Mugtamov, Stanislav Melnikov

Kuban State University, Krasnodar, Russia

Introduction

Nowadays the amount of fertilizers used in agriculture is increasing in order to increase productivity. The most common fertilizer is an ammonium nitrate, which is used worldwide. Nitrate ions from the soil pass into surface waters, pollute pastures, and accumulates in the fruits of plants. Because of the increasing nitrate pollution, its removal from surface waters when obtaining potable water and food products is an actual task.

There are works in which the reduction of nitrate ions occurs on nanoparticles of metals of the platinum group [1], as well as on such as iron and copper [2, 3]. Effective membrane materials can be obtained by incorporating metal catalysts into ion-exchange matrix [4]. However, it is not possible to obtain stable materials when such particles are incorporated into the ion-exchange membrane, since when placed in an electric field; part of the nanoparticles undergoes anodic polarization and dissolves.

The purpose of this work was to create a composite material based on the industrial anion-exchange membrane MA-41, which is capable of selective ion transport, catalyze the reduction reaction of nitrate ions, and study the properties of the resulting material.

Experiments

The MA-41/Pd membrane provided by Bespalov A.V. has a volumetric modification. The need for volumetric modification is because anodic and cathodic polarization of the palladium particles will occur on different sides of the membrane. This allows further deposition of copper nanoparticles on only one side of the membrane, and further prevents oxidation of the reduction products of the nitrate ions at the anode.

Membranes MA-41/Pd with a high content of reduced palladium were obtained by successive "saturation-reduction" cycles.

Introduction of copper nanoparticles to the surface of a modified membrane was carried out by electrochemical method from a solution of copper sulfate, which was supplied to the chambers adjacent to the membrane, a solution of sodium nitrate circulated in the electrode chambers (fig. 1a).

Under the influence of electric current, ions of bivalent copper were reduced on the surface of the platinum-coated membrane MA-41 facing the anode.

Initially, a considerable voltage was applied to the cell for a short time, so that crystal nuclei appeared on the surface of the membrane, then the voltage was lowered, it is necessary for the copper particles to increase in size.

After determining the limiting current, the mass-transfer characteristics of the modified membrane were studied. Measurement of the transfer numbers of nitrate ions through the membrane is necessary to evaluate the removal efficiency of nitrate ions. To do this, a laboratory cell was assembled (Fig. 1b), and the concentration and desalting chambers were connected to containers filled with 200 ml 0.01 M sodium nitrate solution, 0.01 M sodium nitrate solution was fed into the electrode chambers. In order for the concentration difference to be determined using the liquid chromatography method, a current of 3.42 mA was applied per cell for 5 hours.

Calculation of the current efficiency for nitrate ions was carried out according to the equation (1):

$$\eta = \frac{26,8 \cdot V(C_0 - C_{fin})}{iS\tau} \quad (1)$$

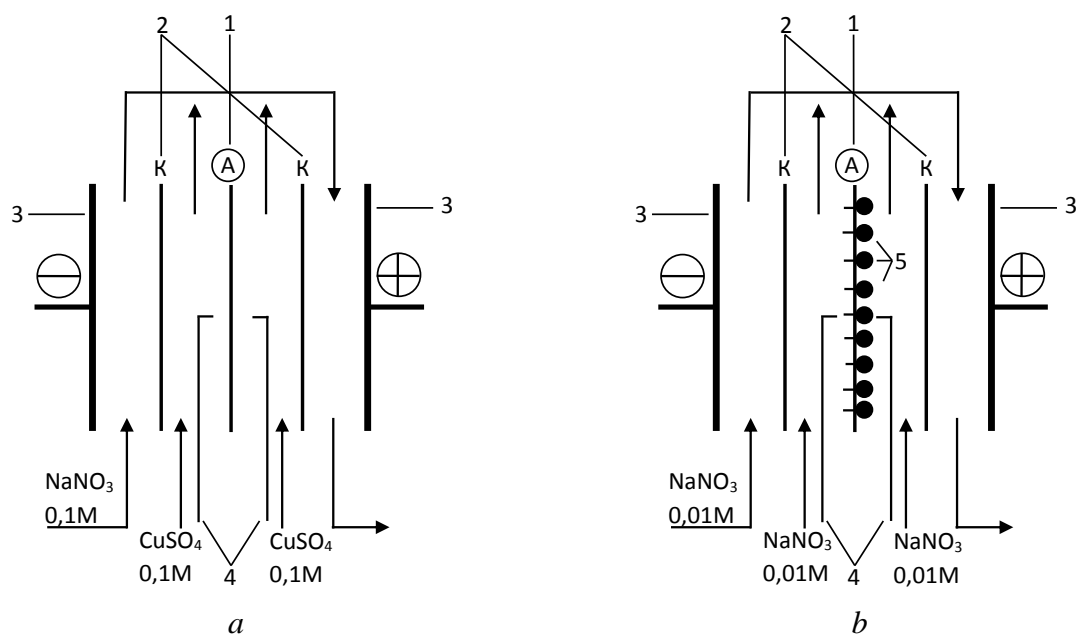


Figure 1. Cell schematics for modifying of the original membrane (a) and for the study of mass transfer characteristics (b). 1 - MA 41 membrane, 2 - MK 40 membrane, 3 - platinized electrodes, 4 - Luggina-Haber capillaries, 5 - copper nanoparticles

Results and Discussion

The modification included several cycles, after each of which a current-voltage characteristic of the obtained membrane was taken. Because of the modification on the current-voltage characteristic of the composite membrane, a "second limiting current" appears (fig. 2a). At low values of the reduced potential jump, the value of the current for the modified membrane is significantly higher than in the original one, which may indicate the electrochemical reaction to the nanoparticles introduced into the membrane (fig. 2b).

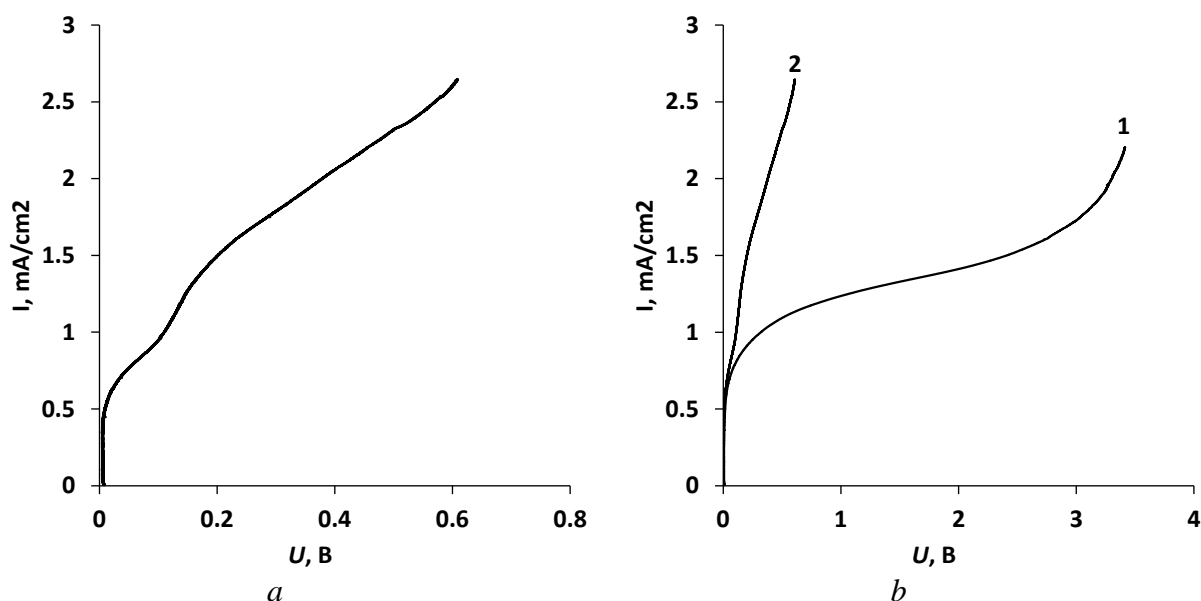
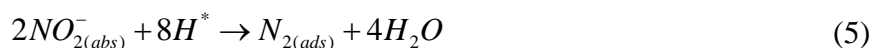
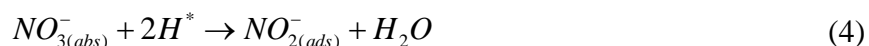


Figure 2. Typical view of the reduced current-voltage curve of the modified membrane (a), a comparison of the current-voltage curves of the initial (1) and modified (2) membranes in a 0.01M NaNO₃(b)

It is assumed that the electrochemical reaction proceeding on copper has the following mechanism:





Nitrate ions passing through the anion-exchange membrane are sorbed on the surface of copper (2) nanoparticles, where the reduction takes place, due to the reaction with atomic hydrogen (4,5), formed electrochemically (3) and released from the palladium volume. Reclamation takes place in several stages.

The initial concentration of sodium nitrate in both chambers at the beginning of the experiment was 0.0094 M, at the end of the experiment in the desalting chamber the concentration was 0.0798 M, in the concentration chamber 0.0109 M. The current yield calculated by the equation for the desalting chamber was 0.55, for the concentration chamber 0.37.

The possibility is shown of synthesizing bimetallic palladium-copper particles stabilized by an ion-exchange membrane matrix. The obtained particles have electrochemical activity with respect to nitrate ions, which is manifested in the appearance of a second limiting current on the current-voltage characteristic of the membrane.

The investigated composites are fairly stable when they are polarized by a direct current, which is confirmed by the invariance of their current-voltage characteristic before and after continuous polarization for 10 hours.

The resulting material selectively transfers ions due to the ion exchange matrix, and also catalyzes the reduction reaction of nitrate ions on bimetallic particles.

Acknowledgments

The present work is supported by the State Task of the Ministry of Education and Science of the Russian Federation, project No. 10.3091.2017 / PP.

References

1. *Safonova T. Ya.* // *Rus. J. Electrochem.*, 1998, Vol. 34, p. 1264.
2. *Macova Z.* // *J. Appl. Electrochem.*, 2005, Vol. 35, p. 1203.
3. *Mossa Hosseini S., Ataie-Ashtiani B., Kholghi M.* // *Desalination*, Vol. 276, p. 214.
4. *Kravchenko T.A., Zolotuhina E.V., Chai`ka M.Iu., Iaroslvtcev A.B.* // *E`lektrohimiia nanokompozitov metall-ionoobmennik. M.: Nauka, 2013. 365 s.*

REAGENT-FREE ELECTRO-MEMBRANE TECHNOLOGY OF PH-CORRECTION OF WATER AND WATER-ORGANIC SOLUTIONS

Victor Zabolotsky, Nikolay Sheldeshov, Stanislav Melnikov, Stanislav Utin
Kuban State University, Krasnodar, Russia, E-mail: vizab@chem.kubsu.ru

Correction of pH of technological solutions is often a necessary part of preconditioning before subsequent stages of processing. Compared with traditional chemical stages of pH correction membrane methods, which use a bipolar membranes, allow to avoid the use of acids and alkalis. This process is possible if the salt is contained in the technological solution in an amount sufficient to obtain the required acid or alkali. To ensure that the use of bipolar membrane is economically justified, the voltage drop across it should be small enough.

The work was aimed at the development of bipolar membranes with improved characteristics containing catalytic additives, further development of the theory of the heterogeneous and homogeneous catalysis on the charged interfaces under direct current polarization and elaboration of processes based on bipolar membranes.

Catalytic additives include carboxylated and phosphorylated hyperbranched polymers based on BoltornTM H20, linear functionalized polymers based on polyvinyl alcohol, microsized and nanosized particles of phosphomolybdic heteropolyacid, nanosized particles of the sol of iron (III) hydroxide, linear and crosslinked ionpolymers (sulphoacidic cationite KU-2, carboxyl cationites KB-2 and KB-4, phosphoacidic cationite KF-1, tertiary and secondary amines containing anionite EDE-10P, polyacrylic acid). Newly synthesized additives were studied by the FTIR, NMR, and scanning-electron spectroscopy while their physic-chemical characteristics were also being studied. Electrochemical characteristics of the bipolar membranes with these additives were studied by the electrochemical impedance spectroscopy and voltammetry. Using the mathematical model developed in the previous stage of the project the limiting water splitting rate constants were found.

The electro dialysis free-reagent process for pH-correction of water was designed. During the tests of industrial electro dialyzer in real working conditions was shown that its operation as a part of the baroelectromembrane complex with productivity of 5 m³/h ensures the stable pH correction of water to a level of not less than 10 (Figure 1). After the treatment by electro dialysis with bipolar membranes solution at the outlet of alkali chambers is mixed with reverse osmosis water and is directed to feeding of boiler. After mixing the pH value of water was ranged 8,5-9,5. Electomembrane complex provides the pH value of boiler feed water, which allows use it for operation of steam boilers in heat-and-power engineering without adding of chemical reagents.

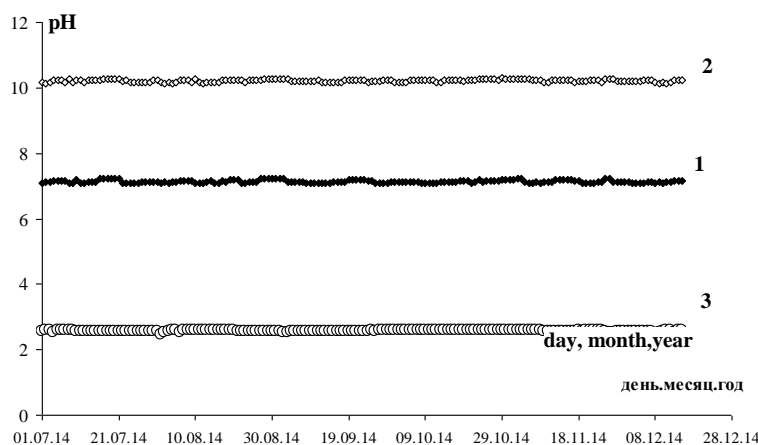


Figure 1. Dependence of treatment water pH on operation time of electro dialyzer. 1 – initial pH value, 2 – pH value at the outlet of alkaline chambers of electro dialyzer, 3 – pH value at the outlet of acidic chambers of electro dialyzer

In order to determine the influence of organic solvents on the generation of lithium hydroxide from technological solutions comprising dimethylacetamide, isobutyl alcohol, water and lithium chloride two processes were studied. In the first process lithium chloride was contained in a previously neutralized technological solution (solution A) comprising 0.25 mol/l lithium chloride, 28.0 wt% N, N-dimethylacetamide, 21.0 wt% isobutyl alcohol and 50 wt % water. In the second process the solution of lithium chloride comprised 0.75 mol/l lithium chloride, 1.49 wt % N, N-dimethylacetamide and 95% water (solution B). Solution B is the concentrate obtained from electro dialysis processing of a neutralized technological solution (solution A).

Both processes were studied in an electro dialysis module with EDS-4/3 bipolar membranes (Figure 2). MB-3 industrial heterogeneous bipolar membrane, MK-40 cation exchange membrane and MA-40 anion-exchange membrane were used in the membrane stack of electro dialysis module. The current density applied to the apparatus was 1 A/dm² and 2 A/dm² for solutions A and B respectively.

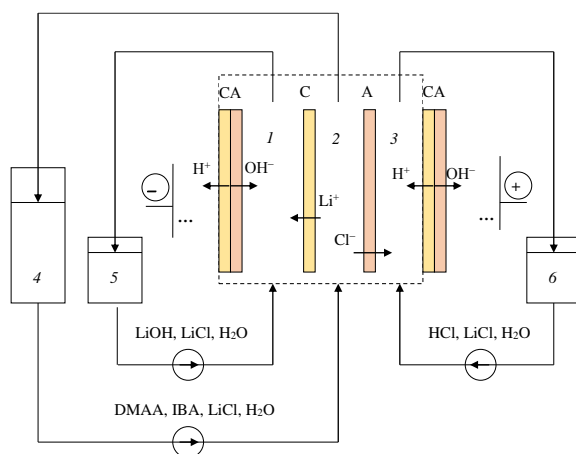


Figure 2. Simplified diagram of test setup for electromembrane electro dialyzer-synthesizer with bipolar membranes intended for reagent-free production of lithium hydroxide and hydrochloric acid from lithium chloride solution. 1 – alkaline chamber; 2 – salt chamber; 3 – acidic chamber; 4 – vessel with lithium chloride solution; 5 – vessel to accumulate lithium hydroxide solution; 6 – vessel to accumulate hydrochloric acid solution. The dotted line shows the unit cell of the membrane stack

Concentrations of acid and alkali increase and the rate of their accumulation decreases over time. This is due to a decrease in the current efficiency of acid and alkali (Figure 3) due to a decrease in the selectivity of bipolar, cation and anion exchange membranes in more concentrated solutions. The decrease in specific energy consumption with increasing acid and alkali concentrations in the solutions is caused by the rapid decrease of unit cell voltage compared with the decrease in current efficiency of acid or alkali. Reduction of specific productivity in the same conditions is caused by a decrease in the rate of accumulation of acid and alkali in the solutions because of increased co-ion transport numbers through the membranes.

Comparison of the specific characteristics of the processes in which the starting salt solutions were A and B solutions is of particular interest. When the salt solution is rich in organic components (solution A) the current efficiency and specific productivity of acid and alkali is less and the specific energy consumption is greater than when the salt solution is depleted in organic components (solution B). Increased energy consumption with increasing concentration of organic components in the saline solution is due to a decrease in conductivity of the solution and increasing the voltage drop in the unit cell. The low conductivity of solution is due to a decrease in ion mobility in the aqueous-organic solution as a result of the increase of its viscosity compared to the aqueous solution.

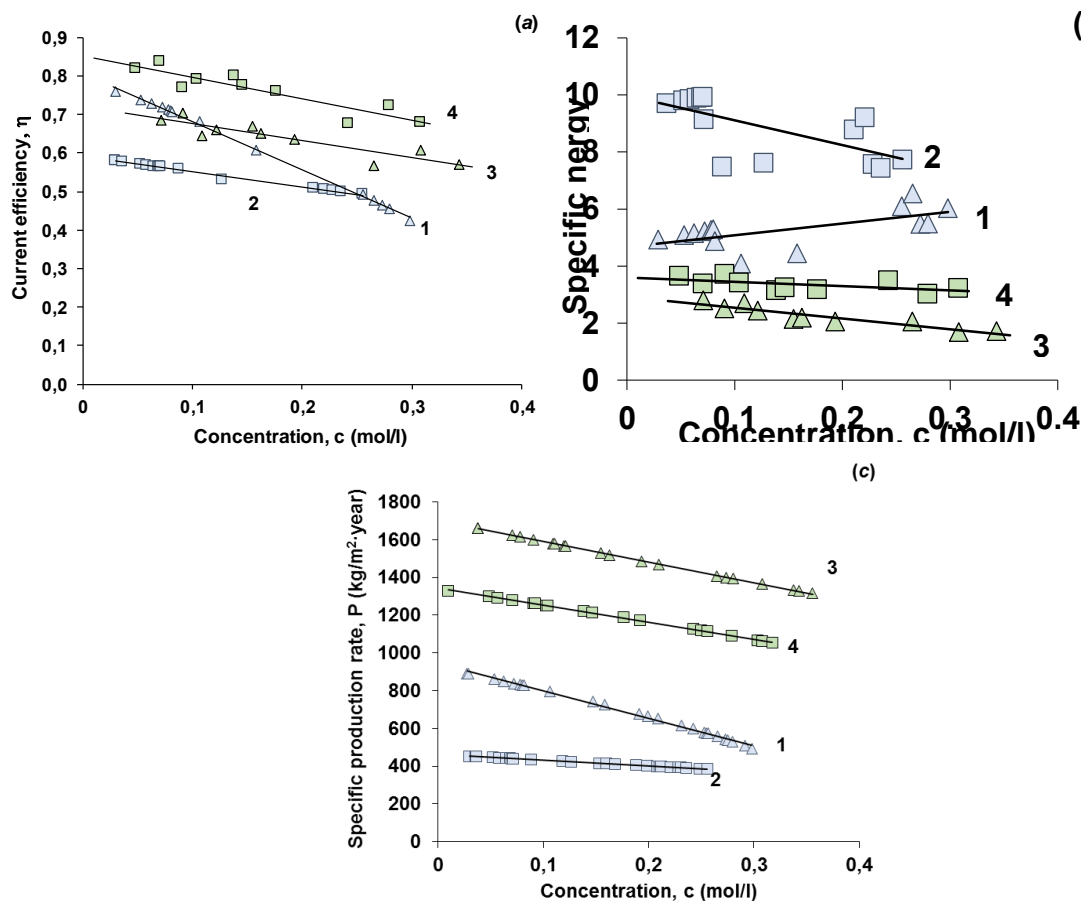


Figure 3. Differential current efficiency of hydrochloric acid (1, 3) and lithium hydroxide (2, 4) (a), specific energy consumption during production of alkali and acid (b) and of specific productivity of membrane stack on alkali and acid (c) on concentration of lithium hydroxide and hydrochloric acid, produced from solutions A (1, 2) and B (3,4)

Reduced current efficiency of the acid and alkali and decreased specific productivity when using solution A could be the result of several factors. Firstly, the electric current strength in the case of solution A was half of that in solution B in order to decrease heating-up of solution A, which has higher resistance. This leads to an increase in co-ion transport numbers in the bipolar membrane and an increase in diffusion losses of acid and alkali into the salt chamber. Secondly, the influence of organic components on the structure of cation and anion exchange membranes may lead to an increase in co-ion leakage through the membranes.

Analysis of the impurities of lithium chloride in producing acid and alkali solutions shows that salt contamination does not exceed 0.019 mol/l and 0.021 mol/l respectively, in the case of solution A, and 0.008 mol/l and 0.05 mol/l in the case of solution B. Contamination of acid by organic compounds (DMAA and IBA) was negligible. Pollution of alkali by dimethylacetamide was less than 0.41%, and by isobutyl alcohol less than 0.1%.

Thus, electrodialysis with bipolar membranes makes it possible to produce lithium hydroxide and hydrochloric acid from aqueous-organic solutions of lithium chloride in which the total mass fraction of DMAA and IBA is in the range 1.8-53%. When the concentration of DMAA and IBA is high (53% wt.) the specific characteristics of the process deteriorate in comparison with solutions with a low concentration (1.8% wt.) of DMAA and IBA in solution.

The present work is supported by the State Task of the Ministry of Education and Science of the Russian Federation, project No. 10.3091.2017 / PP.

THEORETICAL AND EXPERIMENTAL INVESTIGATION OF THE PH CORRECTION PROCESS OF SOFTENED WATER IN LONG ELECTRODIALYSIS CHANNELS WITH BIPOLAR MEMBRANES

Victor Zabolotsky, Polina Vasilenko, Stanislav Utin, Konstantin Lebedev
Kuban State University, Krasnodar, Russia, E-mail: utinstanislav@mail.ru

Introduction

Prediction and calculation of mass-exchange characteristics of industrial electrolysers is an actual problem of modern membrane technology. One of the mathematical methods for scaling of electrolysers is compartmentation method. Works [1-5], devoted to the use of compartmentation method for scaling the characteristics of electrolysis, show satisfactory results in electrolysis desalination and concentration of dilute solutions. At the same time, active development of electrolysis with bipolar membranes makes it necessary to search for mathematical approaches that allow us to scale and predict the characteristics of long membrane channels with bipolar membranes. However, for real natural waters the process of electrolysis is considerably complicated by the presence of a large number of components and the chemical reaction between them.

Experiments

The objects of investigation were two electrolysers with bipolar membranes: with channel length of 10 cm, containing 2 cell pairs, and 40 cm, containing 10 cell pairs. The scheme of cell pair presented in [6]. The studies were carried out on softened water with components content presenting in table 1.

Table 1: Components content of softened water

Initial components in softened water	Cl ⁻	HCO ₃ ⁻	H ₂ CO ₃	SO ₄ ²⁻	Na ⁺
Concentration, mg/l	55	261	7	80	168

Results and Discussion

The modeling principle for theoretical description of the pH correction process of softened water in an electrolyser with bipolar membranes with a channel length of 40 cm, was proposed. This mathematical approach was in dividing the length of the membrane channel into a sufficiently large number of sections with smaller length, located perpendicular to the direction of the solution flow. The calculation was carried out in such a way that the inlet data in the previous section were inlet data for the subsequent section. The mathematical model consisted of combination of algebraic equations describing the balance of chemical reactions and material balance for each component in alkaline and acidic chambers. Calculation of counter-ions transport numbers through anion-exchange membrane is carried out on the basis of theoretical approach, developed in [7]. The current density at corresponding potential U was calculated from formula:

$$i = \frac{F^2}{RT} \frac{U - \frac{RT}{F} \ln \frac{c_{H^+}^2}{c_{H^+}^1}}{\left(\sum_j z_j^2 D_i c_j^1 + \sum_j z_j^2 D_j c_j^2 \right) h}$$

where $c_{H^+}^1, c_{H^+}^2$ – the concentrations of protons in acidic and alkaline chambers respectively; h – inter membrane distance. D – coefficients of ions diffusion in solution. To reduce the mathematical transformations, the calculations were paralleled. Two programs were created that worked simultaneously for both chambers. In the acidic chamber, the calculation was carried out with the transport numbers obtained in the previous step, and then refined with the calculated transfer numbers in the alkaline chamber. Figure 1 shows the dependences of solution pH on channel length of the electrolyser with bipolar membranes. Theoretical calculation shows that the maximal

change in the solution pH at the outlet from the acidic and alkaline chambers occurs in the start section of up to 10 cm, which agrees with the experimental data.

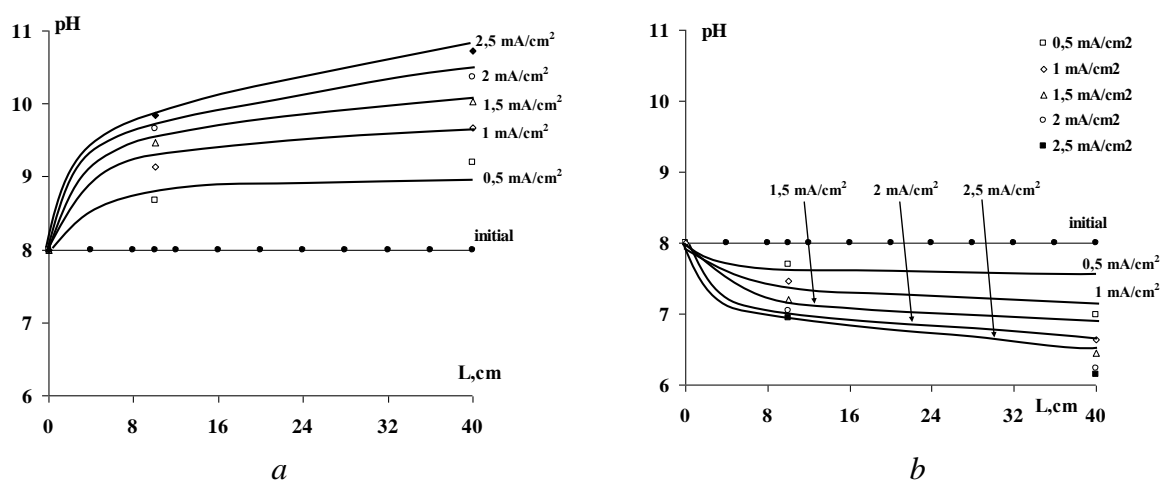


Figure 1. Dependence of solution pH at the outlet of alkaline (a) and acidic (b) chambers with bipolar membranes on channel length at different current densities; Dots – experimental values, curves – calculation by the model

It is shown that the model describing the process of electro dialysis pH correction of multi-component solutions based on thermodynamic equations of ion equilibrium, equations of material balance, kinetic equations for the calculation of transport numbers and compartmentation method, can be used to modeling of long (≈ 40 cm) electro dialysis channels with bipolar membranes.

Acknowledgements

This work was financial supported by RFBR grant and administration of Krasnodar region №16-48-230433r_a.

References

1. Nikonenko V.V., Pismenskaya N.D., Istoshin A.G., Zabolotsky V.I., Shudrenko A.A. // *Electrokhimiya* 2007. V. 43. №9. P. 1125.
2. Zabolotsky V.I., Pismenskaya N.D., Laktionov E.V., Nikonenko V.V. // *Desalination* 1996. V. 107. P. 245.
3. Nikonenko V.V., Pismenskaya N.D., Istoshin A.G., Zabolotsky V.I., Shudrenko A.A. // *Chemical Engineering and Processing* 2008. V. 47. P. 1118.
4. Evangelista. F. // *Desalination* 1987. V. 64. P. 353.
5. Zabolotskii V. I., Melnikov S.S., Demina O.A. // *Electrokhimiya* 2014. V. 50, №1. P. 38.
6. Utin S.V., Zabolotskii V. I., Lebedev K.A. // *Sorbtsionnye i hromatograficheskie processy* 2015. V. 15. №6. P. 811.
7. Lebedev K.A., Nikonenko V.V., Zabolotsky V.I., Gnusin N.P. // *Electrokhimiya*. 1986. V. 22. №5. P. 638.

GALVANIC DEPOSITION OF MULTICOMPONENT ALLOYS INTO THE NANOSIZED PORES OF TRACK MEMBRANES

¹Dmitri Zagorskiy, ^{1,2}Sergey Bedin, ³Sergey Kruglikov, ^{1,4}Ilya Doludenko

¹Center of Crystallography and Photonics of RAS, Leninsky pr.,59, E-mail: dzagorskiy@gmail.com

²Moscow Pedagogical University, Moscow, Russia

³Mendeleev University of Chemical Technology, Miusskaya sq.,9, Moscow, Russia

⁴National Research University Higher School of Economics, Moscow, Russia

Introduction

Matrix synthesis. The obtaining and application of different types of nanomaterials are the main trends at the last time. The method of matrix synthesis are one of the most perspective among other techniques of nanomaterial fabrication [1]. The main idea of method is to fill the pores of specially prepared matrix by any desired material. The obtained structures are replicas of the pores [2]. Different mediums could be used as the matrixes-porous alumina, different zeolits, porous silica, polymer track membranes. Different materials could be used as a “filler”- polymers, dielectrics, some sorts of crystals and metals. The method is actually “two-stage”- the fabrication of the matrix and the “filling” of this matrix. The advantage of such approach is the possibility of independent exposure to different stage of the process and therefore the possibility to change different properties of obtained materials. In this work polymer matrixes were used as the templates and their pores were loaded (electrodeposited) by metals in order to obtain so-called nanowires (NWs).

Experiments and Results

Metals electrodeposition into the pores of different matrixes is investigated by many authors [3]. In our previous works [4,5] we investigated the deposition of pure metals into the pores of track membranes. This paper devoted to deposition of two metals (of iron group) for obtaining of NWs. Two types of structures could be obtained- homogeneous (“alloys”) and heterogeneous-layered structures (“layers”) [6,7]. In our work we used Track membranes with the pores 50-100-200 nm for matrix synthesis of NWs via electrodeposition. Complex electrolytes –containing the ions of both metals- were used. Fig.1 demonstrate the results of deposition of “alloys” Fe-Co and Fe-Ni into the pores of 100 nm diameter.

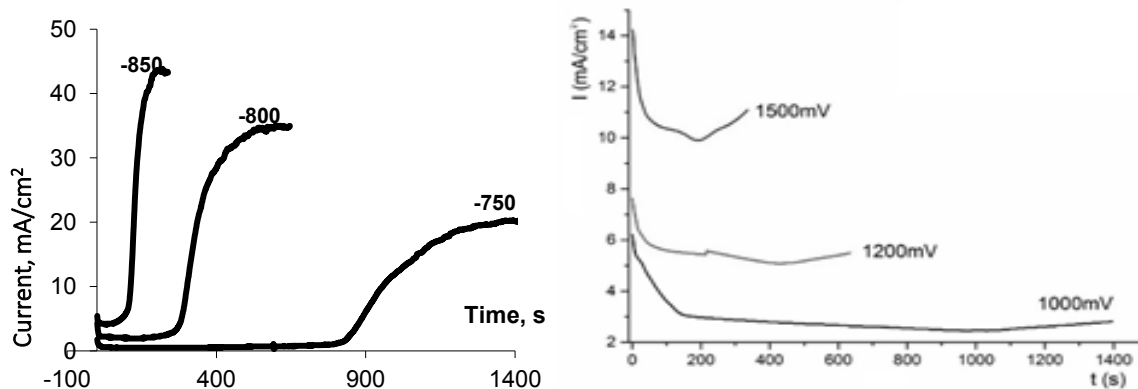


Figure 1. Electrodeposition of alloys Fe-Co (left) and Fe-Ni (right) into the pores of track membranes (100 nm)-dependence of Current on time (for different voltages)

The main features of these processes are the same as for deposition of pure metals. Nevertheless there are some differences: the composition of the NWs could be different from the composition of grooving electrolyte- due to different diffusion mobility of different ions. The grooving conditions could vary at different parts of pores channel- so, we the concentration of both metals could be different at different parts of NWs.

The next part of our work was devoted to fabrication of “layered” NWs. Special regime – “pulse” –Steps with different voltage – was used for this case. Fig.2 demonstrated the obtained results.

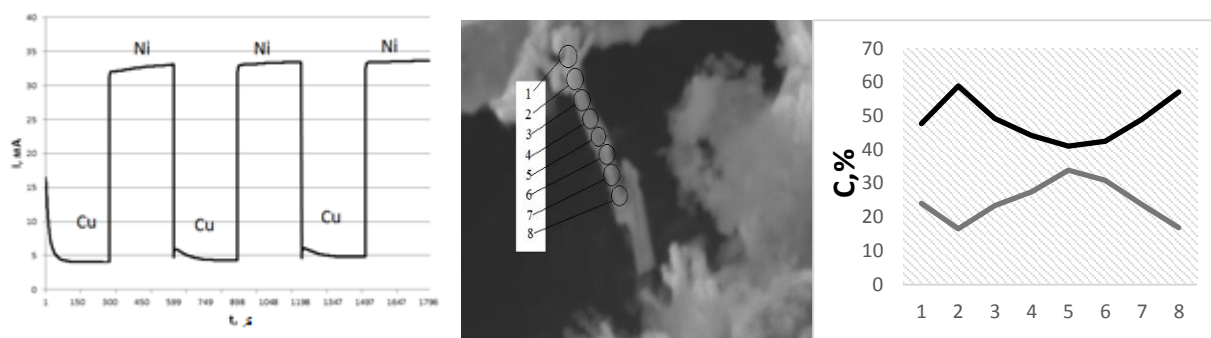


Figure 2. Electrodeposition of layers (Ni/Cu) into the pores: galvanic process (left), SEM image of single NW with the points for elemental analysis (middle), concentrations-on –length dependence (right)

The quantity of layers corresponds to quantity of “steps”. Elemental composition of these layers is different- in accordance to voltage applied during the corresponding stage.

So, by varying the electrodeposition parameters – composition of solution, voltage, time, current –we could obtain different nanostructure.

Asknowlegments

This work was supported by Grant RFBR 15-08-04949, Authors thanks V.Korotkov for preparation of Fe-Co samples and V.Artemov (IC RAS) for SEM-images.

References

1. C. R. Martin. Nanomaterials–A Membrane-Based Approach.//Science 266,1994,1961-1966.
2. Chakarvarti S.K., Vetter J. Template synthesis.// Nucl. Instr. Meth. 1991.V. B 62. p. 109–114.
3. DavidovA.D.,VolginV.M. Template electrodeposition of metals (Review) // Electrochemistry, 2016, V.52, N9, p.905-933 (in Russian).
- 4.Korotkov V., Kudriavtsev V.,Zagorskiy D., Bedin S. Electrodeposition of Cobalt into the micro- and nanosize pores of track membranes.//Galvanotechnic and Surface treatment, 2011, V.XIX, N4, p.23-28 (in Russian).
5. Korotkov V., Kudriavtsev V. Kruglikov S.,Zagorskiy D.,Sulianov S., Bedin S.// Electrodeposition of Metals of Iron group into the pores of track mamtrixes for obtaining of nanowires. // Galvanotechnic and Surface treatment, 2015, V. XXIII, N1, p.24-33 (in Russian).
- 6.T. Ohgai. Fabrication of Functional Metallic Nanowires Using Electrodeposition Technique. //(in “Electrodeposited Nanowires and Their Applications” Book edited by : Nicoleta Lupu, ISBN 978-053-7619-88-6, pp.228, Feb.2010, INTECH, Croatia.
- 7.A.Sugiyama, M.Yoshino, T.Hachisu, T.Osaka. Electrochemical Synthesis of metal alloys for magnetic recording systems. //book- in “Modern Electroplating” ed by M.Schlesinger and M.Paunovic, 2015

EFFECT OF THE TYPE OF FUNCTIONAL GROUPS ON SCALING DURING ELECTRODIALYSIS

Evgenia Zhelonkina, Svetlana Shishkina

Vyatka State University, Moskovskaya st., 36, Kirov, 61000, Russia (*vgu_tep@mail.ru*)

Introduction

Membrane scaling seriously complicates the practical implementation and economic indicators of the electrodialysis process. The most serious problems arise in the demineralization of hard natural waters [1] and solutions containing ions of toxic heavy metals (THM) [2, 3].

Hardly soluble THM hydroxides can have a catalytic effect on the water dissociation reaction [4], which increases the transmembrane transport of H^+ and OH^- ions and leads to significant pH changes in the electrodialysis chambers [5].

It was shown [6] that the anion-exchange membranes can sorb THM co-ions due to form complexes with unprotonated tertiary and secondary aminogroups. These coordination centers also have increased catalytic activity with respect to the water dissociation reaction because they contain water molecules which polarized by metal cations [7].

The purpose of our work was to study the effect of the type of functional groups of the anion-exchange membranes on the formation and properties of hardly soluble precipitates of THM hydroxides.

Experiments

The objects of the study were the MA-40 and MA-41 anion-exchange membranes. The functional groups of the MA-40 membrane are secondary and tertiary amines. The functional groups of the MA-41 membrane are quaternary ammonium bases.

The method of selective polarization of the membranes was used to study the hydrogen and hydroxyl ions fluxes [5]. The solutions contained 0.005 M copper sulfate or nickel sulfate, pH 4-4.2. In solutions, which was taken from the desalting and concentration chambers, pH was measured, the concentrations of metal ions and anions were determined, and fluxes of salt ions and H^+ (OH^-) ions were calculated.

Results and Discussion

In Fig. 1 (a) shows the values of the transport numbers of hydrogen and hydroxyl ions obtained by the electrodialysis of the $CuSO_4$ solution with the use of the MA-40/MK-40 and MA-41/MK-40 membrane pairs. It should be noted that the black precipitate of the copper oxide was observed at the surface of the cation-exchange membrane at current densities $i \geq 5i_{lim}$. The values of the transport numbers of hydrogen ions through the cation-exchange membrane did not exceed 0.2, and the transport numbers of hydroxyl ions were close to zero in the entire region of current densities. As a result, the solutions in the desalting and concentration chambers were acidified. In the case of the MA-41 / MK-40 membrane pair, the transport numbers of the water dissociation products were approximately the same, which led to an acidification of the desalting chamber.

During the electrodialysis of the nickel sulfate solution (Fig. 1b), a green precipitate of nickel hydroxide was observed on the surface of the cation-exchange membrane. According to data by Tanaka [4], this hydroxide has a high catalytic activity with respect to the water dissociation reaction, which is confirmed by sufficiently high values of the transport number of hydrogen ions through the cation-exchange membrane. However, the transport numbers of the hydroxyl ions up to $i = 5i_{lim}$ remains close to zero, but at higher current densities it rapidly reaches a value of 0.6.

It is possible that the low value of t_{OH^-} due to the fact that the MA-40 membrane sorbs copper ions due to form complexes with functional groups [6,7]. Transport of the OH^- ions leads to the formation of hydroxides in the phase of the membrane, which reduces their flow.

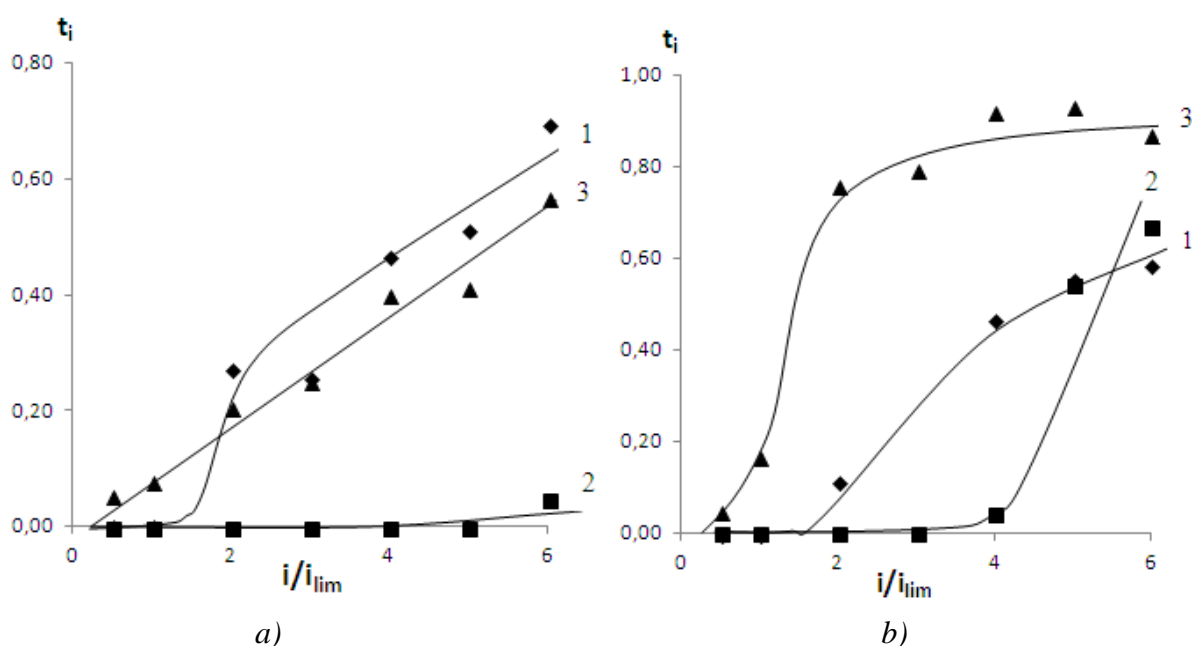


Figure 1- The transport numbers of ions in the CuSO_4 (a) and NiSO_4 (b) solutions: curve 1- the transport numbers of hydroxyl ions through the MA-41 membrane; curve 2 - the transport numbers of hydroxyl ions through the MA-40 membrane; curve 3- the transport numbers of hydrogen ions through the MK-40 membrane

Thus, scaling by the transition metals (copper, nickel) hydroxides on the cation-exchange membrane forms layers which are catalytically active with respect to the water dissociation reaction [4]. This makes it possible to transfer salt ions while the water dissociation reaction proceeds. According to our data, the MA-40 membrane can be used to remove salt ions with simultaneous pH correction.

References

1. Michaylin S, Basinet L. // Adv. Colloid Interface Sci. 2016. V.229. P.34-56.
2. Shishkina S.V., Zhelonkina E.A. // Proceedings of the Russian conference «Membrane-2016». N.Novgorod, 2016. P. 115-117.
3. Shishkina S.V., Zhelonkina E.A., Osokina P. // Proceedings of the International conference «Ion transport in organic and inorganic membranes». Tuapse, 2014. C. 279.
4. Tanaka Y. // Russ. J. Electrochem. 2012. N. 48.№7 P. 739.
5. Shaposhnik V.A., Kozaderova O.A. // Russ. J. Electrochem. 2012.N.48.№ 8.P.870.
6. Shishkina S.V., Pechenkina E.S., Dyukov A.V. // Russ. J. Electrochem. 2006. N. 42. P. 1457.
7. Ganych V.V., Zabolotsky V.I., Sheldeshov N.V. // Russ. J. Electrochem. 1992. N.28. №9.P.1390.

INFLUENCE OF HUMIDITY AND PRESSURE ON SEPARATION OF ETHYLENE/ ETHANE MIXTURES WITH SULFOCATIONITE MEMBRANES

¹Natalia Zhilyaeva, ¹Elena Mironova, ¹Margarita Ermilova, ¹Natalia Orekhova, ²Nina Shevlyakova, ²Margarita Dyakova, ²Vladimir Tverskoy, ^{1,3}Andrey Yaroslavl'tsev

¹A.V.Topchiev Institute of Petrochemical Synthesis, RAS, Moscow, Russia

E-mail: zhilyaeva@ips.ac.ru

²Lomonosov Moscow State University of Fine Chemical Technologies, Moscow, Russia

E-mail: tverskoy@mitht.ru

³Kurnakov Institute of General and Inorganic Chemistry, RAS, Moscow, Russia

E-Mail: yaroslav@igic.ras.ru

Introduction

One of the problems of pure light olefins preparation is the separation of saturated and unsaturated hydrocarbons mixtures. Industrially, this separation is carried out by cryogenic distillation, which is highly energy-intensive. The membrane separation has some advantages in comparison with distillation and adsorption methods due to their low energy consumption, moderate cost and compact design. However, ethylene/ethane separation with the use of conventional membranes has difficulties, being the result of the similar structure and sizes of their molecules. This problem can be solved with the use of membranes of "facilitated" transport due to selective formation of ethylene complexes with carrier. In our opinion the most promising can be ion exchange membranes in H⁺ or Ag⁺ form. Membranes from PE– graft– sulfonated polystyrene (PS) were chosen because of the possibility to change the content of carrier concentration and water uptake by varying the PS grafting degree [1]. The use of Ag⁺ form of investigated membranes showed their effectiveness for ethylene/ethane separation, the separation factor achieves high values up to 120. But these membranes lost gradually the selectivity owing to Ag⁺ ions, which are easily reduced under exposure to light to Ag nanoparticles. The same membranes in H⁺ form appeared to be more stable.

The aim of this work was to study influence of humidity and pressure on a separation process ethylene/ethane mixtures on polymeric sulfocationite membranes.

Experiments

Ion-exchange membranes based on polyethylene (PE), grafted with PS were prepared by the post-radiation graft polymerization of styrene on low-density PE film and the subsequent sulfonation of the grafted PS [1]. The permeability (*P*) of the polymer films was studied in a stainless steel permeation flow cell partitioned into two non-interconnected compartment by a membrane [2]. One of the compartments was fed with the individual gases (ethane and ethylene) or mixtures of ethane and ethylene in various ratios, and the carrier gas (helium) was passed through the other compartment. Both gas streams were humidified by passing through bubblers containing distilled water. The gases passed through the membrane (penetrant) were analyzed on gas chromatograph equipped with a thermal conductivity detector and a chromatographic column packed with Porapak Q, which provides the separation of ethane, ethylene, and water.

Results and Discussion

The changes in humidity mixtures of ethylene with ethane affect the permeability coefficients of the two gases (Fig. 1, 2). From the above, one would expect them to decrease with moisture increasing. However, this pattern is observed only for ethane, which is mainly transferred through a phase of PE. At the same time with a decrease in the degree of polystyrene grafting its permeability coefficient is also reduced. In the case of ethylene, opposite trend takes place - the permeability increases with increasing of humidity. This rule is violated only for the lowest degrees of grafting, when permeability value has remained largely unchanged. In the latter case, the system apparently is in a state close to the *percolation* threshold, ethylene transfer is determined by diffusion through PE and little affected by the humidity of the gas mixture in the range from 30 to 65% (Fig. 1, 2).

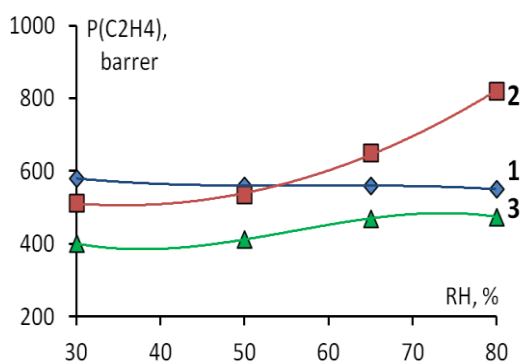


Figure 1. The dependence of the permeability coefficients of ethylene on humidity for the membranes with PS content of 26 % (1); 43 % (2); 55 % (3)

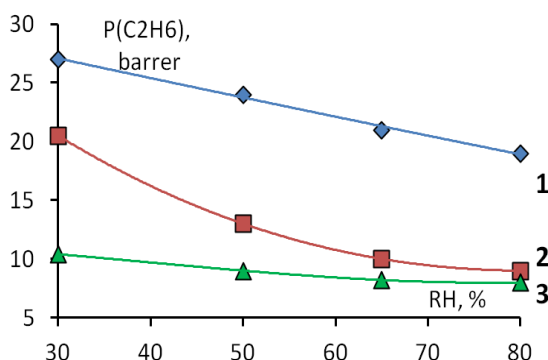


Figure 2. The dependence of the permeability coefficients of ethane on humidity for the membranes with PS content of 26 % (1); 43 % (2); 55 % (3)

The separation factor for this sample is nearly independent of the humidity of the gas mixture, increasing only slightly by lowering the permeability ethane (Fig. 3).

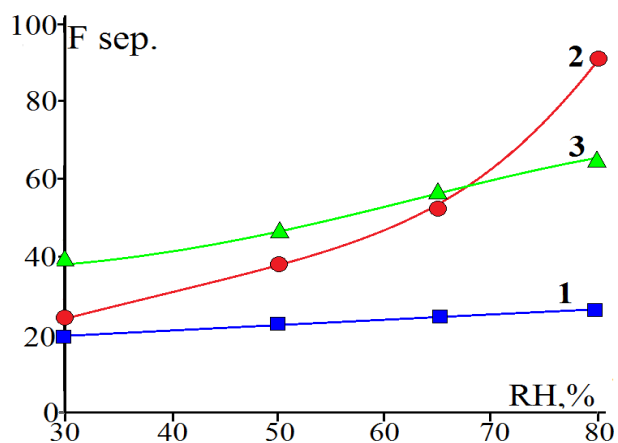


Figure 3. The dependence of ethylene/ethane separation factor on humidity for the membranes with PS content of 26 % (1); 43 % (2); 55 % (3)

With increasing in PS content the percolation threshold is reached, and ethylene transfer occurs mainly through a system of pores and channels of the membrane. Another factor is dominated with increase in humidity. The permeability of ethylene increases owing to increased mobility of its complex with a proton with an increase in moisture content and pore volume (Fig. 1). However, for the highest grafting degree, when a large number of pure water exists in the pore center, permeability of ethylene grows significantly slower (Fig. 1). In this regard, a clear increase in the ethane separation factor (Fig. 3) is observed, the most marked for the sample with PS content equal to 43%.

A study of the effect of the initial ethane and ethylene mixture composition on the transport properties of membranes with different degrees of grafting showed that the ethylene permeability coefficient decreases with an increase in ethylene partial pressure from $10 \cdot 10^2$ Pa to $60 \cdot 10^2$ Pa (Fig. 4). A decrease in the separation coefficient of ethylene is also observed (Fig. 5). Apparently, this is explained by the decrease of the ethylene permeability coefficient with increasing its concentration in the initial ethylene / ethane mixture and is related to the mechanism of its membrane transport [2]. The transfer of gases occurs due to the Langmuir sorption (the so-called double sorption mechanism), in which the penetrant is selectively sorbed by the carrier. Such a carrier, as noted above, is a proton that forms complexes with C_2H_4 . Due to the relatively low mobility of complexes of proton with ethylene, the concentration of protons appears to be a limiting factor in their transfer through membranes, which, with an increase in the initial partial pressure of ethylene, leads to a decrease in its permeability coefficient.

Thus, these results confirm the assumption about the prospect of using of membranes of facilitated transport, based on PE grafted with PSS in hydrogen form, for the separation of ethylene and ethane mixtures.

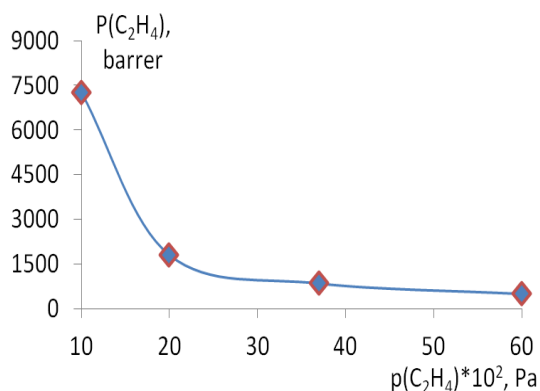


Figure 4. The dependence of the permeability coefficients of ethylene on its partial pressure of the initial mixture for the membrane with PS content of 55 %, $\text{C}_2\text{H}_4:\text{C}_2\text{H}_6 = 6:94$ v./v., humidity – 80%.

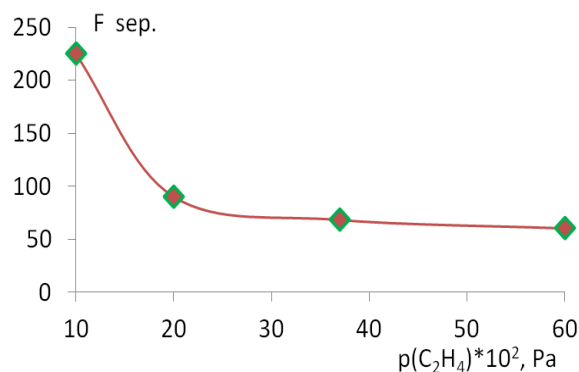


Figure 5. The dependence of the ethylene/ethane separation factor from the partial pressure of ethylene in the initial mixture for the membrane with PS content of 55 %, $\text{C}_2\text{H}_4:\text{C}_2\text{H}_6 = 6:94$ v./v., humidity – 80%.

Conclusions

Effect of "facilitated" ethylene transfer through the ion exchange membranes in the hydrogen form described at the first time. This can permit to optimize the process of a ethane and ethylene mixture separating.

The most selective ethylene extraction was carried out with the use of ion exchange membrane in the hydrogen form at relative humidity of mixture equal to 80% with the ethylene separation factor equal to 97.

References

1. Safronova E.Yu., Golubenko D.V., Shevlyakova N.V., D'yakova M.G., Tverskoi V.A., Dammak L., Grande D., Yaroslavtsev A.B./ New cation exchange membranes based on cross-linked sulfonated polystyrene and polyethylene for power generation systems./ J. Membrane Sci. 2016, V. 515, p. 196–203.
2. Zhilyaeva N.A., Mironova E.Yu., Ermilova M.M., Orekhova N.V., Bondarenko G.N., Dyakova M.G., Shevlyakova N.V., Tverskoy V.A., Yaroslavtsev A.B.// Petroleum chem. 2016. V. 56. P.1034-1041.

FUNCTIONAL MATRIX ACTIVITY OF NANOCOMPOSITES SILVER-ION EXCHANGER IN LOW-TEMPERATURE FORMALDEHYDE OXIDATION

Ekaterina Zolotukhina, Konstantin Gor'kov, Ekaterina Sakardina, Sofia Kleinikova

Institute of Problems of Chemical Physics RAS, Chernogolovka, Russia, *E-mail: zolek.ya@yandex.ru*

Lomonosov Moscow State University, Moscow, Russia, *E-mail: gorkovk@yandex.ru*

Formaldehyde (methanal) and acetaldehyde (ethanal) impurities in water and in alcohols are undesirable substances because of their great carcinogenic (for human) and poisoning (for catalysts in fuel cell) effect. In research practice (in works or research laboratory) fast detection of these impurities is very complicated because of absence of reliable and in situ methods of their detection. Well-known methods for detection of mentioned aliphatic aldehydes (polarography, gas chromatography (GC), spectroscopy) in solution are bulk and expensive or require toxic reagents. This problem is actual for scientist who develops new methods for removing of these pollutants from aqueous or alcohol media. So, reliable aldehyde detection method is necessary in many applications.

For detection of aldehydes we used UV-visible spectroscopy, GC and electrochemical methods. Electrochemical method of aldehydes detection was developed in two different direction. We used potentiodynamic polarization mode for gold microelectrode (25 μm in diameter) in three-electrode electrochemical cell with alkaline alcohol or water solution of corresponding aldehyde (ethanal or methanal). Calibration curve was formed from CV-data (peak current in various concentration of formaldehyde or acetaldehyde) in both oxygen and argon atmospheres. This method gave consistent results in comparison with UV-vis spectroscopy and GC data.

Alternative electrochemical method is amperometric detection of aldehyde by Pd/PPy composites modified electrodes [1]. Pd/PPy composites were formed via one-step&one-pot redox synthetic procedure reported in our previous works [2, 3]. Glassy carbon electrode modified with Pd/PPy powder with Nafion as a binding agent demonstrated high sensitivity and selectivity to formaldehyde in aqueous medium. The role of conjugated polymer matrix in this case is not only electronic conductive carrier, but stabilizer of Pd nanoparticles in their active state. Unfortunately, electrochemical stability of polypyrrole matrix is depended on pH. It was shown, that pH more than 13 leads to degradation of polymer matrix and decreasing of formaldehyde peak current. Nevertheless, one can conclude that electrochemical methods are more perspective and fast for real time aldehyde concentration detection and more applicable for research tasks.

By the help of this method we can investigate the kinetic and dynamic of catalytic oxidation of formaldehyde on silver nanoparticles included in ion exchange matrix. In our recent works we proposed novel silver-anion exchanger composite catalyst for aldehyde (methanal, ethanal) impurities removing (from water and ethanol) [4, 5]. These composites are able to remove aldehydes with 95 % conversion in oxidative catalytic reaction with formation of CO, CO₂ and H₂O as products.

In current work it was shown that ion exchange matrix is not only carrier for catalytic active particles, but its ion exchange properties play the important role in catalytic process. For ion exchange matrix in OH-form the hydroxide ions are involved in formation of methylene glycolate anions from formaldehyde in solution and these species react on the surface of silver particles with formation of CO₂ and H₂O. CO₂ also react with OH-counter ions with formation of carboxyl counter anions. These process is very important for catalytic oxidation of formaldehyde at room temperatures with high conversion. For matrices with other ionic form or with ionogenic centers of cathion-exchange nature catalytic process in the same conditions either does not realize or not so efficient.

It was demonstrated, that well-known mechanism for high-temperature formaldehyde oxidation is not realized. Novel mechanism based on electrochemical reactions was proposed for describing of catalytic oxidation of formaldehyde on silver-ion exchanger nanocomposites.

Acknowledgements

This work was supported by the Russian Foundation for Basic Research (project nos. 15–03–06351 A and 16–38–60164 mol_a_dk).

References

1. Gor'kov K.V., Zolotukhina E.V., Mustafina E.R. *et al.* Electrocatalytic activity of palladium–polypyrrole nanocomposite in the formaldehyde oxidation reaction // Dokl. Phys. Chem. 2016. V. 467. P. 37–40.
2. Magdesieva T.V., Nikitin O.M., Levitsky O.A. *et al.* Polypyrrole-palladium nanoparticles composite as efficient catalyst for Suzuki-Miyaura coupling // J. Molecular Catalysis A: Chem. 2012. V. 353-354. P. 50-57.
3. Magdesieva T.V., Nikitin O.M., Zolotukhina E.V. *et al.* Palladium-polypyrrole nanoparticles-catalyzed Sonogashira coupling // Mend.Comm., 2012. V.22. P. 305-306.
4. Sakardina E.A., Kravchenko T.A., Zolotukhina E.V., Vorotyntsev M.A. Silver/ion exchanger nanocomposites as low-temperature redox-catalysts for methanal oxidation // Electrochimica Acta. 2015. V. 179. P. 364–371.
5. Sakardina E. A., Kravchenko T. A., Kalinichev A. I., Zolotukhina E. V. Catalytic Activity of Silver–Ion Exchanger Nanocomposites in Methanal Oxidation Reaction with Molecular Oxygen // Doklady Physical Chemistry. 2015. V. 464 (1). P. 202–205.

EXPERIMENTAL STUDY OF THE EFFECT OF PULSED ELECTRIC FIELD ON CHRONOAMPEROGRAMS OF NAFION 438

Svetlana Zyryanova, Dmitriy Butylskii, Victor Nikonenko, Natalia Pismenskaya

Membrane Institute, Kuban State University, Krasnodar, Russia, E-mail: zyryanova.s.v@yandex.ru

Introduction

The use of pulsed electric field (PEF) has a long and successful history in galvanotechnics [1], but in the field of separation by membranes this approach is new [2].

The main effects in this case are an increase in the mass transfer rate [3], and a decrease in the rate of membrane scaling [2, 4]. The latter, perhaps, is more important for electrodialysis (ED) applications. In addition, in the PEF mode, the rate of water splitting at the membrane / solution interface decreases, and it becomes possible to work at higher voltages, avoiding problems associated with a change in the pH of desalted and concentrated solutions [2, 3]. Thus, the main obstacles for application of ED in overlimiting current modes, namely: scaling/fouling, reduction of mass transfer and low current efficiency, can be overcome.

Previous works have given the experimental evidence of the positive effect of PEF on electrodialysis of a NaCl solution in underlimiting current mode, and presented the theory of this effect [5]. However, the relationship between the parameters of PEF and ED process remains poorly studied. In this context, the aim of this work is to elucidate the impact of parameters of PEF on the chronoamperograms of Nafion™ 438 membrane.

Experiments

Nafion™ 438 is a perfluorosulfonic acid (PFSA) cation-exchange membrane, combining outstanding chemical resistance with an updated polytetrafluoroethylene (PTFE) monofilament reinforcement (Fig. 1a).

One side of the membrane is rough (Fig.1b), the other is smooth (Fig. 1c). According to the manufacturer's recommendation, the side marked CATH (the rougher side) must be installed facing the cathode.

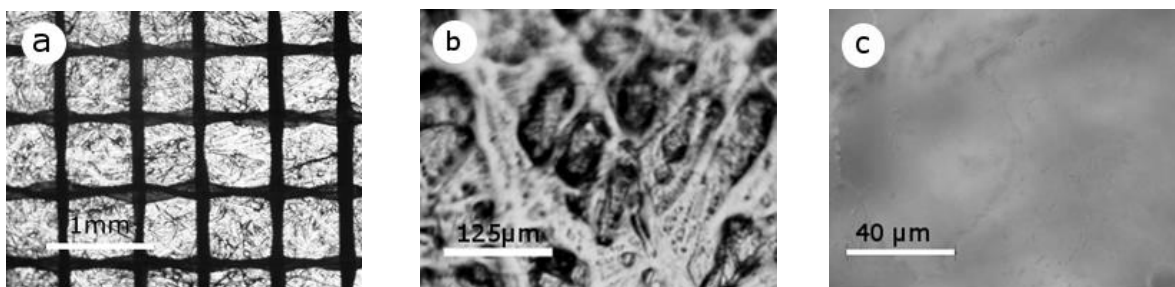


Figure 1. Optic images of wet Nafion 438 membrane. The reinforcing grid is shown in (a), (b) and (c) show the rough and smooth membrane sides, respectively.

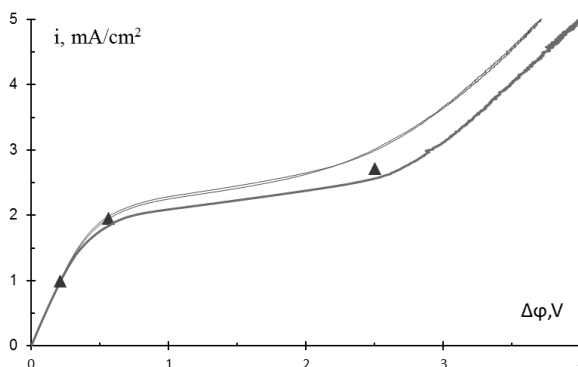


Figure 2. Current-voltage curve of Nafion 438. The triangular dots indicate the current/potential, which were used in measuring the chronoamperograms.

The experimental setup consisted of a membrane cell, hydraulic and measuring systems was described in [6]. A 0.02 M NaCl solution was used. Current-voltage curves (Fig.2) were obtained before and after experiments with PEF. Three points were chosen (i/i_{lim} : 0.5, 1.0, 1.38) to measure chronoamperograms. 15 different frequencies (0,01 Hz -20 Hz) were used. In the pulsed current mode (Fig. 3), a period where a constant voltage was applied (pulse duration T_{on}) was alternated with the period of zero current (T_{off}). Five duty cycles (defined as the ratio of T_{on} to the period $T = T_{on} + T_{off}$) were applied: $\alpha=1/4, 1/3, 1/2, 2/3$ and $3/4$.

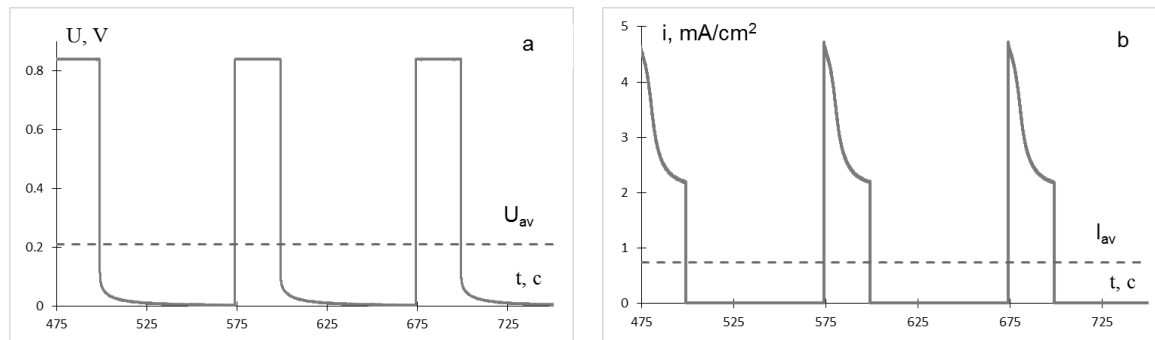


Figure 3. Current and voltage vs. time dependencies in PEF potentiostatic mode, $\alpha=1/4$. The dashed line shows the time-averaged voltage (a) and time-averaged current density I_{av} (b).

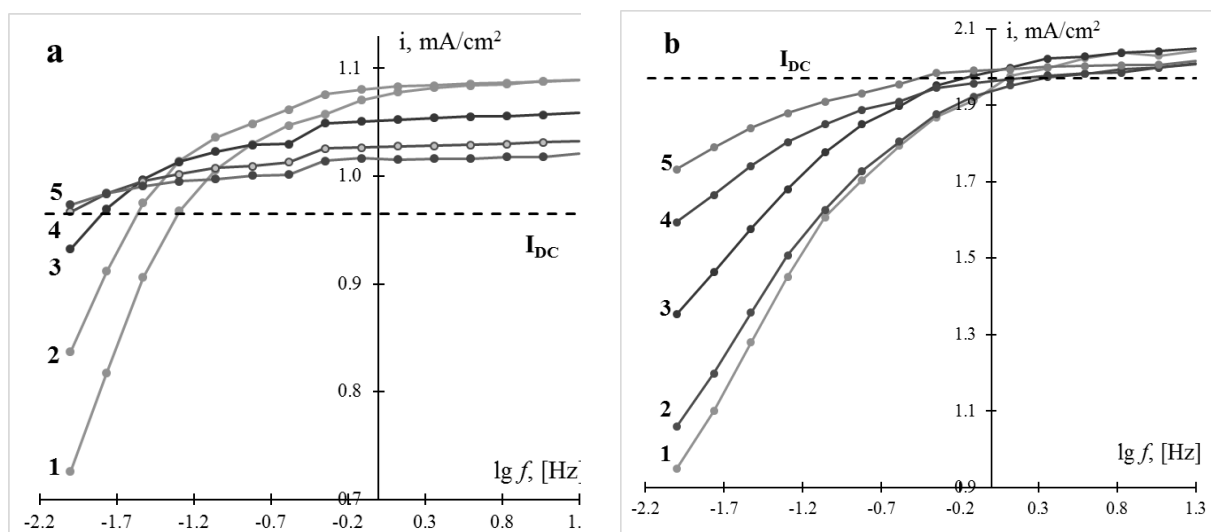
Results and Discussion

From obtained chronoamperograms, in case $i/i_{lim}=0.5$ (Fig. 4a), the time-averaged current density I_{av} in the PEF mode is higher than the current density $I_{DC} = 0.975 \text{ mA/cm}^2$ obtained in the DC mode with a potential jump of 0.21 V, in the high-frequency region. In the low-frequency region, I_{av} in the PEF mode is lower than I_{DC} . The maximum current gain is achieved at $\alpha=1/4$ and $f > 10\text{Hz}$ and is approximately 13% compared to I_{DC} . This result agrees well with the theoretical simulation for underlimiting current mode [5].

In case $i/i_{lim}=1$ (Fig.4b), in the high-frequency region, I_{av} in the PEF mode is slightly higher than the IDC current density obtained in the DC mode with a potential jump of 0.56 V. In the low-frequency region, I_{av} in pulsed current mode is much lower than IDC. The maximum current gain is achieved at $\alpha=1/2$ and is approximately 3.9% compared to IDC.

And in case $i/i_{lim}=1.38$ (Fig.4c), I_{av} in the PEF mode at high-frequencies strongly depends on the duty cycle α : I_{av} is greater than IDC for $\alpha = 1/2$ and $\alpha = 2/3$; and less than IDC for $\alpha = 1/3$ and $\alpha = 1/4$. The maximum current gain is 33% compared to IDC (for $\alpha = 1/2, f = 11.6 \text{ Hz}$).

The fact that the highest gain in current transfer is achieved in the range of overlimiting current densities is apparently explained by the effect of electroconvection.



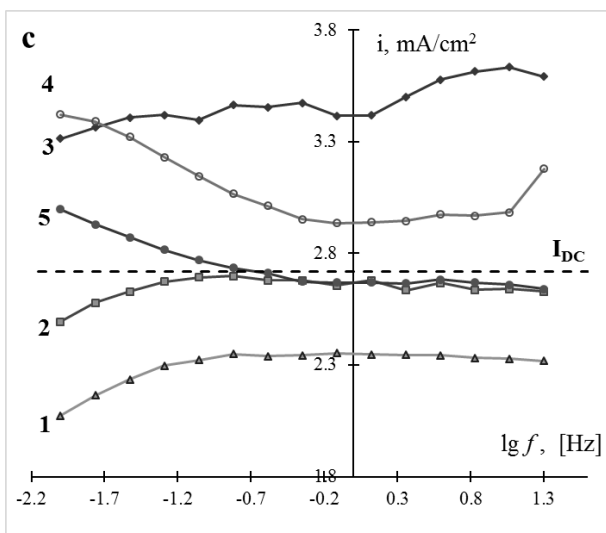


Figure 4. Chronoamperograms of Nafion 438 in PEF mode; the time-averaged potential drop is equal to $\Delta\varphi$ corresponding to $i/i_{lim}=0.5$ (a), 1 (b) and 1.38 (c). The duty cycle $\alpha = 1/4$ (1), $1/3$ (2), $1/2$ (3), $2/3$ (4) and $3/4$ (5).

Conclusion

By varying the values of the PEF parameters, one can achieve an increase in the time-averaged current density in comparison with the DC regime.

Acknowledgements

This investigation was carried out within French-Russian laboratory "Ion-exchange membranes and related processes". The authors are grateful to the Russian Foundation for Basic Research (grant 15-58-16005NCNIL_a) for financial support.

References

1. *Puippe J.C., Leaman F.H.* Theory and practice of pulse plating. Research Parkway, Orlando, Florida: AESF, 1986. 247p.
2. *Mikhaylin S., Bazinet L.* Fouling on ion-exchange membranes: Classification, characterization and strategies of prevention and control // *Adv. Colloid and Interface Sci.* 2016. V. 229. P. 34.
3. *Mishchuk N.A., Koopal L.K.* Intensification of electro dialysis by applying a non-stationary electric field // *Colloids Surf. A.* 2001. V. 176 (2-3). P. 195.
4. *Lee H.-J., Moon S.-H., Tsai S.-P.* Effects of pulsed electric fields on membrane fouling in electro dialysis of NaCl solution containing humate // *Sep. Purif. Technol.* 2002. V. 27 (2). P. 89.
5. *Sistat P., Huguet P., Ruiz B., Pourcelly G., Mareev S.A., Nikonenko V.V.* Effect of pulsed electric field on electro dialysis of a NaCl solution in sub-limiting current regime // *Electrochim. Acta.* 2015. V. 164. P. 267.
6. *Mareev S.A., Butylskii D. Yu., Pismenskaya N.D., Nikonenko V.V.* Chronopotentiometry of ion-exchange membranes in overlimiting current range. Transition time for finite-length diffusion layer, modeling and experiment // *J. Membr. Sci.* 2016. V. 500. P. 171-179.

THIN FILM COMPOSITE PTMSP/PAF MEMBRANES: STUDY OF PHYSICAL AGING

¹Danila Bakhtin, ¹Alexey Volkov, ¹Vladimir Volkov, ¹Valeriy Khotimskiy, ²Leonid Kulikov, ²Anton Maksimov, ²Eduard Karakhanov

¹A.V.Topchiev Institute of Petrochemical Synthesis (TIPS RAS), Moscow, Russian Federation
Email: db2@jps.ac.ru

²Moscow State University, Moscow, Russian Federation

Introduction

Vast majority of the membrane materials used for commercial gas separation membranes or being close to the upper bound on the Robeson diagram are amorphous, glassy polymers due to their high permeability/selectivity and ability to maintain rigid structure under processing conditions [1,2,3,4]. Meanwhile, the gas separation membrane shall meet the following criteria to be taking into account for further applications such as high gas permeability, desired level of selectivity, good mechanical and film forming properties, sufficient resistance under operation conditions, and stable performance during long-term operation. However, the polymeric materials, glassy polymers in particular, are non-equilibrium systems that are tend to relaxation of excess fractional free volume (FFV) due to macrochains rearrangements resulted in the deterioration of membrane permeability with time (so called “aging effect”).

The goal of this work was to evaluate the ability of porous aromatic framework particles (PAF-11) with the size of 150-200 nm to stabilize the performance of the thin film composite membranes with varied thickness of selective layer, based on the most permeable polymeric material PTMSP.

Experiments

PTMSP (TaCl₅/TIBA) and PAF-11 synthesized in [5] were used in this study. The thin top-layer of PTMSP was casted on the porous PAN-support (HZG, Germany) from 0.5 wt.% polymeric solution in chloroform by a kiss-coating technique described elsewhere [6]. In the case of loaded PTMSP layer, PAF-11 fillers were added to polymeric casting solution. It was possible to obtain TFC-membrane samples with size of 10x30 cm for further testing.

Transport characteristics of TFC membranes were monitored by the individual gas permeability (N₂, O₂, CO₂) measured by a volumetric method at room temperature, feed pressure up to 2 bar, permeate pressure was 1 bar. The active membrane surface area *S* was 12.6 cm². In all cases, the gas flux was increased linearly with the respect of trans-membrane pressure that was allowed to determine the gas permeability the graph slope. All gas flux and permeability presented in this work were recalculated to STP conditions.

All obtained membranes were analyzed by scanning electron microscopy (SEM). A high-resolution scanning electron microscope, Hitachi Tabletop Microscope TM3030Plus, was used. Beforehand the samples were immersed to *iso*-propanol to fill-up the pore structure, then fractured in liquid nitrogen and sputtered under vacuum with a thin (5 nm) layer of gold.

Results and Discussion

Figure 1 illustrates SEM visualization of the cross-section for TFC membrane sample. As might be noticed, the PAF-11 fillers are mostly well distributed within the polymer with thanks to the hydrophobic nature of porous particles, and no noticeable aggregation of these particles was observed.

In contrast to the annealing protocol used for fast aging of the dense PTMSP membranes in our recent study [5], all TFC membranes were kept at ambient temperature to monitor their physical aging preventing the possible affect of high temperature on the adhesion of top-layer and performance of PAN-support. Figure 2 presents the change in N₂, and CO₂ permeance of fabricated TFC membranes with the overall thickness of selective layer of 1.7-6.8 μm over the time of about 5000 hours; in addition, the data for TFC membrane with virgin PTMSP layer of 2.8 μm is also provided as a reference. It can be seen that the as-cast membranes showed the very promising gas permeation, but immediate decline in gas permeance occurred, which can be explained by the

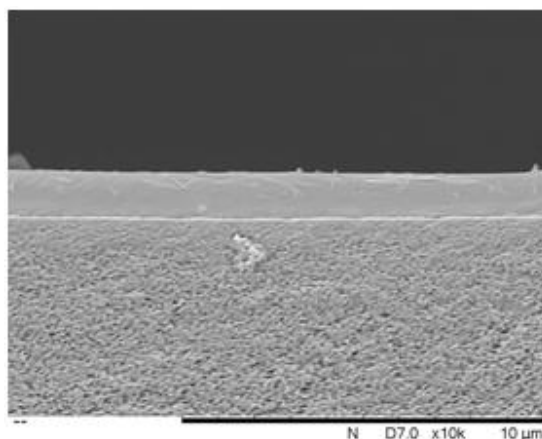


Figure 1. The Cross-Section of PAN/PTMSP TFC Membrane

physical aging of glassy polymer. Worth noting that the composite membranes with loaded PTMSP layer of 1.7, 2.1 and 3.8 μm possessed more rapid decline in gas permeance in contrast to the membrane with virgin PTMSP layer of 2.8 μm . However, the steady state performance was reached within shorter time for PTMSP/PAF-11.

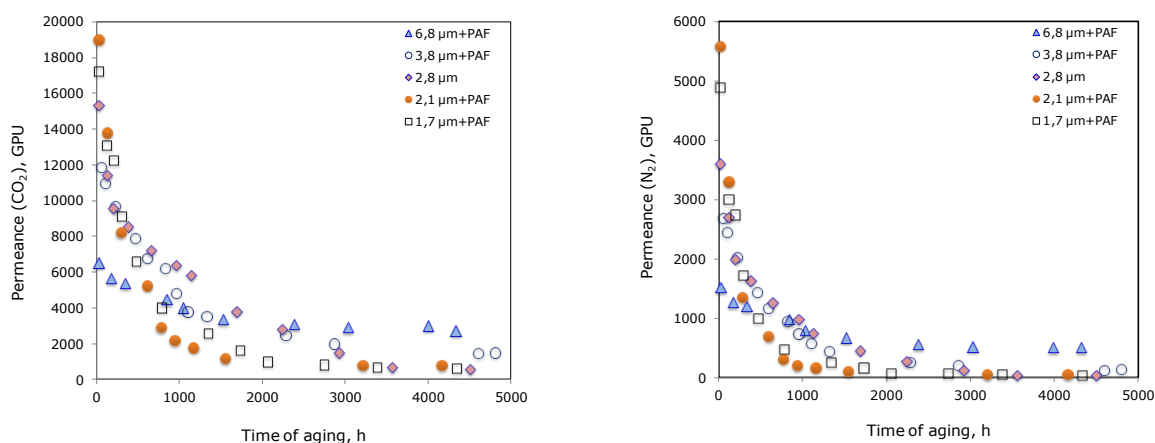


Figure 2. Gas permeance of TFC membranes with different top-layer thickness as a function of aging time.

It was found that the thickness of selective layer plays a major role in the physical aging of TFC membranes. The addition of PAF-11 (10 wt.%) resulted in achieving of faster relaxation and the increase in the resulted gas permeance in contrast with the TFC membranes with virgin PTMSP. The combination of addition of PAF-11 fillers and cross-linking of selective layer allowed to obtain the TFC membrane with N_2 , O_2 and CO_2 permeance of 790, 1250 and 4450 GPU, respectively, and the ideal selectivity $\alpha(\text{O}_2/\text{N}_2)=1.6$ and $\alpha(\text{CO}_2/\text{N}_2)=5.6$. To the best of our knowledge, these are the highest gas permeance values stable in time reported in the literature for the composite membranes based on the high permeability glassy polymers.

References

1. Baker R.W. Membrane technology and applications (2nd ed.), John Wiley & Sons, Ltd, West Sussex, England, 2004.
2. Robeson L.M. The upper bound revisited // J. Membr. Sci. 2008 V. 320. P. 390.
3. Bernardo P., et al. Membrane gas separation. A review/state of the art // Ind. Eng. Chem. Res. 2009 V. 48. P. 4638.
4. Freeman B., et al. Materials science of membranes for gas and vapor separation, John Wiley & Sons, Ltd, West Sussex, England, 2008.
5. Volkov, A. V., et al. Stabilization of gas transport properties of PTMSP with porous aromatic framework: Effect of annealing // J. Membr. Sci. 2016. V. 517. P 80-90.
6. Dibrov G.A., et al. Robust high-permeance PTMSP composite membranes for CO_2 membrane gas desorption at elevated temperatures and pressures // J. Membr. Sci. 2014. V. 470. P. 439.

Index of authors

A		Bazhenov S.	67, 91, 230, 268, 271, 283
Abdrashitov E.	207	Bazinet L.	72
Abonosimov D.	16	Bdiri M.	70, 198
Abonosimov O.	19	Bedin S.	419
Achoh A.	22	Belashova E.	72, 168, 275, 278
Ageev E.	25	Belenov S.	171, 236
Ainetdinov D.	27, 382	Belyakov G.	358
Akberova E.	29, 31, 34, 376, 398	Berekchiian M.	75
Akhmetshina A.	332	Bergmann A.	167
Akimova A.	193	Bespalov A.	86, 241, 367
Alekseenko A.	37, 236	Bessarabov S.	76
Aleshkina D.	40	Bildyukevich A.	91, 268, 271, 283, 286, 394
Ambarnov D.	135	Birukov Yu.	59
Andreeva M.	43, 259	Blonskaya I.	61
Anisimova n.	46	Bobreshova O.	113, 274
Aniskina U.	198	Bocharova A.	78
Anokhina T.	48	Bogdanova Yu.	80
Ansari M.	159	Bograchev D.	83
Antipov A.	51, 54, 56, 281, 282, 340, 361, 385	Bokun V.	207
Antonov S.	48	Bondarenko G.	91, 154
Antropova I.	59, 184	Bondarev D.	86
Apasonovich S.	283	Borisov I.	88, 91, 94, 149, 154, 261, 268, 271
Apel P.	61, 204	Borisova V.	76
Arzaniaeva L.	326	Bouyer D.	97
Atlaskin A.	64, 265, 332	Boyarishcheva A.	100
Azarov S.	349	Brailko O.	209
Azarova T.	349	But A.	86, 405
B		Butylskii D.	103, 254, 428
Badessa T.	46	Bykanova V.	215, 319, 349, 351
Bagryantseva I.	134, 292, 294	C	
Bakhtin D.	67, 88, 154, 402, 431	Chaabane L.	70, 107
Baryshev M.	225	Chérif M.	107, 198
		Cherkasov D.	335, 338

Cretin M.	105	Filippov A.	125, 129, 179
		Fink C.	167
D		Finkelshtein E.	94
Dammak L.	43, 70, 103, 107, 198, 259	Fomenko M.	326
Dankovtseva E.	110	Frants E.	132
Deabate S.	300	G	
Demekhin E.	132, 138, 139	Gaidamaka A.	134
Demina O.	78, 118, 179	Galushka I.	135
Demirci U.	112	Ganchenko G.	132, 138, 139
Denisova T.	113	Ganchenko N.	139
Déon S.	123	Gerasimova E.	114
Dmitrieva T.	59	Gerasimova I.	263
Dmitrieva M.	114	Gil V.	140
Dmitrieva K.	223	Goleva E.	29, 31, 143
Dobrovolsky Yu.	114, 207	Golovaneva N.	322
Dolgopolov S.	238	Golovin U.	210
Doludenko I.	419	Golubenko D.	146, 391
Dolzhikova V.	80	Golubev G.	88, 149, 261
Dontsov A.	388	Gor'kov K.	426
Dotsenko V.	367	Gorbacheva E.	138
Drozdov P.	64	Gorobchenko A.	152, 183
Dyakova M.	423	Grande D.	181
Dzyazko Yu.	295	Grushevenko E.	88, 94, 154, 374
		Gursky V.	358
E		Guterman V.	37, 171, 263
Efimov M.	402		
Eliseev A.	75	H	
Epifanova P.	322	Hapacheva N.	193
Ermilova M.	225, 423	Heidari B.	159
		Heidary F.	157, 159
F		Heidary S.	159
Faddeev N.	116	Hellal F.	70
Falina I.	78, 118, 179, 298, 359	Huguet P.	300
Farnosova E.	322		
Fedorova I.	120	I	
Fedoseeva A.	388	Ibragimov R.	91, 268
Fievet P.	123	Ignatenko V.	48
		Ilyin A.	391

Isaichykava Ya.	286	Kovaleva O.	210, 212
Istakova O.	161, 361	Kozaderova O.	256
Ivanets A.	349	Kozuhova E.	376
K		Kozlova A.	196
Kagramanov G.	322	Kozmai A.	107, 198, 233, 329
Karakhanov E.	431	Kravchenko T.	201, 371
Karavanova Yu.	228, 400	Kristavchuk O.	204
Kardash M.	27, 135, 362, 382	Kritskaya D.	207
Karpenko-Jereb L.	135, 164, 167, 307	Krivoshapkina E.	349
Kasparov M.	217	Kruglikov S.	419
Kasperchik V.	394	Kukushkin V.	204
Kharchenko O.	168, 275	Kulikov L.	431
<u>Kharitonov A.</u>	234	Kuriganova A.	116
Kharitonova T.	307	Kushakova L.	209
Khorokhorina I.	16, 210	Kutuzov K.	374
Khotimskiy V.	431	L	
Kim K.	256	Lakeev S.	59
Kirakosyan S.	171	Larchet C.	43, 70, 103, 107, 198
Kleinikova S.	426	Lavrova G.	291, 294
Klevtsova A.	173	Lazarev S.	16, 19, 210, 212
Kolganov V.	29	Lebedev D.	215, 319, 349, 351
Kolot D.	176	Lebedev K.	22, 217, 345, 376, 417
Konev D.	161, 281, 282, 340, 361, 385	Lebedeva O.	335, 338,
Kononenko N.	43, 179, 181, 289, 382	Leschenko E.	388
Kononov A.	152, 183	Lizunov N.	61
Korchagin S.	356	Loza N.	220, 223, 298
Korotkov D.	29	Loza S.	220, 223, 367
Korovkina A.	46	Lytkina A.	225
Korzhov A.	223	M	
Koshkina O.	59, 184	Magomedbekov E.	59, 184
Kostyanaya M.	186	Maksimov A.	431
Kotenev S.	19	Makulova S.	228
Kovalenko A.	189, 191, 278, 365, 370	Malakhov A.	230
Kovalev N.	100, 193	Malykhin M.	34
Kovalev S.	212		

Mareev S.	103, 152, 183, 233, 251, 254	Novikova S.	244
Markova S.	234	Novitsky E.	261, 374
Matushkina N.	25	Novomlinskiy I.	263
Matveev D.	261	O	
Medvedev O.	324	Orekhova N.	225, 423
Melnikov S.	22, 176, 238, 408, 411, 414	Orelovich O.	61
Menshchikov V.	236	Otvagina K.	265, 332
Mikhaleva O.	238	Ovcharova A.	91, 268, 271, 286
Mikhalin A.	83, 382	P	
Mikhaylin S.	72	Paperj K.	37
Minashkin V.	59	Parshina A.	113, 274
Mironova E.	423	Pavlets A.	37
Mochalova A.	265	Petriev I.	225
Mochalova T.	241	Petrov M.	281, 282
Morozov A.	27, 135	Petrova I.	186
Morozova N.	388	Petukhov D.	75
Moshareva M.	244	Philippova T.	129
Mugtamov O.	411	Pichugov R.	281, 282
Myint O P.	184	Pismenskaya N.	40, 72, 103, 140, 168, 173, 248, 254, 275, 326, 329, 428
N		Pismenskiy A.	189, 191, 278, 365
Naseri E.	159	Pleshivtseva T.	48
Nazyrova E.	246	Plisko T.	283, 286
Nebaikina D.	184	Plotnikova V.	76
Nebavskaya K.	248, 251, 259	Pogosyan K.	289
Nebavskiy A.	251, 254	Polikarpov V.	210
Nechaev A.	204	Polnyi R.	27
Nevakshenova E.	329	Polotskaya G.	316
Nichka V.	233, 251, 254	Polyanskii L.	371
Niftaliev S.	256	Ponomarev A.	207
Nikiforov I.	204	Ponomarev I.	228
Nikonenko V.	72, 103, 107, 140, 181, 183, 198, 233, 248, 254, 259, 275, 300, 303, 370, 428	Ponomareva V.	134, 291, 292, 294
Nosova E.	176,	Ponomarova L.	295
Novak L.	376, 405	Popov R.	212
		Popova D.	298
		Porozhnyy M.	300

Pourcelly G.	303	Sherstneva N.	340
Pridorogina V.	371	Shevlyakova N.	423
Prikhno I.	305	Shishkina S.	421
Prozorovich V.	349	Shiverskiy A.	215, 319, 349, 351
Pulyalina A.	316	Shkirskaaya S.	110, 179, 238, 246, 382
R		Shutova E.	291, 292
Reznichenko A.	209	Simunin M.	215, 319, 351
Roldughin V.	307, 310, 313	Sistat P.	329
Romanyuk N.	220	Sizikova N.	209
Rostovtseva V.	316	Smirnov M.	324
Rybtsev S.	46	Smirnova N.	116, 363
Rychagov A.	83, 382	Smolyanskii A.	59, 184
Ryzhkov I.	215, 319, 349, 351	Sobolev V.	248, 322, 347
S		Sokolova M.	324
Sabbatovskiy K.	248, 322	Solodovnichenko V.	215, 319, 349, 351
Safonova L.	120	Soloshko V.	246
Safronova E.	113, 274, 305	Sosenkin V.	83, 295, 382
Sakardina E.	426	Stenina I.	391
Salashenko M.	298	Strilets I.	362
Samarov A.	324	Strusovskaya N.	25
Sanginov E.	207	Szymczyk A.	123
Sarapulova V.	40, 173, 326, 329	T	
Sazanova T.	265, 332	Talagaeva N.	353
Schatt E.	167	Tatschl R.	167
Sedelkin V.	335, 338	Teplaykov V.	196
Seidova N.	191	Terentyev A.	114
Serdiuk A.	193	Terin D.	135, 356
Sereda O.	340	Timofeev S.	358
Sergeeva I.	347	Titskaya E.	359
Shabatin A.	310, 313	Toikka A.	324
Shalygin M.	196	Tolmachev Yu.	361, 385
Shandryuk G.	154	Trautmann Ch.	61
Shaposhnik V.	46, 343	Tripachev O.	361
Sheldeshov N.	100, 193, 217, 241, 345, 414	Trofimenko E.	374
Shelistov V.	132	Trubyanov M.	64
Shepelev A.	59	Tsyplyaev S.	135, 362

Tverskoy V.	391	Yasnev I.	396
U		Yatsev A.	398
Ulyankina A.	363	Yurova P.	400
Urtenov M.	189, 191, 278, 365, 370	Yushkin A.	48, 402
Urthaler P.	167	Z	
Ushakov N.	94	Zabolotsky V.	22, 86, 100, 118, 193, 217, 223, 241, 345, 367, 376, 405, 408, 411, 414, 417
Utin S.	367, 408, 414, 417	Zagorskiy D.	419
Uzdenova A.	259, 370	Zakharov B.	294
V		Zemtsov L.	402
Vakhnin D.	371	Zhdanov V.	310, 313
Vasil'eva V.	31, 34, 143, 217, 289, 376, 398, 405	Zhelonkina E.	421
Vasilenko P.	417	Zhilyaeva N.	423
Vasilevsky V.	149, 268, 271, 374	Zolotukhina E.	114, 353, 426
Vilensky A.	379	Zyryanova S.	428
Vinogradova L.	316		
Volkovich Yu.	83, 295, 382		
Volkov A.	48, 67, 154, 230, 261, 271, 374, 402, 431		
Volkov V.	88, 91, 94, 149, 186, 268, 271, 431		
Volochaev V.	37, 236		
Vorotyntsev M.	51, 54, 56, 161, 281, 282, 340, 353, 361, 385		
Vorotyntsev I.	64, 265, 332		
Vorotyntsev V.	64		
Vvedenskii A.	388		
Y			
Yakunina T.	27		
Yaroslavtsev A.	146, 186, 225, 228, 244, 305, 391, 400, 423		
Yaskevich A.	394		

Подписано в печать 15.05.2017г. Гарнитура Таймс.
Печать цифровая. Бумага офсетная.
Заказ № 860 Тираж 300 экз.

Отпечатано в типографии «Best Print».
Краснодар. ул. Селезнева 4/А, оф. 49-50.
Тел.: 8 (861) 210-20-16, моб.: 8 (909) 45-48-515
www.bestprint.info, office@bestprint.info



9 785990 677760